ISSN 0021-9673

VOL. 675 NOS. 1 + 2 JULY 22, 1994

COMPLETE IN ONE ISSUE

JOURNAL OF CHROMATOGRAPHY A

INCLUDING ELECTROPHORESIS AND OTHER SEPARATION METHODS

JOURNAL OF CHROMATOGRAPHY A

INCLUDING ELECTROPHORESIS AND OTHER SEPARATION METHODS

Scope. The *Journal of Chromatography A* publishes papers on all aspects of **chromatography, electrophoresis** and related methods. Contributions consist mainly of research papers dealing with chromatographic theory, instrumental developments and their applications. In the *Symposium volumes*, which are under separate editorship, proceedings of symposia on chromatography, electrophoresis and related methods are published. *Journal of Chromatography B: Biomedical Applications* —This journal, which is under separate editorship, deals with the following aspects: developments in and applications of chromatographic and electrophoretic techniques related to clinical diagnosis or alterations during medical treatment; screening and profiling of body fluids or tissues related to the analysis of active substances and to metabolic disorders; drug level monitoring and pharmacokinetic studies; clinical toxicology; forensic medicine; veterinary medicine; occupational medicine; results from basic medical research with direct consequences in clinical practice.

Submission of Papers. The preferred medium of submission is on disk with accompanying manuscript (see *Electronic manuscripts* in the Instructions to Authors, which can be obtained from the publisher, Elsevier Science B.V., P.O. Box 330, 1000 AH Amsterdam, Netherlands). Manuscripts (in English; *four* copies are required) should be submitted to: Editorial Office of *Journal of Chromatography A*, P.O. Box 681, 1000 AR Amsterdam, Netherlands, Telefax (+31-20) 5862 304, or to: The Editor of *Journal of Chromatography B: Biomedical Applications*, P.O. Box 681, 1000 AR Amsterdam, Netherlands. Review articles are invited or proposed in writing to the Editors who welcome suggestions for subjects. An outline of the proposed review should first be forwarded to the Editors for preliminary discussion prior to preparation. Submission of an article is understood to imply that the article is original and unpublished and is not being considered for publication elsewhere. For copyright regulations, see below.

Publication information. *Journal of Chromatography A* (ISSN 0021-9673): for 1994 Vols. 652–682 are scheduled for publication. *Journal of Chromatography B: Biomedical Applications* (ISSN 0378-4347): for 1994 Vols. 652–662 are scheduled for publication. Subscription prices for *Journal of Chromatography A*, *Journal of Chromatography B: Biomedical Applications* or a combined subscription are available upon request from the publisher. Subscriptions are accepted on a prepaid basis only and are entered on a calendar year basis. Issues are sent by surface mail except to the following countries where air delivery via SAL is ensured: Argentina, Australia, Brazil, Canada, China, Hong Kong, India, Israel, Japan, Malaysia, Mexico, New Zealand, Pakistan, Singapore, South Africa, South Korea, Taiwan, Thailand, USA. For all other countries airmail rates are available upon request. Claims for missing issues must be made within six months of our publication (mailing) date. Please address all your requests regarding orders and subscription queries to: Elsevier Science B.V., Journal Department, P.O. Box 211, 1000 AE Amsterdam, Netherlands. Tel.: (+31-20) 5803 642; Fax: (+31-20) 5803 598. Customers in the USA and Canada wishing information on this and other Elsevier journals, please contact Journal Information Center, Elsevier Science Inc., 655 Avenue of the Americas, New York, NY 10010, USA, Tel. (+1-212) 633 3750, Telefax (+1-212) 633 3764.

Abstracts/Contents Lists published in Analytical Abstracts, Biochemical Abstracts, Biological Abstracts, Chemical Abstracts, Chemical Titles, Chromatography Abstracts, Current Awareness in Biological Sciences (CABS), Current Contents/Life Sciences, Current Contents/Physical, Chemical & Earth Sciences, Deep-Sea Research/Part B: Oceanographic Literature Review, Excerpta Medica, Index Medicus, Mass Spectrometry Bulletin, PASCAL-CNRS, Referativnyi Zhurnal, Research Alert and Science Citation Index.

US Mailing Notice. *Journal of Chromatography A* (ISSN 0021-9673) is published weekly (total 52 issues) by Elsevier Science B.V., (Sara Burgerhartstraat 25, P.O. Box 211, 1000 AE Amsterdam, Netherlands). Annual subscription price in the USA US$ 4994.00 (US$ price valid in North, Central and South America only) including air speed delivery. Second class postage paid at Jamaica, NY 11431. **USA POSTMASTERS**: Send address changes to *Journal of Chromatography A*, Publications Expediting, Inc., 200 Meacham Avenue, Elmont, NY 11003. Airfreight and mailing in the USA by Publications Expediting.

See inside back cover for Publication Schedule, Information for Authors and information on Advertisements.

0021-9673/94/$07.00

Printed in the Netherlands

VOL. 675, NOS. 1 + 2 JOURNAL OF CHROMATOGRAPHY A JULY 22, 1994

CONTENTS

(Abstracts/Contents Lists published in Analytical Abstracts, Biochemical Abstracts, Biological Abstracts, Chemical Abstracts, Chemical Titles, Chromatography Abstracts, Current Awareness in Biological Sciences (CABS), Current Contents/Life Sciences, Current Contents/Physical, Chemical & Earth Sciences, Deep-Sea Research/Part B: Oceanographic Literature Review, Excerpta Medica, Index Medicus, Mass Spectrometry Bulletin, PASCAL-CNRS, Referativnyi Zhurnal, Research Alert and Science Citation Index)

REGULAR PAPERS

Column Liquid Chromatography

(Continued overleaf)

Contents (continued)

SHORT COMMUNICATIONS

JOURNAL OF CHROMATOGRAPHY A

VOL. 675 (1994)

JOURNAL OF CHROMATOGRAPHY A

INCLUDING ELECTROPHORESIS AND OTHER SEPARATION METHODS

ELSEVIER

Amsterdam – Lausanne – New York – Oxford – Shannon – Tokyo

J. Chromatogr. A, Vol. 675 (1994)

0021-9673/94/$07.00

Printed in the Netherlands

ELSEVIER

Journal of Chromatography A, 675 (1994) 1–11

JOURNAL OF CHROMATOGRAPHY A

Comparison of the models describing the retention in micellar liquid chromatography with hybrid eluents for a group of benzene derivatives and polycyclic aromatic hydrocarbons

M.A. García, O. Jiménez*, M.L. Marina

Departamento de Química Analítica, Facultad de Ciencias, Universidad de Alcalá de Henares, 28871 Alcalá de Henares, Madrid, Spain

(First received December 20th, 1993; revised manuscript received March 22nd, 1994)

Abstract

Some models for predicting capacity factors of benzene derivatives and some polycyclic aromatic hydrocarbons as a function of surfactant and organic modifier concentrations in micellar liquid chromatography with hybrid eluents have been tested. The surfactants used in this study were hexadecyltrimethylammonium bromide and sodium dodecyl sulphate and as organic modifiers *n*-propanol and *n*-butanol were employed both on C_8 and C_{18} columns.

The equation that best explains the experimental results is $1/k' = A\mu + B\varphi^2 + C\varphi + D\mu\varphi + E$ so we propose the use of this model in conjunction with the appropriate factorial design to predict the solute retention behaviour in micellar liquid chromatography with hybrid eluents.

1. Introduction

Micellar liquid chromatography (MLC) was first described by Armstrong and co-workers in 1979 [1,2]; since then, many reports have been published on the retention dependence of micellar concentrations [3–7], selectivity [4,8–13], and efficiency [14–18].

The primary advantages of this type of liquid chromatography compared to conventional reversed-phase liquid chromatography (RPLC) are low cost and non-toxicity of surfactants *versus* expensive and flammable solvents of chromatographic grade [3,4,19,20], unique selectivity [14,17,18,20–22], compatibility of mobile phases with salts and water-insoluble compounds [18], and shorter equilibration times for gradient elution. Perhaps the main drawback of this separation technique is its reduced efficiency compared to conventional reversed-phase systems [14,17,18,20,23,24], which is probably due to a poor wetting of the stationary phase [14] and restricted mass transfer [14,15].

In MLC, solutes may interact with both the stationary and mobile phases and thus partition equilibria are established between water and stationary phase, between water and micelles, and between micelles and stationary phase [25,26]. If the solute is water-insoluble partition occurs directly between the micelle solute species and the surfactant-coated stationary phase [26–28].

The addition of propanol and more generally short-chain alcohols to the mobile phase improves the chromatographic efficiency but the mechanism of solute retention in such hybrid

* Corresponding author.

0021-9673/94/$07.00
SSDI 0021-9673(94)00292-H

eluents is very complex because alcohol modifiers alter the characteristics of surfactant [7,11,13,27,29,30] and the nature of the surfactant-modified stationary phase [27].

Although the use of hybrid eluents in MLC is a separation technique of widespread application there is a lack of knowledge about the solute retention mechanism. It seems clear that solute retention depends mainly on micelle and organic modifier concentrations and nature, on the nature of the solute, on pH and ionic strength, etc, but more work is needed to establish an equation that permits to predict the retention behaviour of solutes in such complicated systems and thus enable us to exploit the full potential advantages of this separation technique in a more judicious way.

Some authors have explored the possibilities of predicting the solute retention in MLC with hybrid eluents with varying concentrations of surfactant and organic modifier. Thus, Strasters *et al.* [6] using a dimensional space design determined the capacity factors of five mobile phases (four at the corners and the last one at the centre). Then, an equation of the type

$$\log k' = A\mu + B\varphi + C \quad (1)$$

is fitted in each of the four triangle subspaces with three measurements, two at the corners and the central point (μ being the total surfactant concentration and φ the volume fraction of organic modifier).

Torres-Lapasió *et al.* [7] also used the capacity factor of five mobile phases (with different experimental designs) to achieve the constants calculation for different equations and then with all the capacity factors measurements (thirteen mobile phases and five solutes) the prediction errors were calculated. The equations that they checked consisted in linear and quadratic expressions in which the reciprocal or the logarithm of the capacity factor were related to μ and φ. As an example of such expressions we can cite three of them with which the least errors were obtained

$$1/k' = A\mu + B\varphi + C\mu\varphi + D \quad (2)$$

$$1/k' = A\mu + B\varphi^2 + C\varphi + D\mu\varphi + E \quad (3)$$

$$\log k' = A\mu + B\varphi + C\mu\varphi + D \quad (4)$$

The best results were obtained with Eq. 2. It was also indicated that for the catecholamines studied by them and for several aromatic compounds the retention did not follow a linear model ln k' *versus* (μ,φ). However, they only tested the models with an anionic surfactant (sodium dodecyl sulphate, SDS).

The objective of this report is to provide more data for a better understanding of the solute retention mechanism in MLC with hybrid eluents and to find, if possible, an equation to describe it which should allow an easy way to predict the retention of a solute in any mobile phase with a minimum effort.

To study the influence of the nature and concentration of the surfactant and the alcohol on the retention of the solute, we have used the retention data of fifteen benzene and naphthalene derivatives and eight polycyclic aromatic hydrocarbons in micellar mobile phases with different concentrations of hexadecyltrimethylammonium bromide (CTAB) and SDS modified with different percentages of *n*-propanol and *n*-butanol. This study has been made for two columns, octadecylsilica and octylsilica.

2. Experimental

2.1. Apparatus

The Chromatograph consisted of a 1050 pump, a 1050 automatic injector, a 1050 spectrophotometric detector of variable wavelength, and a HP 3394 integrator (all from Hewlett-Packard).

Retention data were obtained with a Spherisorb C_8, 15 cm × 4.0 mm I.D. column ($d_p = 5$ μm) (Teknokroma).

A 0.45-μm filter and filtration system (Millipore) were used.

2.2. Reagents

SDS, CTAB, *n*-propanol and *n*-butanol (all from Merck) were used as received. Water

purified with a Milli-Q system (Millipore) was used.

Benzene derivatives and polycyclic aromatic hydrocarbons were as follows: (1) benzene, (2) benzylic alcohol, (3) benzamide, (4) toluene, (5) benzonitrile, (6) nitrobenzene, (7) phenol, (8) 2-phenylethanol, (9) chlorobenzene, (10) phenylacetonitrile, (11) 3,5-dimethylphenol, (12) naphthalene, (13) 1-naphtol, (14) 2-naphtol, (15) 1-naphthylamine, (16) pyrene, (17) phenanthrene, (18) 2,3-benzofluorene, (19) fluorene, (20) fluoranthene, (21) acenaphtylene, (22) acenaphthene and (23) anthracene.

2.3. Procedure

Micellar mobile phases (with a surfactant concentration from 0.035 to 0.12 *M*) were prepared by dissolving the appropriate amount of surfactants and *n*-propanol or *n*-butanol in water in a ultrasonic bath followed by filtration. Stock solutions of test solutes were prepared in the mobile phase itself and their concentrations were adjusted to permit their detection from the injection of a 20-μl volume of sample. The void volume of the column for SDS micelles was determined from the retention time of the peak originating from the injection of the nitrate anion into the chromatographic system. For CTAB mobile phases, the first deviation of the baseline was employed.

The column and the mobile phase were water jacketed and thermostated at 25 ± 1°C with a circulating water bath.

2.4. Data manipulation

Multiple regression analysis and Box plots were carried out using a SOLO Statistical System [31].

3. Results and discussion

The capacity factors of eight polycyclic aromatic hydrocarbons in a MLC system in the presence of *n*-propanol and *n*-butanol were determined by using SDS and CTAB as surfactants in the mobile phase and a C_8 column. The results of these experiments have been used in this article in conjunction with the results obtained previously for a group of benzene and naphthalene derivatives on C_{18} and C_8 columns with mobile phases of SDS and CTAB without and in the presence of *n*-propanol and *n*-butanol. Table 1 groups all experimental data used in this work. All these data allowed conclusions to be drawn regarding the models which better fit the experimental retention data.

In order to compare models 1 and 2 (Eqs. 2 and 4 in the Introduction section of this article), several factorial designs were employed depend-

Table 1
Summary of experimental data used in this study

Experiment	Compounds	Surfactant and concentration range (*M*)	Alcohol and concentration range (%, v/v)	Column	n^a	Ref.
1	1–23	CTAB (0.035–0.1)	Propanol (0.03–0.1)	C_{18}	345	13, this work
2	1–15	SDS (0.035–0.08)	Butanol (0–0.1)	C_{18}	180	25,32
3	1–15	CTAB (0.05–0.12)	Propanol (0–0.1)	C_8	299	33
4	1–15	CTAB (0.05–0.12)	Butanol (0–0.1)	C_8	292	33
5	1–15	SDS (0.05–0.12)	Propanol (0–0.1)	C_8	300	33
6	1–15	SDS (0.05–0.12)	Butanol (0–0.1)	C_8	300	33
7	16–23	CTAB (0.05–0.12)	Propanol (0.03–0.1)	C_8	112	This work
8	16–23	CTAB (0.05–0.12)	Butanol (0.03–0.1)	C_8	120	This work
9	16–23	SDS (0.05–0.12)	Propanol (0.03–0.1)	C_8	118	This work
10	16–23	SDS (0.05–0.12)	Butanol (0.03–0.1)	C_8	120	This work

[a] *n* = Number of experimental data per experiment (number of mobile phases multiplied by number of compounds).

ing on the hybrid system considered (Fig. 1). As shown in Fig. 1 capacity factors for compounds 16 to 23 were not obtained in the absence of alcohol due to the great retention times of these solutes in such media. With the capacity factors for these five mobile phases (Fig. 1) a multiple regression analysis [31] was achieved for each solute and then capacity factors for all mobile phases were calculated. With both, experimental and predicted capacity factors for models 1 and 2, the relative errors were calculated.

Our results, globally, show that the mean relative errors obtained for Eq. 4 are greater than those for Eq. 2, both for C_8 and C_{18} columns (Fig. 2), which is in agreement with the work reported by Torres-Lapasió *et al.* [7]. This is true in all the systems studied with only one exception that we will discuss later. As shown in Fig. 2 the mean relative errors are low, lesser than 5 and 10% for Eqs. 2 and 4, respectively.

With the aim of studying the influence of the surfactant nature on the errors obtained with

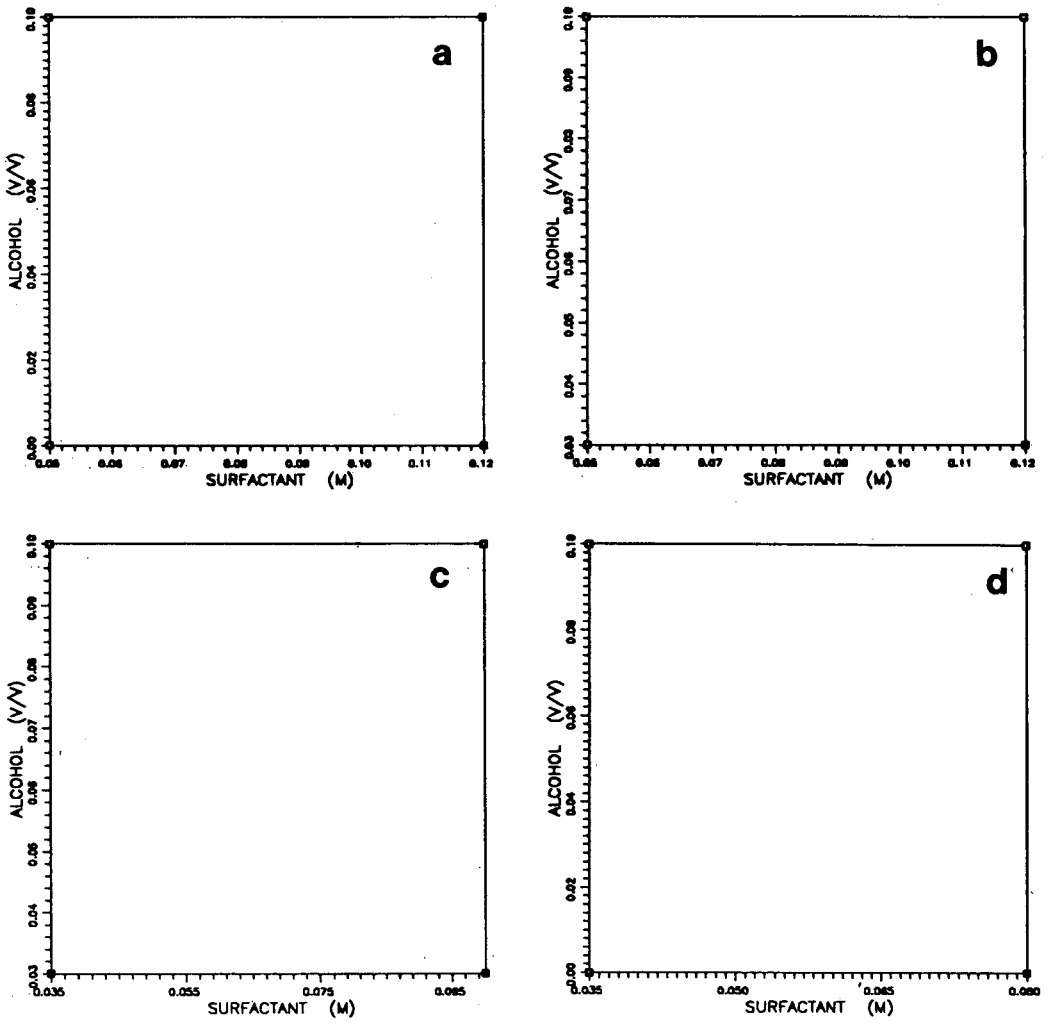

Fig. 1. Factorial designs used in the modellization study for systems (a) CTAB–*n*-propanol, CTAB–*n*-butanol, SDS–*n*-propanol and SDS–*n*-butanol (compounds 1–15 and C_8 column), (b) CTAB–*n*-propanol, CTAB–*n*-butanol, SDS–*n*-propanol and SDS–*n*-butanol (compounds 16–23 and C_8 column), (c) CTAB–*n*-propanol (compounds 1–23 and C_{18} column) and (d) SDS–*n*-butanol (compounds 1–15 and C_{18} column).

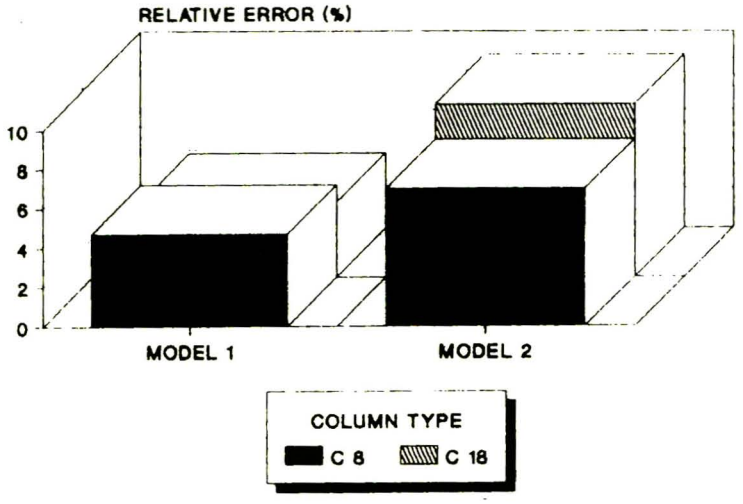

Fig. 2. Mean relative errors (%) for models 1 (Eq. 2) and 2 (Eq. 4) for C_8 and C_{18} columns.

Eqs. 2 and 4, the mean relative errors in hybrid phases of SDS and CTAB modified with the same alcohol were compared. Thus, in Fig. 3a and b the mean relative errors for the fifteen benzene and naphthalene derivatives (1–15) *versus* the type of equation for two different systems (CTAB–butanol and SDS–butanol) are shown. We can observe that in both cases the equation that best explains the experimental results is Eq. 2. Further, the mean relative errors for both equations are lesser when CTAB is used as surfactant. Although the results are not shown, the same conclusions have been found for the systems CTAB–propanol *versus* SDS–propanol with compounds 1–23.

CTAB and SDS are positively and negatively charged surfactants, respectively, so the solutes can interact in a different way with both surfactants. The solutes studied in this work have aromatic rings, so favourable electrostatic interactions between the positively charged CTAB head groups and the unlocated charge of the aromatic ring(s) of the solutes can be expected [25]. Thus, it seems that Eq. 2 better explains the results than Eq. 4 when, both, favourable electrostatic and hydrophobic interactions with micelles are responsible for the solute retention behaviour.

Although it has not been possible to compare the relative errors with both equations when the surfactant nature is modified using a C_{18} column, at least in the systems studied the results show, again, that Eq. 4 grants the poorest prediction of the solute retention behaviour.

In Fig. 3 the relative error of capacity factor prediction with Eqs. 2 and 4 when the hybrid eluents are SDS–propanol (Fig. 3c) and SDS–butanol (Fig. 3b) are shown in order to study the organic modifier nature. As we can observe for both alcohols, the equation that best explains, the experimental results is Eq. 2 being the mean relative errors greater when butanol is used as the organic modifier. Although the results obtained when CTAB is used as surfactant in the hybrid eluent and propanol as organic modifier have not been included in the figure the same conclusions can be drawn. In these systems, CTAB–propanol and CTAB–butanol, the mean relative errors of capacity factors prediction are 2.02 and 3.60% with Eq. 2 and 3.38 and 9.86% with Eq. 4, respectively.

Consequently, the equation that best explains the experimental results for compounds 1–15 is Eq. 2. This is also valid with the polycyclic aromatic compounds 16–23 with a C_{18} column (results not shown). With a C_8 column, as shown in Fig. 4, the relative errors obtained with Eq. 4 are lesser than those obtained with Eq. 2 only when SDS is used as the surfactant and butanol is employed as organic modifier (Fig. 4d), and

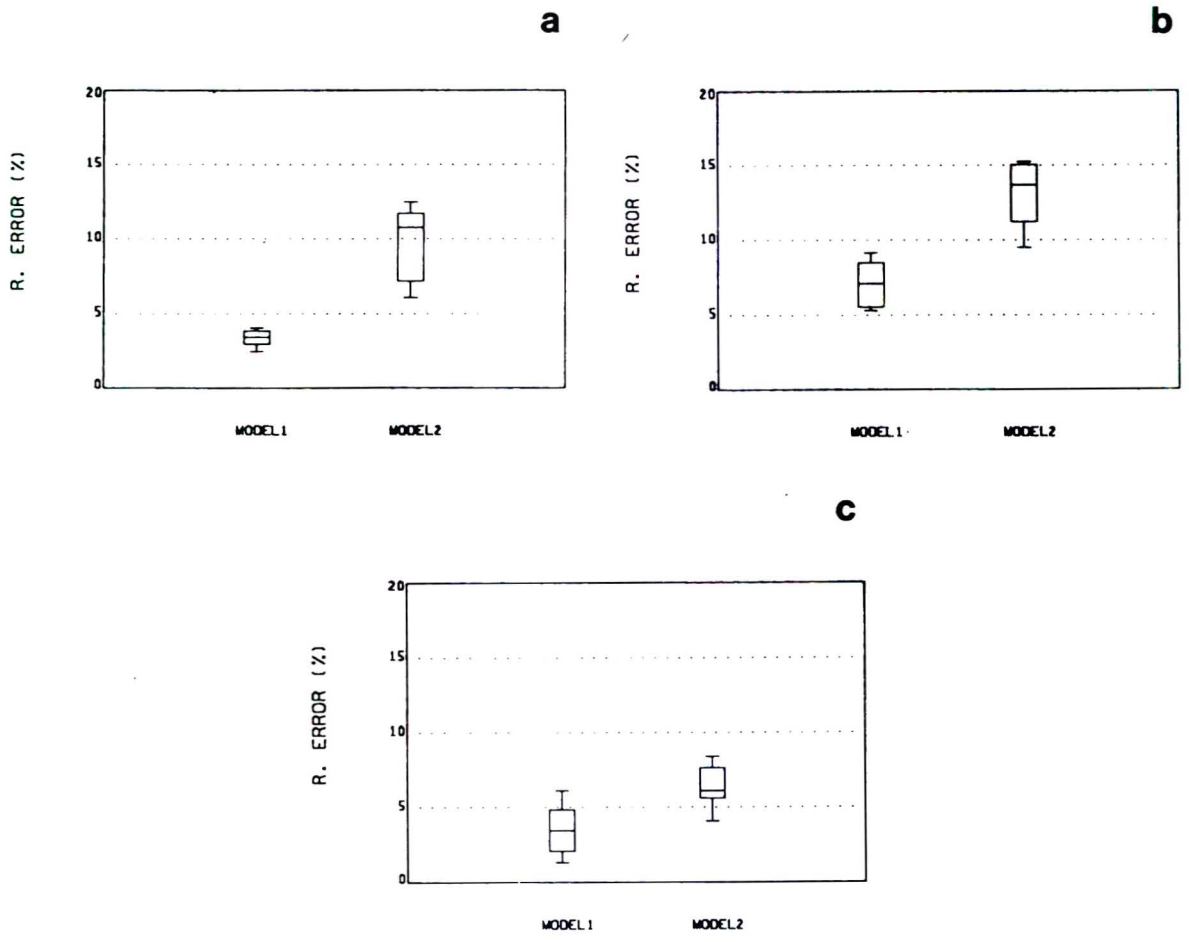

Fig. 3. Box plots for relative (R.) errors *versus* models of capacity factor prediction 1 and 2 for compounds 1–15 and a C_8 column with hybrid systems (a) CTAB–*n*-butanol, (b) SDS–*n*-butanol and (c) SDS–*n*-propanol.

not in the other cases (Fig. 4a–c). In Fig. 4a–c the relative errors *versus* models 1 and 2 are plotted for the hybrid eluents CTAB–propanol, CTAB–butanol and SDS–propanol, respectively. It can be concluded from these figures that changes in surfactant nature and alcohol influence the relative errors obtained for both models. The relative errors are low when CTAB is used as surfactant and they enhance when systems containing SDS are considered. These facts together seem to indicate that both models fail in taking into account some interactions of solutes, and that they are more important in very hydrophobic systems and when solute–micelle interactions are diminished.

Borgerding *et al.* [27] have reported that the amount of sorbed surfactant in the stationary phase decreases with the addition of alcohol modifiers compared to that possible in their absence and that the amount of surfactant desorbed by such additives is proportional to the additive concentration and increases as the hydrophobicity of the additive increases. Thus, one can expect that the amount of surfactant desorbed by butanol is greater than that by propanol. One can also expect that butanol can compete in a greater extent than propanol with the micelle for the interaction of the solutes.

In order to clarify the anomalous behaviour observed in Fig. 4d, another equation (Eq. 3 or model 3 in this discussion) has been included in the retention prediction study with all the com-

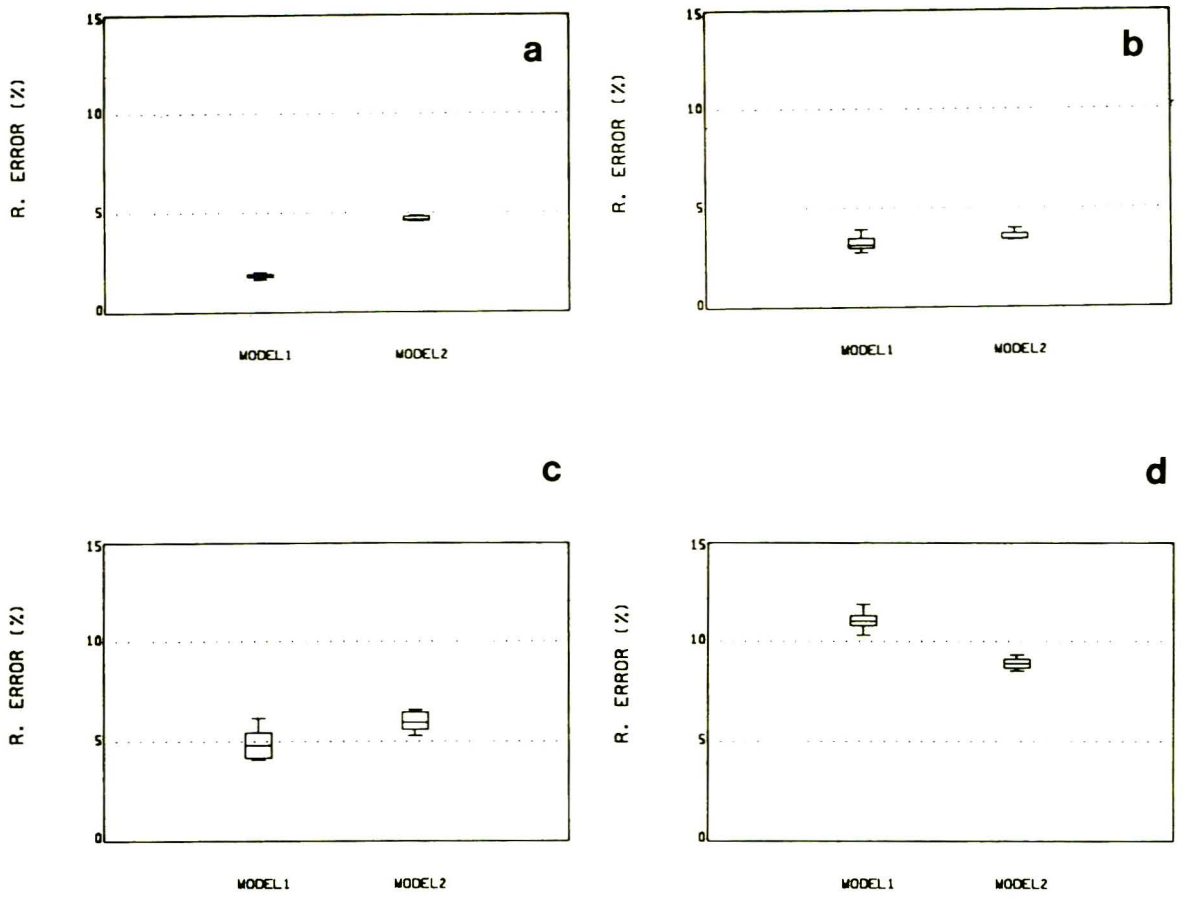

Fig. 4. Box plots for relative errors *versus* models of capacity factor prediction 1 and 2 for compounds 16–23 and a C_8 column with hybrid eluents (a) CTAB–*n*-propanol, (b) CTAB–*n*-butanol, (c) SDS–*n*-propanol and (d) SDS–*n*-butanol.

pounds (1–23) since the dependence of the capacity factor on the concentration of micelles seems to be different from the dependence of the concentration of the modifier [7]. Torres-Lapasió *et al.* [7] have reported that equivalent coefficients (A–E) in both Eqs. 2 and 3 have been obtained for catecholamines and the φ^2 term was negligible compared to the $\mu\varphi$ term. In the case of compounds 16–23 the coefficients (A–E) for Eq. 3 have been calculated and for the system SDS–butanol (with a C_8 column) they are given in Table 2. These results show that for these compounds the term φ^2 is not negligible compared to the $\mu\varphi$ or the μ term. This behaviour is clearly shown in Fig. 5 in which the inverse of the capacity factor for pyrene (compound 16) *versus* φ is plotted for different concentrations of surfactant. It is evident that the relation between $1/k'$ and φ is quadratic and the effect is more pronounced as the surfactant concentration is increased.

Once the necessity of including a term in φ^2 is explained for the most hydrophobic compounds the validity of this equation has been checked with all the compounds in the different systems. The mean relative errors obtained with Eq. 3 are equal or clearly better as compared with those obtained with Eqs. 2 or 4. For instance, in Fig. 6, the relative errors with Eqs. 2, 3 and 4 for the different solutes in two systems (CTAB–propanol and SDS–butanol for a C_8 column) are shown. These two systems represent the best and the worst results for the prediction of solutes capacity factors. In Fig. 6a (CTAB–propanol) it

Table 2
Parameter values for Eq. 3 with the system SDS–*n*-butanol and a C_8 column

Compound	*A*	*B*	*C*	*D*	*E*
16	0.2092	10.1449	−1.2521	8.6939	0.0296
17	0.2653	11.2225	−1.3491	8.3469	0.0320
18	0.1647	12.0061	−1.4949	8.9388	0.0340
19	0.2955	13.0041	−1.5542	8.2449	0.0365
20	0.2184	12.1469	−1.4885	8.6735	0.0344
21	0.3498	13.6612	−1.6768	8.6735	0.0409
22	0.3449	13.3878	−1.5551	7.6939	0.0346
23	0.2600	13.1000	−1.6044	8.5714	0.0371

can be observed that the relative errors are low (individual values below 5%) for all the equations checked but significant differences can be detected among them, for example, for compound 2 the relative error by using model 2 is more than 5-fold higher than that obtained with model 3 and more than 2-fold higher if we compare models 1 and 3. In Fig. 6b the mean relative errors for all the compounds under study and with the three models checked (mobile phases containing SDS and butanol) have been plotted. These values are below 20, 13 and 12% for models 2, 1 and 3, respectively. It is interesting to note that great differences between models 1 or 2 with respect to model 3 are obtained for compounds 16–23 (mean relative errors below 6% for model 3), so apparently the inclusion of the term φ^2 (model 3), previously mentioned, clearly improves the prediction of capacity factors for these compounds.

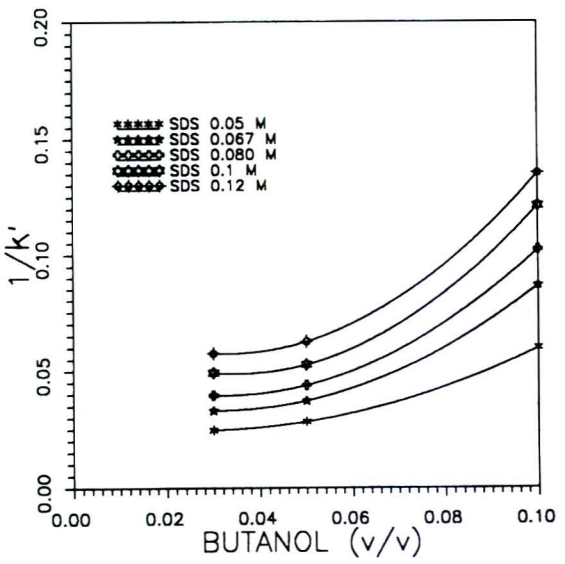

Fig. 5. Variation of the inverse of capacity factor for pyrene as a function of alcohol concentration for some fixed total surfactant concentrations (0.05, 0.067, 0.080, 0.100 and 0.120 *M*). Hybrid eluent containing SDS and butanol.

In Fig. 7 the calculated k' values according to Eq. 3 were plotted against the experimental values for compounds 1–15 (Fig. 7a) and 16–23 (Fig. 7b) both in mobile phases containing CTAB as surfactant and *n*-propanol as organic modifier (C_8 column). The straight lines obtained have slopes values very near to unity and intercepts near zero.

As a consequence of the results obtained in this article, we propose the use of Eq. 3 to describe the retention of a solute in MLC with hybrid eluents due to the fact that this equation is generally more valid than the others proposed.

4. Conclusions

From the results obtained in this work it can be concluded that at least for the group of compounds studied the following statements can be established:

First, the equation $1/k' = A\mu + B\varphi^2 + C\varphi + D\mu\varphi + E$ allows to obtain lower errors in the prediction of the capacity factors for all com-

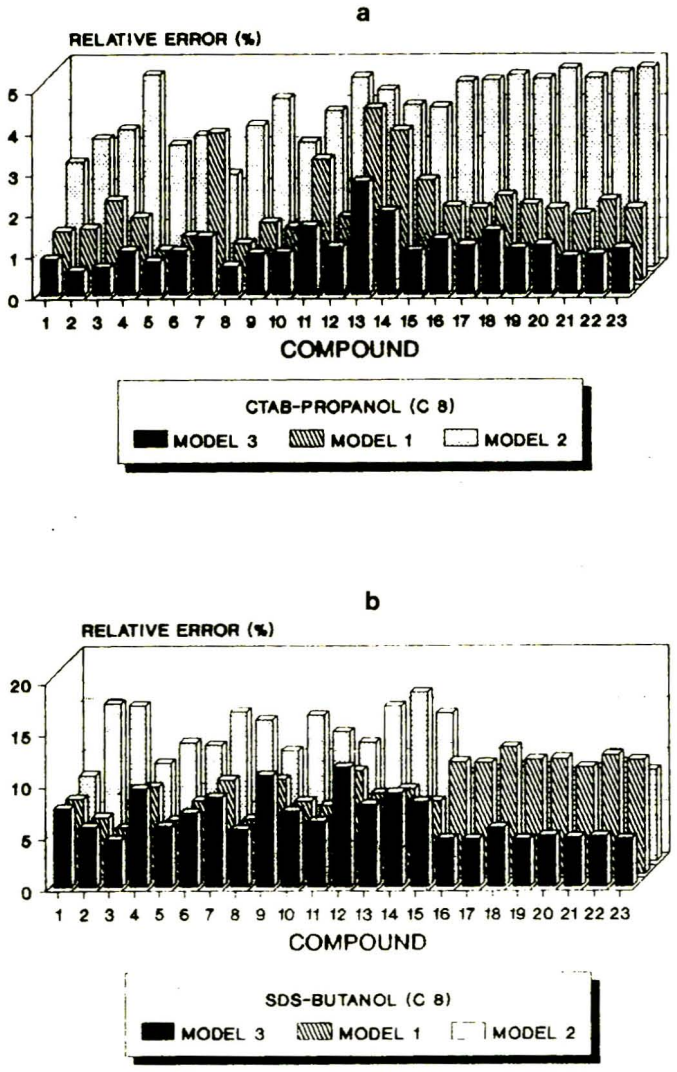

Fig. 6. Relative errors (%) obtained for the capacity factor prediction of compounds 1–23 with models 1, 2 and 3, the hybrid eluents being (a) CTAB–*n*-propanol and (b) SDS–*n*-butanol.

pounds, especially for the more hydrophobic ones. In fact the φ^2 term can be negligible for some compounds but not for these strongly hydrophobic ones. For these compounds, a clearly non-linear variation for $1/k'$ with φ can be obtained.

On the other hand, the nature of surfactant and alcohol used in the mobile phase seem to have an influence on the error obtained in the prediction of the capacity factor; CTAB and *n*-propanol being the surfactant and modifier that allow to decrease the relative errors.

Acknowledgement

We gratefully acknowledge the support of this work through a research project from DGICYT (Spain) (reference PS90-0026).

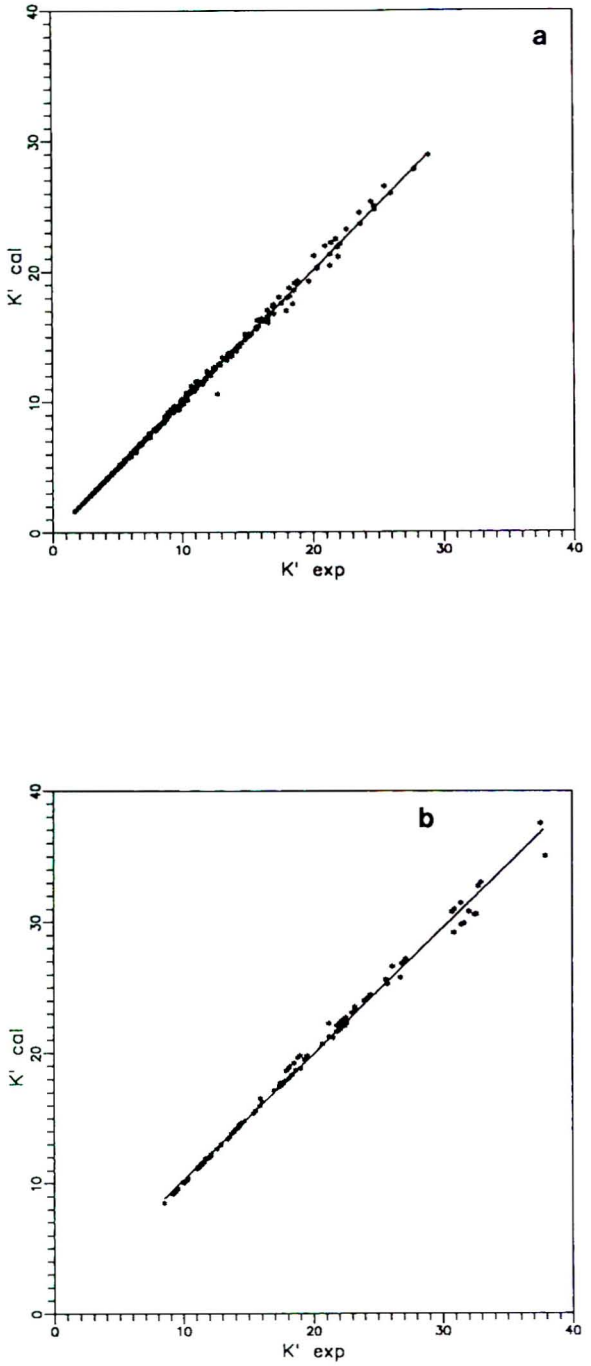

Fig. 7. Variation of calculated k' (K' cal) with model 3 as a function of experimental k' (K' exp) for (a) compounds 1–15 and (b) compounds 16–23 in systems containing CTAB as surfactant and *n*-propanol as organic modifier. (a) $y = 1.008x - 0.068$, $n = 299$; (b) $y = 0.963x + 0.659$, $n = 112$.

References

[1] D.W. Armstrong and R.Q. Terril, *Anal. Chem.*, 51 (1979) 2160.
[2] D.W. Armstrong and M. McNeeely, *Anal. Lett.*, 12 (1979) 1285.
[3] D.W. Armstrong and F. Nome, *Anal. Chem.*, 53 (1981) 1662.
[4] P. Yarmchuck, R. Weinberger, R.F. Hirsch and L.J. Cline Love, *Anal. Chem.*, 54 (1982) 2233.
[5] M. Arunyanart and L.J. Cline love, *Anal. Chem.*, 56 (1984) 1557.
[6] J.K. Strasters, E.D. Breyer, A.H. Rodgers and M.G. Khaledi, *J. Chromatogr.*, 511 (1990) 17.
[7] J.R. Torres-Lapasió, R.M. Villanueva-Camañas, J.M. Sanchis-Mallols, M.J. Medina-Hernández and M.C. García-Alvarez-Coque, *J. Chromatogr.*, 639 (1993) 87.
[8] D.W. Armstrong and G.Y. Stine, *Anal. Chem.*, 55 (1983) 2317.
[9] J.P. Foley and W.E. May, *Anal. Chem.*, 59 (1987) 110.
[10] M.G. Khaledi, *Anal. Chem.*, 60 (1988) 876.
[11] M.G. Khaledi, J.K. Strasters, A.H. Rogers and E.D. Breyer, *Anal. Chem.*, 62 (1990) 130.
[12] A.S. Kord and M.G. Khaledi, *Anal. Chem.*, 64 (1992) 1901.
[13] M.A. García, S. Vera, M. Bombín and M.L. Marina, *J. Chromatogr.*, 646 (1993) 297.
[14] J.G. Dorsey, M.T. DeEchegaray and J.S. Landy, *Anal. Chem.*, 55 (1983) 924.
[15] P. Yarmchuck, R. Weinberger, R.F. Hirsch and L.J. Cline Love, *J. Chromatogr.*, 283 (1984) 47.
[16] M.F. Borgerding, W.L. Hinze, L.D. Stafford, G.W. Fulp, Jr. and W.C. Hamlin, Jr., *Anal. Chem.*, 61 (1989) 1353.
[17] A. Berthod, M.F. Borgerding and W.L. Hinze, *J. Chromatogr.*, 556 (1991) 263.
[18] R. Bailey and R.M. Cassidy, *Anal. Chem.*, 64 (1992) 2277.
[19] R.A. Barford and B.J. Sliwinski, *Anal. Chem.*, 56 (1984) 1554.
[20] A. Berthod, I. Girard and C. Gonnet, *Anal. Chem.*, 58 (1986) 1359.
[21] A. Berthod, I. Girard and C. Gonnet, *Anal. Chem.*, 58 (1986) 1362.
[22] A. Berthod, I. Girard and C. Gonnet, *Anal. Chem.*, 58 (1986) 1356.
[23] F.P. Tomasella, J. Fett and L.J. Cline Love, *Anal. Chem.*, 63 (1991) 474.
[24] A.S. Kord and M.G. Khaledi, *Anal. Chem.*, 64 (1992) 1894.
[25] M.L. Marina, S. Vera and A.R. Rodríguez, *Chromatographia*, 28 (1989) 379.
[26] M.A. Rodríguez-Delgado, M.J. Sánchez, V. González and F. García-Montelongo, *Fresenius' J. Anal. Chem.*, 345 (1993) 748.
[27] M.F. Borgerding, R.L. Williams, Jr., W.L. Hinze and F.H. Quina, *J. Liq. Chromatogr.*, 12 (1989) 1367.

[28] M.F. Borgerding, F.H. Quina, W.L. Hinze, J. Bowermaster and H.M. McNair, *Anal. Chem.*, 60 (1988) 2520.
[29] M.F. Borgerding and W.L. Hinze, *Anal. Chem.*, 57 (1985) 2183.
[30] A. Malliaris. J. Lang, J. Sturm and R. Zana, *J. Phys. Chem.*, 91 (1987) 1475.
[31] *SOLO Statistical System*, BMDP Statistical Software, Los Angeles, CA, 1991.
[32] M.A. García, S. Vera and M.L. Marina, *Chromatographia*, 32 (1991) 148.
[33] M.A. García and M.L. Marina, in preparation.

ELSEVIER

Journal of Chromatography A, 675 (1994) 13–28

JOURNAL OF CHROMATOGRAPHY A

Influence of temperature on dead volume of ODS columns and on *n*-alkane retention in high-performance liquid chromatography

H.J. Möckel

Hahn–Meitner Institut Berlin GmbH, Abt. CC, Glienicker Strasse 100, D-14109 Berlin, Germany

(First received August 13th, 1993; revised manuscript received March 23rd, 1994)

Abstract

Dead volume of ODS columns as determined from the homologous series of *n*-alkanes with *n*-pentane or methanol eluent decreases with increasing temperature. This decrease which occurs in addition to the influence of thermal expansion of the eluent, is thought to be caused by thermal expansion of the stationary phase. Dead volume decreases about 2% per 40°C with *n*-pentane eluent and 5% with methanol eluent. No such decrease is found with a silica column. In addition, there appears to be a slight dependence of exclusion coefficients on temperature.

With *n*-pentane eluent, net retention of *n*-alkanes on ODS is very low (on the order of 1% of retention with methanol eluent). Solutes smaller than eluent molecules (butane to methane) exhibit higher retention times than expected from larger solutes (hexane and higher). With methanol eluent, plots of log capacity factor (a) *versus* carbon number for various temperatures and (b) *versus* inverse temperature for various carbon numbers show common intersection points.

1. Introduction

Influence of temperature on retention in various HPLC systems has been dealt with in numerous investigations [1–23 and references cited therein]. Most of this work was concerned with either structural changes in bonded phases, or with determination of enthalpy and entropy contributions to retention. Only little information is available on the effect of temperature on dead volume. An influence of thermal eluent expansion on dead time has been described by Colin *et al.* [3] and by Krstulovic *et al.* [10]. Recent data by Bidlingmeyer *et al.* [24] indicate a decrease of V_m of 5.2% between 45 and 65°C with uracil as a marker, of 4.3% between 35 and 55°C with acetone as marker, and of 1.5% between 35 and 55°C with ^2H_2O as marker, all at 2 ml/min flow. Laub and Madden [13] calculated V_0 from retention data of the series toluene through butylbenzene and benzyl alcohol through phenylpentanol and found temperature-independent, although strongly scattering V_0 from phenylalkanes, but decreasing values from phenylalkanols, both between 10 and 30°C.

Bidlingmeyers data and some other experimental results [24–28] suggested that dead volume might depend on temperature more strongly than expected from thermal expansion of the mobile phase. A temperature-induced

0021-9673/94/$07.00
SSDI 0021-9673(94)00296-L

change of stationary phase volume has been proposed in this context [26–28]. The present work was performed in order to (i) confirm the existence of this effect, (ii) determine its extent and (iii) investigate the possible influence of temperature on exclusion.

2. Experimental

2.1. Apparatus, columns, chemicals

The HPLC apparatus was assembled from commercial components and combined with various custom-made parts. Pumps were either Gynkotek 300C or Knauer 64. For 15–55°C experiments, pumps were thermostated in an air bath at 25 ± 1°C. For all other experiments, pumps operated at ambient temperature. The eluent was continuously kept under helium. Injection valve was a Valco C6W with air actuator which was run on 0.7–0.8 MPa helium via a pilot valve system [29], yielding switching times around 10 ms. The injector valve was immersed into the column thermostat bath and automatically loaded using a Hamilton Microlab P syringe drive. Eluent feed line (2 m × 0.7 mm I.D.) and column were kept in a water–methanol thermostat/cryostat bath (Haake F3) at a ± 0.02°C level for 15–55°C experiments. At low-temperature experiments, control was probably worse, ± 1°C at best. For detection, a Sicon LCD 200 refractive index detector was used. For higher-temperature work, its thermostating connectors were arranged in series with the column thermostat bath. At low temperature, the optical unit was taken out and mounted in an air-tight box flushed with dry nitrogen to prevent moisture condensation. The data system was PE/Nelson 960 and for some work, Shimadzu CR6A, both giving retention times in minutes with three decimals. It was started by a precision switch mounted on the injection valve drive. Further experimental details have been published elsewhere [30,31,54].

Columns (stainless steel, 250 × 4 mm I.D.) were purchased from Knauer Säulentechnik, Berlin, Germany. Packings were (data on grain and pore size as quoted by manufacturer): (column 1) Eurospher silica 100 Å 5 μm and (column 2) Eurospher ODS 80 Å 5 μm (100 Å base silica) (these two columns had been made as similar as possible, from the same silica batch B911); (column 3) Nucleosil ODS 120 Å 5 μm and (column 4) LiChrospher ODS 100 Å 5 μm.

Eluents methanol (MeOH), *n*-pentane (nC_5) and tetrahydrofuran (THF) were HPLC grade from Riedel-de Haen, Germany. *n*-Alkanes (Aldrich) were of the highest available grade and used as received.

Reproducibility of data in five repetitive runs was 0.2–0.3% R.S.D. in low-temperature experiments. Accuracy was certainly lower due to imperfections in the cryostating apparatus. Reproducibility at higher temperatures (15–55°C) was 0.1% R.S.D. or better. The elution volume of a polystyrene standard (molecular mass $2.95 \cdot 10^6$) in THF eluent at 25°C was taken as interstitial volume. Total liquid volume was measured either gravimetrically or by injecting C^2H_3OH samples with MeOH eluent. Mobile phase volume in pores was calculated from the difference between total liquid volume and interstitial volume.

3. Data treatment

3.1. Corrections

Retention time data t_R from five runs were fed into a computer. If an outlier (> 0.1% R.S.D.) for at least one solute was detected, the run was discarded and another one was started. In low-temperature experiments the R.S.D. limit was correspondingly increased. Outliers occurred sometimes with an insufficient time interval after a new temperature setting. Data were first averaged and pertaining statistical data were calculated (standard deviation and maximum data scatter). Next, averaged data were corrected for thermal expansion or contraction of the eluent and normalized to 25°C. Eq. 1 was used for correction:

$$t_R^*(25°C) = t_R(\tau°C) \cdot \frac{(1 + \gamma \cdot \tau)}{(1 + \gamma \cdot 25)} \quad (1)$$

where $\tau = K - 273 = °C$. This procedure is very similar to that of Colin *et al.* [3]. For MeOH, $\gamma = 0.001199$ and for nC_5, $\gamma = 0.001608/°C$ were taken [32], which is an approximation because γ is the cubic expansion coefficient at 20°C. Actually, expansion coefficients depend on temperature. Expansion of column tube and silica skeleton were not accounted for because expansion coefficient of stainless steel is very small, and no information is available on the thermal behaviour of silica.

If there were any changes in flow-rate, data were further normalized to a flow-rate of 1 ml/min at 25°C which yielded V_R^*. Finally, effective gross retention volumes V_{ms}^{eff} were obtained by subtracting extra column dead volume (at 25°C) from V_R^*. This proved to be important at the given relatively high precision level.

V^{eff} indicates that these data (effective or accessible volume data) are influenced by exclusion effects and may differ considerably from data solely controlled by the thermodynamic partition coefficient K^{th}. V_{ms}^{eff} values were used for calculation of dead volume and of ln k' specified as from "measured data".

Partial steric exclusion effects have recently been described in detail [25,55]. Although exclusion is not the objective of the present work, it will be necessary to discuss a few related effects in order to explain the general shape of measured retention functions. Exclusion refers to volumes contained in pores, the stationary phase volume V_{stat} and the "stagnant" part of mobile phase, V_{mp}. It is accounted for by the exclusion coefficient K^e:

$$V_{mp}^{eff} = V_{mp}K^e \quad (0 \leq K^e \leq 1) \tag{2}$$

$$V_{stat}^{eff} = V_{stat}K^e \tag{3}$$

As net retention volume $V_s = V_{stat}K^{th}$, effective net retention volume becomes

$$V_s^{eff} = V_{stat}K^{th}K^e \quad (0 \leq V_s^{eff} \leq V_s) \tag{4}$$

V_m consists of interstitial volume V_{int} and V_{mp} [56], so effective dead volume is

$$V_m^{eff} = V_{mp}^{eff} + V_{int}$$
$$= V_{mp}K^e + V_{int} \quad (V_{int} \leq V_m^{eff} \leq V_m) \tag{5}$$

In a system which is known to produce no retention at all, measured elution volumes are effective dead volumes, and all observed changes are solely caused by exclusion effects. Then it is easy to determine exclusion coefficients :

$$K^e = \frac{V_m^{eff} - V_{int}}{V_{mp}} = \frac{V_m^{eff} - V_{int}}{V_m - V_{int}} \tag{6}$$

V_{ms}^{eff}, being the sum of net retention volume and dead volume, can be written as

$$V_{ms}^{eff} = (V_{mp} + V_{stat}K^{th})K^e + V_{int}$$
$$= (V_{mp} + V_s)K^e + V_{int} \tag{7}$$

It appears exceedingly difficult to determine K^e in systems producing so much retention that V_s (Eq. 7) is on the order of or greater than V_{mp}. If it is possible to make V_s small enough, Eq. 7 eventually approaches Eq. 5. We have approximated this situation by using *n*-pentane as eluent.

According to the treatment of Giddings *et al.* [33], K^e for "capsule shaped" molecules in a system of cylindrical pores, shows an exponential decrease with increasing ratio of solute length to pore diameter. *n*-Alkanes in non-polar or low-polarity solvents can be regarded as approximately cylindrical or capsule shaped. Their length (or better, mean external length $\bar{L}$ [33]) depends linearly on carbon number n_C. If this dependence is introduced into Giddings *et al.*'s expression for K^e, a generally non-linear decrease of K^e with increasing n_C is found, with pore diameter D_{pore} as parameter. In the range of small- to medium-size alkanes (up to about C_{30}) and larger pores (100 Å and wider), the decrease does not deviate much from linearity. With decreasing pore diameter, K^e decreases, as expected. Furthermore, curvature of K^e *versus* n_C functions may become more evident.

Elution functions $V_R^* = f(n_C)$ in systems assumed to have little or perhaps no retention, SiO_2/C_5 and ODS/C_5, are found to vary from practically linear to visibly curved. They can reasonably well be approximated using first- or higher-order polynomials :

$$V_m^{eff} = f(n_C) = \sum_{i=0}^{i=n} a_i n_c^i \quad (8)$$

Zeroth order coefficient a_0 always gives the maximum dead volume because exclusion vanishes for vanishing solute size,

$$a_0 = V_m = V_{mp} + V_{int} \quad (9)$$

This equation is used in solving Eq. 6.

As a matter of fact, existence of some retention cannot be ruled out with sufficient certainty in practical systems. Since retention as well as exclusion must vanish for vanishing solute size, we assume that the slope of an exclusion function has to be calculated from the first derivative of the elution function at $n_C = 0$. Then, $V_m^{eff} = a_0 + a_1$ in Eq. 6, a_0 and a_1 being 0th and 1st order coefficients of polynomials used to describe measured elution functions.

Exclusion coefficients calculated from low/no retention systems were tentatively applied without modification to retention data obtained with MeOH eluent in order to calculate exclusion-corrected gross retention volume:

$$V_{ms} = \frac{V_{ms}^{eff} - V_{int}}{K^e} + V_{int} \quad (10)$$

This procedure could be an oversimplification because the extent of exclusion might be different in solvents having different properties.

3.2. Dead volume

Dead volume calculation was performed by establishing a function which relates V_{ms} of a series member having $n + 1$ carbon atoms to V_{ms} of the preceding one having n carbon atoms:

$$V_{ms}(n+1) = f[V_{ms}(n)] \quad (11)$$

This function is empirically found to be linear with correlation coefficient on the order of $r = 0.9998$:

$$V_{ms}(n+1) = SL \cdot V_{ms}(n) + IN \quad (12)$$

where SL and IN are slope and intercept, respectively.

While linearity is perfect with exclusion-corrected V_{ms} data, there is a small, but distinctly systematic deviation of non-corrected V_{ms}^{eff} data from linear regression, exceeding experimental data scatter at least by a factor of 10. Using $V_{ms} = V_s + V_m$ and the definition (Eq. 13) of selectivity α:

$$\alpha = V_s(n+1)/V_s(n) \quad (13)$$

it follows that

$$SL = \alpha \quad (14)$$

$$IN = V_m(1 - \alpha) \quad (15)$$

from which V_m is readily obtained.

This process is basically the same as that of Berendsen *et al.* [34]. Calculation yields effective V_m^{eff} which decrease with increasing n_C if measured data V_{ms}^{eff} are used, while V_{ms} data (without contribution from exclusion) yield constant V_m [25,54,55].

4. Results

4.1. Silica column, n-pentane eluent

Experimental retention times of *n*-alkanes C_1–C_{28} at nine temperatures from −15°C to +25°C in 5°C steps on an Eurospher silica column (column 1) are given in Table 1. The following is observed:

(1) Retention times t_R are highest at −15°C and lowest at +25°C for each solute.

(2) At each temperature, t_R of C_1–C_{28} decrease with increasing carbon number n_C. As seen from Fig. 1, this decrease is steepest from C_1 to C_2 and then gradually diminishes. Above $n_C = 6$ it seems to be linear, but data quality is not sufficient to unambiguously rule out some curvature.

Fig. 2 shows V_{ms}^{eff}, which is obtained from the above data (without C_1–C_4) by correction for thermal expansion of the eluent, if necessary for deviating flow-rate, and for extra column dead volume. There is only little temperature dependence left. It is observed that expansion-corrected elution volumes V_{ms}^{eff} increase slightly with increasing temperature. If straight regression

Table 1
n-Alkanes on silica with *n*-pentane eluent

n_C	Experimental retention time (min)								
	−15°C	−10°C	−5°C	0°C	5°C	10°C	15°C	20°C	25°C
1	2.724	2.703	2.692	2.665	2.635	2.621	2.593	2.576	2.555
2	2.673	2.664	2.660	2.625	2.604	2.588	2.568	2.557	2.541
3	2.650	2.642	2.633	2.610	2.590	2.581	2.550	2.540	2.526
4	2.643	2.635	2.623	2.596	2.583	2.557	2.542	2.529	2.512
6	2.632	2.617	2.608	2.582	2.570	2.546	2.533	2.514	2.497
7	2.627	2.613	2.599	2.579	2.565	2.544	2.529	2.509	2.492
9	2.613	2.601	2.587	2.567	2.554	2.532	2.517	2.501	2.482
11	2.599	2.587	2.568	2.553	2.539	2.521	2.505	2.488	2.475
13	2.586	2.570	2.555	2.542	2.527	2.506	2.495	2.480	2.464
15	2.572	2.557	2.543	2.530	2.514	2.495	2.488	2.469	2.459
17	2.566	2.547	2.531	2.515	2.505	2.485	2.477	2.457	2.446
19	2.540	2.528	2.512	2.504	2.488	2.475	2.467	2.448	2.436
22	2.523	2.509	2.494	2.491	2.475	2.458	2.448	2.433	2.419
28	2.521	2.495	2.459	2.454	2.440	2.435	2.421	2.405	2.392

Column 250 × 4 mm Eurospher silica, 100 A; 5 μm (column 1). Eluent nC_5, flow 1 ml/min at 25°C. Column temperature as indicated. Refractive index detection. Experimental retention times averaged from five runs.

lines C_6–C_{28} are extrapolated to $n_C = 0$, all of them but the −15°C line yield almost identical intercepts of 2.523 ± 0.004 ml. Residual deviations are non-systematic and probably due to data scatter. Regression lines for V_{ms}^{eff} can be described by

$$V_{ms}^{eff}(n_C, \tau) = a_0 + a_1(\tau)n_C$$
$$= 2.523 + (-0.00613 + 6.43 \cdot 10^{-5}\,\tau)n_C \quad (16)$$

The temperature effect is small, but it persists if expansion correction is performed using the complete polynomial expression for expansion coefficient γ, and if thermal change of the column tube volume is accounted for.

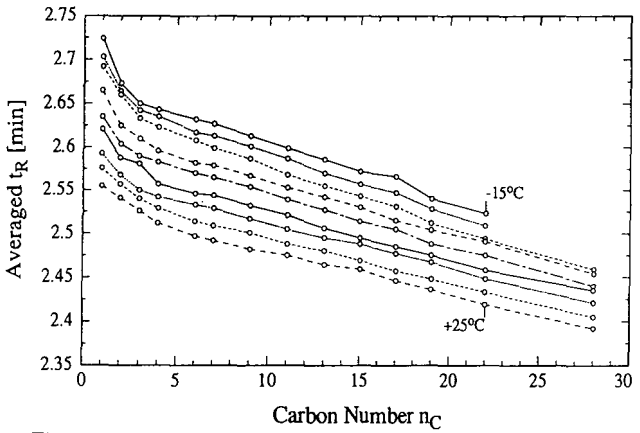

Fig. 1. Experimental retention times, t_R, of *n*-alkanes C_1–C_{28} at temperatures from −15 to +25°C in 5°C steps. Eurospher silica, 100 Å, 5 μm, 250 × 4 mm (column 1). Eluent *n*-pentane. Flow 1 ml/min at 25°C. Refractive index detection.

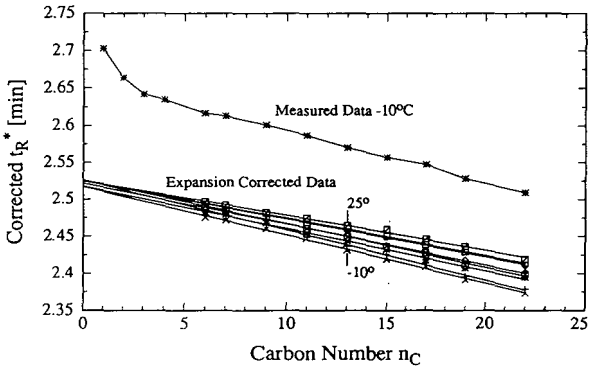

Fig. 2. Expansion-corrected retention times, t_R^*. Same data as in Fig. 1 (without −15° set) but corrected for thermal expansion of eluent, normalized to 25°C. Temperatures from original t_R data set. For comparison, measured t_R (−10°C) trace from Fig. 1 is included.

Liquid volume within the column as determined by weighing with different liquids (*n*-hexane, dichloromethane, carbon tetrachloride) was 2.516 ml and agreed with *n*-hexane data in Fig. 2.

Interstitial volume was found to be $V_{int} = 1.253$ ml at 25°C. The volume of mobile phase residing in pores is calculated to be $V_{mp} = 2.523 - 1.253 = 1.27$ ml at 25°C.

If it was assumed that there is no retention ($V_s = 0$), expansion-corrected elution volumes are effective dead volumes $V_{ms}^{eff} = V_m^{eff}$, and Eq. 9 can be used to determine exclusion coefficients:

$$K^e = 1 - (0.00483 - 5.06 \cdot 10^{-5}\,\tau)n_C \qquad (17)$$

According to this calculation, the pore-entering probability is reduced to about 90% for eicosane on the silica column.

In another calculation, C_1–C_4 were included and elution functions were represented by third-order polynomials. Intercept a_0 was found to be 2.566 ml (S.D. = 0.0056 or 0.2% R.S.D.) for all temperatures except −15°. For the first-order coefficient, $a_1 = -0.01922 + 1.28 \cdot 10^{-4}\,\tau$ was obtained. With these figures, exclusion coefficient K^e is

$$K^e = 1 - (0.0146 - 9.74 \cdot 10^{-5}\,\tau)n_C \qquad (17a)$$

From this equation, a pore-entering probability of 75% is calculated for C_{20}.

4.2. ODS columns, n-pentane eluent

Experimental retention times t_R on the Eurospher ODS column (column 2) are given in Table 2. Fig. 3 shows retention behavior to be similar to that on the parent silica column (column 1). There are three notable differences: (1) t_R values are lower on ODS; (2) t_R of C_6–C_{32} are slightly curved, and curvature is more pronounced at lower temperature; and (3) curves run almost parallel to each other, deviations increase for higher n_C and lower temperature.

Temperature dependence is reduced after correction for thermal expansion of the eluent. Before correction, −10°C t_R data were 0.15 ml higher than +25°C data, after correction, the difference between respective V_R^* data is only

Table 2
n-Alkanes on ODS with *n*-pentane eluent

n_C	Experimental retention time (min)								
	−15°C	−10°C	−5°C	0°C	5°C	10°C	15°C	20°C	25°C
1	2.422	2.369	2.350	2.319	2.300	2.267	2.243	2.227	2.202
2	2.330	2.331	2.312	2.284	2.293	2.242	–	–	–
3	2.310	2.280	2.265	2.241	2.225	2.221	2.179	2.163	2.142
4	2.292	2.263	2.248	2.225	2.209	2.187	2.164	2.147	2.128
6	2.262	2.239	2.221	2.198	2.180	2.152	2.137	2.120	2.098
7	2.250	2.229	2.210	2.186	2.168	2.144	2.126	2.108	2.088
9	2.228	2.208	2.187	2.164	2.144	2.128	2.103	2.087	2.066
11	2.208	2.182	2.168	2.144	2.127	2.107	2.083	2.067	2.048
13	2.191	2.162	2.147	2.125	2.104	2.090	2.066	2.048	2.030
15	2.176	2.143	2.128	2.103	2.085	2.072	2.047	2.030	2.012
17	2.163	2.131	2.112	2.086	2.069	2.053	2.029	2.014	1.997
19	2.152	2.113	2.095	2.068	2.056	2.037	2.014	1.997	1.981
22	2.138	2.102	2.078	2.053	2.039	2.020	1.999	1.984	1.968
24	–	–	–	–	–	–	–	1.961	1.945
28	–	2.072	2.041	2.014	1.988	1.971	1.950	1.933	1.921
32	–	–	2.023	1.983	1.963	1.944	1.924	1.912	1.895

Column 250 × 4 mm Eurospher ODS, 80 Å, 5 μm (column 2). Eluent 1 ml/min nC_5 at 25°C. Column temperature as indicated. Refractive index detection. Experimental retention times averaged from five runs.

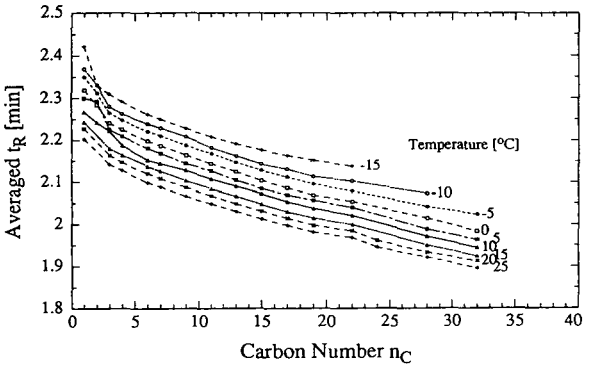

Fig. 3. Experimental retention times, t_R, of *n*-alkanes C_1–C_{28} (C_{32}) at temperatures from −15 to +25°C in 5°C steps. Eurospher ODS, 100 Å, 5 μm, 250 × 4 mm (column 2). Eluent *n*-pentane. Flow 1 ml/min at 25°C. Refractive index detection.

0.03 ml. It was found that C_1–C_{20} data are well approximated by third-order polynomials of n_C. Because determination of polynomial coefficients is strongly influenced by data scatter, data visibly deviating from smooth curves in Fig. 3 were removed (C_{22} and C_{32}).

Intercept a_0 decreases linearly with increasing temperature:

$$a_0 = 2.247 - 0.0015\tau = 2.247(1 - 0.00067\tau) \quad (18)$$

First-order coefficient a_1 increases slightly with increasing temperature:

$$a_1 = -0.0255 + 1.62 \cdot 10^{-4}\,\tau \quad (18a)$$

Coefficients a_2 and a_3 are small and show severe scatter, but some temperature dependence is recognized:

$$a_2 = 9.54 \cdot 10^{-4} - 1.01 \cdot 10^{-5}\,\tau \quad (18b)$$

$$a_3 = -1.5 \cdot 10^{-5} + 1.7 \cdot 10^{-7}\,\tau \quad (18c)$$

Gravimetrically (2.208 ml at 25°C) and chromatographically determined liquid volume agreed reasonably well. Interstitial volume of this column was $V_{int} = 1.182$ ml, the mobile phase volume within pores $V_{mp} = 1.026$ ml, both at 25°C. The difference in V_{mp} between silica (column 1) and ODS derived therefrom (column 2) is 0.263 ml and probably due to space occupied by the bonded layer. Interstitial volume is slightly decreased, possibly because of better packing properties of bonded material [35].

Exclusion coefficients were calculated as shown in the data treatment section, using a_0 and a_1 from Eqs. 18 and 18a only.

$$K^e = \frac{a_0 + a_1 - V_{int}}{a_0 - V_{int}} = 1 - \frac{0.0255 - 1.62 \cdot 10^{-4}\,\tau}{1.099 - 0.0031\tau} n_C \quad (19)$$

This procedure implies the presence of some retention in this system. A rough measure of that retention is given by higher-order coefficients a_2 and a_3.

As seen from Fig. 4, K^e on ODS (solid lines) are lower than on the parent silica (broken lines). This is probably due to narrower pores, but additional entropy effects might be superimposed [36].

Characteristic volume data at 25°C was measured also for the Nucleosil ODS column (column 3) which was later used for experiments with MeOH eluent. Total liquid volume V_{liq} from weighing with MeOH and CH_2Cl_2 (2.028 ml) and from retention of C^2H_3OH in MeOH eluent (2.041 ml) are almost identical. Interstitial volume was determined as described above to be 1.133 ml. Pore volume was calculated as $V_{mp} = 2.028 - 1.133 = 0.895$ ml.

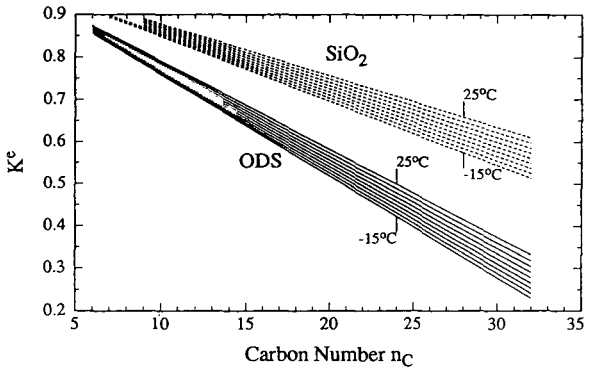

Fig. 4. Dependence of exclusion coefficients K^e on temperature and on solute carbon number for *n*-alkanes on ODS and on parent silica. Calculation based on data in Tables 1 and 2 (see text).

4.3. ODS columns, MeOH eluent

Retention data for *n*-alkanes, measured at 25°C on Eurospher ODS (column 2), averaged from 11 runs is shown in Table 3. Relative standard deviation is of the order of 0.05%. More retention data on this column have been published elsewhere [25]. Exclusion coefficients were calculated via Eq. 19 and applied to $V_{ms}^{eff} - V_{int}$ as shown in Eq. 10. Exclusion-corrected V_{ms} are higher than V_{ms}^{eff} (*e.g.* 3.370 *versus* 3.096 for C_6 up to 14.884 *versus* 10.016 for C_{17}) Sub-sets of V_{ms}^{eff} and of V_{ms} were subject to dead volume calculation [25]. With V_{ms}^{eff}, calculated V_m decreases from 1.866 ml for the C_6 to C_1 sub-set almost linearly to 1.634 ml for the C_{12} to C_{17} sub-set. Corrected V_{ms} yield constant $V_m = 1.862$ ml (0.6% R.S.D.). This value was used to calculate ln k' from V_{ms} ($k' = (V_{ms} - V_m)/V_m$) for all n_C, and ln $k' = -1.38596 + 0.19595 n_C$ with correlation coefficient $r = 0.9999999$ was found.

We have observed with various ODS columns that changing K^e in Eq. 10 by trial and error until constant V_m is obtained yields the same K^e value as determined from experiments with *n*-pentane eluent.

The following experiments were performed in the + 15° to + 55°C range on a Nucleosil ODS column (column 3) with MeOH eluent and *n*-alkane solutes C_6–C_{17}. Table 4 gives retention times averaged over five runs. Exclusion coefficients showed slight temperature dependence which was on the same order of magnitude as observed with nC_5 eluent.

Table 3
n-Alkanes on ODS with methanol eluent

n_C	t_R (min) (average)	S.D. (min)	R.S.D. (%)
6	3.152	0.002	0.08
7	3.384	0.002	0.06
8	3.664	0.002	0.04
9	3.994	0.002	0.05
10	4.388	0.002	0.05
11	4.856	0.002	0.05
12	5.409	0.003	0.05
13	6.065	0.002	0.04
14	6.836	0.003	0.05
15	7.746	0.003	0.04
16	8.815	0.004	0.04
17	10.072	0.006	0.06

Column 250 × 4 mm Eurospher ODS, 80 Å, 5 μm (column 2). Eluent MeOH, flow 1 ml/min at 25°C. Column temperature 25°C. Refractive index detection. Experimental t_R data averaged over 11 runs.

After correction of experimental data for expansion and exclusion, V_{ms} values were used to calculate the dead volume at each temperature. Fig. 5 shows a remarkable dependence of V_m on temperature, V_m being high at 15°C and low at 55°C. This dependence is more pronounced than in Eq. 18. It seems that a second-order polynomial (solid line) fits data better than a first-order one (broken line):

$$V_m = 2.054 - 0.0033\tau + 1.96 \cdot 10^{-5} \tau^2 \qquad (20)$$

It is seen that $V_m = 1.983$ ml at 25°C is slightly lower than V_{liq}.

Similar effects have been found with a variety of ODS columns [26–28]. LiChrospher ODS (column 4) with MeOH eluent is shown as an example in Fig. 6. The nC_{10} trace (squares) was calculated from experimental data, which yield V_m^{eff} depending on both n_C and temperature. After correction for thermal expansion, the slope is somewhat reduced (◇). Triangles show the temperature dependence of V_m as determined with C^2H_3OH as marker. It has been shown that CD_3OH indicates the total eluent volume in the column, immobilized fraction in the stationary phase included [37]. Temperature dependence of this "dead volume" disappears upon correction for thermal expansion (○), as expected from earlier work [10]. The volume found with C^2H_3OH is generally greater than V_m from homologous series. With H_2O as marker, no temperature dependence was seen (asterisks).

From exclusion corrected V_{ms} and temperature dependent V_m (Eq. 20), ln k' displayed in Fig. 7 were calculated. Ln k' increase linearly over carbon number n_C for each temperature:

$$\ln k'(n_C, \tau) = a(\tau) + b(\tau) n_C \qquad (21)$$

Linearity of ln k' over n_C is further documented in Table 5 which shows intercepts a and

Table 4
n-Alkanes on ODS with methanol eluent

n_C	T (K)	t_R (min) (average)	S.D. (min)	Δ_{max} (min)
6	288	3.307	0.0021	0.007
7		3.557	0.0018	0.005
8		3.864	0.0026	0.007
9		4.239	0.0026	0.008
10		4.697	0.0011	0.003
11		5.251	0.0023	0.007
12		5.924	0.0016	0.005
13		6.735	0.0059	0.019
14		7.712	0.0016	0.005
15		8.889	0.0043	0.010
16		10.295	0.0027	0.008
17		11.979	0.0059	0.017
6	293	3.238	0.0019	0.005
7		3.470	0.0021	0.006
8		3.753	0.0012	0.003
9		4.093	0.0026	0.008
10		4.507	0.0022	0.007
11		5.005	0.0026	0.007
12		5.603	0.0027	0.008
13		6.319	0.0022	0.006
14		7.173	0.0024	0.006
15		8.194	0.0022	0.006
16		9.403	0.0043	0.010
17		10.839	0.0056	0.015
6	298	3.180	0.0013	0.004
7		3.396	0.001	0.002
8		3.656	0.001	0.002
9		3.969	0.001	0.002
10		4.345	0.0013	0.004
11		4.795	0.0015	0.004
12		5.331	0.001	0.002
13		5.968	0.0005	0.001
14		6.724	0.001	0.002
15		7.618	0.0012	0.003
16		8.673	0.0019	0.005
17		9.915	0.0018	0.004
6	303	3.121	0.0013	0.003
7		3.321	0.0017	0.005
8		3.562	0.0011	0.003
9		3.850	0.0013	0.004
10		4.190	0.0011	0.003
11		4.599	0.0012	0.003
12		5.081	0.0018	0.005
13		5.650	0.0013	0.004
14		6.320	0.0016	0.005
15		7.109	0.0017	0.005
16		8.033	0.0016	0.005
17		9.115	0.0022	0.005

Table 4 (*continued*)

n_C	T (K)	t_R (min) (average)	S.D. (min)	Δ_{max} (min)
6	308	3.067	0.0004	0.001
7		3.253	0.0004	0.001
8		3.477	0.0008	0.002
9		3.740	0.0004	0.001
10		4.053	0.001	0.003
11		4.423	0.0004	0.001
12		4.857	0.0004	0.001
13		5.366	0.001	0.002
14		5.964	0.0012	0.003
15		6.661	0.003	0.007
16		7.471	0.0028	0.007
17		8.421	0.0035	0.010
6	313	3.013	0.0004	0.001
7		3.187	0.0005	0.001
8		3.395	0.0004	0.001
9		3.638	0.0004	0.001
10		3.926	0.001	0.002
11		4.263	0.0004	0.001
12		4.657	0.0008	0.002
13		5.116	0.001	0.002
14		5.650	0.0004	0.001
15		6.272	0.001	0.003
16		6.994	0.0022	0.006
17		7.825	0.0032	0.008
6	318	2.965	0.0018	0.005
7		3.128	0.0019	0.005
8		3.321	0.0017	0.005
9		3.545	0.0021	0.006
10		3.809	0.0016	0.004
11		4.117	0.0018	0.005
12		4.473	0.0019	0.005
13		4.886	0.0034	0.010
14		5.367	0.0016	0.005
15		5.921	0.0017	0.005
16		6.560	0.0008	0.002
17		7.294	0.0030	0.008
6	323	2.916	0.001	0.002
7		3.068	0.0004	0.001
8		3.247	0.0005	0.001
9		3.455	0.0004	0.001
10		3.696	0.0034	0.009
11		3.978	0.0004	0.001
12		4.303	0.0005	0.001
13		4.676	0.001	0.002
14		5.107	0.0004	0.001
15		5.603	0.0012	0.003
16		6.170	0.0008	0.002
17		6.821	0.0017	0.005

(Continued on p. 22)

Table 4 (*continued*)

n_C	T (K)	t_R (min) (average)	S.D. (min)	Δ_{max} (min)
6	328	2.868	0.0008	0.002
7		3.012	0.0005	0.001
8		3.178	0.0005	0.001
9		3.371	0.001	0.002
10		3.592	0.0005	0.001
11		3.850	0.0013	0.004
12		4.145	0.0013	0.004
13		4.483	0.0008	0.002
14		4.871	0.0019	0.005
15		5.315	0.0015	0.004
16		5.821	0.0012	0.003
17		6.397	0.001	0.003

Column 250 × 4 mm Nucleosil ODS, 120 A; 5 μm (column 3). Eluent 1 ml/min MeOH at 25°C. Column temperature as indicated. Refractive index detection. t_R, raw data, averaged from five runs, includes extra column dead time. S.D. in five runs. Δ_{max} data span, max–min value in five runs.

slopes ***b*** of the respective regression lines, together with correlation coefficients which are high, of the order of $r = 0.999999$.

Regression lines for ln k' have been extrapolated to $n_C = 0$. It is seen from Fig. 7 that ln k' intersect and become independent of temperature at a hypothetical carbon number of *ca.* 4.

In Fig. 8, ln k' values from Fig. 7 have been plotted over $1000 \cdot (1/T)$. Again, plots are linear. There is a small irregularity in the vicinity of 40°C. If ln $k'/(1/T)$ values are extrapolated to

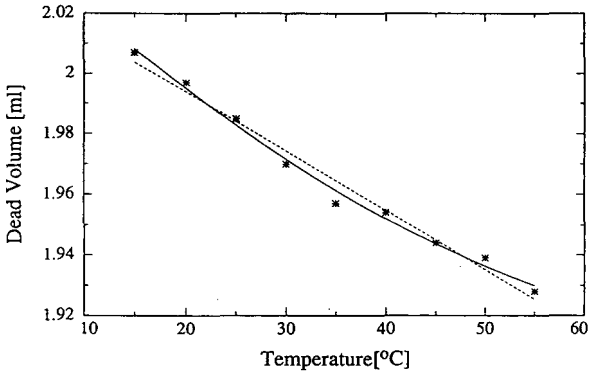

Fig. 5. Dead volume calculated from *n*-alkane retention data in Table 4 (Nucleosil ODS/MeOH, column 3) corrected for thermal expansion and partial exclusion, as function of temperature.

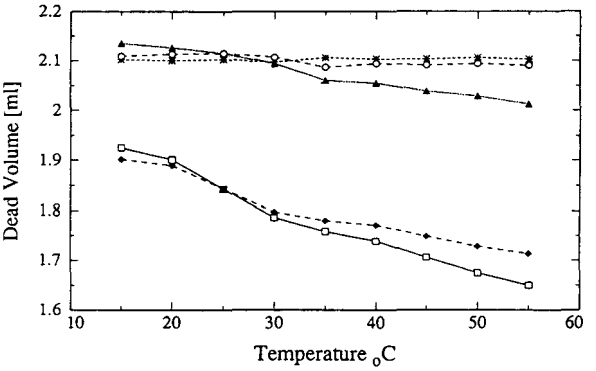

Fig. 6. Dead volume determination on LiChrospher ODS, 100 Å, 5 μm, 250 × 4 mm (column 4) at various temperatures. Eluent methanol. Flow 1 ml/min. □ = solute *n*-decane; ◆ = same data, but corrected for thermal expansion; ▲ = solute C^2H_3OH; ○ = same data, but corrected for thermal expansion; ∗ = solute H_2O.

higher temperatures, all intersect at $(1/T) = 0.00197$ or $\tau = 235$°C.

Slopes ***b*** are linear over $1/T$ with high correlation coefficients. Intercepts ***a*** show moderate deviations from linearity if plotted either over $1/T$ or over T, so the actual temperature dependence of ***a*** cannot be determined from these data.

5. Discussion

5.1. Silica column, n-pentane eluent

The elution function of *n*-alkanes on this silica column is strongly curved in the C_1–C_6 range and almost linear for longer-chain solutes. Actually, a certain degree of non-linearity is anticipated as outlined in the data treatment section. This packing material, however, has nominally 100 Å pores and a relatively wide pore size distribution [25], so that curvature is likely to be small and obscured by data scatter.

It is not quite clear whether smallest solutes C_1–C_4 should be included in the evaluation of exclusion coefficients or not. On one hand, the elution function of alkanes longer than eluent molecules looks fairly linear which suggests that the onset of higher retention times at C_4 may

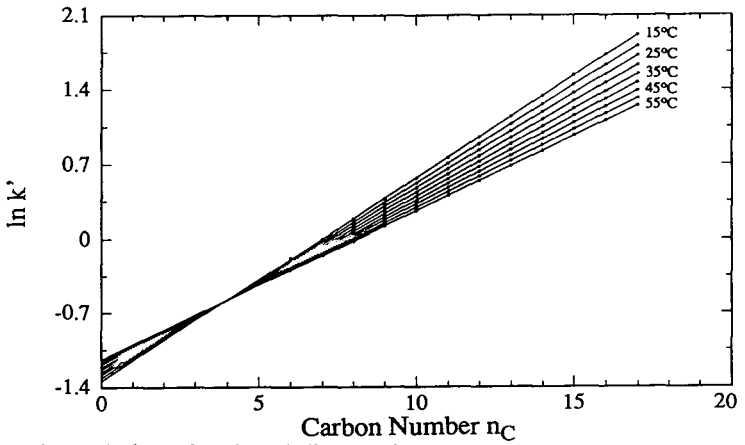

Fig. 7. Logarithm of capacity factor, ln k', as function of alkane carbon number n_C at various temperatures. Data (dots) derived from Table 4 (Nucleosil ODS/MeOH, column 3) corrected for thermal expansion and partial exclusion. Regression lines extrapolated to $n_C = 0$.

Table 5
Parameters of ln $k' = a + bn_C$ with correlation coefficient r

Temperature (°C)	a	b	r
15	−1.49856	0.20735	0.99999987
20	−1.43564	0.19791	0.99999995
25	−1.39008	0.18977	0.99999997
30	−1.34988	0.18206	0.99999998
35	−1.31337	0.17501	0.99999991
40	−1.27102	0.16809	0.99999994
45	−1.23861	0.16153	0.99999991
50	−1.20492	0.15521	0.99999991
55	−1.168	0.14896	0.99999987

Calculation based on data from Table 4.

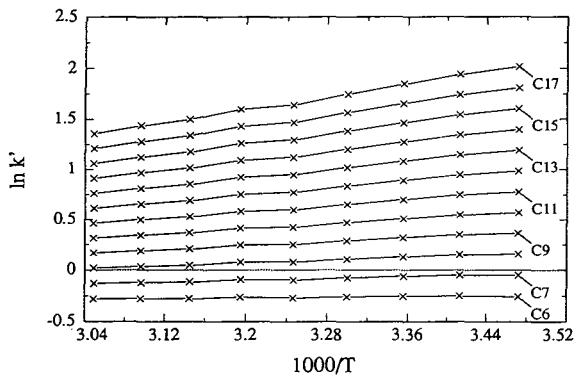

Fig. 8. Data from Fig. 7, plotted as function of $1000/T$ (Van 't Hoff plot) for carbon numbers 6–17.

indicate an extra effect, and C_1 to C_4 should be omitted. On the other hand, molecular cross-section of C_5 and longer alkanes is practically the same as that of C_1. Consequently, alkanes with $n_C > 1$ can enter the same pores as C_1, even if entering probability decreases. Very high concentration of eluent C_5 probably overrides lowered entering probability so that the eluent can effectively use all pores being accessible to C_1. It is mainly for this reason that we prefer to include the smallest solutes in K^e determination. For this purpose, the elution function is described by a third-order polynomial.

Intercept a_0 of third-order polynomials at $n_C = 0$ does not depend on temperature if expansion-corrected data are used. Because retention (if there is any) as well as exclusion must vanish for vanishing molecular dimensions, this intercept can be interpreted as the maximum possible dead volume, which is the sum of V_{int} and V_{mp}.

Results obtained in the SiO_2/nC_5 system suggest that elution volumes of n-alkanes are primarily controlled by exclusion. Temperature dependence of expansion-corrected data is small and in "wrong" order, *i.e.*, higher retention times are found with higher temperature. We assume that ΔH is very small. This may be interpreted using Snyder's displacement model of adsorption chromatography [38,39], in this particular case for non-polar, non-localizing solutes and eluent molecules. Prior to sorption of a

longer-chain alkane, the silica surface is covered with nC_5. Because interaction of alkanes with any surface is purely dispersive, there is no preferred orientation of in-plane sorbed molecules. If an alkane molecule is to get into contact with the silica surface, it has to displace an adequate number of nC_5 molecules. Consequently, net enthalpy of interaction of *n*-alkane solutes with silica is expected to be low. Existing differences between (entropic) activity coefficients of C_6 to C_{17} in nC_5 eluent are assumed to be widely cancelled by similar effects in the sorbed monolayer [38,39], so they are not likely to influence retention significantly.

Overall ΔG^{sorp} is therefore expected to be quite small but not necessarily zero. After exclusion-correction according to Eq. 10 using K^e from Eq. 17a, V_{ms} was obtained. Temperature dependence of V_{int} was accounted for in this calculation. Net retention volume V_s was calculated by subtracting $V_m = a_0$ from V_{ms}. Resulting V_s values are small, increasing almost linearly from *ca.* 0 for smaller solutes to *ca.* 0.3 ml for C_{22}. These values are so small that, regarding inaccuracy of data and uncertainty of the exclusion model, no further comments can be made.

The slight temperature dependence of slope in Eq. 16 suggests K^e to be weakly temperature dependent (see Fig. 4). The reason for this effect is not really clear, but we assume that temperature has a slight influence on exclusion via temperature-dependent diffusion of molecules from mobile phase stream paths to pores. The increase of influence of temperature on K^e with increasing solute size seems to support this hypothesis.

5.2. ODS columns, n-pentane eluent

Exclusion behavior of *n*-alkanes in the ODS/nC_5 system is expected to be similar to that in SiO_2/nC_5 systems. It has been shown [25] that pore size distribution of an ODS packing differs from that of parent silica mainly in the most abundant pore width which is shifted to smaller values. In addition, some pores might get plugged, thus becoming inaccessible to solutes and eluent.

The shift of pore diameters to smaller values must necessarily cause a stronger dependence of exclusion on solute size [33], without changing general characteristics of the exclusion function. Stronger exclusion is expressed in a lower value of K^e, causing a decrease of V_R^* as compared to parent silica, which is seen in experimental results. This suggests that elution functions observed with alkanes in the ODS/nC_5 system may be mainly governed by exclusion, but it seems realistic to assume that thermodynamic effects could be involved, to a certain extent [36].

In order to find exclusion functions, the same formalism as for SiO_2/C_5 was used, because there is no reason to assume that exclusion behaviour should be principally different. Consequently, a linear function of n_C was obtained. Temperature dependence of K^e is practically the same as in the SiO_2/nC_5 system which may indicate that this effect originates in the mobile phase.

Contrary to the SiO_2/nC_5 system, V_m depend on temperature with ODS/nC_5. The fact that dead volume of an ODS column depends on temperature is remarkable and needs explanation. As the only perceivable difference between ODS and SiO_2 columns used in these experiments is the presence of the bonded layer, we assume that the stationary phase expands with increasing temperature. A wetted ODS phase should be regarded as a non-isotropic liquid, the maximum layer thickness of which will probably be on the order of C_{18} chain length in all-trans conformation. Bonded chains are likely to serve as "backbone" of the stationary phase, and sorbed eluent molecules sit in between chains. Depending on eluent polarity and temperature, bonded chain conformation will vary. At low eluent polarity and higher temperature, chains tend to become more mobile and to expand [40], thereby increasing stationary phase volume. Since the total volume available for stationary plus mobile phase varies only very slightly with temperature, an increase of V_{stat} will necessarily cause a decrease of V_m.

Exclusion-corrected V_{ms} were used to calculate V_s, in the same way as shown for SiO_2/nC_5, the only difference being temperature-dependent V_m. Again, V_s values are unusually low. They range from *ca.* 0 for C_1–C_6 to *ca.* 1 ml for C_{32}.

The increase is close to exponential. There is no information about the origin of this retention.

5.3. ODS columns, MeOH eluent

It has been shown in the Results section that ln k' values are strictly linear over n_C in this system at all investigated temperatures. Furthermore, ln k' values increase linearly over $1/T$ for each solute C_6 through C_{17}. The small irregularity observed in Fig. 8 is probably caused by slightly deviating temperatures. It might, however, as well be comparable to effects observed by Tchapla *et al.* [16] and by Cole and coworkers [17,18]. The latter researchers investigated a wide temperature range and found nonlinear Van 't Hoff plots in various systems.

The most remarkable finding seems to be that, also in this much different system, dead volume decreases with increasing temperature. Although data precision is high, it is still not sufficient to exactly determine the functional relation between V_m and temperature. The actual dependence is probably a relatively complicated function of T, due to anisotropy of the stationary phase. It has to be pointed out that temperature dependence of dead volume in the ODS/MeOH system is more pronounced than in the ODS/nC_5 system. This may indicate that the observed effect is not simply expansion of a common liquid, but mainly controlled by bonded chains stretching. Bonded chains are likely to be more compressed in MeOH environment than in nC_5, and the effect of temperature is expected to be stronger.

The linear dependence of ln k' on n_C (Fig. 7 and Table 5) can be described as shown in Eq. 21. This implies that each methylene group in the alkyl chain contributes a constant, additive increment, b, to ln k'. In terms of sorption free energy, this ln k' incrementation may be written as follows

$$\ln k'(n_C, T) = -\frac{\Delta G^{sorp}}{R}\cdot\frac{1}{T} + \ln \phi(T)$$
$$= -\frac{\Delta G_r^{sorb}}{R}\cdot\frac{1}{T} - n_C\cdot\frac{\Delta G_2^{sorp}}{R}\cdot\frac{1}{T} + \ln \phi(T) \quad (22)$$

where ΔG_r^{sorp} and ΔG_2^{sorp} are (formal) increments of terminal groups (two hydrogen atoms) and of a CH_2 group, respectively, to ΔG^{sorp}, and $\phi(T)$ is the phase volume ratio V_{stat}/V_m which does not depend on n_C as data are exclusion-corrected. Eq. 22 is a description of experimental facts using thermodynamic terms, rather than a consequence of thermodynamics. A similar formalism has been used by several other authors [7,11].

It is very unlikely that ΔG^{sorp} depends linearly on n_C without ΔH^{sorp} and ΔS^{sorp} showing the same behavior. It was therefore assumed that ΔH^{sorp} and ΔS^{sorp} can be split into methylene and residual hydrogen contributions as was done with ΔG^{sorp}. This yields

$$\ln k'(n_C, T) = -\frac{\Delta H_r^{sorb}}{R}\cdot\frac{1}{T} - n_C\cdot\frac{\Delta H_2^{sorp}}{R}\cdot\frac{1}{T} + \frac{\Delta S_r^{sorb}}{R} + n_C\cdot\frac{\Delta S_2^{sorp}}{R} + \ln \phi(T) \quad (23)$$

Eq. 23 interprets slope b and intercept a of Eq. 21 in terms of thermodynamic quantities:

$$b = -\frac{\Delta H_2^{sorp}}{R}\cdot\frac{1}{T} + \frac{\Delta S_2^{sorp}}{R} \quad (24)$$

$$a = -\frac{\Delta H_r^{sorp}}{R}\cdot\frac{1}{T} + \frac{\Delta S_r^{sorp}}{R} + \ln \phi(T) \quad (25)$$

I II III

Slope b (Eq. 24) as function of $1/T$ yields another linear relation with $-\Delta H_2^{sorp}/R$ as slope and $\Delta S_2^{sorp}/R$ as intercept. Linearity indicates that ΔH_2^{sorp} and ΔS_2^{sorp} are constant in the investigated temperature range:

$$\Delta H_2^{sorp} = -1142 \text{ J mol}^{-1} \quad (26)$$

$$\Delta S_2^{sorp} = -2.24 \text{ J K}^{-1} \text{ mol}^{-1} \quad (27)$$

Negative ΔH^{sorp} shows that retention of *n*-alkanes is enthalpy driven in the ODS/MeOH system. Negative sorption entropy probably indicates an origin in the sorbed state, where solutes loose most of their degrees of freedom of molecular motion. A (positive) entropy contribution from collapsing cavities seems to be less important in this system [41].

Intercept a (Eq. 25) cannot be evaluated in

this simple way because it contains the phase ratio term. While term I in Eq. 25 is a function of $1/T$, term III has probably a different temperature dependence. From an approach relating reversed-phase retention to molecular surface area [42,43] it can be concluded that the sum of terms I and II of Eq. 25 is approximately equal to $\boldsymbol{b}$. Then

$$\ln \phi \approx \boldsymbol{a} - \boldsymbol{b} \tag{28}$$

From data in Table 5 it is seen that, with this approximation, phase ratio ϕ varies between 0.18 at 15°C and 0.27 at 55°C. With these figures, V_{stat} is calculated to increase from 0.37 ml at 15°C to 0.49 ml at 55°C. The corresponding formal expansion coefficient of the stationary phase is 0.0094 per °C, which is distinctly higher than with a real liquid.

The common intersection point (CIP) of ln $k'/(1/T)$ seems to be similar to the ones reported by Tchapla *et al.* [16]. It means that at hypothetical temperature T_x, all *n*-alkanes C_6–C_{17} would have the same retention, which can occur only if n_C-dependent terms of Eq. 23 cancel at this temperature:

$$\Delta H_2^{sorp} = \Delta S_2^{sorp}\, T_x \tag{29}$$

$$T_x = 509 \text{ K}$$

Eq. 29 is an example of linear free energy relationships in which common intersection points may be encountered and related to entropy–enthalpy compensation effects. The above calculated T_x is called compensation temperature [2,14,42–52].

The CIP of ln k'/n_C functions at different temperatures is rather unexpected. It says that at hypothetical carbon number n_x, retention becomes temperature-independent. This, in turn, requires the sum of temperature-dependent terms to be constant at n_x

$$\ln k' = -\frac{\Delta H_x^{sorp}}{RT} + \frac{\Delta S_x^{sorp}}{R} + \ln \phi(T) = \text{constant} \tag{30}$$

where H_x^{sorb} and ΔS_x^{sorp} are the enthalpy and entropy of sorption of a *n*-alkane having n_x carbon atoms.

The entropy term of Eq. 30 is negative and temperature-independent. The enthalpy term is positive and decreases with increasing temperature. The phase ratio term is negative and becomes less negative with increasing T. In order to keep ln k' constant when T changes, an alteration of the ΔH term appears to be compensated by an opposite change of the ln ϕ term. This result is surprising as it relates phase ratio to heat of sorption or *vice versa*.

6. Conclusions

Experiments have shown that there may be two temperature effects which have not been observed so far:

Temperature dependence of expansion-corrected retention data in the SiO_2/nC_5 system suggests a slight influence of temperature on exclusion, possibly through temperature dependence of diffusion. Similar dependence of K^e on temperature was found in ODS/nC_5 and ODS/MeOH systems.

Maximum dead volume (for $n_C \rightarrow 0$) in ODS/nC_5 and ODS/MeOH systems depends on temperature, even if data are corrected for thermal expansion. No such dependence is found in a silica/nC_5 system. The observed decrease of V_m with increasing temperature is thought to be caused by an increase of stationary phase volume. As a consequence, phase ratio ϕ must necessarily increase with increasing temperature. The usual way to determine heat of sorption from the slope of ln k' over $1/T$ does obviously not yield ΔH proper, but the sum of ΔH and the temperature change of ln ϕ, instead. This problem has been mentioned earlier by Grushka *et al.* [11].

If C^2H_3OH is used as dead volume marker, total liquid volume in the column is found. This value does not depend on temperature in excess of the thermal expansion effect.

n-Alkanes in SiO_2/nC_5 and ODS/nC_5 systems have little retention, and retention times are mainly controlled by exclusion effects. Small solutes CH_4 to C_4H_{10} have higher retention

times than expected from larger homologues, probably due to easier access to narrow pores.

In ODS/MeOH systems, temperature has its strongest influence in the sorption enthalpy term. The occurrence of a common intersection point in the dependence of ln k' on $1/T$ for a set of n-alkanes requires description of ln k' by a relation like Eq. 23, in which compensation of terms can occur. This equation relates constant and additive increments of thermodynamic quantities to a temperature-independent molecular property, in this case to carbon number n_C. Basically, other properties proportional to carbon number may be chosen, as is frequently done with molecular surface area (*e.g.* refs. 42–49,53), which, in turn, is related to cavity energy. Eq. 23 is another example of frequently observed linear free energy relationships in which common intersection points can occur, due to entropy–enthalpy compensation effects [2,14,49–52]. There appears to be another common intersection point in the dependence of ln k' on n_C for different temperatures. This phenomenon leads to a relation between phase ratio and heat of sorption. Its origin is unclear and requires further investigation at a higher data precision level.

7. Symbols and abbreviations

a_i	polynomial coefficient of order i
a	intercept of linear dependence of ln k' on n_C
b	slope of linear dependence of ln k' on n_C
D_{pore}	pore diameter
ΔG^{sorp}	free energy of sorption (standard conditions)
ΔG_r^{sorp}	sorption free energy increment of terminal groups
ΔG_2^{sorp}	sorption free energy increment of 1 CH_2 group
ΔH^{sorp}	sorption enthalpy (standard conditions), same subscripts as with ΔG^{sorp}
IN	intercept of $V_{ms}(n+1)/V_{ms}(n)$ function
k'	capacity factor V_s/V_m
K^e	exclusion coefficient
K^{th}	thermodynamic partition coefficient
$\bar{L}$	mean external length of molecule
n_C	carbon number of molecule
ODS	octadecyl silica
r	correlation coefficient
R	gas constant (8.314 J K^{-1} mol^{-1})
R.S.D.	relative standard deviation in %
ΔS^{sorp}	sorption entropy (standard conditions), same subscripts as with ΔG^{sorp}
S.D.	standard deviation based on (n-1)
SL	slope of $V_{ms}(n+1)/V_{ms}(n)$ function
t_R	experimental retention time
t_R^*	t_R corrected for thermal expansion
T	temperature in K
V_0	dead volume, non-specified
V_R^*	experimental retention volume, corrected for thermal expansion
V_{int}	interstitial volume
V_{liq}	total liquid volume in column
V_m	dead volume (maximum value)
V_m^{eff}	effective (accessible) part of V_m
V_{mp}	volume of mobile phase in pores
V_{mp}^{eff}	effective (accessible) part of V_{mp}
V_{ms}	gross retention volume
V_{ms}^{eff}	effective gross retention volume
V_s	net retention volume
V_s^{eff}	effective net retention volume
V_{stat}	volume of stationary phase
V_{stat}^{eff}	effective (accessible) part of V_{stat}
x	(subscript) refers to conditions at common intersection point
α	selectivity (relative retention), here $V_s(n+1)/V_s(n)$
γ	cubic coefficient of thermal expansion
τ	temperature in°C
ϕ	V_{stat}/V_m = phase ratio

Acknowledgements

The author is greatly indebted to Professor Cs. Horváth, Yale University, for reading the manuscript and for his valuable comments and suggestions.

Andreas Hühmer's efforts in producing most of the experimental results are appreciated.

References

[1] J.H. Knox and G. Vasvari, *J. Chromatogr.*, 83 (1973) 181.
[2] W.R. Melander, D.E. Campbell and Cs. Horváth, *J. Chromatogr.*, 158 (1978) 215.
[3] H. Colin, J.C. Diez-Masa, G. Guiochon, T. Czajkowska and I. Miedziak, *J. Chromatogr.*, 167 (1978) 41.
[4] L.R. Snyder, *J. Chromatogr.*, 179 (1979) 167.
[5] J. Chmielowiec and H. Sawatzky, *J. Chromatogr. Sci.*, 17 (1979) 245.
[6] R.K. Gilpin and W.R. Sisco, *J. Chromatogr.*, 194 (1980) 285.
[7] Gy. Vigh and Z. Varga-Puchony, *J. Chromatogr.*, 196 (1980) 1.
[8] W.R. Melander, J. Stoveken and Cs. Horváth, *J. Chromatogr.*, 199 (1980) 35.
[9] R.K. Gilpin and J.A. Squires, *J. Chromatogr. Sci.*, 19 (1981) 195.
[10] A.M. Krstulovic, H. Colin and G. Guiochon, *Anal. Chem.*, 54 (1982) 2438.
[11] E. Grushka, H. Colin and G. Guiochon, *J. Chromatogr.*, 248 (1982) 325.
[12] W.R. Melander and Cs. Horváth, *Chromatographia*, 18 (1984) 353.
[13] R.J. Laub and S.J. Madden, *J. Liq. Chromatogr.*, 8 (1985) 173.
[14] R.J. Laub and S.J. Madden, *J. Liq. Chromatogr.*, 8 (1985) 187.
[15] H.J. Issaq, S.D. Fox, K. Lindsey, J.H. McConnell and D.E. Weiss, *J. Liq. Chromatogr.*, 10 (1987) 49.
[16] A. Tchapla, S. Heron, H. Colin and G. Guiochon, *Anal. Chem.*, 60 (1988) 1433.
[17] L.A. Cole and J.G. Dorsey, *Anal. Chem.*, 64 (1992) 1317.
[18] L.A. Cole, J.G. Dorsey and K.A. Dill, *Anal. Chem.*, 64 (1992) 1324.
[19] R.G. Bogar, J.G. Thomas and J.B. Callis, *Anal. Chem.*, 56 (1984) 1080.
[20] D. Morel and J. Serpinet, *J. Chromatogr.*, 248 (1982) 231.
[21] J.C. van Miltenburg and W.E. Hammers, *J. Chromatogr.*, 268 (1983) 147.
[22] C. Gonnet, D. Morel, E. Ramamonjinirina, J. Serpinet, P. Claudy and J.M. Letoffe, *J. Chromatogr.*, 330 (1985) 227.
[23] P. Claudy, J.M. Letoffe, C. Gaget, D. Morel and J. Serpinet, *J. Chromatogr.*, 329 (1985) 331.
[24] B.A. Bidlingmeyer, F.V. Warren, A. Weston, C. Nugent and P.M. Froehlich, *J. Chromatogr. Sci.*, 29 (1991) 275.
[25] H.J. Möckel and U. Dreyer, *Chromatographia*, 37 (1993) 179.
[26] A. Braedikow, *Dipl. Thesis*, TFH Berlin, Berlin, 1991.
[27] M. Mann, *Dipl. Thesis*, TFH Berlin, Berlin, 1991.
[28] A. Hühmer, *Dipl. Thesis*, FU Berlin, Berlin, 1993.
[29] M.C. Harvey and S.D. Stearns, *Anal. Chem.*, 56 (1984) 837.
[30] U. Dreyer, *Ph.D. Thesis*, TU Berlin, Berlin, 1992.
[31] U. Dreyer, *Liquidchromatographische Untersuchung gebundener Umkehrphasen: Bedeutung und experimentelle Realisierung hochpräziser Retentionsdaten*, Reports of the Hahn-Meitner Institute, HMI-B 503, Hahn-Meitner Institut Berlin, Berlin, 1992.
[32] R.K. Kirby, T.A. Hahn and B.D. Rothrock, in D.E. Grey (Editor), *American Institute of Physics Handbook*, McGraw-Hill, New York, 1972, p. 4–141.
[33] J.C. Giddings, E. Kucera, C.P. Russell and M.N. Myers, *J. Phys. Chem.*, 72 (1968) 4397.
[34] G.E. Berendsen, P.J. Schoenmakers, L. de Galan, Gy. Vigh, Z. Varga-Puchony and J. Inczedy, *J. Liq. Chromatogr.*, 3 (1980) 1669.
[35] W. Werner and I. Halász, *J. Chromatogr. Sci.*, 18 (1980) 277.
[36] H.J. Möckel and U. Dreyer, *Chromatographia*, 37 (1993) 184 (Editor's comment).
[37] H.J. Möckel and T. Freyholdt, *Chromatographia*, 17 (1983) 215.
[38] L.R. Snyder, *Principles of Adsorption Chromatography (Chromatographic Science Series*, Vol. 3), Marcel Dekker, New York, 1968.
[39] L.R. Snyder, in Cs. Horváth (Editor), *High-Performance Liquid Chromatography —Advances and Perspectives*, Vol. 3, Academic Press, New York, 1983, pp. 157–223.
[40] A.H.T. Chu and S.H. Langer, *J. Chromatogr.*, 389 (1987) 1.
[41] C. Tanford, *The Hydrophobic Effect: Formation of Micelles and Biological Membranes*, Wiley, New York, 1973, pp. 16*ff*.
[42] H.J. Möckel, G. Welter and H. Melzer, *J. Chromatogr.*, 388 (1987) 255.
[43] H.J. Möckel, F. Höfler and H. Melzer, *J. Chromatogr.*, 388 (1987) 267, 275, 285.
[44] E.J. Tierney, J.M. Bellama, G. Eng, F.E. Brinckman and R.B. Johannesen, *J. Chromatogr.*, 441 (1988) 29.
[45] K. Jinno and M. Okamoto, *Chromatographia*, 20 (1984) 677.
[46] K. Jinno and K. Kawasaki, *J. Chromatogr.*, 316 (1984) 1.
[47] N. Funasaki, S. Hada and S. Neya, *J. Chromatogr.*, 361 (1986) 33.
[48] S. Miertus, V. Jakus, E. Matisova, *Chromatographia*, 30 (1990) 144.
[49] R. Lumry and S. Rajender, *Biopolymers*, 9 (1970) 125.
[50] W.R. Melander, *Chem. Phys. Lett.*, 28 (1974) 14.
[51] R.R. Krug, W.G. Hunter and R.A. Grieger, *J. Phys. Chem.*, 80 (1976) 2335, 2341.
[52] M. Kuchar, V. Rejholec, E. Kraus, V. Miller and V. Rabek, *J. Chromatogr.*, 280 (1983) 279.
[53] Cs. Horváth, W. Melander and I. Molnár, *J. Chromatogr.*, 125 (1976) 129.
[54] U. Dreyer, H. Melzer and H.J. Möckel, *J. Chromatogr.*, 592 (1992) 13.
[55] H.J. Möckel, U. Dreyer and H. Melzer, *Fresenius' J. Anal. Chem.*, 342 (1992) 673.
[56] Cs. Horváth and H.J. Lin, *J. Chromatogr.*, 126 (1976) 401.

ELSEVIER

Journal of Chromatography A, 675 (1994) 29–45

JOURNAL OF CHROMATOGRAPHY A

Synthesis and characterization of silica-based aliphatic ion exchangers

Laura A. Ciolino, John G. Dorsey*

Department of Chemistry, University of Cincinnati, Cincinnati, OH 45221-0172, USA

(Received January 25th, 1994)

Abstract

The chemical literature describing preparation of aliphatic ion exchangers is limited, and although such phases are available commercially, the synthetic schemes are proprietary. The course of our research required the preparation of silica-based aliphatic cation and anion exchangers for which the desired base silica and/or ligand properties were not commercially available. We developed synthetic schemes to prepare silica-based aliphatic sulfonic acid, carboxylic acid and quaternary ammonium ion-exchange phases with active exchange capacities of 0.2–0.9 μmol/m^2. Multiple techniques were used to characterize the intermediate and final phases produced in the syntheses, including Fourier transform diffuse reflectance infrared spectroscopy, spot tests, elemental analysis, acid–base titration and elution analysis.

1. Introduction

We recently investigated the feasibility of using chromatographic silica-based stationary phases as substrates for room temperature phosphorescence. The course of our research required the preparation of aliphatic cation and anion exchangers for which the desired base silica and/or ligand properties were not commercially available. Our interest was in both strong and weak aliphatic ion exchangers, specifically sulfonic acids, carboxylic acids, quaternary amines and amines.

A survey of the literature showed that the vast majority of ion exchangers contain aromatic moieties, and the corresponding synthetic schemes rely on the reactivity of the aromatic moiety for success. Aromatic moieties could not be tolerated for our application due to their high phosphorescence background. Of the limited literature describing aliphatic ion exchangers, there are several which describe preparation of alkylsulfonic acids or sulfonates. However, except for the aminoalkyl phases, the aliphatic ion exchangers of interest cannot be directly prepared via a one-step coupling reaction to silica because of cross-reactions which would occur with such functional silanes. Therefore, derivatization schemes to prepare these phases involve the coupling of a precursor silane with silica in the first step, followed by conversion of the precursor functional group to the desired functional group in one or more subsequent reactions. Cleavage of the original silane in the subsequent reaction step(s), and low conversion represent the major problems.

* Corresponding author.

0021-9673/94/$07.00
SSDI 0021-9673(94)00232-X

We investigated synthetic schemes to prepare aliphatic sulfonic acid, carboxylic acid and quaternary ammonium phases. In all cases, we were able to prepare the desired phases with *active* exchange capacities between 0.2 and 0.9 μmol/m^2. Details of the synthetic schemes developed and suggestions for further optimization of the schemes investigated are presented.

Another challenging aspect of synthetic research for derivatized silicas is the characterization of the intermediate and final phases. Characterization comprises both qualitative and quantitative analysis of the attached ligands, including confirmation that the target functional groups are present intact on the surface. The difficulty arises because the "analyte" (attached ligands) represents only a small percentage of the "sample" (derivatized silica), and the sample is an insoluble solid. A combination of techniques must be used in order to provide even an adequate characterization.

Infrared (IR) spectroscopy is the most frequently used tool for functional group analysis of derivatized silicas [1–6], although solid-state NMR has also been used [7–9]. With the availability of Fourier transform diffuse reflectance IR spectroscopy (FT-DRIFT) [10], the IR spectra of solid samples are relatively easy to obtain, but the analysis is still complicated by the large background absorbance of silica. IR bands for the attached ligands can be observed directly only in the limited spectral regions which are free of the background. Signal averaging and background subtraction are frequently used to improve the quality and appearance of the spectra. Sample preparation usually involves dilution of the solid phase in a non-absorbing matrix such as KCl. Murthy and Leyden [11] showed that FT-DRIFT could also be used for quantitative determination of ligand coverage under dilute conditions ($<17\%$ silica phase in KCl matrix) where the Kubelka–Munk function is linear with respect to concentration. In that work, the absorbance for the aminopropyl ligand (CH stretch) was referenced to the silica Si–O combination band at 1870 cm^{-1}. Correlation of the IR response with a second independent method was required for absolute quantitation.

Solid-state NMR has emerged as a powerful tool for the study of derivatized silicas beyond the simple identification of attached ligand functional groups. Solid-state NMR has been used to discriminate modes of attachment for mono-, di- and trifunctional silanes [7], to observe residual adsorbed solvents such as methanol [7,12], and to study the mobility of bonded alkyl chains as a function of chain length and position along the chain [13,14]. This detailed phase characterization comes at the expense of extensive sample preparation (drying under vacuum for hours or days) and sampling time.

Elemental analysis and determination of ion-exchange capacity are the most frequently used tools for quantitative analysis. While elemental analysis is especially useful for one-step coupling reactions, it is virtually impossible to track the course of a multi-step synthetic sequence with such limited information. Another technique which has been used for quantitative analysis is cleavage of the attached silane via acidic or basic hydrolysis followed by GC–MS [15–17] or GC–FID [18–20], but this technique is restricted to silanes which form volatile dimers upon coupling.

In the present study, FT-DRIFT was used in conjunction with wet chemical techniques (spot tests) for the functional group analysis of alkyl-, ester-, thiol- and amine-containing phases. The shape of the acid–base titration curves were used to characterize the cation-exchange phases as strong (sulfonic) or weak (carboxylic) acids. Elemental analysis and exchange capacity determinations (titration or elution) were used for quantitative analysis. The results are presented along with a perspective of the capabilities and limitations of each of the applied techniques.

2. Experimental

The base silicas used and their properties are summarized in Table 1. Prior to derivatization, all silicas were acid washed, and then dried overnight at 150°C under vacuum. Acid washing comprised refluxing in 0.1 *M* HNO_3 overnight followed by water washes to neutrality. All

Table 1
Summary of base silica properties

Silica	Particle diameter (μm)	Pore diameter (Å)	Shape	Specific surface area (m^2/g)
Waters Nova	5	100	Spherical	119
Davisil	20–30	–	Irregular	300
Waters Nova	12	60	Spherical	114
Supelco	5	100	Spherical	175
Waters Resolve	5	90	Spherical	175
Jones Apex PM 300	5	100	Spherical	170

Silicas in order discussed in text. All information based on manufacturers' literature or contact.

silanes were used as received from Huls America. All solvents were Fisher certified-ACS grade, except for methanol which was Fisher HPLC grade. Reaction solvents were distilled just before use as follows: dichloromethane over P_2O_5 under dry nitrogen; dimethylformamide (DMF) over BaO under vacuum; dimethyl sulfoxide (DMSO) over CaH under vacuum; methyl ethyl ketone and toluene over $CaCl_2$ under dry nitrogen. All wash solvents were used as received. Distilled water was filtered through a Barnsted system prior to use. Reagents for all primary coupling reactions, and where noted for secondary reactions, were weighed out in a dry box. All primary coupling reactions were conducted under a dry nitrogen purge.

Diethyl disulfide and octanoic acid were used as received from Sigma. Concentrated hydrochloric and sulfuric acids, and 30% aqueous hydrogen peroxide were used as received from Fisher. A solution of 25% trimethylamine (TMA) in methanol was used as received from Kodak. Dimethylaminopyridine (Nepera) was dried overnight at 80°C and stored in a desiccator prior to use. Sodium iodide (Fisher certified) was recrystallized twice from acetone–diethyl ether, dried *in vacuo* for 2 h at 50°C, then desiccated. Lithium bromide (MCB reagent grade) was dried for two days at 105°C *in vacuo* and desiccated prior to use. Lithium iodide (Sigma anhydrous, 99%) was opened in a dry box and used as received.

Silane and other reagent molar excesses were calculated assuming 5 μmol/m^2 reactive silanols for the silica surface. All silanes were added at a 4 × molar excess. Dimethylaminopyridine (DMAP) catalyst, when used, was added at a 6 × molar excess.

All elemental analyses were performed by Robertson Microlit Labs. Bonding densities (μmol/m^2) were calculated from elemental analyses according to Eq. 1. Eq. 1 is a modification of Berendsen and De Galan's original equation [6] which has been generalized for any element. A blank carbon level of 0.1% was obtained for the Waters 12-μm underivatized silica. This corresponds to a blank "bonding density" of 0.15 μmol/m^2 for a propyldimethylsilane. The percentage of silane cleavage occurring in secondary or tertiary reactions was calculated from the difference in percent of a given element before *vs.* after the reaction.

$$\alpha(\mu\text{mol/m}^2) = \frac{\%E \cdot 10^6}{n_E M_{a,E} S \cdot \left[100 - \left(\frac{\%E}{M_{a,E} n_E}\right) M_{r,L}\right]} \quad (1)$$

where α = bonding density, $\%E$ = mass% element, n_E = number of atoms of element in ligand fragment, $M_{a,E}$ = atomic mass of element, S = specific surface area of silica (m^2/g) and $M_{r,L}$ = molecular mass of ligand fragment attached.

Exchange capacities for cation-exchange

phases were determined by manual titration with 0.01 *M* NaOH, pH electrode detection. A complete titration curve was recorded for each phase. Exchange capacities were calculated from the volume of NaOH required to neutralize the silica dispersion to a pH of 7 for sulfonic acid phases and a pH of 8 for carboxylic acid phases. The solvent was 20% aqueous methanol. Exchange capacities for quaternary ammonium anion-exchange phases were determined by nitrate elution as described by Warth *et al.* [21] The phases were converted to the nitrate form by washing with 0.5 *M* $NaNO_3$ at a pH of 4, and then washed with water to remove the excess nitrate. The bound nitrate was then eluted with 0.05 *M* Na_2SO_4 at a pH of 4, and analyzed by UV spectroscopy using the absorbance at 220 nm. Exchange capacities are reported in units of $\mu mol/m^2$ to allow comparison among ion-exchange phases with base silicas of differing specific surface area. Units of μequiv./g are also reported for consideration of the functional properties of the phases.

DRIFT spectra of the silica and derivatized silica phases were taken using a Bio-Rad FTS 60A FT-IR spectrometer with KBr as reference material. The spectra were taken of the neat phases (no dilution in the KBr reference material) without any special sample preparation, other than to keep the phases dry in a desiccator. Resolution was 8 cm^{-1}, scan speed was 5 kHz, and the aperture was 1 cm^{-1}. An average of 64 scans was taken for each phase. No background subtraction or smoothing was used. The reflectance data were converted to Kubelka–Munk units using the standard Bio-Rad system software. The bands associated with the attached ligands could be observed on top of the silica background in several spectral regions. Because the solid phases were not diluted in KBr, the reflectance values are outside the linear range of the Kubelka–Munk *vs.* concentration relation. Therefore, the IR spectra taken are not considered in a strict quantitative sense. However, our experience shows that the appropriate IR absorbances do increase with increasing bonding density for a variety of bonded phases (alkyl, ester, cyclohexenyl), and also increase as the alkyl chain length increases for reversed phases. Thus, we are satisfied with the semi-quantitative results for the current studies, given that virtually no sample preparation was required.

3. Results and discussion

3.1. Sulfonic acid phases

Several researchers have investigated the preparation of sulfonic acid-derivatized silicas via the attachment of an alkyl thiol ligand and its subsequent oxidation. Weigand *et al.* [22] obtained a maximum exchange capacity of 103 μequiv./g (0.69 $\mu mol/m^2$) using hydrogen peroxide as the oxidizing agent for butyl thiol-derivatized silica. Silane cleavage was 50%. Wheals [23] attached a propyl thiol silane at 1.6 $\mu mol/m^2$ and subsequently oxidized the thiol to the sulfonic acid using potassium permanganate in 1 *M* sulfuric acid. The final phase had a reported exchange capacity of 0.5–0.6 mequiv./g (1.4 $\mu mol/m^2$). The silane cleavage (not reported) was apparently only 13%.

Fazio *et al.* [24] introduced the use of peroxyoctanoic acid in ether for the oxidation of a propylthiol-derivatized silica with the "absence of significant hydrolysis" of the original silane. They reported a bonding density of 4.1 $\mu mol/m^2$ for attachment of the propylthiol-derivatized silica. Using optimized conditions of 6 h in peroxyoctanoic acid in diethyl ether at room temperature, the authors obtained a maximum exchange capacity of 0.34 mequiv./g for the final phase and also stated that a maximum conversion from thiol to sulfonic acid of 50% was achieved. To explain the limited conversion, the authors theorized that the reaction proceeded through a disulfide intermediate so that only thiols adjacent on the silica surface could react to form the sulfonic acid. Isolated thiols would not react.

Because Fazio *et al.* [24] reported minimum silane cleavage, their scheme was chosen for investigation. In addition, a scheme to improve the yield of the thiol-to-sulfonic acid conversion

was devised, assuming that the reaction proceeds through the disulfide intermediate. The revised scheme involves preparation of an intermediate disulfide phase prior to peroxyoctanoic acid oxidation. If indeed isolated thiols are present, they should be converted to the disulfide by the intermediate reaction, and become oxidized to sulfonic acid in the subsequent step. The original scheme of Fazio *et al.* and the revised disulfide intermediate scheme are depicted in Fig. 1.

Set 1: propylthiol attachment

Two sets of propylthiol silane attachments, disulfide couplings, and peroxyoctanoic acid oxidation experiments were conducted using two different base silicas: Waters Nova 5 μm and Davisil. In the first set, a 6-g batch of propylthiol-derivatized Waters silica was prepared by reacting 3-mercaptopropyltrimethoxysilane with silica in toluene overnight under reflux. The reacted phase was washed with methanol (12 ×) and air dried. The final phase had a bonding density of 1.87 μmol/m^2 (%C) or 1.65 μmol/m^2 (%S). The %C calculation assumes that only one of the methoxy leaving groups has reacted and that the other two are still present on the attached ligand. If it assumed that all three methoxy leaving groups are reacted, %C analysis predicts a bonding density of 3.20 μmol/m^2! Due to the ambiguity associated with the carbon analysis, the bonding density associated with the percent sulfur analysis is believed to be more accurate. Sulfur analysis is used to track the course of the reaction.

Set 1: disulfide couplings

Next, two different 2-g portions of the Waters propylthiol silica were reacted in 20–30 ml of 35% diethyldisulfide in DMSO. The reagents were weighed in a dry box and the reactions were conducted under a dry nitrogen blanket. DMSO was used as the solvent because it is also known to oxidize thiols to disulfides [25,26], and should ensure the completeness of the reaction. The reaction conditions were 14 h at 160°C for the first portion and 22 h at 70–96°C (imprecise temperature control) for the second portion. The disulfide reaction was successful as evidenced by a correlated increase in both %C and %S analysis. The Δ%C and Δ%S can be used to calculate the amount of disulfide ligand produced if it is assumed that no silane cleavage occurred. This assumption is made for the benefit of calculation only, and as discussed later, is probably not true. Δ%C and Δ%S calculations gave similar results: *ca.* 1.2 μmol/m^2 of disulfide was obtained for the higher temperature reaction ("high disulfide") *vs.* 0.6 μmol/m^2 for the lower temperature reaction ("low disulfide"). IR spectra were taken of the original thiol, and the high- and

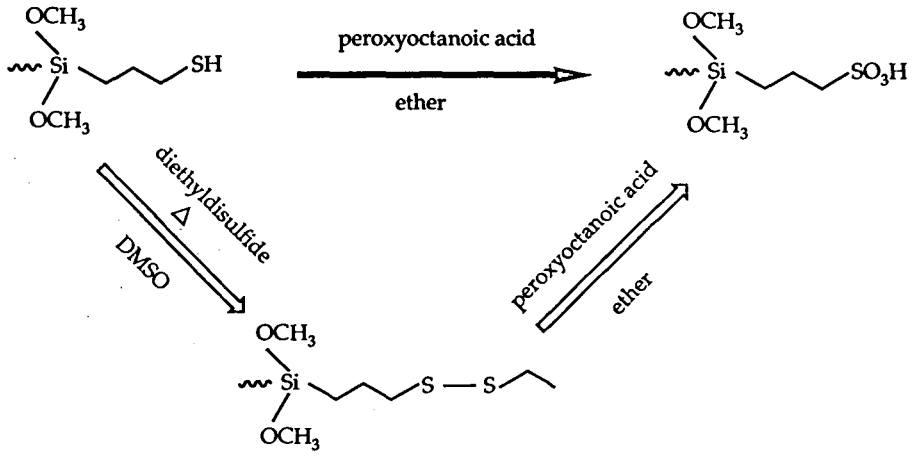

Fig. 1. Schemes to produce a sulfonic acid phase via direct oxidation of a thiol phase according to Fazio *et al.* [24] (solid arrows) or via oxidation of an intermediate disulfide phase (open arrows).

low-disulfide phases. Weak methyl and/or methylene signals could be observed for all three phases in the 3000–2850 cm^{-1} range. The intensity of the 2938 cm^{-1} band increased and the intensity of the 2857 cm^{-1} band decreased in going from the thiol to low-disulfide to high-disulfide phase. The S–H band for the thiol phase was barely discernible at 2579 cm^{-1}. A spot test was able to detect the thiol functional group for the thiol phase as reported at the end of the next section.

Set 1: peroxyoctanoic acid oxidations

The thiol and disulfide phases were subsequently oxidized by reacting 1 g of the phase in 50 ml of 0.4 *M* peroxyoctanoic acid in diethyl ether; the reaction was run for 6 h at room temperature (22°C). Because peroxyoctanoic acid is unstable, it must be prepared just before use. The procedure, previously used by Fazio *et al.* [24], is detailed by Parker *et al.* [27] and involves the stoichiometric reaction of hydrogen peroxide with octanoic acid in concentrated sulfuric acid to produce peroxyoctanoic acid. The freshly prepared peroxyoctanoic acid is extracted into diethyl ether, and the ether solution is washed several times with water to remove traces of sulfuric acid. A 150-ml volume of 0.4 *M* peroxyoctanoic acid in diethyl ether was prepared in this manner and then split into thirds for immediate use in this experiment. Three sulfonic acid phases were produced: oxidized thiol, oxidized "high disulfide" and oxidized "low disulfide". The sulfonic acid phases were washed with methanol (5 ×), water (3 ×), methanol again (3 ×), and then characterized by elemental analysis (%C, %S) and acid–base titration.

In addition to calculating exchange capacities, the acid–base titration curves were used for qualitative phase characterization. The shape of the titration curve identifies the titrated species as a strong or weak acid. The ability to discriminate between strong and weak cation exchangers was demonstrated by titrating a commercial strong cation-exchange phase (Supelco SCX, a propylsulfonic acid phase, base silica 175 m^2/g) and a commercial weak cation-exchange phase

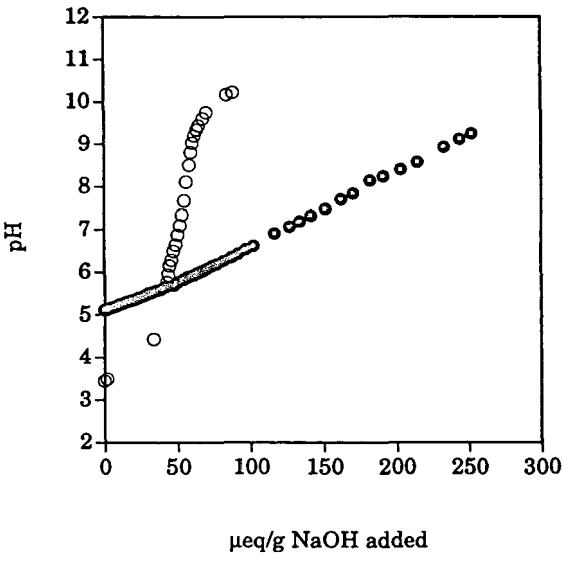

Fig. 2. Acid–base titration of commercial cation-exchange phases: Supelco SCX, a propylsulfonic acid phase (○) and Alltech RP4/Cation, a butanoic acid phase (●).

(Alltech RP4/Cation, a butanoic acid phase, base silica 350 m^2/g). The titration curves are shown in Fig. 2 as pH *vs.* $\mu equiv._{NaOH}/g_{silica}$ added. The titration curve for the sulfonic acid phase is a steep S-shaped curve; the titration curve for the carboxylic acid phase is characteristic of a weak acid. The difference between the shapes of the two titration curves is somewhat exaggerated in this plot because the exchange capacity of the carboxylic acid phase is four times higher than the sulfonic acid phase.

Titration curves for the three Waters sulfonic acid phases are given in Fig. 3, and confirm that strong acid phases were produced. Results show that the highest conversion to sulfonic acid was obtained by direct oxidation of the propylthiol phase (46 μequiv./q), and that disulfide coupling does not increase the final yield. The exchange capacity of the sulfonic acid phase produced from the high-disulfide phase (43 μequiv./g, 160°C) was higher than the capacity of the sulfonic acid phase produced from the low-disulfide phase (29 μequiv./g, 70–96°C). Cleavage of the propylthiol ligand was 24% (%S) based on the direct thiol oxidation case. Silane cleavage could not be calculated for the

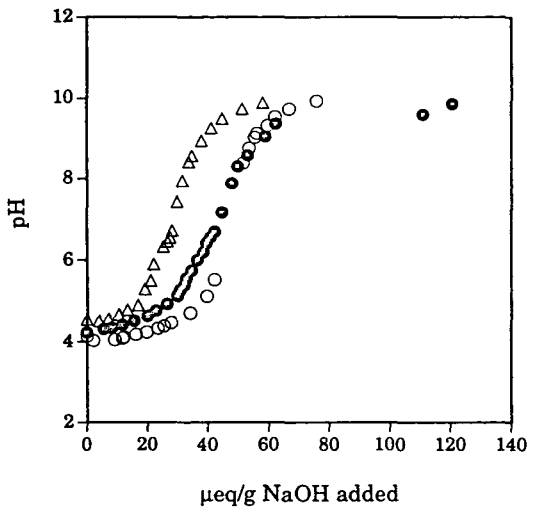

Fig. 3. Acid–base titration of laboratory-made sulfonic acid phases (Waters base silica): oxidized thiol (○), oxidized "high disulfide" (●) and oxidized "low disulfide" (△).

sulfonic acid phases produced from the disulfide phases, because the amount of residual disulfide was unknown.

A spot test was used to determine if unreacted thiol groups were present on the various phases. The test is based on the reaction of alcoholic ammoniacal sodium nitroprusside with thiols [28]; disulfides and sulfonic acids do not react. Four drops of the reagent were added to 30 mg of the phase to be tested in a test tube. A pinkish-purple color develops within 1 min if the test is positive. The propylthiol phase, disulfide phases, sulfonic acid phases and the underivatized Waters silica were all tested in this manner. Only the propylthiol phase gave a positive result.

Set 2

Because the amount of silane cleavage introduced by the disulfide coupling step was unknown, and the sulfonic acid phase produced from the high-disulfide phase had an exchange capacity close to the sulfonic acid phase produced by direct thiol oxidation, a second set of experiments was conducted to determine if a net increase in final sulfonic acid yield could be obtained from disulfide couplings conducted at intermediate temperatures. A higher surface area silica (Davisil, 300 m^2/g) was used to emphasize the difference in μequiv./g exchange capacities. Propylthiol attachment produced a phase with 1.63 (%C) or 1.69 (%S) $\mu mol/m^2$ bonding density consistent with the coverage achieved with the Waters silica. Two disulfide couplings were run at intermediate temperatures: 131 and 119°C, and produced disulfide phases with bonding densities for the disulfide ligand of 0.84 (131°C) and 0.66 (119°C) $\mu mol/m^2$ based on Δ%S; these disulfide bonding densities are intermediate between the bonding densities obtained for the Waters silica 160°C coupling (1.25 $\mu mol/m^2$) and 70–96°C coupling (0.50 $\mu mol/m^2$) as shown in Fig. 4. A good correlation between temperature of the reaction and disulfide "bonding density" is observed.

Peroxyoctanoic acid oxidations using 1.7 *M* peroxyoctanoic acid in diethyl ether were carried out for 6 h at room temperature. A more concentrated reagent was made due to the higher surface area of the silica. Once again, the maximum exchange capacity calculated from the

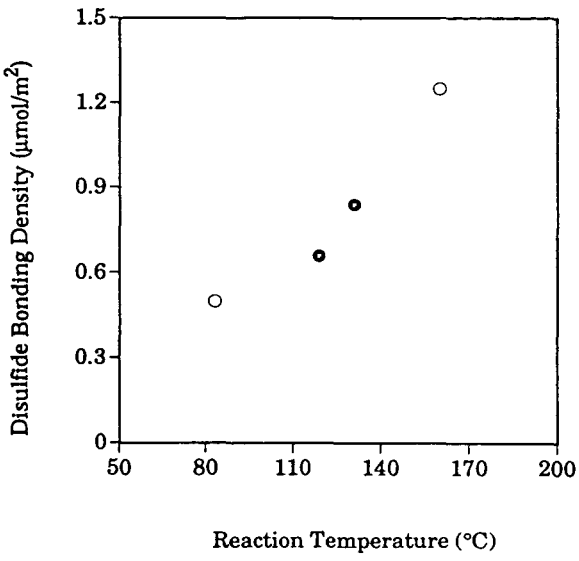

Fig. 4. The effect of reaction temperature on the disulfide coupling step using Waters (○) and Davisil (●) base silicas. The bonding density is calculated from the difference in %S of the phase before *vs.* after reaction and does not account for cleavage of the propylthiol ligands which may occur. The average temperature is used for the lower point of the Waters phase.

titration curves was obtained via direct oxidation of the propylthiol phase (283 μequiv./g), and the sulfonic acid phase produced from the high-disulfide phase (223 μequiv./g, 131°C) had a higher capacity than that produced from the low-disulfide phase (212 μequiv./g, 119°C). The difference was less pronounced because the temperature difference was smaller. Cleavage (%S) based on the direct thiol oxidation phase was 30%.

The exchange capacity of the phase produced in the second set was 0.94 *vs.* 0.39 μmol/m^2 in the first set. The efficiency of the peroxyoctanoic acid oxidation in the second set of reactions (56%) was more than twice as much *vs.* the first (24%) based on the percentage of the original propylthiol ligands that were converted to active sulfonic acid ligands for the direct thiol oxidations. The concentration of peroxyoctanoic acid was four times higher for the second set of reactions (1.7 *M*) *vs.* the first (0.41 *M*), although the actual molar excess was two times lower for the second set (76:1) *vs.* the first (150:1). This indicates that the concentration of peroxyoctanoic acid is likely a key factor in the efficiency of the oxidation reaction, because all other factors and results for the two sets of reactions are similar. This difference in oxidation efficiency is also observed for the disulfide coupled phases.

A commercial propylsulfonic acid phase, Supelco SCX, was characterized for comparison to the laboratory-made phases. Elemental analysis (%S) indicated that the propylsulfur-containing ligand is present at more than 3 μmol/m^2 (assuming 1 S atom per ligand), but the amount of active propylsulfonic acid ligand (exchange capacity) is only 0.3 μmol/m^2. Therefore, only 10% of the propylsulfur ligand precursor was converted to sulfonic acid. The pH of the Supelco SCX silica dispersion prior to titration was *ca.* 3.9, which is slightly lower than the pH of the sulfonic acid phase dispersions produced here, so that the low capacity is not due to preneutralization by the manufacturer. Therefore, the results obtained in this research represent higher yields than at least one commercially available phase.

A spot test using pinacryptol yellow for the detection of sulfonates reagent [29] was evaluated. The test is based on the exchange of the dye reagent's counterion with the sulfonate, and the subsequent effect on the dye's fluorescent properties. Unfortunately, the reagent was available with a methanesulfonate counterion only, and therefore the anion exchange (methanesulfonate *vs.* propylsulfonate) did not change the fluorescent properties significantly enough for visual detection.

The results for the thiol and sulfonic acid phases are summarized in Table 2. Note that the bonding densities calculated from %S analysis correlate with the bonding densities calculated from %C analysis for both the propylthiol phases (part A) and the sulfonic acid phases produced via direct oxidation (part B). The %C calculation assumes that only one of the methoxy groups of the propylthiol silane ligand has reacted. This is a good assumption since the reactions were conducted under anhydrous conditions. The percentage of total ligand which is active can be calculated for the sulfonic acid phases (part B) from the exchange capacity (μmol/m^2) and the bonding density (%S). The percent active ligand is 31% for the Waters sulfonic acid phase and 79% for the Davisil sulfonic acid phase, reiterating the higher conversion obtained in the second set of peroxyoctanoic acid oxidations. Although the conversion was significantly higher in the second set of reactions, the amount of silane cleavage (30%) was not significantly higher than in the first set (24%).

If it is assumed that there is no residual disulfide, the bonding densities calculated from both %S and %C analysis for the sulfonic acid phases produced via the disulfide intermediate (part C) indicate that the *total* amount of ligand is higher than the phases produced by direct oxidation (part B). If residual disulfide is present, then there could actually be less total ligand for these phases. In either case, the final amount of *active* ligand is lower for the sulfonic acid phases produced via the disulfide intermediate. Since it is expected that a disulfide is easier to oxidize than a thiol, it is likely that the lower net

Table 2
Summary of propylthiol and sulfonic acid phases

Silica	Temperature disulfide coupling (°C)	Bonding density (μmol/m^2)		Exchange capacity		Active ligands	Cleavage
		%C	%S	μmol/m^2	μequiv./g	%	%[c]
A. Propylthiol phases							
Waters		1.87[a]	1.65				
Davisil		1.63[a]	1.69				
B. Sulfonic acid phases via direct oxidation of thiol phases							
Waters		1.02[b]	1.25	0.39		31	24
Davisil		1.07[b]	1.19	0.94		79	30
C. Sulfonic acid phases via disulfide intermediate phases							
Waters	70–96	1.21[b,d]	1.50[d]	0.24	29		
Waters	160	1.35[b,d]	1.61[d]	0.36	43		
Davisil	119	1.32[b,d]	1.50[d]	0.71	212		
Davisil	131	1.32[b,d]	1.50[d]	0.74	223		

[a] Calculated assuming 5 carbons per propylthiol ligand.
[b] Calculated assuming 5 carbons per propylsulfonic acid ligand.
[c] Based on sulfur analyses.
[d] Calculated assuming no residual disulfide is present.

yield is due to additional silane cleavage which occurred in the disulfide coupling step.

Fazio *et al.* [24] reported a maximum conversion of 50% for direct oxidation of a thiol phase to a sulfonic acid phase using peroxyoctanoic acid in diethyl ether. We obtained 24 or 56% conversion with the higher conversion corresponding to higher peroxyoctanoic acid concentration. The concentration of peroxyoctanoic acid should be pursued as a key factor in further attempts to optimize this reaction.

3.2. Carboxylic acid, carboxylate phases

There are a few reports of carboxylic acid phases in the literature. Asmus *et al.* [30] prepared a carboxymethylphenyl phase via a three-step reaction sequence: (1) attachment of a chloromethylphenyl ligand, (2) conversion of the chlorine group to a cyano group with CN^- and (3) oxidation of the cyano group with a mixture of concentrated sulfuric and acetic acids. The final phase had a capacity of 130 μequiv./g (0.33 μmol/m^2). Chang *et al.* [31] prepared a carboxymethyl-derivatized silica by attachment of γ-glycoxypropylsilane followed by oxidation with a sodium metaperiodate, potassium carbonate, potassium permanganate reagent. Ion-exchange capacities for two different base silicas were reported in units of $mg_{hemoglobin}/ml_{derivatized\ silica}$ and were 19 (70 m^2/g silica) and 38 (130 m^2/g silica). Caude and Rosset [32] prepared a polymeric carboxylate-derivatized silica by first attaching a vinyl silane and subsequently copolymerizing methacrylic acid with the vinyl silica. An exchange capacity of 2.2 mequiv./g (5.5 μmol/m^2) was reported. Kolla *et al.* prepared a series of polymeric carboxylate-derivatized based on 1:1 butadiene–maleic acid polymers [38]. The preformed butadiene–maleic acid polymers were physisorbed onto silica at several different film thicknesses, and subsequently crosslinked to the silica surface to provide covalent linkage. The resulting exchange capacities were a direct function of film thickness with reported values ranging from 1.1 to 3.9 mmol/g (2.9 to 10 μmol/m^2). Khurana *et al.* [33] used direct coupling of a commercially available carboxylic acid silane

(carboxypropyldimethylchlorosilane) to silica. The reported exchange capacity (acid–base titration) was 90 μequiv./g (0.23 μmol/m^2).

Thus, there appears to be no general way of preparing a carboxylic acid phase, and except for the polymeric phases, the bonding densities of active ion exchanger are low. One scheme that has not been reported is the attachment of an ester-containing silane followed by hydrolysis to the carboxylic acid or carboxylate. A search was conducted to determine a suitable hydrolysis method given that the pH stable range for bonded phases is approximately 2.5 to 7.5. Acids cause cleavage of the silane from the surface (Si–C bond cleavage) and bases dissolve the silica backbone (Si–O bond cleavage).

One hydrolysis technique that appeared promising is the hydrolysis of methyl esters using lithium halide salts in DMF [34]. DMF has been used as a solvent for silane–silica couplings. This scheme is depicted in Fig. 5A. When it became clear that significant silane cleavage (25–50%) did in fact occur with lithium halides in DMF, acidic hydrolysis was also pursued (Fig. 5B). The efficiency of hydrolysis under the acidic conditions tested was also low with significant silane cleavage (50%). Despite the low conversions obtained, both reactions were successful, and the results are presented for the researcher who wishes to continue in this area.

Ester phases

Two different ester silanes were used to prepare ester-derivatized silicas: (10-carbomethoxydecyl)dimethylchlorosilane (C_{11} ester) and 2-(carbomethoxyethyl)methyldichlorosilane (C_3 ester). Reactions were run overnight in refluxing dichloromethane. In most of the reactions, DMAP was added as a catalyst to increase the bonding density. After the reaction was completed, the derivatized silicas were washed three times each with dichloromethane, methanol, methanol–water (1:1), methanol again, and finally, diethyl ether. The silicas were then air dried overnight and stored in a desiccator. The C_{11} ester silane was coupled to Waters Nova 12-μm silica both without and with DMAP catalyst to produce low- and high-bonding-density ester phases of 1.88 and 3.21 μmol/m^2 (%C), respectively. The C_3 ester silane was coupled to both Waters Nova 5-μm and Supelco silicas using DMAP catalyst to produce high-bonding-density phases of 3.08 and 2.96 μmol/m^2, respectively. Results are tabulated in Table 3 (part A). High-bonding-density ester phases (*ca.* 3 μmol/m^2) were consistently produced when the DMAP catalyst was used.

The IR spectrum of the high-bonding-density C_{11} ester phase is given in Fig. 6 *vs.* the spectrum for the underivatized silica. The methylene and carbonyl bands for the ester phase are easily observed on top of the silica background. The carbonyl region comprises a major peak at 1749 cm^{-1} and much smaller peak at 1720 cm^{-1}. The peak at 1749 cm^{-1} corresponds to the normal carbonyl stretch observed for long-chain aliphatic esters. Note the disappearance of the SiOH band at 3738 cm^{-1} (isolated silanols) in going from the underivatized silica to the ester phase.

We expected the spectrum of the low-bonding-

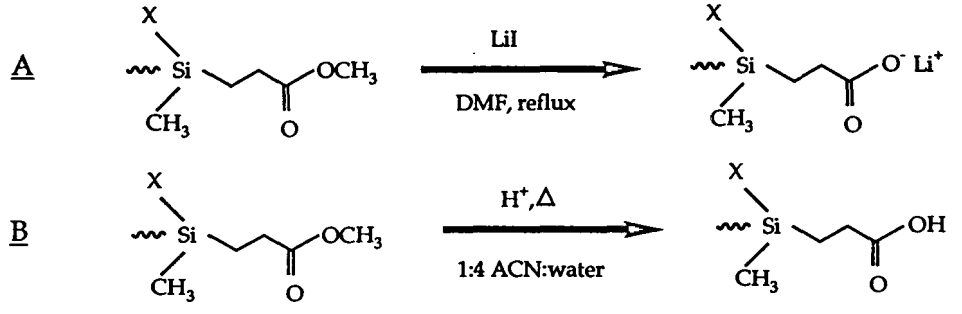

Fig. 5. Schemes to produce carboxylic acid phases based on the hydrolysis of an ester using lithium hydoxide in DMF (A) and aqueous acid (B). ACN = Acetonitrile.

Table 3
Summary of ester and carboxylic acid phases

Silica	Ester chain length	DMAP catalyst	Bonding density (μmol/m^2)	Reaction time (min)	HCl (%)	Reaction temperature (°C)	Exchange capacity		Cleavage (%)
							μmol/m^2	μequiv./g	
A. Ester phases									
Waters Nova 12 μm	C_{11}	No	1.88						
Waters Nova 12 μm	C_{11}	Yes	3.21						
Waters Nova 5 μm	C_3	Yes	3.08						
Supelco	C_3	Yes	2.96						
B. Carboxylic acid phases: lithium iodide/DMF hydrolysis time study									
				2			0.29	34	
				19			0.32	38	
				271			0.26	31	
				328			0.16	19	
C. Carboxylic acid phases: acidic hydrolysis acid level study									
					0.1	92	0.20	34	49
					0.5	92	0.12	21	46
					1	83	0.24	41	41
					5	83	0.23	39	51

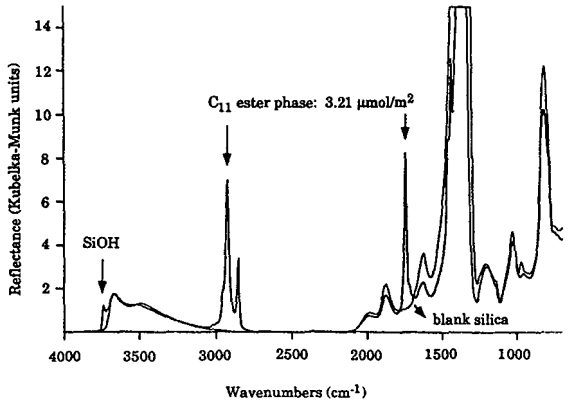

Fig. 6. Diffuse reflectance infrared spectrum of high-bonding-density C_{11} ester phase *vs.* the spectrum of the blank silica. Base silica is Waters Nova 12 μm.

density C_{11} ester phase to resemble the high-bonding-density spectrum but with a lower intensity for the alkyl and carbonyl bands. We did, indeed, observe this in the alkyl region, but the carbonyl bands for the low-bonding-density phase showed a reversal in the relative intensity of the two carbonyl peaks. An enlargement of the carbonyl band region for the two ester phases is given in Fig. 7. The high bonding density phase has a large peak at 1749 cm^{-1} and a much smaller peak at 1720 cm^{-1}, whereas the same peaks in the low-bonding-density phase spectrum are closer in intensity with the 1720

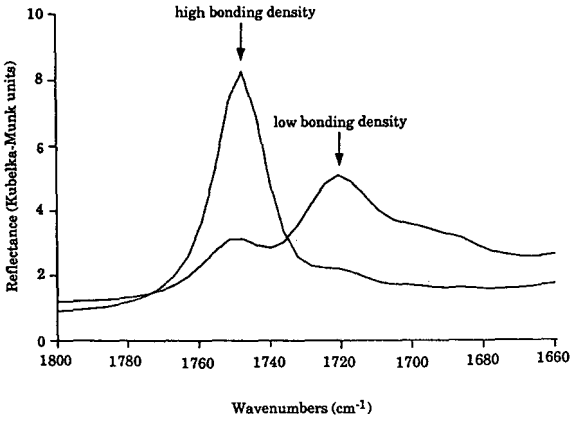

Fig. 7. Diffuse reflectance infrared spectra of high- (3.21 μmol/m^2) and low- (1.88 μmol/m^2) bonding-density C_{11} ester phases. Base silica is Waters Nova 12 μm.

cm^{-1} peak being larger. There are two possibilities to explain the peak at 1720 cm^{-1}: (1) some hydrolysis of the ester has already occurred, and the peak corresponds to carboxylic acid; this possibility was eliminated based on titration with sodium hydroxide; and (2) hydrogen bonding between the carbonyl oxygen of the ester and the silica surface silanols lowers the carbonyl stretching frequency for a given population of the covalently bound ligands; this explanation is consistent with the observed increase in the 1749 cm^{-1} peak in going from low to high bonding density. As the surface becomes more crowded, there is less possibility for the carbonyl moiety, which is at the opposite end of the molecule, to hydrogen bond with the silica surface. An IR spectrum was also taken of the Waters C_3 ester phase. The carbonyl region comprised two equal intensity bands at 1737 and 1716 cm^{-1} showing evidence of a dual ligand population.

Other researchers have seen evidence of ligand-to-surface hydrogen bonding and/or dual ligand populations (free *vs.* surface-hydrogen bonded) in the IR spectra of derivatized silicas. Suffolk and Gilpin [1] deconvoluted the cyano band of cyanoalkylsilanized silicas into high- and low-frequency components which were attributed to hydrogen bonded and free cyano ligands, respectively. Leyden *et al.* [4] attributed the simultaneous shifts of amide I (carbonyl) and amide II bands for acetoacetamide-functionalized silicas to hydrogen bonding of both the amide carbonyl and the amide NH with the silica surface.

Lithium halide hydrolysis

The initial lithium halide hydrolysis experiments were conducted with the C_{11} ester phases. A 1-g amount of the low-bonding-density ester phase was dispersed in 20 ml of DMF, and 0.50 g LiBr (27 × molar excess) were added (all done in dry box). The reaction was run for 3 h under nitrogen purge and reflux conditions. An IR spectrum of the reacted phase showed little to no change in the carbonyl group frequencies or intensities. %C analysis showed that 27% silane cleavage had occurred. The reaction was re-

peated with the high-bonding-density C_{11} ester phase, using a larger LiBr molar excess (71 ×), and a longer reaction time (22 h). The IR spectrum of the reacted phase resembled the IR spectrum of the low-bonding-density ester phase. %C analysis showed that 46% silane cleavage occurred. Our interpretation of these results is that no hydrolysis of the ester occurred in either case, and that the higher amount of cleavage in the second attempt was evident in the IR spectrum.

The original reference for the lithium halide hydrolysis [34] indicated that the rate of hydrolysis was higher for LiI (100% hydrolysis within 1.5 h) than LiBr (100% hydrolysis within 4 h). A final set of experiments was conducted to see if lithium iodide was more reactive. In addition, the reaction was monitored as a function of time because the amount of silane cleavage was observed to increase with time in the previous experiments. The ester phase used was the Waters C_3 methyl ester, and LiI was added at a 26 × excess. Samples of the reacted silica were removed at various time intervals after the reaction mixture began to reflux (total reaction time 5.5 h). The samples were washed with acetone (6 ×), water (6 ×), pH 3.0 HCl (6 ×), water (6 ×) and acetone (3 ×), then air dried and analyzed for exchange capacity. The data are tabulated in Table 3 (part B), and show that the exchange capacity reached its maximum (38 μequiv./g) within the first 20 min and then decreased with time, probably due to subsequent silane cleavage. Silane cleavage was 58% after the first 2 min of the reaction, and 67% after 201 min. The increasing cleavage of the silane from the surface was also observed as a continuing decrease in the intensity of the carbonyl bands in the IR spectra of the reacted phase at 2, 48, 141 and 211 min. There was only a slight change in the carbonyl group frequencies of the original ester *vs.* the hydrolyzed ester phases.

Titration curves for the maximum capacity reacted phase sample, the original ester phase, and the blank silica are given in Fig. 8. The blank silica had a capacity of 8 μequiv./g and the original ester had a capacity of 21 μequiv./g indicating that the ester phase has self-hydrolyzed to a small extent, and show that although the capacity of the reacted phase is low, it is real.

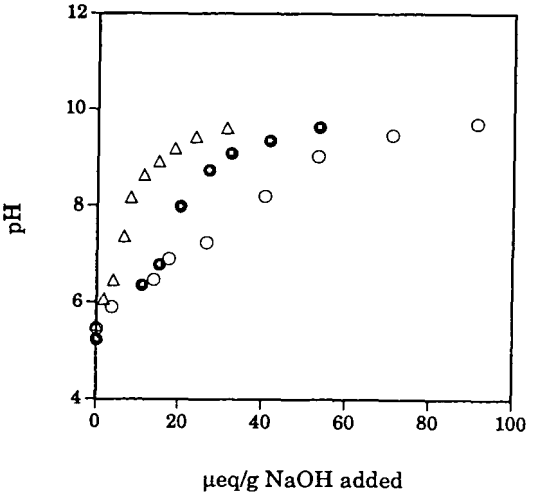

Fig. 8. Acid–base titration of propionic acid phase produced via lithium iodide hydrolysis of a C_3 ester phase (○) *vs.* original C_3 ester phase (●) and blank silica (△). Base silica is Waters Nova 5 μm.

Acidic hydrolysis

The initial acidic hydrolysis experiment was conducted by reacting 1 g of the high-bonding-density C_{11} ester phase in 60 ml of acetonitrile–water (1:1) at a pH of 4 (HCl). The reaction was run under reflux for 22 h. Silane cleavage was extremely low (0.18%) and an IR spectrum of the reacted phase showed no change from the original ester spectrum.

Since there was no evidence of reaction at pH 4, increasing acid levels were tested. The ester phase used was the Supelco C_3 methyl ester. Hydrochloric acid levels of 0.1, 0.5, 1 and 5% were used with a constant reaction time of 22 h. For each of the runs, 1.5 g of the ester phase were dispersed in 20 ml of the acid in acetonitrile–water (1:4). (Acetonitrile is added to promote phase wetting. Less was needed here for the short-chain ester). The temperature for the 0.1 and 0.5% runs was 83°C and for the 1 and 5% runs 92°C. After washing, the final phases were titrated indicating low but real conversion (Fig. 9) and analyzed for %C. Exchange capacities of 21–41 μequiv./g were obtained

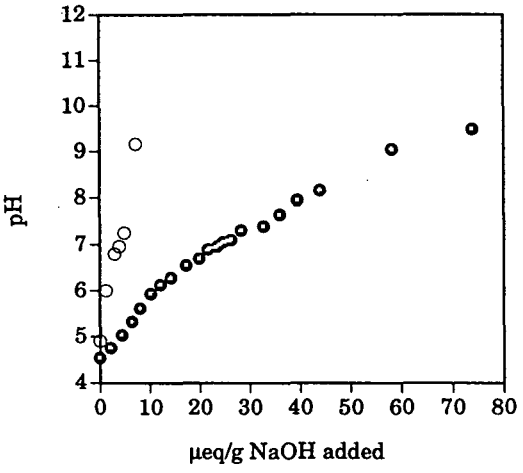

Fig. 9. Acid–base titration of propionic acid phase produced via acidic hydrolysis of a C_3 ester phase (●) *vs.* original C_3 ester phase (○).

(Table 3, part C) *vs.* a capacity of 6 μequiv./g for the original ester. Despite the large range of acid levels tested (a 50:1 concentration range), silane cleavage varied over a narrow range of 41–51%. Capacities are low (21–41 μequiv./g), and the higher capacities were obtained with the higher acid levels, 1 and 5%.

The pH of the 0.1% HCl solution is theoretically 1.6. Based on the initial experiment, no reaction occurred at a pH of 4. Thus, it appears that once a threshold level of acid is reached (somewhere between pH 4 and 1.6), silane cleavage occurs to a significant extent but does not increase in proportion to the additional amount of acid added. Temperature may also be a factor but its effect was not intentionally studied here.

Low conversion to the carboxylate/carboxylic acid and significant ester silane cleavage were obtained for both lithium halide and acid hydrolysis schemes. The capacity of a commercial butanoic acid phase (Alltech RP4/Cation) was 200 μequiv./g (0.57 μmol/m^2). Thus, the capacities obtained via lithium halide or acidic hydrolysis are 2–5 times less than a commercial phase.

It is likely that further optimization of the reaction conditions could improve the net yield for both hydrolysis reactions. The lithium halide reactions were conducted under reflux conditions (153°C). Lower temperatures may provide similar conversion with less cleavage. The relative reactivities of lithium bromide and lithium iodide for ester hydrolysis and silane cleavage should also be investigated.

Silane cleavage from acidic hydrolysis varied from only 41 to 51% over a wide range of acid levels tested (0.1–5%), and there was no definite correlation between acid level and cleavage. Temperature may also be a factor but there are insufficient data to make a conclusion. Two avenues which may be promising to increase the net yield are higher acid levels ($>5\%$) at lower temperatures (<80°C) to increase conversion, and lower acid levels under reflux conditions (100°C) to minimize silane cleavage. High temperature alone does not cause silane cleavage as evidenced by the pH 4 hydrolysis run for which there was less than 0.2% cleavage.

3.3. Quaternary ammonium phases

The synthesis of aliphatic quaternary ammonium-derivatized silica phases has not been reported although these phases are available commercially. A quaternary ammonium silane in which one of the nitrogen substituents is a C_{18} alkyl chain is available from Huls for direct coupling to silica, but shorter-chain versions are not available.

A synthetic route that is frequently used to prepare aromatic quaternary ammonium derivatized silicas involves the direct reaction of a chloroalkyl-derivatized silica with a tertiary amine, or conversion of a chloroalkyl phase to an iodoalkyl phase followed by reaction with a tertiary amine. The aromatic moiety originates from either the chloroalkyl phase [35] or the tertiary amine [36,37]. In the cited references, reaction conditions were adjusted according to the volatility of the amine used. With benzyldimethylamine (boiling range 65–68°C), overnight reflux at 56 to 101°C was used. With TMA (boiling point −4°C), the reaction conditions were one week at 0°C.

The scheme presented here is the reaction between an iodoalkyl precursor phase and TMA

to produce an aliphatic quaternary ammonium phase. The conditions of the reaction are devised so as to speed up the reaction via heat while minimizing loss of the TMA reagent.

Iodoalkyl precursor phases

Iodoalkyl phases were prepared as precursor phases for quaternization. Commercial iodoalkylsilanes are available for direct coupling to silica, and 3-iodopropyltrimethoxysilane was coupled to Waters Resolve silica by reacting overnight in refluxing toluene. After derivatization, the phase was washed 15 times with methanol and then air dried. Elemental analysis (%C, %I) was conducted. The bonding density obtained was 2.57 μmol/m^2 (%C) or 3.28 μmol/m^2 (%I). It has been our experience that bonding densities based on %I are about 30% higher than those based on %C.

Due to the potential for cross-reactivity with the iodine moiety on the silane, conventional catalysts cannot be used to increase the bonding density obtained for iodoalkyl silane couplings. Therefore, an attempt to prepare a higher-bonding-density iodoalkyl phase based on the substitution of a chloroalkyl phase with sodium iodide was made as per Crowther *et al.* [37]. Crowther *et al.* used sodium iodide in methyl ethyl ketone under reflux conditions to convert chloropropyl-derivatized silica to the iodopropyl form.

A high-bonding-density chlorobutyl phase was made by coupling 4-chlorobutyldimethylchlorosilane to Waters Nova 12-μm silica with DMAP catalyst in dichloromethane (overnight, reflux). The resultant phase had a bonding density of 3.40 (%C) or 3.43 (%Cl) μmol/m^2. Next, the chlorobutyl phase was reacted with NaI (15 × excess) in methyl ethyl ketone. The reaction was carried out under a nitrogen purge and reflux conditions for 17 h. The iodobutyl phase was washed as follows: acetone (3 ×), acetone–water (1:1) (10 ×), acetone (7 ×). The phase was air dried and analyzed for %C, %Cl and %I.

The %C was used to calculate the total bonding density after reaction (3.23 μmol/m^2) indicating that minimal silane cleavage occurred (*ca.* 5%). Bonding densities based on %Cl and %I were used to calculate the relative amounts of the chlorobutyl and iodobutyl ligands present, and showed that the sum of chlorobutyl and iodobutyl ligands (2.44 μmol/m^2) was lower than the total bonding density (3.23 μmol/m^2). An explanation for this is that some amount of the haloalkyl ligand was hydrolyzed to the alcohol. The final iodobutyl bonding density (*ca.* 2 μmol/m^2) was lower than that obtained with direct iodopropyl silane attachment (2.6 μmol/m^2).

Quaternization reactions

In the first attempt, a reaction temperature of 15–20°C was maintained by immersing the reaction flask in a circulating water bath, and the reaction flask was capped. A 1-g amount of the iodobutyl phase was dispersed in 10 ml ethanol, and 2 ml of 25% TMA in methanol were added. The reaction was stirred for 24 h, after which another 1-ml aliquot of the TMA reagent was added. The reaction continued for a second 24 h. The phase was washed and elemental analysis was performed. No nitrogen was found indicating that no detectable reaction occurred. Silane cleavage (%C) was 24%.

In the second attempt (Fig. 10), the reaction flask itself was gently heated (34°C) and a condensor containing circulating ethylene glycol–water (1:1) cooled to −7°C was attached. A

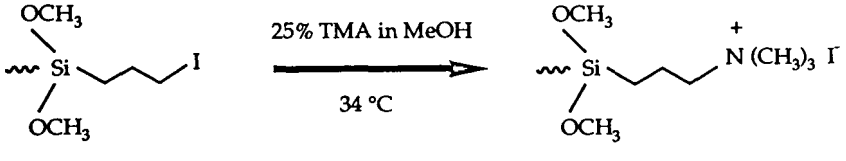

Fig. 10. Scheme to produce a C_3 quaternary ammonium phase based on the reaction of an iodopropyl phase with TMA using heat. Base silica is Waters Resolve.

Table 4
Summary of quaternary ammonium phases

Mode of preparation	Silica	Bonding density (μmol/m^2)		Exchange capacity	
		%C	%N	μmol/m^2	μequiv./g
Commercial silane	Waters Nova 12 μm	1.68	1.84	0.69	79
Quaternization of iodopropyl	Waters Resolve	1.86	0.92	0.52	91

2.6-g amount of the iodopropyl phase was dispersed in 25 ml of 25% TMA in methanol. The reaction was run for 22 h. Elemental analysis showed that quaternization had occurred (nitrogen found). The amount of nitrogen-containing ligand was 0.92 μmol/m^2 (based on %N), and the silane cleavage was 28% (based on %C). The exchange capacity was 0.52 μmol/m^2 (91 μequiv./g).

For comparison, a quaternary ammonium phase was prepared by direct coupling of the commercially available C_{18} quaternary ammonium silane (*n*-octadecyldimethyl[3-(trimethylsilyl)propyl]ammonium chloride) using Waters Nova 12-μm silica. The reaction was conducted overnight in refluxing toluene. A bonding density of 1.68 μmol/m^2 (%C) or 1.84 μmol/m^2 (%N) was obtained. The exchange capacity was 0.69 μmol/m^2.

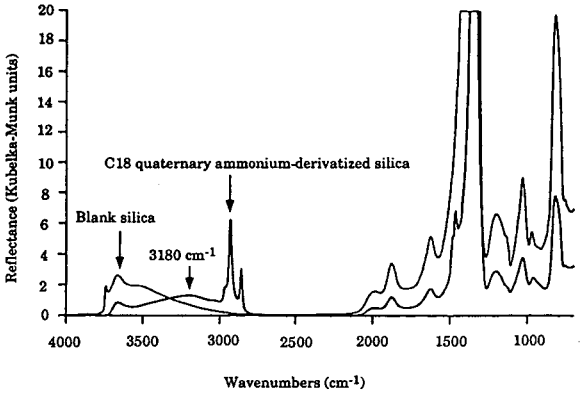

Fig. 11. Diffuse reflectance infrared spectrum of C_{18} quaternary ammonium phase produced via reaction of a commercial silane with Waters Nova 12-μm silica.

An IR spectrum of the C_{18} quaternary ammonium phase was taken, and is shown in Fig. 11 *vs.* the underivatized silica spectrum. The methylene peaks at 2930 and 2860 cm^{-1} are apparent, but there is also a broad band with a peak frequency of 3180 cm^{-1}. This corresponds to an N–H stretch for an ammonium salt, and indicates that the amine is probably not 100% quaternized.

Results for the quaternary ammonium phases are summarized in Table 4. As expected, the %C and %N analyses predict a similar bonding density for the phase produced from coupling of the commercial silane. However, the bonding density calculated from %N is about 50% of the bonding density calculated from %C for the phase produced via the secondary quaternization reaction, which represents a rough estimate of the quaternization efficiency. The amount of active exchanger is less still, about 28% of the total and 57% of the nitrogen-containing ligands, respectively.

Further optimization of the reaction temperature, time and TMA concentration should be investigated for improving the quaternization efficiency. Also, the use of other tertiary alkyl amines which are less volatile than TMA would allow higher reaction temperatures and may give higher yields.

4. Conclusions

The aliphatic ion exchangers produced have active exchange capacities of 0.2–0.9 μmol/m^2. Given that chromatographic silica is readily

available with surface areas up to 550 m^2/g, the synthetic schemes presented can be used to produce phases with active capacities of 100–500 μequiv./g. The suggested steps for further optimization are likely to provide even higher-capacity phases.

Characterization of derivatized silicas continues to represent a challenge to the analytical chemist. Functional group analysis is a key area. The best results are obtained when a combination of complimentary techniques is applied. IR analysis is most useful when the functional group absorbance does not overlap with the silica absorbance background, and when the bonding density of ligands and surface area of the base silica are sufficiently high. Spot tests can be used to supplement IR analysis, and as demonstrated here, can be more sensitive in certain cases.

5. Acknowledgements

The authors are grateful for support of this work by The National Forensic Chemistry Center of the FDA and NIEHS-04908. Special thanks to Sritana Yasui for obtaining all the IR spectra presented. Thanks also to Waters, Davisil, Supelco and Jones for donation of the silicas.

6. References

[1] B.R. Suffolk and R.K. Gilpin, *Anal. Chim. Acta*, 181 (1986) 259.
[2] B.R. Suffolk and R.K. Gilpin, *Anal. Chem.*, 57 (1985) 596.
[3] L. C. Sander, J.B. Callis and L.R. Field, *Anal. Chem.*, 55 (1983) 1068.
[4] D.E. Leyden, D.S. Kendall, L.W. Burggraf, F.J. Pern and N. DeBello, *Anal. Chem.*, 54 (1982) 101.
[5] N. Watanabe, *Chem. Lett.*, (1981) 1373.
[6] G.L. Berendsen and L. de Galan, *J. Liq. Chromatogr.*, 1 (1978) 561.
[7] E. Bayer, K. Albert, J. Reiners, M. Nieder and D. Muller, *J. Chromatogr.*, 264 (1983) 197.
[8] D.E. Leyden, D.S. Kendall and T.G. Waddell, *Anal. Chim. Acta*, 126 (1981) 207.
[9] G.E. Maciel, D.W. Sindorf and V.J. Bartuska, *J. Chromatogr.*, 205 (1981) 438.
[10] M.P. Fuller and P.R. Griffiths, *Anal. Chem.*, 50 (1978) 1906.
[11] R.S.S. Murthy and D.E. Leyden, *Anal. Chem.*, 58 (1986) 1228.
[12] P. Shah, L.B. Rogers and J.C. Fetzer, *J. Chromatogr.*, 388 (1987) 411.
[13] R.C. Ziegler and G.E. Maciel, *J. Am. Chem. Soc.*, 113 (1991) 6349.
[14] M. Gangoda, R.K. Gilpin and B.M. Fung, *J. Magn. Reson.*, 74 (1987) 134.
[15] M. Verzele, P. Mussche and P. Sandra, *J. Chromatogr.*, 190 (1980) 331.
[16] J.B. Crowther, S.D. Fazio, R. Schiksnis, S. Marcus and R.A. Hartwick, *J. Chromatogr.*, 289 (1984) 367.
[17] S.D. Fazio, S.A. Tomellini, H. Shih-Hsien, J.B. Crowther, T.V. Raglione, T.R. Floyd and R.A. Hartwick, *Anal. Chem.*, 57 (1985) 1559.
[18] H. Genieser, D. Gabel and B. Jastorff, *J. Chromatogr.*, 269 (1983) 127.
[19] H. Genieser, D. Gabel and B. Jastorff, *J. Chromatogr.*, 244 (1982) 368.
[20] J. Erard and E.sz. Kováts, *Anal. Chem.*, 54 (1982) 193.
[21] L.M. Warth, R.S. Cooper and J.S. Fritz, *J. Chromatogr.*, 479 (1989) 401.
[22] N. Weigand, I. Sebestian and I. Halász, *J. Chromatogr.*, 102 (1974) 325.
[23] B.B. Wheals, *J. Chromatogr.*, 177 (1979) 263.
[24] S.D. Fazio, J.B. Crowther and R.A. Hartwick, *Chromatographia*, 18 (1984) 216.
[25] T.J. Wallace, *J. Am. Chem. Soc.*, 86 (1964) 2018.
[26] C.N. Yiannios and J.V. Karabinos, *J. Org. Chem.*, 28 (1963) 3246.
[27] W.E. Parker, C. Ricciuti, C.L. Ogg and D. Swern, *J. Am. Chem. Soc.*, 77 (1955) 4037.
[28] G. Toennies and J.L. Kolb, *Anal. Chem.*, 23 (1951) 823.
[29] H. Jork, W. Funk, W. Fischer and H. Wimmer, *Thin Layer Chromatography Reagents and Detection Methods*, Vol. 1a, VCH, New York, 1990.
[30] P.A. Asmus, C. Low and M. Novotny, *J. Chromatogr.*, 123 (1976) 109.
[31] S.H. Chang, K.M. Gooding and F.E. Regnier, *J. Chromatogr.*, 120 (1976) 321.
[32] M. Caude and R. Rosset, *J. Chromatogr. Sci.*, 15 (1977) 405.
[33] A.L. Khurana, E.T. Butts and C. Ho, *J. Liq. Chromatogr.*, 11 (1988) 1615.
[34] P.D.G. Dean, *J. Chem. Soc.*, (1965) 6655.
[35] P.L. Asmus, C. Low and M. Novotny, *J. Chromatogr.*, 119 (1976) 25.
[36] G.B. Cox, C.R. Loscombe, M.J. Slucutt, K. Sugden and J.A. Upfield, *J. Chromatogr.*, 117 (1976) 269.
[37] J.B. Crowther, S.D. Fazio and R.A. Hartwick, *J. Chromatogr.*, 282 (1983) 619.
[38] P. Kolla, J. Kohler and G. Schomburg, *Chromatographia*, 23 (1987) 465.

ELSEVIER

Journal of Chromatography A, 675 (1994) 47–54

JOURNAL OF CHROMATOGRAPHY A

Enrichment technique in an automated liquid microchromatograph with a capillary mixer

Petr Doležel, Miloš Krejčí*, Vladislav Kahle

Institute of Analytical Chemistry, Academy of Sciences of Czech Republic, Veveří 97, 611 42 Brno, Czech Republic

(First received December 20th, 1993; revised manuscript received March 10th, 1994)

Abstract

An automatic device based on a microcolumn liquid chromatograph with a capillary mixer and a laboratory-made fluorescence microcell is described. The device provides adjustment of the sample matrix in such a way that owing to the increase in the analyte capacity factor the sample is enriched on the analytical column. The on-line arrangement of the precolumn, mixer, analytical column and fluorescence detector enables trace amounts of the analyte in the sample to be treated. In the mixer the sample volume eluting from the precolumn (or the sample resulting from an off-line extraction) is mixed with a solvent of low elution strength, then the enrichment of the sample takes place on the analytical column. The device is characterized by a high degree of automation and high reproducibility of the measured data (R.S.D. = 0.8%) with zero losses of the analyte during the enrichment process. The applicability of the system was verified on the examples of determination of six polycyclic aromatic hydrocarbons in an organic extract (acetonitrile) and of the determination of trace amounts of fluoranthene (tens of nanograms per litre) in tap water.

1. Introduction

Typical cases of the determination of trace amounts of analytes in samples are environmental samples and biological samples containing drugs, biologically active substances, ions, toxic substances etc. Trace amounts of the studied substances are often accompanied by further substances present in the sample matrix. The amounts of samples available for analysis are often limited. An important role is played by efficient separation and miniaturization of all parts of the analyser. Both of these requirements are represented by microcolumn liquid chromatography [1–5]. Application of an enrichment technique prior to the determination of trace amounts of analytes is usually necessary. In connection with liquid chromatography, the enrichment by solid-phase extraction is most frequently used [6–8]. Packed precolumns then work as enrichment units [7–11]. Trace determinations require highly sensitive and often selective detection. Automation is important from the point of view of the speed and accuracy of operations performed, mainly with serial analyses.

This paper describes an analytical system connecting the above-mentioned demands for the determination of trace analytes: microcolumn liquid chromatography + enrichment unit + fluorescence detection + automation (the analytical system is controlled by a computer). An

* Corresponding author.

0021-9673/94/$07.00
SSDI 0021-9673(94)00248-8

important element of the whole system is the application of a capillary mixer adjusting the sample matrix so that the analyte capacity factor is increased. Hence, enrichment is carried out not only on the precolumn but also on the head of the analytical column.

2. Theory

Injection on to the analytical column in elution chromatography is limited by the volume V_{max}. The injected volume V_{max} causes a permissible dispersion of the eluated analyte zone [12,13]. V_{max} is proportional to the analytical column dead volume V_{Mcol}, the analyte capacity factor k_{col} and the value of $1/\sqrt{n_{col}}$, where n_{col} is the number of theoretical plates of the analytical column. If there is a sample of volume $V > V_{max}$, direct injection leads to volume overloading of the column. However, injection of the volume V is possible if the analyte capacity factor k_{col} in the sample matrix is increased. This can be performed by application of a mixer [14]. Alternate injection of the sample volume segment and the volume segment of a solvent of low eluting strength (non-eluting solvent) results in mixing of both liquids. This results in the required increase in k_{col}, application of the volume V to the analytical column and, hence, enrichment of the analyte on the column.

Connection of a sorption precolumn with the analytical column is an important means of enrichment of trace amounts of the analyte from the sample. The precolumn can be loaded maximally with a volume V_B which represents the breakthrough volume [7,11]:

$$V_B = V_{Mpre}(1 + k_{pre})\left(1 - \frac{2}{\sqrt{n_{pre}}}\right)$$

where V_{Mpre} is the precolumn dead volume, k_{pre} the analyte capacity factor in the sample matrix in the case of injection on the precolumn and n_{pre} the number of theoretical plates of the precolumn. An increase in k_{pre} leads to an increase in V_B and, hence, to enrichment of the analyte on the precolumn. If the analyte is desorbed from the precolumn in a volume $V_{DES} > V_{max}$, the situation is identical with that as for $V > V_{max}$. Application of a mixer between the precolumn and the analytical column ensures the adjustment of the matrix of the desorbed volume V_{DES} and the possibility of injection on to the analytical column. V_{DES} is mixed with the volume of the non-eluting solvent V_{NS} with a resulting capacity factor k_Σ. The equation

$$\frac{V_{DES} + V_{NS}}{V_{max}} = \frac{k_\Sigma + 1}{k_{col} + 1}$$

describes the possibility of sampling $V_{DES} > V_{max}$ provided that the non-linear dependence of k_Σ on φ_Σ (the volume fraction of the solvent of higher elution strength in the sample matrix). The chromatographic system often used with a reversed phase is characterized by the logarithmic dependence $\log k_\Sigma = f(\varphi_\Sigma)$. This is the important condition so that V_{DES} could be injected completely with the enrichment factor V_{DES}/V_{max}.

3. Experimental

3.1. Apparatus, fluorescence microcell

A schematic diagram of the laboratory-made microcolumn liquid chromatograph [15,16] (Institute of Analytical Chemistry, Brno, Czech Republic) is shown in Fig. 1. The apparatus is controlled by a PMD 85-2 computer (Tesla, Bratislava, Slovak Republic) and connected to a PU 4027 fluorescence detector (Philips, Cambridge, UK) additionally equipped with an FSA emission filter (418-nm cut-off filter) of an FS 950 Fluoromat fluorimeter (Kratos, Ramsey, NJ, USA).

We used a fluorescence flow microcell of our own design with a volume of 0.34 μl, which suits the microcolumn system. It consists of a fused-silica capillary (0.25 mm I.D.). The illuminated part of the microcell is 7 mm long.

3.2. Chemicals

For preparation of the mobile phases and solutions of polycyclic aromatic hydrocarbons

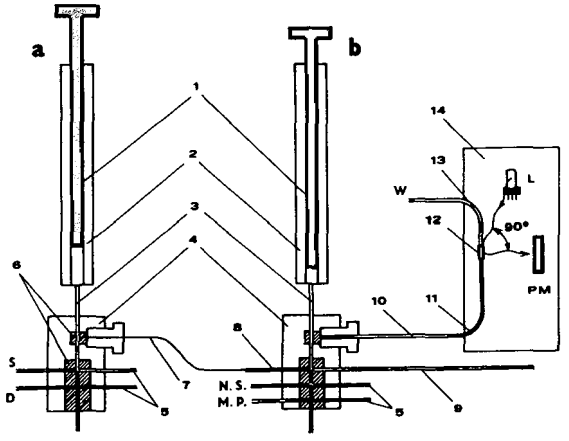

Fig. 1. Connection of the enrichment unit (a) with the analytical unit (b). 1 = Piston; 2 = glass syringe (80 μl); 3 = injection needle (0.3 mm I.D. × 0.5 mm O.D.) provided with a side outlet (0.15 mm I.D.) and closed at the end; 4 = liquid distribution block; 5 = mobile phase and sample inlets; 6 = PTFE seals; 7 = connecting capillary (2.6 μl); 8 = precolumn (50 × 0.31 mm I.D.); 9 = store capillary; 10 = capillary mixer (100 × 0.25 mm I.D.); 11 = analytical column (115 × 0.25 mm I.D.); 12 = fluorescence microcell; 13 = mobile phase waste; 14 = fluorimeter; S = sample; D = solvent for desorption from the precolumn; N.S. = non-eluting solvent; M.P. = mobile phase; W = waste; L = xenon lamp; PM = photomultiplier.

(PAHs), acetonitrile (analytical-reagent grade) and methanol (for HPLC) (Merck, Darmstadt, Germany) were used. Six PAH standards were selected: anthracene, fluoranthene and chrysene (Lachema, Brno, Czech Republic) and pyrene, benzo[*b*]fluoranthene and benzo[*b*]pyrene (Supelco, Belefonte, PA, USA). Stock standard solutions of the PAHs were prepared in acetonitrile at a concentration of 300 mg/l and stored in a refrigerator.

3.3. *Microcolumn, mixer, precolumn, adsorbents, packing*

The analytical column and the mixer were made of two parts of a fused-silica capillary (0.25 mm I.D.) and were connected together by fixing into a glass capillary of larger diameter (0.5 mm I.D.). The length of the mixer capillary was 100 mm and that of the microcolumn 115 mm. At the end of the microcolumn a glass capillary (1 mm × 10 μm I.D.) with a piece of a glass-wool was fixed so that leakage of the sorbent from the microcolumn was prevented. The end of the microcolumn was connected directly with the microcell.

The microcolumn was packed with reserved-phase Separon SGX C_{18} of particle diameter 5 μm (Tessek, Prague, Czech Republic) by a suspension technique from CCl_4 at a pressure 20 MPa.

The capillary precolumn (46 × 0.31 mm I.D.) was packed with the same material and by the same technique as for the analytical column; the particle diameter was 10 μm.

3.4. *Description and function of microchromatograph*

Fig. 1 shows the connection of two laboratory-made microchromatographs: a microchromatograph as an enrichment unit [(a) and Fig. 1] and a microchromatograph as an analytical separation unit [(b) in Fig. 1]. The microcolumn chromatograph has been described previously [15]. The syringe (2) of the microchromatograph with a piston (1) and a needle (3) (Fig. 1) serves for sampling and injection of the mobile phases and the sample. The liquids are pushed out of the needle via a side opening (0.15 mm I.D.) as the end of the needle is blind. The needle passes through the PTFE seal in the liquid distribution block (4). Its movement is controlled by a stepper. The liquid is sucked into a syringe when the side opening in the needle is connected with the inlet to the reservoir (5). The liquid is pushed out of the syringe when the liquid distribution block is adjusted in such a way so that the needle side opening points directly to the mixer and the microcolumn [(b) in Fig. 1] or to the precolumn [(a) in Fig. 1].

3.5. *Sample processing*

Let us consider treating a trace amount of an analyte with enrichment on the precolumn. The sample from the syringe (2) of the enrichment unit [(a) in Fig. 1] is injected on to the precolumn (8). The analyte is retained and the remaining part of the matrix leaves by a store capillary (9). The analyte is desorbed with a solvent of high elution strength and gradually

fills part of the store capillary. The store capillary retains the sample volume desorbed from the precolumn before sampling to the mixer and analytical column. Then the solution of analyte, or a group of analytes, is ready for processing in the analytical separation unit [(b) in Fig. 1].

The sample is injected automatically according to a given programme in the following sequence:

(1) sucking of a sufficient volume (20–50 μl) of the non-eluting solvent into the syringe (2b);

(2) injection of the first volume segment of the non-eluting solvent into the mixer (10);

(3) sucking of the first volume segment of the sample (extract) from the store capillary (9) to the syringe (3b); the needle volume is 2 μl;

(4) injection of the first volume segment of the sample + the second volume segment of the non-eluting solvent into the mixer (10) simultaneously.

The cycle of sample injection with the non-eluting solvent according to steps 3 and 4 is repeated as many times as necessary until the total volume of the extract from the store capillary (9) is transported together with the non-eluting solvent to the mixer and the analytical column. Elution with the mobile phase then follows.

The same injection method can be used in the analysis of an extract resulting from off-line extraction of a sample with a complex matrix. There is the possibility of treating a much higher extract volume in the analytical separation unit in comparison with direct injection of an aliquot of the extract on to the analytical column.

4. Results and discussion

Experiments were designed in such a way that the theoretical assumptions for sample enrichment could be verified practically. Reproducibility of the measured data was established, in addition to the recovery characteristics for the automated microcolumn chromatograph with the enrichment unit. The practical applicability of the device was verified on the example of determination of trace amounts of fluoranthene in tap water and six selected PAHs in the organic extract.

4.1. Chromatographic system

PAHs were selected as test substances with respect to their high affinity for the hydrophobic surface of the stationary phase used. The advantage consists in the application of sensitive fluorescence detection for the determination of these substances. The occurrence of PAHs in the environment needs to be carefully checked owing to their toxicity [17–20]. In most of the experiments fluoranthene (molecular mass 202.26 g/mol) was used. Its concentration in water indicates contamination of the environment by PAHs. The maximum excitation and emission wavelengths of fluoranthene in acetonitrile were found to be $\lambda_{ex} = 350$ nm and $\lambda_{em} = 467$ nm, which are very close to the values in the literature [21].

A chromatographic system with a reversed phase was selected at this type represents about 80% of all applications in liquid chromatography. Using the analytical microcolumn with Separon SGX C_{18} reversed phase, the dependence of the capacity factor k of fluoranthene on the content of acetonitrile in the acetonitrile–water mobile phase was studied. For a volume fraction φ of acetonitrile in the mobile phase in range 0.8–0.4, the logarithmic dependence $\log k = \log k_0 - m\ \varphi$ (correlation coefficient $r = 0.9913$) was found. The values of k and φ are presented in Table 1. For the given range of $\varphi \approx 0.8$–0.4 the values of the constants are $k_0 = 1200$ and $m = 3.67$. With a decrease in φ below 0.4 the values of $\log k$ will increase with a higher slope m than for the measured interval $\varphi \approx 0.8$–0.4. The dependence of $\log k = f(\varphi)$ is an important assumption for analyte enrichment due to addition of a non-eluting solvent to the sample matrix.

The capillary mixer ensures adjustment of the sample matrix (organic extract) by mixing with a non-eluting solvent (water). The function of the mixer is fulfilled by a fused-silica capillary (100 × 0.25 mm I.D.). The capacity of the mixer enables a volume segment of the sample (extract) of 1 μl

Table 1
Dependence of capacity factor of fluoranthene on the acetonitrile content in the mobile phase.

Vol. fraction of CH_3CN (φ)	0.80	0.70	0.60	0.55	0.50	0.45	0.40
k	1.7	3.1	7.0	9.7	16.0	27.5	52.7

to be mixed with a volume segment of the non-eluting solvent. Injection of 1 μl of the extract is the optimum because it fills only the space of the injection needle (3b) of the syringe (2b) (Fig. 1). In the needle the extract is mixed minimally, it does not enter the space of the syringe (2b) and, hence, the analyte losses are eliminated. The volume segment of the non-eluting solvent can be increased as desired. An increase in this volume leads to a decrease in the peak width. With perfect mixing of segments [(3 × 1-μl segments of the sample in 80% CH_3CN) + (3 × 3-μl segments of the non-eluting solvent in 20% CH_3CN) = 12 μl], the contribution to band broadening by the sample volume is negligible and the peak width is 12.1 mm for the experimental conditions used. However, with the real capillary mixer the peak width experimentally measured for the same total sample volume (12 μl) is 13.9 mm. Hence the influence of the total sample volume on band broadening is evident and the volume segments are incompletely mixed. An increase in the volume segment of the non-eluting solvent from 1 to 3 μl leads to only a 4% decrease in the peak width. Therefore, 1 μl of the non-eluting solvent and thus a ratio of segments of 1:1 (μl) were used. A change of the mixer geometry could ensure, if necessary, more perfect mixing of segments.

4.2. Reproducibility, recovery

The reproducibility of the measured data characterizes the precision and the reliability of the tested device. Experiments were performed under the following conditions: injection of 30 μl of 30 μg/l fluoranthene in 40% CH_3CN, desorption from the precolumn with 20 μl of CH_3CN, injection of 9 μl of the extract from the store capillary into the mixer and the analytical column and elution with 80% acetonitrile at a flow-rate of 10 μl/min. The results for seven measurements of the peak area are presented in Table 2. The reproducibility is represented by the value of the relative standard deviation (R.S.D. = 0.8%), calculated according to the equation R.S.D. = $(\sigma_{abs}/\overline{hw}) \cdot 100$, where σ_{abs} is the absolute standard deviation and $\overline{hw}$ is the average value of the product peak height · width. The R.S.D. for tens to hundreds of ppt of fluoranthene in the sample does not exceed 5%. Automation of all the steps during the treatment of the sample contributes to a high accuracy of measurement of the experimental data.

The term recovery is connected here with evaluation of the possible losses during the process of enrichment on the precolumn. The same volume (20 μl) of the same sample (30 μg/l fluoranthene in 40% CH_3CN) was injected

Table 2
Reproducibility of measurements using the automatic microcolumn LC system with the enrichment unit

Parameter	Measurement No.						
	1	2	3	4	5	6	7
Peak height (mm)	154	152	153.5	152	160.5	153	151
Peak width (mm)[a]	6.50	6.50	6.55	6.55	6.20	6.60	6.55
Height · width (mm^2)	1000	988	1005	995	995	1009	990

[a] Peak width at half-height.

(1) directly onto the analytical column (via the mixer) and (2) with enrichment on the precolumn (for measurement conditions, see above). By comparison of the fluoranthene peak areas (see Ratio 2/1 in Table 3), we conclude that during the process of enrichment on the precolumn analyte losses do not occur.

4.3. Example of determination of fluoranthene and PAHs

For the given microcolumn chromatographic system with the fluorescence microcell, a minimum detectable amount, defined by the peak height which is twice the baseline noise, of 8.0 pg of fluoranthene in an injection of 20 μl of a 3 μg/l solution of fluoranthene in 45% methanol was found.

The content of fluoranthene was determined in a sample of tap water, using chromatographic conditions based on the ASTM standard method [22]. A 1-ml sample of water (city of Brno) was adjusted by adding 0.82 ml of methanol to a concentration of 45% methanol in the matrix. The conditions of sample treatment are given in Fig. 2. By the method of standard additions with substraction of the blank, a concentration 120 ng/l of fluoranthene in the original sample of water was found (Fig. 2). The minimum detectable amount found of 8.0 pg of fluoranthene with injection and precolumn loading of up to 800 μl for 45% methanol in the sample matrix determines the detection limit to be 10 ng/l of fluoranthene.

An example of the determination of six selected PAHs in the organic extract (acetonitrile) is presented in Fig. 3. By changing the excitation

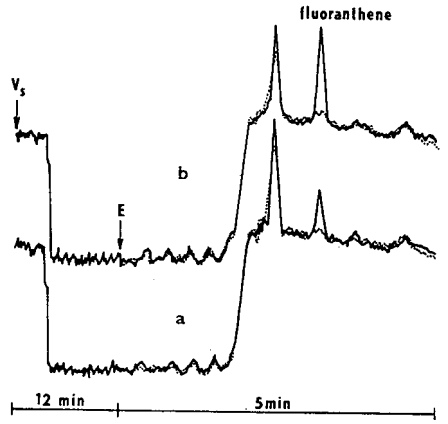

Fig. 2. Determination of fluoranthene in tap water (city of Brno). Mixer, analytical column and precolumn, see Fig. 1. Sampling: 200 μl of water in 45% methanol into the precolumn. Desorption from the precolumn: 19 μl of methanol. V_s = sampling of 14 μl of methanolic extract and 15 μl of distilled water into the mixer and analytical column. E = elution with 90% methanol, flow-rate 5 μl/min. Water analysis (a) without addition of fluoranthene, concentration determined 120 ng/l; (b) with addition of fluoranthene (100 ng/l). Dotted line indicates blank.

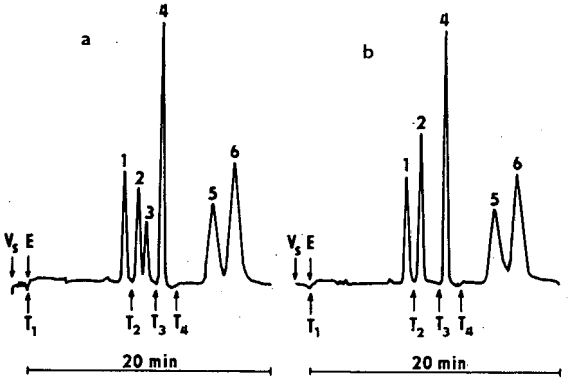

Fig. 3. Determination of six PAHs in acetonitrile. Mixer and analytical column, see Fig. 1. V_s = sampling of 6 μl of PAH solution and 7 μl of water into the mixer and analytical column; E = isocratic elution with 70% acetonitrile. Concentrations: 1 = anthracene, 100; 2 = fluoranthene, 200; 3 = pyrene, 200; 4 = chrysene, 60; 5 = benzo[*b*]fluoranthene, 60; 6 = benzo[*a*]pyrene, 60 μg/l. Emission cut-off filter, 370 nm. (a) Time programming of ($\lambda_{ex}/\lambda_{em}$): $T_1 = 0$ min (350/398 nm); $T_2 = 8.5$ min (330/430 nm); $T_3 = 10.6$ min (264/385 nm); $T_4 = 12.4$ min (300/428 nm). (b) The same conditions as in (a) but $T_2 = 8.5$ min (354/467 nm).

Table 3
Comparison of peak areas in cases 1 and 2 (see text)

Measurement No.	Peak height · width (mm^2)		Ratio 2/1
	Case 1	Case 2	
1	640	630	0.984
2	645	658	1.020
3	652	645	0.989

and emission wavelengths λ_{ex} and λ_{em}, the sensitivity and selectivity of determination can be influenced (the pyrene peak in Fig. 3b was eliminated).

By injection of 6 μl of acetonitrile extract, sample enrichment on the analytical column is obtained. With the fluoranthene sample in 100% acetonitrile we have a maximum volume of 0.4 μl, which is the volume that could be applied directly to the analytical column with the allowed 20% decrease in the separation efficiency. Connection of the mixer with the analytical column, therefore, represents a fifteen times higher enrichment of fluoranthene on the column in case of the acetonitrile extract or the possibility of a fifteen times higher increase in the precolumn volume in case of the sample of water.

4.4. Analyte losses

Analyte losses by sorption on the surface of parts of the apparatus or on the walls of the vessels may represent a difficult problem [17,20,23]. This was also observed in our experiments. We prepared solutions (0.5 ml) of 300 μg/l of fluoranthene in acetonitrile–water mixtures of various composition. We injected 3 μl of these solutions on to the microcolumn via the mixer and the peak area was evaluated. Its decrease with decreasing concentration of acetonitrile in the matrix demonstrates that in the determination of trace amounts this effect has to be taken into account (Fig. 4). The peak height of fluoranthene did not change for up to 2 min after sample preparation in the glass vessel. Addition of a solvent with a high elution strength to the sample matrix is often necessary to prevent analyte losses and then a system mixer is essential to ensure the required enrichment.

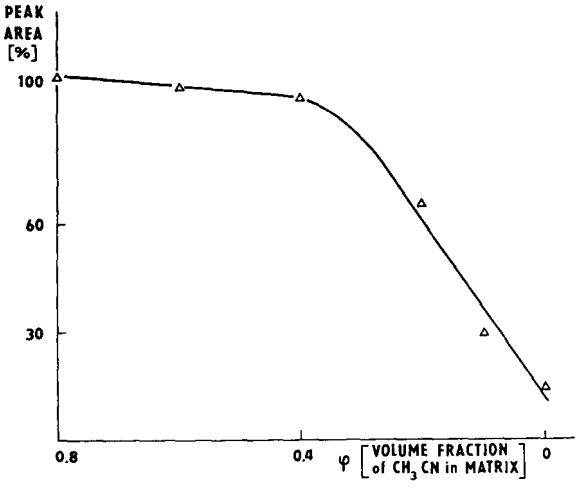

Fig. 4. Adsorption of fluoranthene on the glass surface of the sample flask. Abscissa = content of acetonitrile (φ) in the sample matrix; ordinate = peak area of fluoranthene (%).

5. Conclusions

The application of a microcolumn liquid chromatograph connected on-line with a mixer, enrichment unit and fluorescence microcell has been demonstrated. The device is characterized by automated operation with high reproducibility of the measured data (R.S.D. = 0.8%). The procedure for sample treatment ensures elimination of analyte losses during the process. The analyser permits analyte enrichment from the sample both on the precolumn and on the analytical column connected with the capillary mixer. As a result, the degree of analyte enrichment increases. The applicability of the proposed device was shown by the examples of the determination of trace amounts of fluoranthene in tap water and of six selected PAHs in an acetonitrile extract.

References

[1] P. Kučera (Editor), *Microcolumn High-Performance Liquid Chromatography* (*Journal of Chromatography Library*, Vol. 28), Elsevier, Amsterdam, 1984.
[2] M. Krejčí, *Trace Analysis with Microcolumn Liquid Chromatography* (*Chromatographic Science Series*, Vol. 59), Marcel Dekker, New York, 1992.
[3] M. Novotny and D. Ishii (Editors), *Microcolumn Separations —Columns, Instrumentation and Ancillary Techniques* (*Journal of Chromatography Library*, Vol. 30), Elsevier, Amsterdam, 1985.
[4] D. Ishii (Editor), *Introduction to Microscale HPLC*, VCH, New York, 1988.
[5] M. Novotný, *Anal. Chem.*, 60 (1988) 500A.
[6] I. Liška, J. Krupčík and P.A. Leclerq, *J. High Resolut. Chromatogr.*, 12 (1989) 578.

[7] M.W.F. Nielen, R.W. Frei and U.A. Th. Brinkman, in R.W. Frei and K. Zech (Editors), *Selective Sample Handling and Detection in High-Performance Liquid Chromatography —Part A (Journal of Chromatography Library*, Vol. 39A), Elsevier, Amsterdam, 1988, pp. 5–78.
[8] R. Huber, and K. Zech, in R.W. Frei and K. Zech (Editors), *Selective Sample Handling and Detection in High-Performance Liquid Chromatography —Part B (Journal of Chromatography Library*, Vol. 39B), Elsevier, Amsterdam, 1988, pp. 81–141.
[9] R.E. Shoup and G.S. Mayer, *Anal. Chem.*, 54 (1982) 1164.
[10] S. Bitteur and R. Rosset, *Chromatographia*, 23 (1987) 163.
[11] C.E. Werkhoven-Goewie, U.A. Th. Brinkman and R.W. Frei, *Anal. Chem.*, 53 (1981) 2072.
[12] R.P.W. Scott, *Small Bore Liquid Chromatography Columns*, Wiley, New York, 1984.
[13] P. Kučera, *J. Chromatogr.*, 198 (1980) 93.
[14] R.W. Frei, *Chromatographia*, 15 (1982) 161.
[15] M. Krejčí and V. Kahle, *J. Chromatogr.*, 392 (1987) 133.
[16] M. Krejčí and V. Kahle, *Czech Pat. Appl.*, CS 257657/85 (1985).
[17] H.G. Kicinski, S. Adamek and A. Kettrup, *Chromatographia*, 28 (1989) 203.
[18] *PAHs: Sample Treatment and HPLC Separation*, Chrompack International, Middelburg, Netherlands, 1990.
[19] J. Rzepa, J. Sliwiok, A. Siwek and M. Sajewics, *Chromatogram*, 10, No. 2 (1989) 9.
[20] K. Ogan, E. Katz and W. Slavin, *J. Chromatogr. Sci.*, 16 (1978) 517.
[21] G.G. Guilbault, *Practical Fluorescence*, Marcel Dekker, New York, 1973, p. 614.
[22] *Annual Book of ASTM Standards, Water (II)*, Vol. 11.02, American Society for Testing and Materials, Philadelphia, PA, 1991.
[23] V.F. Eisenbeiss, H. Hein, R. Jöster and G. Naundorf, *Chromatogr. Newsl.*, 6 (1978) 8.

ELSEVIER

Journal of Chromatography A, 675 (1994) 55–64

JOURNAL OF CHROMATOGRAPHY A

Retention characteristics of some selected halogenated environmental pollutants in silica and bonded normal-phase liquid chromatography

Eva Grimvall[☆,a], Conny Östman[*,b]

[a]Department of Analytical Chemistry, Stockholm University, S-106 91 Stockholm, Sweden
[b]Division of Analytical Chemistry, National Institute of Occupational Health, S-171 84 Solna, Sweden

(First received June 29th, 1993; revised manuscript received March 15th, 1994)

Abstract

Seven bonded stationary phases and unmodified silica were investigated regarding their retention properties towards a number of halogenated environmental pollutants including 26 individual polychlorinated biphenyl congeners. No simple retention–structure relationship was found for the polychlorinated biphenyls but a number of phases demonstrated similar selectivities towards the investigated congeners. The retention of compounds with aliphatic carbons were substantially influenced by the presence of hydrogens possessing acidic properties due to inductive effects of adjacent chlorine or oxygen atoms. Solute molecule ether oxygens were shown to promote retention by hydrogen bonding only on silica and phenylpropyl silica. Polybrominated diphenyl ethers demonstrated a complex retention behaviour on the different stationary phases. Indication was found that bromine may be directly involved in the retention mechanism.

1. Introduction

Halogenated environmental pollutants include a number of compound groups who in themselves contain numerous of homologues and isomers. Most methods of determination in complex matrices include one or more liquid chromatographic fractionation steps. Clean-up of chlorinated environmental pollutants performed by chromatographic fractionation traditionally utilise open columns packed with adsorbents like silica, aluminium oxide or Florisil. In recent years the use of high-performance liquid chromatography (HPLC) for clean-up has increased. HPLC provides a much better defined system with higher resolution compared to the packed open columns. It is also possible to choose between various chemically modified bonded stationary phases with different retention properties. A number of HPLC stationary phases have been used in clean-up procedures applied for the analysis of polychlorinated biphenyls (PCBs). Silica has been used in the clean-up procedure for the analysis of PCBs in biota, sediment and atmospheric particles [1], cyanopropyl-modified silica for the determination of PCBs in fish [2], aminopropyl-modified silica for the clean-up of cod liver oil [3] and nitrophenylpropyl-modified

* Corresponding author.
☆ Present address: Division of Analytical Chemistry, National Institute of Occupational Health, S-171 84 Solna, Sweden.

0021-9673/94/$07.00
SSDI 0021-9673(94)00265-B

silica in the determination of PCBs in transformer oil [4]. However, there is a rather limited knowledge regarding the retention behaviour of individual halogenated compounds as well as the numerous groups of halogenated compounds, especially regarding the bonded phases. Silica is the most investigated stationary phase [1,5–10]. Both degree of chlorination and substitution pattern affect the retention order of individual chlorinated biphenyl (CB) congeners. CB congeners with the highest degrees of substitution tend to have a weak retention while retention is stronger for slightly substituted aromatic compounds [6,7]. Anyhow, no general explanation has been found yet for the retention order of all congeners. A number of properties that are recognised as important in liquid chromatography of halogenated compounds are linearity, area, planarity, electron density, ionisation potential, polarisability and dipole moment [10,11]. In recent years electron-donor and electron-acceptor (EDA) phases utilised in both reversed- [12] and normal-phase [13,14] mode have gained some interest. The chemistry of EDA stationary phases has been reviewed by Nondek [15] and Sander and Wise [16].

In the present study the retention properties of a selected number of halogenated environmental pollutants on seven chemically bonded stationary phases and unmodified silica have been investigated.

2. Experimental

2.1. Chemicals

The individual CBs were 18 congeners that have been recommended for analysis by the Nordic Council of Ministers [17]: 2,4,4′-trichlorobiphenyl (CB-28), 2,4,2′,4′-tetrachlorobiphenyl (CB-47), 2,5,2′,5′-tetrachlorobiphenyl (CB-52), 3,4,3′,4′-tetrachlorobiphenyl (CB-77), 2,4,5,2′,5′-pentachlorobiphenyl (CB-101), 2,3,4,3′,4′-pentachlorobiphenyl (CB-105), 2,3,4,5,4′-pentachlorobiphenyl (CB-114), 2,4,5,3′,4′-pentachlorobiphenyl (CB-118), 3,4,5,2′,3′-pentachlorobiphenyl (CB-122), 3,4,5,3′,4′-pentachlorobiphenyl (CB-126), 2,3,4,5,2′,4′,5′-hexachlorobiphenyl (CB-138), 2,4,5,2′,4′,5′-hexachlorobiphenyl (CB-153), 2,3,4,5,3′,4′-hexachlorobiphenyl (CB-156), 2,3,4,3′,4′,5′-hexachlorobiphenyl (CB-157), 2,4,5,3′,4′,5′-hexachlorobiphenyl (CB-167), 3,4,5,3′,4′,5′-hexachlorobiphenyl (CB-169), 2,3,4,5,2′,3′,4′-heptachlorobiphenyl (CB-170) and 2,3,4,5,2′,4′,5′-heptachlorobiphenyl (CB-180) [18]. Eight additional congeners were tested for possible use as internal standards in future analytical procedures for PCBs: 3,5,3′-trichlorobiphenyl (CB-36), 2,3,3′,5′-tetrachlorobiphenyl (CB-58), 3,4,5,4′-tetrachlorobiphenyl (CB-81), 2,4,6,2′,5′-pentachlorobiphenyl (CB-103), 3,4,5,3′,5′-pentachlorobiphenyl (CB-127), 2,4,5,2′,4′,6′-hexachlorobiphenyl (CB-154), 2,3,4,5,3′,4′,5′-heptachlorobiphenyl (CB-189) and 2,3,4,5,6,2′,4′,6′-heptachlorobiphenyl (CB-204). The individual CB congeners were purchased from Ultra Scientific (North Kingstown, Richmond, USA) except CB-189 which was synthesised at the Department of Environmental Chemistry, Stockholm University [19]. A PCB mixture was made by mixing equal amounts of the technical products Aroclor 1221, 1232, 1242, 1248, 1254 and 1260 (Monsanto, MO, USA). Biphenyl was obtained from Merck (Darmstadt, Germany).

The organochlorine pesticides were US Environmental Protection Agency (EPA) reference materials consisting of 1,1-dichloro-2,2-bis(4-chlorophenyl)ethene (*p,p′*-DDE), 1,1,1-trichloro-2,2-bis(4-chlorophenyl)ethane (*p,p′*-DDT), 1,1-dichloro-2,2-bis(4-chlorophenyl)-ethane (p,p′-DDD), *p,p′*-methoxychlor, transnonachlor, aldrin, endrin, dieldrin, heptachlor, heptachlorepoxide, oxychlordane, α- and γ-chlordene, α- and γ-chlordane, α-, β-, γ- and δ-hexachlorocyclohexane, hexachlorobenzene, Toxaphene and Mirex.

Polychlorinated naphthalenes (PCNs) were investigated as a mixture of equal amounts of the technical formulations Halowax 1014, 1051 and 1099 (Koppers, Pittsburgh, PA, USA). Chlorinated paraffins (CPs) consisted of the technical formulations Hüls 40 (C_{18}–C_{26}, 40% Cl) and Hüls 70 (C_{10}–C_{13}, 70% Cl) (Hüls, Germany)

mixed in the proportions 1:1. Polybrominated diphenyl ethers (PBDEs) were investigated as the technical formulations Bromkal 70-5, 79-8 and 82-0 (Chemische Fabrik Kalk, Germany). Bromkal 70-5 has been shown to consist of three major compounds: 2,4,2′,4′-tetrabromodiphenyl ether and two pentabromodiphenyl ethers [20]. Bromkal 79-8 consists of hepta-, octa-. nona- and decabrominated diphenyl ethers [21]. In Bromkal 82-0 the main component is decabromodiphenyl with a small amount of nonabrominated diphenyl ether [21]. Diphenyl ether and 2,4,2′,4′-tetrabromodiphenyl ether were synthesised at the Department of Environmental Chemistry, Stockholm University. Decabromodiphenyl ether originated from Fluka, Germany.

All standard substances were dissolved in either glass-distilled HPLC-grade hexane (Rathburn, UK) or pesticide-grade heptane (Lab-Scan, Dublin, Ireland).

2.2. Stationary phases

Seven bonded normal-phase HPLC stationary phases were characterised. Four columns were obtained from Macherey–Nagel, Germany: nitrophenylpropyl silica (Nucleosil-NO_2, 200 × 4 mm, 5 μm), dimethylaminopropyl silica (Nucleosil-$N(CH_3)_2$, 200 × 4 mm, 5 μm), diol silica (Nucleosil-$(OH)_2$, 250 × 4 mm, 7 μm) and phenylpropyl silica (Nucleosil-C_6H_5, 250 × 4 mm, 7 μm). The other columns were cyanopropyl silica (LiChrosorb-CN, 250 × 4 mm, 5 μm; Merck, Germany), aminopropyl silica (μBondapak-NH_2, 300 × 3.9 mm, 10 μm; Waters, MA, USA) and 2-(1-pyrenyl)ethyldimethylpropyl silica (Cosmosil-PYE, 150 × 4.6 mm, 5 μm; Nacalai Tesque Japan). A column with unmodified silica was also included in the study (μPorasil, 150 × 4.6 mm 10 μm; Waters).

2.3. Instrumentation

The HPLC system consisted of a pump system (Model 590, Waters), an electrically actuated switching valve for reversing the column flow, a UV detector (SPD-2AS, Shimadzu, Japan) and an injector (Model 7125, Rheodyne, CA, USA) equipped with a 200-μl loop. The detector was operated at 225 nm when analysing aromatic compounds, and at 205 nm for all other substances. HPLC-grade hexane (Rathburn) was used as mobile phase at a flow-rate of 1.0 ml/min. The separations were performed at ambient temperature. Pentane (HPLC grade, Rathburn) was used to determine the dead volume of all the HPLC columns. The injected amount varied between 50 and 500 ng for individual compounds and between 500 ng and 5 μg for the technical mixtures.

Capillary GC was used to analyse the fractions collected from the HPLC column outlet. The gas chromatograph was a Varian 3400 (Walnut Creek, CA, USA) equipped with a split/splitless injector and an electron capture detector. The column was a DB-5 (30 m × 0.25 mm, 0.25 μm, J & W Scientific, USA). Hydrogen was used as carrier gas with a column head pressure of 8 p.s.i. (1 p.s.i. = 6894.76 Pa). A make-up gas flow-rate of 30 ml/min of nitrogen was applied to the detector. Temperature settings were as follows: injection port 250°C, detector 310°C, column oven was kept at 80°C for 2 min, followed by a linear temperature increase of 10°C/min up to a final temperature of 310°C which was kept for 10 min. Chromatographic data were registered, stored and processed by an ELDS 900 chromatography data system (Chromatography Data Systems, Svartsjö, Sweden).

2.4. Methodology

The retention properties of compounds like chlorinated paraffins and hexachlorocyclohexanes (HCHs) that have no or little UV absorbance, even at 205 nm, were evaluated by collecting fractions at the HPLC system outlet and subsequently analysing them by GC–electron-capture detection. As a major interest was the isolation of PCBs for application in future analytical procedures, fractions were defined according to the elution of these compounds. A mixture consisting of technical Aroclor products (see *Chemicals* above) was injected. At the time

of the last UV response, the flow was reversed. A single back-flush peak (BF) was then obtained containing all the material with stronger retention than the PCBs. Two fractions were collected. The first (F1) consisted of the material eluting between the dead volume and the time of flow reversal and the second (BF) contained the material in the back flush peak. Both fractions were analysed by GC–electron-capture detection. Estimation of the amounts of compounds found in the fractions was done by comparing the peak areas. To keep track of the variations in retention, CB-118 was injected as every second to tenth injection. The increased frequency was applied when solutes with long retention time were injected. During the experiments the relative standard deviation of the CB-118 retention time was found to be less than 2%.

3. Results and discussion

3.1. Polychlorinated biphenyls

Capacity factors (k') of individual CBs were determined for the different stationary phases and are shown in Table 1. In Fig. 1 the capacity

Table 1
Capacity factors for some individual CB congeners

CB	k'							
	PYE	Cyano	Diol	Phenyl	DMA	Amino	Nitro	Silica
Biphenyl	0.33	0.65	0.63	0.71	0.88	1.08	1.48	2.04
28	0.65	0.42	0.51	0.37	0.61	0.85	0.96	0.76
36	0.73	0.46	0.52	0.32	0.62	0.77	0.98	0.67
47	0.57	0.37	0.50	0.35	0.57	0.77	0.84	0.66
52	0.66	0.51	0.52	0.40	0.55	0.79	0.93	0.75
58	0.74	0.48	0.66	0.43	0.91	0.96	1.05	0.74
77	2.04	0.67	0.81	0.50	1.18	1.67	1.79	0.89
81	1.93	0.55	0.56	0.41	0.59	1.13	1.35	0.76
101	0.71	0.42	0.46	0.35	0.53	0.71	0.81	0.61
103	0.53	0.40	0.42	0.33	0.42	0.62	0.72	0.59
105	1.36	0.59	0.81	0.56	1.25	1.52	1.53	0.89
114	1.17	0.44	0.47	0.35	0.44	0.81	0.99	0.63
118	1.16	0.45	0.48	0.35	0.48	0.84	1.01	0.64
122	1.04	0.55	0.86	0.50	1.36	1.30	1.40	0.88
126	2.72	0.61	0.65	0.44	0.74	1.41	1.62	0.81
127	1.70	0.46	0.44	0.33	0.34	0.82	1.01	0.56
138	0.98	0.47	0.59	0.39	0.68	1.02	1.07	0.71
153	0.82	0.36	0.37	0.29	0.30	0.58	0.71	0.51
154	0.54	0.33	0.36	0.27	0.31	0.62	0.61	0.46
156	1.61	0.48	0.53	0.37	0.54	0.96	1.15	0.64
157	1.74	0.53	0.70	0.43	0.87	1.27	1.37	0.78
167	1.37	0.41	0.41	0.32	0.33	0.70	0.89	0.53
169	3.47	0.57	0.55	0.37	0.42	1.22	1.45	0.67
170	1.28	0.49	0.68	0.40	0.85	1.19	1.21	0.72
180	1.04	0.38	0.40	0.30	0.32	0.66	0.79	0.49
189	1.91	0.43	0.42	0.34	0.33	0.89	1.05	0.53
204	0.41	0.26	0.33	0.23	0.26	0.39	0.49	0.35

The k' values were obtained using hexane as mobile phase at a flow-rate of 1 ml/min and a UV detector set at 225 nm. The variation in retention time as tested by repetitive injections of CB-118 was $<2\%$. The stationary phases are abbreviated as follows: PYE = 2-(1-pyrenyl)-ethyldimethylpropyl silica; Cyano = cyanopropyl silica; Diol = diolpropyl silica; Phenyl = phenylpropyl silica; DMA = dimethylaminopropyl silica; Amino = aminopropyl silica; Nitro = nitrophenylpropyl silica.

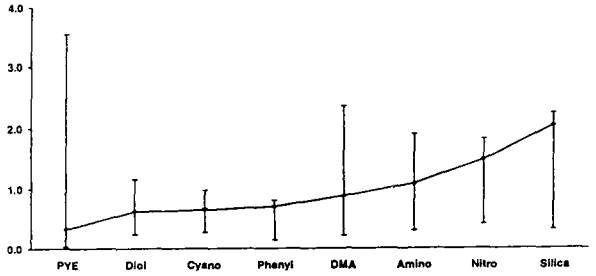

Fig. 1. Retention interval of the commercial PCB mixtures (vertical lines). The capacity factors of biphenyl are shown by diamonds linked together with a horizontal solid line. Column abbreviations as in Table 1. Y-axis represents k'.

factor of biphenyl (linked together with a horizontal line) and the retention interval of the mixture of technical PCB formulations (vertical lines) are plotted for each stationary phase. In general retention was weak. Only the 2-(1-pyrenyl)-ethyldimethylpropyl, nitrophenylpropyl, aminopropyl and dimethylaminopropyl silica phases exhibited $k' > 1$ for any CB congener. The influence on retention of the chloro substitution of biphenyl showed a large variation between the phases. On unmodified silica the introduction of chlorine substituents into biphenyl decreased retention with a factor as large as 5.8 and all investigated CBs had a shorter retention than biphenyl. Similar retention properties were demonstrated by the phenylpropyl silica. Retention was weaker on this column compared to the unmodified silica but the selectivity towards the investigated CBs were similar on both columns with a coefficient of correlation > 0.96 for the linear regression. There were no similarities to the retention behaviour of the 2-(1-pyrenyl)-ethyldimethylpropyl silica demonstrating that there is no significant charge transfer interaction between the single aromatic nucleus on the phenylpropyl group of the phase and the CBs. Thus, the phenylpropyl silica behaved like deactivated unmodified silica towards the investigated CBs. The diolpropyl-modified silica demonstrated a similar selectivity towards CBs as the phenylpropyl silica with a linear regression coefficient > 0.95, but the retention of biphenyl was within the retention interval of the CBs. However, the correlation between diolpropyl silica and unmodified silica was only 0.92.

A totally opposite selectivity towards CBs was demonstrated by the 2-(1-pyrenyl)ethyldimethylpropyl silica phase (PYE). When chlorine was incorporated into the biphenyl solute molecule, retention increased up to 10.5 times. The effect was most pronounced for the coplanar, non-*ortho* CB-77, CB-126 and CB-169. Retention on the PYE stationary phase is highly influenced by solute planarity and this phase has been shown to be excellent for isolating coplanar non-*ortho* CBs and mono-*ortho* CBs from the bulk of PCBs in technical mixtures [13]. Retention is mainly attributed to a charge transfer interaction mechanism were the delocalised aromatic π-electrons of the pyrenyl group of the stationary phase act as electron donors, and the aromatic nuclei of the CB solute molecules having decreased π-electron densities are acting as electron acceptors [13].

Retention of unsubstituted aromatic hydrocarbons on aminopropyl silica is due to a mechanism involving charge-transfer interaction between the n-electrons of the amino nitrogen and the π-electrons of the solute [22]. The same retention mechanism is assumed for the dimethylaminopropyl silica. These two phases demonstrated different selectivities towards the investigated CB congeners. Retention was in general weaker on the latter phase and the coefficient of correlation for a linear regression was < 0.85. This difference in retention properties of these two stationary phases is attributed to steric hindrance of the solute–stationary phase interaction excerted by the methyl groups of the dimethylaminopropyl silica.

The CBs exhibited similar retention orders on the nitrophenylpropyl, aminopropyl and cyanopropyl silica phases. Capacity factors for the investigated CBs obtained from the aminopropyl and cyanopropyl phases were plotted *versus* capacity factors from the nitrophenylpropyl phase. Linear relationships were obtained with regression correlation coefficients better than 0.98 and 0.97 respectively. This implies that a similar retention mechanism may be involved regarding these three stationary phases.

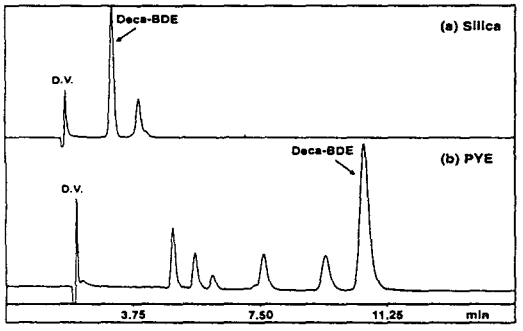

Fig. 2. HPLC chromatogram of the technical PBDE mixture Bromkal 79-8 on a silica (a) and a PYE column (b). D.V. = Dead volume; Deca-BDE = decabromodiphenyl ether.

3.2. Hexachlorobenzene and polychlorinated naphthalenes

Hexachlorobenzene and the chlorinated naphthalenes exhibit short retention times on all investigated stationary phases except PYE. The stronger retention on this phase is attributed to the importance of solute planarity for the solute–stationary phase interaction [13].

3.3. Polybrominated diphenyl ethers

The brominated diphenyl ether (BDE) congeners demonstrate a complex retention behaviour. On both unsubstituted silica and phenylpropyl-modified silica the retention of BDEs decreased by the introduction of bromine in the diphenyl ether molecule (Fig. 2a). A study of retention of BDEs in the system silica gel/*n*-hexane has earlier been performed by De Kok *et al.* [21]. They concluded that "retention tends to decrease with an increasing number of substituents, but this rule is not strictly adhered to". The decrease in retention can be explained in terms of an inductive effect of the bromine substituents decreasing the electron density on the ether oxygen and in the aromatic π-electron nucleus in the solutes. Retention could be reduced by steric hindrance of the solute–stationary phase interaction by the bulky bromine substituents as well. In this study a decrease in retention with an increased number of bromine substituents was also observed on the dimethylaminopropyl silica phase. This effect is attributed to the methyl groups of the stationary phase shielding the interaction between the amino nitrogen and the solute molecule. For all the other bonded stationary phases a reversed behaviour was observed. Retention increased with increasing bromine content (Table 2). The effect was especially pronounced on the nitropropyl-, aminopropyl- and PYE columns. This retention behaviour has previously been found regarding polybrominated biphenyls (PBBs) on aluminium oxide [7]. In contrast to the other bonded phases phenylpropyl silica, as the unsubstituted silica, demonstrated a retention of the unsubstituted

Table 2
Capacity factors for diphenyl ether, and intervals of capacity factors of peaks in technical PBDE mixtures

Compound	k'							
	PYE	Cyano	Diol	Phenyl	DMA	Amino	Nitro	Silica
Diphenyl ether	0.35	0.70	0.67	1.22	0.90	1.05	1.65	4.22
2,4,2',4'-Tetra-BDE	1.17	0.80	0.92	0.67	0.99	1.93	2.28	1.72
Deca-BDE	5.02	0.89	1.24	0.77	0.70	5.25	6.31	0.95
Bromkal 70-5	1.18–1.95	0.74–1.04	0.78–0.91	0.59–0.86	0.65–1.00	1.74–1.93	2.10–2.27	1.29–1.67
Bromkal 79-8	1.83–5.05	0.70–1.16	0.97–1.24	0.64–0.78	0.70–1.09	2.60–5.46	3.17–6.33	0.94–1.39
Bromkal 82-0	2.46–5.01	0.78–1.16	1.10–1.24	0.70–0.78	0.70–0.89	3.68–5.15	4.42–6.31	0.94–1.39

The average degree of bromination is increased in the order 70-5, 79-8 and 82-0 (see Experimental). The k' values were obtained using hexane as mobile phase at a flow-rate of 1 ml/min and a UV detector set at 225 nm. The variation in retention time as tested by repetitive injections of CB-118 was $<2\%$. Column abbreviations as in Table 1.

diphenyl ether that was stronger than for the bromosubstituted derivatives. In the case of the nitrophenyl phase all the PBDEs in the technical formulations detected by UV where shown to elute after the PCB fraction. This implies that the two groups can be completely separated. The PYE column was shown to provide the best selectivity regarding separation of individual BDE congeners (Fig. 2b). Compared to chlorination of biphenyl the effect of bromination of diphenyl ether had a much stronger influence on retention. Bromine have stronger steric effects on the solute–stationary phase interaction due to its size, when compared to chlorine. It also exerts a smaller inductive effect on an aromatic ring system due to its lower electronegativity. Both are properties that decrease interaction with the stationary phase. Since retention increases with increasing bromine substitution, this leads to the conclusion that the increased retention is due to interaction between the stationary phase and the bromine atoms in the solute molecules. This could be explained by the high polarisability of bromine.

3.4. Chlorinated environmental pollutants containing aliphatic carbons

Compared to chlorinated aromatic compounds, a totally different effect on retention is observed when chlorine is introduced into an aliphatic compound. If a chlorine atom is bonded to a carbon with a hydrogen attached to it, there will be a polarisation of the bond and the hydrogen will obtain an acidic character. The inductive effect of the chlorine is additive, so when adding more chlorine substituents to a carbon atom the bond polarisation increases. The effect may extend over more than one carbon atom and reach hydrogens attached to other adjacent carbon atoms. The influence on retention of hydrogens with acidic character have been observed earlier regarding chloro-added polycyclic aromatic hydrocarbons [23]. The present study shows that this kind of acidic hydrogens have a strong influence on the chromatographic retention of environmental pollutants containing aliphatic carbons in their structure (Table 3). The low retention of aldrin and Mirex, two compounds without acidic hydrogens in their structures, enhance the fact that it is not the chlorine atom by itself that causes the retention when bonded to an sp^2-hybridised carbon. The acidic hydrogen effect on retention is demonstrated for a number of compounds, *i.e.* chlordanes, hexachlorocyclohexanes and chlorinated paraffins all exhibited strong retention.

All HCH isomers have six hydrogen atoms with acidic character. By fractionation and subsequent GC analysis of the HPLC effluent it was shown that the four tested HCH isomers eluted after the PCB fraction on all columns except the PYE. The strong retention of HCH is explained by means of the polarised carbon–hydrogen bonds yielding acidic hydrogens being involved in the main retention mechanism. This shall be compared to cyclohexane that eluted with the dead volume and hexachlorobenzene which exhibited k' values ≤ 0.40 on all the stationary phases except PYE. On the PYE column α- and γ-HCH eluted in the PCB fraction, while β- and δ-HCH eluted after. Fractionation of CPs confirmed a strong retention caused by solute acidic hydrogens on all columns except the PYE on which the CPs eluted entirely within the PCB fraction. Acidic hydrogens obviously have only a small influence on retention on a PYE column compared to the other stationary phases.

For the studied chlordane compounds, α- and γ-chlordane and α- and γ-chlordene, the capacity factors increase with an increased number of acidic hydrogens (Table 3). This additivity is well demonstrated by the shift in capacity factor for p,p'-DDT and the related compounds p,p'-DDE and p,p'-DDD (Table 3). On all the investigated stationary phases the elution order was the same: p,p'-DDE, p,p'-DDT and p,p'-DDD. p,p'-DDE has no hydrogen bonded to an aliphatic carbon in the vicinity of any of the chlorine substituents. Hence, the major retention mechanism for p,p'-DDE involves interaction with the aromatic nuclei. For p,p'-DDT, long-range inductive effects of the three chlorine atoms in the 1 position affect the hydrogen in the 2 position of the ethane group. p,p'-DDD finally has one hydrogen atom affected by two adjacent

Table 3
Capacity factors of some organochlorine compounds

Compound	k'							
	PYE	Cyano	Diol	Phenyl	DMA	Amino	Nitro	Silica
HCB	2.21	0.20	0.20	0.25	0.14	0.25	0.40	0.23
PCNs	0.48–21.3	0.22–0.56	0.14–0.66	0.10–0.70	0.13–1.00	0.24–0.98	0.40–1.34	0.05–1.10
PCBs	0.03–3.76	0.25–0.96	0.23–1.16	0.13–0.80	0.20–2.33	0.28–1.87	0.41–1.83	0.31–2.22
p,p'-DDE	0.63	0.56	0.53	0.40	0.55	1.02	1.07	0.91
p,p'-DDT	1.03	1.04	1.09	0.65	1.75	3.16	2.63	1.75
p,p'-DDD	2.57	2.22	2.22	1.26	4.47	9.42	6.80	4.23
α-Chlordene	0.64	0.58	0.59	0.48	0.60	1.00	1.05	1.19
γ-Chlordene	0.68	0.72	0.76	0.56	0.94	1.39	1.38	1.36
α-Chlordane	0.72	1.18	1.28	0.83	2.19	3.91	2.83	2.62
γ-Chlordane	1.55	1.28	1.54	0.86	2.97	5.63	3.56	2.77
Heptachlor	0.44	0.47	0.51	0.39	0.54	0.85	0.87	0.97
Transnonachlor	0.73	1.04	0.98	0.56	1.35	4.64	2.62	1.74
Aldrin	0.36	0.35	0.40	0.29	0.41	0.35	0.64	0.63
Endrin	1.07	2.55	3.26	5.94	4.87	5.81	11.3	41.4
Dieldrin	0.69	2.93	3.88	8.89	7.88	7.78	13.2	53.4
Oxychlordane	0.55	0.83	0.86	0.76	0.99	2.34	1.96	3.16
Heptachloroepoxide	0.62	2.13	2.20	3.31	3.57	5.75	7.88	17.5
p,p-Methoxychlor	1.27	7.43	10.1	>50	34.4	22.9	48.9	>50

The k' values were obtained using hexane as mobile phase at a flow-rate of 1 ml/min and a UV detector set at 225 nm for aromatic compounds and 205 nm for non-aromatic compounds. PCBs and PCNs are commercial mixtures with various degrees of chlorination. The variation in retention time as tested by repetitive injections of CB-118 was $<2\%$. Column abbreviations as in Table 1.

chlorine atoms and one affected by long-range effects. For p,p'-DDT and p,p'-DDD the main retention mechanism involves interaction with the acidic hydrogens or the polarised carbon–hydrogen bond.

The components of Toxaphene, a technical product of polychlorinated camphenes, are spread out in a wide retention interval on the different stationary phases. The camphene structure makes it possible for different chlorinated derivatives to have none or many hydrogens with acidic character.

3.5. Halogenated environmental pollutants containing epoxy or ether groups

Oxygen is more electronegative than chlorine and its presence in the molecular structure induce a similar effect on retention as chlorine. The major influence on retention on the chemically bonded phases involve solute acidic hydrogens interacting with the stationary phase. As shown by the comparison of the retention of biphenyl and diphenyl ether (Tables 1 and 2), hydrogen bonding interaction involving solute ether oxygens does not substantially contribute to retention on any of the bonded phases except phenylpropyl silica. Even the aminopropyl silica did not show any increased retention due to hydrogen bonding with solute ether oxygen. However, on silica a strong retention caused by hydrogen bonding to this kind of oxygen atom was demonstrated.

On all columns except PYE, the highest capacity factor of all the tested compounds was obtained by p,p-methoxychlor (Table 3). This molecule is similar in structure to p,p'-DDT but has the p-chlorine atoms on the phenyl groups substituted by methoxy groups. The oxygen atom in the substituent group is supposed to have a similar influence on the six adjacent hydrogens as is demonstrated by chlorine.

For the compound groups aldrin/endrin/dieldrin and heptachlor/heptachlorepoxide a large increase in capacity factor can be attributed to epoxy groups yielding hydrogens with acidic character (Table 3). Heptachlorepoxide has two acidic hydrogens adjacent to the epoxy group. Oxychlordane is obtained by substituting one of these acidic hydrogens with a chlorine atom. On the bonded phases this yielded a decrease in retention due to the removal of one of the acidic hydrogens. However, on silica oxychlordane exhibit an extremely short retention compared to other compounds containing an epoxy or ether group (Table 3). This can be explained by a decreased strength of hydrogen bonding to this solute oxygen that might be caused by the adjacent chlorine atom counteracting interaction with the silica.

4. Conclusions

When analysing retention data from the different columns it becomes evident that there is no simple structure–retention relationship to be found for the CBs. The nitropropyl, aminopropyl and cyanopropyl phases exhibit similar selectivity towards the investigated CBs, thus implying a similar mechanism of retention. Carbon–hydrogen bond polarisation by adjacent chlorine or oxygen atoms yield hydrogen substituents with an acidic character. These were shown to have a major influence on normal-phase liquid chromatography retention of environmental pollutants having aliphatic carbons in their structure. In contrast to chlorine the retention behaviour of bromine-containing aromatic compounds indicated that bromine itself may be directly involved in the retention mechanism.

For the purpose of clean-up and group isolation of PCBs it was clearly demonstrated that none of the investigated columns were able to provide a complete separation of PCBs from all of the other investigated groups of halogenated environmental pollutants. The best isolation of a PCB fraction would be obtained by using the silica, nitropropyl silica or aminopropyl silica stationary phases. It was also shown that the PYE was the only investigated stationary phase that selectively retained the co-planar toxic CBs from the other CB congeners.

Acknowledgements

The authors wish to thank Åke Bergman and Henrik Kylin for helpful comments and discussions regarding the manuscript and for supplying CB-189 and the EPA pesticide standards. Ulrika Örn is acknowledged for the synthesis of the diphenyl ether and the 2,4,2′,4′-tetrabromodiphenyl ether. Harald Norin is acknowledged for supplying the decabromodiphenyl ether. The project was financially supported by the Swedish National Environmental Protection Board, grant No. 532630-9.

References

[1] G. Petrick, D.E. Schulz and J.C. Duinker, *J. Chromatogr.*, 435 (1988) 241.
[2] H. Hyvönen, T. Auvinen, M.-L. Riekkola and K. Himberg, *J. Microcol. Sep.*, 4 (1992) 123.
[3] M. Schantz, R. Parris, S. Wise, H. Won and R. Turle, *Chemosphere*, 24 (1992) 1687.
[4] V. Nero and R. Hudson, *Anal. Chem.*, 56 (1984) 1041.
[5] U.A.Th. Brinkman, J.W.F.L. Seetz and H.G.M. Reymer, *J. Chromatogr.*, 116 (1976) 353.
[6] U.A.Th. Brinkman, A. de Kok, G. de Vries and H.G.M. Reymer, *J. Chromatogr.*, 128 (1976) 101.
[7] U.A.Th. Brinkman and G. de Vries, *J. Chromatogr.*, 169 (1979) 167.
[8] A. Gillespie and S. Walters, *J. Liq. Chromatogr.*, 9 (1986) 2111.
[9] E. Storr-Hansen, M. Cleeman, T. Cederberg and B. Jansson, *Chemosphere*, 24 (1992) 323.
[10] R.F. Rekker, G. de Vries and G.J. Bijloo, *J. Liq. Chromatogr.*, 12 (1989) 695.
[11] P.G. Seybold and J. Bertrand, *Anal. Chem.*, 65 (1993) 1631.
[12] K. Kimata, K. Hosya, T. Arakai, N. Tanaka, E.R. Barnhart, L.R. Alexander, S. Sirimanne, P.C. McClure, J. Grainger and D.G. Patterson, Jr., *Anal. Chem.*, 65 (1993) 2502.
[13] P. Haglund, L. Asplund, U. Järnberg and B. Jansson, *J. Chromatogr.*, 507 (1990) 389.
[14] L.C. Sander, R.M. Parris and S.A. Wise, *Anal. Chem.*, 63 (1991) 2589.

[15] L. Nondek, *J. Chromatogr.*, 373 (1986) 61.
[16] L.C. Sander and S.A. Wise, *CRC Crit. Rev. Anal. Chem.*, 18 (1987) 299.
[17] U. Ahlborg, A. Hanberg and K. Kenne, *Risk Assessment of Polychlorinated Biphenyls, Nord 1992:26*, Nordic Council of Ministers, Stockholm, 1992, p. 84.
[18] R. Fischer and K. Ballschmitter, *Fresenius' Z. Anal. Chem.*, 335 (1989) 20.
[19] G. Sundström, *Acta Chem. Scand.*, 27 (1973) 600.
[20] G. Sundström and O. Hutzinger, *Chemosphere*, 3 (1976) 187.
[21] J.J. de Kok, A. de Kok and U.A.Th. Brinkman, *J. Chromatogr.*, 171 (1979) 269.
[22] D. Karlesky, D.C. Shelley and I.M. Warner, *J. Liq. Chromatogr.*, 6 (1983) 471.
[23] U. Nilsson and A. Colmsjö, *Chromatographia*, 32 (1991) 334.

ELSEVIER

Journal of Chromatography A, 675 (1994) 65–78

JOURNAL OF CHROMATOGRAPHY A

Phenol oxidase-based biosensors as selective detection units in column liquid chromatography for the determination of phenolic compounds

Fidel Ortega[a], Elena Domínguez[a], Elisabeth Burestedt[b], Jenny Emnéus[b], Lo Gorton[b], György Marko-Varga*[,b]

[a]*Department of Analytical Chemistry, Faculty of Pharmacy, University of Alcalá de Henares, 28 871 Alcalá de Henares, Madrid, Spain*

[b]*Department of Analytical Chemistry, University of Lund, Box 124, 221 00 Lund, Sweden*

(First received October 21st, 1993; revised manuscript received March 23rd, 1994)

Abstract

Amperometric biosensors of two types based on the phenol oxidase tyrosinase (EC 1.18.14.1, monophenol monooxygenase) are presented. The enzyme was immobilised either on solid graphite electrodes or in carbon paste electrodes. The performance of the two biosensors was investigated with respect to immobilisation technique, pH, flow-rate and oxygen dependence. The use of detergents in the mobile phase was shown to greatly influence activity, selectivity, and operational stability of the biosensors.

One of the developed biosensors was further used as a selective and sensitive detector in a column liquid chromatographic system for the determination of phenolic compounds in a spiked wastewater sample.

1. Introduction

Due to the increased awareness of the multitude of problems caused by pollution around the world, environmental protection has taken a more important role in society and moved right into our everyday life and household. Environmental pollution is in many cases the cause of alterations in cellular activities in nature, resulting in a broad spectrum of effects, *e.g.* changes in membrane permeability, mutations of genetic materials and inhibition or acceleration of catalyzed reaction rates in *e.g.* respiration and photosynthesis [1]. A considerable number of organic pollutants, widely distributed throughout the environment, have a phenol-based structure. These phenols and substituted phenols are products of many industrial processes *e.g.* the manufacture of plastics, dyes, drugs, antioxidants and wastewaters from the pulp industry.

Various substituted phenols such as chloro- and nitrophenols are highly toxic to man and aquatic organisms. These two groups of substituted phenols are also known to be the main degradation products of organophosphorous and chlorinated phenoxyacid pesticides [2–4]. Even at low concentrations (< 1 ppb) phenols affect

* Corresponding author.

0021-9673/94/$07.00
SSDI 0021-9673(94)00295-K

the taste and odour of drinking water and fish [5]. As a consequence, the need to determine phenols and related aromatic compounds in the environment has increased over the years, and the screening for these compounds in complex environmental samples has stimulated the development of new detection principles in this area. This also recently led the European Economic Community (EEC) to initiate a research program, within the environmental programme, devoted to the development of biosensors for environmental control.

In the development of biosensors for these target compounds, the complex nature of environmental samples has to be considered [6,7]. In fact, selective detection systems have to be supplemented with adequate sample pretreatment techniques and liquid chromatography when a particular compound has to be monitored [8]. Consequently, the development of these detection units has to run in parallel to the considerations that dictate sample handling and chromatographic separations to make "on-line" systems possible [9].

Chemical derivatisation and reaction detection utilising immobilised enzymes are currently techniques in rapid development [10–12]. In the field of catalytic reaction detection in conjunction with column liquid chromatography (CLC) most studies have focused on the use of immobilised enzymes in solid-phase reactors (IMERs), used either in the pre- or post-column mode [13]. Only recently have enzyme-based amperometric biosensors been utilised as detection units in CLC [14]. We have previously developed IMER-based detection systems for the analysis of various groups of analytes in complex biotechnological samples [8,9,15,16].

We here report on the development of phenol-sensitive amperometric biosensors utilising immobilised tyrosinase (TYRase, EC 1.18.14.1, monophenol monooxygenase) based on both carbon paste (CP) and solid graphite electrodes. These sensors are developed with the intention to be used as selective and sensitive detection units in CLC systems for environmental applications.

2. Experimental

2.1. Carbon paste electrodes

TYRase from mushroom was purchased as a lyophilised powder [Sigma T-7755, 2100 U mg^{-1} solid (lot 71H9685), 4200 U mg^{-1} solid (lot 102H9585) and 8300 U mg^{-1} solid (lot 112H9580) measured as TYRase activity and 860 000 U mg^{-1}, $6 \cdot 10^6$ U mg^{-1} and $1.06 \cdot 10^6$ U mg^{-1}, measured as catecholase activity, respectively] and used without further purification.

Unmodified CP was prepared according to the following: 100 mg of graphite powder (Fluka 50870) and 40 μl of paraffin oil (Fluka 76235) were thoroughly mixed for 20 min in an agate mortar until a homogeneous paste was formed. The unmodified CP was then packed into plastic syringes (1-ml syringe, ONCE, ASIK, Denmark, I.D. 0.85 mm, surface area 0.023 cm^2); 3–4 mm of the syringe tip was left empty so that it could be filled with enzyme-modified graphite paste (see below). Electrical contact was obtained by immersing a silver wire (Aldrich 34, 878-3) into the unmodified CP.

TYRase was immobilised in CP in five different ways. (1) An amount of TYRase equivalent of 1900 U was first dissolved into 300 μl of 0.1 *M* phosphate buffer (pH 6.0) and then added to 100 mg of graphite powder. The enzyme–graphite suspension was mixed at 4°C for 90 min and then dried in a desiccator for 4–5 h at reduced pressure. A 40-μl volume of paraffin oil was then added to the dried enzyme–graphite powder and thoroughly mixed in an agate mortar for 20 min. Additionally six other equivalent TYRase-modified CPs were prepared in this way with the exception that the enzyme–graphite mixtures were exposed to different drying times (between 1.5 and 4.5 h) in the desiccator. (2) An equal amount as above (1900 U) of TYRase powder was taken but added in a dry state directly to the graphite powder and carefully mixed for 10 min in an agate mortar. A 40-μl volume of paraffin oil was then added and the final enzyme-modified carbon paste was prepared as above. (3) A 4.25-mg amount of water-soluble 1-ethyl-3-(3-

dimethylaminopropyl) carbodiimide hydrochloride ("carbodiimide", Sigma E-6383) was dissolved into 300 μl of 0.05 *M* acetate buffer (pH 4.8) and added to 100 mg of graphite. The mixture was stirred for 2 h at 4°C and then thoroughly washed with ultrapure water over a G4 filter. An amount of 1900 U of TYRase was then dissolved into 300 μl of 0.1 *M* phosphate buffer (pH 6.0) and added to the carbodiimide-activated graphite. The enzyme–graphite suspension was stirred for 2 h at ambient temperature and then dried in a desiccator for 4–5 h at reduced pressure. Finally, 40 μl of paraffin oil were added and the enzyme-modified carbon paste was prepared as described above. (4) An initial procedure was used as in (3) with carbodiimide activation of the graphite powder followed by addition of the enzyme dissolved in buffer but here also followed by the addition of glutaraldehyde (Sigma G-5882) to the enzyme carbodiimide-activated graphite. An amount of 1900 U of TYRase was dissolved into 300 μl of 0.1 *M* phosphate buffer (pH 6.0) and added to the carbodiimide-activated graphite followed by the addition of 10 μl of a 25% aqueous solution of glutaraldehyde. Prior to use, any polymerised aldehyde was removed by addition of activated carbon followed by centrifugation at 4°C and the supernatant was stored at −18°C. The mixture was stirred for 2 h at 4°C and then washed thoroughly with 0.1 *M* phosphate buffer (pH 6.0) over a G4 filter. The enzyme–graphite powder was dried for 4–5 h and the CP was prepared as described above. (5) Amounts of 2.0, 3.3 and 10.0 mg bovine serum albumin (BSA, Sigma A-6003) were each dissolved in 200 μl 0.1 *M* phosphate buffer (pH 6.0). The BSA solutions were added to each 100 mg of graphite powder. The BSA–graphite mixtures were stirred for 30 min after which they were dried for 70 min at reduced pressure. Lyophilised dry TYRase (4200 U 100 mg^{-1} graphite) and 40 μl paraffin oil were then added to each of the three different BSA-modified graphite preparations and the CPs were prepared as described above.

Aliquots of the enzyme-modified CPs were then packed into the empty tips of the syringes, prepared with unmodified CP as described above. The electrodes were then gently rubbed on a glass surface so that smooth electrode surfaces were obtained. When not in use the enzyme electrodes were stored in a dry state at 4°C.

2.2. Solid graphite electrodes

Rods of spectrographic graphite (RW 001, 3 mm O.D., Ringsdorff-Werke) were cut, polished on wet fine emery paper, thoroughly washed with deionized water, and allowed to dry at room temperature. They were then heated to 700°C for 90 s in a Muffle furnace. They were then cooled and stored in a desiccator until use.

Two different techniques were assayed for the immobilisation of the enzyme onto the surface of the solid electrodes: physical adsorption and covalent coupling via carbodiimide using glutaraldehyde as cross-linking agent. The covalent coupling was also studied with and without addition of BSA.

The adsorption coupling was made as follows: 12 μl of a TYRase solution (2.4 mg solid, 5040 U ml^{-1} in 0.1 *M* phosphate buffer pH 6) were added to polished ends of graphite rods. Evaporation was allowed to proceed at room temperature for 15 min. The covalent coupling with carbodiimide involves an activation step of the electrode surface described previously [17]. The enzyme was then coupled by dipping the activated electrodes into 0.5 ml of the TYRase solution (2.4 mg solid ml^{-1} in 0.1 *M* phosphate buffer pH 6) containing 1% glutaraldehyde. This binding between the activated carboxylic groups of the electrodes and the amino groups of the enzyme was allowed to proceed for 16 h at 4°C. The enzyme electrodes were then carefully rinsed with 0.1 *M* buffer solution pH 6 and kept at 4°C in the same buffer. When BSA was added, a final concentration of 4 mg BSA ml^{-1} was added in the solution containing the enzyme and glutaraldehyde.

When in use, the enzyme electrodes were press-fitted into a PTFE holder so that only the

flat circular end (0.0731 cm^2) was exposed to the flow [18].

2.3. Apparatus

The electrodes were inserted into a confined wall-jet flow through amperometric cell [18]. The cell was connected to a single-channel flow injection (FI) system consisting of a pneumatically operated injection valve (Cheminert SVA) with an injection volume of 25 μl, a peristaltic pump (Gilson Minipuls 3), and a potentiostat (Zäta Electronics, Lund, Sweden). The enzyme electrode was used as the working electrode, an Ag/AgCl electrode as the reference, and a platinum wire as the counter electrode. All the connections between the different parts of the FI system were made of PTFE tubings (0.5 mm I.D.) and Altex screw couplings. All measurements with the amperometric biosensors were performed at an applied potential of −50 mV *versus* SCE [17].

Phosphate buffers (0.1 *M*) of different pH values were carefully filtered through 0.4-μm pore diameter membranes (Millipore) and degassed and used as carriers in the FI system. Different flow-rates between 0.1 and 1.5 ml min^{-1} were used with 0.1 *M* phosphate buffer (pH 6.0) as the carrier. In some experiments two different detergents, polyoxyethylenesorbitan monolaurate (Tween 20, Sigma P-1379) and polyoxyethylenesorbitan monooleate (Tween 80, Sigma P-1754) were added to the carrier (0.05%, v/v) to investigate their influence on the biosensor activity and stability.

Stock solutions of 100 m*M* of catechol (Sigma C-9510) and phenol (Merck 206) were prepared by dissolving appropriate amounts in acetonitrile or methanol and stored at 4°C. Phosphate buffer was prepared from sodium dihydrogenphosphate and sodium hydroxide. Acetate buffer was prepared from acetic acid and sodium hydroxide. All chemicals used were of analytical grade. HPLC-grade water was produced in a Milli-Q system and was used throughout this work.

To investigate the oxygen dependence of the reactions taking place at the electrode surface, the following experiment was made. Phenol (0.2 m*M* or 2 μM) or 0.1 m*M* catechol solutions were prepared in 0.1 *M* phosphate buffer (pH 6.0) and saturated with air at 40°C for 20 min followed by cooling to room temperature. A steady-state current was obtained by continuously pumping this solution through the FI system also containing the TYRase biosensor. When a steady state was obtained the phenol-containing carrier was continuously deairated by flushing nitrogen through the solution.

Chromatographic analyses were performed using a Hewlett-Packard (HP) 1050 HPLC system with a 20-μl injection loop and a HP 1040 M photodiode array detector coupled to a HP 9000/300 personal computer and HP 9153 C disk drive. A stainless-steel column (250 × 4 mm I.D.) packed with Nucleosil 120 C_{18} material (particle size 5 μm) (Scharlau) was used. The mobile phase was pumped in the isocratic mode at 1 ml min^{-1} and consisted of acetonitrile–0.1 *M* acetate buffer pH 5.0 (20:80, v/v). Detection was effected at 270 nm. The effluent of the photodiode array detector was connected to the inlet of the amperometric cell containing a solid graphite TYRase electrode.

2.4. Sample handling of waste water

The waste water samples were used as obtained from a pulp industry in the south of Sweden. The samples were diluted 10-fold with distilled water, adjusted to pH 5.0, membrane filtrated, and finally subjected to clean-up by solid-phase extraction (SPE). The clean-up column, containing amine ($-NH_2$) functionalities (Sep-Pak, Waters, Milford, MA, USA), was conditioned by using 2 ml of methanol–water (80:20) to remove impurities from the cartridge, followed by 3 ml of water to remove this solvent mixture. The column was finally conditioned with 2 ml of 0.1 *M* phosphate buffer (pH 6.0) which then was removed by 3 ml of water. Next, 1.5 ml of the wastewater were eluted through the SPE column. The purified wastewater sample was then injected into the chromatographic systems.

3. Results and discussion

3.1. Enzymatic reactions

TYRase [19] is a phenol oxidase which preferably oxidises monophenols but is also active on certain diphenols preferably when the OH-groups are located in *ortho*-position. TYRase contains copper as the prosthetic group in the active site which takes part in the oxidation of molecular oxygen to water [20].

The oxidation reaction of monophenols proceeds in two separate consecutive steps, involving molecular oxygen. The first step is referred to the enzyme's hydroxylase activity where phenol is hydroxylated by the aid of molecular oxygen to produce catechol (*o*-hydroquinone). The second step is an oxidation step known as the enzyme's catecholase activity. The catechol formed in the first step is oxidised to an *o*-quinone, whereby the enzyme is oxidised by molecular oxygen to its native form under the production of water.

The entire reaction path, also including the electrochemical step, for the detection of various phenolic compounds at the TYRase-modified electrode is depicted in Fig. 1. The two enzymatic reactions are followed by electrochemical reduction of the enzymatically produced *o*-quinone forming catechol at the electrode surface. The coupling of enzymatic oxidation of catechol and electrochemical reduction of *o*-quinone thus forms a reaction cycle that results in an amplification of the signal response to phenolic compounds. However, quinones suffer from high instability in water and intermediate formation of radicals in both the enzymatic and electrochemical reactions may readily react and polymerise to polyaromatic compounds which have proved to inactivate the enzyme and to foul the electrode [21–24].

Two different electrode configurations were investigated in which the enzyme was immobilised on a solid graphite electrode or in a CP electrode. Both electrode configurations were incorporated into equal wall-jet electrochemical flow cells and their performances were investigated in an FI system, as described in the Experimental section.

3.2. Carbon paste electrodes

Considering the organic composition of a CP, a rather different catalytic behaviour of an enzyme can be predicted [25]. This opens up new possibilities for the detection of analytes, which may not be recognised by the enzyme in a complete aqueous phase, *i.e.*, when it is immobilised on the surface of a solid electrode or in an enzyme reactor [25]. Additionally, the fact that the enzyme is located in an organic phase imposes a distribution of substrates and products between aqueous and organic phases. The CP configuration allows to remove, by pushing down the paste, the outer catalytic layer once the response decreases by fouling and/or instability, giving a new and catalytically active layer. Finally, it has to be stressed that the CP configuration

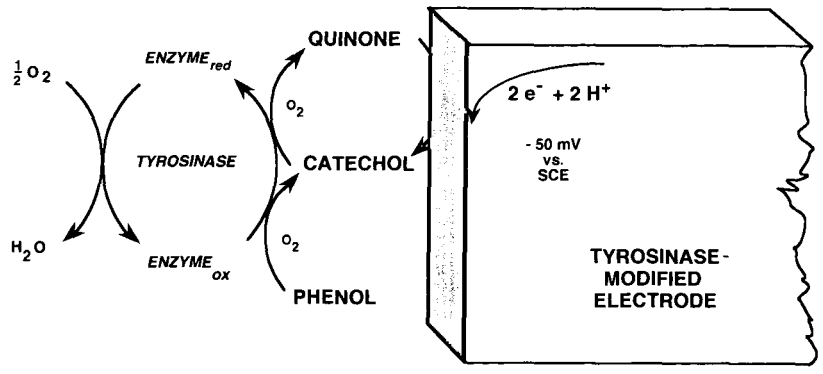

Fig. 1. The reaction sequence for a tyrosinase-modified biosensor, including both the enzymatic and the electrochemical steps.

seems to be a more versatile approach allowing so called bulk modification by the inclusion of various additives needed for an efficient catalysis and fast electron transfer, *e.g.* cofactors, mediators, activators and stabilisers.

In a first attempt when making TYRase-modified CP, the enzyme was physically adsorbed to the graphite powder surface before addition of the pasting liquid. This resulted in an electrode which gave a very low response for catechol (16 nA/m*M*) and a rapid decline of the signal response.

The rapid decline of the signal response with time, as seen in Fig. 2a, has been explained in the literature and it can be due to a number of factors. Bonakdar *et al.* [24] suggested that the rapid decline of the catalytic signal was due to polymerisation reactions followed by the deposition of the produced polyaromatic compounds at the electrode surface. The authors reported a more stable catalytic response of a TYRase-modified CP electrode, by adding the redox-mediator hexacyanoferrate(II) into the paste. The *o*-quinone produced by the enzymatic reaction was thus removed and indirectly monitored amperometrically by the redox-mediator. Wood and Ingraham [26] and Zachariah and Mottola [27] suggested that inactivation of immobilised TYRase was due to reaction inactivation by the substrate. Their explanation was that the nucleophilic lysine groups of the enzyme attack the quinone product, yielding a covalent adduct which blocks the active site of the enzyme. They found that working at concentrations below 10^{-5} *M* did not result in reaction inactivation. A more thorough investigation was therefore made in order to elucidate which factors influence the stability and activity of the TYRase-modified CP electrode.

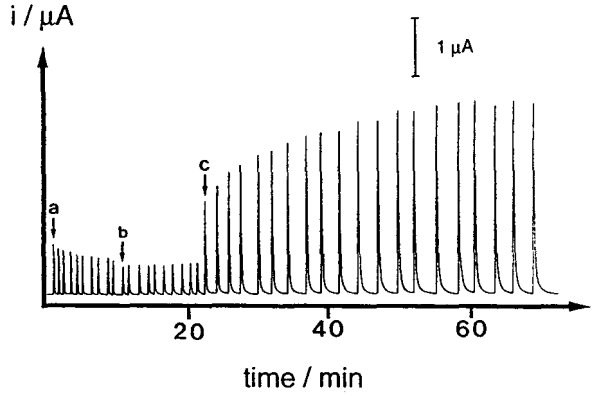

Fig. 2. Flow injection peaks of a 0.2 m*M* catechol solution when the carrier stream in the flow system contains (a) no additive, (b) 0.05% Tween 80 or (c) 0.05% Tween 20. Flow injection conditions as in Fig. 3.

Factors influencing stability and/or activity

It is generally agreed that covalent attachment of an enzyme results in a more stable enzyme preparation compared to immobilisation by pure adsorption. TYRase was therefore immobilised by way of adsorption, covalent coupling with carbodiimide, and covalent coupling with carbodiimide and subsequent cross-linking with glutaraldehyde. The highest catalytic activity was obtained when TYRase was covalently attached with carbodiimide and cross-linking with glutaraldehyde. However, better operational stability was not obtained by changing the immobilisation procedure from pure adsorption to either of the two ways of covalent attachment.

The low catalytic activities obtained in the above experiments were puzzling, since earlier experiments performed in our laboratory using exactly the same conditions gave much higher response for both catechol and phenol (data not shown). In the field of using enzymes in organic media the amount of water surrounding the enzymes in the organic environment is of utmost importance [28–32]. Depending on the type of enzyme, the polarity of the organic solvent, and the hydrophilicity/hydrophobicity of the support used, the necessary water for optimum activity differs. A similar water dependence was found when TYRase-modified CPs were exposed to different drying times in a desiccator (1–4.5 h). It was clearly seen that too much or too little water (short or long drying times, respectively) in the CP electrode resulted in low catalytic responses. Optimum activity was obtained when the enzyme-modified CP was dried for 2.5 h. However, when trying to reproduce some of the former experiments under optimum drying conditions, the catalytic responses of the resulting CP electrodes were extremely irreproducible.

The reason for this is probably that the necessary water content is changing depending on different practical conditions obtained from day to day in the desiccator. When the dry enzyme powder was added by direct admixing with the CP, the response to catechol and phenol increased drastically (data not shown). Apparently, the enzyme powder in its dry state contains the necessary water for full activity, which was indicated by fairly reproducible results obtained for several identical experiments. The immobilisations presented below in this paper were therefore performed by direct admixing of the dry enzyme powder with the CP.

When an enzyme is immobilized on solid supports with large active surfaces, the surface groups on the support can induce conformational changes on the enzyme and thereby blocking the active configuration. Wehtje *et al.* [33] showed that the surface coverage of adsorbed lipase on zeolite had great influence on the inactivation behaviour of the enzyme when used in different organic solvents. If a monolayer of lipase (2–3 mg m^{-2}) was immobilised, a stable enzyme preparation was obtained, whereas when smaller amounts were immobilised, inactivation was pronounced. The authors showed that the latter case could be counteracted by co-immobilising the lipase with an enzymatically inactive protein such as BSA, which thus protects lipase from the inactivating surface groups on the support. Based on these findings we were interested in investigating the role of a protein additive such as BSA on the stability of the CP electrode. The resulting currents for 0.2 m*M* catechol and phenol with different amounts of BSA pre-adsorbed to the CPs are shown in Table 1, columns 2 and 3. It can be seen that the catalytic current for catechol and phenol increases when the graphite is pre-treated with the protein barrier, BSA. The best response for both catechol and phenol was when the graphite was pre-treated with 3.3 mg of BSA. However, it has to be stressed that the stability of the sensor remained unsolved because it was only slightly improved by this pre-treatment. The following work was therefore focused on improving the stability of the CP configuration, particularly since the stability had not been a major problem in previous work with TYRase immobilized in different enzyme configurations [34].

Table 1
Current (i) intensities for 0.2 m*M* catechol and phenol with tyrosinase-modified carbon paste electrodes pre-treated with different amounts of BSA

BSA (mg)	$i_{catechol}$ (μA)	i_{phenol} (μA)	$i_{catechol}$ + Tween 20 (μA)	i_{phenol} + Tween 20 (μA)
0	0.43	–		
2	0.90	0.64	3.0	0.94
3.3	1.78	0.76	2.7	0.98
10	1.26	0.33	1.7	0.42

The flow injection conditions were as in Fig. 3 except that in columns 4 and 5 the carrier also contained 0.05% Tween 20.

Considering the organic nature of the TYRase–CP, a partitioning of substrates and products between an aqueous–oil (W/O) phase has to be considered. Addition of a surfactant could be beneficial for both the partition of substrates at the interface of the electrode and more so for the removal of water-insoluble catalytically produced polymer products from the oil phase of the electrode to the carrier stream. A non-ionic surfactant, Tween 20, was therefore added to the carrier at a concentration of 0.05% (w/w). The currents obtained for the different BSA pre-treated electrodes are presented in Table 1, columns 4 and 5. A further increase of the current in catalytic response was observed by the presence of Tween 20 and the signal remained stable (see below). A second non-ionic surfactant, Tween 80, was also studied and in Fig. 2, it can be observed for a non-BSA pre-treated TYRase–CP electrode, (a) a decline of the signal when no detergent was added to the carrier, (b) a stabilisation of the signal when 0.05% Tween 80 were added to the carrier and (c) a recovering and a pronounced increase of the signal, which eventually levels off to a stable signal, when 0.05% Tween 20 were added to the carrier. With both surfactants the signal remained stable. The reason for the increase in signal with Tween 20 and not with Tween 80, might be related to the difference in length of

the non-polar chains of the surfactants. Tween 20 contains monolaurate (C_{11}) groups and Tween 80 monooleate (C_{17}) groups. It is reasonable to think that a larger molecule, Tween 80, will occupy a larger surface on the electrode and the number of surfactant molecules at the interface will be presumably lower. A specific interaction of the surfactant and the enzyme is also a possible explanation. Ongoing work will contribute to a better knowledge and understanding of surfactants in CP electrodes.

pH dependence

The optimum pH of an enzyme electrode will be determined by the influence on both its catalytic activity and the electrochemical transduction. The pH profile obtained for phenol and catechol with a pH range from 4.0 to 8.0 in the carrier is presented in Fig. 3. The optimum pH for both substrates is 6.0, which was therefore the pH employed in the following experiments presented below.

Flow dependence

The flow dependence of the TYRase-modified CP electrode can be seen in Fig. 4 (left *y*-axis). The signal response for both catechol and phenol decreases with increasing flow-rate. The response is dependent on the combined effect of the rate of mass transfer to the electrode surface, the rate of the enzymatic reaction, and the rate of the electrochemical reduction of the enzyme product. Since mass transfer increases with increasing flow-rate it can be realised that the decrease in signal response with the increase of flow-rate, is largely due to limitations by the enzymatic reaction. In Fig. 4 (right *y*-axis), this is verified by the increase of the current ratio (catechol · phenol^{-1}) with flow-rate. At low flow-rates a larger portion of phenol is converted to product than at high flow-rates, which indicates that the limitation for phenol conversion is mainly caused by the first step in the enzymatic reaction (phenol→catechol).

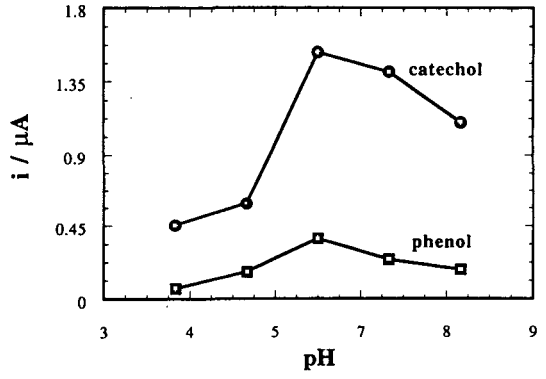

Fig. 3. Variation of the current intensity with pH for 0.2 m*M* catechol and phenol obtained for a tyrosinase-modified carbon paste electrode. A 25-μl volume of 0.2 m*M* catechol was injected into the carrier stream. The carrier was 0.1 *M* phosphate buffer (pH 6.0) and the flow-rate was 0.8 ml min^{-1}. The applied potential was −50 mV *vs.* Ag/AgCl.

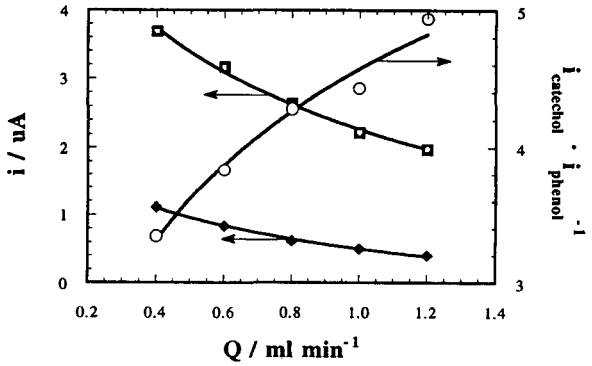

Fig. 4. Variation of the current intensity with the flow-rate (Q) for catechol (□) and phenol (◆) obtained with the tyrosinase-modified carbon paste electrode inserted in a flow injection system. Flow injection conditions as in Fig. 3.

O_2 dependence

As for any oxidase, molecular oxygen is the natural electron acceptor responsible for the reoxidation of the reduced enzyme and its effect has to be considered in the design of the TYRase biosensor. However, when trying to determine the oxygen dependence of the TYRase–CP electrode, very contradictory results were obtained when the same experiment was performed several times. Both oxygen dependence and oxygen

independence for catechol and phenol were found when several identical experiments were performed. A conclusion concerning the oxygen dependence for a TYRase-modified CP electrode was difficult to make and a more thorough investigation is therefore needed.

3.3. Solid graphite electrodes

The solid electrode configuration allows the immobilisation of the enzyme on the porous surface of the spectrographic graphite. Physical and chemical coupling were assayed. Despite the limited surface area of the solid electrode (0.0731 cm^2), the porosity of this material and the preparation of the electrodes by polishing on fine emery paper gives an enhanced micro surface [35] ready to physically adsorb the enzyme molecules. Carbodiimide activation requires carboxylic functionalities from the graphite. It has been shown that an oxidative pre-treatment step of the carboneous material can increase the enzymatic loading and the specific activity of the preparation depending on the specific enzyme [36]. Heating of the electrodes at 700°C for 90 s was chosen as an oxidative cleaning procedure. Glutaraldehyde was added as a cross-linking agent to increase the rigidity of the enzyme molecules by covalent bonds between them. This covalent procedure was also assayed in the presence of BSA. Adsorption of the enzyme yields lower currents than when covalently coupled, but yields significantly higher currents than when covalently coupled in the presence of BSA. It has been previously discussed on the beneficial effect of the addition of BSA on the signal of the TYRase–CP electrode. From the results in Table 2, it seems obvious that BSA has a rather detrimental effect on the current intensity of the solid electrodes.

As stated in the Introduction, the peak shape of the biosensor response plays an important role in avoiding band broadening and loss of chromatographic resolution. The peak shapes of the different TYRase electrodes based on solid graphite are presented in Table 2 as peak width,

Table 2
Current intensities and peak shapes for solid graphite tyrosinase electrodes prepared with three different immobilisation techniques

	i (nA)	$t_{w1/10}$ (s)	$t_{w1/2}$ (s)
Adsorption			
Catechol (20 μM)	1040	33.50	6.25
Phenol (20 μM)	104	111.60	15.60
Covalent EDC + GA			
Catechol (20 μM)	2160	13.50	7.25
Phenol (20 μM)	900	32.10	10.80
Covalent EDC + GA + BSA			
Catechol (20 μM)	344	14.25	6.25
Phenol (20 μM)	80[a]	n.d.	n.d.

EDC = 1-Ethyl-3-(3-dimethylaminopropyl) carbodiimide hydrochloride; GA = glutaraldehyde. The electrodes were assayed in the flow injection mode. The carrier was 0.1 M phosphate buffer (pH 6) and the flow-rate was 0.7 ml min^{-1}. The applied potential was −50 mV *vs.* SCE. n.d. = Not determined; t_w = peak shape (see text); i = current intensity.
[a] 100 μM.

in s, at half and tenth of the peak height ($t_{w1/2}$ and $t_{w1/10}$, respectively). The covalent coupling also gives the most favourable peak shapes *versus* adsorption where broad peaks are obtained. When adsorption of the TYRase on the surface of the electrode was made by dipping the electrode into an enzyme solution (instead of adding 12 μl of enzyme solution on the electrode surface) the peak width became much larger (data not shown). Narrower peaks was observed for catechol compared with those of phenol which proves the influence of the catalytic reaction on the peak dispersion [37]. This fact supports the assumption of the existence of two different active centres in the same enzyme working independently but consecutively for monophenols. In fact, the hydroxylase reaction rate will determine the concentration profile for phenol and consequently any approach which favours this slow kinetic step will also favour the peak shape.

All the following experiments with solid graphite electrodes were therefore made with the

TYRase electrode prepared by covalent coupling and cross-linking with glutaraldehyde.

Effect of Tween 80

A concentration of 0.025% Tween 80 was added into the carrier consisting of 0.1 *M* phosphate buffer pH 6. The flow-rate was kept at 0.7 ml min^{-1}. After 20 consecutive injections of 20 μM catechol, a 40% decrease in response was observed, while in the absence of surfactant this dramatic decrease in response was not seen. It has to be stressed that the addition of a surfactant to the solid electrode was motivated mainly for comparative reasons. The absence of an organic phase in the solid electrode simplifies the reaction mechanism and it makes the addition of a surfactant presumably unnecessary. The decrease in signal response, understood as a catalytic inactivation or a deteriorated electrochemical performance, requires further investigation. It has been reported that amphiphilic molecules aggregate on solid surfaces and reduce the rate of charge transfer from redox couples in solution to gold, tin oxide [38,39], and carboneous [40] electrodes [41].

pH dependence

The pH profile obtained for phenol and catechol, ranging from 4.0 to 9.0 in the carrier, is presented in Fig. 5. For both, phenol and catechol, an optimum is found at pH 6 as for the CP electrode. A sharper decrease for phenol than for catechol is noticeable at higher pH values, while at lower pH values the response for catechol decreases more dramatically than for phenol.

Flow dependence

Fig. 6 shows the variation of the response for a TYRase–solid electrode with the flow-rate. An increase in the current intensity can be expected when assuming that the enzyme is working under first-order conditions. This general behaviour is not observed for the response of this biosensor to injections of phenol. The plateau obtained indicates that at high flow-rates the kinetics of the overall enzymatic and electrochemical steps are the rate-limiting factors for the response.

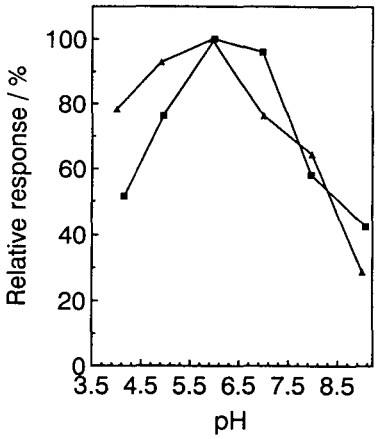

Fig. 5. Variation of the current intensity with the pH obtained with a tyrosinase graphite electrode in the flow injection system. A 25-μl volume of 10 μM phenol (▲) and 25 μl of 20 μM catechol (□) were injected into the carrier stream. The carrier was 0.1 *M* phosphate buffer at different pH values and the flow-rate was 0.7 ml min^{-1}. The applied potential was −50 mV *vs.* SCE.

The faster the phenol plug reaches the electrode surface, the lower enzymatic conversion and additionally, the produced quinone is more easily transported back into the bulk solution. The plateau response is already achieved at 1.1 ml min^{-1} in the flow injection system, and the decrease in response is 60% in relation to the response obtained at low flow-rate. Between 1.1 and 0.1 ml min^{-1} the response increases as a consequence of an increase in the time allowing the sample to be in contact with the enzyme. The flow-rate profile for catechol appears rather different. Increasing the flow-rate between 0.4

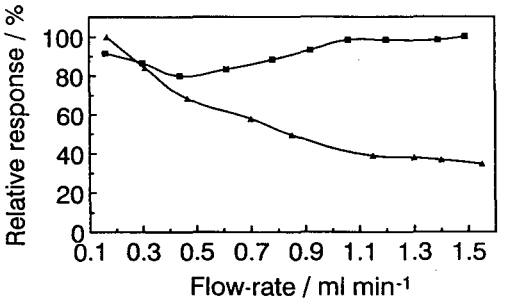

Fig. 6. Variation of the current intensity with the flow-rate obtained with the tyrosinase solid graphite electrode. Same conditions as in Fig. 5.

and 1.0 ml min^{-1} results in an increase of the response showing a mass transport limitation in this flow range, *i.e.* the overall enzymatic and electrochemical reactions are not limiting the current intensity. Similar as for CP electrodes, the behaviour observed for phenol concludes that it is the hydroxylase activity, which is limiting the overall conversion for monophenols. Between 0.4 and 0.1 ml min^{-1} the increase in response can be equally understood considering the longer residence time of the catechol on the surface of the electrode. At higher flow-rates, between 1 and 1.5 min ml^{-1}, the enzymatic oxidation becomes the limiting step, also for catechol.

O_2 dependence

The effect of molecular oxygen was studied in the flow injection system flowing at 0.7 ml min^{-1} for a 2 μM phenol solution (pH 6) in the carrier stream. Once a steady current was achieved with an aerated phenol solution, nitrogen was introduced by sparkling the gas into the carrier stream for 50 min. A decrease of the phenol response could be observed during the time that oxygen was removed from the carrier stream. After 50 min, nitrogen sparkling was stopped and phenol was removed by introducing phosphate buffer into the carrier stream to restore the baseline. Recovery of the response for phenol was evaluated which resulted in that 30% of the TYRase activity was irreversibly lost by anaerobic conditions.

Calibration of solid graphite TYRase electrode

Strictly linear calibration was obtained from 10 nM to 20 μM at pH 6 in the flow injection system with 25-μl injections of catechol at a flow-rate of 0.7 ml min^{-1}. Regression analysis gave an equation $y = 134.05(\pm 0.97) \times + 12.85(\pm 7.07)$, where y is the response in nA and x the catechol concentration in μM, $r = 0.99979$. With a 25-μl injection loop a limit of detection (LOD) of 2.3 nM was calculated from $LOD = y_B + 3s_B$, where y_B and s_B are, respectively, the blank signal and its standard deviation ($n = 10$). The average sensitivity was 0.16 $\mu A/\mu M$.

TYRase-modified solid graphite or CP electrode?

The question whether to use a solid graphite electrode or a CP electrode as the post-column detector for CLC was at this stage not difficult. Since a stable response was not obtained for the CP electrode unless Tween was added to the carrier stream, this configuration was ruled out, otherwise a make-up flow would have been necessary. Additionally, the sensitivity of the solid graphite electrode was generally ten times higher than for the CP electrode. However, ongoing work with TYRase-modified CP electrodes has shown that this type of configuration has a promising future. The sensitivity can be increased considerably by bulk modifying the CP electrode with different types of activators and/or stabilisers (data not shown). Additionally, the noise and background currents are lower than for solid electrode materials. The above-mentioned possibilities and the fact that a whole new catalytic biosensor surface can be obtained by simply removing the outer layer, call for further investigation of the TYRase-modified CP electrode.

3.4. Analysis of industrial wastewater samples

Applications were made as described earlier [16] by comparing the use of UV detection and the use of the TYRase-modified solid graphite electrode as detection device for the CLC system. Wastewater samples were obtained from a pulp industry in the south of Sweden. SPE was introduced as a sample handling step using disposable Sep-Pak columns of the silica-based amino phase type (see Experimental). This SPE step was used to eliminate some of the brown components present in the almost black wastewater samples. Removal of disturbing brown-coloured components such as humic substances and lignin-derived oligomers and polymers, was not complete although the levels were lowered considerably. This was investigated by running UV spectra before and after the clean-up and recovery studies with phenol and *o*-cresol as phenolic standards. Even though a quaternary amine phase (strong anion exchanger) was found

to have a higher sorption capacity for the brown-coloured interferents, these Sep-Pak phases showed much lower recovery values for both phenol and *o*-cresol.

Fig. 7A shows the separation of a wastewater sample spiked with phenol, *p*-cresol and catechol after sample pretreatment, as described in the Experimental section. The phenol peak (peak 2) is somewhat tailing which is probably due to limitations in enzyme reaction kinetics. The blank injection is shown in Fig. 7B and it can be seen that no other peaks are found in the chromatogram. The same sample as above was separated and detected with a UV detector at 270 nm, see Fig. 8. The spiked sample (Fig. 8A) shows many early-eluting compounds in the chromatogram, in spite of that many of these first-eluting compounds were successfully eliminated in the clean-up step. The separation of the blank in Fig. 8B shows the same separation of early-eluting compounds but also the possible background levels of catechol and other polar possible phenolic compounds present in the sample. These could not be confirmed by using

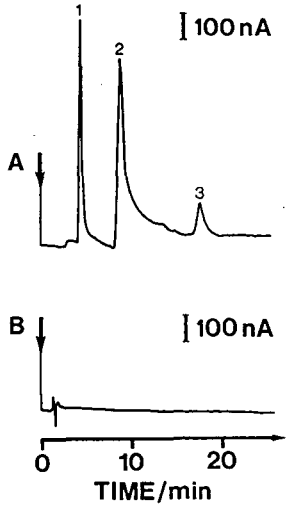

Fig. 7. Chromatographic separation of (A) spiked wastewater and (B) blank samples after solid-phase extraction. Chromatographic conditions: analytical column, silica C_{18} (LiChrospher); mobile phase, acetonitrile–phosphate buffer (100 m*M*, pH 6.2) (5:95); injection volume 20 μl, and an applied potential of −50 mV *vs.* Ag/AgCl. Peaks: 1 = 100 μM catechol; 2 = 100 μM phenol; 3 = 100 μM *p*-cresol.

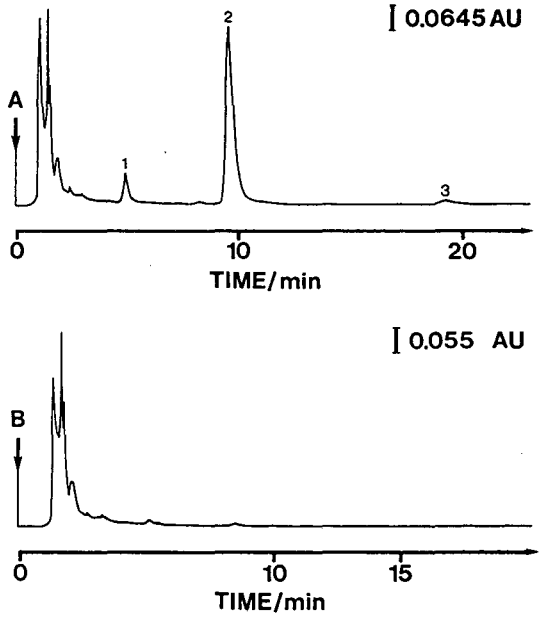

Fig. 8. As Fig. 7, using a diode array detector at 270 nm. Peaks: 1 = 100 μM catechol; 2 = 100 μM phenol; 3 = 100 μM *p*-cresol.

the retention data and the UV spectrum alone. These compounds are not found in the separation of the blank using the enzyme electrode, see Fig. 7B, which is due to the higher selectivity obtained with the TYRase biosensor compared with UV detection. The biosensor is operated in the optimal potential range for electrochemical measurements [in the vicinity of 0 V *versus* the saturated calomel electrode (SCE)]. Here, the enzymatic and electrochemical reactions occur at their optimal reaction rates, the capacitive current switches signs and thus background and noise currents take their lowest value, the electrochemical reduction of molecular oxygen and oxidation of interfering compounds also present in the sample are eliminated and thus not contributing to the analytical signal. Calculation of the concentration of these possible phenolic compounds obtained in Fig. 8A showed that if they were of phenol origin they would readily be detected by the biosensor detection mode. The conclusion can therefore be drawn that these peaks are not of phenol or catechol origin.

4. Conclusions

We have shown that it is possible to obtain a more selective detection system for phenolic compounds by using a TYRase-based biosensor as a post-column detector for CLC compared with UV detection. The TYRase-modified solid graphite electrode was used in the post-column mode, since at this initial stage, the sensitivity and stability of this electrode was greater than with the CP electrode. As mentioned earlier, the CP electrode configuration should not be ruled out since ongoing work has shown that various so-called promoters (activators and/or stabilisers) have shown to have great influence on the CP electrode biosensor performance.

Another matter that should be addressed is the observed instability of the biosensor in the presence of organic modifiers. However, this instability can be improved by casting a membrane on top of the biosensor, thereby protecting the enzyme from the organic solvent. Additionally, the chromatographic separation can be optimized so that lower levels or even pure aqueous mobile phases can be used.

Acknowledgements

Gilson Medical Electronics (Villiers-le-Bel, France), Instrument Lambda (Sollentuna, Sweden) and Pacisa (Madrid, Spain) are gratefully acknowledged for support with instrumentation.

Financial support from the Swedish Board for Technical and Industrial Development (NUTEK), the Swedish Natural Science Research Council (NFR), the DGICYT (Dirección General de Investigación Científica y Técnica, PS 90-0028) and the Commission of European Community, Environment programme (1990-1994) No. EV5V-CT92-0109, is gratefully acknowledged.

References

[1] A.G. Heath, *Water Pollution and Fish Physiology*, CRC Press, Boca Raton, FL, 1987, p. 165.
[2] A. Farran, J. de Pablo and D. Barceló, *J. Chromatogr.*, 445 (1988) 163.
[3] G. Durand, N. de Bertrand and D. Barceló, *J. Chromatogr.*, 554 (1991) 233.
[4] M.K. Fayyad, M.A. Alawi and T.J. El-Ahmed, *Chromatographia*, 28 (1989) 465.
[5] A. G. Huesgen and R. Schuster, *LC · GC Int.*, 4 (1991) 40.
[6] D. J. Munch and C. Frebis, *Environ. Sci. Technol.*, 26 (1992) 921.
[7] K.W. Edgell, E.J. Erb, J.E. Longbotton and V. López-Avila, *J. Assoc. Off. Anal. Chem.*, 75 (1992) 858.
[8] G. Marko-Varga, L. Gorton, E. Domínguez and D. Barceló, *Chromatographia*, 36 (1993) 381.
[9] G. Marko-Varga, E. Domínguez, B. Hahn-Hägerdal, L. Gorton, H. Irth, G.J. de Jong, R.W. Frei and U.A.Th. Brinkman, *J. Chromatogr.*, 523 (1990) 173.
[10] L. Gorton, E. Csöregi, E. Domínguez, J. Emnéus, G. Jönsson- Pettersson, G. Marko-Varga and B. Persson, *Anal. Chim. Acta*, 250 (1991) 203.
[11] G. Marko-Varga and L. Gorton, *Anal. Chim. Acta*, 234 (1990) 13.
[12] R. D. Schmid and W. Künnecke, *J. Biotechnol.*, 14 (1990) 3.
[13] G. Marko-Varga, *Electroanalysis*, 4 (1992) 1.
[14] T. Yao and T. Wasa, *Anal. Chim. Acta*, 209 (1988) 259.
[15] G. Marko-Varga, E. Domínguez, L. Persson, B. Hahn-Hägerdal and L. Gorton, *Autom. Lab. Rob.*, 5 (1993) 11.
[16] G. Marko-Varga, in D. Barceló (Editor), *Modern Techniques in Environmental Analysis*, Elsevier, Amsterdam, 1993, p. 225.
[17] F. Ortega, E. Domínguez, G. Jönsson-Pettersson and L. Gorton, *J. Biotechnol.*, 31 (1993) 289.
[18] R. Appelqvist, G. Marko-Varga, L. Gorton, A. Torstensson and G. Johansson, *Anal. Chim. Acta*, 169 (1985) 237.
[19] IUBMB, *Enzyme Nomenclature*, Academic Press, San Diego, CA, 1992.
[20] B. Malmström G., L.-E. Andreasson and B. Reinhammar, in P. D. Boyer (Editor), *Copper-Containing Oxidases and Superoxide Dismutase*, Vol. 12B, Academic Press, New York, 1975, 507.
[21] N. H. Horowitz, M. Fling and G. Horn, *Methods Enzymol.*, 17A (1970) 615.
[22] L. Macholán and I. Boháčková, *Biológia (Bratislava)*, 43 (1988) 1121.
[23] G.F. Hall, D.J. Best and A.P.F. Turner, *Anal. Chim. Acta*, 213 (1988) 113.
[24] M. Bonakdar, J.L. Vilchez and H.A. Mottola, *J. Electroanal. Chem.*, 266 (1989) 47.
[25] V. Kacaniklic, K. Johansson, G. Marko-Varga, L. Gorton, G. Jönsson-Pettersson and E. Csöregi, *Biosens. Bioelectr.*, in press.
[26] B.J.B. Wood and L.L. Ingraham, *Nature*, 205 (1965) 291.
[27] K. Zachariah and A. Mottola, *Anal. Lett.*, 22 (1989) 1145.

[28] C. Laane, S. Boeren, R. Hilhorst and C. Veeger, in J. Tramper, H.C. Van der Plas and P. Linko (Editors), *Biocatalysis in Organic Synthesis*, Elsevier, Amsterdam, 1985, p. 65.
[29] M. Reslow, P. Adlercreutz and B. Mattiasson, *Eur. J. Biochem.*, 172 (1988) 573.
[30] A. M. Klibanov, *Trends Biochem. Sci.*, 14 (1989) 141.
[31] K. Martinek, N.L. Klyachko, A.V. Kabanov, Y.L. Khmelnitsky and A.V. Levashov, *Biochim. Biophys. Acta*, 981 (1989) 161.
[32] S.H.M. van Erp, E.O. Kamenskaya and Y.L. Khmelnitsky, *Eur. J. Biochem.*, 202 (1991) 379.
[33] E. Wehtje, P. Adlercreutz and B. Mattiasson, *Biotechnol. Bioeng.*, 41 (1993) 171.
[34] F. Ortega, J.L. Cuevas, J.I. Centenera and E. Domínguez, *J. Pharm. Biomed. Anal. Chem.*, 10 (1992) 789.
[35] B. Persson, *Ph.D. Thesis*, University of Lund, Lund, 1990.
[36] J.A. Osborn, R.M. Ianniello, H.J. Wieck, T.F. Decker, S.L. Gordon and A.M. Yacynych, *Biotechnol. Bioeng.*, 24 (1982) 1653.
[37] C.C. Painton and H.A. Mottola, *Anal. Chim. Acta*, 154 (1983) 1.
[38] H.O. Finklea, S. Avery, M. Lynch and T. Furtsch, *Langmuir*, 3 (1987) 409.
[39] M. Gómez, J. Li and A.E. Kaifer, *Langmuir*, 7 (1991) 1797.
[40] R.E. Panzer and P.J. Elving, *J. Electrochem. Soc.*, 119 (1972) 864.
[41] M. Skoog, K. Kronkvist and G. Johansson, *Anal. Chim. Acta*, 269 (1992) 59.

ELSEVIER

Journal of Chromatography A, 675 (1994) 79–88

JOURNAL OF CHROMATOGRAPHY A

Resolution of enantiomers of alcohols and amines by high-performance liquid chromatography after derivatization with a novel fluorescent chiral reagent

Toshimasa Toyo'oka*,[a], Yi-Ming Liu[a], Nobumitsu Hanioka[a], Hideto Jinno[a], Masanori Ando[a], Kazuhiro Imai[b]

[a]*Division of Environmental Chemistry, National Institute of Health Sciences, 1-18-1 Kamiyoga, Setagaya-ku, Tokyo 158, Japan*
[b]*Faculty of Pharmaceutical Sciences, University of Tokyo, 7-3-1 Hongo, Bunkyo-ku, Tokyo 113, Japan*

(First received January 11th, 1994; revised manuscript received March 25th, 1994)

Abstract

4-(2-Chloroformylpyrrolidin-1-yl)-7-nitro-2,1,3-benzoxadiazole [*R*(+)-NBD-Pro-COCl and *S*(−)-NBD-Pro-COCl], optically active tagging reagents, have been synthesized for resolution of enantiomers of amines and alcohols by high-performance liquid chromatography. The reagents react with amino and hydroxyl functional groups in the presence of pyridine to produce the corresponding diastereomers. The optimum excitation and emission wavelengths for the diastereomers in water–acetonitrile (1:1) were approximately 485 nm and 530 nm, respectively. The excitation and emission wavelengths were independent of the amine or alcohol portion of the diastereomer. The resulting diastereomers can usually be efficiently resolved by normal-phase chromatography with *n*-hexane–ethyl acetate as the eluent. When *R*(+)-NBD-Pro-COCl was used as the derivatization reagent, the diastereomers corresponding to the *R*-configurations of amines and alcohols were eluted faster than those from the *S*-configuration. The elution order was reversed when the diastereomers were prepared with *S*(−)-NBD-Pro-COCl. The R_s values of the diastereomers derived from amines and alcohols by normal-phase chromatography are in the range of 3.23–4.32 and 2.99–4.10, respectively. After derivatization with NBD-Pro-COCls the alcohol enantiomers were also separated adequately by a reversed-phase column with a water–acetonitrile mixture.

1. Introduction

High-performance liquid chromatography (HPLC) has been widely accepted for the resolution of chiral molecules [1,2]. The resolution of racemates can be done with chiral stationary phase (CSP) columns. The different types of CSPs have been classified as follows: (1) chiral ligand exchange phases [3], (2) affinity phases [4,5], (3) helical polymer phases [6], (4) cavity phases [7,8] and (5) Pirkle-type phases [9]. Another HPLC technique employs formation of diastereomer with a chiral derivatization reagent [10]. Although the compounds having amino functional groups are easily derivatized with various reagents [11], many of the reagents do not have chiral properties [12–15]. The hydroxyl group is one of most difficult to derivatize due to

* Corresponding author. Present address: School of Pharmaceutical Sciences, University of Shizuoka, 52-1 Yada, Shizuoka 422, Japan.

0021-9673/94/$07.00
SSDI 0021-9673(94)00319-5

the limited reactivity and the relatively poor stability of the reagent and product [16–18]. Therefore, only a few reagents have been used for the resolution of chiral alcohols. There is a need for chiral reagents for alcohols and amines.

We have developed fluorescent chiral derivatization reagents [*S*(−)- and *R*(+) - 4 - (2 - chloroformylpyrrolidin - 1 - yl) - 7 - (N,N-dimethylaminosulfonyl) - 2,1,3-benzoxadiazole (DBD-Pro-COCl)] for alcohols and amines [19–21]. The enantiomers of some alcohols and amines were well separated by reversed-phase and/or normal-phase HPLC. The reagents are relatively stable and react readily with amines and alcohols. The fluorescence characteristics of the resulting diastereomers with excitation at approximately 450 nm and emission at approximately 560 nm are another advantage because these long wavelengths reduce the likelihood of interference. Although the detection limits (10–50 fmol levels) of the method with DBD-Pro-COCl is not superior to that of other methods, detection is improved with use of an argon-ion laser at 488 nm [20].

The objectives of this work were the synthesis of the chiral derivatization reagents [*S*(−)- and *R*(+)-enantiomers of NBD-Pro-COCl], evaluation of their reactivities toward alcohols and amines and the study of the fluorescence characteristics of the resulting diastereomers. HPLC separations of the diastereomers were also investigated by normal-phase and reversed-phase chromatography.

2. Experimental

2.1. Materials and reagents

4-Fluoro-7-nitro-2,1,3-benzoxadiazole (NBD-F) was purchased from Wako Pure Chemicals (Osaka, Japan). 4-(2-Carboxypyrrolidin-1-yl)-7-nitro-2,1,3-benzoxadiazoles [*R*(+)- and *S*(−)-NBD-Pros] were synthesized as previously described [22]. Prolines [*R*(+)- and *S*(−)-enantiomers] were obtained from Sigma (St. Louis, MO, USA). Enantiomers of 2-hexanol, 2-heptanol, 2-nonanol, 1-phenylethanol, 1-(1-naphtyl)-ethylamine (NEA) and 1-phenylethylamine (PEA) were obtained from Wako. Enantiomers of 1-cyclohexylethylamine (CEA) (Fluka, Buchs, Switzerland), oxalyl chloride (Tokyo Kasei, Tokyo, Japan), methylamine (abs. 30% sol.) and pyridine (Wako) were used as received. Ethyl acetate (AcOEt), *n*-hexane, benzene, acetonitrile and water were of HPLC grade (Wako). All other chemicals were of analytical-reagent grade and were used without further purification.

2.2. Apparatus

Proton nuclear magnetic resonance (^{1}H NMR) spectra were recorded on a Varian Jemini-300 (Palo Alto, CA, USA) at 300 MHz using tetramethylsilane (0.00 ppm) as the internal standard. For describing NMR characteristics, the following abbreviations are used: s = singlet, d = doublet, m = multiplet and br = broad. Mass spectra (MS) were recorded on JEOL DX-300 [70 eV, electron-impact ionization (EI)] mass spectrometer (Tokyo, Japan). Infrared spectra were measured using potassium bromide (KBr) discs with a Shimadzu Model IR-460 (Kyoto, Japan). For measurement of excitation and emission spectra, a Hitachi 650-60 fluorescence spectrometer with a 1-cm quartz cell was employed without spectral correction. Optical rotations were measured on a DIP-370 Digital Polarimeter (JASCO, Tokyo, Japan) with 50 × 3.5 mm I.D. cylindrical cell. Melting points (mp) were measured by a Yanagimoto micro melting point apparatus (Tokyo, Japan).

The high-performance liquid chromatograph consisted of two LC-10AD pumps (Shimadzu) and an SCL-10A system controller (Shimadzu). Sample solutions were injected with a SIL-10A auto injector (Shimadzu). The analytical columns were an Inertsil ODS-80A (150 × 4.6 mm I.D., 5 μm) for reversed-phase chromatography and an Inertsil SIL (150 × 4.6 mm I.D., 5 μm) (GL Sciences, Tokyo, Japan) for normal-phase chromatography. The columns were maintained at 40°C with a CTO-10AC column oven (Shimadzu). A Shimadzu RF-10A fluorescence monitor equipped with a 12-μl flow cell was

employed for the detection. The excitation and emission wavelengths were fixed at 485 nm and 530 nm, respectively. The peak areas obtained from the fluorescence monitor were calculated with a C-R7A chromatopac (Shimadzu). All mobile phases were de-gassed with an on-line degasser (DGU-3A, Shimadzu). The flow rate of the eluent was 1.0 ml/min.

2.3. Synthesis of the chiral derivatization reagents

To *S*(−)-4-(2-carboxypyrrolidin-1-yl)-7-nitro-2,1,3-benzoxadiazole [*S*(−)-NBD-Pro] (2.6 g, 9.3 mmol) dissolved in 200 ml of anhydrous dichloromethane was added 10 ml of oxalyl chloride and 0.2 ml of dimethylformamide (DMF). The mixture was stirred for 60 min at room temperature. The solvent was evaporated *in vacuo*. The crystalline precipitate obtained was immediately dissolved in 100 ml of anhydrous benzene and the undissolved materials were filtered off. The filtrate solution was then evaporated under reduced pressure. The remaining crystals were dried in a vacuum desiccator over phosphorous pentoxide (P_2O_5).

S(−)-4-(2-Chloroformylpyrrolidin-1-yl)-7-nitro-2,1,3-benzoxadiazole [*S*(−)-NBD-Pro-COCl]: red-orange crystals; mp. 103–104°C (decomp.); yield 2.4 g (87%); NMR (ppm) in $CDCl_3$, 8.44 (1H, d, $J = 8.9$ Hz, a), 6.17 (1H, d, $J = 8.9$ Hz, b), 5.67 (1H, br, c), 3.86 (2H, br, d), 2.56–2.70 (2H, m, e), 2.14–2.39 (2H, m, f); EI-MS, m/z 296 (M^+); IR (KBr) 1794, 1615, 1555, 1495, 1447, 1325, 1154, 1111, 999, 959, and 708 cm^{-1}; $[\alpha]_D^{20}$ −204.2°, $c = 0.43$ in $CHCl_3$; Analysis: calculated for $C_{11}H_9N_4O_4Cl$, C 44.53, H 3.06, N 18.88; found, C 44.48, H 2.87, N 18.30.

R(+)-4-(2-Chloroformylpyrrolidin-1-yl)-7-nitro-2,1,3-benzoxadiazole [*R*(+)-NBD-Pro-COCl] was also obtained from the reaction of *R*(+)-4-(2-carboxypyrrolidin-1-yl)-7-nitro-2,1,3-benzoxadiazole [*R*(+)-NBD-Pro] and oxalyl chloride in the same manner described above.

R(+)-NBD-Pro-COCl: yield 2.4 g (87%), $[\alpha]_D^{20}$ +208.5°, $c = 0.45$ in $CHCl_3$; Analysis: calculated for $C_{11}H_9N_4O_4Cl$, C 44.53, H 3.06, N 18.88; found, C 44.83, H 2.92, N 18.49. Other instrumental data were the same as those of *S*(−)-NBD-Pro-COCl.

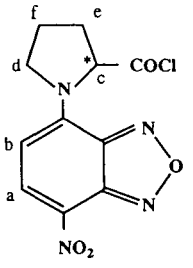

NBD-Pro-COCl

2.4. Reactivity of optically active NBD-Pro-COCl with alcohol and amine enantiomers

Amounts of 50 μl of 10 m*M* NBD-Pro-COCl [*R*(+)- or *S*(−)-enantiomer] in anhydrous benzene, and 50 μl of 2-heptanol or 1-(1-naphtyl)ethylamine (1 m*M* of each enantiomer) in anhydrous benzene containing 2% pyridine were mixed in a 1.5-ml mini-vial (GL Science). The vials were tightly capped and heated for 4 h at 80°C (for derivatization of alcohols) or 50°C (for derivatization of amines). After the fixed time intervals, a vial was removed from the dry heat block, and cooled in ice-water (0–5°C). The reaction was quenched by the addition of 0.9 ml of 1% methylamine in acetonitrile. An aliquot (5 μl) of the diluted solution was automatically injected into an Inertsil ODS-80A, and the fluorescence peak area of the resulting diastereomer was calculated with an integrator. The reagent blanks without alcohols or amines were treated in the same manner.

2.5. HPLC separation of the diastereomers derived from the enantiomers of alcohols or amines

The enantiomers (*ca.* 1 mg each) of alcohols (or amines) were reacted at 80°C (or 50°C) with NBD-Pro-COCl [1 m*M* *R*(+)- or *S*(−)-enantio-

mer] in 1 ml of anhydrous benzene in the presence of 1% pyridine. After 1 h, an aliquot (5 μl) of the solution was injected into Inertsil ODS-80A (reversed-phase column) and Inertsil SIL (normal-phase column). The eluents for reversed-phase and normal-phase chromatography are water–acetonitrile and *n*-hexane–ethyl acetate, respectively. The capacity factor (k'), separation factor (α) and the resolution value (R_s) were calculated from the following equations, respectively.

$$k' = (t_R - t_0)/t_0,\ \alpha = k_2'/k_1',$$
$$R_s = 2(t_{R2} - t_{R1})/(w_1 + w_2)$$

where t_R, t_{R1} and t_{R2} are retention times of the peaks and t_0 is the dead time of the column ($t = 1.3$ min); w_1 and w_2 are the widths of the bases formed by triangulation of the peaks.

For the fluorescent spectra measurements, 50 μl of the solution was injected onto the column and the peak corresponding to the alcohol or amine derivative was collected from outlet of the detector (*ca.* 2-ml portion).

3. Results and discussion

3.1. Synthesis of NBD-Pro-COCl

DBD-Pro-COCls were synthesized from DBD-Pro enantiomers with PCl_5, as described in a previous paper [19]. The yields of *ca.* 60% were adequate, however, oxalyl chloride provided quantitative yields of the acid chlorides. Therefore, oxalyl chloride was also employed for the synthesis of NBD-Pro-COCls [*R*(+)- and *S*(−)-isomers].

Fig. 1 shows the synthetic pathway of the chiral derivatization reagents and the subsequent reactions with enantiomers of alcohols and amines. The direction of the optical rotation of the chiral reagents are the same as those of the starting materials, NBD-Pros. NBD-Pro-COCls and DBD-Pro-COCls are fairly stable as solids. No degradation was observed after storage of three months at 5°C in a refrigerator. As with other acid chloride type reagents reported previously, these reagents gradually decomposed in solution to produce corresponding acids, NBD-

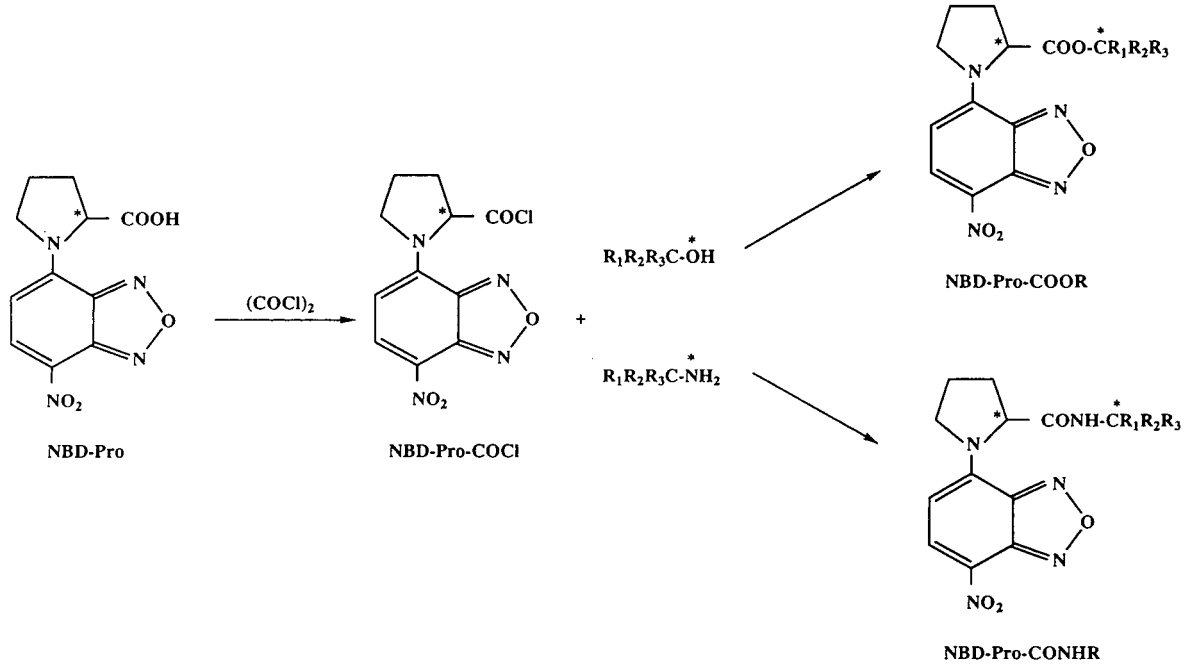

Fig. 1. Synthesis of the chiral derivatization reagents and preparation of diastereomers.

Pro and DBD-Pro. The rates were faster in benzene containing pyridine than without pyridine. Therefore, the reagent solutions should be prepared just prior to use.

Since high optical purity of the tagging reagent is required for the determination of trace amounts of the antipode enantiomer in the presence of a large amount of the enantiomer, the determination of the optical purity of the reagents synthesized was attempted by HPLC with utilizing a few CSP columns such as modified β-cyclodextrin and cellulose as the sorbents. However, the complete separations allowing the determination of the optical purity were not achieved. The limited stability of the reagents in solution is one of difficulties in the analyses. Since no measurable peaks derived from antipode enantiomers are obtained from each pair of the reagents, the optical purities of these reagents seem to be good enough for the determination of racemic alcohols and amines.

3.2. Fluorescence characteristics of the diastereomers

The fluorescence excitation and emission spectra of the diastereomers were measured in acetonitrile–water (1:1). The excitation and emission maxima of the diastereomers derived from amines and alcohols are essentially the same (*ca.* 485 nm and 530 nm, respectively). The results suggest that the fluorescent properties of the diastereomers are dominated by the NBD-Pro structure and independent of the structures of the alcohol or amine analytes. Excitation and emission at long wavelengths provide a distinct advantage in biological samples because there is negligible interference by sample co-extractives, which have no amino and hydroxyl functional groups in the structure.

3.3. Derivatization

As described in our previous work [20], optimal conditions with DBD-Pro-COCls were selected after studies of various parameters affecting the derivatization reaction. The same solvent (benzene), catalyst (pyridine) and temperatures (80 or 50°C) were adopted in the following studies because the reactive site of NBD-Pro-COCl is same of that of DBD-Pro-COCl. The effects of the functional groups (nitro and dimethylaminosufnonyl) at the 7-position of 2,1,3-benzoxadiazole were expected to be negligible. Toluene in the presence of pyridine can also be replaced, instead of the highly toxic benzene. Judging from the results in the previous works [19–21] with DBD-Pro-COCls, it was anticipated that the derivatization of alcohols with NBD-Pro-COCls would be more difficult than the derivatization of amines. In addition, it was necessary to test the reactivity of each reagent enantiomer toward each enantiomer of the chiral molecules because differences in reactivity could give mixtures of diastereomers that would not accurately reflect the isomeric composition. The reactivities of the optically active reagents [*S*(−)- and *R*(+)-NBD-Pro-COCls] toward 2-heptanol and NEA, which were selected as the representative enantiomers of alcohols and amines, were examined separately in benzene solution containing 1% pyridine.

Figs. 2 and 3 show the results of time course studies with 2-heptanol at 80°C and NEA at 50°C. As shown in Fig. 2, the formation of the

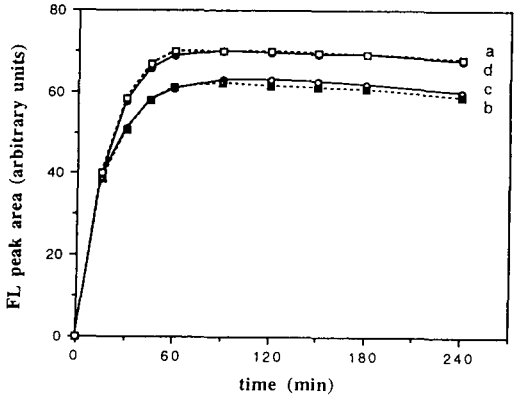

Fig. 2. Time course of diasteromer formations corresponding to 2-heptanol enantiomers with NBD-Pro-COCls at 80°C in benzene containing 1% pyridine. (a) Reaction of *S*(+)-2-heptanol with *R*(+)-NBD-Pro-COCl; (b) *R*(−)-2-heptanol with *R*(+)-NBD-Pro-COCl; (c) *S*(+)-2-heptanol with *S*(−)-NBD-Pro-COCl; (d) *R*(−)-2-heptanol with *S*(−)-NBD-Pro-COCl. HPLC eluent, H_2O–CH_3CN (35:65); other HPLC conditions as in Experimental.

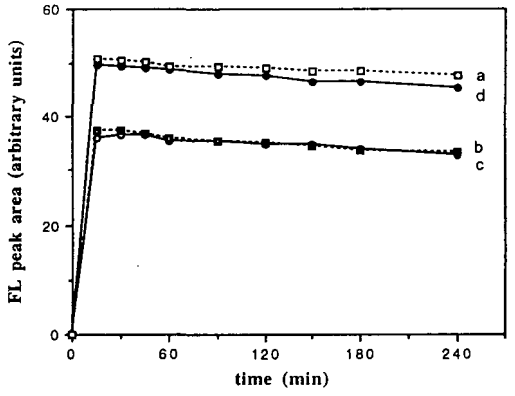

Fig. 3. Time course of diasteromer formations corresponding to NEA enantiomers with NBD-Pro-COCls at 50°C in benzene containing 1% pyridine. (a) Reaction of *S*(−)-NEA with *R*(+)-NBD-Pro-COCl; (b) *R*(+)-NEA with *R*(+)-NBD-Pro-COCl; (c) *S*(−)-NEA with *S*(−)-NBD-Pro-COCl; (d) *R*(+)-NEA with *S*(−)-NBD-Pro-COCl. HPLC eluent, H_2O–CH_3CN (55:45); other HPLC conditions as in Experimental.

diastereomers corresponding to both enantiomers of 2-heptanol increased with heating time and was essentially complete after 90 min. The peak area of the diastereomer, derived from *R*(+)-NBD-Pro-COCl and *S*(+)-2-heptanol, was approximately 10% larger than that of other diastereomer. Similar high intensity was confirmed with the diastereomers derived from *S*(−)-NBD-Pro-COCl and *R*(−)-2-heptanol. Figs. 2 and 3 illustrate that the reaction rates of the NEA isomers with NBD-Pro-COCls were obviously faster than those of 2-heptanol. The reactions were completed after 15 min, even at the temperature of 50°C (Fig. 3). A steady decrease in the peak areas with time was observed for both enantiomers of the reagent. Similar phenomena were observed in the reaction of amine with the reagent. Judging from the curves in Figs. 2 and 3, the derivatives of alcohols and amines seem to be fairly stable. However, exact figures for the stability of the derivatives cannot be given because authentic derivatives are not synthesized yet. The peak areas of the diastereomers, derived from *R*(+)-NBD-Pro-COCl and *S*(−)-NEA or *S*(−)-NBD-Pro-COCl and *R*(+)-NEA, were *ca.* 25% larger than the other diastereomers. The difference of peak areas might be due to the difference of fluorescence quantum yield (ϕ) of the resulting diastereomers. Judging from the reaction curves in Figs. 2 and 3, the reactivities of NBD-Pro-COCls seem to be essentially the same for both enantiomers. Consequently, a 2-h reaction period at 80°C was selected for the derivatization of alcohols and a 30-min reaction period at 50°C in benzene containing 1% pyridine was adopted for the amines.

3.4. HPLC separation of resulting diastereomers

Since intermolecular hydrogen bonding between the derivative and the stationary phase not only contributes to fixation of the conformation, but is also important for the efficient resolution of the diastereomers, the normal-phase column is generally employed together with non-polar organic solvents as a mobile phase. As shown in a previous report [19] some alcohols labelled with DBD-Pro-COCl were well resolved by a silica-gel column with *n*-hexane–ethyl acetate mixture (R_s 3.34–4.48). However, the separations of the diastereomers derived from amines were poor (*e.g.* R_s of PEA, 1.19) [21]. Initially, the separations of each pair of amines labelled with NBD-Pro-COCl were attempted by normal-phase chromatography. The capacity factors (k'), separation factors (α) and resolution values (R_s) for the diastereomers are listed in Table 1. Three amines tested were well resolved by Inertsil SIL column with *n*-hexane–ethyl acetate (55:45) (R_s 3.23–4.32). Both values of R_s and α were independent of the amine. The R_s values obtained with the proposed reagent were higher than those achieved with DBD-Pro-COCl. Similar good resolution was also obtained with the diastereomers of the alcohols (Table 2). The R_s values (2.99–4.10) were slightly smaller than those with DBD-Pro-COCl (R_s 3.23–4.32) [19]. R_s values obtained with the alcohols having greater hydrophobicity, *e.g.* 2-nonanol, were larger than those for alcohols having higher hydrophilicity, *e.g.* 2-hexanol. When *S*(−)-NBD-Pro-COCl was used as the chiral derivatization reagent, the corresponding diastereomers of the *S*-enantiomers of the amines and alcohols

Table 1
HPLC separation of diastereomers derived from S(−)-NBD-Pro-COCl by normal-phase chromatography

Amine	S-enantiomer		R-enantiomer		α	R_s	Eluent
	t_R (min)	k'	t_R (min)	k'			
PEA	10.29	6.91	13.51	9.39	1.36	3.14	A
	13.66	9.51	18.19	12.99	1.37	3.78	B
	19.03	13.64	25.63	18.71	1.37	4.32	C
NEA	8.21	5.32	10.12	6.79	1.28	2.32	A
	10.59	7.15	13.22	9.17	1.28	2.77	B
	14.54	10.19	18.26	13.04	1.28	3.23	C
CEA	9.22	6.09	11.45	7.81	1.28	2.35	A
	11.63	7.94	14.64	10.27	1.29	2.75	B
	15.73	11.10	19.98	14.37	1.29	3.27	C

Column, Inertsil SIL (150 × 4.6 mm I.D., 5 μm) at 40°C; eluent A, *n*-hexane–AcOEt (45:55); eluent B, *n*-hexane–AcOEt (50:50); eluent C, *n*-hexane–AcOEt (55:45); flow rate, 1.0 ml/min, fluorescence detection, ex. 470 nm, em. 540 nm; t_0 = 1.3 min.

elute more rapidly than the *R*-enantiomers. The opposite results were obtained from usage of *R*(+)-DBD-Pro-COCl. No exceptions were observed among all pairs of enantiomers tested. Typical normal-phase chromatograms of the diastereomers formed with *S*(−)-NBD-Pro-COCl are depicted in Fig. 4. The polar compounds, including the hydrolysate of the derivatization reagent, eluted later than the diastereomers. Although the complete resolutions of the enantiomers of amines and alcohols were achieved by normal-phase chromatography, this technique may not be suitable for biological specimens because of sample handling difficulties. There-

Table 2
HPLC separation of diastereomers derived from *R*(+)-NBD-Pro-COCl by normal-phase chromatography

Alcohol	S-enantiomer		R-enantiomer		α	R_s	Eluent
	t_R (min)	k'	t_R (min)	k'			
2-Hexanol	8.64	5.65	7.48	4.75	1.19	1.73	A
	11.92	8.17	10.17	6.82	1.20	2.33	B
	18.17	12.98	15.33	10.80	1.20	2.99	C
2-Heptanol	8.28	5.37	7.01	4.40	1.22	2.10	A
	11.37	7.75	9.47	6.29	1.23	2.45	B
	17.24	12.26	14.14	9.88	1.24	3.26	C
2-Nonanol	7.74	4.95	6.43	3.95	1.25	2.17	A
	10.60	7.16	8.64	5.65	1.27	2.62	B
	15.93	11.26	12.76	8.82	1.28	3.39	C
1-Phenylethanol	12.26	8.43	10.34	6.95	1.21	2.56	A
	17.91	12.78	14.81	10.39	1.23	3.26	B
	28.55	20.96	23.32	16.94	1.24	4.10	C
	5.80	3.46	5.15	2.96	1.17	1.24	D

Column, Inertsil SIL (150 × 4.6 mm I.D., 5 μm) at 40°C; eluent A, *n*-hexane–AcOEt (70:30); eluent B, *n*-hexane–AcOEt (75:25); eluent C, *n*-hexane–AcOEt (80:20); eluent D, *n*-hexane–AcOEt (55:45); flow rate, 1.0 ml/min; fluorescence detection, ex. 470 nm, em. 540 nm; t_0 = 1.3 min.

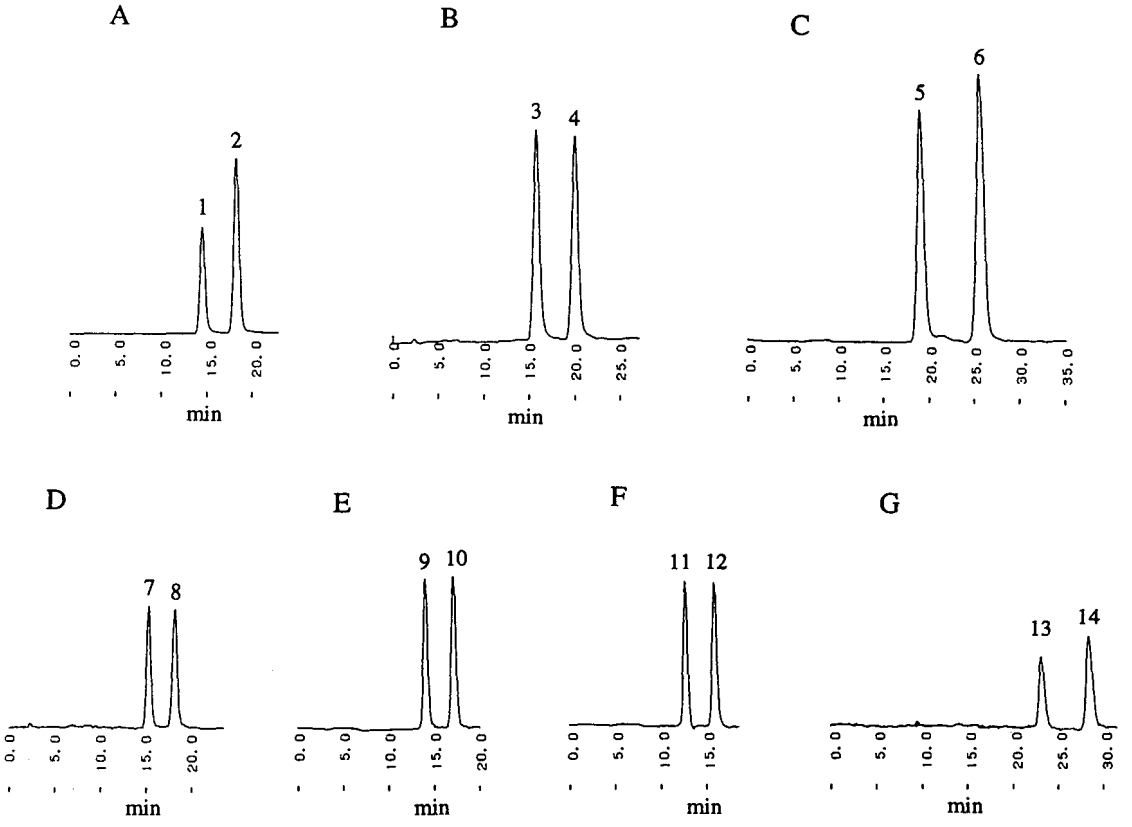

Fig. 4. Chromatograms obtained from the reaction with *S*(−)-NBD-Pro-COCl by normal-phase chromatography. Separation of the resulting diastereomers: (A) NEA; (B) CEA; (C) PEA; (D) 2-hexanol; (E) 2-heptanol; (F) 2-nonanol; (G) 1-phenylethanol. Peaks: 1 = *S*(−)-NEA, 2 = *R*(+)-NEA, 3 = *S*(+)-CEA, 4 = *R*(−)-CEA, 5 = *S*(−)-PEA, 6 = *R*(+)-PEA, 7 = *S*(+)-2-hexanol, 8 = *R*(−)-2-hexanol, 9 = *S*(+)-2-heptanol, 10 = *R*(−)-2-heptanol, 11 = *S*(+)-2-nonanol, 12 = *R*(−)-2-nonanol, 13 = *S*(−)-1-phenylethanol, 14 = *R*(+)-1-phenylethanol. HPLC eluent: *n*-hexane–benzene (55:45) for chromatograms A, B and C; *n*-hexane–benzene (80:20) for chromatograms D, E, F and G. Other HPLC conditions as in Experimental.

fore, the analysis by reversed-phase chromatography with aqueous solvent system was also investigated.

As shown in Table 3, the separation of the diastereomers derived from PEA was incomplete by reversed-phase chromatography; while no separation of the diastereomers obtained from CEA was achieved. Only NEA was resolved, but the R_s value was small (1.65), as compared with normal-phase HPLC. In the case of DBD-Pro-COCl, the R_s values obtained from reversed-phase chromatography were in the following order: CEA > NEA > PEA [21]. On the other hand, the resolution of all pairs of the diastereomers formed from alcohols were perfectly separated (1.55–1.99) (Table 4). However, the R_s values were smaller than those obtained from normal-phase chromatography. The results described above suggest that the formation of hydrogen bonds between the stationary phases and the resulting diastereomers play important roles in the separations. The elution orders were the same as those by normal-phase chromatography, *S*-enantiomers eluted faster than *R*-enantiomers with use of *S*(−)-NBD-Pro-COCl and *R*-enantiomers eluted faster than *S*-enantiomers with use of *R*(+)-NBD-Pro-COCl.

The proposed chiral derivatization reagents [*S*(−)- and *R*(+)-NBD-Pro-COCls] provided excellent resolution of the enantiomers of amines

Table 3
HPLC separation of diastereomers derived from S(−)-NBD-Pro-COCl by reversed-phase chromatography

Amine	S-enantiomer		R-enantiomer		α	R_s	Eluent
	t_R (min)	k′	t_R (min)	k′			
PEA	5.45	3.19	5.24	3.03	1.05	0.42	A
	7.74	4.96	7.35	4.66	1.06	0.77	B
	11.87	8.13	11.87	8.13	1.0	NC [a]	C
NEA	9.58	6.37	9.12	6.02	1.06	0.88	A
	15.58	10.98	14.58	10.21	1.08	1.28	B
	26.68	19.52	24.64	1.96	1.09	1.65	C
CEA	15.46	10.89	15.46	10.89	1.0	NC	B
	26.24	19.19	26.08	19.06	1.01	NC	C

Column, Inertsil ODS-80A (150 × 4.6 mm I.D., 5 μm) at 40°C; eluent A, H_2O–CH_3CN (50:50); eluent B, H_2O–CH_3CN (55:45); eluent C, H_2O–CH_3CN (60:40); flow rate, 1.0 ml/min; fluorescence detection, ex. 470 nm, em. 540 nm; t_0 = 1.3 min
[a] NC = not calculated.

and alcohols by normal-phase and/or reversed-phase HPLC. NBD-Pro-COCl is recommended for the resolution of chiral amines. For the resolution of alcohols, DBD-Pro-COCl might be more suitable judging from the R_s values by normal-phase chromatography (2.99–4.10 *vs.* 3.34–4.48). However, it must be noted that the diastereomers derived from all alcohols and NBD-Pro-COCl can be separated by reversed-phase chromatography. Since the elution order of enantiomers can be changed with the use of the different enantiomer of the chiral reagents

Table 4
HPLC separation of diastereomers derived from R(+)-NBD-Pro-COCl by reversed-phase chromatography

Alcohol	S-enantiomer		R-enantiomer		α	R_s	Eluent
	t_R (min)	k′	t_R (min)	k′			
2-Hexanol	5.90	3.54	5.90	3.54	1.0	NC [a]	E
	7.99	5.15	7.72	4.94	1.04	0.48	F
	11.42	7.79	10.95	7.43	1.05	0.85	A
	17.38	12.37	16.56	11.74	1.05	1.20	B
	28.02	20.55	26.54	19.42	1.06	1.55	C
2-Heptanol	7.75	4.97	7.46	4.74	1.05	0.49	E
	10.98	7.75	10.49	7.07	1.05	0.86	F
	16.39	11.61	15.56	10.97	1.06	1.23	A
	26.17	19.13	24.65	17.96	1.07	1.73	B
	44.39	33.15	41.55	30.96	1.07	1.90	C
2-Nonanol	14.45	10.12	13.67	9.52	1.06	1.25	E
	22.18	16.06	20.85	15.04	1.07	1.61	F
	35.89	26.61	33.51	24.78	1.07	1.99	A
1-Phenylethanol	10.19	6.84	9.81	6.54	1.05	0.66	B
	15.68	11.06	14.92	10.48	1.06	1.17	C
	26.66	19.51	24.99	18.23	1.07	1.75	D

Column, Inertsil ODS-80A (150 × 4.6 mm I.D., 5 μm) at 40°C; eluent A, H_2O–CH_3CN (40:60); eluent B, H_2O–CH_3CN (45:55); eluent C, H_2O–CH_3CN (50:50); eluent D, H_2O–CH_3CN (55:45); eluent E, H_2O–CH_3CN (30:70); eluent F, H_2O–CH_3CN (35:65); flow rate, 1.0 ml/min; fluorescence detection, ex. 470 nm, em. 540 nm; t_0 = 1.3 min
[a] NC = not calculated.

[23,24], the determination of trace amounts of one enantiomer in the presence of much greater amount of the other enantiomer is easily accomplished. The detection limits of the alcohols are in the 10–50 fmol range. Since the excitation wavelengths of the derivatives are close to the argon-ion laser light emission, the determination of the enantiomers of alcohols and amines at attomole level should be possible with laser-induced fluorescence detection [25]. Hence, the proposed method with pre-column derivatization with NBD-Pro-COCl should be suitable for the resolution of chiral amines and alcohols in real samples as is the case with DBD-Pro-COCl. Further studies concerning the resolution of racemic drugs such as β-blockers and herbicides are currently in progress.

Acknowledgement

The authors thank Dr. C.R. Warner, Food and Drug Administration in Washington, DC, for reviewing the manuscript.

References

[1] M. Zief and L.J. Crane (Editors), *Chromatographic Chiral Separation*, Marcel Dekker, New York, 1988.
[2] A.M. Krstulovic (Editor), *Chiral Separation by HPLC*, Ellis Horwood, Chichester, 1989.
[3] G. Gubitz, W. Jellenz and W. Santi, *J. Chromatogr.*, 203 (1981) 377.
[4] S. Allenmark, *Biochem. Biophys. Methods*, 9 (1984) 1.
[5] J. Hermansson, *J. Chromatogr.*, 269 (1983) 71.
[6] Y. Okamoto, *Chemtech*, (1987) 176.
[7] R. Dappen, H. Arm and V.R. Meyer, *J. Chromatogr.*, 373 (1986) 1.
[8] I.W. Wainer and D.E. Drayer (Editors), *Drug Stereochemistry*, Marcel Dekker, New York, 1988.
[9] W.H. Pirkle and T.C. Pochapsky, *Advan. Chromatogr.*, 27 (1987) 73.
[10] R.H. Buch and K. Krummen, *J. Chromatogr.*, 315 (1984) 279.
[11] K. Imai and T. Toyo'oka, in R.W. Frei and K. Zech, (Editors), *Selective Sample Handling and Detection in High-performance Liquid Chromatography (J. Chromatogr. Library*, Vol. 39A), Elsevier, Amsterdam, 1988, p. 209.
[12] J. Goto, M. Hasegawa, S. Nakamura, K. Shimada and T. Nambara, *J. Chromatogr.*, 152 (1978) 413.
[13] D.W. Aswad, *Anal. Biochem.*, 137 (1984) 405.
[14] N. Nimura and T. Kinoshita, *J. Chromatogr.*, 352 (1986) 169.
[15] J. Goto, N. Goto, A. Hikichi and T. Nambara, *J. Liq. Chromatogr.*, 2 (1979) 1179.
[16] K. Sasaki and H. Hirata, *J. Chromatogr.*, 585 (1991) 117.
[17] J. Goto, N. Goto, G. Shao, M. Ito, A. Hongo, S. Nakamura and T. Nambara, *Anal. Sci.*, 6 (1990) 261.
[18] J. Goto, G. Shao, M. Ito, T. Kuriki and T. Nambara, *Anal. Sci.*, 7 (1991) 723.
[19] T. Toyo'oka, M. Ishibashi, T. Terao and K. Imai, *Analyst*, 118 (1993) 759.
[20] T. Toyo'oka, Y.-M. Liu, N. Hanioka, H. Jinno and M. Ando, *Anal. Chim. Acta*, 285 (1994) 343.
[21] T. Toyo'oka, Y.-M. Liu, H. Jinno, N. Hanioka and M. Ando, *Biomed. Chromatogr.*, in press.
[22] T. Toyo'oka, Y. Watanabe and K. Imai, *Anal. Chim. Acta*, 149 (1983) 305.
[23] T. Toyo'oka, M. Ishibashi and T. Terao, *Analyst*, 117 (1992) 727.
[24] T. Toyo'oka, M. Ishibashi and T. Terao, *Anal. Chim. Acta*, 278 (1993) 71.
[25] T. Toyo'oka, M. Ishibashi and T. Terao, *J. Chromatogr.*, 625 (1992) 357.

ELSEVIER

Journal of Chromatography A, 675 (1994) 89–100

JOURNAL OF CHROMATOGRAPHY A

Purification of simian immunodeficiency virus, SIV_{MAC251}, and of its external envelope glycoprotein, gp148☆

Gustav Gilljam[a], Kithmini Siridewa[b,c], Lena Hammar*[,b]

[a]*Department of Clinical Virology, Swedish Institute for Infectious Disease Control, Solna, Sweden*
[b]*Department of Veterinary Virology, Biomedical Center, Box 585, S-751 23 Uppsala, Sweden*
[c]*Department of Biochemistry and Molecular Biology, University of Colombo, Colombo, Sri Lanka*

(First received January 25th, 1994; revised manuscript received March 25th, 1994)

Abstract

Two-phase extraction in a system composed of dextran and polyethylene glycol was used to purify simian immunodeficiency virus, SIV_{MAC251} (*32H* isolate) from 25 l of culture supernatant. The virus partitioned to the interphase with 80% recovery of *gag* peptide p27 and reverse transcriptase and an about 25% recovery of the external *env* glycoprotein, gp148.

The virus was treated with octylglycoside and its subcomponents separated. Two *gag*-p27 containing fractions were obtained; *gag*-1, which also contained reverse transcriptase and nucleopeptides, and *gag*-2, which contained the major portion of the p27. The *env* gp148 was purified by chromatography through a series of lectin columns. The prepared materials are characterized by sodium dodecyl sulphate–polyacrylamide gel electrophoresis and immuno- and lectin blotting.

1. Introduction

In human immunodeficiency virus (HIV) and related viruses the *env* glycoproteins form protrusions from the envelope. These structures are essential for binding of the virus to the target cell and for the infection process, as discussed by Gelderblom [1]. The external *env* glycoprotein is non-covalently attached to the transmembrane glycoprotein and is easily shed into the surrounding medium. After ultracentrifugation its recovery in the virion fraction is usually poor [2,3]. This is probably due to shear forces developing during high spin. Similar labile "knob and socket" mechanisms linking the *env* proteins applies to several retroviruses [4]. Different structural changes occur on release of the external glycoprotein [5,6]. Therefore, in the purification of virus for functional studies, or for use as reference material in vaccine studies, care should be taken to preserve these membrane structures.

In the search for suitable methods to purify retroviruses we tried extraction in aqueous polymer systems [7–11]. With several of the viruses tested we found systems yielding an increased recovery of the external glycoprotein, compared to high spin ultracentrifugation [7–9]. Faced with

* Corresponding author.

☆ Part of this material was presented at the *8th International Conference on Partitioning in Aqueous Two-Phase Systems, Leipzig, August 22–27, 1993.*

0021-9673/94/$07.00
SSDI 0021-9673(94)00313-X

the problem of purifying SIV_{MAC} and its external *env* glycoprotein, gp148, for use within an European Community (EC)-concerted research programme, European vaccine against AIDS (Programme EVA), we applied the two-phase technique to concentrate the virus [10,11]. Purification of gp148 directly from culture supernatant was recently reported [12]. In the present paper we use the virus, concentrated by two-phase extraction, as start material for purification of the glycoprotein.

2. Experimental

2.1. Virus production

Production of virus was established with the SIV_{MAC251} *32H* isolate in roller bottle cultures (500 ml/flask) of the human T-cell line *C8166*. The growth medium RPMI-1640, supplemented with 5% fetal calf serum, 2 m*M* L-glutamine, penicillin (100 IU/ml) and streptomycin (100 μg/l), in 4-(2-hydroxyethyl)-1-piperazineethanesulphonic acid (HEPES) buffer, pH 7.4, was used. The virus was harvested at peak production of reverse transcriptase, day 5 after infection. The flasks (roller bottles) used for culture of infected cells were left standing upright in the incubator the last night before virus harvest, to allow the cells to sediment to the bottom.

2.2. Detergents

Isotridecyl poly(ethylene glycol ether)$_n$ ($n = 7–8$) (ITDP), *n*-octylglucoside and Triton X-100 were from Boehringer Mannheim, Mannheim, Germany and Empigen BB + + (N-dodecyl-N,N-dimethylglycine) was from Calbiochem, La Jolla, CA, USA.

2.3. Monoclonal antibodies and immunochemicals

For analyses by enzyme-linked immunosorbent assay (ELISA) and immunoblot monoclonal antibodies against HIV-2 or SIV proteins were obtained from the Programme EVA (Dr. H. Holmes, NIBSC, Potters Bar, UK). The antibodies were KK33 reactive against the p27, KK7 reactive against the transmembrane glycoprotein, and KK8 and KK12 reactive against the gp148 [13]. For detection alkaline phosphatase or horseradish peroxidase conjugated goat anti-mouse IgG, blotting grade, from Bio-Rad Labs., Richmond, CA, USA, were used.

2.4. ELISA

gp148-ELISA

Polystyrene microtiter plates coated with GNA were used to bind SIV-gp148. The bound glycoprotein was quantified using a monoclonal antibody in a peroxidase-linked immunoassay according to Gilljam [12].

p27-ELISA

The antigen-capture ELISA of Thorstensson *et al.* [14] was used in combination with monoclonal antibody KK33 for detection of SIV-p27.

2.5. Lectin blot analysis

Lectin blotting was performed as earlier described [15,16]. Biotinylated lectins were from Boehringer Mannheim, Vector Labs. (Burlingame, CA, USA) and E-Y Labs. (San Mateo, CA, USA). For detection avidin and biotinylated alkaline phosphatase (ABC-AP kit) from Vector Labs. were used.

2.6. Chromatography gels and columns

Concanavalin A (Con A)-Sepharose and wheat germ agglutinin (WGA)-Sepharose were from Pharmacia, Uppsala, Sweden. These gels were packed, total volumes about 20 ml, in HR16/10 columns (Pharmacia). ProSep-GNA, the affinity column with *Galanthus nivalis* lectin (GNA, Boehringer Mannheim) coupled to pore glass beads (BioProcessing, Durham, UK) was prepared as described by Gilljam [12]. The beads were packed in an 3 × 1 cm column, total volume 2.4 ml. HiTrap-Albumin-Adsorption gel was kindly supplied by Marie Buhre, Pharmacia. It was prepared from NHS-activated HiTrap matrix

(Pharmacia) with antibodies against bovine serum albumin and packed in an 5 × 1 cm column, total volume 4 ml. Agarose-*Ricinus communis* agglutinin 120 (RCA-agarose) was from BioMakor, Rehovot, Israel.

The set of affinity columns used for preparation of *gag*-1 fraction was treated as follows: Con A-Sepharose had been stored and equilibrated against 50 m*M* ammonium acetate, 500 m*M* NaCl, 1 m*M* $MnCl_2$, 1 m*M* $CaCl_2$, pH 6.8. HiTrap-Albumin-Adsorption gel was stored in the same buffer without metal ions. Before sample application both columns were washed with 20 m*M* HEPES, pH 5.0, 0.1% Triton X-100. (The first gel was regenerated with 500 m*M* methyl mannoside in the wash buffer and the second gel with 100 m*M* glycine, pH 2.8.)

The set of affinity columns used for preparation of *gag*-2 fraction was treated as follows: Con A and HiTrap-Albumin-Adsorption gels were stored in the same buffers as used above. Prior to use they were washed with carefully deaerated 20 m*M* Hepes, pH 7.5, 0.01% octylglucoside.

2.7. Preparation of virus, two gag peptide-containing fractions (gag-1 and gag-2) and purification of the external env glycoprotein

General strategy

Infection of cell cultures and harvest at day 5 of cell-free virus containing culture medium. Extraction of virus using a two-phase system with dextran and poly(ethylene glycol) (PEG). Collection of the interphase, which contains the virus. Removal of polymers by centrifugation through a sucrose cushion to obtain the virus fraction. Treatment with octylglycoside. This results in an octylglucoside (OG) soluble fraction and an octylglucoside-insoluble fraction (OG-pellet). The former was used as source for the *gag*-2 fraction and for purification of gp148. The *gag*-1 fraction was prepared from the OG-pellet. Details are given below.

Virus purification

The virus was purified by extraction in a two-phase system with 0.24% (w/w) Dextran T500 (Pharmacia) and 7.2% (w/w) of PEG-6000 (Merck–Schuchardt, Darmstadt, Germany) ($D_{0.24}PEG_{7.2}$) as earlier described [11]. Plastic bags with attached tubing were used as extraction funnels (transfer bags "5L", or for smaller volumes blood bags; Baxter Medical, Bromma, Sweden). Polymer stock solutions were prepared to contain 10 m*M* sodium phosphate, pH 7.4 and 155 m*M* NaCl, in addition to the polymer. With the aid of a peristaltic pump the following solutions were pumped, under sterile conditions, into each 5L bag: 96 g of 10% (w/w) Dextran T500, 3330 ml cell supernatant, taken directly from culture flasks through a sterile 10-ml pipette, and 576 g of 50% (w/w) PEG-6000. The bags were then left hanging in the hood for 4 h, or overnight, during which period the system separated into a large top phase and a small bottom phase (volume ratio about 300:1). The virus accumulated at the interphase (Table 1). The bottom phase was tapped off before collecting the interphase material in a Falcon tube. The tube with the interphase was filled by addition of 8% PEG in phosphate-buffered saline (PBS), turned end over end a couple of times and spun at 1000 *g* for 10 min, in a cell centrifuge, whereby the interphase was sharpened and remainings of the bottom phase separated out. The interphase material was collected and further washed three times by addition of fresh 8% PEG-6000 in a Falcon tube. Finally the interphase material was suspended in PBS (10 m*M* sodium phosphate, pH 7.4, 155 m*M* NaCl) with 1 m*M* dithiothreitol (DTT). Polymers and soluble contaminants were removed by centrifugation through a 30% sucrose layer (over a bottom layer of 60% sucrose) at 12 000 *g* for 16 h at 4°C in a Kontron TFT 71.38 rotor. The virus fraction was collected under the 30% sucrose layer.

Solubilization of virus proteins

The virus was treated with octylglycoside, 3% final concentration, at 4°C for 60 min. It was then diluted 3-fold with 100 m*M* Tris–HCl, pH 8.5, to obtain a final octylglycoside concentration of 1% before centrifugation at 12 000 *g* for 16 h at 4°C (Kontron, rotor TFT 71.38).

Table 1
Recovery of SIV external *env* protein gp148

Fraction	Volume (ml)	Protein concentration (mg/ml)	gp148		
			Total (mg)	Recovery (%)	Purification (fold)
SIV infected cell culture medium	25 000	5	9.8	100	1
Dextran-PEG extraction					
Interphase	85	12	2.55	26	32
Bottom phase	52	–	0.005	0.1	–
Virus fraction	200	0.51	2.4	25	300
Lectin-affinity chromatography					
env gp148 fraction from GNA column	8	0.13	1.04	11	12 600

Preparation of gag-1 fraction

The OG-pellet, which contained the major portion of reverse transcriptase (RT) in addition to *gag* proteins was suspended in 10% Triton X-100 and frozen at −70°C. It was thawed and 10 m*M* Tris–HCl, pH 8.5, added to obtain a final Triton X-100 concentration of 1%, cleared by centrifugation at 100 000 *g* (Kontron, rotor TST 41.14) for 60 min. The supernatant was dialyzed, first against 20 m*M* HEPES, pH 7.5, 1 m*M* DTT, 0.5% Triton X-100, then against carefully deaerated 20 m*M* HEPES, pH 5.0, 0.1% Triton X-100.

The dialyzed material was passed over the combined Con A-Sepharose and HiTrap-Albumin-Adsorption columns. Sodium chloride was added to 25 m*M* and pH corrected to 7.5 by addition of NaOH before a final centrifugation as above. The protein content was determined relative to bovine serum albumin on trichloroacetic acid-precipitated samples. The material, *gag*-1 fraction, was diluted with 20 m*M* HEPES, 25 m*M* NaCl, pH 7.5, 0.1% Triton X-100, to a protein concentration of 1 mg/ml before sampling. The material was stored frozen at −70°C.

Preparation of gag-2 fraction

The material solubilized by octylglucoside was directly applied to similar chromatographic removal of glycoproteins and albumin as the *gag*-1 fraction by passing through a set of affinity columns. After the first passage the material was extensively dialyzed against carefully deaerated 20 m*M* HEPES, 0.01% octylglucoside, pH 7.5. The obtained opalescent material was supplemented with octylglucoside to 0.1% and centrifuged at 3000 *g* for 15 h (Sorvall, rotor SS34). It was then again passed over the regenerated affinity columns and concentrated by freeze drying to about half volume. Thawed material was dialyzed against 20 m*M* HEPES, 0.1% octylglucoside, pH 8.0, sterile filtered and diluted with the same buffer to a protein concentration of 1 mg/ml. It was stored frozen at −70°C.

Purification of external SIV env glycoprotein, gp148

The gp148 contained in the OG-soluble fraction was adsorbed on Con A-Sepharose. Before elution of the glycoprotein with 500 m*M* methyl mannoside, the column was extensively washed with 10 m*M* Tris–HCl, pH 7.5, 155 m*M* NaCl (TBS). The methyl mannoside eluate was directly applied to a WGA-Sepharose column equilibrated against TBS. This column was eluted with 100 m*M* N-acetylglucosamine (GlcNAc) in TBS and the eluate directly applied to a column with ProSep-GNA. This column was washed as shown

in Fig. 4. The SIV gp148 was eluted with 500 m*M* methyl mannoside. The purified material was sampled and stored at −70°C. During preparation the material was kept at 4–8°C.

3. Results and discussion

3.1. Two-phase extraction

There were two main reasons to apply two-phase extraction for the purification of SIV_{MAC}. First the method is convenient to use with large volumes of infectious material. Second the method has a potential for recovery of native structures [11]. In this study we concentrated SIV from a batch of 25 l by direct mix of cell supernatant and polymer stock solutions. After 4 h the phases had separated and the virus could be recovered from the interphase, 300-fold concentrated. Fig. 1 shows the presence of different virus proteins in the interphase material. SIV prepared in this way has been used for vaccine studies [17] and as source for preparation of the external *env* glycoprotein for the same purpose. In addition to the two-phase extraction we included a centrifugation step to obtain the virus free of polymers. This was done by centrifugation through a sucrose layer, overnight at 12 000 *g*. In the virus fraction the recovery of the reverse transcriptase activity and gag-p27 were about 80%. The yield of gp148 was about 25%. Loss of gp148 during re-extraction and centrifugation was minimal (Table 1), which points to the glycoprotein being associated with the virion.

3.2. Solubilization and gag fractions

In our initial studies the detergent ITDP was tried for the solubilization of the virus components. With HIV-2 this non-ionic mild detergent exclusively solubilized the external *env* glycoprotein without much leakage of *gag* proteins. With SIV_{MAC} the solubilization of gp148 was poor. We therefore used octylglucoside. This has an about 10-fold higher critical micelle concentration than ITDP. However, it has the advantage of a small micelle size ($M_r \approx 8000$), which makes it dialyzable.

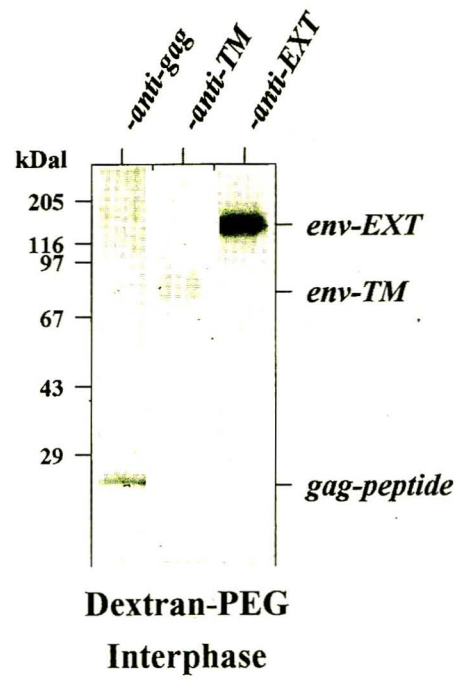

Fig. 1. SIV components recovered in the interphase in a two-phase system composed of infected cell culture supernatant, 0.24% (w/w) Dextran T500 and 7.2% (w/w) PEG-6000 as demonstrated by western blotting; the blots were probed with monoclonal antibodies against *gag*-p27 (gag-peptide), the transmembrane *env* protein (env-TM) and the *env*-gp148 (env-EXT). kDal = kilodaltons.

Treatment of the virus preparation with octylglucoside resulted in the solubilization of the major portion of gp148 and gag-p27. However, the major portion of reverse transcriptase and small *gag* peptides as well as about 5% of the p27 remained in the OG-pellet. They were solubilized by Triton X-100, depleted of N-glycosylated proteins and albumin and finally recovered as the *gag*-1 fraction. OG-soluble material was further processed to yield the *gag*-2 fraction and purified gp148.

Two fractions of *gag* protein has earlier been observed after treatment of HIV with octylglucoside and other detergents [18]. Contrary to this report we recover the major portion of the *env* proteins in the soluble fraction.

The peptide pattern of *gag*-1 and *gag*-2 fractions are shown in Fig. 2. Calculated from staining intensity of p27 and albumin bands in

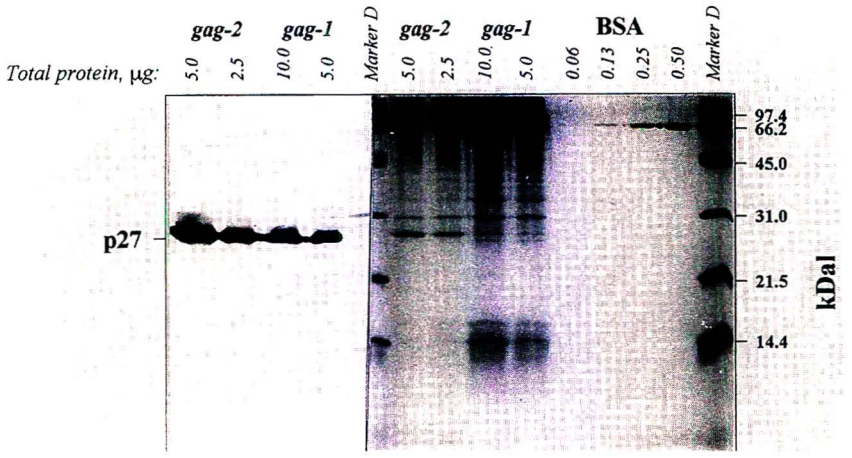

Fig. 2. SDS-PAGE and western-blot analysis of *gag*-1 and *gag*-2 fractions prepared as outlined in the Experimental section; right-hand panel shows a SDS-PAGE gel after Commassie staining. Samples of the *gag* fractions and of bovine serum albumin (BSA) were run in parallel. The amount of total protein in the applied samples and the molecular mass of marker peptides are indicated. Left-hand panel shows a western blot run with a section of the same gel. This is probed with a monoclonal anti-*gag*-protein antibody.

the Commassie stained sodium dodecyl sulphate–polyacrylamide gel electrophoresis (SDS-PAGE) gel the p27 constitutes 2–4% of total protein in *gag*-1 fraction and 10–12% in the *gag*-2 fraction. This gives the estimated value of 30 μg/ml in the *gag*-1 and 110 μg/ml in the *gag*-2 preparation. This gives that the total yield of p27 from a 25-l culture was 840 μg (28 ml, 30 μg/ml) in the *gag*-1 fraction and 16.5 mg (150 ml, 110 μg/ml) in the *gag*-2 fraction. Both were prepared to hold a total protein concentration of 1 mg/ml.

Immunoblot of the *gag*-1 fraction (Fig. 3, not all blots are shown) with sera from HIV-2 infected humans (h-213, h-277) show, in addition to that of p27, bands at M_r 15 000, 22 000, 36 000, 44 000 and 50 000 which may represent virus peptides. The M_r 44 000 peptide binds jacalin (JAC, Fig. 3), peanut agglutinin (PNA), and the lectins from *Ricinus communis* and *Aleuria auratia* (RCA and AAA, Fig. 3), but not the lectins from *Ulex europaeus* (UEA-I) or *Lotus tetragonolobus* (Lot). The lectin binding pattern indicate an O-linked glycoconjugate with non-sialylated Galβ1→3GalNAc (Gal = galactose) core and fucose linked in such a way that it is recognized by AAA but not by UEA-I or Lot.

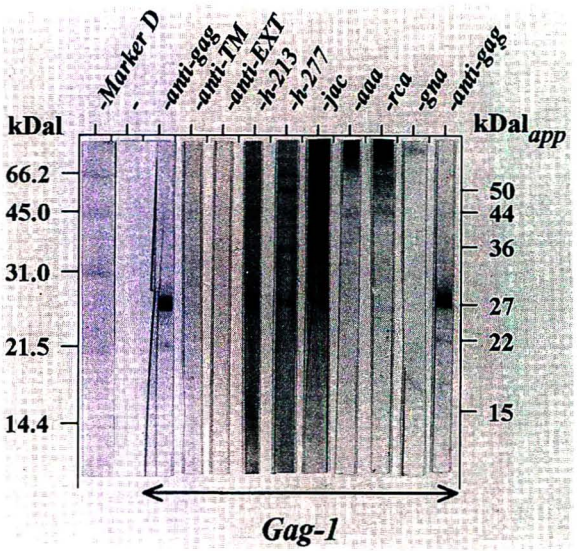

Fig. 3. Western and lectin blot analyses of the *gag*-1 fraction. The probes were monoclonal antibodies against SIV proteins (anti-*gag*, anti-TM and anti-EXT), human HIV-2 positive sera (h-213, h-277), and the lectins JAC, AAA, RCA-agl and GNA. Lectin abbreviations are explained in Table 2. Estimated molecular mass of peptides revealed by probing with the human sera are shown at the right. Marker peptides are indicated to the left.

A narrow band in the region is labeled by *Pisum sativum* agglutinin (PSA) and lentil lectin (LCA) indicative of mannose. There is no binding of GNA (Fig. 3). A summery of the lectins, the abbreviations used and reported main specificity is given in Table 2.

3.3. Purification of gp148

It may be noted that in the presence of octylglucoside the gp148 was not adsorbed to Lentil-Sepharose (Pharmacia). The binding to Con A-Sepharose was not impaired. Therefore the Con A-Sepharose was used to withdraw the glycoprotein from the virus lysate.

The lectin columns (Con A→WGA→GNA) were combined so that the eluting sugar in one system should not affect the binding to the next. The elution profile from the GNA column is shown in Fig. 4. It was found essential to carefully wash the column before elution with α-methylmannoside in order to obtain the desired purity and a sharp elution of the gp148. If the column was washed with only TBS before elution with methylmannoside a broad elution peak was obtained. If eluted with the mannoside in 1 *M* NaCl the peak was sharpened but contaminating proteins present, as shown in sample c of Fig. 5B. Small peptide contaminants were removed by washing the column with high salt before application of methyl mannoside (sample b, Fig. 5B). However, washing the column with the detergent Empigen, as in the Fig. 4A chromatogram, resulted in a sharp elution of gp148 by methyl mannoside. The purity of the gp148 preparation is demonstrated in Fig. 5 (gp148, Fig. 5A and B). Fig. 4B shows UV spectra of the elution peaks from the chromatogram. The gp148-containing methyl mannoside fraction shows a typical protein spectrum

Table 2
List of lectins used

Abbreviation	Source	Main specificity
AAA	*Aleuria aurantia*	α(1-6)-linked Fuc
BSL-1	*Bandeiraea simplicifolia* seeds	α-GalNAc, α-Gal, Blgr.AandB
BSL-2	*Bandeiraea simplicifolia* seeds	α-/β-GlcNAc
Con A	*Canavalia ensiformis* (Jack been) seeds	α-Man
DBA	*Dolichos biflorus* (Horse gram) seeds	GalNAc(α-1,3)GalNAc, α-Gal, Blgr.A1
DSL	*Datura stramonium* (Thorn apple) seeds	GlcNAc(β-1,4)GlcNAc, terminal LacNAc-
ECL	*Erythrina cristagalli* (Coral tree) seeds	Gal(β-1,4)GlcNAc, GalNAc
GNA	*Galanthus nivalis* (Snow drop) bulb	terminal Man(α-1,3)Man-
JAC, jacalin	*Artocarpus integrifolia* (Jackfruit) seeds	O-linked Gal(β-1,3)GalNAc, α-Gal
LCA	*Lens culinaris* (lentil) seeds	α-Man
Lot	*Lotus tetragonolobus* (Asparagus pea)	α-L-Fuc, Blgr.H(0)
LPA	*Limulus polyhemus* (Horseshoe crab)	NANA, mucins, phosphorylcholin
MAA	*Maackia amurensis*	α(2-3)-linked NANA
PHA-E	*Phaseolus vulgaris* (red kidney bean)	Red cell specific saccharide
PHA-L	*Phaseolus vulgaris* (red kidney bean)	Lymphocyte specific saccharide
PNA	*Arachis hypogaea* (peanuts)	Gal(β-1,3)GalNAc-, Gal-
PSA	*Pisum sativum* (garden pea) seeds	terminal α-Man-, or α-Glc-
RCA-agl	*Ricinus communis* (castor beans) seeds	β-Gal-, β-GalNAc-
RCA-tox	*Ricinus communis* (castor beans) seeds	β-Gal-, βGalNAc-
SJA	*Sophora japonica* (Jap. pagoda tree) seeds	terminal GalNAc-, terminal Gal-
STL	*Solanum tuberosum* (potato) tubers	*oligo*-GlcNAc, MurNAc
UEA-I	*Ulex europaeus* (Furze gorse) seeds	α-Fuc, Blgr.A2, Blgr.H(0)
VVL	*Vicia villosa* (hairy vetch) seeds	GalNAc(α)-Ser/Thr, Blgr.A1,Tn
WGA	*Triticum vulgaris* (wheat germ)	GlcNAc(β-1,4)GlcNAc, NANA
sWGA	-succinylated WGA	terminal GalNAc(β-1,4)GlcNAc

Fuc = Fucose; Blgr. = blood group; Man = mannose; Lac = lactose; NANA = N-acetylneuramic acid (sialic acid); other abbreviations defined in text.

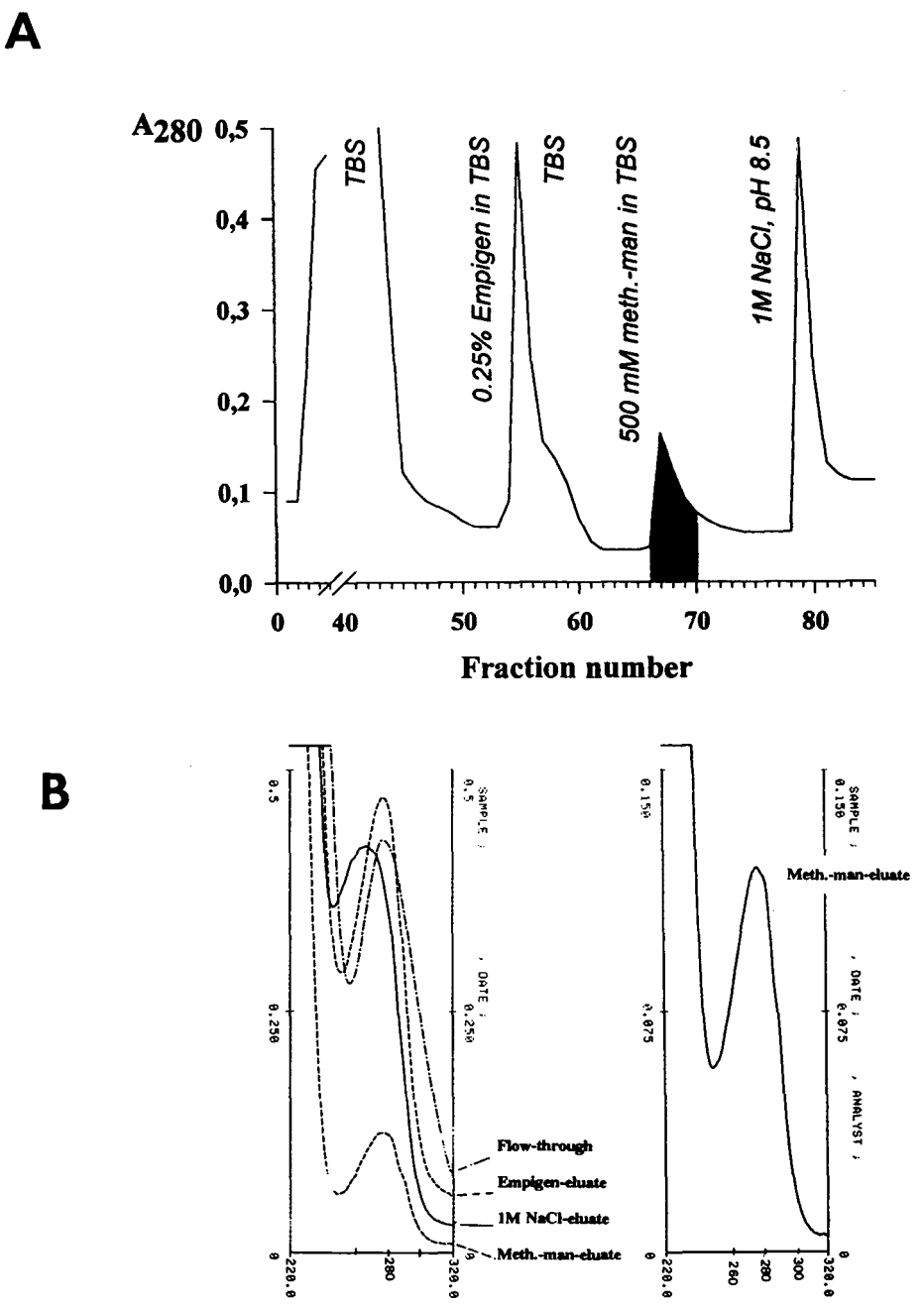

Fig. 4. Chromatography on ProSep-GNA, 30 × 8 mm. Sample: GlcNAc fraction obtained from the WGA column (see Experimental section). (A) Chromatogram showing the protein profile (A_{280}) and the buffer changes. The gp148 was found in the fraction eluted with 500 m*M* methyl mannoside (black). (B) The UV spectrum of the gp148 fraction (Meth.-man-eluate) is compared to those of the other fractions from the chromatogram shown in (A). To the right: The intensity axis is expanded to show the protein type spectrum of the gp148 fraction (Meth.-man-eluate).

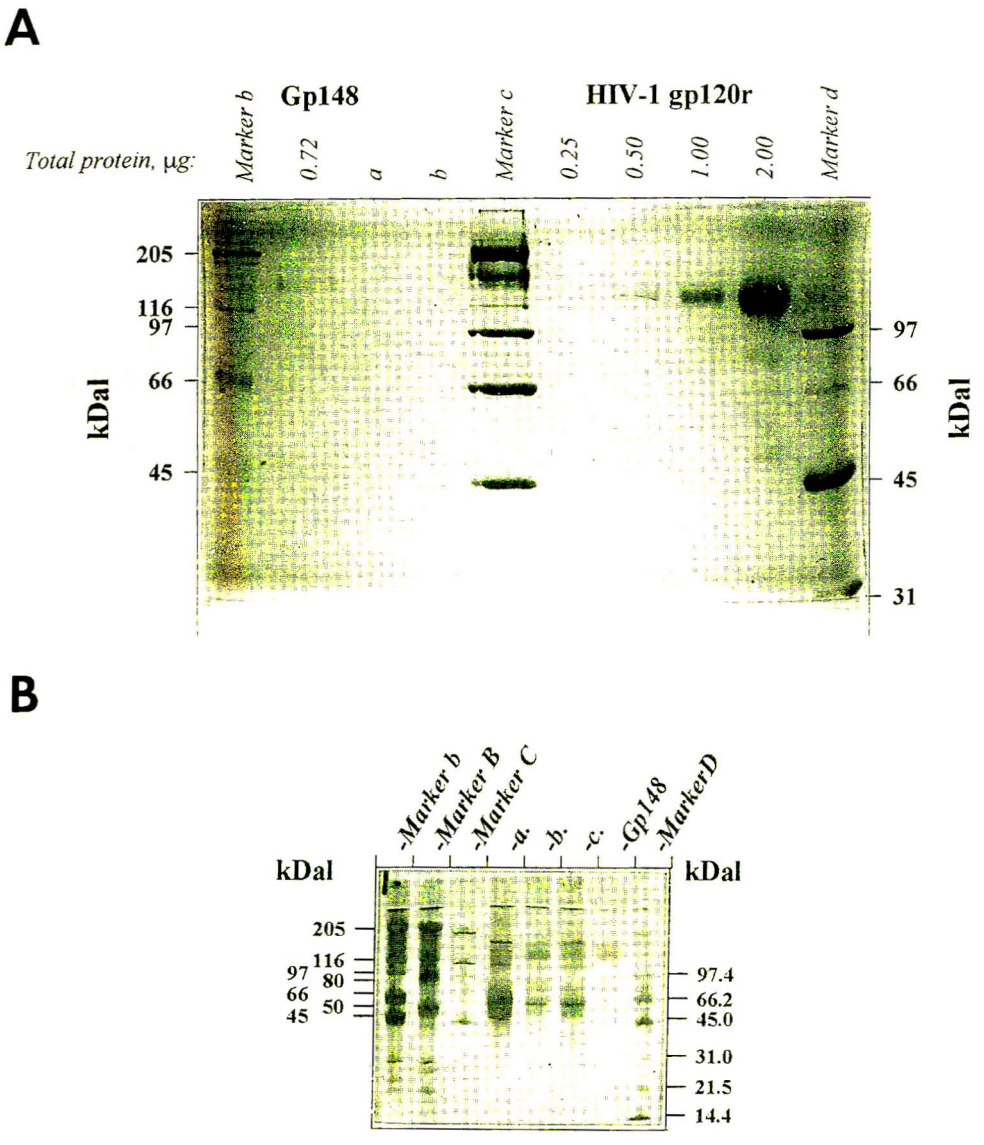

Fig. 5. (A) SDS-PAGE of the purified gp148 and a recombinant HIV-1_{IIIB}-gp120. The gel is stained with Commassie Brilliant Blue. The amount of applied protein is indicated above the gel. (B) SDS-PAGE (PhastSys, Pharmacia) with silver staining of the gel to show the peptide profile of purified gp148, obtained as the meth.-man fraction from ProSep-GNA chromatography according to the elution scheme in Fig. 4A. Sample a is the flow through from the same run. Sample b is the methyl mannoside fraction from a similar run in which the Empigen washing step was exchanged for by a wash with 1 *M* NaCl and sample c is the eluate obtained with 500 m*M* methyl mannoside in 1 *M* NaCl when the Empigen step was omitted.

(Meth.-man-eluate, Fig. 4B). A shoulder at about 290 nm may reflect the relatively high content of tryptophan relative to tyrosine (17:21) in the protein, as judged from the predicted amino acid sequence [19]. Material eluted with 1 *M* NaCl at elevated pH showed λ_{max} at 260 nm (Fig. 4B).

Protein content in the gp148 preparation was determined, with the same result, by UV spectroscopy and by the Bradford technique [20],

using thyroglobulin as standard. A comparison of staining intensity of the gp148 band in the SDS-PAGE gel with that of known amounts of a recombinant HIV-1 gp120 (rgp120) run in parallel (Fig. 5A), points to gp148 representing the full protein content in the applied sample. The silver stained gel in Fig. 5B, lane "gp148", shows that contaminants represent less than 1%. The purity is also revealed by the single band obtained in electroblot analyses with a large panel of lectins as probes (Fig. 6).

The recovery of the gp148 from the virus fraction was 45% and that obtained through the full purification procedure was about 10% (Table 1). Thus, from 25 l of infected cell culture about 1 mg of purified gp148 was obtained (Table 1).

3.4. Lectin blot analysis

Lectin blot analyses were done to give a view of the possible character of the oligosaccharides of gp148. These analyses (Fig. 6) point to the presence of high mannose type as well as complex type N-linked oligosaccharides in the gp148. This is in analogy with findings for SIV_{SM} [21] and HIV-1 [22–26]. As with SIV_{SM} [21] there seems to be ample presence of lactosamine containing saccharides. Hansen gives arguments and evidence for the presence of O-linked oligosaccharides in HIV [27]. With SIV gp148 the binding of jacalin and a weak signal from *Vicia villosa* lectin (JAC and VVL, Fig. 6, bottom right hand panel) indicate the possible presence of O-linked sugars. However, the peanut agglutinin blot was negative (PNA, Fig. 6, top right hand panel). Jacalin has been reported to block HIV-1 infection *in vitro* [28]. It was assumed not to bind to HIV-gp120, but to share similarities in its amino acid sequence with a stretch in the second conserved region of the glycoprotein and thereby exert its effect [28].

The lectin blot technique [15] may help in deciding on a suitable strategy for glycoprotein purification or analysis. The selectivity of GNA for gp148 among the glycoproteins of the solubilized virus fraction is evident from the lectin blot analysis (Fig 6, gna, bottom left hand panel). Other lectins that may be of use in the purification of the virus glycoprotein are those from *Erythrina cristagalli* (specificity for lactosamine) and *Aleuria aurantia* (specificity for α-fucose) (see Fig. 6, ECL and AAA, bottom left hand panel). However, both of these lectins also bind an $M_r \approx 100\,000$ glycopeptide as the main contaminant and are therefore not selective for gp148 to the same extent as the GNA.

GNA selectively binds terminal α-1,3-, and/or α-1,6-mannose residuals in oligosaccharides or in protein glycoconjugates [29,30]. Such structures, if present in mature extracellular proteins, are usually not exposed. Their presence in the external *env* protein seems to be a feature in common for different HIV isolates [31–34]. Consequently GNA, a similar lectin or mannan antibody, should constitute a general affinity method for the purification of these glycoproteins. This has been explored by Gilljam [12] for purification of the external *env* protein from HIV-1 and HIV-2 as well as from SIV.

4. Concluding remarks

In this paper we have advised a strategy for the purification of SIV_{MAC} from large volumes of culture fluid and for the subsequent fractionation of its sub-components. The good recovery of reverse transcriptase activity in the concentrated virus indicate a well preserved virion. The recovery of the external glycoprotein was not exceptional but may reflect the amount *de facto* attached to the envelope of the mature virus, as discussed above. HIV-1 gp120, when concentrated with a similar system, was recovered to a much higher extent (about 60%) [9]. However, this is a different virus and cell system and there may be differences in the kinetics of glycoprotein shedding from the cell surface and virus maturation [35].

Although the dextran–PEG system works well with several retroviruses [11] we have earlier found that other systems may be more advantageous when it comes to the recovery of the external *env* protein [7–9,11]. Therefore, it is possible that the extraction conditions can be better optimized for the SIV glycoprotein. How-

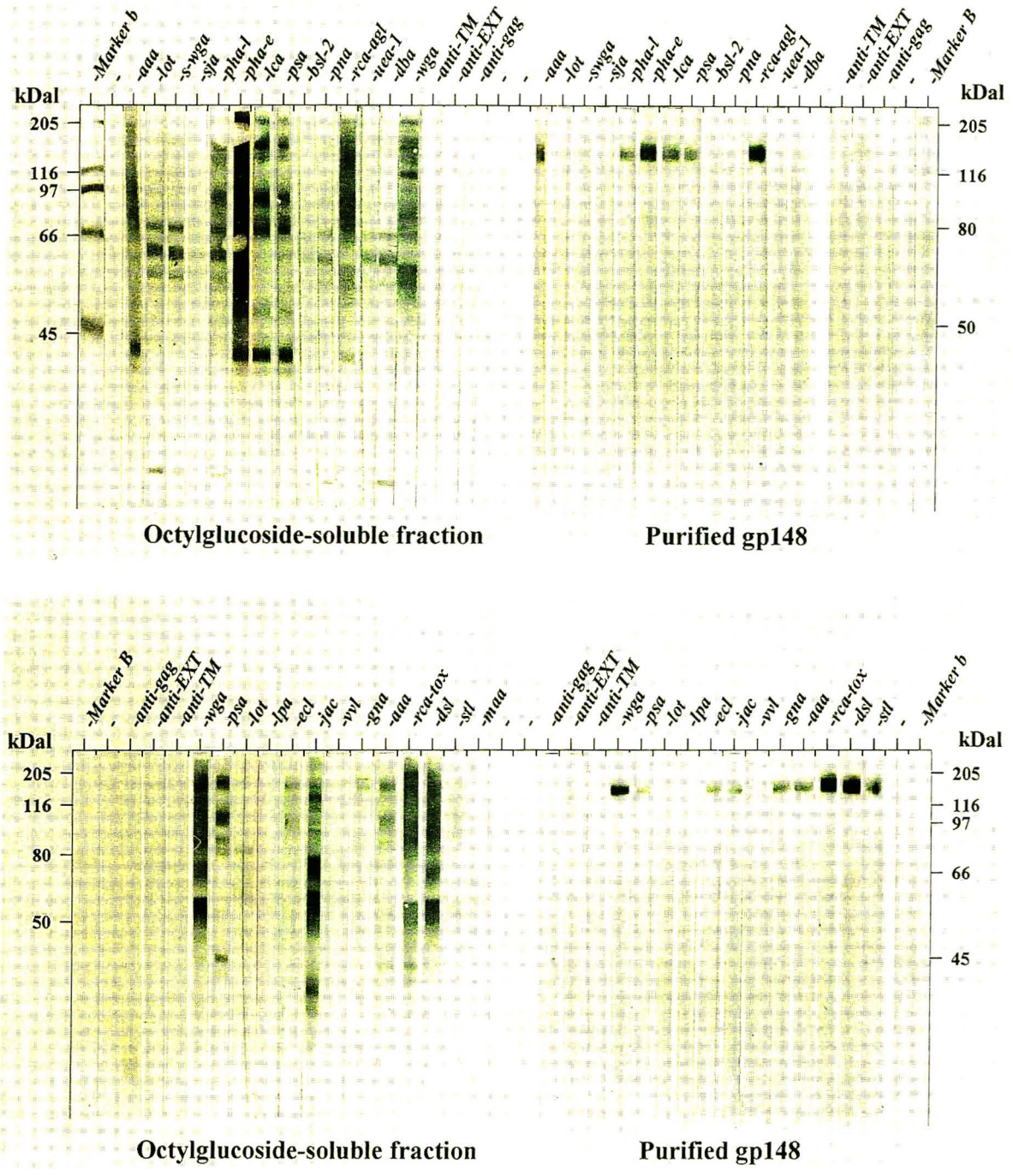

Fig. 6. Lectin and immunoblot analyses of octylglucoside soluble fraction (left-hand panels) from the extracted SIV preparation and of the purified gp148 (right-hand panels). Top and bottom panels show blots from two different SDS-PAGE gels. Markers are included at the outer borders. The probes are indicated above the blots. Lectin abbreviations are explained in Table 2.

ever, in the present case we appreciate the well documented biocompatibility and inert nature of the dextran and PEG, which ensures that traces of the polymers in the purified products will not cause major problems in the utilization of the prepared material.

Acknowledgements

Many thanks are due to Professor Britta Wahren and her staff at the HIV laboratory, Department of Clinical Virology, Swedish Institute for Infectious Disease Control, Solna, Sweden. This study was supported by grants from the EC-concerted research programme: European vaccine against AIDS (Programme EVA), National Institute for Biological Standards and Control, Potters Bar, UK, and from the Swedish Medical Research Council (09932), the Swedish Cancer Society (3205-B91) and "Trygghetsstiftelsen", Stockholm, Sweden. K.S. held a scholarship from the International Science Programme in the Chemical Sciences at the University of Uppsala, Uppsala, Sweden.

References

[1] H.R. Gelderblom, *AIDS*, 5 (1991) 617.
[2] S.W. Pyle, J.W. Bess, G. Robey and P. Fischinger, *AIDS Res. Human Retrovir.*, 3 (1987) 387.
[3] S.W. Pyle, G.C. Dubois, G. Robey and P.J. Fischinger, *J. Virol.*, 62 (1988) 2258.
[4] T.F. Schulz, B.A. Jameson, L. Lopalco, A.G. Siccardi, R.A. Weiss and J.P. Moore, *AIDS Res. Human Retrovir.*, 8 (1992) 1571.
[5] J.S. Allan, E.M. Whitehead, K. Strout, M. Short, P. Kanda, T.K. Hart and P.J. Bugelski, *AIDS Res. Human Retrovir.*, 8 (1992) 2011.
[6] D.J. Looney, S. Hayashi, M. Nicklas, R.R. Redfield, S. Broder, F. Wong-Staal and H. Mitsuya, *J. Acquired Immune Defic. Syndr.*, 3 (1990) 649.
[7] L. Hammar, S. Eriksson, K. Malm and B. Morein, *J. Virol. Methods*, 24 (1989) 91.
[8] L. Hammar, M. Merza, K. Malm, S. Eriksson and B. Morein, *Biotechnol. Appl. Biochem.*, 11 (1989) 296.
[9] L. Hammar and G. Gilljam, *AIDS Res. Human Retrovir.*, 6 (1990) 1379.
[10] L. Hammar, G. Gilljam and B. Wahren, in *Programme EVA Workshop: Challenges and Strategies for AIDS Vaccine Development, Rome, 1992.*
[11] L. Hammar, *Methods Enzymol.*, 228 (1994) 640.
[12] G. Gilljam, *AIDS Res. Human Retrovir.*, 9 (1993) 431.
[13] K.A. Kent, L. Gritz, G. Stallard, M.P. Cranage, C. Collignon, C. Thiriart, T. Corcoran, P. Silvera and E.J. Stott, *AIDS*, 5 (1991) 829.
[14] R. Thorstensson, L. Walther, P. Putkonen, J. Albert and G. Biberfeld, *J. Aquired Immune Defic. Syndr.*, 4 (1991) 374.
[15] S. Eriksson, R. Bhikhabhai and L. Hammar, *Pharmacia PhastSystem, Application File No. 301*, Pharmacia, Uppsala, 1989.
[16] L. Hammar, S. Eriksson and B. Morein, *AIDS Res. Human Retrovir.*, 5 (1989) 495.
[17] P. de Vries, J.L. Heeney, J. Boes, M.E.M. Dings, E.G.J. Hulskotte, R. Dubbes, W. Koornstra, P. ten Haaft, L. Åkerblom, S. Eriksson, B. Morein, S. Norley and A.D.E. Osterhaus, (1994) in preparation.
[18] A.G. Bukrinskaya and N.K. Sharova, *Arch. Virol.*, 110 (1990) 287.
[19] N. Almond, A. Jenkins, A. Slade, A. Heath, M. Cranage and P. Kitchin, *AIDS Res. Human Retrovir.*, 8 (1992) 77.
[20] M. Bradford, *Anal. Biochem.*, 72 (1976) 248.
[21] C. Holschbach, J. Schneider and H. Geyer, *Biochem. J.*, 267 (1990) 759.
[22] H. Geyer, C. Holschbach, G. Hunsmann and J. Schneider, *J. Biol. Chem.*, 263 (1988) 11760.
[23] C.K. Leonard, M.W. Spellman, L. Riddle, R.J. Harris, J.N. Thomas and T.J. Gregory, *J. Biol. Chem.*, 265 (1990) 10373.
[24] T. Mizuochi, M.W. Spellman, M. Larkin, J. Solomon, L. Basa and T. Feizi, *Biochem. J.*, 254 (1988) 599.
[25] T. Mizuochi, T.J. Matthews, M. Kato, J. Hamako, K. Titani, J. Solomon and T. Feizi, *J. Biol. Chem.*, 265 (1990) 8519.
[26] T. Mizuochi, *Nippon Rinsho*, 50 (1992) 1419.
[27] J.-E. Hansen, *APMIS*, 100 Suppl 27 (1992) 96.
[28] J. Favero, P. Corbeau, M. Nicolas, M. Benkirane, G. Travé, J.E.F. Dixon, P. Aucouturier, S. Rasheed, J.W. Parker, J.P. Liautard, C. Devaux and J. Dornand, *Eur. J. Immunol.*, 23 (1993) 179.
[29] N. Shibuya, I.J. Goldstein and E.J.M. Van Damme, *J. Biol. Chem.*, 263 (1988) 729.
[30] H. Kaku and I. Goldstein, *Methods Enzymol.*, 179 (1989) 327.
[31] W.E.G. Muller, P. Reuter, M. Schaffrath, H.C. Schröder and I. Winkler, *AIDS-Forsch.*, 4 (1989) 465.
[32] W.E. Muller, H.C. Schroder, P. Reuter, A. Maidhof, G. Uhlenbruck and I. Winkler, *AIDS*, 4 (1990) 159.
[33] J. Balzarini, D. Schols, J. Neyts, E.J.M. Van Damme, W. Peumans and E. De Clercq, *Antimicrob. Ag. Chemother.*, 35 (1991) 410.
[34] J. Balzarini, J. Neyts and D. Schols, *Antiviral Res.*, 18 (1992) 191.
[35] P.J. Greenaway and G.H. Farrar, *Animal Cell Biotechnol.*, 4 (1990) 379.

ELSEVIER

Journal of Chromatography A, 675 (1994) 101–112

JOURNAL OF CHROMATOGRAPHY A

Preparative isolation of recombinant human insulin-like growth factor 1 by reversed-phase high-performance liquid chromatography

Charles V. Olson*[,a], David H. Reifsnyder[a], Eleanor Canova-Davis[b], Victor T. Ling[b], Stuart E. Builder[a]

[a]*Department of Recovery Process Research and Development, Genentech Inc., 460 Point San Bruno Boulevard, South San Francisco, CA 94080, USA*

[b]*Department of Medicinal and Analytical Chemistry, Genentech Inc., 460 Point San Bruno Boulevard, South San Francisco, CA 94080, USA*

(First received January 4th, 1994; revised manuscript received March 8th, 1994)

Abstract

The isolation of recombinant human insulin-like growth factor 1 (rhIGF-1) is complicated by the presence of several rhIGF-1 variants which co-purify using conventional chromatographic media. These species consist primarily of a methionine-sulfoxide variant of the properly folded molecule and a misfolded form and its respective methionine-sulfoxide variant. An analytical reversed-phase high-performance liquid chromatography procedure using a 5-μm C_{18} column, an acetonitrile–trifluoroacetic acid (TFA) isocratic elution, and elevated temperature gives baseline resolution of the four species. Using this analytical method as a development tool, a process-scale chromatography step was established. The 5-μm analytical packing material was replaced with a larger-size particle to reduce back-pressure and cost. Since the TFA counter-ion binds tightly to proteins and is difficult to subsequently dissociate, a combination of acetic acid and NaCl was substituted. Isocratic separations are not good process options due to problems with reproducibility and control. A shallow gradient elution using premixed mobile phase buffers at the same linear velocity was found to give an equivalent separation at low load levels and minimized solvent degassing. However, at higher loading there was a loss of resolution. A matrix of various buffers was evaluated for their effects on separation. Elevated pH resulted in a significant shift in both the elution order and relative retention times of the principal rh-IGF-1 variants, resulting in a substantial increase in effective capacity. An increase in the ionic strength further improved resolution. Several different media were evaluated with regard to particle size, shape and pore diameter using the improved mobile phase. The new conditions were scaled up 1305-fold and resulted in superimposable chromatograms, 96% recovery and >99% purity. Thus, by optimizing the pH, ionic strength and temperature, a high-capacity preparative separation of rhIGF-1 from its related fermentation variants was obtained.

1. Introduction

Human insulin-like growth factor-1 (IGF-1) is a peptide of M_r 7649 with a pI of 8.4 [1,2] belonging to a family of somatomedins with insulin-like and mitogenic biological activities which modulate the action of growth hormone [3–6]. IGF-1 has hypoglycemic effects similar to

* Corresponding author.

0021-9673/94/$07.00
SSDI 0021-9673(94)00238-5

insulin but also promotes positive nitrogen balance [7,8]. Due to this range of activities, IGF-1 is being tested in humans for uses ranging from wound healing to the reversal of whole-body catabolic states [9].

Genetically engineered biopharmaceuticals are typically purified from a supernatant containing a variety of diverse host cell contaminants. The recombinant human IGF-1 (rhIGF-1) peptide was isolated through a recovery process which utilized conventional low-pressure chromatography. However, the final process pool contained several variant species of rhIGF-1 which were difficult to separate. In this paper we describe a systematic optimization strategy for the purification of rhIGF-1 from its related fermentation variants using reversed-phase high-performance liquid chromatography (RP-HPLC).

2. Experimental

2.1. Reagents

The following chemicals were used: HPLC-grade acetonitrile (ACN; J.T. Baker, Phillipsburg, NJ, USA); HPLC-grade trifluoroacetic acid (TFA; Pierce, Rockford, IL, USA); analytical reagent-grade NaCl, dibasic sodium phosphate, hydrochloric acid, sodium hydroxide and acetic acid (HAc) (Mallinckrodt, Paris, KY, USA). All aqueous mobile phases were made using purified water. pH adjustment was done with HCl or NaOH. All buffers were 0.2-μm-filtered prior to use.

Analytical RP-HPLC was performed on a 25 × 0.46 cm stainless-steel column pre-packed with 5-μm, 300-Å, trifunctional, Vydac C_{18} spherical silica (Separations Group, Hesperia, CA, USA). The development of preparative RP-HPLC methods was carried out using a 30 × 0.39 cm stainless-steel column pre-packed with 15-μm, 300-Å, monofunctional, Waters C_4 spherical silica (Millipore, Waters Chromatography Division, Milford, MA, USA). The other preparative RP-HPLC columns which were evaluated include: Bakerbond C_4 (J.T. Baker); YMC-C_8 (Yamamura, Morris Plains, NJ, USA); Kromasil C_8 (Eka Nobel, Surte, Sweden); Amicon C_8 (Amicon, Danvers, MA, USA); Impaq C_4 (PQ Corp., Valley Forge, PA, USA); PLRP-S (Polymer Labs., Amherst, MA, USA); Eurosil-Bioselect (Paxxis, Belmont, CA, USA). Pilot- and process-scale RP-HPLC were performed using the Waters C_4 packed in 30 × 4.7 cm and 60 × 10 cm radial compression cartridges, respectively.

Additional chemicals purchased for electrophoresis include: premixed Tris–glycine and Tris–tricine sodium dodecyl sulfate (SDS) buffers (Novex, San Diego, CA, USA); methanol (J.T. Baker); Coomassie R-250 and Coomassie G-250 (Eastman Kodak, Rochester, NY, USA); sulfuric acid and glycerol (Mallinckrodt); trichloroacetic acid (Fisher Scientific, Fairlawn, NJ, USA).

2.2. Equipment

The Vydac C_{18} RP-HPLC analysis and Waters C_4 preparative RP-HPLC methods development were both carried out on a Hewlett-Packard 1090 HPLC system (Hewlett-Packard, North Hollywood, CA, USA), equipped with a ternary gradient system and diode-array detector. The pilot-scale RP-HPLC was done using a Waters DeltaPrep 600-E controller, LC-3000 pumping system fitted with 180 ml/min heads and a 30 × 4.7 cm PrepPak radial compression module (RCM). The preparative RP-HPLC was accomplished using a Biotage KiloPrep-250 system (Biotage, Charlottesville, VA, USA) and a 60 × 10 cm RCM.

2.3. Analysis

Purity was assessed by 12% SDS–polyacrylamide gel electrophoresis (PAGE) (Integrated Separation Systems, Hyde Park, MA, USA), pH 3.5–9.5 isoelectric focusing (IEF) gels (Pharmacia LKB Biotechnology, Piscataway, NJ, USA), and analytical RP-HPLC using a 25 × 0.46 cm Vydac C_{18} column and Hewlett-Packard 1090 HPLC system. The SDS gels were run with Tris–tricine buffers [10] and Coomassie-R250

stained [11]. The low-percentage-polyacrylamide IEF gels could not be stained with silver or Coomassie R-250 because the IGF-1 diffuses out during the staining procedure. The gels were therefore stained in the absence of alcohol with Coomassie G-250 [12].

3. Results and discussion

3.1. Analytical separation

A preparative-scale RP-HPLC step in the down-stream processing of recombinant proteins is typically implemented late in the recovery scheme. This strategy is utilized to help maximize the efficiency of the separation and the column lifetime by removing the majority of the contaminants during previous purification steps. The RP-HPLC step for rhIGF-1 was developed after several conventional low-pressure chromatographic steps had produced a partially purified process pool primarily containing rhIGF-1 and its variants. The pool appeared to be homogeneous by SDS-PAGE and IEF analysis (Fig. 1A and B). However, RP-HPLC analysis on a 25 × 0.46 cm Vydac C_{18} column using a 10–60% ACN/50 min gradient at 22°C revealed that other species were present (Fig. 1C). The expanded chromatogram (Fig. 1C, inset) shows two major peaks and some minor peaks. These minor later eluting peaks are immunoreactive to antibodies directed against IGF-1 and appear to be sequential multimeric species of IGF-1 by immuno-blot analysis (data not shown). Using the same column at elevated temperature (50°C), an isocratic separation baseline resolved the mixture into its four respective constituents (Fig. 1D) [13]. N-Terminal sequence, peptide mapping, RP-HPLC and mass spectrometry analysis (data not shown) were performed on the four collected peaks which identified them as rhIGF-1, a methionine-sulfoxide variant, a misfolded form, and the respective misfolded-methionine-sulfoxide form. These results are consistent with those previously reported [14–16].

3.2. Initial scale-up considerations

The two initial development goals were finding a suitable replacement buffer for TFA and translating the analytical separation of rhIGF-1 variants to preparative media. The TFA counter-ion used in the analytical separation appeared to form a tight ion pair with the product and was difficult to remove in subsequent process steps. This strong ion-pair interaction has been previously observed for synthetic peptides [17]. A similar separation to 0.1% TFA, 28.5% ACN was achieved on the Vydac C_{18} column by using a low-ionic-strength acetate–halide pH 3 buffer (20 m*M* HAc, 20 m*M* NaCl) in 27.5% ACN (Fig. 2). The beneficial ion-pairing effects of NaCl in RP-HPLC have been previously reported [18]. HAc or NaCl levels higher than 20 m*M* showed no further increase in resolution. The retention times were stabilized by changing the elution conditions from isocratic to a very shallow linear gradient, 27–28% ACN over 40 min.

The acetate buffer mobile phase optimized on the Vydac C_{18} column was adapted to a Waters C_4 preparative medium packed in a 30 × 0.39 cm column (Fig. 3A). The shorter C_4 alkyl chain substitution was chosen to maximize product recovery [19]. Irreversible binding of insulin and proinsulin to C_{18} stationary phases has recently been reported [20]. Using the acetate buffer at 50°C, four peak fractions were collected during a shallow gradient elution, 27–28% ACN over 40 min. Fractions 1–4 were analyzed on the Vydac C_{18} column as described above with the following modifications. To increase analytical throughput, a rapid, near-isocratic (27–28% ACN with 0.1% TFA) method was developed by increasing the flow-rate from 0.5 to 2 ml/min. The gradient volume was kept constant by shortening the duration from 40 to 10 min. Vydac C_{18} analysis of the four peak fractions collected during the Waters C_4 preparative chromatography confirmed that the elution order of the rhIGF-1 species using the acetate buffer was identical to the order observed initially with TFA (Fig. 3B).

As increasing levels of protein are consecutive-

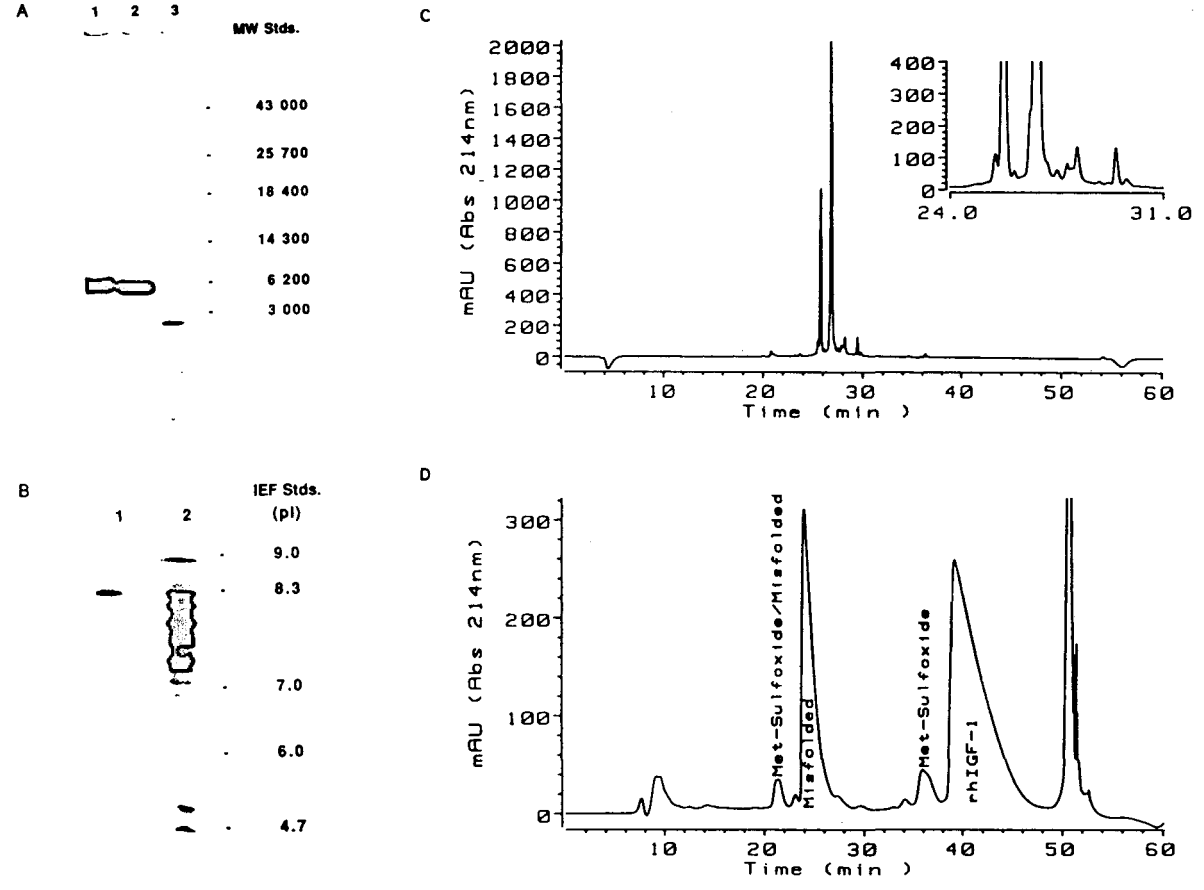

Fig. 1. Characterization of starting material. (A) Analysis by Tris–tricine SDS-PAGE. Samples of a partially purified rhIGF-1 process pool and molecular mass standards (MW Stds.) were loaded as follows: lanes: 1 = process pool, non-reduced, 2 μg rhIGF-1; 2 = process pool, reduced, 2 μg rhIGF-1; 3 = low-molecular-mass standards, reduced. The gel was stained with Coomassie-R250. (B) Analysis by IEF. Process pool sample and p*I* standards were loaded as follows: lanes: 1 = rhIGF-1, 10 μg; 2 = p*I* standards. The gel was stained with Coomassie-G250. (C) Gradient RP-HPLC analysis. The chromatography was performed on a 5-μm Vydac C_{18} column using a 10-60% ACN gradient over 50 min, 0.1% TFA, 1 ml/min, 22°C. The process pool sample was diluted 5-fold into the initial mobile phase and 250 μl were loaded. The inset shows an expanded view of the later-eluting peaks. (D) Isocratic RP-HPLC analysis. The chromatography was performed isocratically on a 5-μm Vydac C_{18} column at 28.5% ACN, 0.1% TFA, 0.5 ml/min, 50°C. The process pool sample was diluted 10-fold into the mobile phase and 25 μl were loaded. After 40 min, the column was washed with 60% ACN to remove the more hydrophobic species. The four predominant rhIGF-1 variants are labeled on the chromatogram.

ly loaded onto a RP-HPLC column, from an analytical load to a preparative mass overload condition, the non-linear elution peak profile takes the shape of a right triangle [21]. When a mixture of components is loaded to this level, the highly concentrated leading edge of a product peak can be displaced forward during the elution into the next less hydrophobic species while the dilute trailing edge continues to elute true. This observation is thought to be due to a combination of the various component equilibrium isotherms and the intrinsic column efficiency [22–24]. For most separations, the optimal condition is usually achieved by maximizing the difference in retention time between the product and any leading edge contaminants, thereby effectively augmenting the effective capacity of the separation. The effective capacity

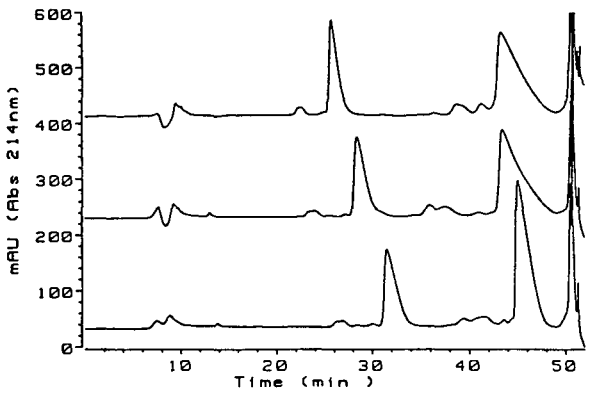

Fig. 2. Counter-ion substitution and gradient optimization. The chromatography was performed at 50°C on a 5-μm Vydac C_{18} column at 0.5 ml/min; isocratically at 28.5% ACN–0.1% TFA (upper trace); isocratically at 27.5% ACN, 20 m*M* HAc, 20 m*M* NaCl (middle trace); or with 20 m*M* HAc, 20 m*M* NaCl using a shallow 27–28% ACN/40 min gradient (lower trace).

is defined as the dynamic capacity (mg) of well resolved product per unit bed volume (ml). When the capacity of the C_4 column using the acetate buffer mobile phase was evaluated the non-linear profile became apparent. Even moderate loading (50 μg of rhIGF-1/ml bed volume) caused a loss in resolution between the product and the leading edge variants (Fig. 3C).

3.3. Parameter evaluation

After transferring the analytical method to a preparative medium, the second goal was to optimize the selectivity of the mobile phase for enhanced resolution which would ultimately translate to higher effective capacity. However, the evaluation of even a limited number of variables increases as a power function of the combinations. Therefore, to efficiently optimize this system, a limited three-dimensional set of conditions was established within the framework of the following parameters: pH (3, 5 and 7), buffer concentration (20 and 100 m*M*) and temperature (22 and 50°C). For this screen the solvent was limited to ACN and the counter-ions to sodium, chloride, phosphate and acetate. These conditions were chosen following considerations of buffer–solvent compatibility, instru-

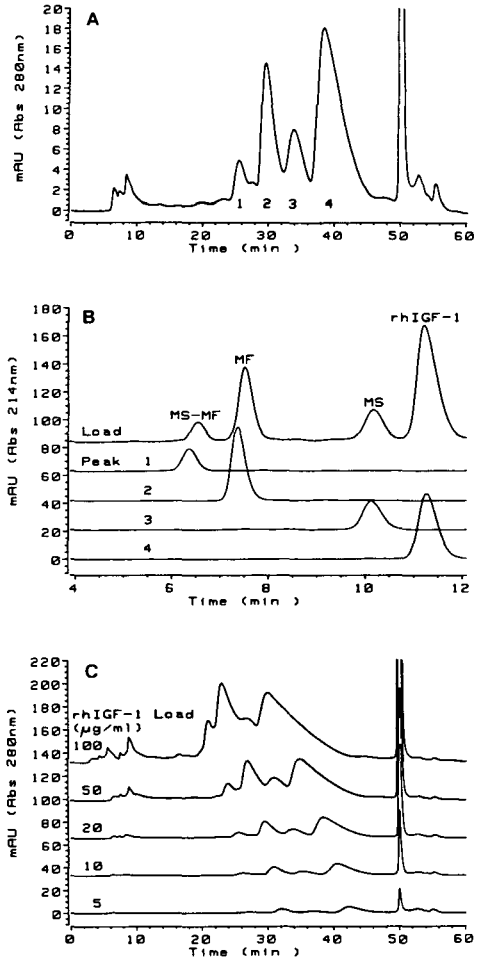

Fig. 3. Preparative evaluation of acetate buffer pH 3 mobile phase. (A) Analytical separation on preparative media. The preparative chromatography was performed on an analytical-size, 30 × 0.39 cm, 15-μm Waters C_4 column: 27–28% ACN/40 min, 20 m*M* HAc, 20 m*M* NaCl, pH 3, 0.5 ml/min, 50°C. rhIGF-1 (20 μg) was loaded onto the column and four peak fractions were collected. (B) Analysis of peak fractions. The rapid analytical chromatography was performed on a 5-μm Vydac C_{18} column using a modified version of the initial analysis (Fig. 1D). The flow-rate was increased to 2 ml/min at 50°C. A 28–29% ACN/10 min gradient, with 0.1% TFA, maintained a constant gradient volume. The fractions collected from (A) were diluted two-fold with water and 100 μl were injected. The four predominant rhIGF-1 species are labeled on the chromatogram: 1 = methionine-sulfoxide/misfolded (MS-MF); 2 = misfolded (MF); 3 = methionine-sulfoxide (MS); 4 = rhIGF-1. (C) Effective loading capacity. The chromatography was performed as in (A). Increasing levels of rhIGF-1 were sequentially loaded onto the column from 5 to 100 μg rhIGHF-1/ml bed volume.

mentation limits and potential molecular instability.

A Waters C_4 column was equilibrated and loaded at 10% ACN for each mobile phase counter-ion condition, then ramped over 1 min to the initial gradient condition. The solvent level was adjusted such that the rhIGF-1 would elute during a 1% ACN gradient over 40 min. Low load levels (20 μg rhIGF-1/ml bed volume) were used throughout the evaluation to allow easy peak identification. Comparing the acetate buffer mobile phase Waters C_4 chromatography at 22 and 50°C resulted in a dramatic peak sharpening (Fig. 4A and B). This effect is

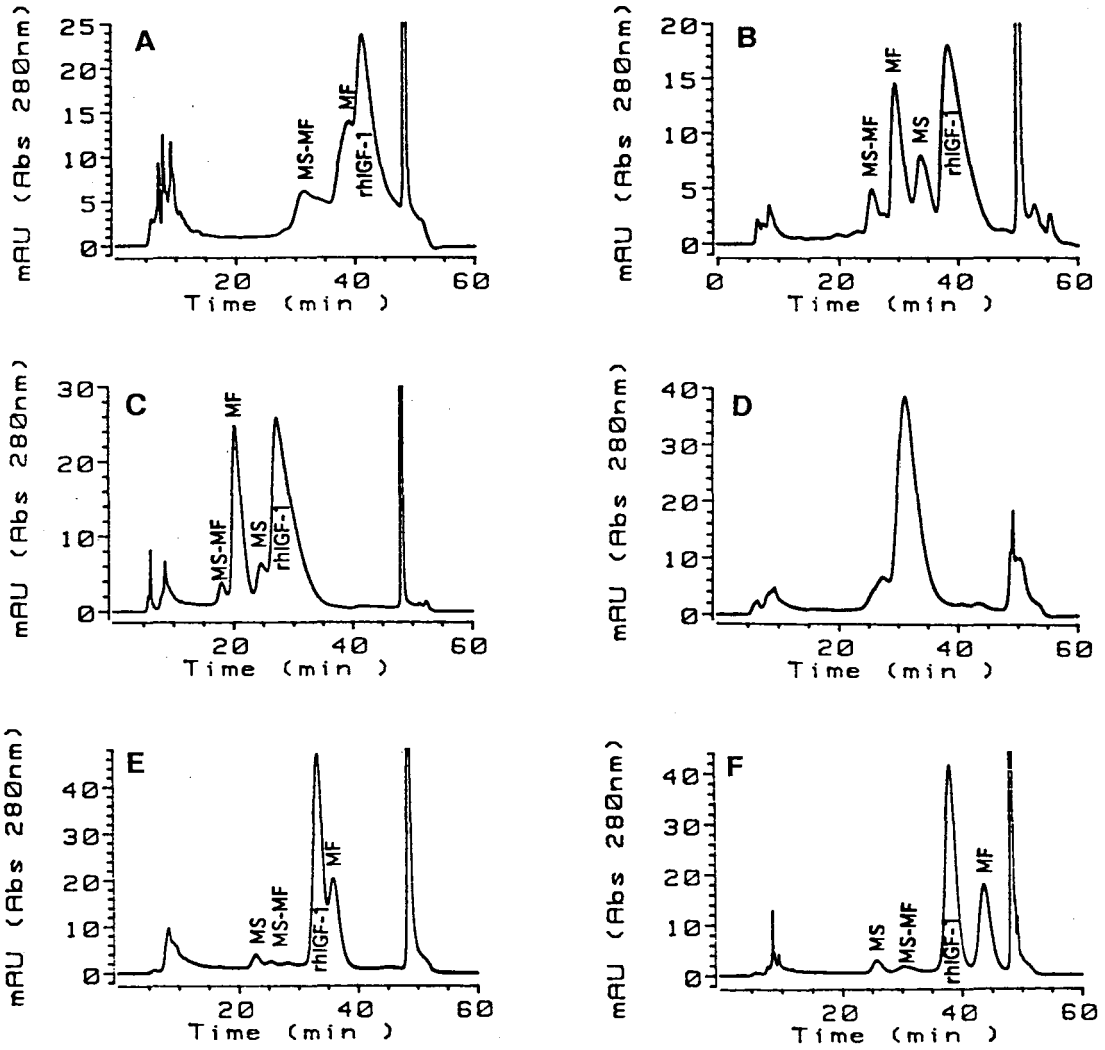

Fig. 4. Optimization of pH and ionic strength. The chromatography was performed on an analytical-size, 30 × 0.39 cm, 15-μm Waters C_4 column equilibrated in 10% ACN and the respective counter-ion. The % ACN was ramped in 1 min to the initial gradient condition. The solvent strength was independently modified such that the rhIGF-1 would elute during a near-isocratic 1% ACN/40 min gradient at 0.7 ml/min. The load level was maintained at 20 μg rhIGF-1/ml bed volume. The four predominant rhIGF-1 species are labeled on the chromatogram: methionine-sulfoxide/misfolded (MS-MF), misfolded (MF), methionine-sulfoxide (MS) and rhIGF-1. (A) 20 m*M* HAc, 20 m*M* NaCl, pH 3, 22°C, 26–27% ACN; (B) 20 m*M* HAc, 20 m*M* NaCl, pH 3, 50°C, 27–28% ACN; (C) 20 m*M* H_3PO_4, 20 m*M* NaCl, pH 3, 50°C, 27–28% ACN; (D) 20 m*M* HAc, 20 m*M* NaCl, pH 5, 50°C, 26–27% ACN; (E) 20 m*M* Na_2HPO_4, pH 7, 50°C, 23–24% ACN; (F) 100 m*M* Na2HPO4, pH 7, 50°C, 23–24% ACN.

presumably due to increased diffusivity through a viscosity mediated decrease in the resistance to mass transfer [25]. Since the higher-temperature effects appeared generally beneficial, the 50°C condition was maintained in all subsequent experiments. Concerning product stability, material generated at the higher temperature was biologically active. However, activity may be compromised at temperatures higher than 50°C. Changing the counter-ion from 20 m*M* acetate buffer (HAc–NaCl) to 20 m*M* phosphate buffer (20 m*M* H_3PO_4 + 20 m*M* NaCl, pH adjusted to 3 with NaOH) while maintaining the pH at 3 had no major effect on resolution (Fig. 4C). Increasing the pH from 3 to 5 using acetate buffer caused all four species to co-elute (Fig. 4D). However, a significant change in selectivity resulting in a further shift in both relative retention time and elution order of the four rhIGF-1 variants occurred with an increase in the pH using 20 m*M* phosphate buffer, pH 7 (20 m*M* Na_2HPO_4, pH adjusted to 7 with HCl, Fig. 4E). Based on peak area, it was shown that the misfolded peak eluted after the main rhIGF-1 peak and the methionine-sulfoxide peak shifted from the leading edge of the product to the beginning of the gradient. The gradient conditions necessary for elution changed from 26–27% (pH 3) to 23–24% ACN (pH 7). The optimum conditions were achieved by raising the buffer concentration from 20 to 100 m*M* phosphate (Fig. 4F). Enhanced resolution correlated with an increase in peak symmetry (Table 1). This change in selectivity with increased pH could be caused by an ion-pair suppression of hydrophilic or non-specific ionic interactions of rhIGF-1 with the base matrix [26], an observation also made for other basic molecules [27]. Alternatively, if the solubility of rhIGF-1 is enhanced in the 100 m*M* phosphate buffer pH 7 mobile phase, it could potentiate rapid partitioning and a concomitantly sharper peak shape [28].

Four peak fractions were isolated from the optimized (100 m*M* phosphate–ACN, pH 7, 50°C) Waters C_4 preparative chromatography conditions (Fig. 5A). Analysis on the Vydac C_{18} column confirmed the relative mobility of the rhIGF-1 variants (Fig. 5B). A fifth variant which was apparently co-migrating with the main rhIGF-1 peak using the acetate buffer is now well resolved (peak 2 analysis) and was identified as a hydroxamate species [13]. By starting with the protein load level used during the methods development and then increasing the load in subsequent runs by a factor of two, the optimized chromatography appears to have an effective capacity >1000 μg rhIGF-1 product/ml of bed volume (Fig. 5C). This 100-fold enhancement in the effective capacity between the initial acetate and optimized phosphate mobile phases is primarily due to the misfolded rhIGF-1 peak shift and the 5-fold increase in the difference in relative retention times between rhIGF-1 and the less hydrophobic variant species, and is especially pronounced during non-linear elution due to mass overloading, as described earlier.

Additional analytical size columns packed with a variety of preparative RP-HPLC media from

Table 1
Effects of pH and buffer concentration on resolution and peak symmetry

Counter-ion	pH	Buffer concentration(m*M*)	Temperature (°C)	Main, A_s	Main/Met, R_s	Main/Mis, R_s
HAc + NaCl	3	20	22	0.64	*	0.28
HAc + NaCl	3	20	50	0.37	0.65	1.51
H_3PO_4 + NaCl	3	20	50	0.29	0.47	1.39
HAc + NaCl	5	20	50	*	*	*
Na_2HPO_4	7	20	50	0.70	2.97	0.74
Na_2HPO_4	7	100	50	0.78	3.48	1.51

* = Peaks overlap. Main peak symmetry [19], $A_s = B/A$, where A, B = half peak width from vertical line from peak apex. Resolution, $R_s = 1.18(t_{R,2} - t_{R,1})/(w_2 + w_1)$, where t_R = retention time and w = peak width at half peak height. Main/Met = R_s between main IGF-1 peak and met-sulfoxide peak; Main/Mis = R_s between main IGF-1 peak and misfolded peak.

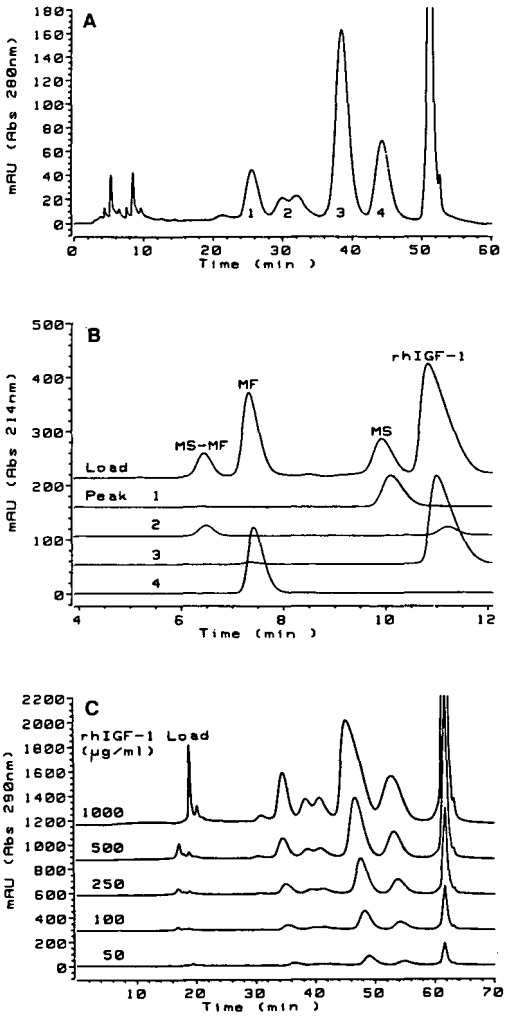

Fig. 5. Preparative evaluation of 100 m*M* phosphate buffer pH 7 mobile phase. (A) Differential selectivity at pH 7. The preparative chromatography was performed on a 15-μm Waters C_4 column using the optimized conditions (Fig. 4F), 23–24% ACN/40 min, 100 m*M* Na_2HPO_4, pH 7, 0.7 ml/min, 50°C. rhIGF-1 (100 μg) was loaded onto the column and four peak fractions were collected. (B) Analysis confirms shift in retention times. The rapid analytical chromatography was performed on a 5-μm Vydac C_{18} column as in Fig. 3B. The fractions collected from (A) were diluted two-fold with water and 100 μl were injected. The order of elution of the species was altered as labeled on the chromatogram: 1 = methionine-sulfoxide (MS); 2 = methionine-sulfoxide/misfolded (MS-MF) and a second rhIGF-1 co-eluting peak; 3 = rhIGF-1; 4 = misfolded (MF). (C) Effective loading capacity. The chromatography was performed as in (A). Increasing levels of rhIGF-1 were sequentially loaded onto the column from 50 to 1000 μg rhIGF-1/ml bed volume.

other suppliers were evaluated using the optimized 100 m*M* phosphate buffer, pH 7, ACN mobile phase (Fig. 6A–F). The conditions were adjusted as necessary for each individual column in order to have the product elute within a similar gradient slope (1% ACN gradient per 40 min). Chromatography on the various media resulted in similar profiles, independent of base matrix (silica or polymer), alkyl chain length (C_4 or C_8) or pore diameter (200–300 Å). Differences in particle size (7–20 μm) and pore diameter can significantly alter surface area and appear to affect resolution. The Amicon medium was unable to resolve the different variants under these conditions, although it was not independently optimized further to improve the separation.

3.4. Scale-up

The optimized preparative chromatography was scaled in two stages. The Hewlett-Packard 1090 HPLC system used for method development delivers precise solvent blending by utilizing separate dual-syringe metering pumps for each reservoir to determine composition and flow, and is accurate even when using neat aqueous and organic phases. When neat solvents were tested with either the pilot-scale Waters DeltaPrep or preparative-scale Biotage KiloPrep instruments, neither one had the absolute accuracy to deliver the 1% gradient needed for the separation. These chromatographs use low-pressure mixing with solenoid-based gradient formation. This problem was overcome by premixing the 100 m*M* phosphate buffer with 20% ACN (A buffer) and 40% ACN (B buffer). In addition, these premixed buffers required no further degassing to prevent cavitation. The Waters RCM and cartridge format of column scale-up was chosen for its ability to easily and economically utilize the same column hardware for different products, in addition to the radial compression technology, *per se*. Of the columns tested, the Waters C_4 medium appeared to have comparable resolution and was readily available in the cartridge format. A counter-current heat exchanger

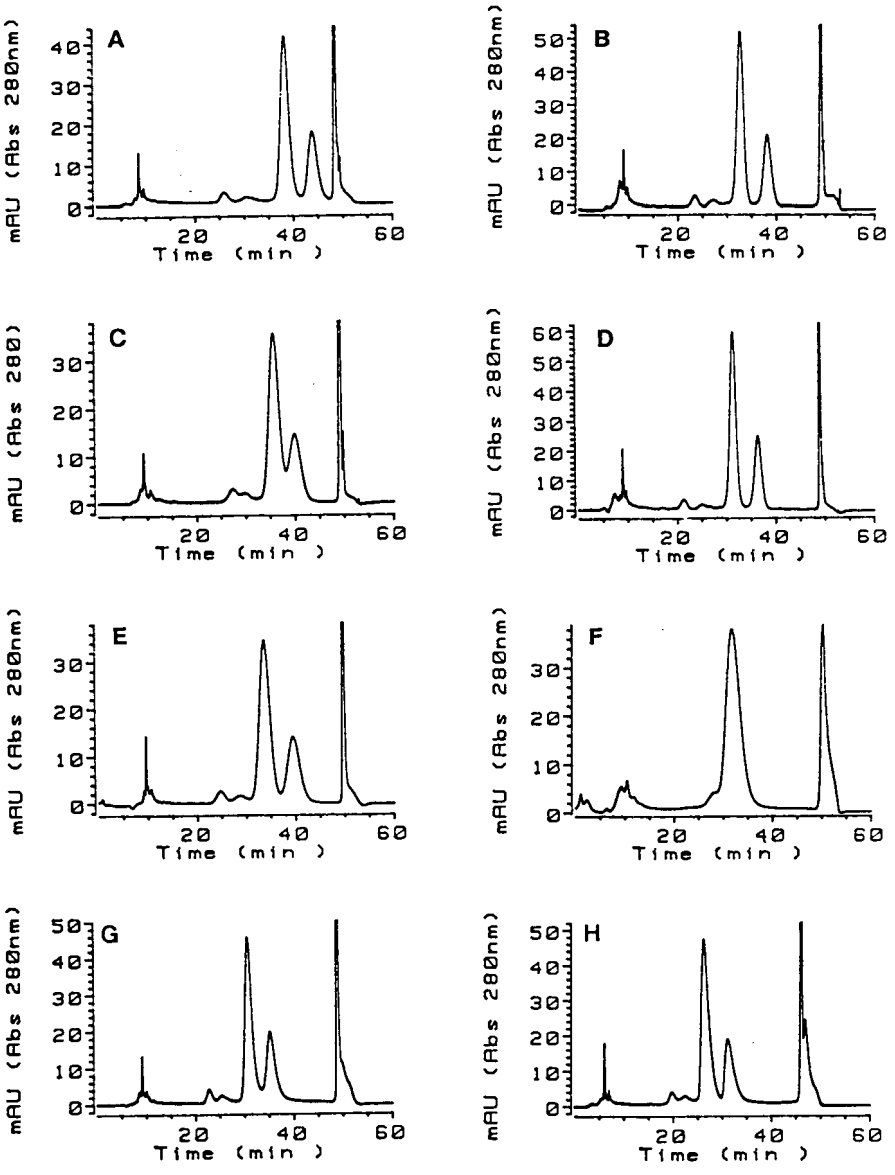

Fig. 6. Comparison of different preparative media. The chromatography in each case was performed on columns with similar geometry, using the optimized 100 m*M* phosphate buffer pH 7 mobile phase, 0.7 ml/min, 50°C. The load level was maintained at 20 μg rhIGF-1/ml bed volume. (A) Waters C_4, 15 μm, 300 Å, 23–24% ACN; (B) YMC-C_8, 15 μm, 300 Å, 23.5–24.5% ACN; (C) Baker C_4, 15 μm, 275 Å, 22.5–23.5% ACN; (D) Kromasil C_8, 10 μm, 200 Å, 25–26% ACN; (E) Impaq C_4, 20 μm, 200 Å, 25–26% ACN; (F) Amicon C_8, 20 μm, 250 Å, 26–27% ACN; (G) PLRP-S, 8 μm, 300 Å, 23–24% ACN; (H) Eurosil C_4, 7 μm, 300 Å, 21.5–22.5% ACN.

and recirculating water bath was placed in-line with the column and the temperature of the column inlet and outlet monitored with thermocouples to maintain a 50°C mobile phase throughout the separation.

The first scale increase from the Hewlett-Pac-

kard 1090 to the Waters Delta-Prep System involved a 145-fold increase in cross-sectional area at constant column length, from the analytical size 30 × 0.39 cm (3.58 ml bed volume) stainless-steel column to a 30 × 4.7 cm (520 ml) radial compression cartridge. By using the same gradient slope of 1% ACN over 40 min and maintaining the residence time at approximately 5 min (5.76 cm/min), the flow-rate was increased to 100 ml/min with identical chromatography. To initiate a sequence of cycles, a single blank run through the system fully equilibrated the column from room temperature to 50°C (as measured at the column outlet) with a 1°C temperature drop across the column.

The second scale increase from the Waters DeltaPrep to the Biotage KiloPrep System was accomplished in both column dimensions. The cross-sectional area was increased 4.5-fold and the length 2-fold to a 60 × 10 cm (4.71 l) cartridge for an additional 9-fold, or an overall total of 1305-fold scale-up relative to the analytical column. Since the bed geometry had changed, the flow-rate was adjusted based on a linear velocity to 450 ml/min, using a proportionately larger heat-exchanger. The cycle time was increased to account for the slower flow-rate, maintaining the same relative gradient volume. The chromatogram was similar to those from the analytical and pilot scale runs. The purity of the collected product peak was >99% rhIGF-1, as assessed by the Vydac C_{18} analysis. At load levels of 1000 μg rhIGF-1/ml of bed volume, 4.5 g of product can be processed per cycle in the large RCM. The mass balance of product across the column at the various scales is identical (Table 2).

4. Conclusions

Because of its stable structure, small size, and relatively hydrophobic character, the selectivity of RP-HPLC was utilized to isolate rhIGF-1 from its fermentation variants. Procedures utilizing RP-HPLC have been published for many molecules [29], and are included in the purification of native, synthetic and rhIGF-1 [14,30–34], However, few papers have shown a systematic optimization of a preparative RP-HPLC isolation step of a recombinant protein resulting in pharmaceutical purity [35]. Preparative chromatography differs from analytical chromatography in three principal ways which dictate the approach of the respective methods development. (a) Purity—when isolating a single species from a complex mixture, only the resolution of the product from its closest eluting neighbors is of interest. In addition, the use of mobile phase solvents and modifying agents whose pharmacological safety is questionable, especially if they interact tightly with the product and whose removal necessitates validation, should be restricted. (b) Effective capacity—high yield, recovery and throughput should be developed in parallel with an optimized separation to address questions relating to process economics and feasibility. (c) Molecular integrity—bioactivity of the product must be maintained.

The practical limitations of process-scale RP-HPLC include the high cost of small-particle high-efficiency packing material and the high-pressure equipment needed to generate moderate flow-rates [36]. Assuming that the integrity of the molecule is not compromised by the potentially denaturing conditions of reversed-phase

Table 2
Recovery of rhIGF-1 during RP-HPLC scale-up

Column	Dimensions (cm)	Bed volume	Scale-up	Purity	Recovery	
					Mass	%
Analytical	30 × 0.39	3.58 ml	1-fold	>99	3.5 mg	97
Pilot RCM	30 × 4.7	520 ml	145-fold	>99	0.5 g	96
Prep RCM	60 × 10	4.71 L	1305-fold	>99	4.5 g	96

chromatography, the approach of large-scale HPLC process development has typically had three stages [21,37]. First, develop a high resolution separation using 2–5-μm media. Second, transfer that method to a 15–40-μm particle with similar surface chemistry. Third, modify the method as needed for optimal process considerations. Each change in medium can result in another cycle of optimization.

For this RP-HPLC isolation of rhIGF-1, a conventional low-pressure development methodology was utilized. Initially, a sensitive, rapid, high-resolution analytical separation was developed which could be used to both identify closely related species of rhIGF-1 and quantitate the level of product. The selectivity of the initial analytical and preparative methods was similar. However, as the components in the methods diverged the selectivity was significantly altered. Then the RP-HPLC analysis using the analytical method became justifiable. Using preparative-size media packed in a small column with easily scalable geometry, parameters based on various pH and ionic strength buffers, counter-ions, temperatures, and media were evaluated. As the other analytical techniques of SDS-PAGE and IEF utilized during process development were unable to adequately quantitate the level of rhIGF-1 variants, the rapid RP-HPLC analytical chromatography became the principal technique to monitor the progress of the development effort, analyze for product purity and determine yield and effective capacity. When an acceptable set of preparative conditions was elucidated, a 1000-fold scale-up of the separation was achieved based on the chromatographic principles of constant linear velocity or residence time.

The bulk of the literature describing protein purification via preparative RP-HPLC typically describes a multi-peak, high-resolution analytical procedure being directly transferred to a larger bed volume. The columns are typically 1–2.5 cm in diameter, contain 5-μm media and the method is scaled 5–10-fold using analytical instrumentation. This approach is satisfactory from a research perspective for isolating micrograms or even milligrams of protein. However, for pharmaceutical manufacturing where grams or kilograms of ultrapure product are required, a different developmental format should be applied. As described in this paper, a systematic evaluation of practical process parameters using medium-particle preparative media will facilitate translating an analytical RP-HPLC method into a high-capacity preparative recovery step. Chromatographic optimization should center on factors which influence selectivity, focusing on maximizing the band spacing between the product and its closest eluting neighbors. Since non-linear elution profiles occur during mass overload conditions, the first less hydrophobic contaminant to the product peak will be of particular interest. Special attention should be given to buffer conditions known to enhance product solubility. Subsequently, scaling-up the chromatography 10–1000-fold or more using preparative equipment is straightforward.

References

[1] E. Rinderknecht and R.E. Humbel, *Proc. Natl. Acad. Sci. U.S.A.*, 73 (1976) 2365.
[2] E. Rinderknecht and R.E. Humbel, *J. Biol. Chem.*, 253 (1978) 2769.
[3] J.J. Van Wyk, L.E. Underwood, R.L. Hintz, S.J. Voina and R.P. Weaver, *Recent Prog. Horm. Res.*, 30 (1974) 259.
[4] M. Binoux, *Ann. Endocrinol.*, 41 (1980) 157.
[5] D.R. Clemmons and J.J. Van Wyk, *Handb. Exp. Pharmacol.*, 57 (1981) 161.
[6] R.C. Baxter, *Adv. Clin. Chem.*, 25 (1986) 49.
[7] E. Underwood, R. Clemmons, M. Moss, A.J. D'Ercole and J.M. Ketelsleger, *Hormone Res.*, 24 (1986) 166.
[8] H.P. Guler, J. Zapf and E.R. Froesch, *N. Eng. J. Med.*, 317 (1987) 137.
[9] H.P. Guler, J. Zapf, E. Scheiwiller and E.R. Froesch, *Proc. Natl. Sci. U.S.A.*, 85 (1988) 4889.
[10] H. Schagger and G. Von Jagow, *Anal. Biochem.*, 166 (1987) 368.
[11] A.T. Andrews, *Electrophoresis,* Oxford University Press, New York, 1986.
[12] V. Neuhoff, N. Arnold, D. Taube and W. Ehrhardt, *Electrophoresis*, 9 (1988) 255.
[13] E. Canova-Davis, M. Eng, V. Mukku, D.H. Reifsnyder, C.V. Olson and V.T. Ling, *Biochem J.*, 285 (1992) 207.
[14] G. Forsberg, G. Palm, A. Ekebacke, S. Josephson and M. Hartmanis, *Biochem. J.*, 271 (1990) 357.
[15] F. Raschdorf, R. Dahinden, W. Maerki, W.J. Richter and J.P. Merryweather, *Biomed. Environ. Mass Spectrom.*, 16 (1988) 3.

[16] M. Iwai, M. Massakazu, K. Tamura, Y. Ishii, H. Yamada and M. Niwa, *J. Biochem. (Tokyo)*, 106 (1989) 949.
[17] T.F. Gabriel, *Int. J. Peptide Protein Res.*, 30 (1987) 40.
[18] M.J. O'Hare and E.C. Nice, *J. Chromatogr.*, 171 (1979) 209.
[19] E.C. Nice, M.W. Capp, N. Cooke and M.J. O'Hara, *J. Chromatogr.*, 218 (1981) 569.
[20] S. Linde and B.S. Welinder, *J. Chromatogr.*, 536 (1991) 43.
[21] G.B. Cox and L.R. Snyder, *LC·GC*, 6 (1988) 894.
[22] S. Golshan-Shirazi and G. Guiochon, *Am. Biotech. Lab.*, 8 (1990) 24.
[23] P. Gareil, *Prep. Chrom.*, 1 (1991) 195.
[24] Y.B. Yang, K. Harrison, D. Carr and G. Guiochon, *J. Chromatogr.*, 590 (1992) 35.
[25] M.T. Tyn and T.W. Gusek, *Biotechnol. Bioeng.*, 35 (1990) 327.
[26] Cs. Horváth and W. Melander, *J. Chromatogr. Sci.*, 15 (1977) 393.
[27] R.J.M. Vervoort, F.A. Maris and H. Hindriks, *J. Chromatogr.*, 623 (1992) 207.
[28] K. Krummen and R.W. Frei, *J. Chromatogr.*, 132 (1977) 27.
[29] B.A. Bidlingmeyer (Editor), *Preparative Liquid Chromatography*, Elsevier, Amsterdam, 1987.
[30] M.E. Svoboda, J.J. Van Wyk, D.G. Klapper, R.E. Fellows, F.E. Grissom and R.J. Schlueter, *Biochemistry*, 19 (1980) 790.
[31] H.J. Cornell, N.M. Boughdady and A.C. Herrington, *Prep. Biochem.*, 14 (1984) 123.
[32] P.E. Petrides, R.L. Hintz, P. Bohlen and J.E. Shively, *Endocrinology*, 118 (1986) 2034.
[33] H.J. Cornell and P.H. Brady, *J. Chromatogr.*, 421 (1987) 61.
[34] G.L. Francis, K.A. McNeil, J.C. Wallace, F.J. Ballard and P.C. Owens, *Endocrinology*, 124 (1989) 1173.
[35] E.P. Kroeff, R.A. Owens, E.L. Campbell, R.D. Johnson and H.I. Marks, *J. Chromatogr.*, 461 (1989) 45.
[36] R.M. Nicoud and H. Colin, *LC·GC*, 8 (1990) 24.
[37] L.R. Snyder, J.L. Glajch and J.J. Kirkland, *Practical HPLC Method Development*, Wiley-Interscience, New York, 1988.

ELSEVIER

Journal of Chromatography A, 675 (1994) 113–122

JOURNAL OF CHROMATOGRAPHY A

Non-denaturing assay for the determination of the potency of recombinant bovine somatotropin by high-performance size-exclusion chromatography

Jen P. Chang*[,a], R. Craig Tucker[b], Barbara F. Ghrist[b], Mark R. Coleman[a]

[a]*Lilly Research Laboratories, Eli Lilly and Co., P.O. Box 708, Greenfield, IN 46140, USA*

[b]*Lilly Research Laboratories, Eli Lilly and Co., Indianapolis, IN 46285, USA*

(First received February 18th, 1993; revised manuscript received March 18th, 1994)

Abstract

A non-denaturing high-performance size-exclusion chromatographic method has been developed for the determination of the potency of recombinant bovine somatotropin (rbST) in bulk materials. A Spherogel TSK 3000 PW column containing a polymer base packing material with very hydrophilic bonded surface was used in this method. Ammonium hydrogencarbonate buffer pH 9.0, was used as the mobile phase. This method was shown to be non-denaturing by rat mass-gain assay and radioreceptor assay. The optimization for the separation and determination of rbST has been investigated. The method was validated for the determination of rbST in bulk materials.

In addition, rbST soluble aggregates formed in the production process due to protein association, used to be found in bulk materials. The behavior of rbST soluble aggregates in ammonium hydrogencarbonate solutions have been studied. The bio-inactive aggregates can be separated by the method developed in this study. The high–low chromatographic technique has been used to estimate rbST soluble aggregates in bulk materials.

1. Introduction

Recombinant DNA-derived bovine somatotropin (rbST) is under development for increased milk production and improvement of efficiency of production in lactating dairy cows. It is important to establish an assay for the determination of the potency of rbST for quality control. Several methods for determination of human growth hormone have been reported [1–5] but only a few publications for the quantification of rbST were found in the literature [6–8]. For years, the potency of rbST has been estimated by a rat mass-gain method [9]. Recently, a radioreceptor assay has been developed for the biopotency of rbST [10]. This method appears to be more accurate than the rat mass-gain method. However, these assays are time-consuming and less reproducible to be used to quantify rbST in routine analysis. In this case, it could be considered to determine the potency by physico-chemical techniques. In recent years, reversed-phase high-performance liquid chromatography (RP-HPLC) has been employed for rbST determination [7,8]. Nevertheless, RP-HPLC was not an appropriate method for the determination of rbST potency because of the denaturation and degradation produced in the chromatographic

* Corresponding author.

0021-9673/94/$07.00
SSDI 0021-9673(94)00281-D

process by acidic medium and organic solvents used in the mobile phase. The results obtained in the study of the effect of acidification indicated that bovine growth hormone results in increased unfolding of the hormone as the pH in solution was reduced from 5 to 2 [11]). High-performance size-exclusion chromatography (HPSEC) has been employed to assay rbST [6–8] but these methods cannot be used as potency assays because of the denaturation in mobile phases containing sodium dodecyl sulfate (SDS) or 6 *M* guanidine hydrochloride (Gn · HCl), in the methods.

rbST is composed of 199 amino acids [12] with a molecular mass of 22 818. rbST shows a stronger hydrophobicity (calculated value 478) [13] because of 69 hydrophobic amino acids including 28 leucine, 14 alanine, 14 phenylalanine and 7 isoleucines in the molecule. Selection of a stationary phase in SEC for this protein was difficult. The packing materials used in SEC for rbST potency determination had to be very hydrophilic. Consequently, the strong hydrophobic protein rbST would not be adsorbed on the packing material surface in the SEC process. Most HPLC packing materials are made of silica gel as a supporting base and can only be used at pH lower than 7.4. rbST maintains bioactivity in weak alkaline solution. Therefore, polymer-base packing materials with hydrophilic bonded surface would be available for the separation and determination of rbST potency.

Based upon the requirements mentioned above, a non-denaturing HPSEC assay was developed in this study for the determination of rbST potency in bulk materials. Spherogel TSK 3000 PW column containing a polymer-base packing material with very hydrophilic bonded surface was applied in this method with ammonium hydrogencarbonate buffer used as a mobile phase. This method was shown to be non-denaturing by rat mass-gain assay and radioreceptor assay. The optimal conditions which include control of salt concentration, pH in the mobile phases and flow-rate, have been investigated for the separation and determination of rbST. This method has been validated for the determination of rbST in bulk materials.

rbST soluble aggregates formed in the production process due to protein association, used to be found in bulk materials. These aggregates are bio-inactive. Therefore, it is important to develop a method to determine rbST soluble aggregates for quality control.

In pharmaceutical analysis, often a reference standard is not available for each component, mostly only for main components. In this case, an alternative method was required to use for the quantitation of impurities in samples. High–low chromatography is a technique that can be employed to estimate trace impurities in samples [14]. Generally, the high–low approach utilizes a pair of sample solutions with a higher concentration and a lower concentration. In the chromatogram obtained from a higher-concentration sample solution, the main component response is off-scale and the impurity peak response is in the linear range of the detection system. The main component peak response in the solution with a lower-concentration sample concentration, 1 to 50 or 100 dilution of the higher-concentration sample solution, was quantitated in the linear region of the detection system. The percentage of the impurity can be calculated by comparing the peak responses in the pair of chromatograms because the concentration difference between the two solutions is known. The limitation of this approach is that it requires close peak absorptivity between the main component and the impurity if UV–visible detection is used. In addition, the selection of chromatographic conditions is important to provide accurate results.

In this study, the high–low chromatographic technique was used to estimate soluble aggregates in rbST bulk materials. Behavior of rbST soluble aggregates in solutions has also been investigated.

2. Experimental

2.1. Chemicals and reagents

All reagents were of analytical-reagent grade and were used without further purification. Water was obtained from a Millipore Milli-Q water purification system. SDS (Aldrich, Mil-

waukee, WI, USA) and Gn·HCl (Sigma, St. Louis, MO, USA) were used as denaturing agents. Protein standards were obtained from Sigma molecular mass marker kits. The rbST reference standard and bulk materials were obtained from Eli Lilly and Company (Indianapolis, IN, USA).

2.2. Chromatography

The majority of the study was performed with a Waters 625 LC system with a 991+ photodiode array detector and a WISP 712 autosampler (Waters Chromatography, Milford, MA, USA). The validation work was carried out on a Beckman System Gold HPLC system (Fullerton, CA, USA) consisting of a Model 126 solvent delivery system, a Model 166 variable-wavelength detector, and a Model 507 autosampler. All measurements were monitored at 280 nm. Spherogel TSK 3000 PW columns (300 × 7.5 mm I.D.) (Beckman, Palo Alto, CA, USA) and TSK gel G2500PWXL column (300 × 7.8 mm I.D.) (TosoHaas, Montgomeryville, PA, USA) were employed for most of the studies except as indicated. The mobile phase was 0.2 *M* ammonium hydrogencarbonate adjusted to pH 9 with NaOH. Ammonium hydrogencarbonate 0.2 *M* (pH 9) with 1% SDS was used as a mobile phase in the SDS SEC study. All separations were achieved at room temperature with a flow-rate of 0.5 ml/min. The injection volume was 20 μl. The quantity of rbST present in the samples was calculated by constructing a linear regression plot of concentration of rbST in mg/ml *versus* peak area. All chromatographic data were collected, stored and analyzed on a HP-1000 computer system (Hewlett-Packard, San Fernando, CA, USA).

2.3. Sample and reference standard preparation

Samples were typically prepared at a concentration of 0.5–0.8 mg/ml in the mobile phase. To minimize incomplete dissolution, an aliquot of mobile phase was added and the sample solution was allowed to stand at room temperature for 30 min. After that the solution was gently shaken for 5–10 min and then diluted to volume. To remove insoluble substances, sample solutions were filtered through an acrodisc low protein binding filter (0.45 μm) prior to chromatography. rbST reference standards were immediately prepared in mobile phase at three concentrations ranging between 0.1–1.0 mg/ml.

2.4. High–low chromatography

In high–low chromatography, a 10 mg/ml solution of rbST sample was prepared in the mobile phase and filtered through an Acrodisc filter (0.45 μm) as a high-concentration sample solution. A low-concentration sample solution was obtained by making a 1 to 50 dilution of the high-concentration sample solution with the mobile phase. Both solutions were chromatographed under identical experimental conditions. The percentage of minor components (soluble aggregates) can be calculated as

$$\% \text{ Soluble aggregates} = (A_{SA}/50)/[A_M + (A_{SA}/50)] \cdot 100$$

where A_{SA} is the peak response of the soluble aggregates that was measured from the high-concentration chromatogram and A_M is the peak response of rbST main component from the low-concentration chromatogram.

3. Results and discussion

3.1. Separation

Fig. 1 shows chromatograms of three rbST lots that were obtained on a Spherogel TSK 3000PW column with 0.2 *M* ammonium hydrogencarbonate (pH 9.0) mobile phase. In the chromatograms, a main peak at 840 s in all three samples was identified as the rbST monomer. Peaks eluting around 590 s, the total exclusion volume of the column, in chromatograms B and C may be rbST soluble aggregates with very high molecular mass. No aggregates were found in lot 001 but lot 003 contains higher than 30% soluble aggregates, and lot 002 had approximately 7%

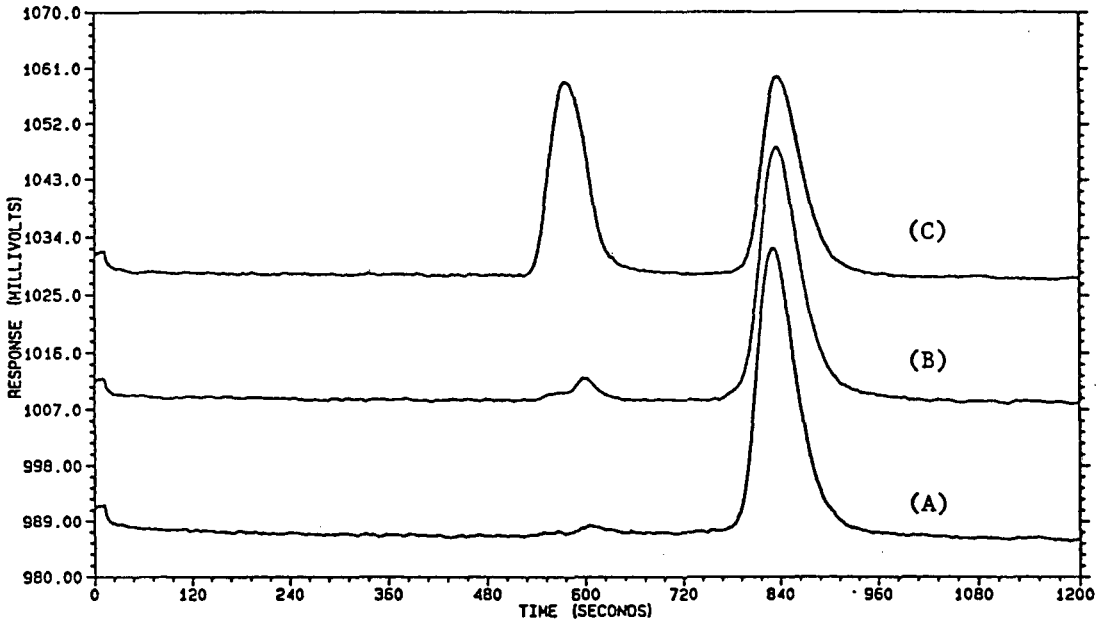

Fig. 1. SEC chromatograms of rbST sample lots. Column: TSK Spherogel 3000 PW (300 × 7.5 mm). Mobile phase: 0.2 *M* ammonium hydrogencarbonate (pH 9) in water. Flow-rate: 0.5 ml/min. Sample concentration: 1 mg/ml. Injection volume: 20 μl. (A) lot 001; (B) lot 002; (C) lot 003.

soluble aggregates. In order to obtain high column efficiency in the separation, a TSK 2500PWXL column packed with 5-μm polymer-base packing material had been tried to use for the separation of rbST. The poor resolution between rbST soluble aggregates and monomer, that is due to smaller permeation volume of this packing material, was found even though a sharper peak of the rbST monomer was obtained on this column.

3.2. Molecular mass measurement

The apparent molecular masses of rbST monomer and soluble aggregates were determined in 0.1 *M* NH_4HCO_3–0.1 *M* NaCl solution based upon a standard protein calibration curve (Fig. 2, plot A). Using several lots, the molecular mass of the rbST monomer was found to be 23 800. The molecular mass of the soluble aggregates was determined to be larger than 400 000 because it eluted at the total exclusion volume of the column. The molecular mass of rbST monomer was also examined in a mobile phase containing denaturing agents such as SDS and Gn · HCl. The higher molecular mass was obtained in a mobile phase containing SDS ($M_r \approx 25\,000$) and Gn · HCl (34 000). This may be due to unfolding of the protein [15,16] and an increase in molecular size of the SDS–protein complex.

3.3. Optimal HPLC conditions

The effect of ammonium hydrogencarbonate concentration on the elution time of rbST was investigated. A typical plot of elution time (t_e) *versus* buffer concentration [NH_4HCO_3] is shown in Fig. 3, plot A. A slight change in elution time was observed as the ammonium hydrogencarbonate concentration ranged from 0.1 to 0.4 *M*. Elution time increased more rapidly above 0.4 *M* ammonium hydrogencarbonate. The peak area of rbST monomer did not change in the concentration of ammonium hydrogencarbonate below 0.7 *M*, but dramatically decreased when increasing the salt

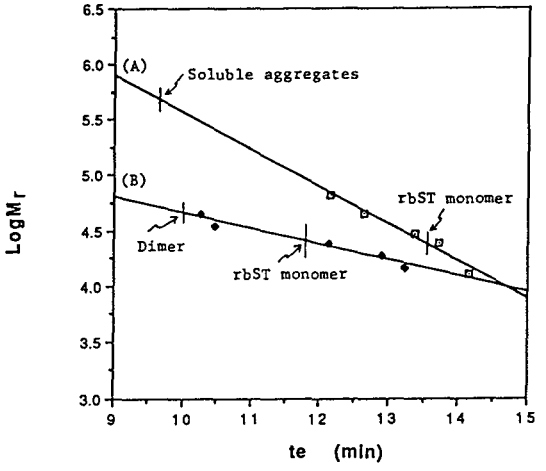

Fig. 2. Molecular mass calibration plots for TSK Spherogel 3000 PW column. Plot A: Mobile phase is 0.1 *M* ammonium hydrogencarbonate–0.1 *M* NaCl (pH 9.0) solution. *y*-Intercept = 8.94; slope = 0.337; correlation coefficient = 0.961. Protein standards: bovine serum albumin (M_r 66 000); ovalbumin (M_r 45 000); carbonic anhydrase (M_r 29 000); trypsinogen (M_r 24 000); cytochrome *c* (M_r 12 400). Plot B: Mobile phase is 1% SDS in 0.2 *M* ammonium hydrogencarbonate solution (pH 9.0). *y*-Intercept = 6.10; slope = 0.144; correlation coefficient = 0.959. Protein standards: ovalbumin (M_r 45 000); pepsin (M_r 34 700); trypsinogen (M_r 24 000); β-lactoglobulin (M_r 18 400); lysozyme (M_r 14 300). Flow-rate = 0.5 ml/min. The concentration of protein standards is 1 mg/ml in water. Injection volume is 20 μl.

concentration to higher than 0.7 *M*. This was due to the salting-out effect of the protein (Fig. 4, plot A).

A 0.2 *M* ammonium hydrogencarbonate solution was selected as a mobile phase for the study of pH effect. When increasing the pH in the mobile phase, the elution time of the rbST monomer remains constant but the peak area was slightly increased (Fig. 5, plot A).

The behavior of soluble aggregates in hydrogencarbonate solution has also been investigated. The solubility of rbST soluble aggregates was strongly effected by pH and hydrogencarbonate concentration in solution. Increasing hydrogencarbonate concentration to higher than 0.1 *M* caused the solubility of soluble aggregates to sharply decrease because of the strong salting-out effect of the huge molecules (Fig. 4, plot B). Soluble aggregates precipitate in the 0.2 *M* hydrogencarbonate solution at pH below 8.5.

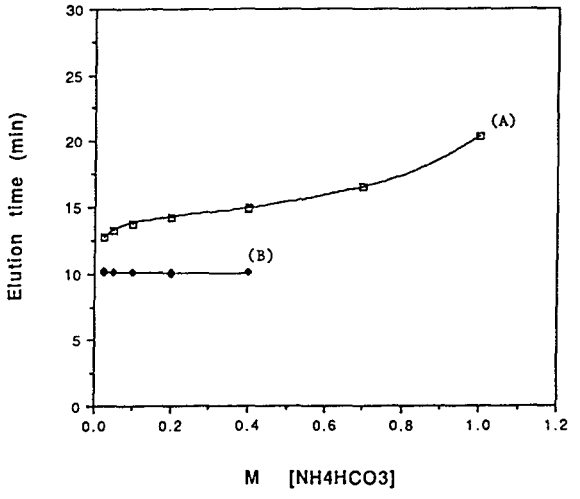

Fig. 3. Effect of hydrogencarbonate concentration on retention times. Same conditions as in Fig. 1 except the concentration of bicarbonate in the mobile phase changed from 0.025 to 1 *M*. The rbST sample used in this experiment is lot 003. Plot A: rbST monomer; plot B: rbST soluble aggregates.

The solubility increases with increasing pH to 9.5 and then remains no significant change until pH 10.5 (Fig. 5, plot B). These results demonstrated that rbST soluble aggregates can be removed in buffer solutions with pH below 8. No significant influence of pH and salt concentration on elution

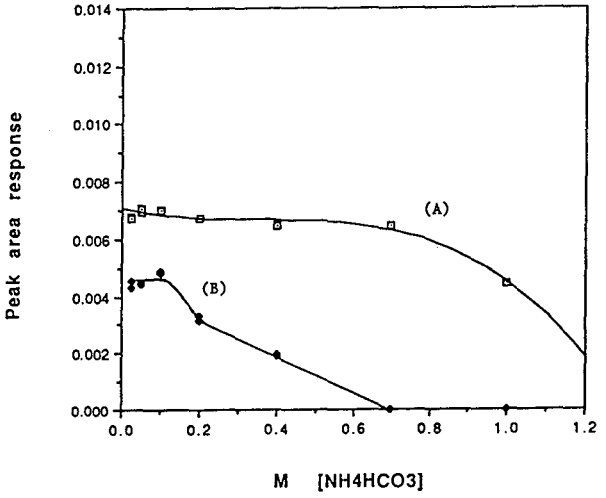

Fig. 4. Effect of hydrogencarbonate concentration on peak areas. Same conditions as in Fig. 3. Plot A: rbST monomer; plot B: rbST soluble aggregates.

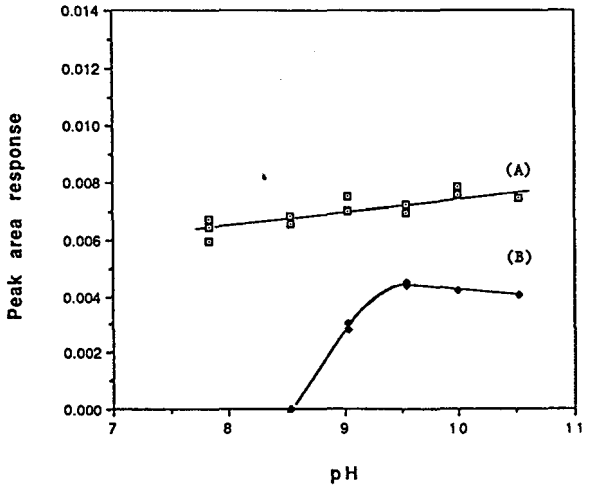

Fig. 5. Effect of pH variation in the mobile phase on the peak area of bST. Same condition as in Fig. 1. Plot A: rbST monomer; plot B: rbST aggregates.

time of the soluble aggregates was found in this study

The optimal flow-rate in this method was 0.5 ml/min. A flow-rate of 0.3 ml/min results in equivalent efficiency but nearly doubles the run time. A higher flow-rate of 1.0 ml/min results in the rbST main peak being partially overlapped with the void peak.

3.4. Non-denaturation

The non-denaturation of the rbST monomer in the separation has been confirmed by rat mass-gain assay and radioreceptor assay. Two different lots, 003 and 004, were used in this study. Lot 004 contained less than 1% aggregates, but more than 30% of soluble aggregates were present in lot 003. The rbST monomer in both lots was semi-preparatively separated and collected under the same experimental conditions as described above. The bioactivity of the monomer fractions collected from both lots was measured by the rat mass-gain assay and found to be close to that of the reference standard (Table 1). The soluble aggregates fraction collected from lot 003 showed no bioactivity by the rat mass-gain assay.

Results obtained in the radioreceptor assay (RRA) for the lot 003 and the reference standard were consistent with that in rat mass-gain assay. It indicated that the bioactivity of rbST monomer collected in both samples remains identical but the soluble aggregates collected from lot 003 showed no bioactivity using the radioreceptor assay (Table 1). A linear correlation was found between chromatography and radioreceptor data in different lots of bulk materials. A relatively poor correlation coefficient of 0.845 was obtained due to the limitation of the reproducibility of the RRA method.

The results obtained in this study clearly indicated that the separation conditions in this study can be applied to establish a non-denaturing potency assay for determination of rbST in bulk materials.

3.5. Soluble aggregates and dimer

The formation of rbST aggregates during the production process has been recognized. In order to identify the soluble aggregates, a num-

Table 1
Bioactivity confirmation by rat mass-gain assay (RMGA) and radioreceptor assay (RRA)

	Potency (IU/mg) RMGA			RRA	
	RS	Lot 004	Lot 003	RS	Lot 003
rbST Main component					
Original solution	1.25	1.04		1.2	1.1
Collected in SEC		1.29	1.19	1.2	1.1
rbST aggregates collected			0		0

RS = Reference standard.

ber of experiments were carried out in this study. The UV spectrum provided by on-line photodiode array detector in the chromatographic process of lot 003 demonstrated that the UV profiles of both rbST monomer and soluble aggregates are very similar. A slight differentiation at 250–270 nm (Fig. 6) for both proteins may be due to the change in environment of the aromatic amino acids in the molecule after aggregation.

The stability of rbST soluble aggregates in hydrogencarbonate solution has been investigated. The isolated soluble aggregates are relatively stable in pH > 9 ammonium hydrogencarbonate solution at least for 9 h, particularly at low concentration.

Denaturing agents, such as detergents, Gn · HCl and urea, decompose rbST aggregates into denatured monomer [15–17]. As 1% SDS was added to the mobile phase, the aggregate peaks in lot 002 and 003 disappeared in the chromatograms as shown in Fig. 7. rbST monomer peak was broadened and a small peak was found in front of the main peak that may be a covalent bond dimer of rbST. Similar results were obtained in a 0.2 *M* NH_4HCO_3, pH 9 mobile phase containing 6 *M* Gn · HCl.

To confirm the above presumption, the soluble aggregate fraction was collected from lot 003 in the system consisting of a TSK 3000 PW column and 0.2 *M* ammonium hydrogencarbonate mobile phase. The collected fraction was mixed 1:1 with 2% SDS solution and re-chromatographed on the same column with a 1% SDS–0.2 *M* NH_4HCO_3 mobile phase. An identical profile and elution time were obtained as the SDS-monomer peak The same results were obtained in the mobile phase with Gn · HCl. These results illustrated that in the presence of denaturing agents in solutions, rbST soluble aggregates (non-covalent bonded) would be decomposed into denaturated monomer. It is important to realize that if rbST soluble aggregates existed in bulk material, an excessively high result would

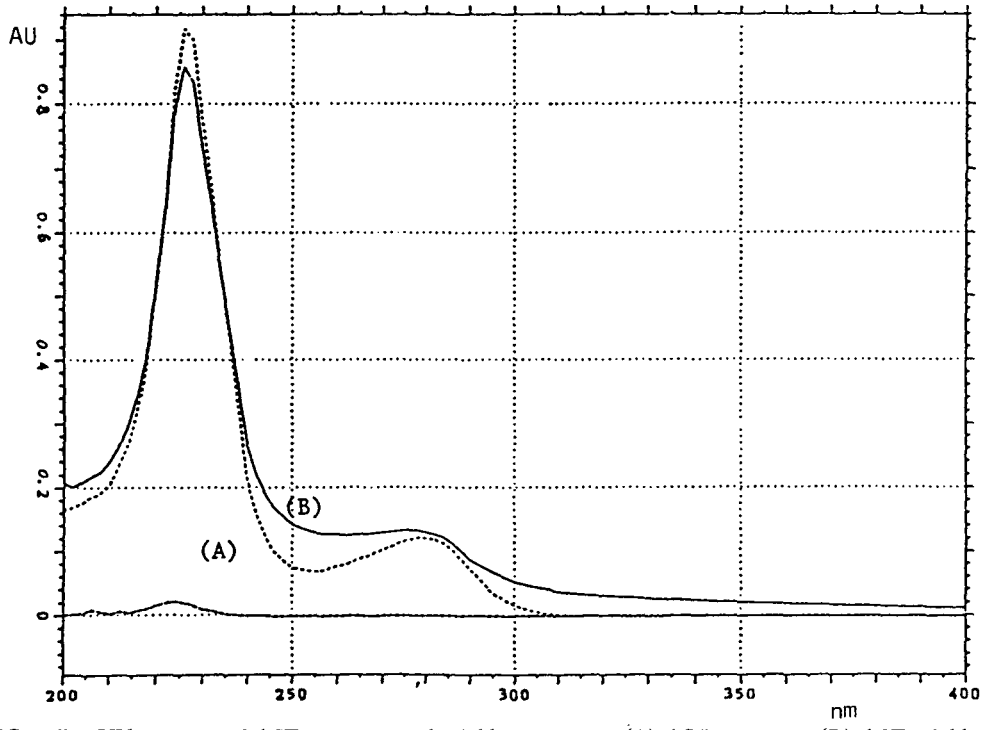

Fig. 6. HPSEC on-line UV spectrum of rbST monomer and soluble aggregates. (A) rbST monomer, (B) rbST soluble aggregates. Chromatographic conditions as in Fig. 1.

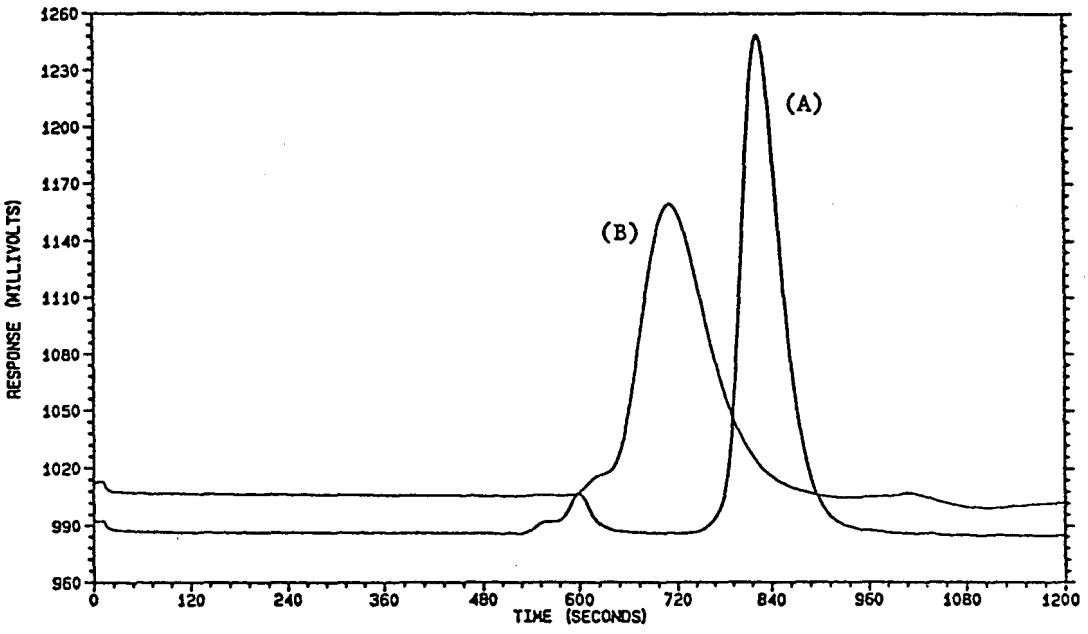

Fig. 7. SDS SEC chromatograms of lot 002 bulk material. Column: TSK Spherogel 3000 PW (300 × 7.5mm). (A) In 0.2 *M* ammonium hydrogencarbonate (pH 9.0); (B) in the mobile phase A with 1% SDS. Sample concentration: 1 mg/ml; flow-rate: 0.5 ml/min.

be obtained in quantitative work by these denaturing analytical procedure [6–8] because of the decomposition of aggregates.

The above results also indicated that the covalent bonded dimer of rbST may be present in rbST lots. The rbST covalent bonded dimer, mostly in low concentration (<3%), cannot be completely resolved in the system of a TSK 3000 PW column and pH 9 ammonium hydrogencarbonate because of the limitation of the less efficiency of polymer packing materials. In the presence of denaturing agents such as SDS and Gn · HCl in the mobile phase, however, the resolution increased and covalent bonded dimer could be separated from the rbST monomer (Fig. 7). It provides a possibility to estimate rbST dimer by using the high–low chromatographic technique or normalization procedure. The molecular mass of covalent bonded dimer in SDS–NH_4HCO_3 mobile phase has been estimated to be 46 000 by utilizing standard protein calibration curve as shown in Fig. 3. The further study for the characterization of rbST dimer has been carrying out in our laboratory,

3.6. Quantification and validation for rbST monomer

Quantification of rbST monomer was achieved using an external standard for the determination of rbST monomer potency. The linearity of rbST monomer in 0.2 *M* ammonium hydrogencarbonate mobile phase was measured by preparing a number of rbST reference standard solutions with different concentrations. The linear regression analysis was performed in the concentration range from 0.1 to 1 mg/ml. The correlation coefficient ranged from 0.9998 to 1.000 and the average relative standard deviation (R.S.D.) was 1.36%.

The precision of this method was evaluated by three days using two different chromatography systems, three different columns and three different lots of rbST bulk materials. The average

Table 2
Estimation of rbST soluble aggregates by high–low chromatography

Sample lot	Soluble aggregates (%)	R.S.D. (%)
002	8.8	4.6
008	0.76	5.0

R.S.D. of rbST monomer measured was less than 2.8% and the reproducibility of elution time was less than 0.18%.

The recovery study for rbST monomer was carried out by addition of reference standard at two different concentrations in the bulk material solutions. The recoveries obtained in this experiment ranged from 101 to 104%.

The stability of the rbST monomer in solution was measured at room temperature by using three rbST reference standard solutions at different concentrations. The rbST content in freshly prepared solutions was determined and then compared with the data obtained from an aged solutions which were stored at room temperature for 30 h. Data obtained in this experiment indicated that no significant change in results was found within 30 h.

3.7. Estimation of soluble aggregates

A single sample high–low procedure described in the Experimental section with a dilution ratio of 50 was used in this study. Good correlation was found between peak response of soluble aggregates and concentration in the range from 0.014 to 0.362 mg/ml. The results obtained for two rbST lots are listed in Table 2.

4. Conclusions

(1) The non-denaturing HPSEC assay developed in this paper provides for the accurate and precise determination of rbST potency in bulk materials. The non-denaturation of this method was confirmed by rat mass-gain assay and RRA.

(2) The rbST soluble aggregates can be resolved from the monomer in this method and estimated by the high–low chromatographic technique.

(3) The experimental results demonstrate that in the presence of denaturing agents such as SDS and Gn · HCl, non-covalent bonded aggregates dissociate to rbST. Thus, an increase in rbST monomer content is obtained when denaturing mobile phases are used in the assay.

Acknowledgements

The authors thank Dr. Bruce H. Frank, Dr. Ralph M. Riggin and Dr. Gregory F. Needham for very useful discussions; Dr. Eugene L. Inman, Mr. J. Matt Rodewald and Mr. Daniel J. Sweeney for reviewing the manuscript and Mr. Paul A. Record for the rat mass-gain assay.

References

[1] J. Fogh, B. Dineson, B. Hansen, K. Jorgensen, P. Nilsson and H.H. Sorensin, *Pharmeuropa*, 3 (1991) 25–28.
[2] A.W. Purcell, M.I. Aguilar and M.T.W. Hearn, *J. Chromatogr.*, 476 (1989) 113–23.
[3] R.M. Riggin, G.K. Dorulla and D.J. Miner, *Anal. Biochem.*, 167 (1987) 199–209.
[4] R.M. Riggin, C.J. Shaar, G.K. Dorulla, D.S. Lefeber and D.J. Miner, *J. Chromatogr.*, 435 (1988) 307–318.
[5] A.F. Bristow and S.L. Jeffcoate, *Pharmeuropa*, 3 (1991) 3.
[6] J.D. Stodola, J.S. Walker, P.W. Dame and L.C. Eaton, *J. Chromatogr.*, 357 (1986) 423–428.
[7] M.J. Hageman, J.M. Bauer, P.L. Possert and R.T. Darrington, *J. Agric. Food Chem.*, 40 (1992) 348–355.
[8] B.D. Violand, M. Takano, D.F. Curran and L.A. Bentle, *J. Protein Chem.*, 8 (1989) 619–628.
[9] W. Marx, M.E. Simpson and H.M. Evans, *Endocrinology*, 30 (1941) 1–10.
[10] B.F.D. Ghrist, unpublished results.
[11] H.G. Burger, H. Edelhoch and P.G. Condliffe, *J. Biol. Chem.*, 241 (449) 1966.
[12] Somidobove (somatotropin ox); USAN and the USP dictionary of drug names (1961–1990) cumulative list, 551.

[13] E.C. Rickard, M.M. Strohl and R.G. Nielson, *Anal. Biochem.*, 197 (1991) 197.
[14] E.L. Inman and H.J. Tenbarge, *J. Chromatogr. Sci.*, 26 (1988) 89–94.
[15] H.A. Havel, E.W. Kauffman, S.M. Plaisted and D.N. Brems, *Biochemistry*, 25 (1986) 6533–6538.
[16] D.N. Brems, S, M. Plaisted, H.A. Havel, E.W. Kauffman, J.D. Stodola, L.C. Eaton and R.D. White, *Biochemistry*, 24 (1985) 7662–7668.
[17] D.N. Brems, S.M. Plaisted, E.W. Kauffman and H.A. Havel, *Biochemistry*, 25 (1986) 6539–6543.

ELSEVIER

Journal of Chromatography A, 675 (1994) 123–128

JOURNAL OF CHROMATOGRAPHY A

Determination of spectinomycin using cation-exchange chromatography with pulsed amperometric detection

Joseph G. Phillips*[,a], Carole Simmonds[b]

[a]*Analytical Sciences, SmithKline Beecham Pharmaceuticals, 709 Swedeland Road, PO Box 1539, King of Prussia, PA 19406, USA*

[b]*Department of Chemistry, Loughborough University of Technology, Loughborough, Leicestershire LE11 3TU, UK*

(First received May 11th, 1993; revised manuscript received March 15th, 1994)

Abstract

An isocratic HPLC method was developed for the determination of spectinomycin dihydrochloride pentahydrate. The method is based on cation-exchange chromatography with pulsed-amperometric detection. The method was optimised for the separation of spectinomycin, actinamine and actinospectinoic acid on a Dionex IonPac CS3 column at ambient temperature with 150 m*M* sodium acetate (pH 6) mobile phase. Detector response with respect to sodium hydroxide concentration was investigated using cyclic voltammetry. A three-step pulse sequence with a sampling potential of + 0.05 V was used for detection. The *k'* values for spectinomycin and related impurities were insensitive to column temperature changes in the range 21–50°C and show only minor variations to pH changes in the range 5.0–6.0. The method is linear and unbiased for the determination of spectinomycin over the concentration range 25–200 μg/ml for 50-μl injections. Two-day precision data for the method show within-sample R.S.D.s in the range 0.3–1.0% and between-day R.S.D.s in the range 0.3–0.9%. The limits of detection and quantitation determined for spectinomycin are 0.02 μg and 0.06 μg on-column, respectively. The method is suitable for the analysis of drug-substance.

1. Introduction

Spectinomycin is a broad-spectrum antibiotic used in the treatment of Gram negative organism infections. It is manufactured mainly as the *R-cis* form of the dihydrochloride pentahydrate salt. In aqueous and organo–aqueous solutions anomerisation occurs resulting in an equilibrium mixture of the *R-cis*, *S-cis*, *R-trans* and *S-trans* forms [1]. The keto form also hydrates readily to produce the *gem*-diol form [2,3]. Acid degradation leads to the formation of actinamine, whilst base degradation produces actinospectinoic acid [3].

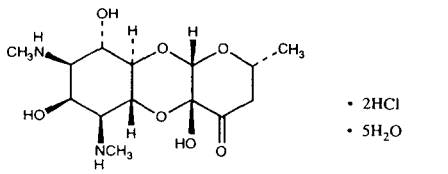

R-cis spectinomycin dihydrochloride pentahydrate

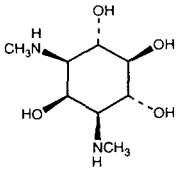

actinamine

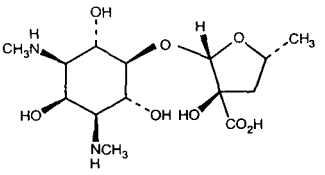

actinospectinoic acid

* Corresponding author.

0021-9673/94/$07.00
SSDI 0021-9673(94)00287-J

Under reversed-phase equilibrium conditions, spectinomycin quickly equilibrates to a mixture of diol and keto form. The diol form has no chromophore and the keto form has no significant chromophore. Therefore, the determination of spectinomycin by HPLC with UV detection requires complex derivatisation procedures [4,5]. Also, these methods do not adequately resolve and quantify the anomers to express potency and they suffer from variability caused by lack of control of the stereoisomeric equilibrium. Although electrochemical detection using controlled potential coulometry has been applied to the determination of spectinomycin [6], the repeatability of the method is characteristically poor due to contamination of the electrode surface.

The method described in this report applies cation-exchange chromatography to elute spectinomycin anomers as a single peak and pulsed-amperometric detection for low limit of detection, good signal-to-noise ratio and low method variability.

2. Experimental

2.1. Materials

Spectinomycin dihydrochloride pentahydrate, actinamine and actinospectinoic acid were supplied by Upjohn (Crawley, UK). All other chemicals were analytical reagent grade supplied by Fisons (Loughborough, UK). Water was purified using a Millipore Milli-Q system (Waters, Watford, UK). All solvents and solutions were degassed under vacuum, purged with helium and maintained under a head of helium during use.

2.2. Cyclic voltammetry

Since base is essential for pulsed-amperometric detection (for oxidation) of polyhydroxy compounds [7], the effect of different concentrations of sodium hydroxide on the detector response to spectinomycin was assessed using cyclic voltammetry. This was conducted using a Metrohm VA Detector E611 with a gold working electrode, a stainless-steel auxiliary electrode and Ag/AgCl reference electrode, a Metrohm VA Scanner E612 and a Gould HR 2000 X-Y recorder. Voltammograms of four 3 m*M* solutions of spectinomycin in 150 m*M* sodium acetate and varying amounts of sodium hydroxide (12.5, 25.0, 50.0 and 100.0 m*M*) as well as of the corresponding blank solutions (without spectinomycin) were recorded. A scanning range of −0.30 to +0.10 V and a scan speed of 50 mV/s were used.

2.3. Chromatography

All chromatograms were generated using a Dionex metal-free quaternary gradient pump; a Dionex pulsed-amperometric detector with gold working electrode, a stainless-steel auxiliary electrode and Ag/AgCl reference electrode; a LDC Constametric III post-column pump; a Dionex metal-free rotary injection valve with a 50-μl injection loop; a Dionex IonPac CS3 column (250 mm × 4 mm I.D.) and Dionex CG3 guard column (25 mm × 4 mm I.D.); a Shimadzu CTO-6A column oven and a Spectra Physics SP4290 computing integrator. The system was operated using a column flow-rate of 1 ml/min; a sample injection volume of 50 μl; a column pressure of 6.2 MPa and a post-column flow-rate of 1.5 ml/min. The pulsed-amperometric detector was used with a rise-time filter setting of 3.0 s and an output range of 1 μA.

Optimisation was conducted for isocratic elution using sodium acetate mobile phase at concentrations in the range 150–250 m*M*, mobile phase pH at values in the range 5–6 and column temperature at values in the range 21–50°C. Validation was conducted for linearity of response to concentrations of spectinomycin in the range 25–200 μg/ml, limits of detection and quantitation for signal-to-noise ratios of 3 and 10, respectively, and two-day precision for triplicate injections of three solutions of spectinomycin at concentrations of approximately 75, 100 and 125 μg/ml.

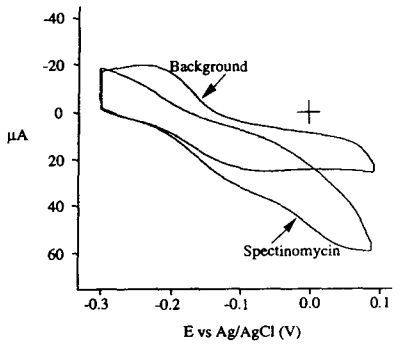

Fig. 1. Cyclic voltammogram (labelled *background*) for a solution of 150 m*M* sodium acetate and 100.0 m*M* sodium hydroxide (pH 12.6). Cyclic voltammogram (labelled *spectinomycin*) for 3 m*M* spectinomycin in 150 m*M* sodium acetate and 100.0 m*M* sodium hydroxide (pH 12.6). The scan speed was 50 mV/s. The origin of the plots is indicated by (+).

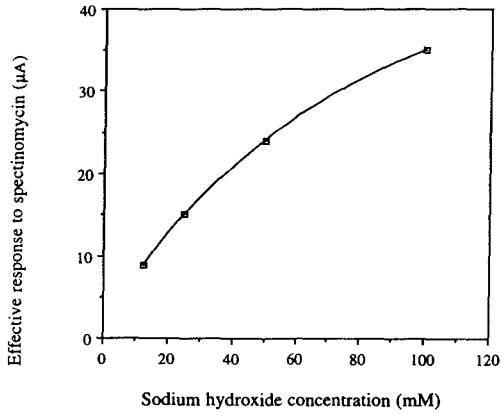

Fig. 2. Relationship between effective response to 3 m*M* spectinomycin and sodium hydroxide concentration. The effective response for spectinomycin is derived from the cyclic voltammograms by subtraction of the maximum background current from the maximum current recorded for the analyte solution.

3. Results and discussion

The cyclic voltammograms (example shown in Fig. 1) show that the maximum current for the blank solutions is reached at approximately −0.05 V. The values obtained for the maximum current measured for the blank solutions (Table 1) varied with each experiment conducted. The lowest (25 μA) and highest (72.5 μA) values obtained were for the blank solutions containing 100.0 m*M* sodium hydroxide and 50.0 m*M* sodium hydroxide, respectively. For the 3 m*M* spectinomycin solutions, the maximum current measured occurred at +0.1 V for those solutions containing 12.5, 25.0 or 100.0 m*M* sodium hydroxide. The cyclic voltammogram for the spectinomycin solution containing 50.0 m*M* sodium hydroxide showed a maximum response at −0.03 V which decreases by 4 μA at 0 V and show no further significant decrease at 0.1 V. This solution gave the largest value of 96.5 μA for current measured and the corresponding blank solution gave the largest background current measured (72.5 μA). The largest effective response to spectinomycin was 35 μA (Table 1). This value was obtained for the 3 m*M* spectinomycin solution containing 100.0 m*M* sodium hydroxide after subtraction of the current measured for the corresponding blank solution. A plot of the effective response to spectinomycin *versus* concentration of sodium hydroxide is shown in Fig. 2. The solid line for the plot is interpolated to a simple curve. A similar response curve was obtained in a comparable study reported for carbohydrates [8].

The results show that under the conditions

Table 1
Maximum measured current for blank solutions and spectinomycin solutions derived from the cyclic voltammograms

Sodium hydroxide concentration (m*M*)	Maximum blank solution current (μA)	Maximum sample solution current (μA)	Effective response to analyte (μA)
12.5	37.5	46.3	8.8
25.0	26.3	41.3	15.0
50.0	72.5	96.5	24.0
100.0	25.0	60.0	35.0

used for the cyclic voltammetry, an increase in amperometric response to spectinomycin with respect to increasing sodium hydroxide concentration is obtained. This indicates that even though spectinomycin degrades in alkaline solution, its amperometric detection in sodium hydroxide can be achieved. At sodium hydroxide concentrations between of 25–100 m*M* the current due to the background for potential values between −0.1 to +0.1 V does not interfere with the detection of spectinomycin. Using pulsed amperometry, a measuring potential between −0.1 to +0.1 V and a sodium hydroxide concentration between 25–100 m*M* should provide detection of spectinomycin following chromatographic separation with sodium acetate. However, sodium hydroxide must be added post-column to avoid on-column degradation of spectinomycin.

With cyclic voltammetry, the measured current for spectinomycin in 100 m*M* sodium hydroxide rose sharply to 58.5 μA at +0.05 V, at an approximate rate of 192 μA/V. Beyond +0.05 V the increase in current to 60 μA at +0.1 V was at a much slower rate. For pulsed-amperometric detection of spectinomycin, a measuring potential of +0.05 V was used, since beyond this potential the increase in amperometric response is minimal. Additionally, at higher measuring potentials, interference due to oxidation of unknown components that may be present in real samples would be greater. A measuring potential of +0.05 V during pulsed-amperometric detection of spectinomycin should not give an unduly high background current since the cyclic voltammograms show no significant change in the current for the blank solutions between −0.05 and +0.10 V.

A three-step pulse-sequence (Fig. 3) was used for the pulsed-amperometric detection of spectinomycin, actinospectinoic acid and actinamine following separation by cation-exchange chromatography and post-column addition of 100.0 m*M* sodium hydroxide (33.3 m*M* effective concentration). The pulse-sequence used +0.05 V sampling potential with a 100-ms delay-time and 380-ms measuring-time. The oxidation potential to clean the electrode was +0.60 V for 120 ms

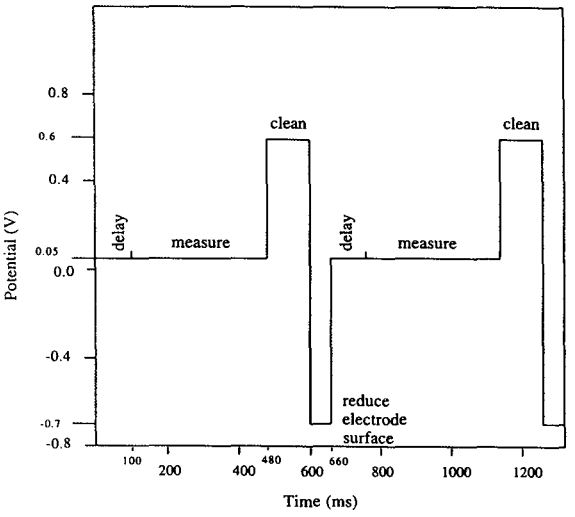

Fig. 3. Pulse sequence for the detection of spectinomycin, actinospectinoic acid and actinamine using a gold working electrode, a stainless-steel auxiliary electrode and an Ag/AgCl reference electrode.

and the reduction potential to activate the electrode surface was −0.70 V for 60 ms. The separation of the components of interest was optimised with respect to mobile phase (sodium acetate) concentration, mobile phase pH and column temperature. The k' values (Table 2) for spectinomycin, actinamine and actinospectinoic for the sodium acetate mobile phase at concentrations in the range 150–250 m*M* show that the best separation is achieved at 150 m*M* sodium acetate. Satisfactory separation of the three components is achieved at all concentrations of sodium acetate investigated and the time for analysis is significantly reduced with increasing concentrations of sodium acetate. However, resolution of other minor unknown impurities that elute close to actinospectinoic acid and spectinomycin is only adequately accomplished at 150 m*M* sodium acetate concentration. The mobile phase pH over the narrow range of 5.0 to 6.0 does not interfere significantly with the resolution of the components as shown by the k' values (Table 2). Mobile phase pH outside these values caused acid- and base-catalysed degradation of spectinomycin. The results in Table 2 also show that k' is independent of changes in temperature over the range 21–50°C. Fig. 4

Table 2
Changes in k' with respect to changes in pH, column temperature and sodium acetate concentration

	k'		
	Actinospectinoic acid	Spectinomycin	Actinamine
pH			
5.0	0.20	4.65	5.59
5.5	0.20	4.38	5.39
6.0	0.20	5.39	5.26
Temperature (°C)			
21	0.24	4.26	5.42
30	0.31	4.29	5.52
40	0.31	4.29	5.59
50	0.31	4.26	5.73
Sodium acetate (mM)			
150	0.39	8.18	9.77
200	0.23	4.32	5.34
250	0.11	3.07	3.75

shows a typical chromatogram for a 50-μl injection of a solution containing spectinomycin, actinamine and actinospectinoic acid, each at a concentration of 50 μg/ml in 150 m*M* sodium acetate. The sample was chromatographed using 150 m*M* sodium acetate mobile phase (pH 6) and 21°C column temperature. At the sample concentration used, the detector response to all three components is above 300 nA. The peaks labelled 1 and 2 are minor impurities found in actinospectinoic acid. The peak labelled 3 is a minor impurity found in actinamine. The analysis time for the method is 15 min. Under the chromatographic conditions applied throughout this study the spectinomycin anomers consistently eluted as a single peak. The co-elution of the anomers allows easy quantification of the potency of spectinomycin based on a single major component.

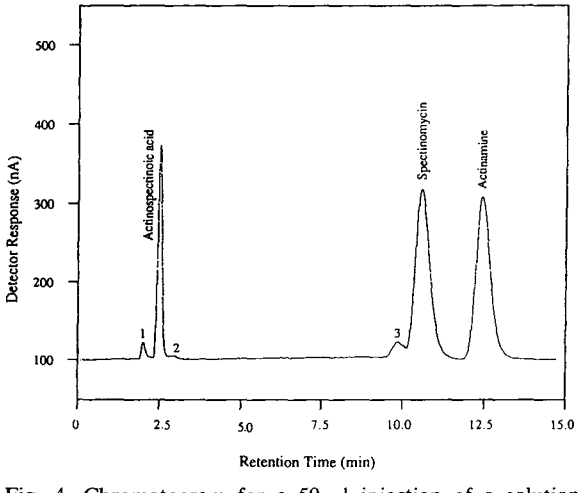

Fig. 4. Chromatogram for a 50-μl injection of a solution containing spectinomycin, actinamine and actinospectinoic acid. Each are at a concentration of 50 μg/ml in 150 m*M* sodium acetate. The sample was chromatographed using 150 m*M* sodium acetate mobile phase (pH 6) and 21°C column temperature. The peaks labelled 1, 2 and 3 are minor impurities in actinospectinoic acid and actinamine.

Least squares linear regression for spectinomycin at concentrations between 25–200 μg/ml *versus* peak area response gave an equation for the line of $y = -1.27 \cdot 10^{-4} + 4313.6x$ and $r^2 = 1$. The response to spectinomycin over the concentration range examined is therefore linear and unbiased, thus, supporting a proposal for nominal sample concentrations of 50–100 μg/ml for weight based assay and 100–200 μg/ml for determination of impurities. Results for the two-day precision study for spectinomycin solutions at concentrations of 74.78, 99.81 and 124.87 μg/ml (Table 3) show within-sample R.S.D.s in the range 0.3–1.0% and between-day R.S.D.s in the range 0.3–0.9%. The limit of detection of spec-

Table 3
Two-day peak area precision data for solutions of spectinomycin

	Spectinomycin concentration (μg/ml)		
	Sample 1 74.78	Sample 2 99.81	Sample 3 124.87
Day 1			
	308 411	408 518	573 924
	307 512	407 296	581 563
	309 131	410 719	580 987
Mean	308 351	408 844	575 491
R.S.D. (%)	0.3	0.4	1.0
Day 2			
	310 512	410 823	582 134
	312 306	409 513	583 479
	309 151	408 791	579 352
Mean	310 656	409 709	581 655
R.S.D. (%)	0.5	0.3	0.4
Overall mean	309 503	409 276	578 573
Overall R.S.D. (%)	0.6	0.3	0.9

tinomycin was determined as 0.02 μg on-column and the limit of quantitation was estimated as 0.06 μg on-column.

4. Conclusion

The results of these studies show that the method developed resolves spectinomycin and its known degradation products. Under the conditions of the method the anomers of spectinomycin elute as a single peak, thus reducing the variability seen with non-ion-exchange methods. The method is linear and unbiased between 25–200% of a nominal sample concentration of 100 μg/ml and shows a limit of detection of 20 ng on-column.

Acknowledgement

The authors would like to thank Upjohn Limited (Crawley, UK) for the samples of spectinomycin, actinamine and actinospectinoic acid.

References

[1] D.R. White, R.D. Birkenmeyer, R.C. Thomas, S.A. Mizsak and V.H. Wiley, *Aminocyclitol Antibiotics* (*ACS Symposium Series*, No. 125), American Chemical Society, Washington, DC, 1980, p.111.
[2] P.F. Wiley, A.D. Argoudelis and H. Hoeksema, *J. Am. Chem. Soc.*, 85 (1963) 2652.
[3] W. Rosenbrook Jr., *Jpn. J. Antibiot.*, 32 (Suppl.) (1979) S211.
[4] H.N. Myers and J.V. Rindler, *J. Chromatogr.*, 176 (1979) 103.
[5] K. Tsuji and K.M. Jenkins, *J. Chromatogr.*, 333 (1985) 365.
[6] L. Elrod Jr., J.F. Bower and S.L. Messener, *Pharm. Res.*, 5 (1988) 664.
[7] R.D. Rocklin and C.A. Pohl, *J. Liq. Chromatogr.*, 6 (1983) 1577.
[8] T. Soga, Y. Inoue and K. Yamaguchi, *J. Chromatogr.*, 625 (1992) 151.

ELSEVIER

Journal of Chromatography A, 675 (1994) 129–139

JOURNAL OF CHROMATOGRAPHY A

Simultaneous use of size-exclusion chromatography and photon correlation spectroscopy for the characterization of poly(lactic acid) nanoparticles

P. Huve[a], T. Verrecchia[a], D. Bazile*[,a], C. Vauthier[b], P. Couvreur[b]

[a]*Rhone Poulenc Rorer, IBP-PHTEC, New Drug Delivery System Unit, 20 Avenue R. Aron, 92165 Antony Cedex, France*
[b]*Laboratoire de Physico-Chimie, Pharmacotechnie et Biopharmacie, URA CNRS 1218, 5 Avenue J.B. Clement, 92296 Chatenay Malabry Cedex, France*

(First received June 10th, 1993; revised manuscript received December 7th, 1993)

Abstract

Fetuin-coated poly(lactic acid) particles of size range 50–200 nm were prepared by an emulsion, microfluidization and solvent evaporation method. The separation of ^{14}C-labelled particles made with ^{125}I-labelled protein by size-exclusion chromatography (SEC) was followed by the measurement, in each collected fraction, of the average diameter of the particles by photon correlation spectroscopy, absorbance and concentrations by radioactivity counting. In one experiment, this showed that the dependence of the specific turbidity of the particles on their diameter correlated well with Mie's theory. A first approximation of the particle size distribution could also be obtained together with the separation capacities of Sepharose CL-2B and Sephacryl S1000, in addition to the amount of bound protein per unit surface area of the particles. Thus, the simultaneous use of size-exclusion chromatography and photon correlation spectroscopy was found to be a powerful tool that needed neither column dispersion function analysis nor any column standardization.

1. Introduction

Nanoparticles have attracted growing interest as site-specific drug-delivery devices. However, their use for *in vivo* administration is restricted by the fast uptake by the macrophages of the mononuclear phagocytes system [1]. Biodegradable and biocompatible poly(lactic acid)–fetuin nanoparticles have been designed to avoid this uptake. The uptake mechanism is complicated and depends greatly on the physico-chemical characteristics of the particles such as surface properties and size [2]. Hence precise characterization of the particles is required. The particle size distribution (PSD) of the nanoparticles must be known so as to be sure that there are no multiple populations of particles, each with a different behaviour. From another point of view, in order to assess the role of the coated protein layer at the surface of the nanoparticles, the amount of fetuin associated with the nanoparticles must be measured. Further, in addition to the precise characteristics of the particles, preparing such well defined nanoparticles is necessary in order to test their *in vivo* fate and to understand the uptake mechanism.

The average size of the studied particles is around 100 nm [3]. Various methods have been

* Corresponding author.

0021-9673/94/$07.00
SSDI 0021-9673(94)00159-7

proposed in order to characterize the size and the size distribution of such submicron particles populations including photon correlation spectroscopy (PCS), size-exclusion chromatography (SEC) and, more recently, field-flow fractionation (FFF). Further, the separation of the particles as a function of their size could be achieved by both SEC and Split-flow thin (SPLITT)-FFF (SFFF). However, poly(lactic acid) nanoparticles could be polydisperse in both size and density. If the size and the size polydispersity can be well described by PCS, no previous analysis of the density is necessary.

FFF appeared to be a versatile tool for submicron particle analysis. So far, two main subtechniques have been proposed, one based on multigravitational field (SFFF) and the other on a hydrodynamic separation. The use and applications of these techniques have been reviewed recently by Giddings [4]. In SFFF, the separation of the particles resulted from a balance between the size and the density or the mass of the particles. These combined effects led to a complex separation mechanism involving a steric-like elution mechanism [5], inertia [6] or lubrification forces [7] when high external fields were applied.

Thus, in order to obtain a separation of the nanoparticles as a function of their size, SEC has been prefered to SFFF. SEC is based only on a size-driven separation and does not involve density or other parameters. Further, it is inexpensive and has been in use for over a decade [8,9,10]. With SEC, the separation is not perfect, however, because of the axial dispersion of the chromatographic system, which gives a broad peak for a narrow particle size distribution (PSD) [8,10,11]. All chromatographic systems used for particle analysis may be considered as an operator (CH), defined in Eq. 1, which translates the PSD into a chromatogram. A PSD, hereafter denoted N, is a normalized function of the variable diameter ($\boldsymbol{d}_p$), that gives the proportion of particles, in number, which have this diameter. The percentage of the total number of particles whose diameters lie between $\boldsymbol{d}_p$ and $\boldsymbol{d}_p + d\boldsymbol{d}_p$ is given by $100N[\boldsymbol{d}_p]d\boldsymbol{d}_p$. Thus, a particle suspension is characterized if N and the total number of particles (or particle number concentration), n, are given.

A chromatogram is a function C of the elution volume, giving either the concentration of particles present at a volume v or the optical density (OD) induced by those particles. The operator CH which corresponds to the mathematical expression of the chromatographic system is given by the equation

$$C[v] = CH(nN)[v] \tag{1}$$

The common hypothesis for this operator (which is true for not too concentrated samples) is that particles do not interfere with each other during the process [8]. Therefore, CH is a linear operator. This means that the chromatogram obtained after the injection of a mixture of two suspensions, n_1N_1 and n_2N_2 is

$$CH(n_1N_1 + n_2N_2)[v] = n_1CH(N_1)[v] + n_2CH(N_2)[v] \tag{2}$$

Of course, this hypothesis is easy to test with three successive experiments.

In order to illustrate the effect of the axial dispersion of real systems, let us consider a perfectly monodisperse suspension, composed with 100% of particles whose diameter is exactly $\boldsymbol{d}_p$, called $\delta(\boldsymbol{d}_p)$, or Dirac distribution. The Dirac distribution has been prefered to Poisson or Gaussian models because it gives simpler equations which are sufficient for the purpose of this work. As the chromatographic system is not perfect, the chromatogram obtained will not show a sharp curve [8,10]; it is transformed by the chromatographic system into a chromatogram $CH(\delta(\boldsymbol{d}_p))[v]$, hereafter denoted $G[\boldsymbol{d}_p, v]$. The maximum of $CH(\delta(\boldsymbol{d}_p))$ is denoted $V_e[\boldsymbol{d}_p]$, V_e being the characteristic function of the system that gives the mean elution volume of a sample whose diameter is $\boldsymbol{d}_p$. As any suspension nN can be expressed as [8,11]

$$nN[\varphi] = \int_0^\infty nN[d_p]\delta(d_p)[\varphi]dd_p \tag{3}$$

then, as CH is also a continuous operator (closely related suspensions have closely related chromatograms), we have

$$CH(nN)[v] = \int_0^\infty nN[d_p]G[d_p, v]dd_p \tag{4}$$

G is called the dispersion function of the chromatographic system [8,11,12].

If the system was perfect, for a given value d_0 of d_p, $G[d_0, v]$ would be equal to $\delta(V_e[d_0])[v]$. Hence, for such a system, $CH(nN)[v] = nN[V_e^{-1}[v]]$, which means that the PSD of the suspension could be read directly from the chromatogram, whether the particle diameter at volume v is measured or is deduced from prior knowledge of V_e [10].

For systems that are not perfect, the chromatogram obtained from a detector (usually a spectrophotometer) needs further processing to retrieve the real PSD. This processing requires the knowledge of the chromatographic system axial dispersion function G, which can be calculated using suspensions with perfectly known PSD [8,9,10,12]. Of course, once the function has been calculated, any change in the chromatographic system must be avoided.

An alternative to this method is to use SEC just as a separating tool to obtain in each collection fraction a relatively monodisperse suspension, whose diameter is measured by PCS (a method that is much more accurate on monodisperse suspensions).

This paper shows that the combination of SEC and PCS allowed the dependence of the particle specific turbidity on their diameter to be obtained in a one-step experiment. Simultaneously, an approximation of the PSD of the suspension was obtained, in addition to a measure of the amount of protein bound to the nanoparticles.

2. Experimental

2.1. Materials

Methylene chloride (CH_2Cl_2) was purchased from Prolabo. Fetuin, a glycoprotein from foetal calf serum, was obtained from Sigma Chimie (F2379); it was further purified as described [13,14] (purification control by electrophoresis). ^{125}I-labelled fetuin was obtained by a classical method. Briefly, to 0.5 mCi $Na^{125}I$ (Amersham) were added, successively, 20 μl of 0.13 M phosphate buffer (pH 7.4), 5 μl of 1 mg ml^{-1} protein solution and 10 μl of 1 mg ml^{-1} chloramine T solution. Two minutes later, after shaking for 20 s, 20 μl of 0.6 mg ml^{-1} metabisulphite solution were added together with 100 μl of the same buffer. Free iodine was separated from the protein on a 3-ml G-5 column (Pharmacia–LKB).

The poly(lactic acid) used was PLA 50 from Phusis with M_r 47 000. ^{14}C-labelled PLA 50 (M_r 18 000) was purchased from DuPont (specific activity 7.8 mCi g^{-1}); it contained water-soluble fragments which where removed by water–methylene chloride partitioning (purification control by gel permeation chromatography).

2.2. Radioactivity counting

^{14}C Radioactivity counting was performed on a Beckman LS6000IC counter by mixing 0.5 ml of sample with 5 ml of Ready Solv HP (Beckman). ^{125}I radioactivity counting was performed on a Berthold LB 2111 γ-counter. When both ^{125}I and ^{14}C were counted together and if the ^{125}I activity did not exceed 5% of the ^{14}C one activity, it was checked that no interference occurred.

2.3. Preparation of nanoparticles

Nanoparticles were prepared by solvent evaporation of an oil-in-water emulsion [15]. First, 1.5 ml of methylene chloride solution containing 100 mg of the polymer (a mixture consisting of 1% labelled and 99% unlabelled PLA 50) was pre-emulsified by stirring (10 000 rpm for 1 min) in 10 ml of a 10 mg ml^{-1} fetuin aqueous solution with the aid of an Ultra-Turrax homogenizer (type T25; Bioblock). Then, the pre-emulsion was completed and homogenized with a Microfluidizer 110S (Microfluidics). In this apparatus, the pre-emulsion is pumped into a specially designed chamber in which fluid sheets interact at ultra-high velocity and pressure. Microchannels within the chamber provide an extremely focused interaction zone of turbulence causing the release of energy amid cavitation and shear forces, causing break-up of the droplets of the pre-emulsion. For the preparation of the

nanoparticles, the pre-emulsion was introduced into the microfluidizer at a pressure of 6 bar. Finally, methylene chloride present in the emulsion obtained after microfluidization was evaporated under vacuum, giving a colloidal suspension of nanoparticles which was filtered on a 1.2-μm filter.

2.4. Size-exclusion chromatography

A concentrated particle suspension (110 nm, 1 ml) was injected on to a Sepharose CL-2B-containing XK16-100 chromatographic column (100 cm × 16 mm I.D.) (Pharmacia). Elution was performed with 0.13 *M* phosphate buffer (pH 7.4) at a flow-rate of 0.1 ml min^{-1}. Fractions of 2 ml were collected automatically and analysed later. Sephacryl S1000 gel was also used under the same conditions (the Pharmacia FPLC system was used).

The sample of concentrated particle suspension was prepared according to the following procedure. Freshly prepared particles were concentrated tenfold by centrifugation: 10 ml of the suspension were centrifuged for 30 min at 25 000 rpm (4°C) in a T865 rotor, OTD Combi Sorvall ultracentrifuge. The supernatant was discarded and 1 ml of 0.13 *M* phosphate buffer (pH 7.4) was added. The particles were resuspended by gentle shearing. When accurate determination of particle concentration was needed, ^{14}C-labelled particles were used.

2.5. Particle diameter

The intensity average particle diameter of each fraction was measured by PCS. This technique measures the time-dependent light-scattering fluctuations from particles under Brownian agitation from which a correlation function is established using an autocorrelator. The characteristic translation diffusion coefficient obtained directly from this measurement is related to the size of the particles according to the Stokes–Einstein law [16]. The PCS apparatus used was a Brookaven BI 90 particle sizer. Each measurement took 3 min.

2.6. Spectrophotometry

Absorbance measurements (wavelengths from 200 to 1100 nm) were made on a Perkin-Elmer UV–Vis Lambda 2 spectrophotometer with a 1-cm optical path length quartz cell.

2.7. Computations

All calculations were made using Sigma Plot 3.01 on an IBM-compatible PC.

3. Results

The measurement of particle mean diameters in each collected fraction was performed after separation of the nanoparticle suspension (intensity average diameter 110 nm) on a Sephacryl S1000 packed column (Fig. 1). To agree with

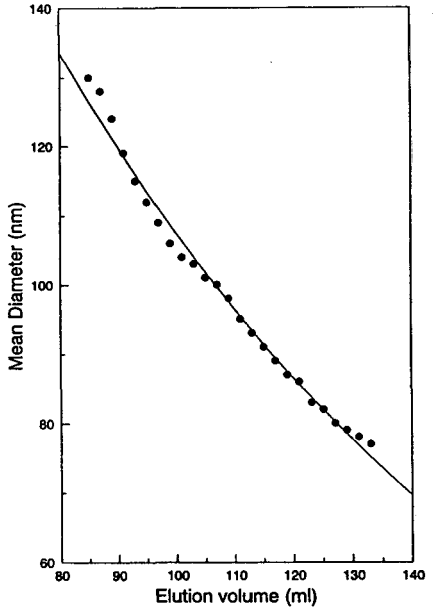

Fig. 1. Separation of 110-nm intensity average diameter PLA–fetuin nanoparticles on Sephacryl S1000 (XK16-100 column). The average diameter of the particles in each collected fraction is plotted as a function of the elution volume. The values correspond approximately ($r^2 = 0.99$) to $d = 318 \exp(-0.01086v)$, where v is the volume in ml and d the diameter in nm.

usual representation of chromatographic data, an exponential regression was calculated, giving

$$\ln d = \ln(318) - 0.01086(v) \quad (r^2 = 0.990) \qquad (5)$$

where d is the intensity average diameter (in nm) and v the elution volume (in ml).

In fact, the separation was nearly linear in the range studied, corresponding approximately to a 1-nm drop mer ml. The total volume of the column was *ca.* 200 ml but the void volume could not be determined accurately. It could be estimated to be 70 ml using 400-nm particles (results not shown).

When the same experiment was performed on Sepharose CL-2B gel with the same type of nanoparticles of 107-nm intensity average diameter, a different general shape of the curve was obtained (Fig. 2). Expecially when ln d was represented as a function of the elution volume, the superposition of two distinct slopes was obvious. The four-parameter exponential regression analysis gave

$$d = 307 \exp(-0.01087v) + 156 \exp[-0.25\ (v - 72)] \quad (r^2 = 0.997) \qquad (6)$$

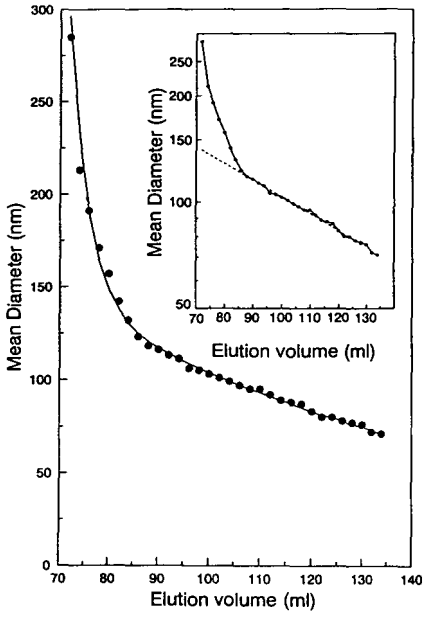

Fig. 2. Separation of 107-nm intensity average diameter PLA–fetuin nanoparticles on Sepharose CL-2B (XK16-100 column). The mean diameter of the particles in each collected fraction is plotted as a function of the elution volume. The values correspond approximately ($r^2 = 0.997$) to $d = 307 \exp(-0.01087v) + 156 \exp[-0.25\ (v - 72)]$.

This complex equation simplified into a linear expression around a 90-ml volume. Then the slope of this linear part took almost the same value as that obtained for the Sephacryl S1000 gel separation and the curves in Figs. 1 and 2 are almost superimposable. In fact, a 1-nm drop was observed for a 1-ml increase in elution volume, as for the Sephacryl S1000 gel. The total volume of the column was 200 ml, whereas the total volume of the eluent was 176 ml (determined by injection of free ^{125}I). The void volume corresponded to the transition between the two slopes at 85 ml [8].

In the two preceding cases, the material loss during the process was very low, and more than 99% of the expected radioactivity was recovered [8]. The Sepharose CL-2B gel was chosen because in the collected fractions, the PCS measurement indicated a much lower polydispersity value. The half-width of the 86–134 ml fraction was *ca.* 5 nm. Owing to the two separation phenomena, this gel also gave a wider diameter range. When larger particles were injected, the mean diameter measured at a given elution volume increased slightly (less than 5 nm variations), whereas a slight decrease in the mean diameter was observed after injection of smaller particles. This was in agreement with colloid SEC theory [8].

In the Sepharose CL-2B experiment (Fig. 3), the use of ^{14}C-labelled particles and the on-line measurement of the absorbance at 405 nm permitted the variation of the 405 nm absorbance/polymer concentration ratio to be represented as a function of particle diameter. This curve is compared in Fig. 4 with the calculated values obtained from ref. 17. According to Mie's theory [18], the absorbance of spherical particles in an aqueous suspension can be expressed as:

$$A = \varepsilon l C \qquad (7)$$

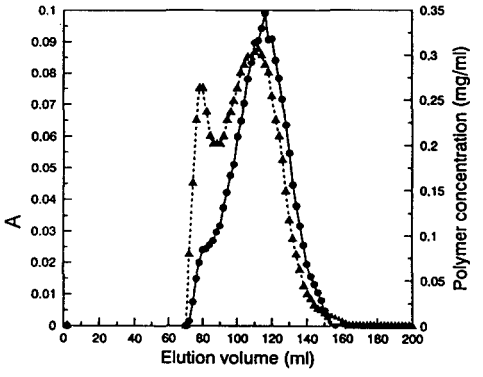

Fig. 3. Chromatograph of the separation of 107-nm ^{14}C-labelled PLA–fetuin particles by Sepharose CL-2B SEC. Absorbance at 405 nm (left-hand axis) (▲) and polymer concentration (right-hand axis) (●) are plotted *versus* the elution volume. The values of particle diameters are shown in Fig. 2.

where l is the optical path length (usually 1 cm), C is the particle mass concentration and ε is the specific turbidity, which in turn can be expressed as

$$\varepsilon = Q[d/\lambda, m(\lambda)]/\lambda \quad (8)$$

where λ is the wavelength, d the particle diameter and m their refractive index, relative to the refractive index of water. Q is a complex function and the values presented in Fig. 4 were computed assuming that the particles showed no absorbance at the wavelength studied for the indicated values of m.

The experimental values seemed to produce a curve whose shape was similar to the theoretical shape for an m value between 1.1 and 1.05. The comparison between the experimental results and theoretical values was done more precisely. In fact, in the diameter range 0–400 nm, the theoretical curves could nearly be superimposed (Fig. 5) by multiplying the ordinates by an appropriate K constant which is a function of the refractive index of the particles, m. This constant K was chosen for the refractive index of the particles $m = 1.1$ curve so as to fit the experimental data and all other K values were calculated as being the best constant to superimpose the other

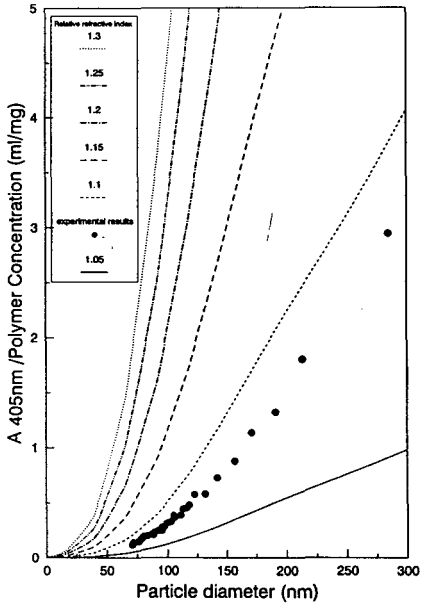

Fig. 4. Absorbance/polymer concentration ratio (proportional to specific turbidity) as a function of particle diameter. Experimental data and six theoretical curves calculated from ref. 9 with the indicated relative refractive indexes are compared.

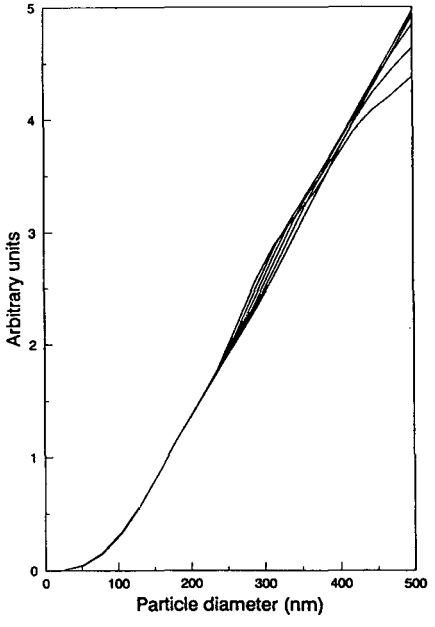

Fig. 5. Superimposition of the six previous theoretical curves after the multiplication of each of them by an appropriate $K(m)$ constant (m is the refractive index).

curves on this new curve. As the ordinates have no physical sense after the multiplication by K, "arbitrary" units were used in Fig. 5. The variation of K with m could be approximated with a third-order interpolation (Fig. 6). The superimposition of the curves, although not perfect, allowed ε to be expressed as

$$\varepsilon = K(m)F(d/\lambda)/\lambda \quad (9)$$

with only a minor approximation in the 0–400-nm diameter range. For example, in Fig. 5, in the worst case of 300-nm particles, a 1.5% error would be made by deducing the $m = 1.05$ curve from the $m = 1.1$ curve. Should the $m = 1.1$ curve be used to fit the experimental values, an even smaller error would be expected.

In order to fit the experimental data, the nearest theoretical curve ($m = 1.1$ in Fig. 4) was used. The best $K(m)$ constant was calculated and the value of m was deduced from Fig. 6 (giving $m = 1.08$). The comparison between the calculated curve and the experimental data obtained with poly(lactic acid)–fetuin nanoparticles is shown in Fig. 7. To agree with theory, the particles should be given an absolute refractive index: $1.08 \cdot 1.33 = 1.44$, where 1.33 is the refractive index of water.

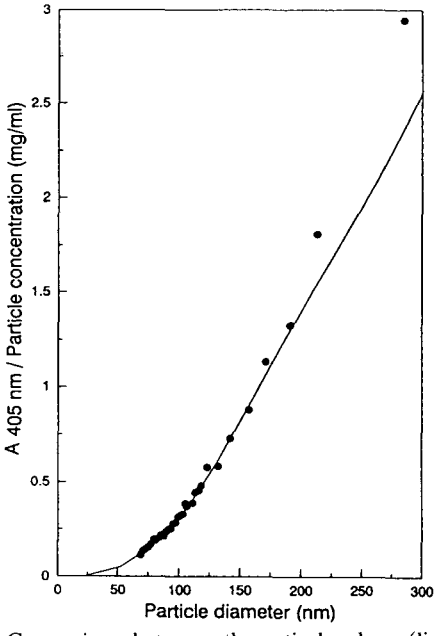

Fig. 7. Comparison between theoretical values (line) and experimental results (O). Adaptation of the $m = 1.1$ theoretical curve which gives the best fit with experimental data. The $K(m)$ constant used corresponds to a relative refractive index $m = 1.08$. The absolute refractive index of particles should be $1.08 \cdot 1.33 = 1.44$.

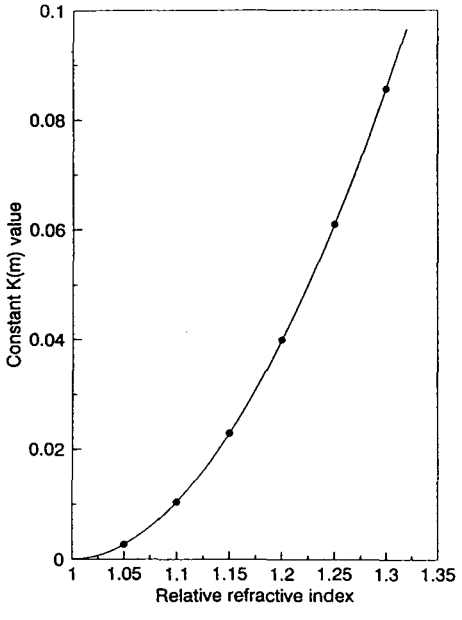

Fig. 6. Third-order interpolated curve that gives the relationship between the m and K values.

The same measurements could also be considered as a first estimation of the particle size distribution of the initial nanoparticle suspension (intensity average diameter measured by PCS of 110 nm). From Fig. 2, the diameter range could be estimated in each fraction, whereas the particle mass concentration was estimated in the same fraction using ^{14}C radioactivity measurements. As the value of the particle concentration by scattering intensity is proportional to the absorbance at 405 nm, the value of the particle concentration by number could be deduced from one of the above concentration values and from the particle diameter. For monodisperse particles the particle mass concentration M is proportional to nd^3, where d is the particle diameter and n the particle concentration by number.

To draw the PSD shown in Fig. 8, the particle concentration measured in each fraction was

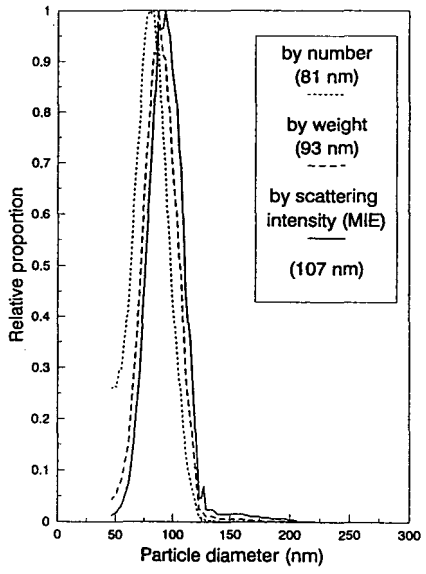

Fig. 8. First-approximation PSD deduced from experimental results. Particle concentration determined by ^{14}C counting was weighted to account for the diameter interval in the corresponding fraction (corresponding average diameter in nm). The average diameter calculated from those data were 81 nm by number, 93 nm by mass and 107 nm by scattering intensity.

divided by the width of the range of diameters in the fraction, in order to obtain the relative proportion for each size. The resulting histogram was smoothed for the sake of clarity only. The three mean diameters given in Fig. 8 were calculated using the equation

$$\text{mean diameter} = \sum dC(d) \Big/ \sum C(d) \qquad (10)$$

where C is the concentration by number, by mass or by scattering intensity and d is the diameter (in nm) [11].

Although it was not the main objective of this experiment, the use of ^{125}I-labelled fetuin allowed the measurement, in addition, of the amount of protein eluted in each fraction with the particles. As the free protein is eluted clearly after the particles (Fig. 9), it was considered that the amount of protein present in the earliest fractions corresponded to fetuin firmly bound to nanoparticles. If the amount of bound protein per unit mass of particles was represented (Fig. 10) as a function of the inverse of the particle diameter, and despite important experimental errors, a linear dependence between these parameters could be evidenced.

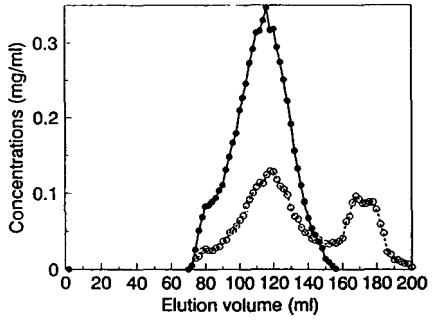

Fig. 9. Chromatograph of the separation of 107-nm ^{14}C-labelled PLA–^{125}I-labelled fetuin particles by Sepharose CL-2B SEC. ○ = Fetuin; ● = polymer concentration. The values of particle diameters are shown in Fig. 2.

4. Discussion

The main question that arises from these results is how accurate they are. In other words,

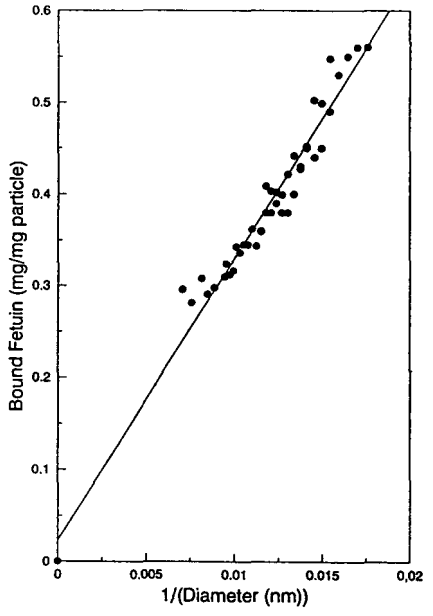

Fig. 10. Amount of bound protein per unit mass of the polymer as a function of the inverse diameter.

it is questionable if the SEC separation was sufficiently efficient to give a reliable particle PSD and an invariant curve for the variation of the particle diameter as a function of the elution volume.

The first result to be considered is the variation of the specific turbidity of the particles as a function of the diameter. A clear correlation was observed between experimental data and calculated values for $m = 1.08$ (Fig. 7). Only two experimental values corresponding to the larger particles were very erroneous owing to the very low values of both the absorbance and concentration. The relationship obtained between specific turbidity and particle diameter has been confirmed for relatively monodisperse PLA–albumin nanoparticles (not shown). No difference was noted compared with monodisperse PLA–fetuin nanoparticles. This means that the nature of the protein did not really matter as the absorbance of this protein was negligible at 405 nm. This relationship can now be used as a method to evaluate the nanoparticle concentration, with a 0.03 mg ml^{-1} accuracy for 100-nm particles. It could also be used as a measure of particle diameter if the concentration is known.

However, one drawback of this method is the need to have no specific absorbance at the wavelength used. However, even though the method has been standardized for a 405-nm wavelength, the curve can be used at any other wavelength. In fact, $\varepsilon = K(m)F(d/\lambda)/\lambda$ (Eq. 9) and the standardized curve is

$$\varepsilon = f_{405}(d) = K(m)F(d/405)/405 \quad (11)$$

If λ has to be changed:

$$\varepsilon = f_{405}(405d/\lambda) \cdot 405/\lambda \quad (12)$$

This means that the value of ε at λ may be obtained for particles whose diameter is d by calculating the value of ε at 405 nm for particles whose diameter is $405d/\lambda$ and then multiplying this value by $405/\lambda$. As the absorbance (200–1100 nm) of each fraction has been measured and when this value was large enough, Eq. 12 was easily confirmed for λ (350–1100 nm). For $\lambda < 350$ nm the absorbance of the protein was found to be no longer negligible (results not shown). In the same way, Eq. 12 could be used for particles larger than 500 nm for which the approximation made that $Q[d/\lambda, m(\lambda)]/\lambda = K(m)F(d/\lambda)/\lambda$ was no longer valid at $\lambda = 405$ nm. Hence it is only necessary that $405d/\lambda < 500$ nm. Then, the only limitation remains to maintain a sufficient signal at high wavelength.

Another drawback of the proposed method for particle concentration determination is much more difficult to bypass as it concerns its sensitivity to the polydispersity of the measured sample. For example, in the case of a 1 g l^{-1} mixture of 100- and 150-nm diameter particles in equal proportions, the absorbance at 405 nm is $A = 0.5[0.32 + (0.32 \cdot 1.5^2)] = 0.52$ and the intensity average diameter becomes $[100 + (150 \cdot 1.5^2)]/(1 + 1.5^2) = 135$ nm; ε read on the curve is then 0.56 l g^{-1} cm^{-1}. This gives a measured concentration value of 0.9 g l^{-1} instead of 1 g l^{-1}, *i.e.*, a 10% error. In fact, owing to its great sensitivity to polydispersity, this law should not be used for polydisperse samples. However, as the results obtained correlated well with the theory, it was concluded that the particle population in each fraction was not too polydisperse. This was further confirmed by photon correlation measurements that gave in each fraction a very low value for polydispersity. This showed that G was probably a skewed function.

In a second step, it should be highlighted that the curves plotted in Figs. 1 and 2 represent only an approximation of the universal calibration curve $\boldsymbol{d}_p = V_e^{-1}(v)$ of the two gels used. The values of diameters that are plotted as a function of v are the PCS intensity average diameters measured in the collected fractions. As such, and according SEC theory [9], they should depend on the nature of the injected suspension. Indeed, experimentally, changing the nature of the injected suspension did change the obtained $\boldsymbol{d}_p$–v relationship, but at most 5-nm variations were observed. A universal curve would be obtained only by injecting perfectly monodisperse samples, each of a well defined diameter. This goal could be achieved, for example, by re-injecting each collected fraction and re-measuring its PSD. However, this was not possible experimentally because, under these conditions, too low ab-

sorbance values would have been obtained. Indeed, if the collected fraction at a given volume v was injected again indefinitely, the value of the diameter in the volume v fraction would converge exactly to $V_e^{-1}(v)$. This means that what has been done here is the first step of a converging process. This means that the average diameter measured in each fraction was probably approximately equal to the standard value. Hence the injection of a single suspension with a broad distribution was sufficient to obtain a good approximation of the column standard calibration graph. Therefore, it is an easy method for standardizing SEC.

A further analysis of Figs. 1 and 2 highlighted that in the case of Sepharose CL-2B, the double-sloped curve was typical of two phenomena: for particles smaller than 125 nm, efficient separation by SEC occurred, whereas two effects are responsible for the separation of the large particles: the usual SEC separation and hydrodynamic separation [8,9,10]. We cannot exclude SEC separation of the large particles because a small proportion of large pores exists in the gel in any case. Further, the numerical results obtained showed that Sephacryl S1000 has only slightly larger pores than Sepharose CL-2B, which is in agreement with their respective standard dextran separation capacities (Pharmacia data).

The next question, which is not totally independent of the above considerations, deals with the reliability of the PSD determination. Of course, to have access to the real PSD, each fraction should have been re-injected and its own PSD determined again, in a converging process. As the measured diameter in a given fraction v was close to $V_e^{-1}(v)$, it could be concluded that the PSD obtained was certainly close to the real value. As a confirmation of this, it should be mentioned that the intensity average diameter calculated from SEC and PCS data (107 nm) was equal to the diameter measured before injection by PCS (107 nm). As generally supposed [8,10], the experimental PSD was found to be close to a log-normal distribution.

Finally, SEC was used to determine the amount of protein bound to nanoparticles. However, as the amount of ^{125}I used was low (in order not to interfere with other measurements), there was a great experimental dispersion, partially balanced by the large number of experimental data. The amount of protein bound per unit mass of polymer was found to be inversely proportional to the particle diameter. This result confirmed previous experiments performed with human serum albumin–PLA particles [3]. This proportionality means that the total amount of bound protein was also proportional to the specific surface area of the particles. With fetuin, the slope of the curve gave approximately 7 mg of bound protein per square metre of particle surface, which was twice the value found with albumin after desorption. This observation could be explained by the affinity of fetuin for itself. It was noteworthy that after desorption and washing, approximately half of the initially bound fetuin remained associated with the polymer. The final values, after washing, of the amount of bound protein are then the same for fetuin and albumin [3]. The fact that this constant proportion of protein remained bound on particles is probably the reason why no particle aggregation upset the experimentation.

5. Conclusions

The present results have shown that the combination of SEC, PCS and turbidity measurements may be considered as an alternative to the mathematical standardization of SEC for the characterization of colloidal suspensions. This method was found to be easy to use, fast and needed no rigorous column maintenance. However, concentrated samples were needed in order to obtain a sufficient signal for PCS measurements. This method has been applied to study the light scattering of colloidal particles, which was found to correlate well with Mie's theory. The resulting calibration graph could be used to determine the concentration of monodisperse particle samples with a known diameter. Also, an accurate approximation of PSD was obtained. Finally, the separation of the particles by SEC, followed by PCS and radioactivity counting in

each fraction, is proposed for determining the amount of ^{125}I-labelled protein bound to the nanoparticles.

6. References

[1] L. Illum and S.S. Davis, in P. Buri and A. Gumma (Editors), *Drug Targeting*, Elsevier, Amsterdam, 1985, pp. 65–80.
[2] R.L. Juliano, *Adv. Drug Delivery Rev.*, 2 (1988) 31–54.
[3] T. Verrecchia, P. Huve, D.V. Bazile, M. Veillard, G. Spenlehauer and P. Couvreur, *J. Biomed. Mater. Res.*, 27 (1993) 1019–1028.
[4] J.C. Giddings, *Science*, 260 (1993) 1456–1465.
[5] S. Lee and J.C. Giddings, *Anal. Chem.*, 60 (1988) 2328.
[6] J. Pazourek and J. Chmelik, *Chromatographia*, 35 (1993) 591–596.
[7] P.S. Williams, T. Koch and J.C. Giddings, *Chem. Eng. Commun.*, 111 (1992) 121.
[8] A. Penlidis, A.E. Hamielec and J.F. MacGregor, *J. Liq. Chromatogr.*, 6 (1983) 179–217.
[9] M.G. Styring, J.A.J. Honig and A.E. Hamielec, *J. Liq. Chromatogr.*, 9 (1986) 3505–3541.
[10] T. Kourti, A. Penlidis, A.E. Hamielec and J.F. MacGregor, *Polym. Mater. Sci. Eng.*, 53 (1985) 147–151.
[11] A.E. Hamielec, *J. Chromatogr. Sci.*, 25 (1985) 117–160.
[12] T. Ishige, S.-I. Lee and A.E. Hamielec, *J. Appl. Polym. Sci.*, 15 (1971) 1607–1622.
[13] J. Marti and S. Aliau, *Biochim. Biophys. Acta*, 303 (1973) 348–359.
[14] D.S. Salomon, M. Bano, K.B. Smith and W.R. Kidwell, *J. Biol. Chem.*, 257 (1982) 14093–14101.
[15] D.V. Bazile, C. Ropert, P. Huve, T. Verrecchia, M. Marlard, A. Frydman, M. Veillard and G. Spenlehauer, *Biomaterials*, 13 (1992) 1093–1102.
[16] A. Einstein, *Investigation on the Theory of the Brownian Movement*, Dover, New York, 1956.
[17] W. Heller and W.J. Pangonis, *J. Chem. Phys.*, 26 (1957) 498–506.
[18] G. Mie, *Ann. Phys. (Leipzig)*, 25 (1908) 377–445.

ELSEVIER

Journal of Chromatography A, 675 (1994) 141–147

JOURNAL OF CHROMATOGRAPHY A

Column-switching techniques in the analysis of phosphate by ion chromatography ☆

M.T. Galceran*, M. Diez

Departament de Química Analítica. Universitat de Barcelona, Av. Diagonal 647, 08028 Barcelona, Spain

(First received December 6th, 1993; revised manuscript received March 7th, 1994)

Abstract

A comparative study of ion chromatography systems for the analysis of phosphate in samples with high levels of sulphate has been performed. Two low-capacity ion-exchange columns, a high-capacity column and switching systems with direct transfer and with loop transfer have been studied. A high-capacity column permits the determination of phosphate in samples with sulphate-to-phosphate ratio of 5000:10 (mg/l), but at this sulphate level the detection limit for phosphate was relatively high (200 ng). For the column-switching systems, switching time and phosphate detection limits have been studied. A low detection limit (50 ng) was obtained using direct-transfer column switching at sulphate concentrations of 4000 mg/l. A similar detection limit was obtained using a loop-transfer column-switching system with a high-capacity column as a primary column for levels of sulphate of 5000 mg/l. Their applicability for the analysis of water samples is demonstrated.

1. Introduction

Ion chromatography (IC) is an effective technique to determine trace anions in a variety of samples but its application to sample matrices of extreme ionic strength shows some difficulties. Anions at relatively low concentrations (100–1000 mg/l) often cause overload and peaks become broad because of the low capacity of the ion exchanger used (less than 0.1 mequiv./g). Moreover, high concentrations of ionic compounds in this kind of sample induce retention time variability, loss of chromatographic efficiency and resolution, decrease in the column lifetime and increase in the background of the conductivity detector.

Several procedures have been suggested to overcome the adverse effects of matrix ions. The concentration of these ions in the sample can be reduced prior to the analysis by using a suitable precolumn filled with an ion-exchange resin [1–5], hollow-fibre ion-exchange membranes [6,7], dialysis through membranes [8,9] or electrodialysis [10–13]. The use of the interfering ion as the eluent [14,15] and the use of gradient IC [16] have also been proposed for samples containing high ratios of ion concentrations.

Few methods are proposed for the elimination of sulphate in highly saline samples but the use of precolumns with ion-exchange resins in the barium form is recommended [3–5]; this pro-

* Corresponding author.

☆ Presented at the *22nd Annual Meeting of the Spanish Chromatography Group, Barcelona, October 20–22, 1993.*

0021-9673/94/$07.00
SSDI 0021-9673(94)00277-G

cedure is time consuming and the recoveries of phosphate are low [5].

Commercial columns with moderate capacity, because of their length, can give better resolutions and may be used in the analysis of samples with anions at different concentrations. We studied the applicability of one of these columns to the analysis of phosphate in samples with high levels of sulphate. The highest sulphate-to-phosphate ratio that allows the determination of phosphate was established and the detection limit for phosphate at different ratios was calculated.

On the other hand, on-line multidimensional chromatography permits complex samples to be broken down into manageable portions, resulting in improved speed, precision and chromatographic resolution. Column switching involves the cleanup and separation of multicomponent mixtures by on-line selective transfer of a fraction from one chromatographic column to one or more secondary columns for additional separation. These techniques have been used for the elimination of chloride from different samples, such as concentrated inorganic acids, water and brine [17–20], of weak organic acid anions in water [21] or large amounts of interferent compounds in the determination of sulphite in a variety of samples [22,23]. Few applications of these methods have been described for the elimination of sulphate in saline samples [21,24], and none of them has been used for the analysis of phosphate. In this study column-switching techniques with direct or with loop transfer for the elimination of sulphate in saline samples before phosphate determination are described. Column-switching time and detection limits for samples with different sulphate-to-phosphate ratios are established.

2. Experimental

2.1. Instruments

The liquid chromatograph consisted of an LKB (Bromma, Sweden) Model 2150 pump, a Rheodyne (Cotati, CA, USA) Model 7125 valve (100-μl loop), a Rheodyne Model 7000 valve and a Metrohm (Herisau, Switzerland) Model 690 conductivity detector. A data processor, Chromatopac C-R3A (Shimadzu, Kyoto, Japan), was used. Two different anion-exchange analytical columns, both based on aminated polymethacrylate resin (exchange capacity 30 μequiv./g), were used. These were a Waters (Milford, MA, USA) IC Pak A (50 × 4.6 mm I.D.; particle size 10 μm) and a high-capacity Waters IC Pak A HC (150 × 4.6 mm I.D.; particle size 10 μm).

2.2. Materials

Salts of the common anions, of analytical-reagent grade or better, were obtained from different suppliers. A 1000 mg/l stock solution of each anion was prepared and used for further dilutions. For samples with high levels of sulphate a 20 000 mg/l stock solution of this anion was prepared and used for further dilutions. Water was purified using a Culligan system and filtered through a 0.45-μm membrane.

Sodium gluconate (97%), boric acid, glycerine (87%) and acetonitrile were obtained from Merck (Darmstadt, Germany). Sodium tetraborate was obtained from Carlo Erba (Milan, Italy).

2.3. Chromatographic conditions

Non-suppressed IC with conductimetric detection using borate–gluconate [1.3 m*M* tetraborate, 5.8 m*M* boric acid, 1.3 m*M* gluconate, 5 g/l glycerine (pH 8.5) and 120 ml/l acetonitrile] at 1 ml/min with a Waters IC Pak A and two Waters IC Pak A on-line, and at 2 ml/min with a Waters IC Pak A HC was used for the determination of phosphate. All eluents were prepared daily, filtered and degassed.

2.4. Column-switching systems

The flow diagram of the column-switching system A, direct transfer, is shown in Fig. 1. This system was equipped with two Waters IC Pak A columns on-line. The primary mobile phase entered the valve (IN) and flushed the primary

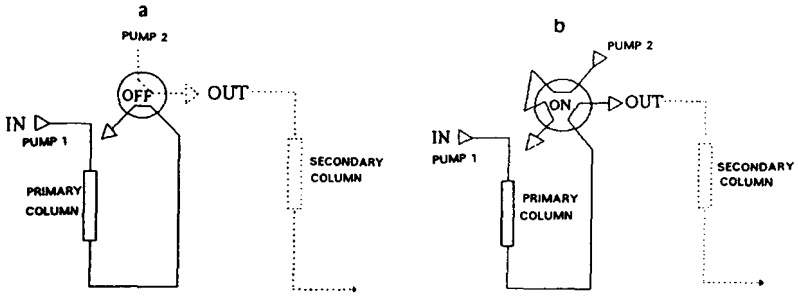

Fig. 1. Column-switching system A. (a) Elution of primary column. (b) Transfer on to the secondary column with primary eluent.

column (Fig. 1a). When the analyte eluted, the switching valve was rotated into the transfer position (ON) (Fig. 1b). The separated analyte fraction was directed through the OUT port to the secondary column; then the valve was rotated back and the secondary mobile phase (PUMP 2) started to elute the analyte from the secondary column.

The column-switching system B was the same as system A, except that it was equipped with a sample loop (2 ml) between the two columns and the primary was a high-capacity column, IC Pak A HC and the secondary an IC Pak A. The primary and secondary columns were not connected on-line during the transfer period to avoid excessive pressure on the columns during the transfer. The analyte effluent from the primary column was collected in a loop and reinjected into the secondary column.

3. Results and discussion

Borate–gluconate is a mobile phase that permits sensitive detection and efficient separation in IC using aminated polymethacrylate columns. To examine the effect of high levels of sulphate on the resolution between sulphate and phosphate using borate–gluconate as mobile phase, samples with 10 mg/l of phosphate and different concentrations of sulphate from 100 to 5000 mg/l were analyzed.

A low-capacity (5 cm), two on-line low-capacity columns and a high-capacity column (15 cm) were used. In Table 1 data for the separation of sulphate and phosphate with different columns are given. For sulphate concentration below 500 mg/l baseline resolution between phosphate and sulphate was always attained. In Fig. 2 the chromatograms obtained with a low-capacity column for samples with sulphate-to-phosphate ratios of 100:10 (mg/l) and 500:10 (mg/l) are shown. An increase in the amount of sulphate gave worse separation and, at 1000 mg/l of sulphate, no separation at all was observed due to the overloading of the sample anions on a low-capacity ion-exchange resin. Although an improvement in resolution between phosphate and sulphate can be obtained at pH lower than 8.5 a decrease in the eluting strength of the eluent occurred, giving higher retention times and worse detection limits. An increase in the column capacity may give better results. For two columns connected on-line enough resolution can be obtained until ratios 4000:10 as can be seen in Fig. 3A. At higher sulphate concentration the phosphate and sulphate peaks co-eluted.

At higher sulphate concentration, 5000 mg/l, only a high-capacity column allowed the separation of phosphate (Fig. 3B), although a distortion of the peaks occurred due to the high level of sulphate. It must be pointed out that the performance of the analysis was strongly dependent on the behaviour of the column, retention time and resolution decreased considerably after 100 injections at this sulphate concentration.

Table 1 shows that the retention time of the phosphate decreased with an increase in the amount of sulphate. This decrease can be explained since sulphate is a stronger eluent than borate–gluconate. With a large sulphate loading,

Table 1
Separation of sulphate and phosphate in anion-exchange columns

SO_4^{2-}:PO_4^{3-} (mg/l)	Columns					
	Low-capacity column		Two low-capacity columns		High-capacity column	
	t_R (min)	Δt (min)	t_R (min)	Δt (min)	t_R (min)	Δt (min)
100:10	13.2	4.3	24.1	8.1	22.6	8.6
500:10	12.1	2.1	23.8	6.1	22.5	6.8
1000:10	Coelution		23.2	5.0	22.1	5.8
2000:10	Coelution		22.8	4.2	21.8	4.1
2500:10	Coelution		22.6	3.5	21.3	3.6
3000:10	Coelution		21.9	2.7	20.9	3.0
3500:10	Coelution		21.5	2.1	20.5	2.6
4000:10	Coelution		21.2	1.6	20.3	2.3
4500:10	Coelution		Coelution		20.1	2.0
5000:10	Coelution		Coelution		19.7	1.9

it can be assumed that the borate–gluconate eluent ion is partially replaced by sulphate ion, which leads to a decrease in the retention times.

3.1. Column-switching procedures

For the analysis of phosphate in a highly concentrated matrix of sulphate two column-switching systems were studied. System A (see Fig. 1) used a direct-transfer technique, and system B a loop-transfer one.

In both techniques, the system was initially assembled with only the primary column in order to determine the column-switching time interval, which is the time between the onset of the analytical peak and its complete elution. For high amounts of sulphate, since the primary column was overload, the column-switching time for each sample must be determined using the coupled system. For example in Fig. 4 the results obtained when switching from 10 to 13 min, from 6 to 8 min and from 3 to 6 min for a sample with a sulphate-to-phosphate ratio of 5000:10 (mg/l) are given, the highest recoveries (71.3%) were obtained when switching from 6 to 8 min. Samples with less sulphate gave higher recoveries of phosphate; for example for samples with a sulphate-to-phosphate ratio of 4000:10 the recovery was 92.5%.

Calibration for phosphate in samples with different levels of sulphate was carried out using the standard addition method; peak area was used as the response. The correlation data show good linearity for phosphate; for example for samples with 5000 mg/l of sulphate the correlation coefficient for phosphate (5–25 mg/l) was 0.9989.

To determine the reproducibility of the technique eight replicate determinations of 10 mg/l of phosphate were carried out for the optimum column-switching time. The relative standard deviation (R.S.D.) of peak areas was 1.5%.

Detection limits for phosphate were calculated as a response higher than three times the standard deviation of the background noise. The values obtained using a low-capacity, two on-line low-capacity columns, a high-capacity column and the column-switching systems are given in Table 2. A low detection limit (5 ng) was obtained with a low-capacity column for samples without sulphate, but there was an increase in the detection limit when columns with higher capacity were used or when the sulphate content was raised. This increase was more pronounced at high levels of sulphate and may be related to a distortion in the phosphate peak and in the baseline. In the column-switching system with direct transfer, phosphate detection limits re-

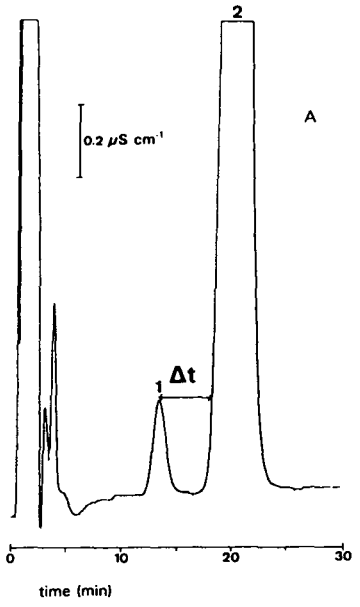

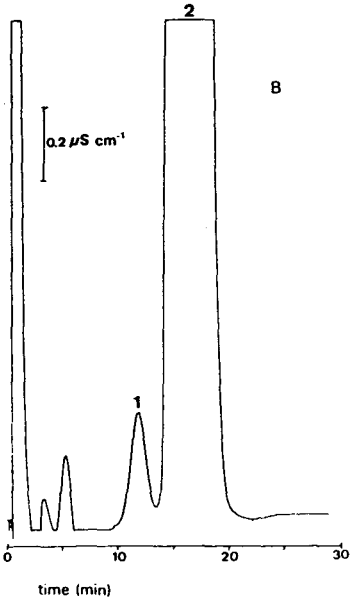

Fig. 2. Chromatograms of the separation of phosphate and sulphate with a low-capacity column (1 ml/min). (A) Sulphate-to-phosphate ratio 100:10 (mg/l), (B) sulphate-to-phosphate ratio 500:10 (mg/l). Peaks: $1 = HPO_4^{2-}$; $2 = SO_4^{2-}$.

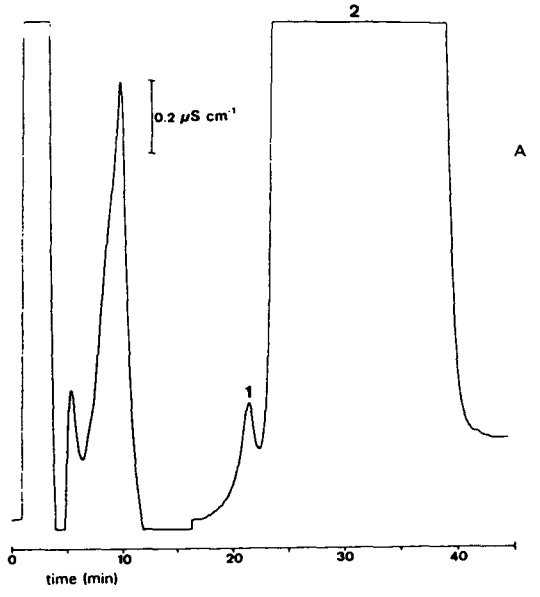

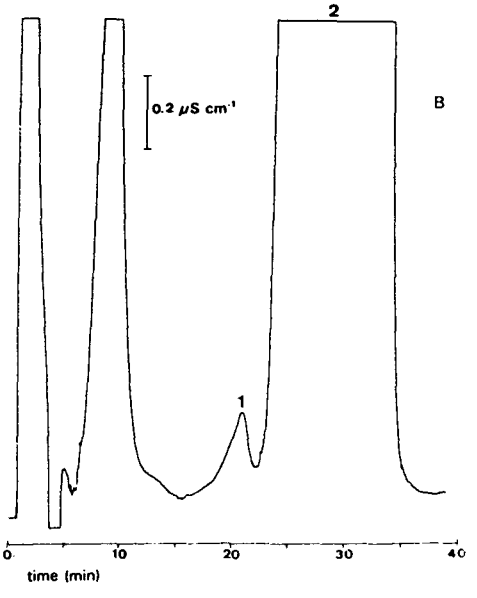

Fig. 3. Chromatograms of the separation of phosphate and sulphate. (A) Two low-capacity columns on-line (1 ml/min), sulphate-to-phosphate ratio 4000:10 (mg/l); (B) high-capacity column (2 ml/min), sulphate-to-phosphate ratio 5000:10 (mg/l). Peaks: $1 = HPO_4^{2-}$; $2 = SO_4^{2-}$.

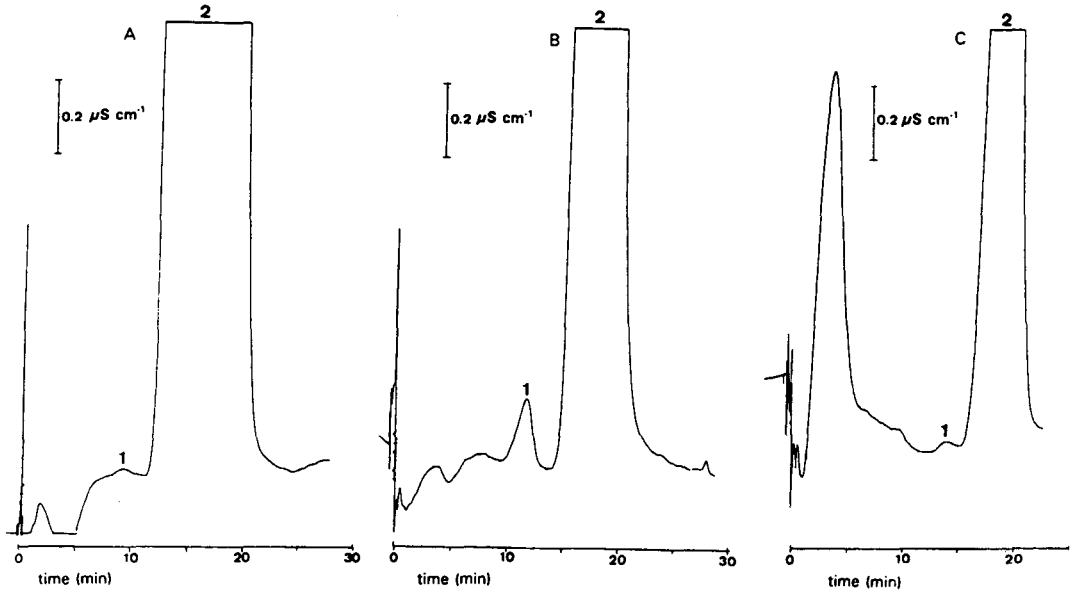

Fig. 4. Chromatograms of the optimization of column-switching time with direct transfer (system A). (A) Column-switching time from 10 to 13 min, (B) column-switching time from 6 to 8 min, (C) column-switching time from 3 to 6 min. Peaks: 1 = HPO_4^{2-}; 2 = SO_4^{2-}.

mained constant for sulphate concentrations between 100 and 1000 mg/l. This behaviour was due to the elimination of the sulphate ion. When the concentration of sulphate increased to 4000 mg/l a rise in the detection limit was observed but this was always lower than that obtained with the other systems. Using a column-switching system with loop transfer and a high-capacity column, higher detection limits for low levels of sulphate were observed related with a diffusion of the solute in the loop, which gives broad peaks. Detection limits were similar for all sulphate concentrations; so for samples with high levels of sulphate the best detection limits were obtained using the switching system. This can be explained due to the high capacity of the primary column, which prevents overloading, and as a result no sulphate enters in the secondary column.

The analysis time using column-switching techniques was 30 min, similar to the time needed for the analysis with a high-capacity column. The

Table 2
Detection limits obtained with different systems

System	Detection limit (ng)					
	SO_4^{2-} concentration (mg/l)					
	0	100	500	1000	4000	5000
Low-capacity column	5	8	35	–	–	–
Two low-capacity columns on-line	15	20	40	50	150	–
High-capacity column	25	35	50	60	80	200
Column switching direct transfer	15	20	20	20	50	100
Column switching loop transfer	35	35	40	40	40	50

reequilibration time before the injection of a second sample can be eliminated if the primary column is continuously flushed with the mobile phase.

To show the applicability of the method in samples with high levels of sulphate, column-switching system A was used for the analysis of synthetic samples with a sulphate-to-phosphate ratio of 5000:10 (mg/l) using the standard addition method; the R.S.D. was 3.4% ($n = 5$).

4. Conclusions

Different IC systems for the analysis of phosphate in samples with high excess of sulphate were compared. For sulphate-to-phosphate ratios lower than 500:10 (mg/l) low-capacity columns can be used. A high-capacity column or two low-capacity columns on-line are needed for samples with sulphate levels between 500 and 4000 mg/l. In samples with a high excess of sulphate, column-switching techniques give better results. Low detection limits for phosphate, at the ng level, in samples with high levels of sulphate, 4000–5000 mg/l, were obtained using column switching with direct or loop transfer. These procedures are reproducible, have high recoveries, are faster than other conventional off-line methods of elimination of sulphate and can be proposed for the analysis of phosphate in highly saline samples. Further applications of the technique are now being studied.

References

[1] P.R. Haddad, *J. Chromatogr.*, 482 (1989) 267.
[2] S.Y. Tyree, Jr. and M.A.O. Bynum, *Limnol. Oceanogr.*, 29 (1984) 1337.
[3] R. Saari-Nordhaus, J.M. Anderson Jr. and I.K. Henderson, *Am. Lab.*, 22 (1990) 18.
[4] I.K. Henderson, R. Saari-Nordhaus and J.M. Anderson, Jr., *J. Chromatogr.*, 546 (1991) 61.
[5] M.T. Galceran, M. Diez and L. Paniagua, *J. Chromatogr.*, 657 (1993) 77.
[6] P.E. Jackson and W.R. Jones, *J. Chromatogr.*, 538 (1991) 497.
[7] W.R. Jones and P. Jandik, *J. Chromatogr. Sci.*, 27 (1989) 449.
[8] J.A. Cox and N. Tanaka, *Anal. Chem.*, 57 (1985) 383.
[9] J.A. Cox and E. Dabek-Zlotorzynska, *Anal. Chem.*, 59 (1987) 534.
[10] Y. Okamoto, N. Sakamoto, M. Yamamoto and T. Kumamaru, *J. Chromatogr.*, 539 (1991) 221.
[11] P.R. Haddad, S. Laksana and R.G. Simons, *J. Chromatogr.*, 640 (1993) 135.
[12] A. Siriraks and J. Stillian, *J. Chromatogr.*, 640 (1993) 151.
[13] S. Laksana and P.R. Haddad, *J. Chromatogr.*, 602 (1992) 57.
[14] P. Pastore, I. Lavagnini, A. Boaretto and F. Magno, *J. Chromatogr.*, 475 (1989) 331.
[15] Marheni, P.R. Haddad and A.R. Mutaggari, *J. Chromatogr.*, 546 (1991) 221.
[16] D.T. Gjerde, D.J. Cox, P. Jandik and J.B. Li, *J. Chromatogr.*, 546 (1991) 151.
[17] M. Murayama, M. Suzuki and S. Takitani, *J. Chromatogr.*, 466 (1989) 355.
[18] A. Siriraks, C.A. Pohl and M. Toefan, *J. Chromatogr.*, 602 (1992) 89.
[19] P.F. Subosa, K. Kihara, S. Rokushika, H. Hatano, T. Murayama, T. Kubota and Y. Hanaoka, *J. Chromatogr. Sci.*, 27 (1989) 680.
[20] P.J. Naish, *Analyst*, 109 (1984) 809.
[21] A.A. Ivanov, I.N. Voloschchik and O.A. Shpigun, *J. Anal. Chem. USSR*, 44 (1989) 569.
[22] S.R. Villaseñor, *Anal. Chem.*, 63 (1991) 1362.
[23] S.R. Villaseñor, *J. Chromatogr.*, 602 (1992) 155.
[24] T.B. Hoover and G.D. Yager, *Anal. Chem.*, 56 (1984) 221.

ELSEVIER

Journal of Chromatography A, 675 (1994) 149–154

JOURNAL OF CHROMATOGRAPHY A

Determination of arsenic compounds using inductively coupled plasma mass spectrometry with ion chromatography

Yoshinori Inoue*,[a], Katsuhiko Kawabata[a], Hiromitsu Takahashi[b], Ginji Endo[c]

[a]*Division of R & D, Yokogawa Analytical Systems Inc., 11-19 Nakacho 2-chome, Musashino-shi, Tokyo 180, Japan*
[b]*Matsushita Science Center of Industrial Hygiene, 7-6 Tonoshima-machi, Kadoma-shi, Osaka 571, Japan*
[c]*Department of Preventive Medicine and Environmental Health, Osaka City University, Medical School, 4-54 Asahi-machi 1-chome, Abeno-ku, Osaka 545, Japan*

(First received December 7th, 1993; revised manuscript received March 15th, 1994)

Abstract

A combined system of inductively coupled plasma mass spectrometry (ICP-MS) with ion chromatography (IC) has been used for the determination of arsenic compounds. Arsenous acid (As^{III}), monomethylarsonic acid (MMAs), dimethylarsinic acid (DMAs), trimethylarsine oxide (TMAsO) and arsenobetaine were separated by anion-exchange chromatography. Subsequently eluates were directly introduced into ICP-MS and detected at m/z 75. Separation parameters were optimized for the arsenic compounds as follows: column, two Excelpak ICS-A35 columns (150 mm × 4.6 mm I.D. each) packed with polymer-based hydrophilic anion-exchange resin (ion-exchange capacity: 0.15 mequiv./g dry); mobile phase, $10 \cdot 10^{-3}$ *M* tartaric acid; flow-rate, 1.0 ml/min; column temperature, 50°C; injection volume, 20 μl. The detection limits for the five arsenic compounds were from 0.22 to 0.44 μg/l as an As element. The repeatability was better than 5% (relative standard deviation) for all arsenic compounds. The IC–ICP-MS system was applied to the determination of arsenic compounds in the urine of DMAs-exposed rats. As^{III}, MMAs, DMAs and TMAsO were detected in the urine.

1. Introduction

Arsenic compounds have been documented as a human carcinogen to the skin and lungs [1]. Most mammals including humans are able to methylate inorganoarsenic compounds to monomethylarsonic acid (MMAs) and dimethylarsinic acid (DMAs) [2]. In experimental rats, necrosis of proximal tubules and necrosis of renal papilla were observed in rats by oral administration of DMAs [3]. On the other hand, AsBe, which is regarded as a non-toxic organoarsenic compound, is rich in sea food and is directly eliminated with urine. Therefore, speciation analysis of arsenic compounds is required in order to evaluate the exposure.

At present, several analytical procedures for arsenic compounds have been reported. For speciation of arsenic compounds, the most commonly used technique is the application of chromatography with different detection systems [4–10]. Inductively coupled plasma mass spectrometry (ICP-MS) is a sensitive, accurate and precise analytical tool for ultra-trace multielemental and isotopic analysis. However, this method does not give any information on specia-

* Corresponding author.

0021-9673/94/$07.00
SSDI 0021-9673(94)00260-G

tion. On the other hand, ion chromatography (IC) is a good separation method for the speciation study of inorganic ions, but lack of sensitivity is a problem for determination of arsenic compounds in biological samples. Because of the ease of combination of ICP-MS with high-performance liquid chromatography, several researchers have applied ICP-MS as a liquid chromatography detector [8–10]. Shibata and Morita [10] have reported a separation of fifteen arsenic compounds in the natural samples, using ion-pair liquid chromatography.

Urine is troublesome to handle because of its higher salt concentration, compared with arsenic compounds' concentrations. The urine matrix causes column overloading, and which results in peak broadening. Furthermore, interference from the polyatomic ion $^{40}Ar^{35}Cl^{+}$ at m/z 75 due to a high content of chloride in the urine has been observed [11–13]. In this case, high dilution of the urine with pure water might be necessary in order to solve this problem [13].

In this paper, we applied IC as a separation device, and inorganic and organic arsenic compounds were separated by an anion-exchange mode. The IC eluate was directly introduced into the ICP-MS system, and the arsenic compounds were detected. The separation parameters were optimized for the five arsenic compounds. The combination of IC and ICP-MS was applied to the determination of the five arsenic compounds in the urine from DMAs-exposed rat.

2. Experimental

2.1. ICP-MS

The ICP-MS instrument used in this experiment was Model PMS 2000 from Yokogawa Analytical Systems (Tokyo, Japan) and operational conditions are described in Table 1. A Scott-type spray chamber, maintained at 0°C by means of Peltier type thermoelectric module, Fassel type torch (Fujiwara Seisakusyo, Tokyo, Japan) and concentric glass nebulizer (Precision Glassblowing, CO, USA) were used in the experiment. For data acquisition of IC–ICP-MS, the selected ion monitoring (SIM) mode was used. For tuning of ICP-MS, 0.01 mg/l of yttrium (Y) solution was analyzed. The system was tuned to get maximum signal for Y by monitoring m/z 89 and changing a bias of lenses.

Table 1
ICP-MS operational conditions

Instrument	PMS 2000
Radio frequency forward power	1.3 kW
Radio frequency reflected power	< 5 W
Plasma gas flow	Ar 18 l/min
Auxiliary gas flow	Ar 1.0 l/min
Carrier gas flow	Ar 0.88 l/min
Sampling depth	5 mm from load coil
Monitoring mass	m/z 75
Dwell time	0.5 s
Times of scan	1 time

2.2. Ion chromatography

The ion chromatograph used in this experiment was Model IC 7000 from Yokogawa Analytical Systems. As to the separation column, Excelpak ICS-A35 (Yokogawa Analytical Systems) was chosen. The ICS-A35 column is 150 mm × 4.6 mm I.D., packed with polymer-based hydrophilic anion-exchange resin (a diameter of 10 μm) with 0.15 mequiv./g dry. Unless otherwise mentioned, the ion chromatograph was operated under the following conditions: mobile phase flow-rate 1.0 ml/min and injection volume 20 μl. A 800 mm × 0.3 mm I.D. poly(ethylenetetrafluoroethylene) (ETFE) tube was used for connection between the column and the nebulizer of ICP-MS. The IC–ICP-MS system is schematically illustrated in Fig. 1.

2.3. Reagents

Arsenic compounds used during this experiment are listed in Table 2. Trimethylarsine oxide (TMAsO) was obtained by oxidation of trimethylarsine (TMAs) with 30% hydrogen peroxide. Pure water was obtained from Milli-Q/SP system (Nihon Millipore, Tokyo, Japan). Stock solutions (100 mg/l) of each arsenic compound were prepared by dissolving each reagent with

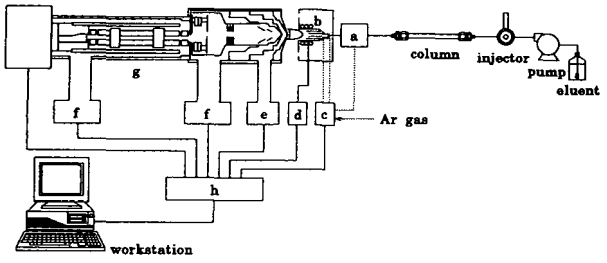

Fig. 1. Schematic flow diagram of IC–ICP-MS system. a = Nebulizer/spray chamber; b = ICP torch; c = gas controller; d = radio frequency power; e = rotary pump; f = oil diffusion pump; g = quadrupole mass filter; h = system controller.

pure water and stored in a refrigerator. Analytical solutions were prepared by diluting the stock solutions to the adequate arsenic compound concentration. Analytical-reagent grade of tartaric acid, 25% ammonium hydroxide and 30% hydrogen peroxide were purchased from Wako (Osaka, Japan).

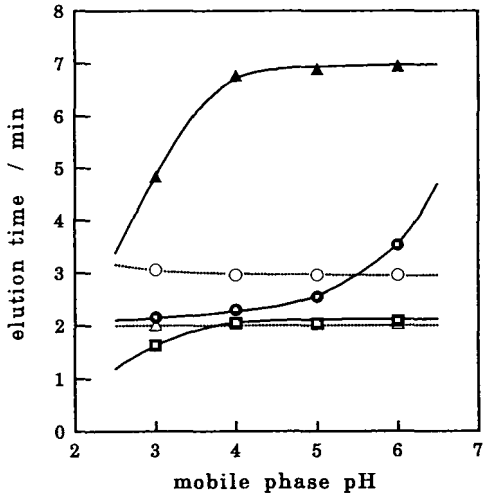

Fig. 2. Dependence of the elution time on the mobile phase pH for five arsenic compounds. Column, Excelpak ICS-A35; mobile phase, $1 \cdot 10^{-3}$ *M* tartaric acid, pH adjusted by 30% ammonium hydroxide; flow-rate, 1.0 ml/min; column temperature, 40°C. Sample (injection volume 20 μl): ▲ = MMAs; ● = DMAs; ■ = TMAsO; △ = AsBe; ○ = As^{III}.

3. Results and discussion

3.1. Separation of arsenic compounds

First, the effect of mobile phase pH was examined. Fig. 2 shows the relationship between the retention time of five arsenic compounds and the mobile phase pH on Excelpak ICS-A35. The retention time of MMAs, DMAs and TMAsO was increased as the mobile phase pH increased. On the other hand, the retention time of As^{III} and AsBe was not changed as the mobile phase pH increased. That means that As^{III} and AsBe do not fully exchange to the stationary phase, because As^{III} (p*K*a 8.78) does almost not ionize and AsBe is a cationic compound in this pH range. As^{III} does not seem to be retained by ion-exchange interaction with ion-exchange groups, but is retained by hydrophilic interaction with hydrophilic groups on packing materials. At pH ≥ 4.0, TMAsO was not separated from AsBe. Lower pH demonstrated the best separation for the five arsenic compounds.

Second, the effect of the mobile phase concentration was examined at a fixed mobile phase pH of 3. The concentration of tartaric acid as the mobile phase was varied from $1 \cdot 10^{-3}$ to $5 \cdot 10^{-3}$ *M*. The retention time of MMAs was rapidly decreased as the mobile phase concentration

Table 2
Arsenic compounds

Compounds	Manufacturer
Arsenous acid (As^{III}) monosodium salt	Wako, Osaka, Japan
Arsenic acid (As^{V}) disodium salt	Wako
Monomethylarsonic acid (MMAs)	Tri Chemical Lab., Kanagawa, Japan
Dimethylarsinic acid (DMAs)	Sigma, St. Louis, MO, USA
Trimethylarsine (TMAs)	Strem Chemicals, Newburyport, MA, USA
Arsenobetaine (AsBe)	Tri Chemical Lab.

increased. The separation between DMAs and AsBe was not improved by changing the mobile phase concentration. These operational conditions were not suitable for this study because of lack of separation capability. Therefore, the ICS-A35 column was combined with another ICS-A35 column to increase the number of theoretical plates.

Fig. 3 shows the relationship between the retention time of five arsenic compounds and the mobile phase concentration on two ICS-A35 columns. The retention times of arsenic compounds were hardly affected by the mobile phase concentration except for the retention time of MMAs and As^{III}. However, the retention time of MMAs rapidly decreased and the retention time of As^{III} increased as the mobile phase concentration increased. The order of their retention was changed at $4.5 \cdot 10^{-3}$ *M* tartaric acid. On the other hand, the retention time of AsBe was slightly decreased and the separation between AsBe and DMAs was improved.

Next, the effect of column temperature was examined. The column temperature hardly affected the retention time of arsenic compounds. However, a higher column temperature improved the resolution and the peak shape of the arsenic compounds.

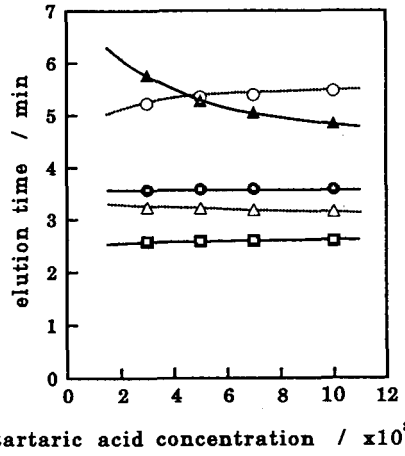

Fig. 3. Dependence of the elution time on the mobile phase concentration for five arsenic compounds. Column, two Excelpak ICS-A35 columns; mobile phase pH, 3.5; flow-rate, 1.0 ml/min; column temperature, 50°C. Sample and injection volume as in Fig 2.

Table 3
Optimized IC operational conditions

Instrument	IC7000
Column	Two Excelpak ICS-A35 columns (150 mm × 4.6 mm I.D. each)
Mobile phase	$10 \cdot 10^{-3}$ *M* tartaric acid
Flow-rate	1.0 ml/min
Column temperature	50°C
Detection	ICP-MS
Monitoring mass	*m/z* 75
Injection volume	20 μl

The optimized IC operational conditions based on these results are described in Table 3. A chromatogram of the five standard arsenic compounds is shown in Fig. 4. The concentration of the five arsenic compounds were 1 mg/l each as As. Arsenate (As^{V}) was not added to the sample solution. The five arsenic compounds and arsenate were completely separated within 15 min.

3.2. Detection limit and reproducibility

The detection limits and reproducibility of the IC–ICP-MS method were determined for the five arsenic compounds. Table 4 gives the detection limits and the reproducibility for the five arsenic compounds calculated from 1.0 mg/l standard solution by injecting a 20-μl sample. The detection limits were calculated from 10 times the square root of blank signal. The reproducibility for 0.1 mg/l standard arsenic compound was obtained from three replicates of the peak area.

Since the temperature of plasma is very high (over 6000 K), arsenic compounds are decomposed and turned into As, O, H and C ions. That means that the sensitivity of arsenic compounds as As does not depend upon the structure of arsenic compounds. When the concentrations of arsenic compounds as As are the same, each compound has to give the same sensitivity at *m/z* 75, giving the same area on the chromatogram. Good agreement was obtained for TMAsO, AsBe and DMAs, but MMAs and As^{III} were smaller than expected. When a standard solution of each arsenic compounds, *i.e.* TMAsO, AsBe and DMAs was injected, each

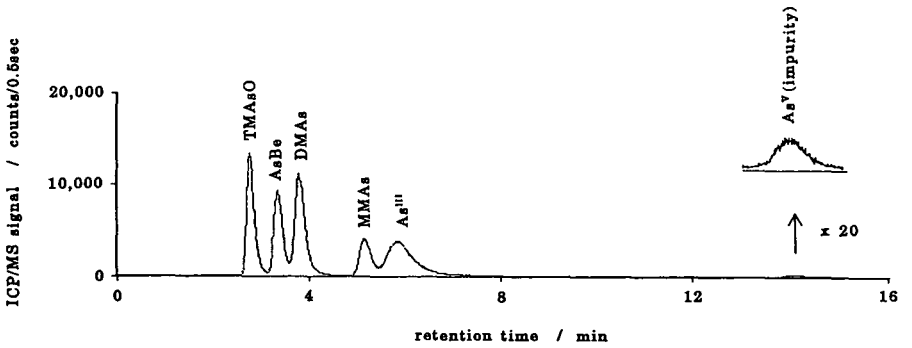

Fig. 4. Chromatograms of five standard arsenic compounds. Conditions as in Tables 2 and 3. Sample concentration: 1 mg/l each.

arsenic species gave almost the same peak area. But when these standard solutions were mixed, TMAsO gave a relatively larger peak area and AsBe a relatively smaller peak area. We assume that AsBe was decomposed in the mixed standard solution, and turned into TMAsO. In the case of MMAs, lack of purity seems to be a main reason. As^{III} was ultimately oxidized to AsV by oxygen in the solution.

3.3. Interference of chloride

In ICP-MS, interference of the polyatomic ion $^{40}Ar^{35}Cl^{+}$ at m/z 75 due to high chloride content in the sample solution has been observed [11–13]. The ArCl ion is formed by combination of chloride in sample solution with argon as the plasma gas. In order to decrease the ArCl ion, addition of a few percent nitrogen to the plasma gas has been employed [14]. However, formation of the ArCl ion cannot be completely depressed by plasma gas control on ICP such as diluting with a few percent of nitrogen. To solve the interference of ArCl, chloride in the sample solution should be removed or separated by some pretreatment before introducing into ICP-MS. Another approach was to separate the arsenic compounds from chloride in sample solution by using liquid chromatography [10,12,13,15,16]. However, the retention time of chloride was close to those of MMAs and TMAsO on an ODS column with ion-pair chromatography [10] and the chloride in urine affected the determination of several μg/l of arsenic compounds. So anion-exchange chromatography was used to separate the arsenic compounds from chloride in the sample solution. In order to check the ArCl ion interference at m/z 75, a 1000 mg/l chloride solution was analyzed under the same conditions. Under these conditions, ArCl ion was not detected and no peaks at m/z 35 and 37 were observed.

Table 4
Detection limits and reproducibility

Arsenic compounds	Detection limits (μg/l)	R.S.D. (%) ($n = 3$)
As^{III}	0.39	3.9
MMAs	0.44	4.9
DMAs	0.28	4.1
TMAsO	0.25	4.7
AsBe	0.22	3.2

3.4. Determination of arsenic compounds in rat urine

The IC–ICP-MS system was applied to the determination of arsenic compounds in urine of DMAs-exposed rats. The urine was obtained from rats which were given 50 and 100 mg DMAs/l in drinking water for 4 weeks. The urine was diluted 20 times by deionized water and 50 μl of the diluted urine were injected into the IC–ICP-MS system. Chromatograms of the diluted urine are shown in Fig. 5. As^{III}, MMAs, DMAs and TMAsO were detected in the urine of DMAs-exposed rat. Not all the DMAs seems to be directly eliminated with the urine; a part was metabolized to MMAs, TMAsO and As^{III}.

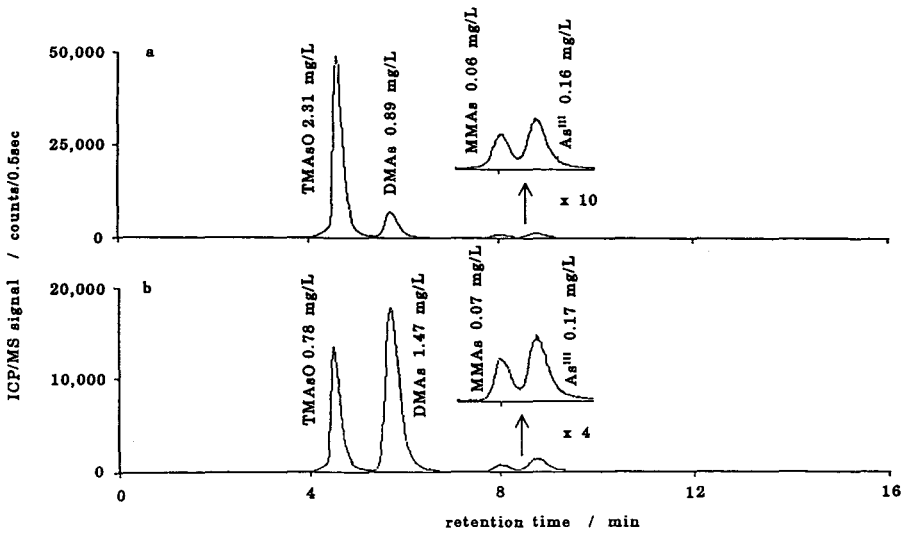

Fig. 5. Chromatograms of arsenic compounds in the urine of DMAs-exposed rats. Conditions as in Tables 2 and 3 except for the injection volume. Sample: (a) 50 mg/l DMAs and (b) 100 mg/l DMAs in drinking water. Injection volume: 50 μl each.

4. Conclusions

An analytical method for the speciation of arsenic compounds is presented. As^{III}, MMAs, DMAs, TMAsO and AsBe were completely separated within 10 min by the IC–ICP-MS method without any interference of ArCl. The detection limits of the five arsenic compounds were better than $4.5 \cdot 10^{-4}$ mg/l. As far as the reproducibility was concerned, the R.S.D. (n = 3) was better than 5%. The IC–ICP-MS system was a sensitive speciation method for arsenic compounds in the urine of DMAs-exposed rats. The IC–ICP-MS system not only demonstrated good detection limits, but also facilitated the sample preparation process. The IC–ICP-MS system will be useful for biological monitoring of arsenic compounds.

References

[1] *IARC Sci. Publ.*, 23 (1980) 39.
[2] M. Vahter, L. Friberg, B. Rahnster, A. Nygren and P. Nolinder, *Int. Arch. Occup. Environ. Health*, 57 (1986) 79.
[3] T. Murai, H. Iwata, T. Otoshi, G. Endo, S. Horiguchi and S. Fukushima, *Toxicology Lett.*, 66 (1993) 53.
[4] M. Morita, T. Uehiro and K. Fuwa, *Anal. Chem.*, 53 (1981) 1806.
[5] F. Brinckman, K. Jewett, W. Iverson, K. Irgolic, K. Ehrhardt and R. Stockton, *J. Chromatogr.*, 191 (1980) 31.
[6] J. Laurence, P. Michalik, G. Tam and H. Conacher, *J. Agric. Food Chem.*, 34 (1986) 315.
[7] J. Blais, G. Momplaisir and W. Marshall, *Anal. Chem.*, 62 (1990) 1161.
[8] J. Thompson and R. Houk, *Anal. Chem.*, 58 (1986) 2541.
[9] D. Beauchemin, M. Bendas, S. Berman, J. McLaren, K. Siu and R. Sturgeon, *Anal. Chem.*, 60 (1988) 2209.
[10] Y. Shibata and M. Morita, *Anal. Sci.*, 5 (1989) 107.
[11] M. Vaughan and G. Horlick, *Appl. Spectros.*, 40 (1986) 434.
[12] B.S. Sheppard, J.A. Caruso, D.T. Heitkemper and K.A. Wolnik, *Analyst*, 117 (1992) 971.
[13] B.S. Sheppard, W.-L. Shen, J.A. Caruso, D.T. Heitkemper and F.L. Fricke, *J. Anal. At. Spectrom.*, 5 (1990) 431.
[14] S. Branch, L. Ebdon, M. Ford, M. Foulkes and P. O'Neill, *J. Anal. At. Spectrom.*, 6 (1991) 151.
[15] Y. Shibata and M. Morita, *Anal. Chem.*, 61 (1989) 2116.
[16] E.H. Larsen, G. Pritzl and S.H. Hansen, *J. Anal. At. Spectrom.*, 8 (1993) 557.

ELSEVIER

Journal of Chromatography A, 675 (1994) 155–175

JOURNAL OF CHROMATOGRAPHY A

Multichannel chromatography and on-line spectra from a flame photometric detector

Brian Millier, Xun-Yun Sun[1], Walter A. Aue*

Department of Chemistry, Dalhousie University, Halifax, Nova Scotia B3H 4J3, Canada

(First received November 9th, 1993; revised manuscript received March 23rd, 1994)

Abstract

A rotating variable interference filter has been incorporated into a flame photometric detector to acquire and simultaneously display low-resolution spectra that are diagnostic for eluting peaks. In its present form this approach yields ten chromatograms (for ten different wavelength segments) that are stored in the computer for subsequent data manipulation such as baseline correction and curve smoothing; three-dimensional display; peak and noise diagnostics; and magnification, subtraction, or elemental correlation of chromatograms. A third, spectral dimension is thus added to the conventional two, chromatographic dimensions of retention time and analyte intensity. The three-dimensional performance is at present accompanied by an order-of-magnitude loss in detection limit and linear range. Typical one-segment (*i.e.* 5% dwell time) elemental detectabilities, at $S/N_{p\text{-}p} = 2$, are $7 \cdot 10^{-13}$ g P/s (via HPO*), $3 \cdot 10^{-11}$ g S/s (S_2^*), $7 \cdot 10^{-12}$ g Ge/s (GeH*) and $4 \cdot 10^{-12}$ g Ru/s.

1. Introduction

As texts on instrumental analysis are fond of pointing out, chromatography and spectroscopy are complements, not competitors, by nature. Chromatography separates but rarely identifies compounds; spectroscopy performs the opposite role. Significant analytical advances can therefore result if the two techniques are properly joined.

But analytical advances can result not only from two instruments symbiotically joined, they can also result from one instrument parasitically enriched (as in this study). It is not surprising, then, that practitioners of either chromatography or spectroscopy should have sought to lend their favourite technique certain features that, in effect, imported or imitated the strength of the other. This may have involved the improvement of dispersion and/or the addition of a further physical or chemical dimension. Instruments offering several dimensions (sectors, channels, columns, etc.) have indeed become commonplace.

Nor is the advantage of multidimensional operation restricted to chromatography and spectroscopy. Other types of reactive and unreactive flow systems on one hand, and sensing systems based on mass, radiation, electron exchange, etc., on the other, have similarly benefitted. As a consequence, the fundamental and technical resources on which this study is able to draw are far too general and numerous to list in any detail. Suffice it to state that both concept

* Corresponding author.

[1] Present address: Environmental Trace Substances Centre, Room 207, University of Missouri–Columbia, Sinclair Road, Columbia, MO, USA.

0021-9673/94/$07.00
SSDI 0021-9673(94)00294-J

and execution of this specific project rely on ample and, we hope, obvious precedents.

Our specific project was to obtain spectra from analytes as they pass through the flame photometric detector (FPD) [1–4]. This well-known detector monitors luminescence, but it does not measure its spectral distribution during analysis. Yet, with some twenty elements now known to respond in the FPD —and further ones likely to follow suit— instantaneous acquisition of spectra from eluting peaks could be of significant value: for the injection of one-shot-only samples, for compound confirmation or identification, for selective multi-element determination, and so forth. The potential merit of adding spectral information to the response of the FPD increased vastly when this detector expanded its purview from volatiles to non-volatiles, *i.e.* from gas chromatography to liquid chromatography, supercritical fluid chromatography and capillary electrophoresis (as well as to various non-chromatographic monitoring techniques).

We did not want to join a typical *spectrometer* to the gas chromatograph; this has been done before in various ways and with varying degrees of success. Rather, we wanted to take the simplistic approach of modifying the FPD so that it could procure spectra on the side and on the fly.

Procuring spectra on the fly is, however, quite difficult. The difficulty lies in the very low intensity and the short duration of the luminescent episodes that constitute the peaks of a chromatogram. The FPD differs strongly in this regard from systems that radiate more intensely (where, for instance, multisensor arrays may be used); or from systems that can be arrested in time (where, for instance, an analyte peak trapped in the detector cuvette may be repeatedly scanned to determine its absorption or fluorescence spectrum).

Under analytically relevant conditions, then, weak spectra in the FPD are difficult to obtain even from continuous analyte inputs. Gleaning them from peaks that stay in the detector for only a few seconds raises that level of difficulty by orders of magnitude.

Furthermore, if spectral information is to facilitate such analytical tasks as the assessment of peak purity, the correction of background radiation, and the correlation of wavelength-dependent chromatograms, the spectra have to be acquired at a rate that is much faster than the peak's passage through the detector. Roughly but typically, 10-s chromatographic peaks thus require 1/10-s spectral scans. It would appear that the simplest, least expensive, and (in terms of light throughput) most efficient means of procuring spectral information should be a rotating variable interference filter.

If such a filter is used to monitor response at different wavelength ranges every tenth of a second, the filter wheel must revolve at 600 rpm. How many samples should reasonably be taken during one of its revolutions —*i.e.* how broad should be the discretely monitored wavelength regions— depends on the bandpass of the filter, the width of the beam, and the ability of the monitoring system to accommodate the data influx. Not only does the monitoring system —a photomultiplier tube (PMT) with high-speed amplifier and dedicated computer— have to record the data, but it also has to prepare them for simultaneous appearance on the screen.

The screen should display the immediate spectrum together with the developing chromatogram, and both need to be smoothed for convenient viewing. Beyond the acquisition phase discussed in this report, the algorithms must also be capable of handling a wide variety of chromatographic and spectral manipulations of the stored raw data, such as integration, subtraction, correlation, normalization, baseline correction, digital smoothing, three-dimensional display, spectral comparison, noise analysis, etc.

Given these demands, it seems reasonable to limit each file at the outset to about half an hour of chromatographic acquisition time, and to restrict the number of spectral segments to ten (a combination that already comprises about $2 \cdot 10^5$ raw data points). The optical bandpass of the variable filter wheel (17 nm maximum between 400 and 700 nm) would easily support a higher number of spectral segments, but ten channels are considered adequate for a first try. If successful, that try should allow a more knowledgeable,

hence more refined choice of time and wavelength parameters in subsequent designs. Besides, the measure of success at this stage is not how close the new spectral information comes to the performance of a conventional spectrometer, but how much it adds to the capabilities of the FPD. Spectra, *per se*, are not the objective; the analytical information that can be obtained from them, is.

This project, coming as it does from an academic realm of characteristically limited means, became feasible only through recent developments in the hardware and software capabilities of personal computers (PCs). In this context we intend, by choice as well as by necessity, to keep the price tag of additional components significantly below the price of a simple, single-channel FPD.

Equally commensurate with academic means is the decision to design and build the acquisition system in a series of *modular* components, so that these could be used individually for other layouts, assemblies and purposes. As one illustrative example of this strategy, the rotating filter wheel and the high-speed signal acquisition assembly could be used to transmit data not only to a computer but also to a digital storage oscilloscope. This oscilloscope could sum and read the data —from passing peaks if need be but more importantly and typically from a *continuous* input such as a stream of analyte, a background emission, a non-chromatographic sensor signal or, for that matter, any long-term luminescence phenomenon— with (close to) the best resolution of which the variable interference filter is capable.

Given the low *absolute* light intensity of the chemiluminescence, the inherent optical limitations of the interference filter, the longer distance and hence the narrower direct-light transmission cone from the flame to the PMT (a cone that is, furthermore, severely restricted by the mandatory filter aperture), it seems that some use of inexpensive optical devices is required to boost the light throughput and bring it closer to that of a conventional FPD channel.

Mirrors [1,5] and lenses [5,6] have been used in some FPDs, although most modern models favour direct observation of the flame (and that for good reason). The inclusion of optical elements is of little help, sensitivity-wise (*cf.* ref. 7), if the noise is mainly due to flame flicker or chromatographic fluctuations.

In our case it is not. However, the merit or demerit of adding a mirror and/or a lens is still not as easy to predict as it would be for a more conventional type of spectroscopy. One of the reasons for that is the shape of the FPD flame or, more to the point, the space the various luminescences occupy. That space depends not only on the obvious conditions of flow-rates and burner dimensions, but also on the nature of the analyte element, on the various emitters from that element (if there are more than one), and, quite disturbingly, on the amount of analyte —not to mention the nature and amount of various co-elutants and contaminants.

The luminescences associated with chromatographic peaks are unique and fascinating spectacles to watch: the variation of their colours and shapes seems infinite. The luminescent space can vary from lanceolate to ovoid, to prolate and oblate spheroid, and even to spherical and cylindrical (the latter, for instance, in the case of a surface luminescence on the quartz chimney); it can also fill *all* of the accessible FPD interior. The volume of the luminescent space can thus change from a few to a few thousand mm^3 (under the same flow conditions!). For instance, the blue luminescence of sulphur can sometimes be observed to appear —vague, weak, and seemingly out of nowhere— in the whole detector volume (peak start); then become stronger and contract into a brilliantly blue flame at the detector jet tip (peak apex); then again weaken in intensity, diffuse all over the detector volume, and slowly fade out (peak end). The theoretical explanation for this phenomenon is straightforward, given the second-order kinetics of the blue S_2 bands, but its enhanced detection via mirrors or lenses is not. The second-order kinetics of sulphur may be regarded a special effect, but first-order emitters, too, can be surprisingly varied in the size and shape, layers and colours of their luminescences. This distinguishes the FPD from the usually much larger, high-energy

flames and plasmas of atomic emission spectroscopy, whose visible shape is changed but little by the presence of analyte.

Thus, the old spectroscopic motto: "project the image of the flame onto the aperture" may be difficult to follow in the case of the FPD. The best one can hope for is to collect a reasonably large portion of light from the polymorphous luminescences and pass most of that light, in as concentrated a beam as possible, through the filter and on to the PMT. The desideratum here is not projection but power, not image but intensity.

2. Experimental

The circular variable interference filter was (initially) positioned between the cooling coils and the PMT of the same Shimadzu FPD we had been using for the last two decades (a Shimadzu GC-4BMPF). The circular filter rotates in a light-tight casing with 1-in. (1 in. = 2.54 cm) diameter entrance and exit ports. The PMT output is processed by (1) a separate high-speed, high-gain amplifier assembly, and then forwarded to (2) the data acquisition circuitry located inside (3) the computer. These three discrete units, as well as some simple optical devices for adjusting the light beam, will be described anon.

First, however, we need to mention the rationale behind the division of circuitry elements into three discrete units. To minimize noise, the high-speed PMT amplifier is given its own shielded enclosure and dedicated power supply. The only other circuit in the amplifier assembly is a minor one, providing power to the optical switch. This unit, which is located in the filter wheel assembly, provides a synchronization signal. The filter wheel assembly includes an integral speed control circuit to stabilize the rotational speed of the wheel. When set up in this fashion, these two units could be interfaced to, for instance, the earlier mentioned digital storage oscilloscope for better spectral resolution. Here, though, they are connected to a custom-built data-acquisition board that, by virtue of residing directly on the PC's ISA bus, allows fast data collection.

2.1. Filter wheel assembly

The filter wheel (item 57496; Oriel Corporation, 250 Long Beach Boulevard, Stratford, CT 06497, USA) is a 4-in. diameter disk with a semicircular variable interference filter section that, over 172° at a dispersion of 1.75 nm/degree, covers the 400–700 nm wavelength range with a 17-nm maximum bandpass and a 15% minimum transmission (according to Oriel specifications). The 180° opaque section acts to balance the wheel for spinning. A filter unit encompassing the full 360° would have been more desirable in terms of higher resolution and proportionately longer light collection, but such a filter is not available "off-the-shelf" to the best of our knowledge.

The filter housing uses two matching square pieces of aluminum stock, machined out to accommodate the filter wheel inside. The wheel rotates past the 1-in. diameter input and output (PMT) ports, both of which are partially covered by two, roughly vertical strips of black tape that run parallel to the filter radius (*i.e.* along isochromes) and form the desired aperture between them. The wheel is mounted on a 1/4-in. shaft held by a double-bearing assembly, and is turned by a small d.c. motor (with integral tachometer) via two pulleys and a flat belt. The ratio of the motor pulley to the filter pulley is 0.263, *i.e.* a motor speed of 2281 rpm produces the desired filter speed of 10 revolutions/s.

The rotational filter speed is very stable, owing to the motor and speed control board taken from an old Tandon 5-1/4 floppy disk drive assembly. (This type of assembly was used in the extremely popular IBM PC and is now available for next to nothing through many outlets.) The stability of rotation is based on the combination of the tachometer (built into the motor) and the pulse-width-modulated feedback controller. The 12 V d.c. needed to drive the motor/controller are provided by a dedicated 12 V, 1.5 A power supply.

A small optical switch assembly is positioned

opposite, *i.e.* 180° from, the light beam. When the filter wheel rotates to a position that allows light to pass from the inlet port to the PMT port, the optical switch finds its light path blocked, resulting in the change of signal state needed to trigger data acquisition. The trigger pulse occurs at the transparent-to-opaque transition, *i.e.* when, on the opposite side, the 400 nm edge of the variable filter just passes the centre of the inlet/PMT ports. This means —given equal time slices for observing each wavelength region— that the first segment will collect only about half the light that would be needed for a quantitative comparison of its intensity with that of subsequent segments. This boundary distortion (which owes its existence to an initial design flaw) could be corrected in either software or hardware, particularly if the spectral profiles of various emitters need to be retained in the form familiar to most analysts.

2.2. High-speed, high-gain PMT pre-amplifier assembly

Fig. 1 describes the pre-amplifier assembly. An OP-07 operational amplifier is used for current-to-voltage amplification. The gain at this stage is 10^8 V/A. Bucking current is introduced through a 1000-MΩ resistor to the input of this amplifier. A 10-turn potentiometer adjusts the bucking current to accommodate various possible PMTs and the range of voltages used to drive them.

A second stage of amplification provides a further gain of 10 as well as a polarity inversion: the latter results in the negative output signal the data acquisition assembly expects.

A built-in power supply serves both the pre-amplifier and the optical switch in the filter wheel assembly. Also, a single resistor is used as a load for the phototransistor in the optical switch. As mentioned earlier, the circuit is designed to allow the filter wheel and the pre-amplifier to operate independently of the data acquisition assembly. This permits the instrumentation to be used for other purposes, *e.g.* for feeding purely spectral data of higher resolution to a suitable collection and readout system.

2.3. Data acquisition assembly

This functional block is custom-designed owing to the somewhat unusual requirements of the rotating filter wheel. Some of these requirements are:

(1) The unit has to be able to synchronize its data collection with a single trigger pulse per revolution of the wheel.

(2) The digitization of the PMT signal has to comprise (in time) essentially all of the particular filter segment that is being monitored by the PMT tube. This appears necessary because the light capable of reaching the PMT through the 1-in. diameter beam containment, the focussing lens, the aperture(s), and the variable interference filter is already very low; and it is further reduced by a factor of 20 for each segment (in the case of a 10-segment acquisition from a filter wheel that is 50% opaque). A gated integrator is used in that function, followed by a fast 12-bit analog-to-digital converter.

(3) The unit has to accommodate a wide dynamic range of signals; hence offers a computer-controlled gain circuit.

Fig. 2 shows the data acquisition assembly, which is based on a JDR Microdevices PR-2 prototype board. This is an 8-bit PC board with all buffering and decoding circuitry already present, including the well-designed power and ground planes necessary for proper analog operation. The 8-bit board was chosen because most of the peripheral integrated circuits (ICs) are 8-bit devices.

The timing circuitry will be discussed first. Its heart is an 8253-5 programmable interval timer, U9. This IC contains three 16-bit counter/timers, all of which are clocked by a 1.0-MHz quartz module, U1. Timer 1 is turned on by the synchronisation signal from the filter wheel (after conditioning by Q1 and U5:A, an inverter). The output of timer 1 consists of ten 1.0-μs pulses, one for each segment. The actual number of pulses can be changed in software: *ten* segments happens to be the initial, arbitrary choice of this study. The ten pulses then (a) set the flip-flop U8:A and generate an interrupt to the PC, and (b) trigger (through gate U5:D and inverter

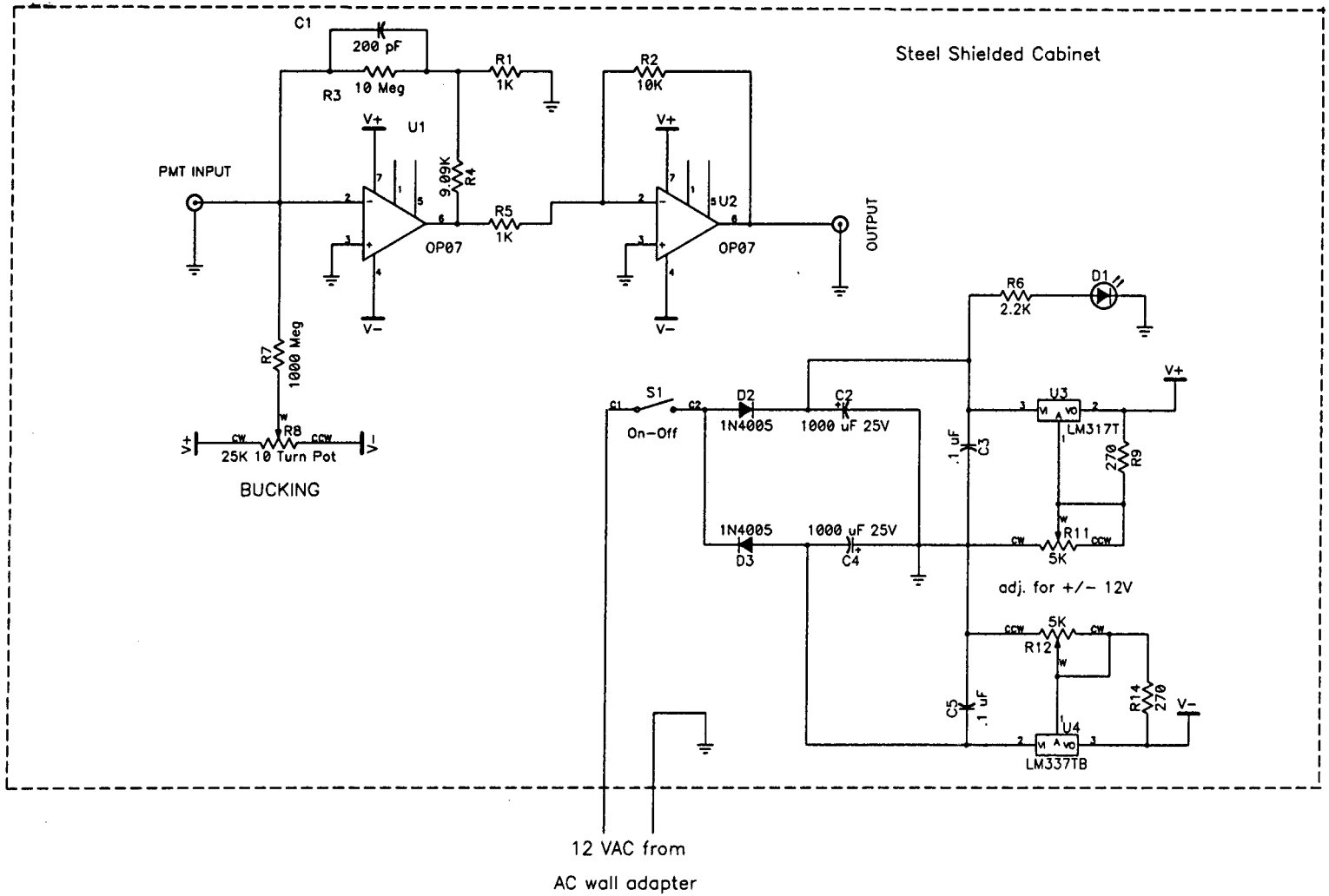

Fig. 1. Amplifier assembly. K = kΩ; Meg = MΩ. AC voltage is supplied to 10 Turn Potentiometer

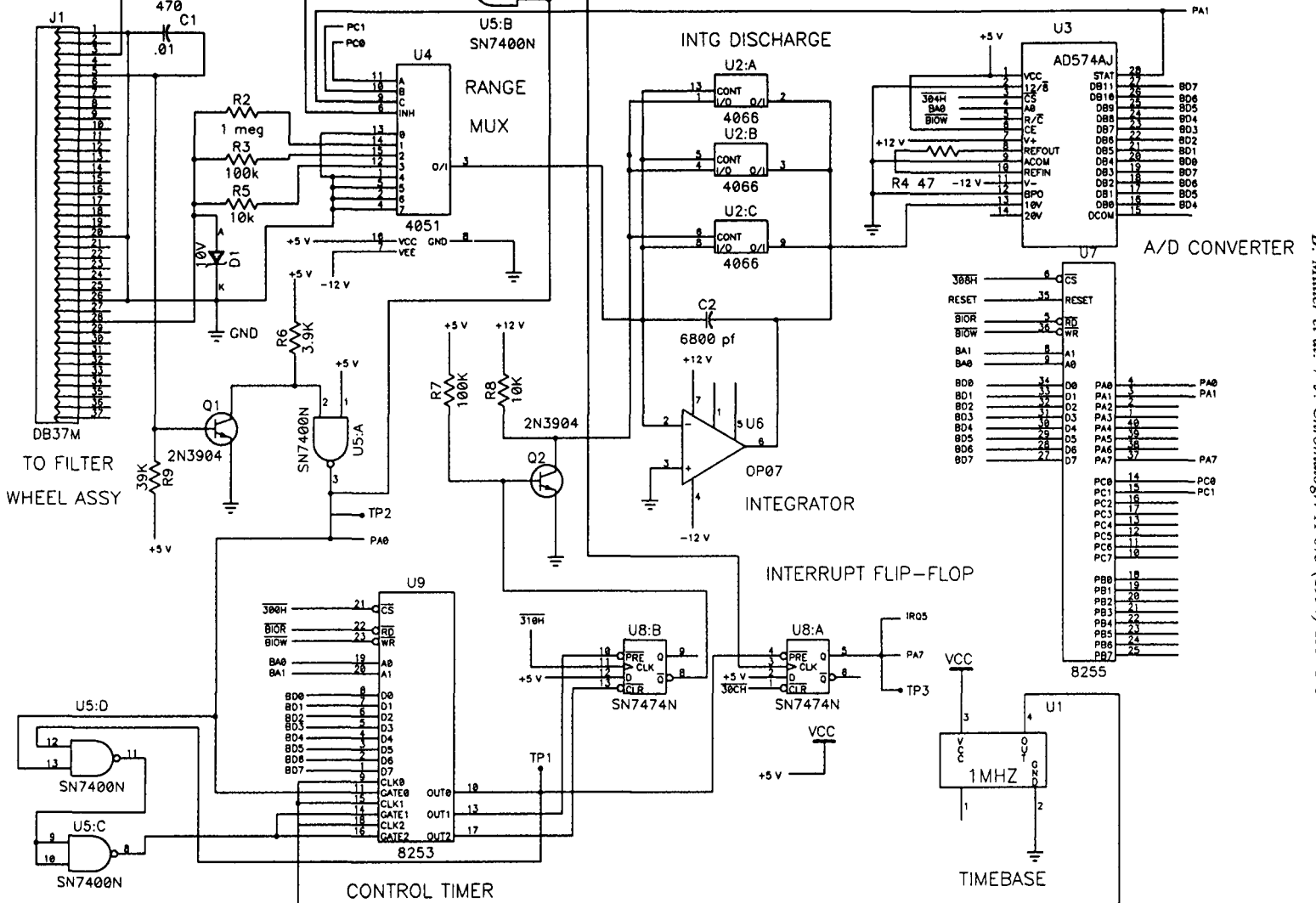
J1
DB37M
TO FILTER
WHEEL ASSY
470
C1
.01
R2
1 meg
R3
100k
R5
10k
D1
GND
R6
3.9K
Q1
2N3904
39K
R9
U4
4051
RANGE
MUX
U5:B
SN7400N
PC1
PC0
+5 V
-12 V
VCC
VEE
GND
SN7400N
U5:A
TP2
PA0
R7
100K
R8
10K
2N3904
Q2
U2:A
U2:B
U2:C
4066
INTG DISCHARGE
C2
6800 pf
OP07
U6
INTEGRATOR
U3
AD574AJ
R4 47
-12 V
A/D CONVERTER
PA1
U7
8255
PA0
PA1
PA7
PC0
PC1
U9
8253
CONTROL TIMER
U5:D
U5:C
SN7400N
U8:B
U8:A
SN7474N
INTERRUPT FLIP-FLOP
IRQ5
PA7
TP3
TP1
VCC
U1
1MHZ
TIMEBASE

U5:C) timers 2 and 3, which are configured as programmable monostables. Each of the timers uses a different delay time, the net result being that the flip-flop U8:B will discharge the integrating capacitor for a fixed time after U3, the analog-to-digital converter (ADC), has completed its job. The actual command to perform the conversion is provided by a "write" to the ADC, initiated by code in the interrupt service routine, and triggered when U8:A asserts the IRQ5 line to the PC.

The signal path will be discussed next. The low-level current from the PMT is amplified externally by the high-speed pre-amplifier assembly and enters the data acquisition board as a signal of negative polarity. A zener diode, D1, limits this signal to a range of +0.6 to −10 V. An analog multiplexer IC, U4, is used in conjunction with three resistors, R2, R3 and R5, to select three sensitivity ranges with decade spacing. With the chosen integration time of 5 ms (less capacitor discharge time) and an integration capacitor of 6800 pF, the 10-V full-scale ADC input is reached with input voltages of 13.6, 1.36 and 0.136 V. The actual integrator comprises the OP-07 operational amplifier, U6, and the 6800 pF capacitor. A quad bilateral CMOS switch, U2, is used to discharge the capacitor. Since U2 operates from a +12 V supply, Q2 is needed as a level shifter to provide enough voltage for control of U2.

The output of the integrator feeds directly the +10 V input of the AD574AJ ADC. The busy-status output of the ADC is monitored via input port A of U7, an 8255 parallel peripheral interface (PPI) IC. While the ADC is performing the conversion, the status output is high: this signal is fed to an address input of U4, the input multiplexer, which in turn feeds a zero volt signal to the integrator to keep it constant during A/D conversion. As well, U5:B feeds the inhibit input of the multiplexer with the result that the integrator is disconnected from any signal while the opaque half of the filter wheel intercepts the light beam.

Two bits of output port C (U7), namely PC0 and PC1, are used to set the multiplexer address, thereby setting the integrator gain in three decade-related steps.

2.4. Software

The software operates in two discrete sections for (1) the acquisition stage and (2) the manipulation and documentation stage. This division of labour is not arbitrary but owes its existence —primarily though not exclusively— to the different technical demands placed upon hardware and software by two disparate operational stages.

Above all: during the acquisition stage the computer must collect the data coming from the filter wheel quickly and reliably. This task requires an interrupt service routine. The routine must have a very short latency time (the maximum time the data acquisition hardware has to wait before the host computer "services" it). It must also have a high priority so that it is never disabled or "masked out" for any length of time. For this reason we use a compiled QuickBasic program in conjunction with an assembly language interrupt service routine driver, running under DOS-5 or -6. (Our attempts to write software running under Microsoft Windows 3.1 were unsuccessful: Windows is a non-preemptive multitasking system —resulting, occasionally, in an interrupt latency time too long for this application, and thereby causing the loss of data and synchronization with the filter wheel.)

No such time constraints exist in the manipulation/documentation section of the software. The many advantages of the Microsoft Windows environment clearly favour it for this application. We chose to use the Visual Basic language, running under Windows. Some of its advantages are: (1) access to a multi-window graphic user interface (GUI), (2) support for different printers/plotters providing hardcopy output and (3) support for numerous large arrays that are limited only by (in our case) 8 megabytes of installed memory.

Data are transferred from the acquisition program to the manipulation/documentation program using files. Owing to QuickBasic's binary file size limitations, a single run (ten parallel chromatograms) is saved as ten separate segment files all sharing the same primary filename. This name is also used for an appended file containing the operator's "yellow notepad" (which actually

appears on the screen in bright yellow colour, demanding that experimental conditions be properly recorded).

2.5. Computer

The acquisition and manipulation software makes use of the following hardware: (1) an Intel 486-class central processing unit (CPU) running at 33 MHz with 8 megabytes of memory, (2) a video local bus (VLB) VGA Video card to speed up the graphics display (about four times), (3) a 120 megabyte (15 ms access time) hard disk drive that, with the DOS-6 disk-doubling software, provides about 230 megabytes of disk space for the large files, and (4) a "15-in." NEC VGA monitor that displays the graphics in colour and with adequate resolution. (Item 1 is required for acquisition, while items 2 through 4 are used primarily for ease of operation.)

2.6. Data smoothing

Data smoothing is available either from an unweighted moving-average called "AVG" (an extremely simple but still highly effective filter that requests the operator's definition of the number of surrounding signals to be considered for each data point, and that is offered both for the acquisition screen and the full manipulation stage); or through a Hamming-window type "FIR" (finite impulse response) low-pass digital filter with fully variable cut-off (that, because of its longer processing time and —for our particular chromatograms— only marginally better performance, is supplied at the manipulation stage only). The FIR digital filter gives the operator the choice of a cut-off frequency and the choice of 32, 64 or 128 taps for different filter "orders". Of the three, the 128-tap filter provides the sharpest cut-off, of course, but it also requires the longest processing time: about 40 s for one typical segment, *i.e.* for one fixed-wavelength chromatogram of *ca.* 20 min duration. In the manipulation mode, the moving-average-filtered chromatogram can be saved for later treatment. In the acquisition mode, however, it is abandoned as the screen image fades and only the *raw* data are stored in the computer's memory (a process that differs from the behaviour of some chromatographic integrating systems or, for that matter, from the behaviour of the human brain).

For sensitivity comparisons, data are smoothed by two conventional treatments: the FIR digital filter as described above, or an analog ("RC") filter. The latter, used here between Shimadzu electrometer and recorder, is a conventional, simple three-pole filter, that offers a series of time constants in the 0.1–10-s range (Fig. 3). Both filters are set such that only a small (less than 10%) reduction in peak height occurs.

2.7. Optical layout

As discussed in the Introduction, maximizing light throughput and minimizing the spread of the beam at the plane of the variable filter is an act of necessity. It is also a matter of compromise for different detector conditions and analytes, at least if inexpensive optical elements are to be used in essentially fixed positions. Fig. 4 shows a schematic of the simple layout that is being used in this study.

To facilitate the use of inexpensive optical components, the FPD flame is raised to the centre of the *ca.* 1-in. diameter cylindrical light path. To improve light transfer through the tunnels, ports and apertures, a first-surface mirror ($f = 10$ mm, 25 mm diameter, item 43 464; Edmund Scientific, 101 E. Gloucester Pike, Barrington, NJ 08007-1380, USA) is held, and moved to the most advantageous position behind the flame, by a laterally adjustable piston. To narrow the effective optical bandpass, a double convex lens ($f = 25$ mm, 25 mm diameter, Edmund Scientific 32 490) is installed at about focal distance from the front side of the rotating filter. The head-on PMT is mounted close to the filter's back side in order to intercept most of the light beam. (Fig. 4 suggests that the PMT should be mounted closer still: this mount awaits the next progression of the wheel.)

Fig. 4, while to scale, is nevertheless approximate. The light rays (which are drawn here for viewer's convenience only) appear to originate from a point source rather than from a vaguely defined and often shapeshifting luminescence.

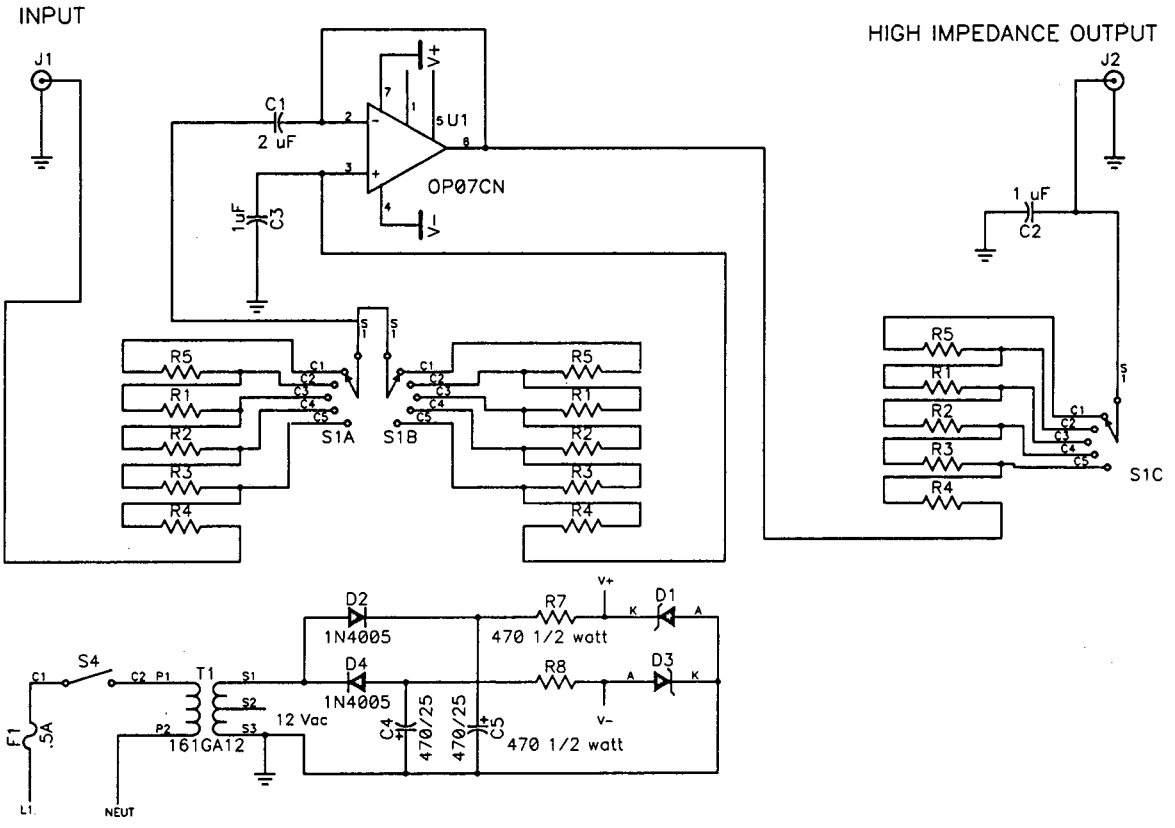

Fig. 3. Analog filter. R1 = 1.5 MΩ; R2 = 680 kΩ; R3 = 680 kΩ; R4 = 8.2 kΩ; R5 = 2.2 MΩ; C1 = 2 μF; C2 and C3 = 1 μF.

To make up for these vagaries, the back mirror can be moved back and forth —from the outside and under operating conditions— in order to optimize light throughput on an empirical basis for different elements and conditions.

2.8. Miscellaneous

The FPD's Hamamatsu R-374 PMT is driven by (typically) −700 to −900 V from a laboratory-built −70 to −1270 V power supply. Separations are carried out on a several-years-old 100 × 0.3 cm I.D. borosilicate column packed with 5% OV-101 on Chromosorb W, 100–120 mesh (150–125 μm) and operated with *ca.* 26 ml/min of nitrogen carrier gas. Injections of tetraethyllead are used as needed to reduce the background luminescence, particularly when the quartz chimney is installed.

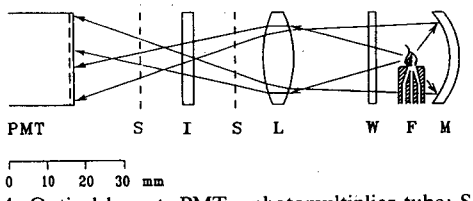

Fig. 4. Optical layout. PMT = photomultiplier tube; S = slit; I = interference filter; L = lens; W = window; F = flame; M = mirror.

In this study the detection limit is determined for a *single* segment. However, it can just as easily be determined for the "total" chromatogram (*i.e.* the sum of ten segments); or for any combination, subtraction or correlation chromatogram. The computer offers "DL" ("detection limit") routines for both amount and flow; these are based on either the root-mean-square calculation or the peak-to-peak measurement of the baseline noise, at the two common signal-to-noise (*S/N*) ratios of 3 and 2, respectively.

Thus, for the more lenient $S/RMS = 3$ definition,

$$DL = 3 \cdot \frac{RMS}{S} \cdot A \text{ (g or mol)}$$

or

$$DL = 3 \cdot \frac{RMS}{S} \cdot \frac{A}{w_{60.7}} \text{ (g/s or mol/s);}$$

and for the much stricter $S/N_{p\text{-}p} = 2$ definition,

$$DL = 2 \cdot \frac{N_{p\text{-}p}}{S} \cdot A \text{ (g or mol)}$$

or

$$DL = 2 \cdot \frac{N_{p\text{-}p}}{S} \cdot \frac{A}{w_{60.7}} \text{ (g/s or mol/s);}$$

where S is the signal (peak height), RMS is the root-mean-square noise of the baseline (equal for Gaussian noise to σ_b), A is the amount injected (in g or mol), $w_{60.7}$ is the width of the peak (in s) at 60.7% of its height (equal in a Gaussian peak to $2\sigma_p$) and $N_{p\text{-}p}$ is the peak-to-peak fluctuation of the baseline, with drift and spikes excluded.

3. Results and discussion

3.1. Data acquisition vs. data manipulation

This report deals with the primary process —data acquisition and simultaneous presentation— of what may be termed "time-multiplexed non-dispersive spectrometry" [8] of chromatographic effluents. As discussed, the secondary process (data manipulation) is both conceptually and physically separate, and will be touched in this report only as far as is necessary to characterize the performance of the "three-dimensional" (3-D) FPD and its data acquisition system.

There are several reasons why data acquisition and data manipulation are treated as two different processes. The main reason, at least for this study, is electronic and has been mentioned in the Experimental section: During a sample run —*i.e.* while the present computer is acquiring chromatographic-cum-spectral ("chromspec") data and, after smoothing, is displaying them as moving averages on the screen— it is fully occupied with that task.

But there are also reasons of a non-electronic nature for distinguishing between the acquisition process and the manipulation process (two processes as different in time and effort as catching a rabbit and cooking it). For instance, the physical separation of the two stages offers the operator the chance to attain the desired balance between time spent watching the chromatogram taking shape and being recorded on one computer, and the time spent scanning and perhaps manipulating separations that have been stored earlier on another computer. As it happens, different laboratories differ greatly in the fraction of time they allocate to these two distinct types of activity. Such time allocation depends on whether the particular brand of chromatography involves routine analysis, analytical development, or exploratory research; whether it runs automatically, requires occasional attention, or calls for human intervention in the separation process; and even whether it takes place in a civil-service, industrial or academic setting.

Yet another reason for separating the acquisition from the manipulation-cum-documentation functions is conceptual and concerns the potentially much wider use of the still developing methodologies. A rotating circular variable interference filter pretty well needs its own specialized acquisition algorithm. However, such a filter could also be used in various other types of luminescence monitoring. Furthermore, such a filter is only one of the many potential multichannel signal sources, including some non-optical and non-chromatographic ones, that could benefit from the diagnostic, preparative and descriptive capabilities of the growing manipulation software[a] (into which Windows-based adaptations of our earlier algorithmic efforts [9–11] might eventually be incorporated).

[a] Researchers interested in these programs for non-commercial purposes are invited to contact the first author for source codes and/or copies.

3.2. Operator controls

While the data acquisition functions are (and, given the fleeting nature of their task, must be) automatic, most of the data manipulation functions are interactive. The experienced operator, [whose recognition of chromatographic and spectral shapes (signal and noise patterns) is superior to that of the computer, and whose common sense and analytical motivation are essential for the task] is allowed wide latitude in measuring, correlating, manipulating, interpreting and reporting of data. The transitory acquisition functions must therefore safely commit to memory *the complete set of raw data* —although the simultaneous appearance of both the chosen-segment chromatogram and the prevailing spectrum uses simple moving averages to quiet an otherwise agitated screen. The operator is given the choice of the number of data points to be averaged (how wide to open the window) and will do so with the expected peak width and baseline noise in mind; the operator is also given the choice of the particular segment (which wavelength region to look at) and will do so in accordance with the nature of the sample and the purpose of the analysis.

It is also possible for the operator to specify, in either acquisition or manipulation mode, a weighting factor for each spectral segment. This routine can produce spectra that are roughly corrected for the response profile of the PMT and the transmission characteristics of the variable filter, as well as for possible border effects (*i.e.* effects relating to total light throughput, wavelength gradation and spectral cut-off) in the first and/or last spectral segment. Its formal attractiveness notwithstanding, the primary merit of this intensity-weighting routine is spectroscopic rather than chromatographic.

3.3. An alternative approach to data acquisition

Despite the success of the electronic approach taken in this study, we believe that the many advantages of the Visual Basic/Windows environment should not remain restricted to the (slow) manipulation program, but should be made available to the (fast) acquisition program as well. We assume that this could best be accomplished by using a microprocessor-based data acquisition controller, either in the form of a free-standing unit interfaced to the host computer via a serial RS-232 or IEEE-488 data link, or in the form of a board built into the host computer (as in the present unit). This would eliminate the critical timing constraints that have so far made it impossible to run Visual Basic under Windows for data acquisition. If the QuickBasic limitation were removed, the data acquisition arrays could become much larger and allow higher optical resolution through the use of a larger number of spectral segments.

3.4. Visual system performance

How well does the on-line system perform? It is difficult to depict for documentation purposes the visual display offered by the data acquisition program, because photographs of the CRT screen are of notoriously poor quality. As a substitute, a "window dump" of the manipulation mode's "SCOUT" routine is exhibited here in Fig. 5. The acquisition mode's developing chromatogram and its spectral vignette look very much the same —except for being coloured on the screen and, of course, for terminating there at the arrow marking the present.

The SCOUT routine of the manipulation program allows the operator to move said arrow (in cursor form) along a stored chromatogram and watch the spectra of peaks pop up accordingly: this routine can serve as an operator-controlled recapitulation of what had happened initially and automatically in the ephemeral acquisition process. It is easy for the experienced operator to watch the "spectra" change in real time and recognize the FPD-active elements of peaks passing through the detector in the acquisition mode; or to follow SCOUT's arrow in the similar pursuit of peaks passing through the algorithmic gate in the manipulation mode. In Fig. 5, the peak marked by the time arrow (cursor) is that of tetramethyltin and the spectral window accordingly shows the green SnOH and the red SnH emission —albeit only in the form of ten

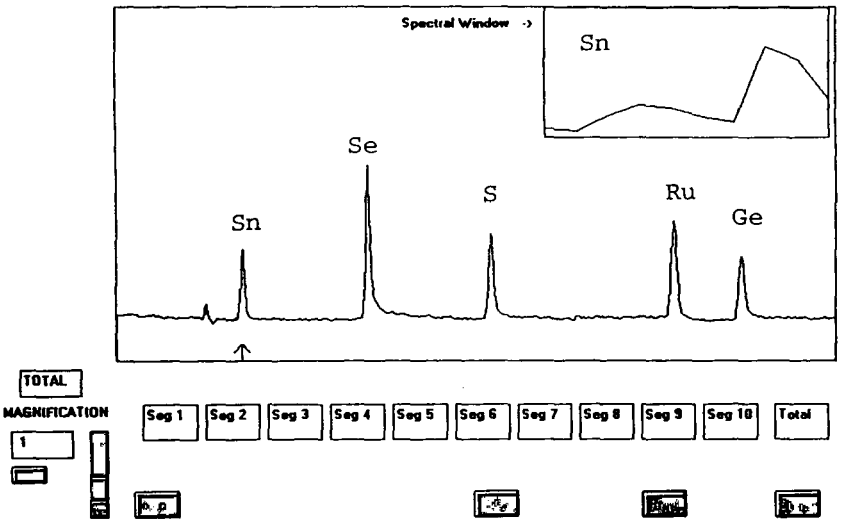

Fig. 5. Chromatogram and spectrum, similar to screen image seen during data acquisition. First segment intensity multiplied by two (see text for further explanations). Compounds: Sn = tetramethyltin; Se = dimethyldiselenide; S = di-*tert.*-butyldisulphide; Ru = ruthenocene (dicyclopentadienylruthenium); Ge = tetra-*n*-butylgermane. Hydrogen 50 ml/min, air 40 ml/min.

segment intensity points connected by *straight* lines (with the first datum, from *ca.* 400 nm, and the last datum, from *ca.* 700 nm, located in the window frame).

Fig. 6 records further the spectral windows as SCOUT's arrow targets the next four peaks of Fig. 5. These peaks are due to dimethyldiselenide, di-*tert.*-butyldisulphide, dicyclopentadienylruthenium and tetra-*n*-butylgermanium. Their "spectra" are hence characteristic of selenium (Se_2), sulphur (S_2 plus a trace of HSO at the red border), ruthenium (emitter unidentified but possibly RuH) and germanium (GeH).

(Note that it may be preferable —and less objectionable to spectroscopists proper— to speak here of "spectral envelopes" rather than of "spectra". A rough summation of the combined effects of filter bandpass, port apertures and segment scan time shows the effective half-height bandpass to be typically in the 60-nm range. Since the formal segment is only 30 nm (18°, 5 ms) wide, this means that the wavelength regions of the ten actually monitored segments do overlap considerably: a consequence of collecting light as much and as long as reasonably possible. Yet this matters little in terms of elemental recognition: the resulting spectra, though broadened by acquisition and cornered by display, are nevertheless well reproducible and therefore diagnostic of their parent ele-

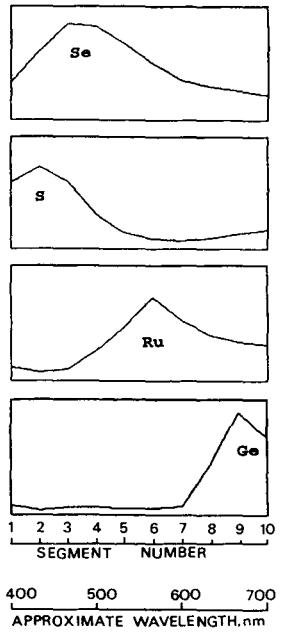

Fig. 6. Spectral windows as obtained by moving the SCOUT arrow (cursor) through four peaks of Fig. 5.

ments. The wheel turns for elemental recognition, not spectral definition: *other* methodologies should be chosen if a heretofore unknown spectrum happens to be in need of measurement.)

To provide a synopsis of the information typically forwarded by the detector in the acquisition mode, we have to call again on the graphic capabilities of the manipulation software. Fig. 7 shows a "3-D" representation, with axis labels added manually and with each peak defined according to its FPD-active element. The chromatographic traces are smoothed by digital filtering and sent to the printer, not as a window dump but in (graphically) high resolution.

3.5. Use of chromspec readouts

The likes of Fig. 7 can serve as overviews of particular separations. Such graphs allow the operator to decide at a glance what spectral region(s) best to use for single-wavelength analysis and report. This task can be carried out directly, *i.e.* with the stored segment serving as the data base; or, requiring a second run, with the wheel stopped at the desired wavelength; or, if sensitivity is the overriding issue but additional work is not, with a suitable fixed-wavelength interference filter mounted in a conventional FPD channel. Further information might be obtained from such 3-D representations about the spectral behaviour of the solvent peak and the baseline and, more importantly, about the best spectral conditions at which to conduct quantitation, introduce matrix subtraction [9], improve selectivity vis-a-vis other sample components, and produce response-ratio [10] or CONDAC [11] chromatograms.

CONDAC ("conditional access") chromatograms use the distinct response ratios characteristic of FPD-active elements to accept peaks of only one element and reject all others. An example, which uses the data of Fig. 7, is shown in Fig. 8. The analyst is offered wide reign by the current ten (as compared to the earlier two [9–11]) channels: several spectrally different conditions are now available for producing background-corrected, element-specific or otherwise correlated chromatograms.

It is even easy to leaf through the spectral envelopes (which are stacked parallel to the *y* axis in Fig. 7) for tentative identification of

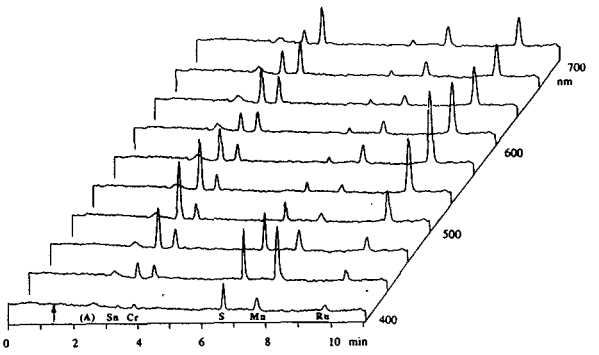

Fig. 7. A typical "3-D" separation. Compounds: A = 1 μl acetone (solvent); Sn = tetramethyltin; Cr = chromiumhexacarbonyl; S = di-*tert.*-butyldisulphide; Mn = methylcyclopentadienylmanganesetricarbonyl; Ru = ruthenocene. Hydrogen 30 ml/min, air 80 ml/min. First segment intensity multiplied by two. Graphic high-resolution mode. Labels added.

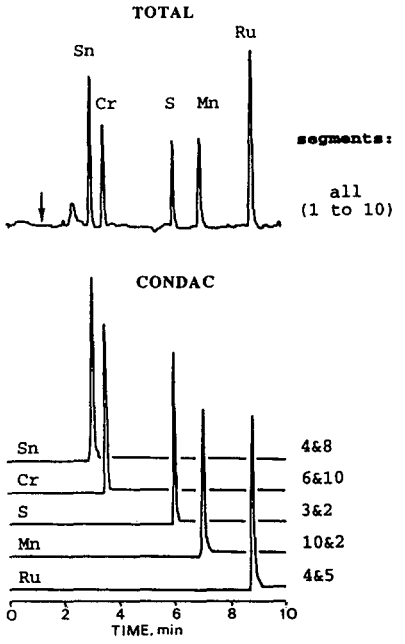

Fig. 8. Typical CONDAC [11] chromatograms from various segment combinations as indicated. Compounds: Sn = 2 ng tetramethyltin; Cr = 10 ng chromiumhexacarbonyl; S = 6 ng di-*tert.*-butyldisulphide; Mn = 20 ng methylcyclopentadienylmanganesetricarbonyl; Ru = 5 ng ruthenocene. Hydrogen 300 ml/min, air 80 ml/min. Without quartz chimney.

elements, for detailed comparison of spectrally similar peaks or for temporal assessment of peak purity. It may be justifiedly asked in this context why we did not portray the chromspec data in the customary protuberant 3-D topography. While easy to obtain, such technicoloured portraits may have turned out more confusing than revealing. Being staid chromatographers, we decided to outline only the chromatograms (time dimension) and leave the spectra (colour dimension) to the imagination of the viewer. Still, even a simple 3-D chromspec plot such as Fig. 7 efficiently represents the essence of the chromatographic and spectral information that is being collected by the acquisition program. Clearly the 3-D plot comprises more and broader information than the conventional, *i.e.* 2-D, chromatogram or spectrum.

3.6. 3-D vs. 2-D: the spectral dimension

Although analysts (or instrument companies) generally prefer 3-D to 2-D —that is, more information (or potential profit) to less— it must be noted that a higher number of physical or chemical dimensions can also mean a shorter or noisier range for any or all of them. In other words, a compromise has to be reached among the various instrumental settings that influence analytical and spectral performance.

Just to mention one example: the number of spectral segments (simultaneous chromatograms) is linked to the spectral resolution on one hand, and the useable signal range on the other. Obviously, the greater the number of segments the higher the spectral resolution. In a semicircular variable filter, divided into ten equitemporal segments during one revolution of the wheel mount, each segment can be monitored at most 5% of the time. Unless $1/f$ noise prevails —which it does not in our case— this means a loss in S/N ratio as compared to a conventional FPD channel. This loss will generally increase with the total number of segments available. In turn, the lower the S/N ratio the less precise the analysis and the shorter its working range. The addition of spectral information thus brings with it a deletion of the lowest part of the calibration curve, *i.e.* a shortening of the response dimension.

Further insight into the analytical quality of data from the acquisition mode can be obtained by using the manipulation mode's "TRICHROM" routine. In this routine the screen displays three chromatograms selected by the operator. To facilitate orientation, a "total" chromatogram, *i.e.* the sum of all ten segment chromatograms (divided by 10 to fit the screen) is usually selected as one of the three. The operator can scale (compress or expand) either the intensity axis or the time axis or both. In the former case, the signal "magnification factor" appears on the left side of the chromatogram. Fig. 9 shows a typical example of a "total" plus two segment chromatograms in the form of a window-dump. Note that the window-dump, while including some function buttons, does not include the constantly updated information that appears automatically on the bottom of the screen to keep the operator informed of the true chromatographic retention time and signal intensity.

To have available ten chromatograms from different wavelengths (or any time slice or additive/subtractive combination thereof, as obtained conveniently by using the "PIZZA" routine of the manipulation program) allows the operator to select the segments that offer the best selectivity, matrix suppression, quantitation, etc. If different peaks contain different heteroelements, the latter can be identified and processed at suitably different wavelengths. If a peak contains more than one FPD-active heteroelement, the elemental ratio can be estimated (similar to the classic case of thiophosphates [12]).

Several other, less obvious advantages may be hidden in this gratuitously available spectral information. For instance, the 3-D FPD may allow the operator to understand and perhaps even control the chemical nature of the baseline (background luminescence). Certain luminescent features may be intrinsic (*e.g.* arise from the oxyhydrogen flame), but many others may be extrinsic (*e.g.* derive from stationary phase bleed during temperature programming; from carrier

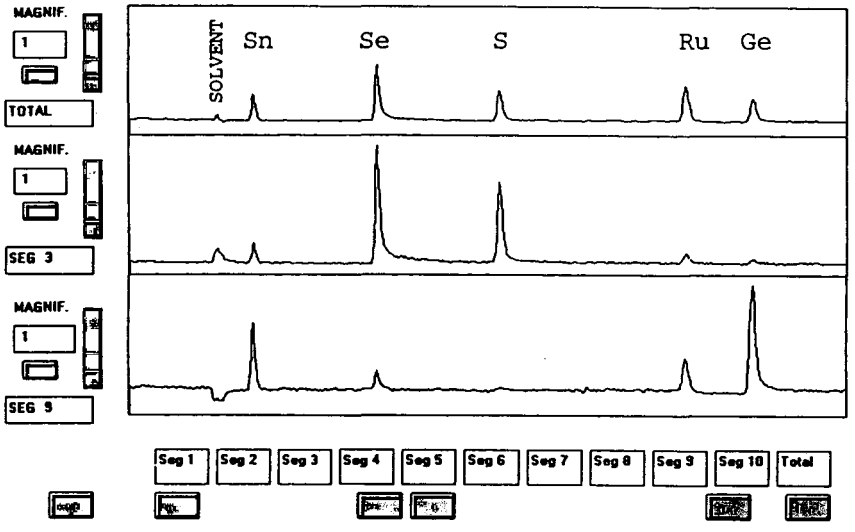

Fig. 9. A typical "TRICHROM" display used for data comparison and manipulation (window-dump only), from the chromatographic run shown in Fig. 5.

gas contamination; or, most insidiously, from injection port, column or detector memory). Our preliminary experience with the wheel system strongly suggests the presence of such temporary effects (which are, of course, also present in the 2-D FPD, but go unnoticed there). For instance, the spectral envelope of the baseline luminescence often changes from evening to morning and, less surprisingly, from one experimental series to the other. Also, the 3-D FPD may allow the operator insight into the behaviour of certain species that at the same time luminesce and quench luminescence —their own and that of other analytes— as in the well-known case of hydrocarbonaceous matrices [3,4,13].

There is little doubt that the immediate state of the FPD influences analyte response in various ways. Willy-nilly, once the computer starts turning out background spectra alongside analyte spectra, the former will be noticed and, in turn, benefit the latter —not just for the obvious spectral correction routines, but also for the diagnostic and prophylactic value of treating contaminating samples and contaminated detectors. However, only time will tell whether such information on potential background interferences and undesirable detector memories will prove a panacea for analysis or merely a placebo for the analyst.

3.7. 3-D vs. 2-D: the S/N ratio

The primary reason for Fig. 9 to be shown here is the visual appearance of the chromatograms, the selectivity they represent, the range of information they convey and —as a hint only— the breadth of manipulation they invite. However, opening a new dimension would be meaningless without ensuring that its sensitivity is up to its tasks. Under typical FPD conditions, the sensitivity of the wheel will almost unavoidably be lower than that of a conventional channel —but the important question is by how much. (If baseline noise were exclusively due to flame flicker, or to other slow chemical and chromatographic fluctuations, detection limits for the regular and the 3-D channel would obviously be comparable.)

When the filter wheel is simply inserted between the original Shimadzu cooling connector and the PMT housing, large amounts of various compounds have to be injected to be seen. This is due to a variety of reasons; some major, some minor. To start with a minor one: the new signal

path (from high-speed amplifier to ADC to digital filter to printer) produces S/N ratios that are estimated to be worse (by a factor of about two) than those from the old signal path (from electrometer to analog filter to stripchart recorder —both starting from the same flame and wheel arrangement, of course).

That a rotating filter produces lower S/N ratios than a stationary one is fairly obvious under shot-noise-limited conditions. What may be less obvious, however, is that the extent of this effect depends on the spectral nature of the measured peak. The largest difference between the filter rotating and the filter stationary occurs when the peak emits in only one of the ten wavelength regions; if, on the other hand, its emission is spread out over all ten, the difference is smaller. A similar argument obtains in the comparison of the "best segment" *vs.* the "total" chromatogram from the rotating filter. If the peak consists of a spectral continuum, the S/N ratio of the single wavelength segment is decidedly lower than that of all ten segments combined; if the peak consists of a sharp spectral feature, the opposite may be the case.

If we are willing to assume an idealized set of circumstances, *e.g.* that the noise is random, that electronic and timing effects are negligible, and so forth and so on, it becomes easy to put numbers to these various relationships [14]. A factor of three $(10^{1/2})$ is most often present in such theoretical comparisons. In actual cases it should be less; and in no case should it exceed ten. Exploratory experiments carried out with the filter rotating *vs.* stationary, and with compounds of manganese *vs.* ruthenium, are generally in agreement with these theoretical estimates. Observed from a different experimental angle, the "total" chromatogram from the rotating filter wheel (via the computer) has an S/N ratio that is, generally and typically, three to four times worse than that of the stationary filter wheel (via the electrometer).

3.8. A detour: FPD noise characteristics

We should include at this point a consideration that, though largely speculative, is of particular importance for the wheel system. Earlier we had mentioned that the S/N ratio cannot be improved in the case of flame flicker. That is conventional wisdom for a single-channel instrument such as the common FPD, but is not necessarily true for dual- or multiple-wavelength instruments. If noise, regardless of its origin, should contain components of a frequency lower than the temporal resolution of the monitoring system, such components could be effectively suppressed to produce a higher S/N ratio.

Typical chromatograms like those shown in Figs. 5, 7 and 9 are electronically filtered to remove fast noise; however, sizeable amounts of apparently slow noise are still in evidence. Noise components with frequencies near that of the analyte peak can obviously not be removed by simple data smoothing. They could, however, be removed by the subtraction capability of the PIZZA menu (as well as by a variety of other techniques). Our peaks are generally wider than 10 s, while our temporal resolution of the raw data, in the worse case, is narrower than 100 ms: this seems to offer an opportunity to improve the S/N ratio. (It also offered the bait that lured us into attempting correlated dual-channel chromatography some years ago: our earlier two-PMT attempt to reduce noise failed —but the experimental set-up, once in existence, earned its keep by offering other analytically meritorious features [9,15]).

In the case of the spectral wheel, the present one-PMT attempt to reduce noise by subtracting scaled segment chromatograms failed likewise. In fact, the noise of the subtraction chromatogram was larger than the noise of either of the two constituent chromatograms; by a factor close to the square root of two. That number suggests random, uncorrelated noise. But how can noise with a time constant above, say, 1 s not be correlated, *i.e.* not be simultaneously present in two channels whose segment acquisition time is only 5 ms and whose repetition time is only 100 ms?

A plausible answer is that the "true" (= initial) noise contains, in fact, no low-frequency components —at least none strong enough to make a difference. What appears as

low-frequency components in Figs. 5, 7 and 9 (as well as in the later Fig. 10) is really the result of random fluctuations that are fast enough (>200 Hz) to escape correlation by the wheel. These uncorrelated fast fluctuations (after summation by the gated integrator) merge during the data-smoothing process into the much slower fluctuations *unique* to each segment. This later type of noise, in contrast to genuine flame flicker, PMT drift, etc., cannot be cancelled by time/wavelength multiplexing. While operational distinctions between initial and filtered noise are rarely drawn, and consequences of noise frequency shifts on baseline correction and detection limits rarely explored, they are of obvious importance for the present case. For one, they can help the analyst decide which S/N losses can be avoided or ameliorated, and which can not.

3.9. 3-D vs. 2-D: detection limits

The major S/N loss is due to the diminution of light on its way from the flame to the PMT tube. When the wheel is merely being inserted between the existing detector block (including the connecting light tunnel carrying the cooling coils) and the existing PMT housing, the S/N ratio is very poor. With *all* the mechanical and optical adjustments described in the Experimental section in place, the S/N ratio improves about fifty-fold (as measured with ruthenocene).

Yet, the improved FPD channel with wheel is still not quite as sensitive as the conventional FPD channel without, an experimental finding easily anticipated on optic and electronic grounds. While as authors we could be considered obliged to put hard numbers to this difference in sensitivity, it should be understood that any such number may depend heavily on the nature of the element being tested and the flow conditions chosen to test it. The most meaningful comparison indeed should be one that is typical in its scope, reasonable in its execution and fair in its assessment.

One such proof-of-the-pudding comparison can be carried out by simply determining the detection limits of a few sensitive and, in their spectral behaviour, disparate elements with the rotating filter wheel; and to use just a *single* segment (which corresponds to monitoring the flame at a given wavelength only 5% of the time) for the calculation. The conditions for this test of detector performance are those suited to each *individual* element: the results can hence be legitimately compared with the known detection limits of the same elements as determined at optimized conditions in the conventional FPD. The two old FPD protagonists, phosphorus and sulphur, appear in their familiar roles. The deuteragonists germanium and ruthenium are less familiar actors on the analytical stage, but are included here to round out the cast. In a series of four separate runs, 100 pg of tris(pentafluorophenyl)phosphine, 1 ng of thianaphthene (benzo[*b*]thiophene), 500 pg of tetra-*n*-butylgermanium and 100 pg of ruthenocene are tested in individually optimized settings.

In the case of sulphur, a narrow quartz chimney surrounds the detector jet, and the flow conditions are those that suit the S_2 emission (the conventional quadratic sulphur response of the FPD [1–4, *cf.* ref. 16]). The quartz chimney is also used for phosphorus and germanium, but is removed for ruthenium. Phosphorus is tested last to minimize possible detector contamination.

The $S/RMS = 3$ detection limits for one-segment chromatograms in the rotating-wheel FPD arrangement are $1 \cdot 10^{-11}$ g tris(pentafluorophenyl)phosphine or $2 \cdot 10^{-13}$ g P/s for phosphorus (via HPO*), $8 \cdot 10^{-11}$ g thianaphthene or $9 \cdot 10^{-12}$ g S/s for sulphur (S_2^*), $3 \cdot 10^{-11}$ g tetra-*n*-butylgermanium or $2 \cdot 10^{-12}$ g Ge/s for germanium (GeH*) and $2 \cdot 10^{-11}$ g ruthenocene or $2 \cdot 10^{-12}$ g Ru/s for ruthenium. The $S/N_{p\text{-}p} = 2$ detection limits are $7 \cdot 10^{-13}$ g P/s, $3 \cdot 10^{-11}$ g S/s, $7 \cdot 10^{-12}$ g Ge/s and $4 \cdot 10^{-12}$ g Ru/s. (The numbers for sulphur may be low since the computer-based calculation of the detection limit uses a *linear* extrapolation. However, many calibration curves for "quadratic" sulphur actually do become linear as they approach the minimum detectable amount.)

For general comparison: Dressler [3] states that "the minimum detectable mass rate ranges from about $1 \cdot 10^{-13}$ g/s to $2 \cdot 10^{-12}$ g/s of P for phosphorus compounds and from about $2 \cdot 10^{-12}$

g/s to $5 \cdot 10^{-11}$ g/s of S for sulphur compounds" (his reference numbers deleted). Our own group —using the same but then much younger gas chromatograph— found the relevant minimum detectable flows at $S/N_{p\text{-}p} = 2$ to be $2 \cdot 10^{-13}$ g Ge/s (as GeH) [17], and $4 \cdot 10^{-13}$ g Ru/s (at 526 nm; emitter unidentified but possibly RuH) [18].

The corresponding detection limits from the wheel are by no means the lowest possible, but are those we consider reasonable under the circumstances. What is "possible" in this context and what "reasonable" needs to be briefly discussed in order to allow the reader an informed evaluation of the quoted figures of merit.

Since most emissions in the FPD cover several segments (compare Fig. 6), the one-segment limits of detection are generally worse than those of multi-segment or all-segment, (*i.e.* "total") chromatograms. This is analogous to the behaviour of the conventional FPD operating with a narrowband *vs.* a broadband *vs.* no interference filter. The rotating wheel is therefore being evaluated in this regard on a *worst*-performance basis. Yet the *single*-segment detection limit is closer in spectral nature to that of the conventional, *i.e.* fixed-wavelength FPD. Also, there may be good practical reasons for using a *single*-segment chromatogram despite its poorer sensitivity: its *selectivity* is more often than not higher than that of the "total" chromatogram.

The detailed calculation of detection limits has been described in the Experimental section. Note that the wider term "detection limit" denotes a computer routine that, in our case, characterizes *detector* performance; this differs from the narrower literature definition which refers to a *total* analytical method [19]. In order to remain "reasonable", data smoothing is restricted here to settings that reduce the analyte peak height by no more than 10% —despite the fact that higher S/N ratios can be obtained if that restriction is ignored. The baseline interval used for the measurement of noise spans about twenty standard deviations of the analyte peak.

Comparisons between detection limits of segmented (3-D FPD) *vs.* continuous (2-D FPD) response reveal some interesting differences. For instance, the conversion factors between the *RMS*- and $N_{p\text{-}p}$-based types of detection limits differ, suggesting a different character (distribution) of noise for 3-D and 2-D modes. Also, the conversion factor between the two definitions clearly depends on the extent of data smoothing. The detailed description/explanation of such effects is, however, lengthy and not essential to this paper; it will be given elsewhere [20].

While in our role as authors we have become habituated to reporting *two* types of detection limits, each for both injected mass and detected flow of analyte, we have been doing so primarily to placate the discriminating referee and accommodate the inquiring reviewer. Left to our own predilections, however, we would simply provide a typical chromatographic peak with enough noise around, *i.e.* a chromatogram taken within range of the detection limit. For any kindred chromatographer bent on carrying out detectability and noise assessments according to personal or local preferences, we therefore offer in Fig. 10 some single-segment peaks from the rotating filter wheel. Segment numbers and 1-min time units are indicated on the individual abscissae. These chromatograms are FIR-filtered; however, AVG and RC filters would have produced very similar results [20].

From this comparison it seems that (very approximately and highly analyte- and condition-dependent) the new 3-D FPD is about one decade less sensitive than the conventional 2-D FPD and that, consequently, its linear range is about one power-of-ten shorter. That loss seems reasonable at the present state of affairs, given that the absolute light level of chemiluminescence is low and that "noise", primarily if not exclusively, appears to consist of photon shot noise [14].

In comparison with a regular 2-D FPD channel, the 3-D FPD's high-speed electronics may contribute to S/N loss by a factor around 2 (a mainly experimental estimate); and the 5% dwell time for each segment could be considered responsible for a loss factor of $(100/5)^{1/2} = 4.5$ (given a square-root dependence of the S/N ratio on sampling time). The light transmission of the variable filter is lower than that of a typical fixed-wavelength interference filter, and the need

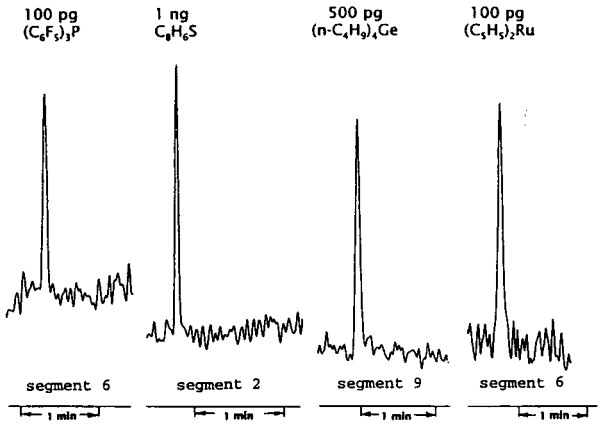

Fig. 10. Typical single-segment peaks near the detection limit. Composite picture in graphically high-resolution mode from selected windows at different wavelength regions (segment numbers), flow conditions, extents of background luminescence, and time scales. Tetraethyllead injections were used prior to the experiment to reduce the luminescent background. Compounds and conditions from left to right (all flows in ml/min): 100 pg tris(pentafluorophenyl)phosphine, 200 hydrogen, 40 air, PMT −860 V, quartz chimney present, variable filter segment 6; 1 ng thianaphthene, 50 hydrogen, 30 air, PMT −830 V, chimney present, segment 2; 500 pg tetra-*n*-butylgermanium, 50 hydrogen, 40 air, PMT −830 V, chimney present, segment 9; 100 pg ruthenocene, 300 hydrogen, 80 air, PMT −800 V, chimney absent, segment 6. Data are FIR filtered close to a 10% reduction in analyte peak height.

to focus the poorly defined beam on the variable filter through not too wide an aperture must add to the photon deficit. On the other side of the ledger, centering the flame and backing it up by a mirror improves light throughput considerably (this may also help a conventional FPD channel although, because of the shorter light path and the much higher light level of the latter, far less so than the wheel system). While matters of sensitivity are condition- and analyte-dependent, and by far not as straightforward as they are made to appear in this short account, the nigh inevitable one-order-of-magnitude loss seems a relatively minor (and still introductory) price to pay for the value added.

But this also invites a value-added tax to be imposed on the goods and services the FPD offers: when the rotating variable interference filter adds wavelength as an instantaneous third dimension to the FPD, it also increases its complexity and hence its acquisition and maintenance costs. In our case, the main initial cost was the US$ 1000 filter itself. A suitable computer/monitor/printer combination may be available second-hand in many laboratories; newly purchased it would require an additional US$ 2000. This seems commensurate with the price of a simple gas chromatograph with single-channel FPD (about US$ 10 000).

Whether a lower sensitivity, a higher price, and a greater complexity can be justified by the information content of a third, spectral dimension has yet to be determined (and should in any case be heavily dependent on the particular analytical demands and conditions). It would appear, however, that the revolving spectral wheel may yet provide one of the simplest and least expensive third dimensions ever added to analytical instrumentation.

3.10. A different type of filter wheel?

The wheel is, however, still far from perfect. Light throughput, hence sensitivity, could undoubtedly be improved. Also, the available wavelength range could be changed to serve particular analytical requirements, for instance by installing custom-made variable filters of smaller, wider, or simply different (*e.g.* UV, IR) optical range. Yet, a *variable-wavelength* filter may, in fact, not be the best choice for many analytical applications.

A possibly better arrangement may involve conventional *fixed-wavelength* 1-in. diameter interference filters held in, say, eight filter holders set in close proximity and radial symmetry over 360° into a metal wheel, with eight acquisition triggers commensurately positioned on (or, alternatively, with eight holes drilled through) its rim to intercept (or pass) the IR trigger beam. In this manner, a variety of advantages could be realized. First, no acquisition time would be "wasted" on an opaque semicircle, or on wavelength regions of only minor interest (as is the case now). Second, any wavelength (*e.g.* typically optimized FPD wavelengths such as 394 or 405 nm for S_2^*, 525 nm for HPO*, etc.) could be

used —and these could range from UV to IR. Third, such conventional filters would inherently produce better resolution (*i.e.* their bandpass, typically 10 nm, would not be degraded by temporal segmentation or beam spread effects). Also, their transmission would typically be better than that of the variable filter. Fourth, the choice which wavelengths to monitor could be adjusted perfectly (subject only to the availability of filters) to analytical tasks (such as background correction and other correlational approaches [9–11]) that rely on the constancy of spectral response ratios [21]. Fifth, a wheel of this nature could also be used for many non-chromatographic purposes, *e.g.* analyzing simple solutions [Na, K, Ca, etc. (*cf.* ref. 22)] by flame photometry, monitoring spectrally classifiable meteorological and astronomical events, following and/or stimulating the response of bioluminescent communities, testing various types of weak natural or stimulated luminescences in inorganic materials, etc. Sixth, the wheel could serve equally well as a (computer-controlled, multiwavelength, pulsed) light *source*. Several other applications seem fairly obvious.

Though sorely tempted to do so, our group shall not be able to develop further wheels, owing to current constraints on electronic and programming support. We do hope, however, that other laboratories see fit to put their own spin on this interesting topic.

Acknowledgements

This research was financially supported by NSERC grant A-9604. The suggestions and highly skilled support by the Department's Machine Shop (Cecil Eisener) and Electronics Shop (Chris Wright) are gratefully acknowledged. Without their help, this study would not have been possible. Thanks are also due to H. Singh for help in revising this manuscript.

References

[1] S.S. Brody and J.E. Chaney, *J. Gas Chromatogr.*, 4 (1966) 42.
[2] S. Kapila, D.O. Duebelbeis, S.E. Manahan, in R.M. Harrison and S. Rapsomanikis (Editors), *Environmental Analysis Using Chromatography Interfaced with Atomic Spectroscopy* (*Ellis Horwood Series in Analytical Chemistry*), Wiley, Chichester, 1989, pp. 76–95.
[3] M. Dressler, *Selective Gas Chromatographic Detectors* (*Journal of Chromatography Library*, Vol. 36) Elsevier, Amsterdam, 1986, pp. 133–160.
[4] S.O. Farwell and C.J. Barinaga, *J. Chromatogr. Sci.*, 24 (1986) 483.
[5] P.W. Grant, in D.H. Desty (Editor), *Gas Chromatography 1958* (*Proc. Symp., Amsterdam, May 1958*), Butterworth, London, 1958, pp. 153–163; as cited in D. Jentzsch and E. Otte, *Detektoren in der Gas-Chromatographie*, Akademische Verlagsgesellschaft, Frankfurt/Main, 1970, pp. 177–178.
[6] P.L. Patterson, R.L. Howe and A. Abu-Shumays, *Anal. Chem.*, 50 (1978) 339.
[7] M.L. Selucky, *Chromatographia*, 4 (1971) 425.
[8] K.W. Busch and M.A. Busch, *Multielement Detection Systems for Spectrochemical Analysis*, Wiley, New York, 1990, pp. 612–613.
[9] W.A. Aue, B. Millier and X.-Y. Sun, *Can. J. Chem.*, 70 (1992) 1143.
[10] B. Millier, X.-Y. Sun and W.A. Aue, *Anal. Chem.*, 65 (1993) 104.
[11] W.A. Aue, B. Millier and X.-Y. Sun, *Anal. Chem.*, 63 (1991) 2951.
[12] M.C. Bowman and M. Beroza, *Anal. Chem.*, 40 (1968) 1448.
[13] W.A. Aue and X.-Y. Sun, *J. Chromatogr.*, 641 (1993) 291.
[14] J.D. Ingle, Jr. and S.R. Crouch, *Spectrochemical Analysis*, Prentice Hall, Englewood Cliffs, NJ, 1988, Ch. 5.
[15] W.A. Aue, B. Millier and X.-Y. Sun, *Anal. Chem.*, 62 (1990) 2453.
[16] W.A. Aue and X.-Y. Sun, *J. Chromatogr.*, 633 (1993) 151.
[17] C.G. Flinn and W.A. Aue, *J. Chromatogr.*, 186 (1979) 299.
[18] X.-Y. Sun and W.A. Aue, *Can. J. Chem.*, 67 (1989) 897.
[19] Analytical Methods Committee, Royal Society of Chemistry, *Analyst*, 112 (1987) 199.
[20] X.-Y. Sun, B. Millier, C.W. Warren, H. Singh and W.A. Aue, *J. Chromatogr.*, submitted for publication.
[21] X.-Y. Sun and W.A. Aue, *J. Chromatogr. A*, 667 (1994) 191.
[22] F.W.J. Garton, J.L. Waddingham, P.C. Wildy, H.M. Davis and S.I. Hawkins, *U.K.A.E.A. Res. Rep. AERE R4141*; as cited in J.B. Dawson, D.J. Ellis and R. Milner, *Spectrochim. Acta*, 23B (1968) 695.

ELSEVIER

Journal of Chromatography A, 675 (1994) 177–187

JOURNAL OF CHROMATOGRAPHY A

Combined solvent extraction–purge and trap method for the determination of volatile organic compounds in sediments ☆

Osvaldo C. Amaral, Lourdes Olivella, Joan O. Grimalt*, Joan Albaiges

Department of Environmental Chemistry (CID–CSIC), Jordi Girona 18, 08034-Barcelona, Catalonia, Spain

(First received December 22nd, 1993; revised manuscript received February 28th, 1994)

Abstract

A method involving methanol solvent extraction (SE) and purge and trap (PT) was evaluated for the determination of chlorinated volatile organic compounds (VOC) in sediments. The method was tested by means of standard solutions encompassing twenty chlorinated compounds with boiling points ranging between 24 and 150°C (at 1 atm = 101 325 Pa). Detection limits (0.05–0.4 μg/g), linearity ranges and recoveries (only 1% average losses by glassware manipulation and 7.5% losses after water sediment suspension with standards and methanol extraction) show the suitability of the method for the determination of chlorinated VOC in environmental samples. A specific advantage of this method is the possibility of storage of the VOC methanol extracts for long periods of time at −20°C without significant alteration of the quantitative results. In the conditions of the study, the average recovery of individual VOCs after storage for 50 days was 89%.

1. Introduction

Man has traditionally disposed of wastes in the most expedient and economic way possible. Residues have been stored in sites of marginal commercial value or near the industrial facilities where they have been generated. Soil, sediment and groundwater pollution are the main problems resulting from these activities. In this respect, the widespread use of volatile organic compounds (VOCs) for industrial applications has very often resulted in this type of compound appearing to be associated with waste lixiviation problems, producing adverse effects on the environment and human health [1].

Accurate mass balances of the VOCs present in polluted sediments are essential for reliable environmental impact studies and feasible remedial programmes. Unfortunately, VOC determination in soils and sediments has not been completely mastered [1]. The efficient extraction (purging) of volatile chemical species from solid matrices if far more difficult than from waters and no specific method is generally accepted in the literature. Thus, methods involving soil extraction with organic solvents (*i.e.*, *n*-hexane [2], *n*-pentane [3] and *n*-pentane–propan-2-ol [3]) and subsequent analysis by gas chromatography (GC) have been proposed. Other methods are based on headspace GC analysis of soil samples heated within capped vials after addition of water [4–8] or methyl glycol (propylene glycol) [9]. In other cases the samples are introduced within canisters or Tedlar bags and the outgassed

* Corresponding author.

☆ Presented at the *22nd Annual Meeting of the Spanish Chromatography Group, Barcelona, October 20–22, 1993.*

0021-9673/94/$07.00
SSDI 0021-9673(94)00199-J

compounds are introduced into a GC system by means of a gas sample valve [10].

Other approaches take advantage of the purge and trap (PT) methods developed for the routine determination of VOCs in water [11,12]. In general, the range of application of these methods has been extended to solid matrices by thermal vaporization of soil or sediment samples (sometimes after addition of water or methanol) and VOC trapping in adsorption tubes packed with Tenax resins [13–18]. An important advantage of these modified procedures is their applicability to the analysis of large series of samples with relatively simple handling when the tubes are submitted to GC analysis in combination with automated thermal desorbers (ATDs).

Unfortunately, this type of approach has recently been reported to give significantly poorer quantitative results, in terms of analytical precision and recovery, than the procedures based on the headspace method [7,8]. This drawback appears to be particularly important for low-boiling organochlorinated solvents such as methylene chloride, trichloroethane, trichloroethylene and tetrachloroethylene. Volatilization losses occurring during sample transfer from the storage vial to the purging vessel seem to be at the origin of this problem [8]. Attempts to minimize these volatilization effects by reduction of soil, water and glassware temperature have been unsuccessful in preventing these losses [8].

In view of these results, an alternative approach to be investigated concerns the combination of solvent extraction and PT methods, that is, sample extraction with a hydrophilic solvent, dilution within a large volume of water and PT analysis by the usual method, a combination that avoids any soil or sediment transfer between different vials. On the other hand, solvent transfer from the extraction to the purge containers can be performed with gas-tight syringes, which avoids volatilization losses. This type of solvent extraction–PT (SE–PT) application has been successfully developed for the determination of gasoline hydrocarbons in soils [19] and, in addition, avoids the need for immediate instrumental analysis of the soils or sediments after sampling. In this study, the possibilities for the analysis of organochlorinated hydrocarbons were investigated. Recoveries, detection limits and linearity ranges for 20 compounds encompassing a boiling temperature range between 24 and 150°C (1 atm), from trichlorofluoromethane to bromoform, were evaluated.

2. Experimental

2.1. Materials

Samples were stored in 40-ml screw-capped vials sealed with 0.010-in. thick 0.25-mm diameter Teflon-faced silicone-rubber septa (Model 2-3285; Supelco, Bellefonte, PA, USA). Methanol extracts were stored in 2-ml crimp-topped vials (Model 5181-3375; Hewlett-packard, Palo Alto, CA, USA) and kept at −20°C until analysis. PT was performed with a Supelco Model 6-4713 modified purging device containing a glass frit of medium porosity (10–15 μm). Water and methanol solutions were transferred with 10-μl and 5-ml PTFE Luer Lock (150-mm needle) syringes (Models 701N and 1005TLL, respectively; Hamilton, Bonaduz, Switzerland).

All standards were obtained from Supelco (Environmental Analytical Standard Series). Residue analysis methanol was purchased from Merck (Darmstadt, Germany). Tenax TA (60–80 mesh) was obtained from Perkin-Elmer (Norwalk, CT, USA). About 180 mg of this adsorbent were packed in 8.8 cm × 4 mm I.D. stainless-steel tubes (Model L4270123; Perkin-Elmer) and plugged between silanized glass-wool inserts (Model 54120790; Perkin-Elmer). Ultrapure helium (Quality 5.3; Abello Linde, Barcelona, Spain) was used as the carrier and purge gas. This gas was additionally purified with two serially connected hydrocarbon (Model 7971; Chrompack, Middelburg, Netherlands) and oxygen (Model 7970; Chrompack) filters.

2.2. Conditioning of the adsorption tubes

The tubes were cleaned by passage of 100 ml/min of helium while heating at 250, 300, 325 and 350°C for successive periods of 30 min each.

They were then tested by GC analysis using the ATD injector. Blank requirements were that no chromatographic peaks under the electron-capture or flame ionization detectors equivalent to 10 pg should be observed.

2.3. Sampling

About 1–3-g sediment sample aliquots were obtained from a water reservoir receiving the discharges from an organochlorinated solvent factory (Flix, Spain) and from an estuary contaminated with spillages from a chemical chlorine complex where organochlorine solvents were produced (Alagoas, Brazil). The samples were introduced into pre-weighed 40-ml screw-capped vials containing 5 ml of methanol. After closing the vial, the sediment suspension was shaken vigorously for 5 min and stored at 4°C in a freezer free from organic solvent vapours and let to settle. In the laboratory, 2 ml of the supernatant methanol extracts were taken with a syringe and introduced into 2-ml vials without leaving a headspace. These vials were sealed with an aluminum seal holding an 11-mm PTFE-faced septum and stored at −20°C.

2.4. Purge and trap

A 200-μl volume of the methanolic extracts was diluted in 100 ml of Milli-Q-purified water and 5 ml of this water were introduced into the PT device by means of a 5-ml syringe. This water aliquot was purged with helium at a flow-rate of 40 ml/min for 11 min. All the purging gas was passed through a Tenax TA tube fitted to the system by means of Model 404-1 PTFE ferrules held with 1/4-in. Swagelock connections. The tubes were subsequently introduced into the ATD system.

2.5. Instrumental analysis

A Perkin-Elmer ATD Model 400A coupled to a Perkin-Elmer Autosystem gas chromatograph equipped with flame ionization and electron-capture detectors connected in parallel were used in all analyses. The adsorption tubes were heated at 300°C for 5 min while passing helium through at a flow-rate of 260 ml/min. About 20% of the desorbed compounds were collected in a cryofocusing trap cooled to −30°C. This percentage was controlled by an inlet split which diverted 210 ml/min of the desorption gas to a vent and 50 ml/min to the cold trap. After the tube desorption period, the cryofocusing trap was heated to 300°C at 40°C/s with a holding time of 10 ml. A helium flow-rate of 16 ml/min was used to purge the cold trap during this period. When leaving the trap, the vaporized compounds were divided further by a second split which vented 8 ml/min to the outlet and directed 8 ml/min (about 50%) towards the GC instrument. Thus, only about 10% of the initial amounts of compounds present in the adsorption tubes were allowed to enter the GC column. At the outlet of the column a Y-type glass tight connection diverted about half of the eluting flow to each detector. The transfer line between the ATD instrument and the gas chromatograph was heated at 225°C.

All analyses were performed with a 75 m × 0.53 mm I.D. DB-624 (film thickness 3 μm) megabore capillary column (catalogue No. 125-1374; J&W Scientific, Folsom, CA, USA). Helium (8 ml/min) was used as the carrier gas. The column was heated from 40°C (holding time 5 min) to 160°C (holding time 1 min) at 5°C/min and then to 210°C (holding time 5 min) at 10°C/min. The electron-capture detector was heated at 290°C and nitrogen (34 ml/min) was used as the make-up gas. The flame ionization detector was heated at 250°C. Hydrogen (45 ml/min) and air (430 ml/min) were used to keep the flame at the operative chromatographic conditions.

2.6. Quantification

Two standard mixtures were used for quantification. One was prepared with trichlorofluoromethane, 1,1-dichloroethylene, dichloromethane, 1,1-dichloroethane, chloroform, carbon tetrachloride, trichloroethylene, 1,2-dichloropropane, 2-chloroethyl vinyl ether, 1,1,2-trichloroethane, tetrachloroethylene and dibromochloromethane. The other contained *trans-*

1,2-dichloroethylene, 1,1,1-trichloroethane, 1,2-dichloroethane, bromodichloromethane, *trans*-1,3-dichloropropene, *cis*-1,3-dichloropropene, bromoform and 1,1,2,2-tetrachloroethane. Various methanol solutions of each compound at concentrations between 0.4 and 10 μg/ml were prepared with these mixtures. Reference solutions for 1,2,3-trichloropropane and hexachlorobutadiene were prepared separately. These solutions were stored in the above-mentioned aluminium-sealed vials and kept at −20°C. After 2 weeks of storage they were always discarded and new series of diluted standards were prepared.

Aliquots of 4 μl of all these solutions were introduced into volumetric flasks containing 10 ml of Milli-Q-purified water. The flasks were capped and shaken vigorously and 5 ml of the water were introduced into the PT device. The standard volatile compounds were trapped in adsorption tubes and these were analysed in the ATD–GC system. Peak-area integration of the chromatograms corresponding to these tubes resulted into 22 reference straight lines allowing the individual calibration of the compounds identified in the samples.

2.7. Recovery tests

About 1–3 g of sediment were introduced into a 40-ml vial together with 5 ml of methanol and 20 μl of the above-mentioned two standard mixtures containing each compound at a concentration of 200 μg/ml. The vials were capped, shaken and left to equilibrate for 24 h at 4°C. Then, 2 ml of the supernatant methanol were introduced into aluminum-sealed vials and an aliquot (200 μl) of this solution was diluted in 100 ml of Milli-Q-purified water and analysed by the PT method following the above-indicated procedure. Alternatively, the methanol solutions were stored at −20°C for 50 days and analysed by the PT method after dilution of a 200-μl aliquot in 100 ml of Milli-Q-purified water. Leak tests not including the introduction of sediment into the 40-ml vials were also performed. In these tests, the methanol solutions were only stored at −20°C in the aluminum-capped vials for 24 h.

3. Results and discussion

Representative chromatograms of the two standard mixtures used for quantification and the recovery tests are shown in Fig. 1. The DB-624 column used affords baseline resolution of all peaks. This column, under the above-indicated operating conditions, also provides a baseline-resolved chromatogram when the two standard mixtures are analysed jointly. However, these operating conditions are critical to achieve the separation of chloroform, 1,1,1-trichloromethane, carbon tetrachloride and 1,2-dichloroethane and also for the separation of 2-chloroethyl vinyl ether and *trans*-1,3-dichloropropene. Two other compounds that are difficult to separate, 1,1,2,2-tetrachloroethane and 1,2,3-trichloropropane (not included in these standard mixtures), were also resolved with this DB-624 column.

3.1. Response factors, limits of detection and range of linearity

The different peak areas in the chromatograms of the standard mixtures shown in Fig. 1 illustrate the wide diversity of the electron-capture detection (ECD) response factors for each compound. These factors (area units per μg of compound) are listed in Table 1, where they are expressed by reference to that of 1,1-dichloroethylene. As expected, they are essentially dependent on the number and type (*i.e.*, fluorine, chlorine, bromine) of halogen atoms in each compound. The relative differences may be higher than three orders of magnitude.

These different response factors give rise to significant differences in detection limits and linear concentration ranges for each VOC. Thus, the observed limits of detection and ranges of linearity on analysis with this SE-PT method are also given in Table 1. In general, there is a good correspondence between response factors and limits of detection. However, it must be noted that the values shown in Table 1 are only guidelines, not necessarily absolute minimum values. The SE–PT method used in this study has been designed for the analysis of VOC

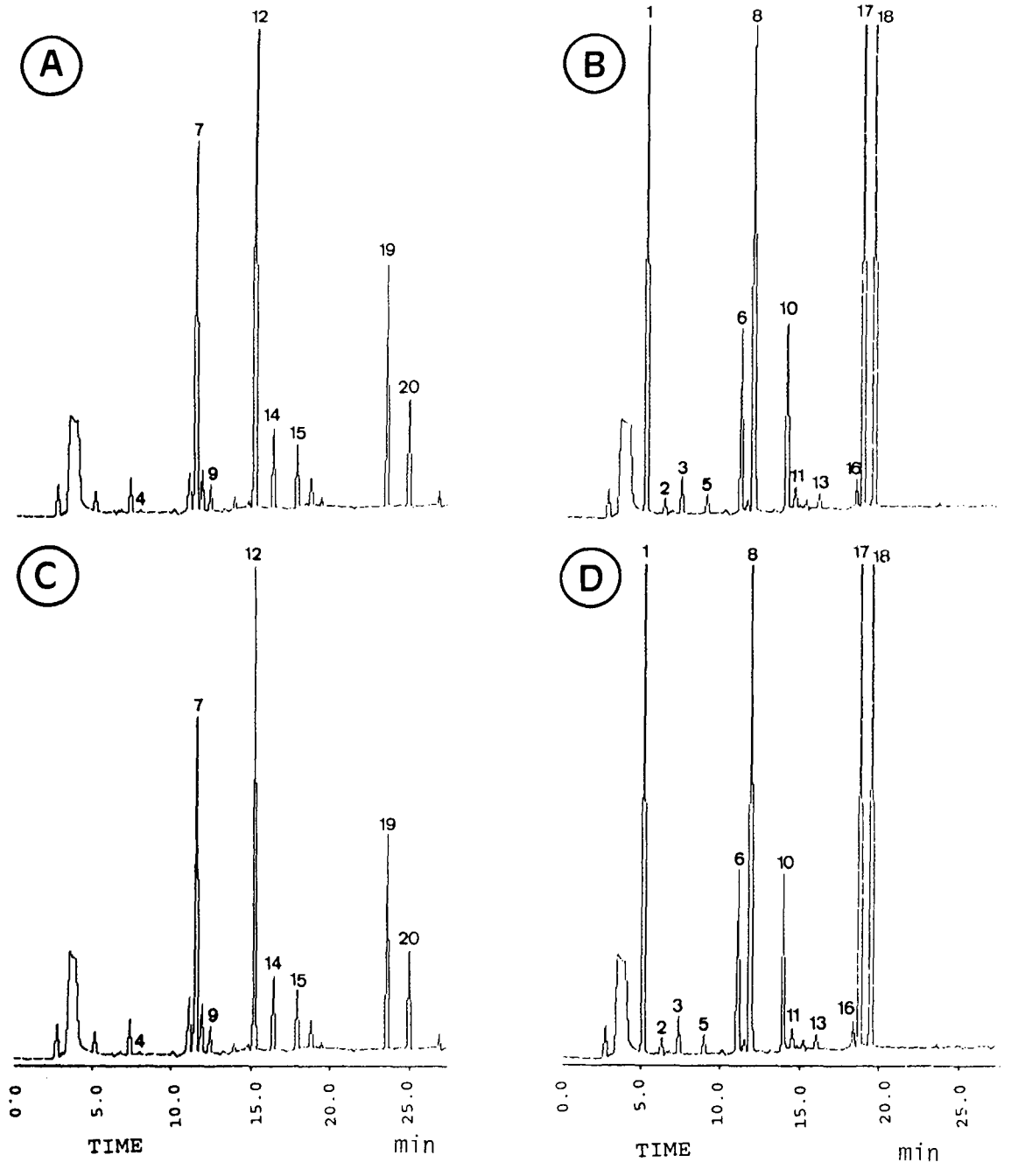

Fig. 1. Chromatograms of the standard mixtures used in the evaluation of the SE–PT method. (A and B) original mixtures; (C and D) recovered methanol extracts after water suspension with sediment and storage at −20°C for 24 h. Peak numbers refer to compound identification in Table 1.

Table 1
Detection limits, ranges of linearity and response factors (relative to 1,1-dichloroethylene) for 22 volatile organic compounds commonly encountered in sediments

No.	Compound	Detection limit (μg/g)	Linearity range (ng)		Response factor (area/μg)
			Lower	Upper	
1	Trichlorofluoromethane	0.05	0.04	40	1600
2	1,1-Dichloroethylene	0.40	0.20	400	1
3	Dichloromethane	0.10	0.10	200	100
4	*trans*-1,2-Dichloroethylene	0.10	0.05	400	13
5	1,1-Dichloroethane	0.10	0.10	100	90
6	Chloroform	0.10	0.04	40	52
7	1,1,1-Trichloroethane	0.05	0.04	40	1300
8	Carbon tetrachloride	0.05	0.02	20	2900
9	1,2-Dichloroethane	0.05	0.4	40	140
10	Trichloroethylene	0.10	0.08	20	790
11	1,2-dichloropropane	0.50	0.20	200	81
12	Bromodichloromethane	0.05	0.02	40	1600
13	2-Chloroethyl vinyl ether	0.10	0.10	200	57
14	*trans*-1,3-Dichloropropene	0.10	0.10	200	180
15	*cis*-1,3-Dichloropropene	0.10	0.10	200	160
16	1,1,2-Trichloroethane	0.10	0.40	200	110
17	Tetrachloroethylene	0.20	0.10	20	2300
18	Dibromochloromethane	0.05	0.05	20	1800
19	Bromoform	0.20	0.10	200	240
20	1,1,2,2-Tetrachloroethane	0.05	0.02	200	250
21	1,2,3-Trichloropropane	0.10	0.10	100	140
22	Hexachlorobutadiene	0.05	0.02	40	5500

mixtures, not for single compounds. Therefore, the working conditions and general evaluation were established following this criterion. Lower detection limits would be achieved if the method only involved the analysis of compounds having the highest response factors. In comparison with detection limits reported in the literature, those in Table 1 are lower than for methods such as those involving solvent extraction and GC [2], but higher than for PT methods with the direct vaporization of soil or sediment samples [16,18].

The ranges of linearity for the individual VOCs are also reported in Table 1. These values are expressed as the absolute amount in nanograms introduced into the PT device. According to the split flows of the ATD–GC system, the VOC amounts effectively arriving at the electron-capture detector represent only about 5% of the tabulated values. Again, the amounts indicated in Table 1 do not correspond to the detailed study of each compound but to the differences between compounds observed in the general evaluation of the method for the analysis of the standard mixtures shown in Fig. 1. According to these linearity ranges, a suitable working interval for all compounds is 0.4–20 ng. This interval has found to be adequate for the analysis of all field samples considered.

3.2. Recoveries

The performance of the SE–PT method (Table 2) was evaluated by means of diverse recovery tests. The leak tests (see Experimental) resulted in recoveries of 94–105% with an average value of 99%. The most volatile compound, trichlorofluoromethane, shows the lowest recovery, 94%, and the highest standard deviation, 17% ($n = 3$). The recoveries higher than 100% may correspond to slight contamination due to

Table 2
Results corresponding to the recovery experiments of the 20 compounds included in the two reference mixtures used for quantification (units in μg/ml of methanol; 100% recovery corresponds to 0.8 μg/ml)

No.	Compound	Leak test, only glassware ($n = 3$)		Sand, 24 h (mean, $n = 2$)	Silt, 24 h (mean, $n = 2$)	Sediment, 24 h ($n = 4$)		Sediment, 50 days ($n = 4$)	
		Mean	S.D.			Mean	S.D.	Mean	S.D.
1	Trichlorofluoromethane	0.75	0.14	0.87	0.89	0.88	0.032	0.66	0.087
2	1,1-Dichloroethylene	0.79	0.050	0.84	0.80	0.83	0.030	0.72	0.022
3	Dichloromethane	0.84	0.040	0.88	0.92	0.90	0.087	0.74	0.033
4	*trans*-1,2-Dichloroethylene	0.80	0.021	0.65	0.70	0.67	0.078	0.69	0.045
5	1,1-Dichloroethane	0.83	0.060	0.81	0.77	0.79	0.051	0.76	0.038
6	Chloroform	0.82	0.025	0.80	0.78	0.79	0.032	0.76	0.048
7	1,1,1-Trichloroethane	0.79	0.010	0.70	0.66	0.68	0.037	0.66	0.072
8	Carbon tetrachloride	0.79	0.0	0.78	0.76	0.77	0.014	0.72	0.017
9	1,2-Dichloroethane	0.80	0.0058	0.73	0.73	0.73	0.028	0.70	0.045
10	Trichloroethylene	0.77	0.010	0.72	0.68	0.70	0.029	0.72	0.029
11	1,2-Dichloropropane	0.79	0.012	0.77	0.74	0.76	0.025	0.73	0.029
12	Bromodichloromethane	0.79	0.0058	0.75	0.74	0.75	0.015	0.75	0.024
13	2-Chloroethyl vinyl ether	0.76	0.12	0.67	0.87	0.73	0.13	0.65	0.11
14	*trans*-1,3-Dichloropropene	0.79	0.020	0.69	0.67	0.68	0.025	1.07	0.051
15	*cis*-1,3-Dichloropropene	0.79	0.017	0.70	0.68	0.69	0.022	0.38	0.021
16	1,1,2-Trichloroethane	0.76	0.11	0.65	0.70	0.68	0.13	0.64	0.041
17	Tetrachloroethylene	0.78	0.012	0.76	0.76	0.76	0.0096	0.73	0.024
18	Dibromochloromethane	0.77	0.070	0.69	0.82	0.73	0.10	0.74	0.028
19	Bromoform	0.78	0.020	0.71	0.69	0.70	0.017	0.69	0.033
20	1,1,2,2-Tetrachloroethane	0.76	0.040	0.70	0.64	0.67	0.048	0.69	0.047
	All compounds	0.79		0.74	0.75	0.74		0.71	

the presence of VOCs in the atmosphere of the laboratory.

Two types of solid matrices, a sand (20% water content, 0.27% organic carbon) and a silt (17% water content, 0.64% organic carbon), were used for the tests involving a suspension of the standard solution with sediments. The results are illustrated in Fig. 1, where the chromatograms corresponding to the standard mixtures and to the recovered methanol extracts after suspension in silt are shown. In the two series of experiments the recoveries ranged between 81 and 110% (average 92.5%) and between 80 and 115% (average 94%) for sand and silt, respectively (Table 2). The Student's *t*-test evaluation of the average values obtained with the two types of sediments showed no significant difference for any of the VOCs included in the study. For this reason, the results corresponding to both series of sediments were grouped together, averaged and used for comparison with other tests.

These average results are also given in Table 2. Their comparison with the leak test described above indicates a general trend to lower VOC recoveries in the presence of sediments. Thus, the total average recoveries of the experiments with and without sediments are 92.5% and 99%, respectively. Conversely, in the case of the most volatile compounds, trichlorofluoromethane, 1,1-dichloroethylene, dichloromethane [boiling points at 1 atm (101 325 Pa) = 24, 37 and 40°C, respectively], the average recoveries of the sediment suspension tests do not show any further decrease, which points to a very limited interaction between these VOCs and the sedimentary matrices. In this respect, none of the average recoveries of these three compounds show significant differences between the two experiments when evaluated with the Student's *t*-test.

The general trend to lower recoveries in the presence of sediments is influenced by the amount of sediment used for suspension. This is shown in Fig. 2, where the results of diverse recovery tests in the presence of various amounts of sediments are represented for selected VOCs. A slight decrease in recoveries with increasing amounts of sediment is observed. In principle, sample amounts of the order of 1 g are preferred although limits of detection (and hence VOC concentrations in the sediments under study) will also have to be taken into account.

One of the main advantages sought by this combined SE–PT method concerns the lack of dependence between the sampling and analytical operations. The methanol extracts can be stored at −20°C in the aluminium-sealed vials for extended periods of time, which allows large numbers of samples to be taken without the need for immediate instrumental analysis. In order to test the effectiveness of this approach, VOC losses after long periods of storage were tested. For this purpose, the methanol extracts obtained after the sediment suspension experiments were stored at −20°C in the aluminium-sealed vials for 50 days and analysed again after this period. The results are also given in Table 2. The recoveries range between 80 and 95% (results for *trans*- and *cis*-1,3-dichloropropene not included) with an average value of 89%. That is, the losses after this long period of storage only represent an additional VOC loss of 4% in relation to the initial recovery values. This small loss indicates that the differences are not significant for most VOCs when evaluated with the Student's *t*-test.

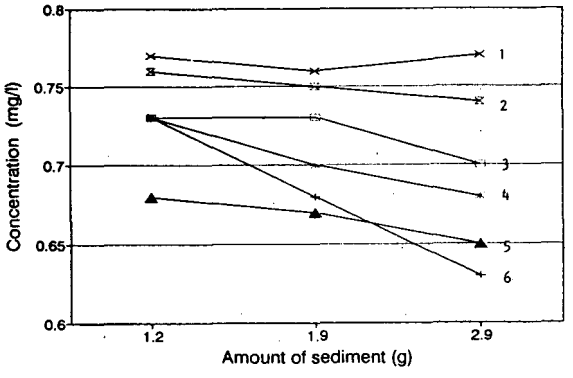

Fig. 2. Recovered concentrations of selected VOC on water suspension with increasing amounts of sediment. 1 = CCl_4; 2 = tetrachloroethylene; 3 = dibromochloroethane; 4 = 1,2-dichloroethane; 5 = 1,1,2-trichloroethane; 6 = 2-chloroethyl vinyl ether.

However, with the most volatile compounds, trichlorofluoromethane, 1,1-dichloroethylene and dichloromethane, the Student's *t*-test shows that the average recovery differences, −14, −8 and −6%, respectively, are significant (confidence levels 99.5, 99.5 and 97.5%, respectively). This is probably due to vapour losses during the long period of 50 days despite storage at −20°C. Significant differences were also observed with the two perchlorinated compounds, carbon tetrachloride and tetrachloroethylene (−6 and −4%, Student's *t*-test confidence levels of 99.5 and 95%, respectively). It is known that these two solvents may undergo oxidation in humid conditions [20–22] and the decrease in concentration seems more likely to be due to this type of process occurring during the long storage period than to evaporation losses that are not observed with other more volatile compounds.

Another interesting aspect concerns *trans*- and *cis*-1,3-dichloropropene, with significant differences in average values at the 99.95% confidence level. Nevertheless, the concentrations of these two compounds are decreased for the *cis* isomer, 0.38 μg/ml, and increased for the *trans* isomer, 1.07 μg/ml. If the concentrations of both species are averaged, 0.72 μg/ml (S.D. 0.37 μg/ml), there is no significant decrease in the total amount of 1,3-dichloropropene which corresponds to a conversion of the *cis* into the *trans* isomer during the 50 days of storage at −20°C.

3.3. Real case studies

Several chromatograms corresponding to sediments collected in aquatic systems situated in the area of influence of two organochlorinated solvent factories are shown in Fig. 3. The concentrations are given in Table 3. Fig. 3A corresponds to sediments collected near a chemical factory situated in Flix and Fig. 3B and C correspond to chromatograms from sediments

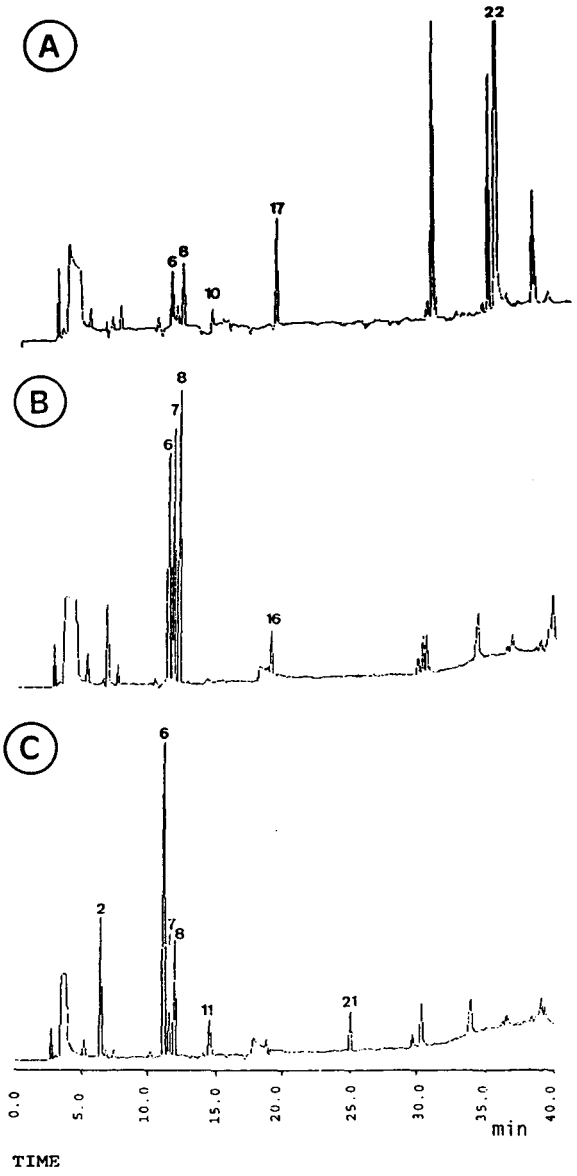

Fig. 3. Chromatograms showing the VOC extracts from sediments collected in (A) Flix and (B and C) Alagoas (see Table 3). Peak numbers refer to Table 2.

sampled in the chlorochemical complex of Alagoas (Brazil). These chromatograms are generated from the analysis of 1–3 g of sediment and, after the dilution steps determined in the GC–PT method, correspond to the effective injection of the extract equivalent to a sample amount of 2–6 mg. This procedure allowed the determination of all trace VOCs present in the samples. However, further dilution (fivefold) was required for quantification of one major compound, hexachlorobutadiene (No. 22 in Fig. 3A).

Three compounds are common to all three samples, chloroform, 1,1,1-trichloroethane and carbon tetrachloride, which correspond to solvents usually synthesized in these types of factories. Carbon tetrachloride may also be a side-product generated in the synthesis of other organochlorinated solvents. As indicated above, the operating conditions selected for the DB-624 column used in this study allow the baseline resolution of these three compounds. Other VOCs, *i.e.*, trichloroethylene, 1,2-dichloropropane, 1,1,2-trichloroethane, tetrachloroethylene, 1,2,3-trichloropropane and hexachlorobutadiene, only occur in some of the samples. In this respect, hexachlorobutadiene (71 μg/g) is a characteristic compound of the air, waters and sediments surrounding the Flix factory and 1,2-di- and 1,2,3-trichloropropane (26 and 10 μg/g, respectively) were used as raw materials in the Alagoas complex.

4. Conclusions

The limits of detection and linearity ranges of the combined SE–PT method considered in this study were tested for a group of 20 standard halogenated VOCs. The results showed that the method provides suitable parameters for the determination of volatile organochlorinated compounds in sediments. These standards were also used for diverse recovery calculations showing that, on average, only 1% of the individual amounts is lost in the glassware manipulations. Further, recovery experiments involving water sediment suspensions with the standards and storage of the methanol extracts for 1 and 50 days resulted in average losses of 7.5 and 11%, respectively. These relatively small values show the usefulness of the method and confirm that, with the system and conditions of storage select-

Table 3
VOC concentrations (μg/g) in sediments from aquatic systems receiving discharges from organochlorinated solvent factories

No.	Compound	Flix (A)	Alagoas (B)	Alagoas (C)
2	1,1-Dichloroethylene	n.d.[a]	n.d.	22
6	Chloroform	0.2	0.3	0.6
7	1,1,1-Trichloroethane	n.d.	1.0	0.4
8	Carbon tetrachloride	0.1	0.2	0.1
10	Trichloroethylene	0.1	n.d.	n.d.
11	1,2-Dichloropropane	n.d.	n.d.	26
16	1,1,2-Trichloroethane	n.d.	0.2	n.d.
17	Tetrachloroethylene	0.3	n.d.	n.d.
21	1,2,3-Trichloropropane	n.d.	n.d.	10
22	Hexachlorobutadiene	71	n.d.	n.d.

[a] n.d. = Not detected.

ed in this study, the concentration measurements are not significantly affected by long delay periods between sampling and analysis. Hence the present SE–PT method appears to be particularly useful in applications where the long distances between the area of study and the instrumental equipment do not allow the immediate determination of the VOC species. In fact, after 50 days of storage no significant decrease in VOC concentration was observed except for the more volatile compounds such as trichlorofluoromethane, 1,1-dichloroethylene and dichloromethane (boiling points at 1 atm lower than 40°C), two perchlorinated compounds, carbon tetrachloride and tetrachloroethylene, and the 1,3-dichloropropenes, among which a conversion from the *cis* to the *trans* isomer is observed.

Acknowledgements

This work was sponsored by the Junta de Residus of the Generalitat de Catalunya (Catalan Autonomous Government). O.C.A. is grateful for a fellowship grant from the Conselho Nacional de Desenvolvimento Científico e Tecnológico de Brazil.

References

[1] H.J.Th. Bloemen and J. Burn (Editors), *Chemistry and Analysis of Volatile Organic Compounds in the Environment*, Blackie, London, 1993.
[2] I.R. DeLeon, M.A. Maberry, E.B. Overton, C.K. Raschke, P.C. Remele, C.F. Steele, V.L. Warren and J.L. Laseter, *J. Chromatogr. Sci.*, 18 (1980) 85.
[3] R.L. Siegrist and P.D. Jenssen, *Environ. Sci. Technol.*, 24 (1990) 1387.
[4] V.D. Roe, M.J. Lacy, J.D. Stuart and G.A. Robbins, *Anal. Chem.*, 61 (1989) 2584.
[5] M.R. Milana, A. Maggio, M. Denaro, R. Feliciani and L. Gramiccioni, *J. Chromatogr.*, 552 (1991) 205.
[6] A. Maggio, M.R. Milana, M. Denaro, R. Feliciani and L. Gramiccioni, *J. High Resolut. Chromatogr.*, 14 (1991) 618.
[7] A.D. Hewitt, P.D. Miyares, D.C. Leggett and T.F. Jenkins, *Environ. Sci. Technol.*, 26 (1992) 1932.
[8] T.C. Voice and B. Kolb, *Environ. Sci. Technol.*, 27 (1993) 709.
[9] A. Preuss and R. Attig, *Fresenius' Z. Anal. Chem.*, 325 (1986) 531.
[10] N. Kirshen and E. Almasi, *J. High Resolut. Chromatogr.*, 14 (1991) 484.
[11] *Methods for Organic Chemical Analysis of Municipal and Industrial Wastewater*; *EPA-600/4-82-057*, US Environmental Protection Agency, Washington, DC, 1982.
[12] *Methods for the Determination of Organic Compounds in Drinking Water*; *EPA-600/4-88-039*, US Environmental Protection Agency, Washington, DC, 1988.
[13] M.H. Hiatt, *Anal. Chem.*, 53 (1981) 1541.
[14] M.J. Charles and M.S. Simmons, *Anal. Chem.*, 59 (1987) 1217.

[15] A. Bianchi and M.S. Varney, *J. High Resolut. Chromatogr.*, 12 (1989) 184.
[16] A. Bianchi, M.S. Varney and J. Phillips, *J. Chromatogr.*, 542 (1991) 413.
[17] Y. Yokouchi and M. Sano, *J. Chromatogr.*, 555 (1991) 297.
[18] X. Yan, K.R. Carney and E.B. Overton, *J. Chromatogr. Sci.*, 30 (1992) 491.
[19] J.L. Parr, G. Walters and M. Hoffman, in P.T. Kostecki and E.J. Calabrese (Editors), *Hydrocarbon Contaminated Soil and Groundwater*, Vol. 1, Lewis, Chelsea, MI, 1991, p. 105.
[20] K.C. Bailey and W.E.S. Hickson, *J. Chem. Soc.*, (1941) 145.
[21] M.R.A. Rao and B.S. Rao, *J. Indian Chem. Soc.*, 12 (1935) 322.
[22] M.R.A. Rao and B.S. Rao, *Chem. Zentralbl.*, I (1936) 1389.

ELSEVIER

Journal of Chromatography A, 675 (1994) 189–204

JOURNAL OF CHROMATOGRAPHY A

Supercritical fluid extraction of polychlorinated biphenyls from lyophilized fish tissue

Søren Bøwadt*[,a], Berit Johansson[a], Palle Fruekilde[a], Michael Hansen[a], Daniele Zilli[a], Bo Larsen[a], Jacob de Boer[b]

[a]*Environment Institute, CEC Joint Research Centre, TP 290, I-21020 Ispra (VA), Italy*

[b]*Netherlands Institute for Fisheries Research, P.O. Box 68, 1970 AB IJmuiden, Netherlands*

(First received January 28th, 1994; revised manuscript received March 22nd, 1994)

Abstract

A method for the rapid interference free analysis of polychlorinated biphenyl congeners (chlorinated biphenyls, CBs) in lyophilized fish tissue is presented. The method was developed on a lyophilized tuna muscle tissue that contained 2.8% lipid (dry mass based), and native CB concentrations in the range of 3–84 ng/g. Sample preparation was made by supercritical fluid extraction using pure CO_2 as extraction fluid. Analysis by high-resolution gas chromatography–electron-capture detection analysis was carried out with on-column injection on two parallel coupled columns, a 60 m DB-17 column and a series combination of a 25 m SIL-8 column and a 25 m HT-5 column. Supercritical fluid extraction was compared with Soxhlet extraction and found to give quantitative recoveries, detection limits of 0.5–2 ng/g and standard deviations of less than 5% on average. The developed method was confirmed on nine different lyophilized fish samples which contained 6.1–26.5% lipid (dry mass based), and native CB concentrations in the range 0.8–134 ng/g.

1. Introduction

The analysis of polychlorinated biphenyls (PCBs) plays an important role in the monitoring of environmental contamination [1]. Because fish are the main source of PCBs in the diet, they constitute a key matrix in the monitoring of these compounds [2]. PCBs accumulate in the lipid (fat) fraction of the tissue and previous extraction procedures anticipate the lipids and the PCBs to be extracted together [3]. This, however, also creates the major problem associated with the analysis of lipid-containing samples *i.e.* the tedious separation of lipids from analytes of interest in order not to ruin the final determination. Lipid separation is normally performed by gel permeation or column chromatography using Florisil or alumina [3–5]. The lipids can be divided into different groups, ranging from non-polar to more polar. Some lipids are bound to the tissue while others form the group of "free lipids" [3].

The most common method for the extraction of PCBs from lipid-containing matrices is Soxhlet extraction applied with a mixture of polar and non-polar solvents. Another generally applied

* Corresponding author. Present address: University of North Dakota, EERC, P.O. Box 9018, Grand Forks, ND 58202, USA.

SSDI 0021-9673(94)00290-P

the PCBs with a light aliphatic hydrocarbon. This method is believed to give the most thorough extraction of PCBs from fatty tissues, especially when the ratio of bound to "free" lipids is high [3]. Unfortunately, saponification is rather laborious. Also, some chlorinated pesticides that are often determined simultaneously, are destroyed during saponification [3]. For this reason Soxhlet has been a more popular choice for extraction of PCBs from animal tissues. As long as Soxhlet extraction is carried out with a mixture of polar and non-polar solvents for an adequate amount of time, this method is also thought to give quantitative recovery of PCBs [3].

Supercritical fluid extraction (SFE) has become increasingly popular in the recent years, and the number of reports on applications for different analytes in diverse matrices is rapidly growing [6–10]. There has, however, been a lack of thoroughly tested SFE methods for the routine monitoring of PCBs in environmental matrices which could replace conventional procedures. This is evident, as most of the published data on SFE have been acquired on spiked samples. When applied to real contaminated samples, SFE was found to be much more difficult than initially thought [11,12]. Therefore further effort is still required in the method development of SFE. It has previously been demonstrated that SFE with solid-phase trapping has the potential of simultaneous extraction, clean-up and concentration of PCBs from different matrices [13–16]. Although somewhat more complicated than conventional trapping in SFE (cryo and liquid trapping), solid-phase trapping is highly efficient and seems well suited for automation and consequently for routine analysis.

SFE of fatty matrices has been carried out on a number of occasions [7,13,17–20]. But in several of these reports the purpose of the extraction has been to get a quantitative yield of lipids rather than the associated analytes. This would also in most cases give high recoveries of PCBs and other lipid-soluble compounds but has the drawback of necessitating a following clean-up step before the final analysis by gas chomatography (GC) with electron-capture detection (ECD) or mass spectrometry (MS). The application of SFE to the analysis of PCBs in fish has only been reported a few times [21–23], and until now never for quantitative analysis of tissues contaminated with native PCB congeners (CBs) at low ng/g levels.

The principal objective of the work presented here was to investigate the use of SFE with solid-phase trapping in the analysis of fish tissues contaminated with native CBs at levels down to a few ng/g. Because many biological samples today are lyophilized in order to facilitate storage, lyophilized fish tissues were to be used instead of raw tissues. A secondary aim was to develop a method suitable for routine usage necessitating a minimum of labour and time consumption.

2. Materials and methods

2.1. Chemicals

The CBs used in this study were obtained as neat crystals from the Community Bureau of Reference (BCR), Brussels, Belgium (IUPAC numbers 28, 52, 101, 105, 118, 128, 138, 149, 153, 156, 170 and 180). The DDE and DDT standards were obtained from Supelco in a solution of known purity and concentration. All dilutions were made gravimetrically in isooctane.

The solvents used (acetone, *n*-hexane, *n*-heptane, isooctane and dichloromethane) were all pesticide grade (Merck, Darmstadt, Germany). The CO_2 and the methanol (MeOH)-modified CO_2 were all obtained as SFE/SFC grade from SIAD, Milan, Italy.

2.2. Fish samples

Nine fish samples (see Table 2) were collected at different sites of Lake Lugano. Depending on the size of the fish one or more were used in the following process. The edible parts of the fish were filleted, grinded with a meat grinder and lyophilized. The lyophilisation was done at 5°C for 48 h. After lyophilisation the dry muscle

tissue was ground in a mechanical grinding device (contact surfaces in ZrO_2) until a fine homogeneous powder was obtained. The powder was then sieved to remove remaining fibres, filled into sealed glass containers and stored at 5°C in darkness. In cases where more than one fish were used for one sample, dry mass and lipid content (based on dry mass) were calculated as an average (Table 2) [24].

The same procedure was used for the tuna fish (*Katsuwonus pelamis)* that was collected in the Mediterranean Sea. This fish had a dry mass of 18.5% and a lipid content of 2.8% (based on dry mass). This lyophilized tuna muscle tissue has been produced at the Environment Institute JRC Ispra, and a certification procedure for various elements and organic compounds is in course[a].

All lake fish (except perch III) were subjected to acid silica clean-up after SFE. This was essential because otherwise gradual column deterioration following on-column injection would occur. This step can be omitted if splitless injection is used instead of on-column. Extracts were loaded on a 10 cm × 3 mm column with activated silica impregnated with 40% (w/w) sulphuric acid (conc.) and eluted with 50 ml *n*-hexane. The eluent was evaporated and the residues were re-dissolved in 1.8 ml isooctane.

2.3. Supercritical fluid extraction

All the work presented was performed with a Hewlett-Packard 7680A supercritical fluid extractor. Fish extractions were prepared as follows: 2-g portions of lyophilized fish powder were mixed with 7 g of anhydrous Na_2SO_4 and packed into 7-ml extraction cells. In our experience on SFE with other types of matrices [14,15], pure CO_2 with a density of 0.75 g/ml (218 bar and 60°C) and a supercritical fluid flow of 1 ml/min normally gives high recoveries of PCBs with very little interfering compounds in the final *n*-heptane eluent. Therefore pure CO_2, without any kind of modifier, was chosen for the SFE to minimize the solubilisation of lipid from the lyophilized muscle tissues.

The method was developed on a tuna fish sample and the supercritical fluid extractions were compared using the following three sets of conditions:

COND-1: 30 min dynamic extraction with pure CO_2 at a density of 0.75 g/ml (218 bar) at 60°C with a flow of 1 ml/min.

COND-2: 10 min static extraction with pure CO_2 at a density of 0.75 g/ml (218 bar) at 60°C followed by 30 min dynamic extraction at the same density and temperature and with a flow of 1 ml/min.

COND-3: 10 min static extraction with pure CO_2 at a density of 0.75 g/ml (378 bar) at 97°C followed by 30 min dynamic extraction at the same density and temperature and with a flow of 1 ml/min.

The completeness of the extractions were examined using sequential extractions. Two different sequences were used:

SEQ-1: step A: identical to the one described under COND-2 above, followed by step B: 30 min dynamic extraction with CO_2 + 5% MeOH (same density, temperature and flow) followed by step C: 30 min dynamic extraction with pure CO_2 (density, temperature and flow as in COND-3).

SEQ-2: step A: identical to the one described under COND-3 above, followed by step B: 30 min dynamic extraction with CO_2 + 5% MeOH (same density, temperature and flow).

Finally the lakefish was analysed using the conditions COND-2 except for perch III, where the conditions COND-1 were used.

For all extractions the nozzle temperature was kept constant at 45°C and the trap was kept at a temperature of 20°C when pure CO_2 was used but 65°C when methanol was used as modifier [14].

The trap was filled with approximately 1 ml Florisil (0.16–0.25 mm particle size) as trapping material and was eluted with 2 × 1.5 ml *n*-heptane, then 1 × 1.5 ml dichloromethane followed by 2 × 1.5 ml *n*-heptane after the end of each individual extraction. A 50-μl volume of internal

[a] For further information please contact H. Muntau or M. Bianchi, Environment Institute, CEC Joint Research Centre (JRC), I-21020 Ispra, Italy.

standard (PCB 35 and PCB 169, at 2.16 ng/μl and 0.43 ng/μl, respectively) was added to the individual fractions and the final volume was adjusted to 1.8 ml with *n*-heptane resulting in internal standard concentrations of *ca.* 60 pg/ml for PCB 35 and *ca.* 12 pg/ml for PCB 169.

2.4. Soxhlet extraction

Aliquots of 2 g of lyophilized fish powder were mixed with 7 g of anhydrous Na_2SO_4 and extracted with 250 ml of *n*-hexane–acetone (2:3) for 18 h. The solvents were evaporated on a rotary evaporator at 30°C, the residues were weighed (to determine the lipid content) and dissolved in 10 ml of *n*-hexane. Extracts were loaded on a 15 cm × 6 mm column with activated silica impregnated with 40% (w/w) sulphuric acid and eluted with 50 ml *n*-hexane. The eluent was evaporated and the residues were re-dissolved in 1.5 ml isooctane. Internal standards were added (PCB 35 and 169, as for the supercritical fluid extractions) and the final volume was adjusted to 1.8 ml with isooctane.

The extractions at the laboratory in IJmuiden were performed with 500 ml *n*-pentane–dichloromethane (1:1) for 12 h. Clean-up was carried out over 15 g alumina (6% water) and fractionation over 1.8 g silica (1.5% water) [25].

2.5. Dual-column gas chromatography

The extracts were analysed using a pressure-controlled Hewlett-Packard (HP) 5890 II gas chromatograph equipped with heatable on-column injector (run in oven track mode) and two ^{63}Ni electron-capture detectors held at 300°C [purged with 60 ml/min of argon–methane (90:10)] and a HP 7673A auto sampler.

Aliquots (1 μl) of the extracts were on-column injected on two parallel coupled columns, a 60 m × 0.25 mm, 0.25 μm 50% diphenyl-dimethyl-siloxane DB-17 column (J & W Scientific) and a series combination of a 25 m × 0.25 mm, 0.25 μm 5% diphenyl-dimethyl-siloxane SIL-8 column (Chrompack) and a 25 m × 0.22 mm, 0.10 μm 1,7-dicarba-closo-dodecarborane-dimethyl-polysiloxane HT-5 column (Scientific Glass Engineering). The columns were installed in the GC oven together with a deactivated 2 m × 0.53 mm fused-silica retention gap using a quick-seal glass "T".

The GC oven program was the following: initial temperature 90°C, retained for 2 min, then increased at a rate of 20°C/min to 170°C, retained for 7.5 min, then increasing at a rate of 3°C/min to 275°C retained for 10 min. Hydrogen linear velocity was approximately 43 cm/s, held constant by the pressure-controlled inlet throughout the whole temperature programme (starting pressure 1.7 atm at 90°C; 1 atm = 101 325 Pa). This choice of columns and GC conditions has previously been shown to give optimum separation of CBs and organochlorine pesticides [26].

Quantitative measurements of CBs and pesticides were performed using peak heights after a 7-point multilevel calibration curve (5-point for the pesticides) using the power fit calibration routine provided with the HP Chem 3365 software. CBs were calibrated in the concentration interval of 1.7 to 573 pg/μl where the intervals for the pesticides were 6.3 to 200 pg/μl (see Table 3 for the exact individual calibration range for the fish powder). Standards were injected after every fifth sample to determine deterioration of separation or drift. New calibrations were performed if the results for the standards drifted by more than 10%.

Chromatograms shown in Figs. 1–3 were performed on a 50 m × 0.22 mm, 0.25 μm 5% diphenyl-1,7-dicarba-closo-dodecarborane-dimethyl-polysiloxane HT-8 column (Scientific Glass Engineering) run under identical conditions as described above.

The GC analyses at the laboratory in IJmuiden were performed with a Perkin-Elmer 8320 gas chromatograph with splitless injection (injector temperature 270°C) and a ^{63}Ni electron-capture detector held at 360°C using 60 ml/min nitrogen as purge gas. The GC was equipped with a 50 m × 0.15 mm (0.30 μm film thickness) CP-Sil 19

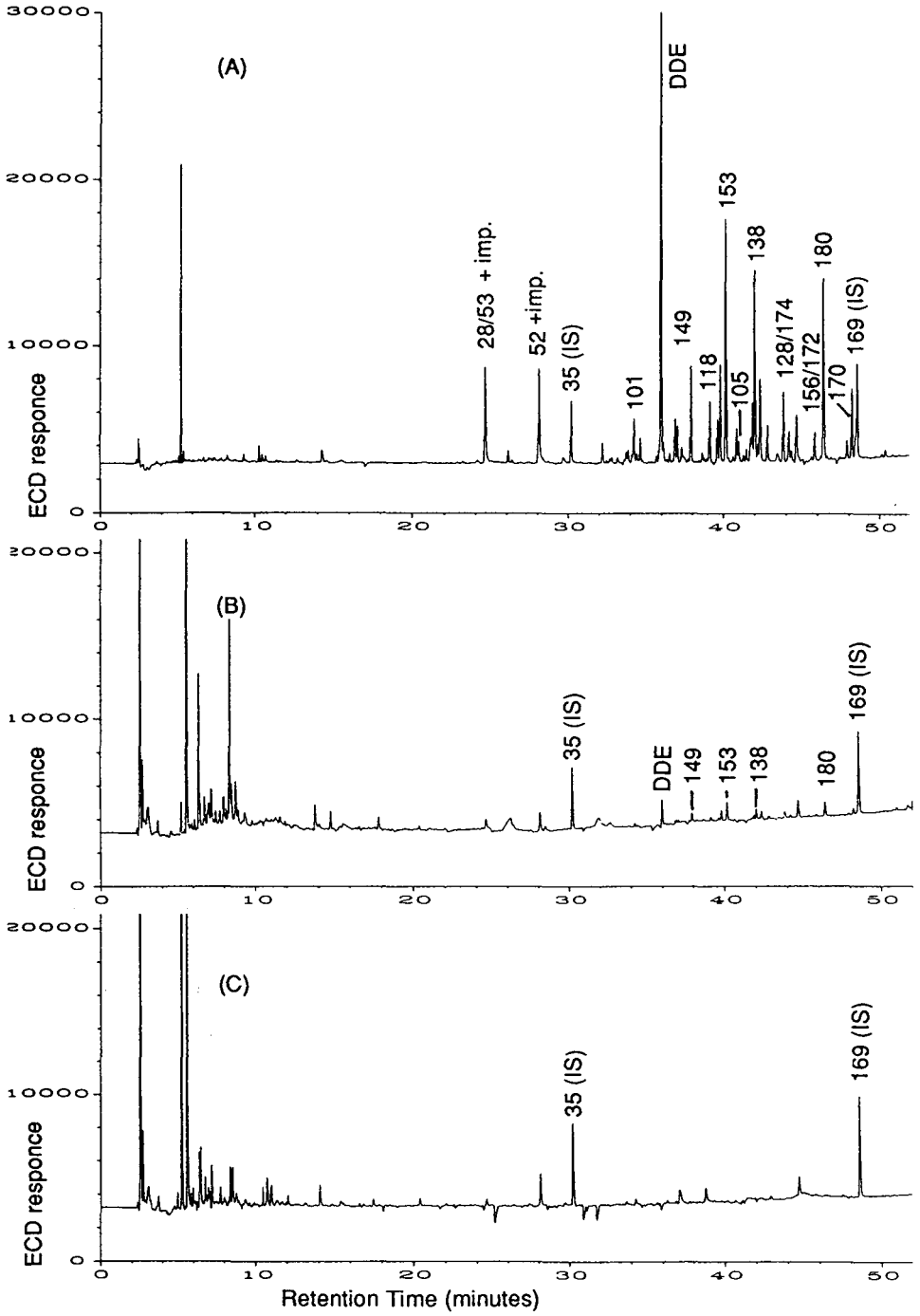

Fig. 1. GC–ECD chromatograms (HT-8) of sequential extractions (SEQ-1) of the lyophilized tuna muscle tissue: (A) 2 g of lyophilized tuna extracted by SFE with pure CO_2 (10 min static and 30 min dynamic, 0.75 g/ml, 218 atm, 60°C, 1 ml/min), (B) 30 min dynamic extraction with CO_2 + 5% MeOH of the tuna tissue already extracted in A (same SFE parameters as A), (C) 30 min dynamic extraction with pure CO_2 (0.75 g/ml, 378 atm, 97°C, 1 ml/min) of the tuna tissue already extracted in B.

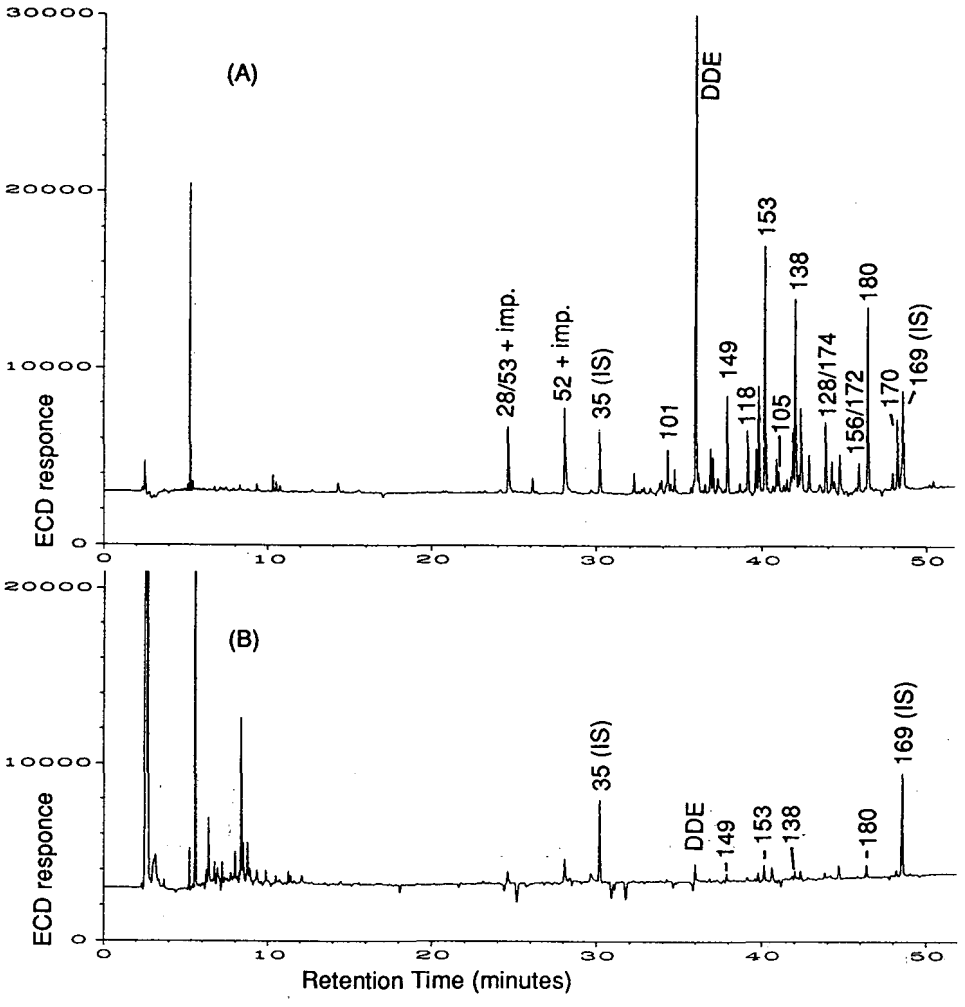

Fig. 2. GC–ECD chromatograms (HT-8) of sequential extractions (SEQ-2) of the lyophilized tuna muscle tissue: (A) 2 g of lyophilized tuna extracted by SFE with pure CO_2 (10 min static and 30 min dynamic, 0.75 g/ml, 378 atm, 97°C, 1 ml/min), (B) 30 min dynamic extraction with CO_2 + 5% MeOH of the tuna tissue already extracted in A (same SFE parameters as A).

column run with hydrogen as carrier gas at a linear gas velocity of 35 cm/s [27].

3. Results and discussion

3.1. Method development: SFE at different conditions compared with Soxhlet extraction

The developing experiments were carried out on a lyophilized tuna muscle tissue which was available in large quantities and was known to be contaminated with PCBs at easily detectable levels[a].

The supercritical fluid extractions were carried out under three rather similar conditions and the results compared with Soxhlet. The results are listed in Table 1. It can easily be seen that the fully dynamical extraction conditions (COND-1) give 10–25% lower recoveries than Soxhlet.

[a] For further information please contact H. Muntau or M. Bianchi, Environment Institute, CEC Joint Research Centre, I-21020, Italy.

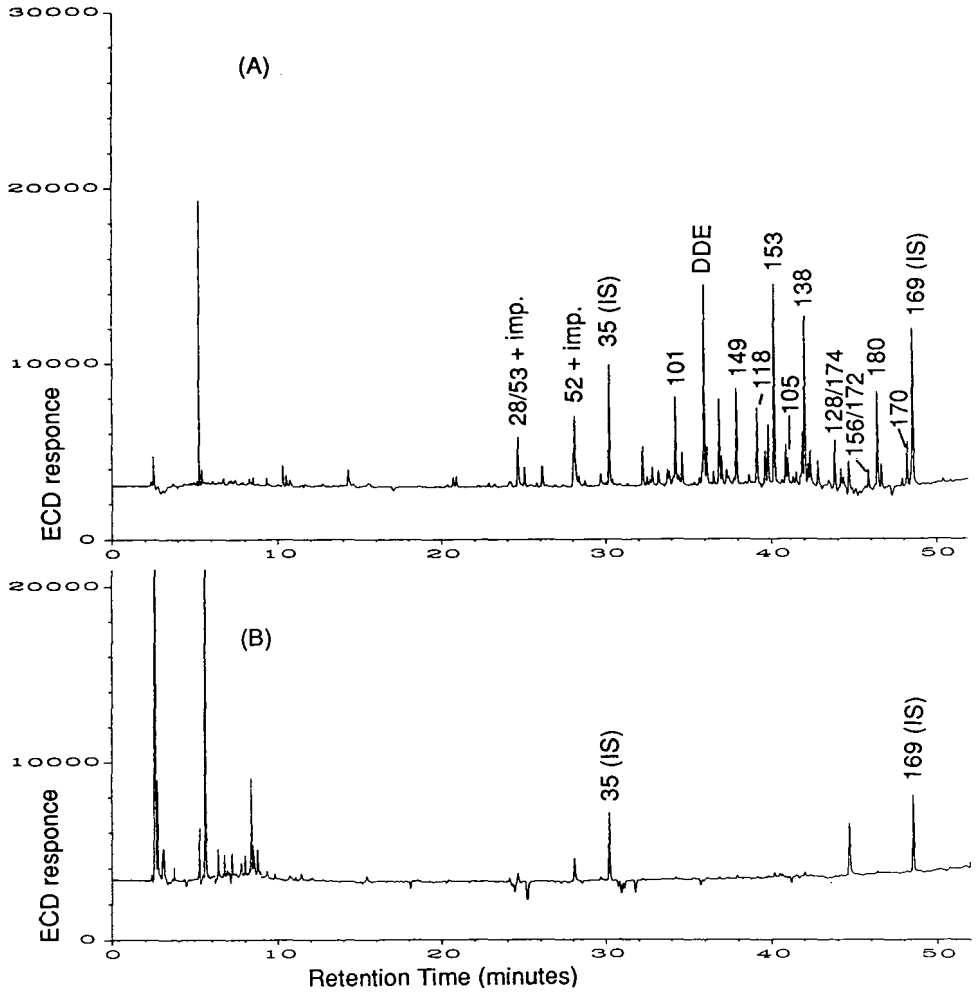

Fig. 3. GC–ECD chromatograms (HT-8) of sequential extractions (SEQ-2) of the lyophilized tench muscle tissue: (A) 2 g of lyophilized tench extracted by SFE with pure CO_2 (10 min static and 30 min dynamic, 0.75 g/ml, 378 atm, 97°C, 1 ml/min), (B) 30 min dynamic extraction with CO_2 + 5% MeOH of the tench tissue already extracted in A (same SFE parameters as A).

However by adding a 10-min static extraction step (COND-2), values virtually identical to the Soxhlet values were obtained. In the third set of experiments the temperature was raised to 97°C while keeping the density constant (COND-3). The reason for this was that it has been reported that extraction at higher temperature rather than higher density results in a more exhaustive extraction [11,28]. Also in our case we have higher recoveries of CBs, but the differences are generally too low to be significant. One drawback to the extraction at high temperature, however, was that the eluents contained interfering compounds in concentrations too high to inject directly for GC–ECD without a previous clean-up. Using these conditions results in the loss of easy automatization contrary to the extraction at lower temperature (60°C) where additional clean-up is not necessary.

From Table 1, it can also be seen, that the standard deviations for extractions performed at COND-1 and COND-3 are significantly higher than for COND-2 and Soxhlet which are of the same magnitude. For the data under COND-1

Table 1
Comparison of Soxhlet extraction with SFE using different extraction conditions for a tuna muscle tissue

PCB	SFE, COND-1		SFE, COND-2		SFE, COND-3		Soxhlet	
	Mean (ng/g dry mass)	S.D. (ng/g)	Mean (ng/g dry mass)	S.D. (ng/g)	Mean (ng/g dry mass)	S.D. (ng/g)	Mean (ng/g dry mass)	S.D. (ng/g)
28	<1	–	<1	–	<1	–	<1	–
52	2.1	0.5	3.1	0.1	3.4	0.2	3.1	0.1
101	12.7	1.3	16.9	0.3	18.6	1.1	16.9	0.2
105	6.8	0.3	6.9	0.1	7.7	0.2	7.2	0.3
118	20.3	1.6	23.5	0.4	23.4	0.8	23.4	0.3
128	6.3	0.3	7.1	0.2	7.8	0.2	7.1	0.1
138	59.1	3.3	62.0	1.4	58.8	2.1	62.4	1.4
149	25.5	1.7	34.4	1.1	36.5	1.3	33.1	0.9
153	67.0	4.2	84.0	2.2	83.1	3.1	79.6	2.6
156	4.6	0.3	4.5	0.1	4.9	0.3	4.4	0.1
170	9.7	0.5	12.0	0.4	13.7	0.2	11.5	0.2
180	41.7	1.7	50.2	1.0	50.9	1.7	49.0	0.7

COND-1 = 30 min dynamic extraction with carbon dioxide at 60°C, without clean-up (four replicates); COND-2 = 10 min static and 30 min dynamic extraction with carbon dioxide at 60°C, without clean-up (four replicates); COND-3 = 10 min static and 30 min dynamic extraction with carbon dioxide at 97°C, with clean-up (five replicates); Soxhlet = 18 h with 250 ml hexane–acetone (2:3), with clean-up (two replicates). S.D. = Standard deviation.

this is probably explained by an incomplete extraction, while for the data under COND-3 the more complex sample handling together with the larger amount of co-extracted compounds (lipids etc.) possibly leads to higher standard deviations.

3.2. Method development: effect of sequential extractions

In the past couple of years a number of results have been published proving that Soxhlet extraction does not necessarily give exhaustive extraction even at optimized conditions [11,29]. Recently a three-step method for the validation of a quantitative SFE method has been proposed [28]:

(1) Determination of the recovery with known concentrations of spiked compounds.

(2) Comparison of the recoveries of native analytes with those achieved using conventionally accepted extraction methods (including the use of standard reference materials).

(3) Performing multiple sequential extractions of the same sample with increasingly stronger extraction conditions.

The present SFE method (COND-2) was validated according to this three-step approach:

(1) For the system used in these experiments, studies on spiked samples demonstrating the trapping ability as well as on a certified reference material (CRM 392, sewage sludge) have been published elsewhere [14,15].

(2) The SFE method was compared with Soxhlet extraction (Table 1).

(3) Two different sequential extractions were conducted on the tuna fish.

The chromatograms resulting from the sequential extractions together with the different parameters used can be seen in Figs. 1 and 2. It is apparent that the first extraction, both at 60°C (SEQ-1) and 97°C (SEQ-2), is not completely exhaustive. In both cases the second extraction with CO_2 + 5% MeOH (known to increase extraction efficiency for most target analytes [8–12]) releases 5–8% additional CBs together with impurities and lipids. These findings demonstrate that relying on a single technique for validation of a method can result in misleading conclusions. The last extraction with pure CO_2 (Fig. 1C) at 97°C only extracts additional impurities and

lipids with no trace of PCBs. The conclusion is that it is only possible to talk about quantitative or near-quantitative recovery if a sequential extraction with increasing strength of extraction has been performed (this does not only apply to SFE but also to other methods).

When sequential extractions were performed on a fish with higher lipid content, however, no additional extractable PCB was observed. Fig. 3 shows the sequential extraction for the tench that has a lipid content of 9.4% (based on dry mass) —more than three times greater than the tuna fish (2.8%). As the bound lipid content in fish is normally around 2.5% [3], the ratio of bound to free lipid for the tuna is very high which makes this fish quite difficult to analyse in comparison with other more-lipid-containing fish. Given that the difference in extraction efficiency for COND-2 and COND-3 is almost negligible, and since the eluates from COND-2 are considerably cleaner, it was decided to use the parameters in COND-2 for method confirmation on nine different lake fish.

3.3. Method confirmation using unknown lyophilized fish samples

The developed SFE method was applied to nine different lyophilized fish sampled in Lake Lugano in the course of a larger survey [24]. The fish investigated are listed in Table 2 together with their respective dry mass, lipid content (based on the dry mass) and the total number of fish used for lyophilization. The fish were selected to represent the largest possible differences in dry mass and in lipid content. With this selection it was hoped also to find large differences in the contents of PCBs, DDT, DDE and DDD between the different fish species and in this way to provide the strictest possible test for the proposed method. As a comparison Soxhlet extraction for 18 h with 250 ml hexane–acetone (2:3) was selected, which was also used for the tuna fish.

During the analysis of the selected fish it was realised that there was a difference using the SFE method on lean fish and on fat fish. For the lean fish such as the tuna no problems concerning lipids in the eluent were experienced. But as the lipid content of the fish increased also the lipid content in the eluent increased. Even if the eluents only contained relatively small amounts of lipids, their prolonged injection (on-column) in GC–ECD were leading to a gradual deteriorating of the resolution of the columns and necessitating a replacement of the retention gap. Because no GC–ECD with split–splitless injection was available (that would minimize the problem substantially), it was decided to do a fast clean-up over acid silica (40% sulphuric acid) for all the lake fish concerned, except for the leanest fish (perch III) that was also ex-

Table 2
Details on the nine fish used for method confirmation

Fish	Dry mass (%)	Fat content (%)[a]	No. of fish used[b]
Bleak (*Alburnus alburnus*)	23.8	26.5	30
Largemouth bass (*Micropterus salmoides*)	22.3	17.0	4
Carp (*Cyprinius carpio*)	21.8	16.1	1
Burbot (*Lota lota*)	18.6	11.8	8
Pike perch (*Stizostedion lucioperca*)	25.0	9.7	1
Tench (*Tinca tinca*)	30.2	9.4	1
Perch I (*Perca fluviatilis*)	21.9	8.9	11
Perch II (*Perca fluviatilis*)	20.1	8.2	8
Perch III (*Perca fluviatilis*)	22.0	6.1	11

[a] Calculation of fat content is based on the dry mass.
[b] The number of fish used for lyophilization in the pooled samples.

tracted without the static step of 10 min. We did, however, analyse some of the extracts before clean-up by GC–MS with split–splitless injection without detecting any effect on the resolution of the column. To take full advantage of the method it is therefore recommendable to use splitless injection for routine analysis of lyophilized fish samples with lipid contents higher than 8–10%.

Table 3 shows the calibrated range for the lyophilized fish tissue according to the specifications in the Materials and methods section together with the detection limits for the method and the column used for quantification. The detection limits were established as the lowest amount of CBs as well as DDT, DDE and DDD detected in the lyophilized muscle tissue samples giving a signal-to-noise ratio greater than 10. No attempt was made to concentrate the extracts further, which means that a detection limit of 2 ng/g dry mass corresponds to an injected amount of approximately 1 pg/compound that is split (1:1) on the two columns. In environmental samples it is not likely that concentrations below our detection limits may cause any concern for the CBs considered in this study.

Generally, there was a good agreement between quantifications on the two different columns used. The choice of what congener to be quantified on which column was based on the knowledge of possible co-elutions [30] (Table 3). In a few cases where obvious interferences were encountered, the lowest results of the two columns were accepted as the results closest to the true value.

In Table 4 the quantitative results of the SFE are listed together with the values from Soxhlet extraction for comparison. The highest amounts of pollutants were generally found in largemouth bass with up to 134 ng/g of CB 153 and 129 ng/g of DDE, whereas the lowest amounts were found in burbut with down to 0.77 ng/g of CB 156 and less than 2 ng/g of DDT. The large dynamic range of concentrations for which the method works satisfactory is worth noting. The relative standard deviations are on average around 5%, lowest with 1–2% for the highest concentrations and highest with approximately 10% for the concentrations close to the detection limits. The relative standard deviations for the SFE experiments are generally of the same

Table 3
Analytical details on the method used for method confirmation

PCB	Calibrated range (ng/g dry mass)[a]	Detection limit (ng/g dry mass)[b]	Column used for quantitation[c]
28	2.8–300	1.5	SIL-8–HT-5
52	4.8–516	1.5	SIL-8–HT-5
101	3.4–366	1	SIL-8–HT-5
105	1.7–183	1	DB-17
118	2.0–216	1.5	SIL-8–HT-5
128	1.7–183	0.5	SIL-8–HT-5
138	2.2–236	1	DB-17
149	2.7–293	1	SIL-8–HT-5
153	1.9–210	1	SIL-8–HT-5
156	1.4–150	0.5	SIL-8–HT-5
170	1.7–181	1	SIL-8–HT-5
180	1.6–168	1	SIL-8–HT-5
DDE	5.9–183	2	SIL-8–HT-5
DDD	5.9–183	2	DB-17
DDT	5.9–183	2	SIL-8–HT-5

[a] The calibrated range for the fish powder according to the specifications in the Materials and methods section.
[b] Detection limits are the lowest amounts of CBs, DDT, DDE and DDD giving a $S/N > 10$.
[c] In general values quantified on the listed columns were used; when the other column was giving smaller values for one type of fish values from this column were used.

Table 4
Comparison of Soxhlet and SFE on nine fish samples

Fish	PCB (ng/g dry mass)	Soxhlet (mean ± S.D.), (ng/g dry mass)	SFE, COND-2 (mean ± S.D.), (ng/g dry mass)	Relative recovery (Soxhlet = 100) (%)
Bleak	28	4.0 ± 0.2	4.6 ± 0.1	114
	52	12.6 ± 0.9	15.3 ± 0.8	122
	101	30.7 ± 1.8	37.0 ± 1.2	120
	105	7.1 ± 0.3	8.1 ± 0.4	114
	118	24.3 ± 0.9	27.4 ± 1.0	113
	128	5.3 ± 0.3	6.0 ± 0.3	113
	138	34.7 ± 0.3	38.4 ± 0.8	111
	149	28.0 ± 1.9	33.8 ± 1.5	121
	153	44.9 ± 3.1	51.7 ± 1.8	115
	156	2.7 ± 0.1	3.2 ± 0.2	118
	170	4.9 ± 0.4	5.4 ± 0.2	111
	180	21.4 ± 0.6	23.2 ± 0.7	108
	DDE	82.5 ± 4.6	89.5 ± 2.8	108
	DDD	12.0 ± 0.8	13.1 ± 0.8	108
	DDT	3.6 ± 0.2	4.0 ± 0.2	110
Largemouth bass	28	5.7 ± 0.3	5.6 ± 0.2	98
	52	19.1 ± 0.3	19.1 ± 0.3	100
	101	62.1 ± 1.3	64.6 ± 1.6	104
	105	15.0 ± 0.7	16.2 ± 0.7	108
	118	52.5 ± 2.1	55.8 ± 1.7	106
	128	12.1 ± 0.6	13.1 ± 0.1	108
	138	98.6 ± 4.5	107 ± 4.6	108
	149	59.7 ± 1.4	62.6 ± 1.5	105
	153	126 ± 5.1	134 ± 3.8	106
	156	7.7 ± 0.2	8.0 ± 0.1	104
	170	14.9 ± 0.8	15.6 ± 0.3	105
	180	68.5 ± 3.6	74.7 ± 1.2	109
	DDE	129 ± 7.2	141 ± 6.4	110
	DDD	10.0 ± 0.2	18.1 ± 0.9	181
	DDT	12.2 ± 0.7	14.2 ± 0.5	116
Carp	28	3.4 ± 0.4	3.7 ± 0.1	107
	52	11.4 ± 1.3	12.0 ± 0.2	105
	101	24.0 ± 2.6	25.1 ± 0.7	104
	105	4.5 ± 0.5	5.0 ± 0.1	111
	118	20.2 ± 2.3	20.7 ± 0.4	102
	128	4.3 ± 0.5	4.6 ± 0.1	105
	138	34.8 ± 3.8	39.9 ± 0.6	115
	149	21.9 ± 2.2	22.2 ± 0.8	101
	153	43.8 ± 4.5	45.1 ± 0.6	103
	156	2.8 ± 0.3	3.3 ± 0.2	115
	170	5.9 ± 0.5	6.1 ± 0.1	104
	180	25.9 ± 2.7	27.9 ± 0.3	108
	DDE	43.8 ± 4.0	43.6 ± 0.6	100
	DDD	7.4 ± 1.0	8.1 ± 0.2	110
	DDT	3.7 ± 0.5	3.8 ± 0.1	103

(Continued on page 200)

Table 4 (*continued*)

Fish	PCB (ng/g dry mass)	Soxhlet (mean ± S.D.), (ng/g dry mass)	SFE, COND-2 (mean ± S.D.), (ng/g dry mass)	Relative recovery (Soxhlet = 100) (%)
Burbot	28	< 1	< 1	–
	52	2.4 ± 0.1	2.5 ± 0.2	104
	101	4.7 ± 0.2	4.7 ± 0.2	100
	105	1.4 ± 0.1	1.4 ± 0.1	100
	118	4.4 ± 0.4	4.2 ± 0.2	96
	128	1.2 ± 0.0	1.2 ± 0.1	98
	138	6.4 ± 0.1	7.0 ± 0.2	108
	149	2.7 ± 0.2	2.9 ± 0.1	108
	153	9.0 ± 0.3	9.0 ± 0.2	100
	156	0.8 ± 0.1	0.8 ± 0.1	103
	170	1.4 ± 0.0	1.4 ± 0.1	106
	180	4.7 ± 0.1	4.8 ± 0.1	102
	DDE	14.2 ± 0.2	13.3 ± 0.3	94
	DDD	2.7 ± 0.1	2.5 ± 0.1	93
	DDT	< 2	< 2	–
Pike perch	28	2.5 ± 0.1	2.6 ± 0.1	100
	52	7.1 ± 0.4	7.2 ± 0.4	102
	101	18.8 ± 0.8	19.2 ± 0.5	102
	105	4.5 ± 0.1	4.4 ± 0.1	99
	118	14.3 ± 0.3	15.2 ± 0.6	106
	128	3.4 ± 0.1	3.5 ± 0.1	103
	138	21.3 ± 0.1	22.6 ± 0.5	106
	149	16.5 ± 1.0	17.5 ± 0.5	106
	153	29.7 ± 1.2	31.1 ± 0.7	105
	156	1.7 ± 0.1	1.7 ± 0.1	102
	170	3.4 ± 0.2	3.7 ± 0.1	108
	180	13.5 ± 0.3	13.9 ± 0.3	103
	DDE	47.7 ± 1.6	49.9 ± 0.7	105
	DDD	6.6 ± 0.2	6.8 ± 0.1	103
	DDT	3.0 ± 0.1	3.4 ± 0.2	111
Tench	28	3.1 ± 0.2	3.1 ± 0.1	99
	52	9.5 ± 0.1	10.8 ± 0.2	114
	101	31.9 ± 1.5	36.4 ± 0.6	114
	105	7.2 ± 0.4	8.1 ± 0.2	113
	118	27.8 ± 1.1	30.4 ± 0.4	109
	128	6.4 ± 0.2	7.1 ± 0.1	111
	138	52.2 ± 2.1	59.8 ± 1.4	114
	149	28.8 ± 1.1	33.6 ± 0.5	117
	153	62.6 ± 2.6	68.9 ± 0.8	110
	156	4.0 ± 0.2	4.6 ± 0.1	116
	170	7.6 ± 0.3	8.6 ± 0.1	114
	180	32.3 ± 0.9	36.6 ± 0.8	113
	DDE	65.0 ± 2.2	70.4 ± 1.4	108
	DDD	6.7 ± 0.9	11.1 ± 0.2	166
	DDT	12.6 ± 0.3	15.2 ± 0.2	120

Table 4 (*continued*)

Fish	PCB	Soxhlet (mean ± S.D.), (ng/g dry mass)	SFE, COND-2 (mean ± S.D.), (ng/g dry mass)	Relative recovery (Soxhlet = 100) (%)
Perch I	28	3.0 ± 0.1	3.2 ± 0.1	106
	52	8.1 ± 0.1	9.6 ± 0.4	118
	101	29.7 ± 0.7	34.0 ± 1.0	115
	105	6.6 ± 0.1	7.3 ± 0.2	110
	118	26.1 ± 0.8	28.2 ± 0.1	108
	128	6.4 ± 0.1	6.9 ± 0.2	108
	138	54.8 ± 1.3	59.5 ± 1.7	109
	149	28.7 ± 0.4	33.6 ± 1.1	117
	153	62.6 ± 1.2	70.7 ± 2.0	113
	156	4.1 ± 0.1	4.7 ± 0.0	113
	170	8.0 ± 0.2	8.8 ± 0.4	110
	180	33.8 ± 0.9	36.8 ± 0.9	109
	DDE	62.5 ± 2.4	64.9 ± 1.6	104
	DDD	8.9 ± 0.1	10.4 ± 0.2	117
	DDT	11.2 ± 0.1	13.1 ± 0.2	117
Perch II	28	2.0 ± 0.1	2.0 ± 0.2	99
	52	7.3 ± 1.0	8.0 ± 0.4	110
	101	23.2 ± 2.6	26.0 ± 1.3	112
	105	5.1 ± 0.1	5.8 ± 0.4	114
	118	18.9 ± 1.4	21.2 ± 1.0	112
	128	4.8 ± 0.4	5.3 ± 0.2	110
	138	33.6 ± 0.6	40.9 ± 1.8	122
	149	23.5 ± 3.0	26.8 ± 1.2	114
	153	43.8 ± 4.7	48.9 ± 2.4	112
	156	2.6 ± 0.1	3.1 ± 0.1	117
	170	5.5 ± 0.6	6.3 ± 0.3	113
	180	22.6 ± 1.7	25.7 ± 1.0	114
	DDE	47.6 ± 3.6	51.9 ± 1.9	109
	DDD	9.6 ± 0.1	10.7 ± 0.7	111
	DDT	15.4 ± 1.2	17.8 ± 0.8	116
Perch III	28	1.7 ± 0.1	1.6 ± 0.1	96
	52	5.2 ± 0.2	4.8 ± 1.5	93
	101	16.2 ± 0.1	15.3 ± 3.2	94
	105	4.1 ± 0.1	4.1 ± 0.3	100
	118	14.2 ± 0.2	15.4 ± 1.5	108
	128	3.4 ± 0.1	3.6 ± 0.2	104
	138	27.2 ± 0.4	26.8 ± 0.9	99
	149	17.5 ± 0.4	17.6 ± 1.7	100
	153	31.2 ± 0.9	28.5 ± 3.4	91
	156	2.1 ± 0.1	2.1 ± 0.3	97
	170	4.2 ± 0.3	3.8 ± 0.3	89
	180	16.4 ± 0.6	15.9 ± 0.6	97
	DDE	30.4 ± 0.1	27.2 ± 2.7	89
	DDD	8.0 ± 0.2	8.5 ± 0.6	106
	DDT	6.0 ± 0.6	6.0 ± 0.2	101

COND-1 = 30 min dynamic extraction with carbon dioxide at 60°C, without clean-up (four replicates); COND-2 = 10 min static and 30 min dynamic extraction with carbon dioxide at 60°C, with clean-up (four replicates); Soxhlet = 18 h with 250 ml hexane–acetone (2:3), with clean-up (two replicates).

magnitude as for the Soxhlet extractions with a tendency to be a little smaller. The recovery ranges from 89 to 181% (in comparison with Soxhlet). The obvious outliers with a DDD recovery of 181 and 166% for largemouth bass and burbut most probably derives from the acid silica clean-up of the Soxhlet extracts. Usually the CBs elute first followed by DDE, DDT and finally DDD when silica clean-up is performed with a non-polar hydrocarbon as eluent [2]. It is likely that an elution volume of only 50 ml in some cases is to small for complete recovery of DDD and DDT from the larger amounts of acid silica necessary for the clean-up of the Soxhlet extracts.

The average recoveries of the SFE experiment in comparison with Soxhlet point to a significant higher recovery for SFE when performed with the COND-2 parameters. This means that the Soxhlet extractions under the given conditions are not quantitative for all the fish investigated. Furthermore, there does not seem to be any obvious reason for some of the fish giving higher recovery with SFE, because no correlation with either the relative dry mass or the lipid content is visible. Natural variations from one fish to another could be the reason. Comparing the average recoveries for perch III (lipid content 6.1%; extracted with COND-1) with the values for the other fish (extracted with COND-2), it is obvious that there is a difference. This difference, however, is not as large as should be expected from the data comparison on the tuna fish extractions. This could mean that the conditions required to extract PCBs with SFE from fatty fish are somewhat milder than conditions for lean fish.

3.4. Independent determination of PCB levels in tuna and tench

Quantitative determinations from analysis of the same sample with different methods are usually closer when performed by the same laboratory than those obtained from different laboratories. Evidently, this is because methods, calibration standards, GC system, injection technique and column choice vary between different laboratories. In order to have a final test of the present method, an extra independent analysis of the tuna and the tench was conducted in the laboratory of the Institute in IJmuiden. Independent means that the laboratory in IJmuiden was using their normal equipment and CB standards for the analysis without knowing the concentrations of individual CBs.

The result can be seen in Table 5. Overall, there is a good agreement between the results of the two laboratories. For some CBs, the values from Soxhlet 2 (IJmuiden) are a little higher than both Soxhlet 1 (Ispra) and SFE (COND-2). However, the difference is not significant, as the Soxhlet 2 analyses were performed on a single GC column (CP-Sil 19) [27,31], while the other analyses were performed on a dual-column system, from which the lowest value was selected to eliminate the possibility of interference. International intercomparisons on PCB analysis show a mean error of 10–15% [32,33]. Seen in this light, the comparison especially between SFE and Soxhlet 2 seems very reasonable.

4. Conclusions

Off-line SFE and GC–ECD (with the right choice of extraction parameters, GC injector and GC columns) has the potential of performing interference free congener specific analysis of native PCBs and related compounds on a routine basis in lyophilized fish tissues without the use of any manual work-up between extraction and GC analysis. With this combination of techniques the time ($\leq$2 h) and labour requirements can be reduced by nearly an order of magnitude in comparison with conventional methods for low ng/g levels of native pollutants. Also the analysis can be performed without losing accuracy and precision, because SFE in this respect is at least as good as Soxhlet extraction. This study demonstrates the importance of sequential extractions in the validation of quantitative SFE methods in addition to comparison with conventional procedures. Finally this study points to the need for sufficient similarity in sample composition when performing method development of a

Table 5
Comparison of SFE with Soxhlet extraction using different and independent methods

PCB	Tuna					Tench				
	SFE, COND-2		Soxhlet 1		Soxhlet 2	SFE, COND-2		Soxhlet 1		Soxhlet 2
	Mean (ng/g dry mass)	S.D. (ng/g)	Mean (ng/g dry mass)	S.D. (ng/g)	Single experiment (ng/g dry mass)	Mean (ng/g dry mass)	S.D. (ng/g)	Mean (ng/g dry mass)	S.D. (ng/g)	Single experiment (ng/g dry mass)
28	<1	–	<1	–	<1	3.1	0.1	3.1	0.2	4.1
52	3.1	0.1	3.1	0.1	3.0	10.8	0.2	9.5	0.1	11
101	16.9	0.3	16.9	0.2	22	36.4	0.6	31.9	1.5	38
105	6.9	0.1	7.2	0.3	8.8	8.1	0.2	7.2	0.4	11
118	23.5	0.4	23.4	0.3	26	30.4	0.4	27.8	1.1	32
128	7.1	0.2	7.1	0.1	8.9	7.1	0.1	6.4	0.2	8.6
138	62	1.4	62.4	1.4	65[a]	59.8	1.4	52.2	2.1	58[a]
149	34.4	1.1	33.1	0.9	37	33.6	0.5	28.8	1.1	34
153	84	2.2	79.6	2.5	100	68.9	0.8	62.6	2.6	77
156	4.5	0.1	4.4	0.1	5.0	4.6	0.1	4.0	0.2	4.6
170	12	0.4	11.5	0.2	22[b]	8.6	0.1	7.6	0.3	16[b]
180	50.2	1.0	49.0	0.7	51	36.6	0.8	32.3	0.9	32

COND-2 = 10 min static and 30 min dynamic extraction with carbon dioxide at 60°C (four replicates); Soxhlet 1 = 18 h with 250 ml hexane–acetone (2:3) (two replicates), Ispra; Soxhlet 2 = 12 h with 500 ml pentane–dichloromethane (1:1), single experiment, single column (CP-Sil 19), IJmuiden.
[a] PCB 163 constitutes more than 20% of the value of PCB 138.
[b] Most likely there is a non-PCB interference in the determination of PCB 170.

specific matrix, as just the difference in lipid content in a sample can be enough to change the optimal extraction conditions.

Acknowledgements

The authors are grateful to Hewlett-Packard Italiana S.p.A., Cernusco S/N, Milan, Italy and especially to Giuseppe Candolfi and Costanza Rovida, for making the HP 7680A SFE extractor available.

Finally, we would like to thank Herbert Muntau and Michele Bianchi (Environment Institute, JRC, Ispra, Italy) for valuable help and discussions throughout this work.

References

[1] V. Lang, *J. Chromatogr.*, 595 (1992) 1.
[2] O. Hutzinger, S. Safe and V. Zitko, *The Chemistry of PCBs*, CRC Press, Cleveland, OH, 1974.
[3] J. de Boer, *Chemosphere*, 17 (1988) 1803.
[4] D.L. Stalling, R.C. Tindle and J.L. Johnson, *J. Assoc. Offic. Anal. Chem.*, 55 (1972) 32.
[5] J.D. McKinney, L. Moore, A. Prokopet and D.B. Walters, *J. Assoc. Offic. Anal. Chem.*, 67 (1984) 122.
[6] S.B. Hawthorne, M.S. Krieger and D.J. Miller, *Anal. Chem.*, 61 (1989) 736.
[7] J.W. King, *J. Chromatogr. Sci.*, 17 (1989) 355.
[8] S.B. Hawthorne, *Anal. Chem.*, 62 (1990) 633A.
[9] S.B. Hawthorne, D.J. Miller and J.J. Langenfeld, in K. Jinno (Editor), *Hyphenated Techniques in Supercritical Fluid Chromatography and Extraction (Journal of Chromatography Library*, Vol. 53), Elsevier, Amsterdam, 1992, p. 225.
[10] J.W. King, J.E. France, in B. Wenclawiak (Editor), *Analysis with Supercritical Fluids: Extraction and Chromatography*, Springer, Berlin, 1992, p. 32.
[11] J.J. Langenfeld, S.B. Hawthorne, D.J. Miller and J. Pawliszyn, *Anal. Chem.*, 65 (1993) 338.
[12] M.D. Burford, S.B. Hawthorne and D.J. Miller, *Anal. Chem.*, 65 (1993) 1497.
[13] F. David, M. Verschuere and P. Sandra, *Fresenius' J. Anal. Chem.*, 344 (1992) 479.
[14] S. Bøwadt, B. Johansson, F. Pelusio, B. Larsen and C. Rovida, *J. Chromatogr.*, 662 (1994) 428.

[15] S. Bøwadt and B. Johansson, *Anal. Chem.*, 66 (1994) 667.
[16] N.L. Porter, A.F. Rynaski, R.E. Cambell, M. Saunders, B.E. Richter, J.T. Swanson, R.B. Nielsen and B.J. Murphy, *J. Chromatogr. Sci.*, 30 (1992) 367.
[17] E. Stahl, E. Schutz and H.K. Mangold, *J. Agric. Food Chem.*, 28 (1980) 1153.
[18] A.C. Eldridge, J.P. Friedrich, K. Warner and W.F. Kwolek, *J. Food Sci.*, 51 (1986) 584.
[19] M.T.G. Hierro and G. Santa-Maria, *Food Chem.*, 45 (1992) 189.
[20] D.L. Stalling, S. Said, K.C. Kuo and J.J. Stunkel, *J. Chromatogr. Sci.*, 30 (1992) 486.
[21] K.S. Nam, S. Kapila, D.S. Viswanath, T.E. Clevenger, J. Johansson and A.F. Yanders, *Chemosphere*, 19 (1989) 33.
[22] H.R. Johansen, G. Becher and T. Greibrokk, *Fresenius' J. Anal. Chem.*, 344 (1992) 486.
[23] F. David, A. Kot, E. Vanluchene, E. Sippola and P. Sandra, in P. Sandra (Editor), *Proceedings of the 15th International Symposium on Capillary Chromatography*, Hüthig, Heidelberg, 1993, p. 1572.
[24] H. Muntau, D. Zilli, M. Bianchi, S. Bøwadt and B. Johansson, unpublished results.
[25] J. de Boer, *Chemosphere*, 17 (1988) 1811.
[26] M.S. Rahman, S. Bøwadt and B. Larsen, *J. High Resolut. Chromatogr.*, 16 (1993) 731.
[27] J. de Boer and Q.T. Dao, *J. High Resolut. Chromatogr.*, 12 (1989) 755.
[28] S.B. Hawthorne, D.J. Miller, M.D. Burford, J.J. Langenfeld, S.E. Eckert-Tilotta and P.K. Louie, *J. Chromatogr.*, 642 (1993) 301.
[29] S.E. Eckert-Tilotta, S.B. Hawthorne and D.J. Miller, *Fuel*, 72 (1993) 1015.
[30] S. Bøwadt, H. Skejø-Andresen, L. Montanarella and B. Larsen, *Int. J. Environ. Anal. Chem.*, in press.
[31] B. Larsen, S. Bøwadt and R. Tilio, *Int. J. Environ. Anal. Chem.*, 47 (1992) 47.
[32] J. de Boer and J. van der Meer, *Cooperative Research Report on the ICES/-IOC/OSPACOM CB Intercomparison in Marine Media, Step 3b*, International Council for Exploration of the Sea, Copenhagen, 1993.
[33] J. de Boer, J.C. Duinker, J.A. Calder and J. van der Meer, *J. Assoc. Off. Anal. Chem.*, 75 (1992) 1054.

ELSEVIER

Journal of Chromatography A, 675 (1994) 205–211

JOURNAL OF CHROMATOGRAPHY A

Homologue distributions of polychlorinated terphenyls by high-resolution gas chromatography and high-resolution mass spectrometry

J. Caixach[a], J. Rivera*[,a], M.T. Galceran[b], F.J. Santos[b]

[a]*Laboratori d'Espectrometria de Masses, CID–CSIC, Jordi Girona 18, 08034-Barcelona, Spain*

[b]*Departament de Química Analítica, Universitat de Barcelona, Diagonal 647, 08028-Barcelona, Spain*

(First received February 1st, 1994; revised manuscript received March 10th, 1994)

Abstract

The use of high-resolution gas chromatography–high-resolution mass spectrometry in the selected-ion monitoring mode (HRGC–HRMS-SIM) to study the distribution of polychlorinated terphenyls (PCTs) in commercial and environmental samples is proposed. Interferences in the detection and measurement of the $M^{+\cdot}$ ions due to chromatographic co-elution of PCT congeners were observed. In this paper, the interfering contribution of the $[M-2Cl]^+$ fragment from the terphenyl homologues with an additional two chlorine atoms was eliminated using HRMS at a resolving power between 30 000 and 35 000. Homologue distributions of PCTs in commercial mixtures, Aroclor 5460 and Leromoll 141, and in samples of shellfish from the Ebro Delta (Catalonia, Spain) are proposed.

1. Introduction

Polychlorinated terphenyls (PCTs) and polychlorinated biphenyls (PCBs) are structurally and toxicologically related classes of anthropogenic compounds that have been identified as potentially serious environmental hazards. They have certain physical properties such as high heat capacity, chemical stability and electrical properties that make them desirable for a number of industrial uses [1]; however, the application of PCTs has always been more limited than that of PCBs.

Reports on the determination of PCTs are rare in the literature, particularly when compared with those concerning PCBs. Nevertheless, they have been detected in river water [2], soils and sediments [3–6], biological samples [5,7–11], food packaging [12,13] and human tissue [7,14–16].

Analyses for PCTs have proved to be difficult because of the complexity of the mixtures and the high boiling points of the heavily chlorinated congeners. Poor resolution in gas chromatography using packed chromatographic columns prevented their determination with PCBs and related compounds in the 1970s. More recently, using open-tubular columns, stationary phase thermal stability problems and very long retention times detracted environmental analytical chemists from further research to confirm the presence of these pollutants in environmental samples.

Two additional problems have been found in

* Corresponding author.

0021-9673/94/$07.00
SSDI 0021-9673(94)00252-5

the determination of PCTs by high-resolution gas chromatography: co-elution of the lower chlorinated PCT congeners with some PCBs and the unavailability of individual standards. The separation between the highly chlorinated PCBs and the low-chlorinated PCTs can be achieved using sufficiently long capillary columns and low-resolution mass spectrometry. Moreover, the unavailability of individual standards can be overcome by using Aroclor or other technical mixtures as secondary standards, but the compositions of these formulations are not known. Gas chromatography–mass spectrometry can be used to elucidate the composition of these mixtures but interferences in the measurement of the molecular ions were observed [15], preventing the identification of the homologues. In a previous paper [11], the approximate distribution of the homologues for Aroclor 5432, Aroclor 5460 and Leromoll 141 using low-resolution mass spectrometry was proposed.

The detection and measurement of the $M^{+\cdot}$ ions produced by a member of a given isomer group may be interfered with by the $[M-2Cl]^+$ fragment ions of homologues with two additional chlorine atoms [11,15]. To discriminate between the molecular and interfering ions, high-resolution mass spectrometry was necessary. In this work, the determination of PCTs was performed by high-resolution gas chromatography–high-resolution mass spectrometry (HRGC–HRMS) at a resolving power between 30 000 and 35 000, and the homologue distributions for Aroclor 5460 and Leromoll 141 were proposed. The presence of these compounds in samples of shellfish from the Ebro Delta (Catalonia, Spain) was investigated.

2. Experimental

2.1. Chemicals

Aroclor 5460 PCT mixture was purchased from Chem-Service (West Chester, PA, USA) and the commercial product Leromoll 141 was a gift from Dr. U.A.Th. Brinkman (Amsterdam, Netherlands). Standard solutions of PCT mixtures containing 10 mg/l of individual Aroclor 5460 and Leromoll 141 were prepared in isooctane for residue analysis (Carlo Erba, Milan, Italy).

2.2. Apparatus

HRGC–HRMS analyses were performed on a Hewlett-Packard (Palo Alto, CA, USA) Model 5890 Series II gas chromatograph interfaced to a VG AutoSpec-Q (VG Instruments, Manchester, UK) with an OPUS 1.0 data system interface and DEC VAX 3100 Workstation for data processing. A DB-5 fused-silica column (J&W Scientific, Folsom, CA, USA) capillary column (60 m × 0.25 mm I.D., 0.25 μm film thickness) was used with helium as the carrier gas at a linear velocity of 25 cm/s. The temperature programme was from 90°C (held for 3 min) to 200°C (held for 1 min) at 20°C/min, and then from 200 to 310°C (held for 30 min) a 2.5°C/min. The injector temperature was kept at 275°C, using the splitless mode.

The HRGC–HRMS-selected ion monitoring (SIM) mode operating conditions were as follows: ion source and interface temperatures, 280 and 290°C, respectively; ionization energy, 70 eV (electron impact mode); monitored ions and the interfering ions as shown in Table 1. The resolving power was kept between 30 000 and 35 000 (10% valley definition), using m/z 404.9760 of pentafluorokerosene (PFK) as lockmass. SIM at an accelerating voltage of 8000 V, dwell time 80 ms and delay time 20 ms was used. The total scan cycle was 1.6 s. Verification of the resolution in the working mass range was obtained by measuring the PFK reference peaks on a mass-calibrated oscilloscope. The theoretical relative abundance of the isotopes of carbon (^{12}C, ^{13}C), hydrogen (^{1}H, ^{2}H, ^{3}H) and chlorine (^{35}Cl, ^{37}Cl), were taken into account in order to calculate the exact masses of PCTs. The two major molecular ions of each PCT homologue were used for mass monitoring.

For HRGC–low-resolution (LR) MS the full-scan mode at a resolving power of 1000 and a mass range between 100 to 750 m/z at 1 s per

decade were used. The working conditions for selected-ion monitoring (LRMS-SIM) were described in a previous paper [11].

3. Results and discussion

The EI mass spectra of the PCTs gave an intense molecular ion $M^{+\cdot}$, as can be seen in Fig. 1, where the full-scan EI spectrum of a nona-CT from Aroclor 5460 is given as an example. The molecular ion and the fragment ions showed the typical expected clustering due to the chlorine isotopes. In addition, a relatively intense fragment due to $[M-2Cl]^+$ and a small fragment ion due to $[M-Cl]^+$ appeared. The fragment $[M-2Cl]^+$ provided an interfering cluster for the molecular ion from the PCT homologues with two fewer chlorine atoms. In Fig. 2, the EI mass spectrum of the molecular region for hepta-CT is given.

For each formulation of PCTs the $[M-2Cl]^+$ interferences were important for the main homologues. Thus nona-CTs interfered with hepta-CTs and deca-CTs interfered with octa-CTs for Aroclor 5460. Leromoll 141 showed interferences from hepta-CTs with the penta-CTs and octa-CTs with the hexa-CTs. As an example, the hepta- and nona-CT LRMS-SIM profiles showing interference of nona-CTs with hepta-CTs for Aroclor 5460 are given in Fig. 3. To calculate the homologue distribution, no co-elution between homologues containing two additional chlorine atoms can be assumed and the contribution of the $[M-2Cl]^+$ can be eliminated. In a previous paper [11], the results obtained using this approach were given. To discriminate between the $M^{+\cdot}$ and the $[M-2Cl]^+$ ions, HRMS was required.

The selected ion monitored, the interfering ion for each homologue and the resolution, calculated at 10% valley definition, are given in Table 1. The nona-CTs molecular cluster ions that gave the mass which interfered with the hepta-CTs molecular ion are given as an example in Fig. 4. As can be observed, the loss of two chlorine atoms as two ^{35}Cl, two ^{37}Cl or one ^{35}Cl and one ^{37}Cl gave the same $[M-2Cl]^+$ cluster fragment. In order to avoid this interference, a resolution of 25 300 was required.

The use of the resolution indicated in Table 1 allowed the elimination of the MS interference

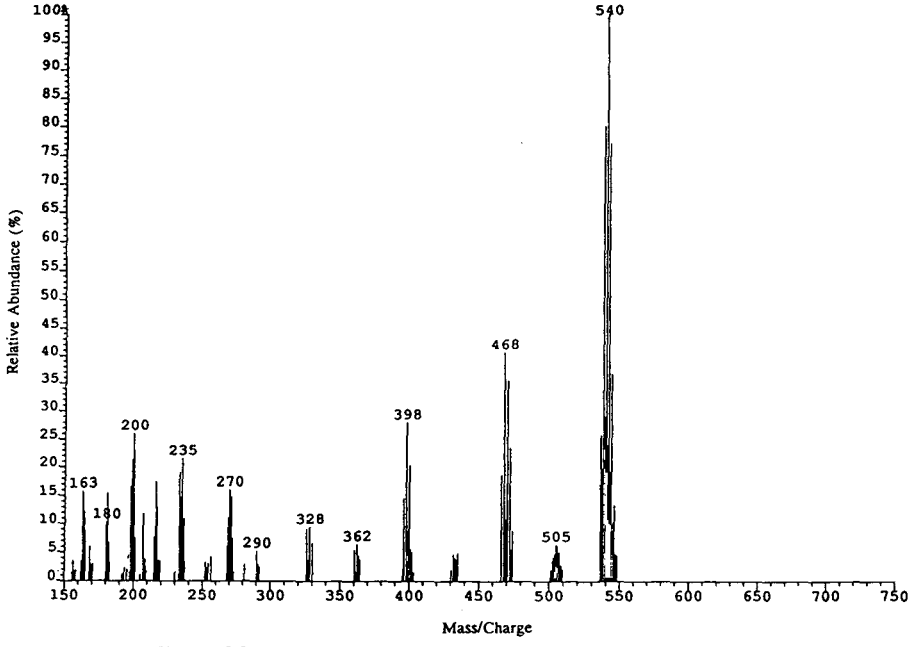

Fig. 1. Mass spectrum of a nonachloroterphenyl in Aroclor 5460.

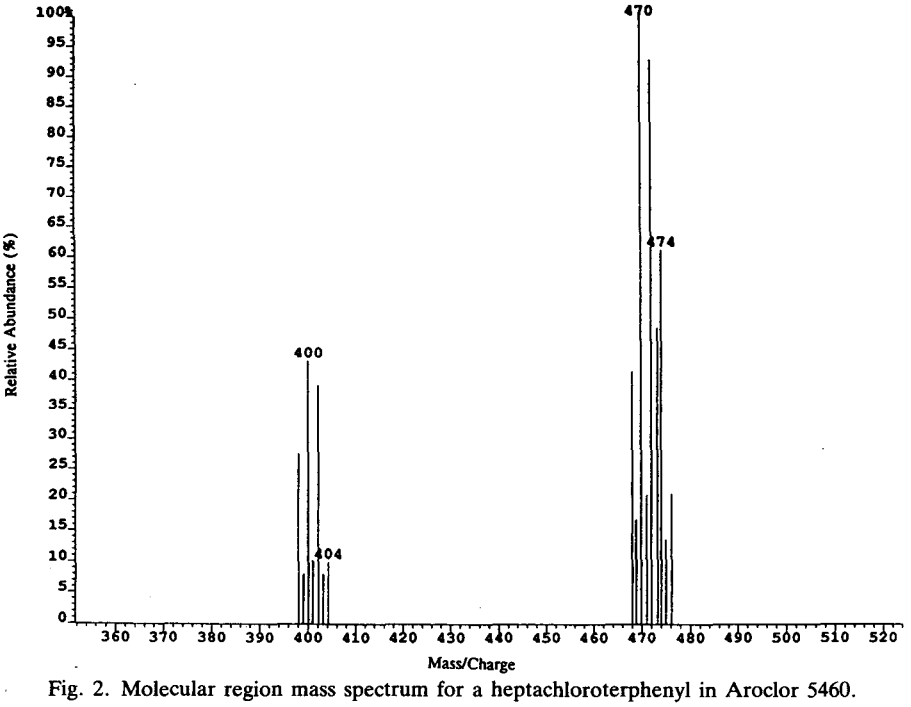

Fig. 2. Molecular region mass spectrum for a heptachloroterphenyl in Aroclor 5460.

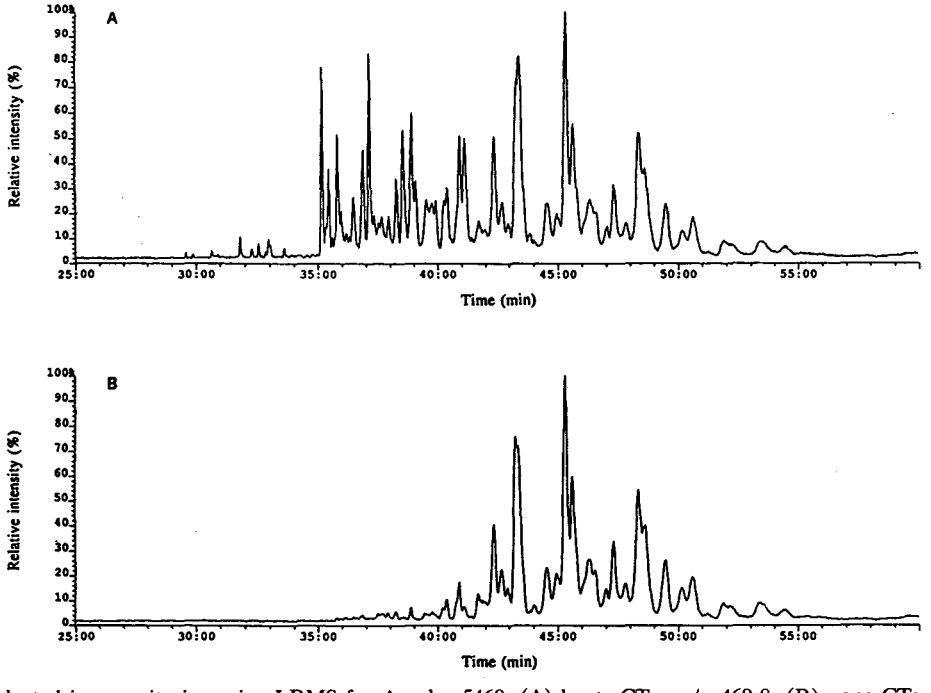

Fig. 3. Selected ion monitoring using LRMS for Aroclor 5460; (A) hepta-CTs, m/z 469.8; (B) nona-CTs, m/z 537.8.

Table 1
Calculated resolution and exact masses used for interfering and monitored ions

Homologue	Monitored m/z	Interfering m/z	Resolution[a]
Penta-CTs	401.9117	401.8931	21 600
	403.9088	403.8902	21 700
Hexa-CTs	435.8728	435.8542	23 400
	437.8698	437.8512	23 500
Hepta-CTs	469.8338	469.8152	25 300
	471.8308	471.8122	25 400
Octa-CTs	503.7948	503.7762	27 100
	505.7919	505.7733	27 200
Nona-CTs	537.7558	537.7372	28 900
	539.7529	539.7343	29 000
Deca-CTs	573.7139	573.6953	30 800
	575.7110	575.6924	31 000
Undeca-CTs	607.6750	607.6564	32 700
	609.6720	609.6534	32 800
Dodeca-CTs	641.6360	641.6174	34 500
	643.6330	643.6144	34 600

[a] Resolution calculated at 10% valley definition.

from $[M-2Cl]^+$. Fig. 5 shows the HRGC–LRMS-SIM profile for the hepta-CTs and the HRGC–HRMS-SIM profiles for the hepta- and nona-CTs. Co-elution of hepta- and nona-CTs between 35 and 40 min was observed. Integration of the HRMS-SIM profiles provided a quantitative determination for each chlorinated homologous family.

Table 2
Homologue distributions for Aroclor 5460 and Leromoll 141

Homologues	Percentage of homologues			
	Aroclor 5460		Leromoll 141	
	LRMS	HRMS	LRMS	HRMS
Penta-CTs	–[a]	–	14	12.0
Hexa-CTs	<1	0.9	28	30.2
Hepta-CTs	6	10.4	30	42.6
Octa-CTs	17	45.7	27	14.1
Nona-CTs	42	29.4	1	0.7
Deca-CTs	28	11.9	–	0.4
Undeca-CTs	6	1.2	–	–
Dodeca-CTs	–	<0.5	–	–

[a] – = Not detected.

The homologue distributions for Aroclor 5460 and Leromoll 141 calculated by HRMS are given in Table 2. These values indicated that Aroclor 5460 was mainly constituted by terphenyls with seven to ten chlorine atoms with a maximum of octa-CTs, and that Leromoll 141 was mainly composed of terphenyls with five to eight chlorine atoms with a maximum of hepta-CTs. A comparison between these percentages and those

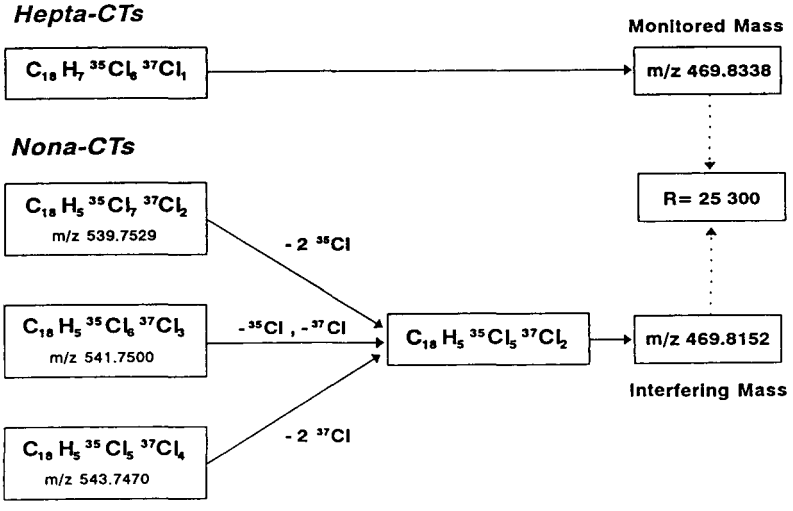

Fig. 4. Interferent mass of nona-CTs on the hepta-CTs monitored molecular mass for Aroclor 5460.

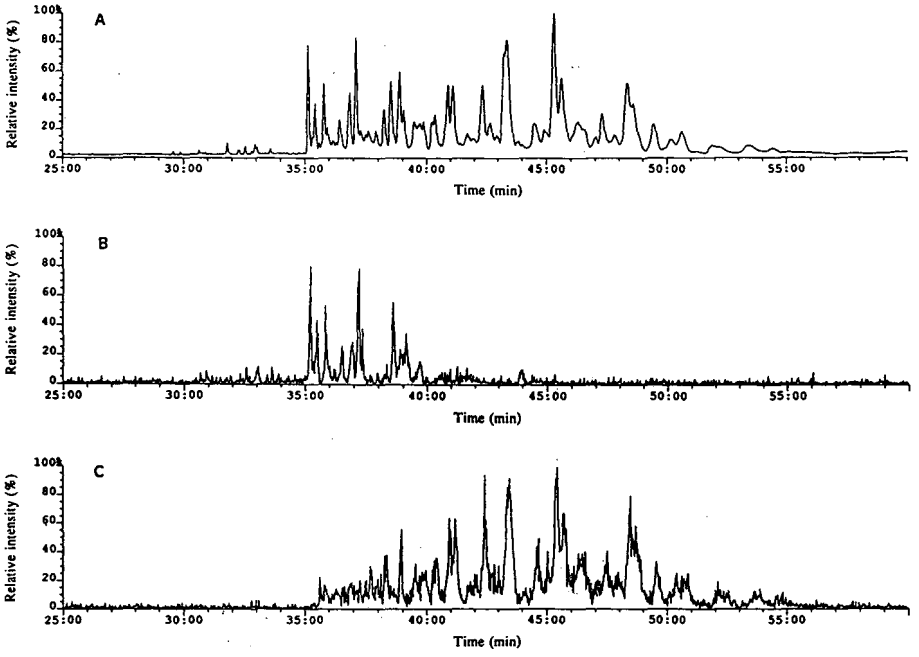

Fig. 5. Selected ion monitoring using (A) LRMS for hepta-CTs, m/z 469.8, and HRMS for (B) hepta-CTs, m/z 469.8338 and (C) nona-CTs after loss of two chlorine atoms, m/z 469.8152.

calculated previously using LRMS showed differences in the data for the octa-, nona-, deca- and undeca-CTs for Aroclor 5460 and hepta- and octa-CTs for Leromoll 141. These differences were due to the simultaneous co-elution of some iomers with different degrees of chlorination.

PCTs were found in samples of shellfish from the Ebro Delta (Catalonia, Spain) collected in

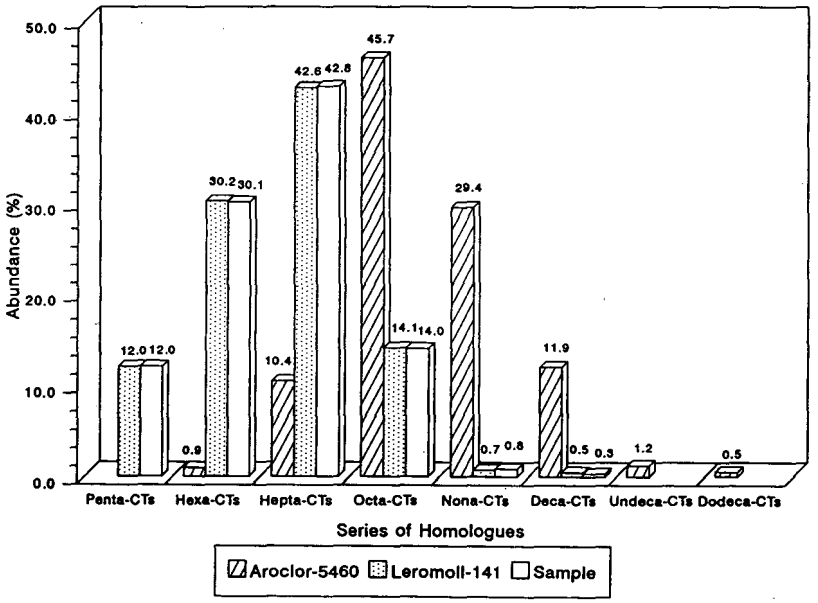

Fig. 6. Homologue distributions for Aroclor 5460, Leromoll 141 and a sample of shellfish.

1989 [11]. For identification purposes, HRGC–HRMS-SIM was applied to samples with high levels of PCTs. The homologue distributions obtained for Aroclor 5460, Leromoll 141 and the shellfish samples are given in Fig. 6. Identical compositions in the last two were observed, so the terphenyls detected in the shellfish samples are due to Leromoll 141 formulations or similar.

4. Conclusions

The homologue distribution of PCTs in the commercial mixtures Aroclor 5460 and Leromoll 141 calculated using HRGC–HRMS-SIM was proposed. HRMS with a resolving power between 30 000 and 35 000 was needed. Previously, the correct homologue compositions of Aroclor 5460 and Leromoll 141 had not been reported in the literature data. These homologue distributions would allow the source of PCTs in real samples to be determined and could be considered as reference values for the determination of the degree of chlorination of each PCT in commercial formulations and environmental samples.

5. References

[1] R.D. Kimbrough and A.A. Jensen (Editors), *Halogenated Biphenyls, Terphenyls, Naphthalenes, Dibenzodioxins, and Related Compounds*, Elsevier/North-Holland Biomedical Press, Amsterdam, 2nd ed., 1989.

[2] J. Freudenthal and P.A. Grere, *Bull. Environ. Contam. Toxicol.*, 10 (1973) 108.

[3] C.L. Stratton and J.B. Sosebeer, Jr., *Environ. Sci. Technol.*, 13 (1976) 1229.

[4] E.T. Furlong, D.S. Carter and R.A.J. Hites, *Great Lakes Res.*, 14 (1988) 447.

[5] R.C. Hale, J. Greares, K. Gallagher and G.G. Vados, *Environ. Sci. Technol.*, 24 (1990) 1727.

[6] F.I. Onuska, K.A. Terry, S. Rokushika and H. Hatano, *J. High Resolut. Chromatogr.*, 13 (1990) 317.

[7] R.C. Hale, E. Bush, K. Gallagher, J.L. Gundersen and R.F. Mothershead, *J. Chromatogr.*, 539 (1991) 141.

[8] A.A. Jensen and K.F. Jörgensen, *Sci. Total Environ.*, 27 (1983) 231.

[9] L. Renberg, G. Sundström and L. Reutergårdh, *Chemosphere*, 6 (1978) 477.

[10] G.F. Fries and G.S. Marrow, *J. Assoc. Off. Anal. Chem.*, 56 (1973) 1002.

[11] M.T. Galceran, F.J. Santos, J. Caixach, F. Ventura and J. Rivera, *J. Chromatogr.*, 643 (1993) 399–408.

[12] D.C. Villeneuve, L.M. Reynolds, G.H. Thomas and W.E.J. Phillips, *J. Assoc. Off. Anal. Chem.*, 56 (1973) 999.

[13] G.H. Thomas and L.M. Reynolds, *Bull. Environ. Contam. Toxicol.*, 10 (1973) 37.

[14] M. Doguchi, S. Fukano and F. Ushro, *Bull. Environ. Contam. Toxicol.*, 11 (1974) 111.

[15] L.H. Wright, R.G. Lewis, L.H. Crist, G.W. Sovocool and J.M. Simpson, *J. Anal. Toxicol.*, 2 (1978) 76.

[16] I. Watanabe, T. Yakushiji and N. Kunita, *Bull. Environ. Contam. Toxicol.*, 25 (1980) 810.

ELSEVIER

Journal of Chromatography A, 675 (1994) 213–218

JOURNAL OF CHROMATOGRAPHY A

Determination of residues of phenoxy acid herbicides in soil and cereals by gas chromatography–ion trap detection ☆

C. Sánchez-Brunete, A.I. García-Valcárcel, J.L. Tadeo*

Departamento de Protección Vegetal CIT-INIA, Apdo 8111, 28080 Madrid, Spain

(First received December 6th, 1993; revised manuscript received March 14th, 1994)

Abstract

The analysis of several phenoxy acids in soil and cereals was carried out by gas chromatography with ion trap detection, after derivatization with BF_3–methanol. Soil was extracted with methylene chloride, at acidic pH, on an orbit shaker, and plants were extracted with a 0.1 *M* NaOH solution in a Sorvall homogenizer. The extracts were cleaned up by liquid–liquid partition, the organic solvents evaporated and residues methylated. Herbicides residues were determined by gas chromatography–ion trap detection on a BP-1 capillary column with helium as carrier gas. Recovery through the method was studied in the range of 0.2 to 2 μg/g and was found higher than 80% for each herbicide in both matrixes. Residues of phenoxy acids were determined by selecting the base peak of their spectra, after acquisition of the total-ion chromatogram of the sample. The limit of detection in the selected-ion mode was 0.005 μg/g in soil and 0.04 μg/g in plant samples.

1. Introduction

Phenoxy acids are an important group of herbicides widely used to control broad leaf weeds. (2,4-Dichlorophenoxy)acetic acid (2,4-D), (4-chloro-2-methylphenoxy)acetic acid (MCPA) and (4-chloro-2-methylphenoxy)-propionic acid (MCPP or mecoprop) are the phenoxy acid herbicides most used in Spanish winter cereals, due to their low cost and good selectivity.

Several organic solvents, like acetonitrile, acetone, diethyl ether and methylene chloride, have been proposed for extraction of phenoxy acids from soils and cereals [1–5].

Determination of phenoxy acid residues has been usually carried out, after esterification, by gas chromatography (GC) with electron-capture detection [6,7], although other methods, like reversed-phase liquid chromatography [8,9], have been used too.

Capillary GC is a technique with high selectivity and sensitivity, suitable for the determination of multiple components, at residue level, in environmental samples [10]. Nevertheless, phenoxy acids are highly polar and with inadequate volatility to allow direct GC analysis. Conversion of acids into the corresponding methyl esters has been accomplished using diazomethane [11], or boron trifluoride–methanol [12]. Other reagents have also been used to

* Corresponding author.

☆ Presented at the *22nd Annual Meeting of the Spanish Chromatography Group, Barcelona, October 20–22, 1993.*

0021-9673/94/$07.00
SSDI 0021-9673(94)00261-7

obtain halogenated alkyl esters [13–15], in order to improve the response of electron-capture detector, especially important for compounds with a low halogen content, like MCPA and MCPP.

The purpose of this paper is to study the determination of several commonly used phenoxy acids, in soil and cereal samples, at trace level. The proposed methods are based on the determination by GC with the highly sensitive and specific ion trap detection (ITD), after esterification of the acids with BF_3–methanol.

2. Experimental

2.1. Chemicals

Herbicide standards were obtained from commercial sources. The compounds used were 2,4-D from Condor (Middlesex, UK), MCPA and MCPP from Akzo (Rotterdam, Netherlands).

The internal standard solution of MCPA propyl ester was prepared in the laboratory. A 2-ml volume of acetyl chloride–propanol (1:5), previously cooled, was added to 50 mg of MCPA and the mixture heated at 100°C in a sand bath for 1 h. After cooling, 2 ml of acetate buffer (pH 4.6) were added and the solution transferred to a 100-ml volumetric flask with methanol.

All solvents used were analytical-reagent grade from Panreac (Spain). Boron trifluoride–methanol was purchased from Merck (Germany).

2.2. Equipment

GC–ITD analysis was performed with a Perkin-Elmer 8500 chromatograph equipped with a Finnigan ion trap detector. A fused-silica capillary column, BP-1 (12 m × 0.22 mm I.D.) bonded phase, 0.25 μm film thickness, was used with helium as carrier gas at 10 p.s.i.g. (1 p.s.i. = 6894.76 Pa). The oven temperature was held at 85°C for 1 min, programmed to 250°C at 25°C/min and then held for 5 min. A 2-μl volume was injected splitless, with the split valve closed for 1 min.

2.3. Mass spectrometric acquisition parameters

The following conditions were used: transfer line temperature, 250°C; mass range, 40–350 u; scan rate, 0.5 s/scan, 2-μscans; radio frequency voltage, 1.1 MHz and 0–7.5 kV; automatic gain control, from 78 μs to 25 ms; solvent delay, 3 min.

2.4. Procedure

Soil (20 g) was extracted with 100 ml of methylene chloride, plus 15 ml of water acidified to pH 1.2 with 9 *M* H_2SO_4, on an orbit shaker for 1 h. Solvent was decanted and soil extracted again with another 100 ml of methylene chloride. The flask content was filtered under suction through Whatman No. 1 filter paper and Celite, and the filter cake washed twice with 50 ml of methylene chloride. The extract was transferred to a separatory funnel and extracted twice with 75 ml of 0.05 *M* NaOH (pH 8–9). The aqueous phase was acidified to pH 1.6 with 9 *M* H_2SO_4 and extracted with methylene chloride (2 × 100 ml). The organic phase was filtered through anhydrous sodium sulphate and solvent was evaporated to dryness using a rotary evaporator.

Plant samples (5 g) were extracted with 0.1 *M* NaOH (2 × 25 ml) in a Sorvall homogenizer, based on a previously published method [16]. The extract was filtered under suction and the filter cake washed twice with 5 ml of the basic aqueous solution. To the extract, 25 ml of saturated sodium chloride solution were added, the pH was lowered to near 5 by the addition of 2 *M* H_2SO_4, the solution let stand for 15 min and the liquid decanted. Then the pH of the solution was lowered to approximately 1, the solution was transferred to a separatory funnel and extracted with diethyl ether (2 × 50 ml). The organic phase was extracted with 0.5 *M* $NaHCO_3$ (2 × 25 ml), the combined aqueous solution acidified to pH 1 by adding carefully 3 *M* H_2SO_4 (10 ml), and extracted with chloroform (2 × 25 ml). The organic phase was filtered through anhydrous sodium sulphate and solvent concentrated to dryness under vacuum.

2.5. Esterification

The residue from the extraction procedure was transferred to a tube with methanol (1–2 ml) and 4 ml of BF_3–methanol were added. The mixture was heated at 70°C for 30 min in a water bath. After cooling the reaction mixture in an ice bath, 10 ml of hexane and 10 ml of water were added, the tube shaked for 1 min and then the hexane phase was transferred to a 10-ml tube, dried over sodium sulphate and analyzed by GC.

3. Results and discussion

Phenoxy acid herbicides, applied in the form of salts or esters, are mainly found in the acid form in soils, since ester hydrolysis to the parent compounds occurs in a few days, under field conditions [17]. Extraction of phenoxy acids from soil samples has been carried out with different solvents at acidic or basic pH [1,10,18]. In our case, the acidic extraction with methylene chloride produced cleaner extracts than those obtained at basic pH.

Acidic herbicides have been extracted from plant samples with organic [19] or aqueous [16] solvents. These compounds are best released from plant tissues at basic pH and several authors included a hydrolytic step through extraction with alkaline aqueous solutions [20]. Cereals were extracted following a previously reported method [16] and good results were obtained with this procedure.

Esterification of phenoxy acids, prior to GC determination, has been accomplished by BF_3–methanol [21], a reagent less dangerous than diazomethane, and good conversion of the three studied herbicides was obtained.

Fig. 1 shows the total ion chromatogram, acquired in the electron impact (EI) mode, of the methyl esters of 2,4-D, MCPA and MCPP, 2 ng each, and the internal standard, the propyl ester of MCPA, 5 ng. Their retention times together with the main ions of their mass spectra are shown in Table 1. The molecular ion is abundant in the mass spectra of these compounds, being the base peak of the spectrum for MCPA and MCPP methyl esters. The spectrum of 2,4-D methyl ester shows the base peak at m/z 199. Other remarkable peaks of 2,4-D, MCPA and MCPP spectra are observed at m/z 175, 155 and 169, respectively, caused by the loss of the $-COOCH_3$ fragment. Also, loss of the $-CH_2-COOCH_3$ fragment is important in the MCPA ester. The internal standard shows the molecular ion m/z 242, as the base peak, and the ions m/z 141 and 125 caused by loss of the fragments $-CH_2-COO-(CH_2)_2-CH_3$ and $-O-CH_2-COO-(CH_2)_2-CH_3$, respectively (Table 1).

Residues of phenoxy acids were determined by selecting the base peaks of their spectra, after acquisition of the total ion chromatogram of the sample. The ions m/z 228, 214, 199 and 242 were selected for MCPP, MCPA, 2,4-D and the internal standard, respectively. The concentration was determined by comparing the ratio of the areas in the mass chromatogram of selected ions in the sample with the ratio found for mixtures of known concentration of the herbicides and the internal standard.

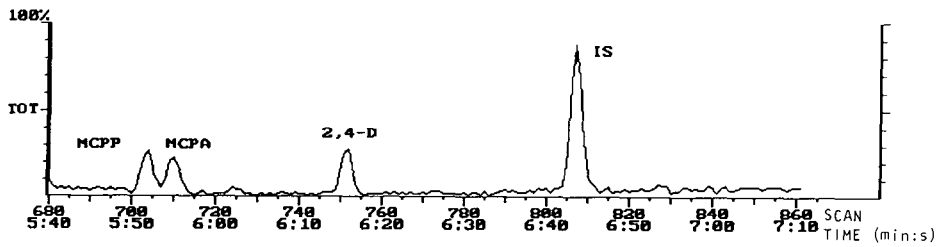

Fig. 1. Total ion chromatogram of the internal standard (IS) and the methyl esters of 2,4-D, MCPA and MCPP. A 5-ng amount of IS and 2 ng of each phenoxy acid were injected.

Table 1
GC retention times (t_R) and main ions in the EI mass spectra of methyl esters of phenoxy acids

Herbicide (methyl ester)	t_R (min)	m/z[a]	Fragment ion assignments
2,4-D	6.16	*199*	$[M - Cl]^+$
		235	$[M]^{+\cdot}$
		175	$[M\text{-}COOCH_3]^+$
MCPA	5.56	*214*	$[M]^{+\cdot}$
		155	$[M - COOCH_3]^+$
		141	$[M - CH_2COOCH_3]^+$
		125	$[M - OCH_2COOCH_3]^+$
MCPP	5.52	*228*	$[M]^{+\cdot}$
		169	$[M - COOCH_3]^+$
		141	$[M - CH(CH_3)COOCH_3]^+$
IS[b]	6.43	*242*	$[M]^{+\cdot}$
		125	$[M - OCH_2COO(CH_2)_2CH_3]^+$
		141	$[M - CH_2COO(CH_2)_2CH_3]^+$

[a] Base peak in italics.
[b] Internal standard: propyl ester of MCPA.

Recovery through the analytical method was studied with soil and cereals samples spiked before extraction by addition of 0.2, 1 and 2 μg/g of herbicides. The average recoveries varied from 80 to 106%, with a relative standard deviation between 1 and 12% (Table 2).

The detection limit of the GC–ITD method, with the total ion current, was near 0.01 μg/g for soil and 0.1 μg/g for plant samples. These limits can be improved with selected-ion monitoring (SIM) down to 0.005 μg/g for soil and 0.04 μg/g for plant samples (Fig. 2).

Soil from a cereal field, treated with MCPP, was sampled several months after treatment. The

Table 2
Recovery of phenoxy acids added to soil and plant samples

Herbicide	Added (μg/g)	Soil (mean ± S.D., %) (n = 4–6)	Plant (mean ± S.D., %) (n = 4)
MCPP	0.2	106.0 ± 2.1	95.5 ± 6.3
	1.0	89.7 ± 8.0	101.0 ± 7.0
	2.0	97.0 ± 12.0	96.5 ± 6.3
MCPA	0.2	80.5 ± 6.3	104.0 ± 6.3
	1.0	91.7 ± 8.3	99.3 ± 10.3
	2.0	102.0 ± 10.2	100.0 ± 1.4
2,4-D	0.2	89.0 ± 1.4	96.0 ± 8.4
	1.0	87.5 ± 12.7	103.0 ± 7.0
	2.0	89.3 ± 6.2	97.0 ± 2.4

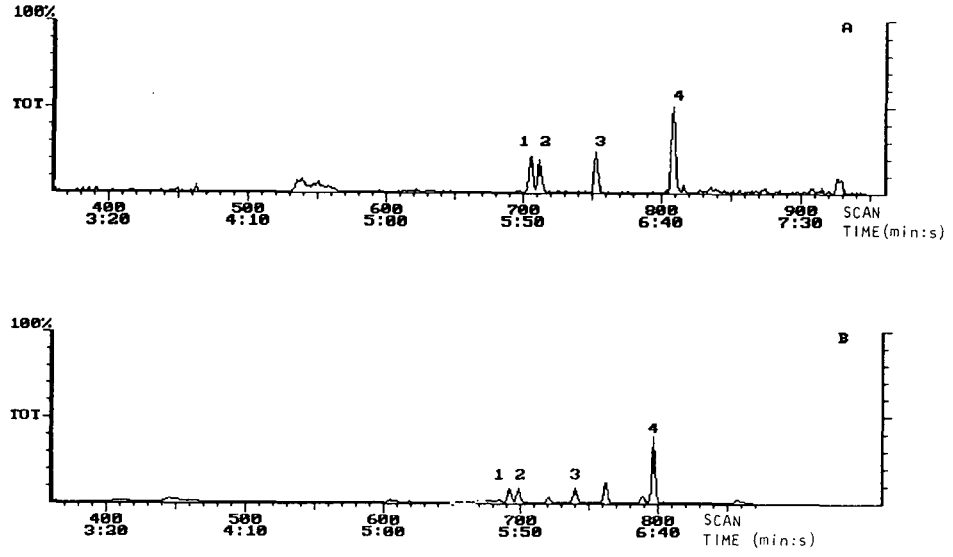

Fig. 2. SIM chromatograms of soil and plant extracts. (A) Soil sample (0.005 μg/g), (B) plant sample (0.04 μg/g). 1 = MCPP, 2 = MCPA, 3 = 2,4-D and 4 = internal standard.

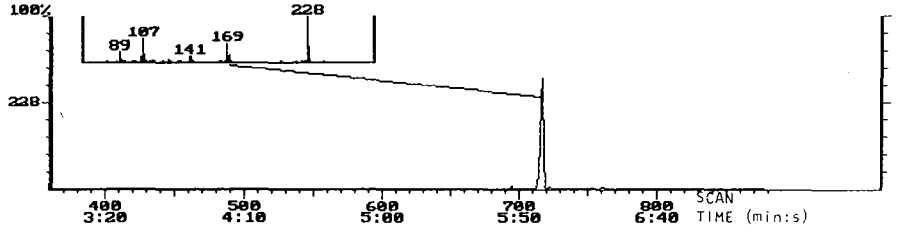

Fig. 3. Mass chromatogram (ion 228) of a treated soil sample (0.19 μg/g of MCPP).

sample was analyzed with the described method and MCPP was determined (0.19 μg/g) and identified by its mass spectrum (Fig. 3).

The proposed methods are reproducible and sensitive enough for determination of 2,4-D, MCPA and MCPP in soil and cereals, at residue level, by GC–ITD.

References

[1] R. Punkayastha, *J. Agr. Food Chem.*, 22 (1974) 453–458.
[2] S.U. Khan, *J. Assoc. Off. Anal. Chem.*, 58 (1975) 1027–1030.
[3] D.W. Woodham, W.G. Mitchell, C.D. Loftis and C.W. Collier, *J. Agric. Food Chem.*, 19 (1971) 186–188.
[4] G.R. Leather and L.E. Forrence, *J. Environ. Qual.*, 11 (1982) 345–347.
[5] A.E. Smith, *J. Assoc. Off. Anal. Chem.*, 67 (1984) 794–798.
[6] A. Adolfsson-Erici and L. Renberg, *Chemosphere*, 23 (1991) 845–854.
[7] C.S. Feung, R.H. Hamilton and R.O. Mumma, *J. Agric. Food Chem.*, 24 (1976) 1013–1015.
[8] H. Ruckendorfer and W. Lindners, *Int. J. Environ. Anal. Chem.*, 18 (1984) 87–99.
[9] J. Pribyl and F. Herzel, *J. Chromatogr.*, 153 (1978) 399–408.
[10] T. Tsukioka and T. Murakami, *J. Chromatogr.*, 469 (1989) 351–359.
[11] M. Osadchuk, E. Salahub and P. Robinson, *J. Assoc. Off. Anal. Chem.*, 60 (1977) 1324–1327.

[12] C.R. Sell and J.C. Maitlen, *J. Agric. Food Chem.*, 31 (1983) 572–575.
[13] H. Agemian and A.S. Chau, *J. Assoc. Off. Anal. Chem.*, 60 (1977) 1070–1076.
[14] H. Siltanen and R. Mutanen, *Chromatographia*, 20 (1985) 685–688.
[15] A.S. Chau and K. Terry, *J. Assoc. Off. Anal. Chem.*, 59 (1976) 633–636.
[16] A.J. Cessna, *Pestic. Sci.*, 30 (1990) 141–147.
[17] A.E. Smith, *Weed Res.*, 16 (1976) 19–22.
[18] H.B. Lee and Y.A.S. Chau, *J. Assoc. Off. Anal. Chem.*, 66 (1983) 1023–1028.
[19] R.H. Hamilton, J. Hunter, J.K. Hall and C.D. Ercegovich, *J. Agric. Food Chem.*, 19 (1971) 480–483.
[20] A.E. Smith, *J. Assoc. Off. Anal. Chem.*, 67 (1984) 794–798.
[21] W.P. Cochrane, *J. Chromatogr. Sci.*, 17 (1979) 124–136.

ELSEVIER

Journal of Chromatography A, 675 (1994) 219–225

JOURNAL OF CHROMATOGRAPHY A

Use of capillary electrophoresis–electrospray ionization mass spectrometry in the analysis of synthetic peptides

Kenneth J. Rosnack, Justin G. Stroh*, David H. Singleton, Bradley C. Guarino, Glenn C. Andrews

Central Research Division, Pfizer Inc., Groton, CT 06340, USA

(First received January 22nd, 1994; revised manuscript received April 6th, 1994)

Abstract

We have constructed a capillary electrophoresis (CE) system with UV detection and have successfully interfaced it to an electrospray ionization mass spectrometry (ES-MS) system. A synthesized fragment of heregulin-β (212–226) was thought to be a single component by re-injection into an HPLC system, but results from CE–UV–ES-MS indicated that a dehydration product was present in the desired peptide sample. A synthetic heregulin-α (177–241) was isolated by preparative HPLC, but re-injection on an analytical system indicated a tailing peak. CE–UV–ES-MS indicated a mixture whose two major components were of the same nominal molecular mass (within experimental error), suggesting the presence of an isomer or a deamidation product. The results show that CE–UV–ES-MS can be used as an orthogonal analytical technique to solve practical problems encountered in peptide synthesis laboratories.

1. Introduction

Peptides of biological interest in the molecular mass range 500–8000 are often synthesized using an automated peptide synthesizer. Crude reaction products are usually purified using preparative reversed-phase HPLC with UV detection which in most cases produces a peptide that is 95% pure by area. When multiple peaks are observed in the chromatogram, identification entails isolation of the fraction and amino acid analysis, N-terminal sequencing, or mass spectrometry (MS). Occasionally a single HPLC peak is actually a mixture of co-eluting peptides or peptides that cannot be fully resolved using HPLC. When this is the case, capillary electrophoresis (CE) with UV detection may be employed as an orthogonal analytical method due to its superior resolving power [1–3].

While analytical CE has superior resolving power, its major drawback is that sample volumes (nanoliter injections) and sample amounts (femtomoles) are low, severely limiting the methods by which the identity of a peak may be determined. Semi-preparative CE [4,5] is possible but is difficult and time consuming. One approach to this problem is to interface CE directly with MS [6–11] to obtain the necessary

* Corresponding author.

0021-9673/94/$07.00
SSDI 0021-9673(94)00373-H

resolving power coupled with analytical sensitivity. In this article, we report on the interfacing of a CE system with electrospray ionization (ES) MS, and on the use of the system for the analysis of synthetic peptide mixtures.

2. Experimental

2.1. Mass spectrometer and electrospray interface

All experiments were performed on a Finnigan MAT TSQ700 triple quadrupole mass spectrometer (Finnigan, San Jose, CA, USA) equipped with an electrospray ionization source (Analytica of Branford, Branford, CT, USA). The source was operated at −3500 V and 20–50 nA in positive ion mode. A coaxial sheath liquid consisting of 2-methoxyethanol (Aldrich, Milwaukee, WI, USA) at a flow-rate of 1 μl/min was used for direct-infusion ES-MS while a 50:50 mixture of isopropanol–1% aqueous acetic acid at a flow-rate of 4 μl/min was used for the CE–ES-MS experiments. Nitrogen was used as the curtain gas and the coaxial sheath gas. The curtain gas was set at 15 p.s.i. (1 p.s.i. = 6894.76 Pa) for all experiments. For direct-infusion ES-MS experiments, the sheath gas was set at 22 p.s.i. while the CE–ES-MS experiments required 13 p.s.i. with the flow controller wide open.

The manufacturer-supplied electrospray probe was used for the direct-infusion experiments while a modified version was used for the CE–ES-MS experiments [12–14]. The modified version of the electrospray probe replaces the stainless-steel sample needle with a 375 μm O.D. polyimide fused-silica tubing used in the CE portion of the experiment. The stainless-steel tubing used for the coaxial liquid sheath was replaced with a section of 22-gauge stainless-steel tubing (0.028 in. O.D. × 0.016 in. I.D.; 1 in. = 2.54 cm; Scientific Instrument Services, Ringoes, NJ, USA) to accommodate the fused-silica CE capillary. The tip of the 22-gauge tubing was rounded and polished to improve electrospray stability. The orifice in the gas sheath probe tip was enlarged to accommodate the 22-gauge tubing. The fused-silica CE capillary terminated flush with the edge of the 22-gauge stainless-steel tubing. Many of the above design changes have been described by Thompson et al. [12].

The mass spectrometer was tuned and calibrated using horse heart cytochrome *c* and glucagon, respectively. Profile mode spectra (peaks presented in analog format) were collected at a scan time of 3.5 s, averaging 32 scans. Spectra were smoothed using a seven-point smoothing routine. Profile mode provides the best accuracy of the data but rapidly consumes disk storage space. Centroid spectra (profile data converted to bar graph format) were collected at a scan time of 2 s. These spectra were averaged over 10–25 scans and were background subtracted. Centroid data files are considerably smaller than profile data files and hence were used in collecting the CE–UV–ES-MS data. Electropherograms were smoothed using a seven-point routine and were also baseline corrected. The molecular mass as well as the multiply charged peaks in the profile and centroid spectra were identified using a "deconvolution algorithm" [15] and an "averaging algorithm" [15] using Finnigan's Biotech software. All numbers shown in the mass spectra are observed m/z values while the "observed mass" in the figure captions and text refers to the observed molecular mass of the compound.

2.2. HPLC

The HPLC analysis was performed on a Beckman System Gold (Beckman Instruments, Fullerton, CA, USA). The chromatography was performed using a linear gradient consisting of 0.1% aqueous trifluoroacetic acid (TFA) and 0.1% TFA in acetonitrile on a Waters C_{18} μBondapak 300 × 3.9 mm column (Waters, Division of Millipore, Milford, MA, USA).

2.3. Capillary electrophoresis

A CE system was constructed in our laboratory and consisted of commercially available

components and a fabricated Plexiglass housing. A Spellman CZE1000R 30 kV power supply (Spellman, Plainview, NY, USA) and a Spectra-Physics Spectra 100 UV–Vis detector (Spectra-Physics Analytical, San Jose, CA, USA) comprised the main components of the system. The CE columns were made from 75 μm I.D. × 375 μm O.D. fused-silica (Polymicro Technologies, Phoenix, AZ, USA) capillary tubing. Uncoated capillary columns were 110 cm in length while linear polyacrylamide-coated columns [16] (made in our laboratory) were 90 cm. Both the untreated and linear polyacrylamide columns were used for CE–UV and CE–UV–ES-MS analysis. The bradykinin–magainin spacer peptide (MSP) mixture and heregulin-β fragment were run on the untreated fused-silica CE columns while the heregulin-α sample was run on the linear polyacrylamide-coated CE columns. The internally coated polyacrylamide columns were found to minimize adsorption of peptides and small proteins to the capillary wall. The absence of electroosmotic flow in the polyacrylamide column did not affect the performance of the CE–ES-MS system. Approximately 1 mm of the fused silica's external polyimide coating was removed 40 cm from the inlet side of the capillary to provide a window for the UV detector.

The polyacrylamide-coated CE column was washed with 100 μl of distilled water followed by 100 μl of the background electrolyte, while the untreated capillary was washed first with 100 m*M* NaOH followed by distilled water and the background electrolyte. Samples were siphon-infused into the CE column by inserting the column inlet into the sample vial and then elevating the column inlet 25 cm above the outlet for approximately 10 s. This procedure produced an injection volume of approximately 10 nl. Bulk flow was minimized in the CE capillary by adjusting the height of the anode reservoir with respect to the electrospray probe using the procedure described by Thompson and co-workers [12]. Samples were electrophoresed at 275 V/cm with resulting currents of 1–12 μA depending on the background electrolyte. UV detection was performed at 214–220 nm, 0.005 AUFS and 0.3 s rise time.

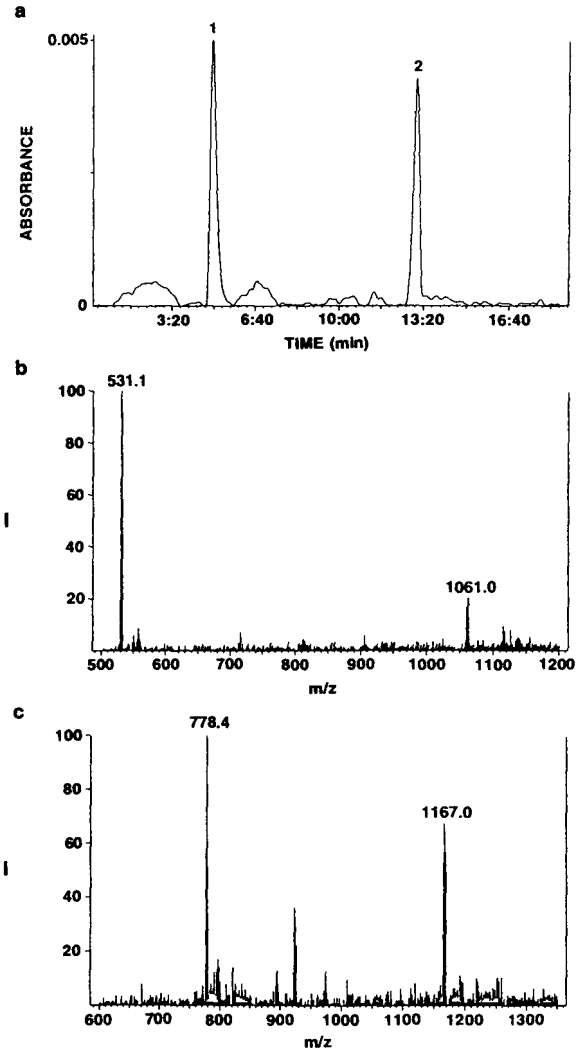

Fig. 1. (a) CE–UV electropherogram of bradykinin (peak 1, ca. 10 pmol) and magainin spacer peptide (peak 2, ca. 5 pmol) mixture. CE analysis was performed using a 110-cm untreated fused-silica column with 20 m*M* ammonium acetate (pH 5.5) as the background electrolyte. (b) Averaged mass spectrum of bradykinin (calculated M_r 1060.2) from the CE–UV–ES-MS analysis of peak 1. The observed M_r was 1059.9. (c) Averaged mass spectrum of magainin spacer peptide (calculated M_r 2332.4) from the CE–UV–ES-MS analysis of peak 2. The observed M_r was 2332.1.

2.4. Sample preparation

Cytochrome *c* (Sigma, St. Louis, MO, USA) and glucagon (Boehringer Mannheim, In-

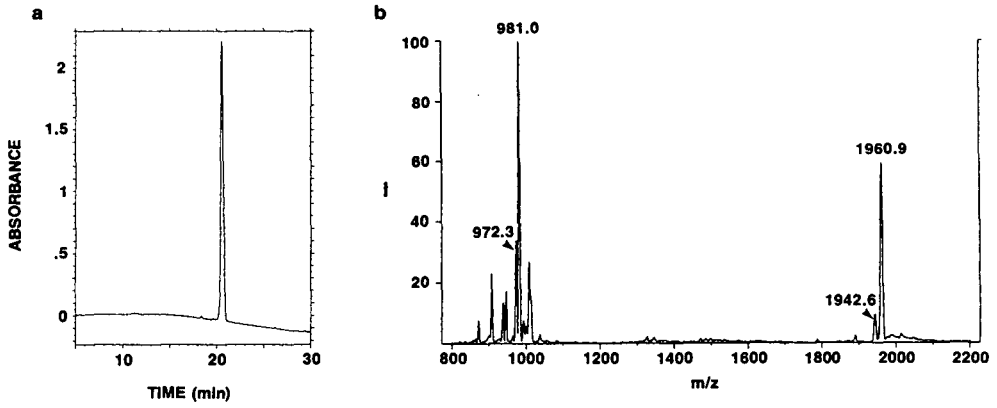

Fig. 2. (a) Reversed-phase analytical HPLC–UV chromatogram of the heregulin-β fragment (calculated M_r 1959.8). HPLC gradient was 0–80% acetonitrile (0.1% TFA) over 30 min. (b) Direct infusion ES profile mass spectrum of the heregulin-β fragment The observed M_r of 1959.9 (MH^+: 1960.9) corresponds to the intact peptide while the observed M_r of 1942.4 corresponds to a potential dehydration product.

dianapolis, IN, USA) standards, used in the tuning and calibration of the mass spectrometer, were dissolved in 0.1% TFA at 10 pmol/μl. They were infused at 1 μl/min into the mass spectrometer. Bradykinin (Sigma), MSP (Peninsula Labs., Belmont, CA, USA), and heregulin-α [17] (prepared in our laboratory), used in the CE–ES-MS experiments, were dissolved at 1 μg/μl in 0.1% TFA. A truncated synthetic heregulin-β [17] peptide Ac-C(Acm)PNEFTGDRC(Acm)QNYVM-NH_2 (prepared in our laboratory; Acm = acetamidomethyl) was dissolved to 1 μg/ml in distilled water.

The peptides were synthesized on an ABI Model 430A (Applied Biosystems, Foster City, CA, USA) solid-phase synthesizer using a *tert.*-butoxycarbonyl (Boc) protocol with capping. The ABI system employs 1-hydroxybenzotriazol (HOBT) active ester coupling using standard amino acids and N-methylpyrrolidone (NMP)-based chemistry. All samples were run as received.

The background electrolyte for heregulin-α was 20 m*M* ϵ-amino-*n*-caproic acid (EACA) [12,18] (Sigma) adjusted to pH 4.6 using glacial acetic acid. All other samples were run using 10–20 m*M* ammonium acetate (Sigma) adjusted to pH 5.5 using glacial acetic acid.

3. Results and discussion

To demonstrate a working and viable CE–ES-MS system, bradykinin (calculated molecular mass 1060.2) and MSP (calculated molecular mass 2332.4) were used as a test mixture. Fig. 1a shows the CE–UV electropherogram resulting from an approximately 10-nl injection of bradykinin (ca. 10 pmol) and MSP (ca. 5 pmol) test mixture onto a 1.1 m untreated fused-silica column using a background electrolyte of 20 m*M* ammonium acetate (pH 5.5). Bradykinin was the first peak to elute followed by MSP approximately 14 min later. The mass spectra of the bradykinin and MSP are presented in Fig. 1b and c, respectively. Both the electropherogram and mass spectra show that this particular system can be used for analysis of peptide mixtures in the low picogram range.

3.1. Heregulin-β

The heregulins [17] are specific activators of the $p180^{erbB4}$ gene [19], which has been implicated in breast and ovarian cancers. A fragment of heregulin-β (212–226), Ac-C(Acm)-PNEFTGDRC(Acm)QNYVM-NH_2 (calculated molecular mass 1959.8), was synthesized and

further purified by preparative HPLC. Although the isolate was thought to be a single component by re-injection into the HPLC system (Fig. 2a), a direct-infusion ES-MS (Fig. 2b) spectrum of the isolate indicated a possible dehydration impurity. The peaks at m/z 1960.9 and 981.0 correspond to the singly $(M + H)^+$ and doubly $(M + 2H)^{2+}$ charged ions, respectively, for the desired peptide. The peaks at m/z 1942.6 and 972.3 arise from the singly and doubly charged ions, respectively, of a dehydration product $(M - 18)$. It was not known whether this dehydration product was produced by the electrospray process or whether it was truly an impurity in the sample. Since a mixture was not indicated by HPLC, we performed a CE analysis to determine if the impurity was present in the truncated heregulin-β sample. A CE–UV electropherogram of the truncated heregulin-β sample is shown in Fig. 3a. Two components were found in the sample (Fig. 3a). A CE–MS mass spectrum of the minor component (peak 1) is presented in Fig. 3b. The peak at m/z 971.8 corresponds to the doubly charged ion of a dehydration product which has an observed molecular mass of 1941.6. The observed mass is in close agreement with the calculated mass of 1941.8 even though the signal obtained is very weak. Peak 2, whose mass spectrum is shown in Fig. 3c, is the desired peptide. The peak at m/z 1961.3 is the $(M + H)^+$ for the desired peptide (calculated molecular mass 1959.8) while the peak at m/z 981.2 is the doubly charged species. The observed and calculated mass agree within the expected error of a fast centroid scan analysis.

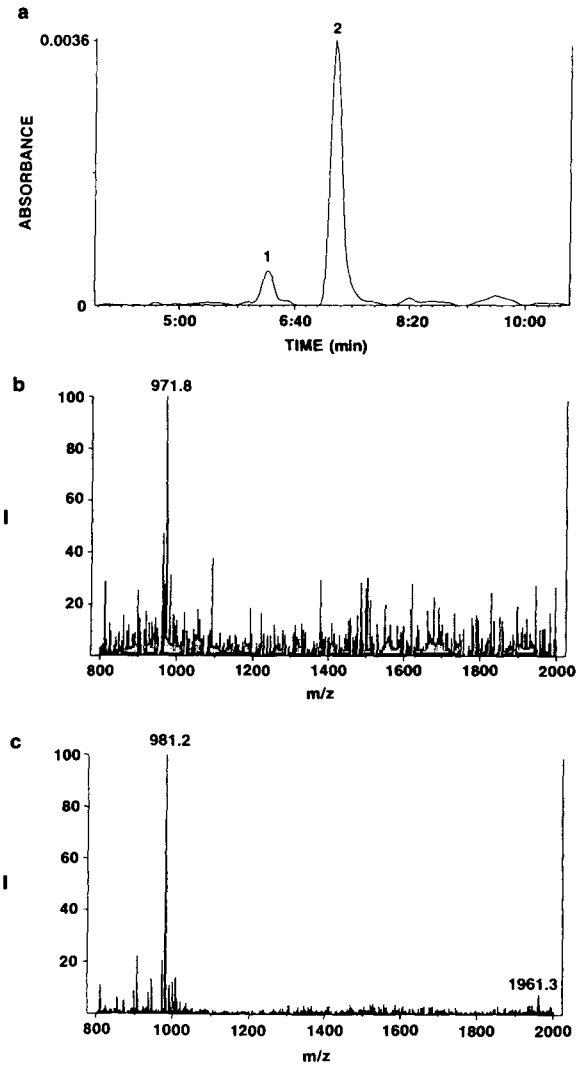

Fig. 3. (a) CE–UV electropherogram of the heregulin-β fragment (ca. 5 pmol). CE analysis was performed using a 110-cm untreated fused-silica column with 10 mM ammonium acetate (pH 5.5) as the background electrolyte. (b) Averaged mass spectrum of peak 1 from the CE–UV–ES-MS analysis of the heregulin-β fragment sample. The observed M_r based on the doubly charged ion is 1941.6 and corresponds to a dehydration product. (c) Averaged mass spectrum of peak 2 from the CE–UV–ES-MS analysis of the heregulin-β fragment sample. The observed M_r was 1960.4 and corresponds to the intact peptide.

3.2. Heregulin-α

A second problem that we analyzed using CE–ES-MS involved a synthetic 63 amino acid peptide, heregulin-α (177–241) which has the sequence: SHLVKCAEKEKTFCVNGGECFMVKDLSNPSRYLCKCQPGFTGARCTENVPMKVQNQEKAEELY. This peptide was synthesized and isolated using HPLC. The HPLC–UV data indicated a single component, although there was some broadening of the peak (see Fig. 4a) which was thought to be due to overlapping peaks. Direct-infusion ES-MS indicated a single molecular mass, so any impurity present was

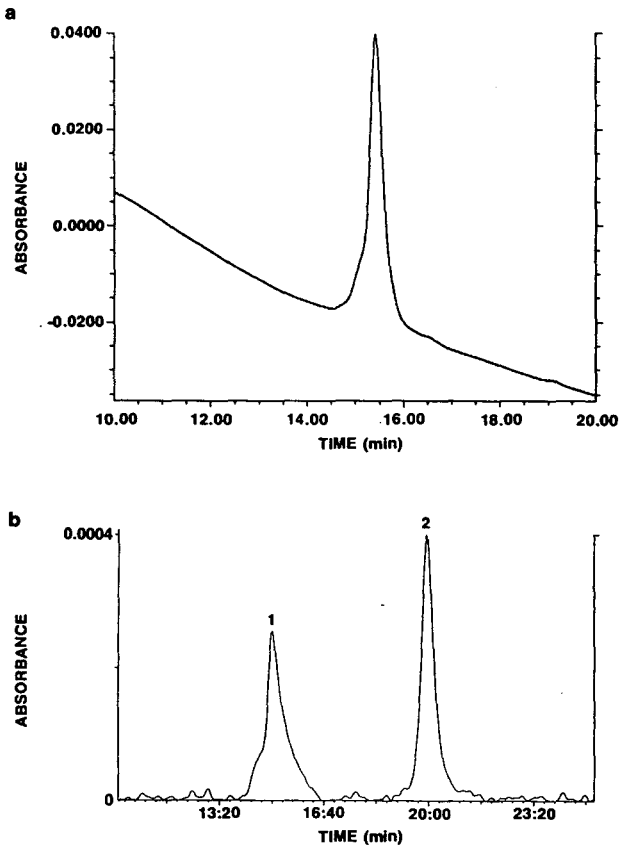

Fig. 4. (a) HPLC–UV chromatogram of the heregulin-α sample. (calculated M_r 7113.3). HPLC gradient was 10–60% acetonitrile (0.1% TFA) over 45 min. (b) CE–UV electropherogram of the heregulin-α sample. CE analysis was performed on a 90-cm linear polyacrylamide-coated capillary using 20 mM EACA (pH 4.6) as the background electrolyte. Peak numbers refer to Fig. 5.

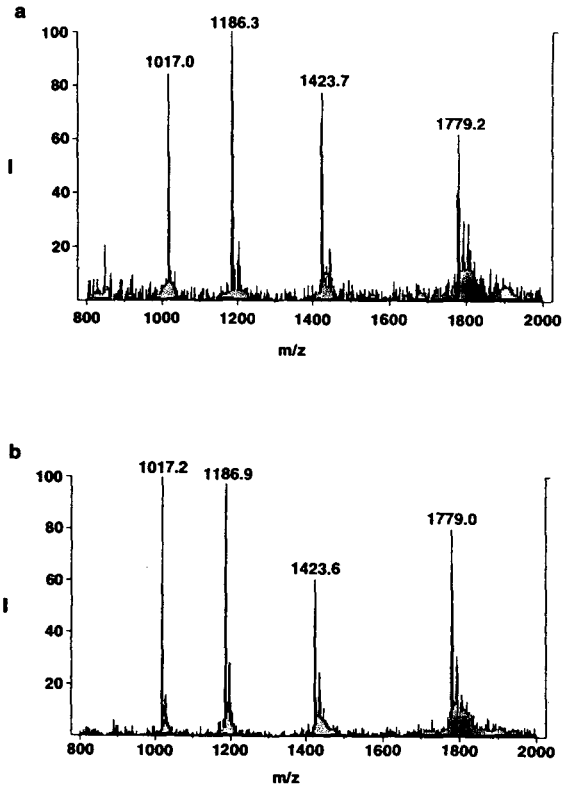

Fig. 5. (a) Averaged mass spectrum of peak 1 found in the CE–UV–ES-MS analysis of the heregulin-α sample (Fig. 4b). The observed M_r was 7113.0. (b) Averaged mass spectrum of peak 2 found in the CE–UV–ES-MS analysis of the heregulin-α sample (Fig. 4b). The observed M_r was 7112.6.

likely an isomer of the desired material. CE–UV–ES-MS was performed on this sample due to concern over the broadening of the peak in the HPLC. The CE–UV electropherogram, indicating two components, is shown in Fig. 4b. The CE–MS spectra for the two components are found in Fig. 5a and b. The two peaks give identical mass spectra, which suggests two possibilities: first, that the two components are isomeric due to differences in the disulfide bonding pattern or second, that one component contains a single deamidation (loss of 1 u) of one of the four asparagines or three glutamines in this peptide. As for the first possibility, a difference in three-dimensional structure resulting from different disulfide bonding patterns could cause differences in charge availability and hence differences in elution times in the CE analysis. As for the second possibility, a difference of 1 u at mass 7113 would appear as the same nominal mass within the error of the present instrumentation. Although the power of CE–MS in solving problems in peptide synthesis is readily apparent in this example, at the present time we cannot use it to distinguish between these two possibilities.

4. Conclusions

We have successfully interfaced a CE system to a TSQ700 mass spectrometer and have demonstrated that CE, with its superior resolving power, can separate complex synthetic peptide mixtures when reversed-phase HPLC cannot. Although low sample loading is a drawback to the CE technique, coupling CE to MS overcomes the problem and utilizes the mass-resolving capability and high sensitivity of the spectrometer for structure analysis of the mixture. CE–UV–ES-MS is a powerful complimentary analytical technique for solving practical problems encountered in a peptide synthesis laboratory.

Acknowledgement

We greatly appreciate the assistance on CE technology provided to us by Dr. Paul Vouros and co-workers, Department of Chemistry, Northeastern University, Boston, MA, USA.

References

[1] F. Foret and P. Boček, *Electrophoresis*, 11 (1990) 661–664.
[2] A. Guttman, A.S. Cohen, D.N. Heiger and B.L. Karger, *Anal. Chem.*, 62 (1990) 137–141.
[3] J.W. Jorgenson and K.D. Lukacs, *Science*, 222 (1983) 266–272.
[4] M. Albin, S.-M. Chen, A. Louie, C. Pairaud, J. Colburn and J. Wiktorowicz, *Anal. Biochem.*, 206 (1992) 382–388.
[5] N. Banke, K. Hansen and I. Diers, *J. Chromatogr.*, 559 (1991) 325–335.
[6] F. Garcia and J.D. Henion, *Anal. Chem.*, 64 (1992) 985–990.
[7] J.A. Olivares, N.T. Nguyen, C.R. Yonker and R.D. Smith, *Anal. Chem.*, 59 (1987) 1230–1232.
[8] T. Wachs, J.C. Conboy, F. Garcia and J.D. Henion, *J. Chromatogr. Sci.*, 29 (1991) 357–366.
[9] R.D. Smith, H.R. Udseth, C.J. Barinaga and C.G. Edmonds, *J. Chromatogr.*, 559 (1991) 197–208.
[10] M.A. Moseley, L.J. Deterding, K.B. Tomer and J.W. Jorgenson, *Anal. Chem.*, 63 (1991) 109–114.
[11] E.D. Lee, W. Muck, J.D. Henion and T.R. Covey, *Biomed. Environ. Mass Spectrom.*, 18 (1989) 844–850.
[12] T.J. Thompson, F. Foret, P. Vouros and B.L. Karger, *Anal. Chem.*, 65 (1993) 900–906.
[13] R.D. Smith, C.J. Barinaga and H.R. Udseth, *Anal. Chem.*, 60 (1988) 1948–1952.
[14] S.K. Chowdhury and B.T. Chait, *Anal. Chem.*, 63 (1991) 1660–1664.
[15] M. Mann, C.K. Meng and J.B. Fenn, *Anal. Chem.*, 61 (1991) 1702–1708.
[16] S. Hjertén, *J. Chromatogr.*, 347 (1985) 191–198.
[17] W.E. Holmes, M.X. Sliwkowski, R.W. Akita, W.J. Henzel, J. Lee, J.W. Park, D. Yansura, N. Abadi, H. Raab, G.D. Lewis, M. Shepard, W.-J. Kuang, W.I. Wood, D.V. Goeddel and R.L. Vandlen, *Science*, 256 (1992) 1205–1210.
[18] F. Foret, E. Szoko and B.L. Karger, *J. Chromatogr.*, 608 (1992) 3–12.
[19] G.D. Plowman, J.M. Green, J.-M. Culouscou, G.W. Carlton, V.M. Rothwell and S. Buckley, *Nature*, 366 (1993) 473–475.

ELSEVIER

Journal of Chromatography A, 675 (1994) 227–236

JOURNAL OF CHROMATOGRAPHY A

Determination of metal cations by capillary electrophoresis Effect of background carrier and complexing agents

Y.-H. Lee, T.-I. Lin*

Department of Chemistry, National Taiwan University, Taipei 106, Taiwan

(First received November 26th, 1993; revised manuscript received March 2nd,1994)

Abstract

The determination of trace metals in aqueous samples can be readily accomplished by capillary electrophoresis (CE) via indirect absorbance detection. Methods for simultaneously determining alkali, alkaline earth and transition metal ions and Group IB, IIB and IVA metals ions were developed. Imidazole, benzylamine, ephedrine or pyridine was used as the carrier buffer and the background absorbance provider. Glycolic acid, α-hydroxyisobutyric acid or succinic acid was used as the complexing agent. The elements determined were Li, Na, K, Cs, Mg, Ca, Sr, Ba, Cr, Mn, Fe, Co, Ni, Cu, Zn, Cd, Ag, Al and Pb. All ions could be separated in less than 15 min. In most instances reported here, more than a dozen ions could be separated in 5–10 min. All peaks were well separated and baseline resolved (*i.e.*, no peaks overlapped), except Ag and Al, which required a separate and additional analysis. The detection limit was in the range 0.02 (Na)–208 ppb (Cr) with the electrokinetic injection mode (10 kV, 5 s). The reproducibility was 1% for the migration time and better than 5% for the peak height for most metal ions. The calibration graphs were linear for most ions in the concentration range 10^{-5}–10^{-3} M ($R^2 = 0.9995$–0.9999) using the hydrodynamic injection mode. Concentrations lower than 10^{-5} M can be determined using the electrokinetic injection mode, but the calibration graph is not linear. The methods developed here are well suited for determining metal ions in a variety of real samples.

1. Introduction

The determination of metal ions in various samples is important for obvious reasons. Reliable and rapid techniques are needed for the determination of metal ions in medicines, soil samples, drinking water, etc. Metal ions can be determined by a number of techniques, including various atomic spectroscopic methods, electrochemical methods and ion chromatography [1,2]. A separation tool which has been rapidly developing is capillary electrophoresis (CE). Since a UV absorption detector is readily available in all commercial capillary electrophoresis systems, the development of indirect UV absorption detection has made metal ion determination by CE an attractive alternative.

Foret *et al.* [3] utilized indirect UV detection to demonstrate the separation of fourteen lanthanide cations by CE with the aid of a complexing agent, α-hydroxyisobutyric acid (HIBA), and creatinine as a UV-absorbing co-ion. Wildman *et al.* [4] and Weston and co-workers [5–7] investigated the factors affecting the separation of metal cations and optimized the detection sensitivity for metal cations using indirect photometric detection. They showed that a mixture of ninetten alkali, alkaline earth and lanthanide

* Corresponding author.

0021-9673/94/$07.00
SSDI 0021-9673(94)00220-4

metal cations can be baseline resolved in less than 2 min. Beck and Engelhardt [8] investigated several background carrier electrolytes (BCE) for indirect UV detection and found imidazole to be suitable for the separation of metal ions, amines and amino alcohols. They recently reported [9] a new buffer system consisting of *p*-aminopyridine and 2-hydroxybutyric acid for the separation of some transition metals. Timerbaev *et al.* [10] used 8-hydroxyquinoline-5-sulphonic acid for the CE of the transition and alkaline earth metals as precolumn-formed chelates with direct UV detection. Aguilar *et al.* [11] and Buchberger *et al.* [12] reported a detection scheme for the CE determination of Fe, Cu, Ni, Cr, Hg, Pd, Ag, Cd, Zn and Co cations using cyanide complexes by direct UV detection. Chen and Cassidy [13] evaluated several experimental parameters, *e.g.*, indirect detection reagents, pH, complexing agents and type of capillary surfaces, that would affect the separation of metal ions by CE and optimized the conditions for the separation of 26 metal ions. Shi and Fritz [14] described the use of several complexing agents, including phthalate, tartrate, HIBA and lactate, for the separation of 27 metal ions in only 6 min. Recently, we have investigated the role of complexing agents and pH on the CE separation of alkali and alkaline earth metal ions [15]. Using various mono-, di- and tricarboxylic and hydroxycarboxylic acids as complexing agents and imidazole as the background carrier for indirect UV absorbance detection, we showed that the metal ions could be completely separated in less than 2 min with a maximum resolution of 15 and a number of theoretical plates as high as 750 000 per metre.

We report here CE methods for analyzing a mixture of nineteen metal ions (Li, Na, K, Cs, Mg, Ca, Sr, Ba, Cr, Mn, Fe, Co, Ni, Cu, Zn, Cd, Ag, Al and Pb) (alkali metals and Ag ions are monovalent, Al and Cr ions are trivalent, all other ions are divalent; charges are omitted for brevity). Detection of metal ions was accomplished by indirect UV absorbance measurement. Imidazole, benzylamine, ephedrine and pyridine were investigated as carrier buffers and background absorbance providers. Glycolic and succinic acid and HIBA were employed as metal-complexing agents.

2. Experimental

2.1. Chemicals

All metal ion solutions were prepared from their nitrate salts, except Fe(II) (chloride salt). Stock standard solutions (1.0×10^{-2} *M*) were prepared, mixed and diluted to the specified concentrations used in different CE runs. All chemicals used, including various BCE and complexing agents, were of analytical-reagent grade from several vendors. Doubly deionized water prepared with a Milli-Q system (Millipore, Bedford, MA, USA) or doubly deionized distilled water was used exclusively for all solutions. The water blank was routinely checked for contamination by trace amounts of alkali and alkaline earth metal ions.

2.2. Buffers and pH adjustment

The running buffer contained 5 or 10 m*M* of BCE. The pH was varied as specified in the figures, being adjusted by adding a 1 *M* stock solution of complexing agent to the desired pH of 4.0 or 4.5 depending on the experiments. The concentration of the complexing acid varied from 5.7 to 16 m*M* (calculated by the volume added) as specified in the figures.

2.3. Apparatus

CE experiments were carried out in a fully automated Spectra Phoresis Model 1000 instrument (Spectra-Physics, San Jose, CA, USA). The system was equipped with a rapid scanning UV–Vis detector with 5-nm wavelength resolution. In most instances reported here, the detector wavelength was fixed at 254 nm (for pyridine) or 210 nm (all others) in order to obtain a more stable and less noisy baseline. The instrument was also equipped with an autosampler, a capillary cartridge and a solid-state Peltier temperature control unit. A personal computer (486 IBM

AT-compatible PC) was used to control the instrument settings, data acquisition and analysis with the vendor-provided software. The separation capillaries (bare fused silica) from Polymicro Technologies (Phoenix, AZ USA) were 75 μm I.D. (365 μm O.D.) × 70 cm (63 cm to the detector) for the determination of the mobilities of background carriers and 75 μm I.D. (365 μm O.D.) × 90 cm (83 cm to the detector) for the separation of mixtures of metal ions. UV–Vis absorption spectra of BCE and complexing agents were measured with a Hitachi (Tokyo, Japan) U-2000 double-beam scanning spectrophotometer.

2.4. Electrophoretic procedures

Prior to first use, a new capillary was subjected to a standard wash cycle, and subsequent runs were carried out according to the established procedure [15]. Sample injection was carried out in either the electrokinetic (EK) or hydrodynamic (HD) mode as specified in the figures and tables. The separation run was at a constant voltage of +25 kV at a constant temperature of 25°C and with a current of 4–12 μA. The capillary was also washed with 0.1 *M* NaOH and deionized water as a daily routine. All buffer solutions were freshly prepared, filtered through 0.20-μm membranes and degassed under vacuum for 10 min.

2.5. Electrophoretic mobility determination

Benzyl alcohol was added to samples as a neutral marker for the electrophoretic mobility determination. The mobilities of the various BCE under the specified CE conditions were determined in 10 m*M* sodium acetate buffer (pH 4.0 or 4.5). Samples were injected in the HD mode for 1 s. Detection was made by rapidly scanning the UV absorbance over the range 200–300 nm, which allowed a positive identification of the background provider. Electroosmotic mobility, μ_{eo}, was calculated by the following equation:

$$\mu_{eo} = l_d l_t / t_m V \ (\mathrm{cm^2\ V^{-1}\ s^{-1}})$$

$$\mu_e = \mu_{obs} - \mu_{eo}$$

where l_d and l_t are the length of the capillary to the detector and the total length of the capillary, respectively, V is the running voltage and t_m is the migration time of the neutral marker (benzyl alcohol). The electrophoretic mobility of the background carrier electrolyte, μ_e, was obtained by subtracting μ_{eo} from the observed mobility μ_{obs}.

2.6. Identification of metal peaks in electropherograms

Peak identification for a specific metal ion was carried out after a complete baseline separation of all peaks had been established under the given conditions specified in the figures. Standards that contained only a single metal ion were run under the same conditions. The migration time of the known ion was compared with those in the mixture of metals. Since the reproducibility of migration time was about 0.2% in the HD injection mode and about 1% in the EK injection mode (see the Results and Discussion), this approach was fairly reliable. Also, trace amounts of K and Na were sometimes present in the diluent, the retention of which served as an internal marker for adjusting small discrepancies in the migration time. Alternatively, samples were spiked with standards containing only single metal species and the peak with increased height was identified.

3. Results and discussion

3.1. Separation of metal ions in different background electrolytes

Seventeen metal ions could be separated in CE using imidazole, pyridine or benzylamine as the BCE with the addition of glycolic acid as the complexing agent. Previous studies have shown that in order to achieve a good separation of analytes, the mobilities of the analyte ions must match that of the BCE [7,8]. The mobilities of the BCE used in this work were determined and

Table 1
Mobilities and pK_a values of various BCE

BCE	pK_a[a]	Mobility[b] ($cm^2\ kV^{-1}\ s^{-1}$)	
		pH 4.0	pH 4.5
Imidazole	6.95	0.511	0.507
Pyridine	5.25	0.472	0.416
Benzylamine	9.33	0.373	0.352
Ephedrine	10.14	0.283	0.280

[a] From ref. 16.
[b] See Experimental for details.

are listed in Table 1 along with their pK_a values. The positions where these background carriers appear in the electrophoregram are indicated by upward arrows in the figures. The mobility of imidazole matched best with the alkali and alkaline earth metal ions (they have higher mobilities), hence in this buffer these metal ions were better separated than the other ions (see Fig. 1). The migration order of the seventeen metal ions is as follows: (1) Cs, (2) K, (3) Ba, (4) Sr, (5) Na, (6) Ca, (7) Mg, (8) Mn, (9) Cr, (10) Fe, (11) Cd, (12) Li, (13) Co, (14) Ni, (15) Pb, (16) Zn, (17) Cu. In all of the following figures, these peaks will be referred to by arabic numerals 1–17. In imidazole, peaks 10 and 11 (Fe, Cd) and peaks 12 and 13 (Li, Co) were not baseline resolved. Ni, Pb and Zn ions (peaks 14–16) that migrated more slowly showed peak trailing and had broader peak widths. Cu ion migrated the slowest and had the highest retention (about 13 min *vs.* 5.4–10.4 min for other peaks) with considerable peak trailing. Presumably the last four ions formed complexes with glycolic acid that have higher stability constants.

The migration order of these seventeen ions was the same in all three BCE. However, the resolution depended on the mobility of the BCE used. In imidazole the resolution for the last four peaks was poor because the mobility of BCE was too fast, and hence incompatible with these four metals. Pyridine, which had a lower mobility than imidazole, provided a better separation for the transition metal ions than the other BCE that were tried. Comparing the CE performed in imidazole, the most noticeable difference was the better separation between Fe and Cd peaks, and a complete baseline resolution of Li and Co

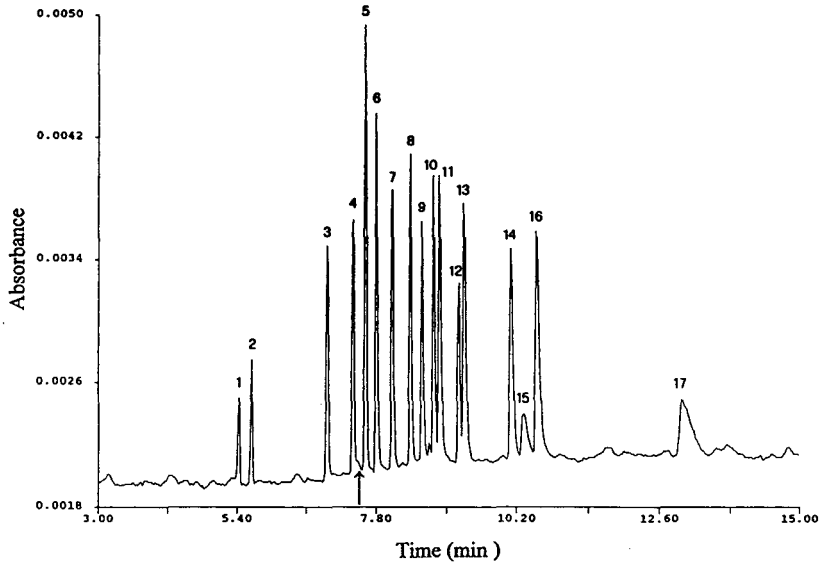

Fig. 1. Electrophoretic separation of seventeen metal ions using 10 m*M* imidazole–13 m*M* glycolic acid (pH 4.0). 1 = Cs; 2 = K; 3 = Ba; 4 = Sr; 5 = Na; 6 = Ca; 7 = Mg, 8 = Mn; 9 = Cr; 10 = Fe; 11 = Cd; 12 = Li; 13 = Co; 14 = Ni; 15 = Pb; 16 = Zn; 17 = Cu. Metal ions migrate in the same order in all figures. The upward arrow indicates the migration position of imidazole.

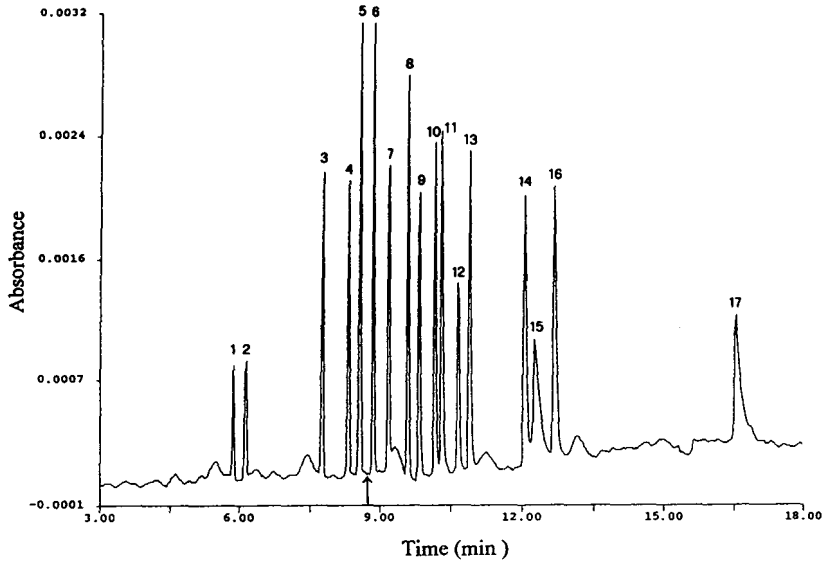

Fig. 2. Electrophoretic separation of seventeen metal ions using 10 m*M* pyridine–12 m*M* glycolic acid (pH 4.0). The upward arrow indicates the migration position of pyridine. Peaks as in Fig. 1.

peaks (Fig. 2). The Pb and Cu peaks were also higher. The number of theoretical plates, N, in pyridine was higher for the last four ions than in the imidazole buffer. In benzylamine the five slower migrating ions all had sharper peaks (and hence higher N); however, Cd and Li were poorly separated (Fig. 3).

We thought that adding ephedrine (lowest mobility among the four) might improve the resolution of the last four peaks. A mixed BCE

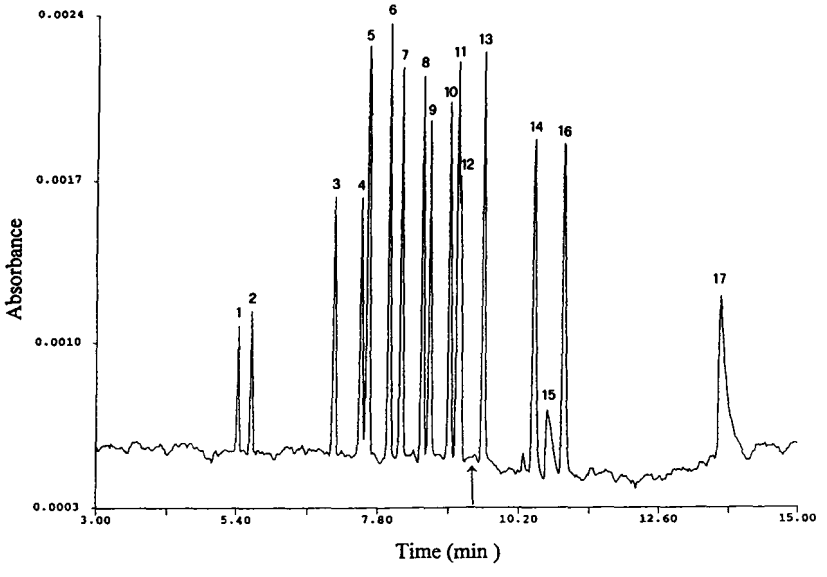

Fig. 3. Electrophoretic separation of seventeen metal ions using 10 m*M* benzylamine–16 m*M* glycolic acid (pH 4.0). The upward arrow indicates the migration position of benzylamine. Peaks as in Fig. 1.

containing 5 m*M* imidazole and 5 m*M* ephedrine with 12.2 m*M* glycolic acid (pH 4.0) was investigated, since in imidazole the migration time is shorter while the addition of ephedrine (smallest mobility among the four) may improve the performance of the last four peaks. Indeed, the Pb, Zn and Cu peaks (migration time unchanged as in 10 m*M* imidazole) were all considerably sharper in the mixed BCE than in the absence of ephedrine (Fig. 4). However, the separations between Fe and Cd and between Li and Co were poor. Thus, for samples in which analysis for the last four ions is more important, running CE in mixed BCE will improve their determination. The electroosmotic flow increased as the pH increased from 4.0 to 4.5, hence the CE separation time could be shortened at higher pH. However, we found that at pH 4.5 the resolution was inferior to that at pH 4.0 when monoprotic acids were used as the complexing agents. The resolution of the electropherogram was very sensitive to pH, as reported previously for alkali and alkali earth metal ions [15]. Overall, running CE in 10 m*M* pyridine combined with 12 m*M* glycolic acid at pH 4.0 seems to give the best performance.

3.2. Effect of the complexing agent on CE separation

Several previous studies [3,6,15] have shown that HIBA is an effective complexing agent for separating alkali and alkaline earth metal cations by CE. We showed that succinic acid and several other dicarboxylic acids are also useful complexing agents for similar applications [15]. Previously, we tried CE for the seventeen cations using 10 m*M* imidazole and 14.6 m*M* HIBA at pH 4.0. Under such conditions, the Na–Ca, Cr–Fe, Cd–Li and Ni–Pb peaks could not be completely resolved [17]. The effects of imidazole and HIBA were investigated by lowering their concentrations to 5 and 6.75 m*M* (pH 4.0), respectively. The separation of certain metal cations was improved; in particular, the Ca, Na, Cr, Fe and Pb peaks were all well separated. However, the separation of Mn–Cd was poor and the Ni peak became merged with the Li peak (Fig. 5). The migration order of these seventeen ions also changes, indicating that the complexing agent has a strong effect particularly on the mobility of the divalent cations. The effect of succinic acid as a complexing agent was investigated. CE was

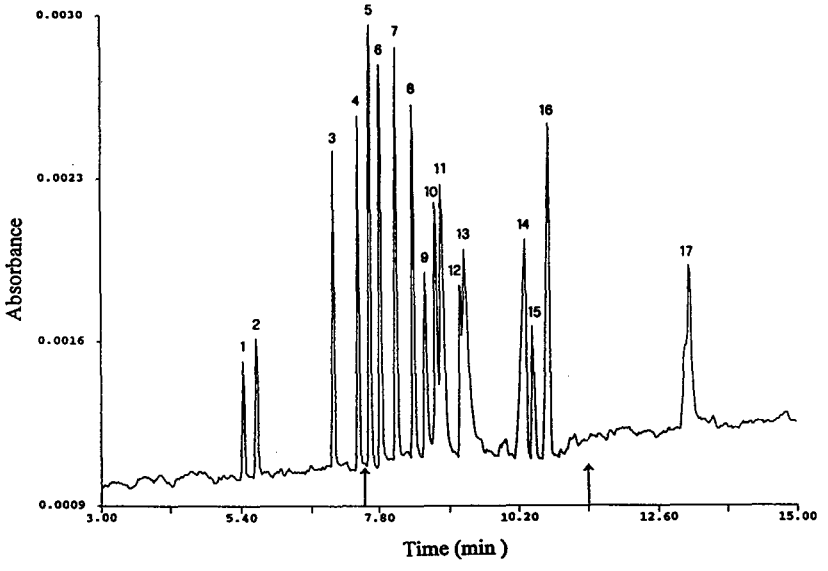

Fig. 4. Electrophoretic separation of seventeen metal ions using 5 m*M* imidazole–5 m*M* ephedrine–12.2 m*M* glycolic acid (pH 4.0). The left arrow indicates the migration position of imidazole and the right arrow that of ephedrine. Peaks as in Fig. 1.

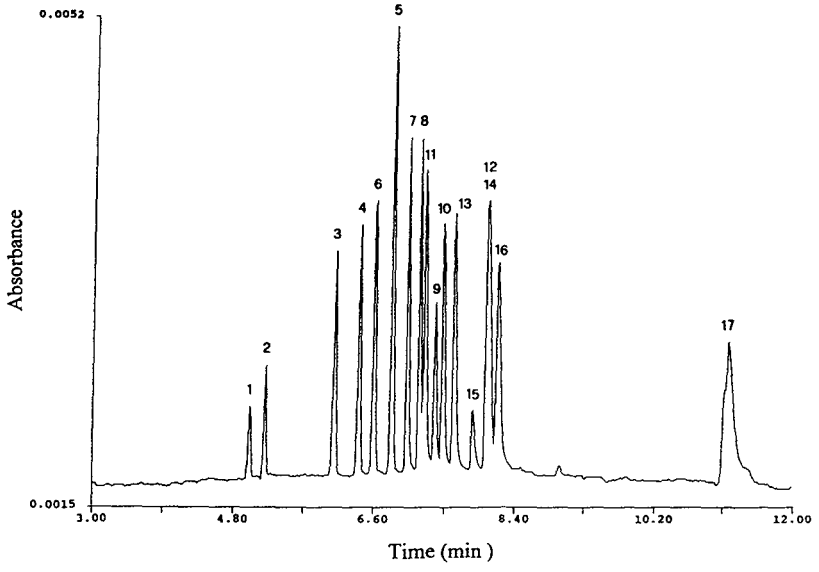

Fig. 5. Electrophoretic separation of seventeen metal ions using 5 m*M* imidazole–6.75 m*M* HIBA (pH 4.0). Peak 14 is Ni merged with the Li peak. Peaks as in Fig. 1.

performed using 10 m*M* imidazole and 9.7 m*M* succinic acid (pH 4.5), using 10 m*M* pyridine and 7.5 m*M* succinic acid (pH 4.5) and using 5 m*M* benzylamine and 5.75 m*M* succinic acid (pH 4.5). In all three buffers, which contained succinic acid as the complexing agent, the separations of metal cations were inferior to those obtained using glycolic acid. The results support the previous notion that the complexing agent plays a more important role than the background carrier in resolving ions whose mobilities were close and therefore could not be separated without the addition of a particular complexing agent.

3.3. CE determination of silver and aluminium cations

The determination of Ag and Al when mixed with the alkali and alkaline earth metal ions is a challenging problem. Numerous combinations of different compositions of BCE and complexing agents have been tried without complete success. Al and Ag cations could be separated from the seventeen ions in the previous analysis only in pyridine (5 m*M*), with the pH adjusted to 3.2 by sulphuric acid, which also acted as a complexing agent [15]. However, the electropherogram of the mixture of nineteen metal ions showed that the transition metal and Pb ions (peaks 8–11 and 13–17 in Fig. 2) overlapped with the alkali and alkaline earth metal ions (peaks 3–7 and 12 in Fig. 2). For clarity, in Fig. 6, the electropherogram of Al mixed with Ag and eight other alkaline and alkaline earth metal is shown. Using sulphuric acid at pH 3.2, the Al peak trailed behind all other cations except Cr. Thus, under the above conditions, the trivalent ions were the slowest migrating ions. In the above analysis, adjustment of the pH to low acidity was necessary in order to prevent precipitation of $Al(OH)_3$. Sulphuric acid was most suitable as it formed complexes with divalent cations and retarded the migration of Ba (behind Na), and thus provided a window for Ag to migrate between K and Na. Separation of Al and Cr from other ions could be obtained at pH 3.5 but only at pH 3.2 could the two trivalent ion peaks be resolved (Cr trailed behind Al). Also, it should be noted that using any complexing agent other than sulphuric acid would cause Al peak to overlap with other divalent cation peaks. For

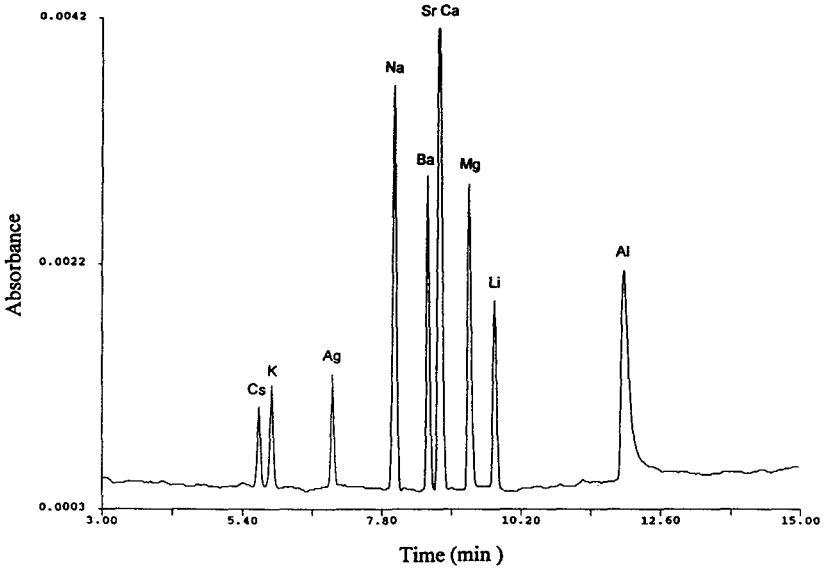

Fig. 6. Electrophoretic separation of Ag and Al from the mixtures with alkali and alkaline earth cations using 5 m*M* pyridine with the pH adjusted to 3.2 with sulphuric acid.

example, if glycolic acid (3–6 m*M*), which strongly affects the mobility of alkaline earth metal cations [15] and Al ion is used, several peaks would merge and the Al peak would be buried. Therefore, it is very difficult (if not impossible) to resolve all nineteen ions in a single CE analysis. For the determination of Ag and Al, an additional run is necessary.

3.4. Reproducibility, quantification, linearity and detection limit

The reproducibility of the CE method was studied by making five consecutive runs with all seventeen ions present at 10 m*M* with pyridine as the BCE (as in Fig. 2). Two injection modes were studied, a 3-s HD mode and a 3-s EK mode at +10 kV. The precisions in terms of relative standard deviation (R.S.D.) for the EK and ED modes are shown in Table 2. Both injection modes provided excellent precision for the migration time. Good precision could be obtained for peak height or area for most ions, with the exception of the ions where the mobilities were considerably different from the BCE, *e.g.*, Cu in the EK mode and Cs and K in the HD mode. The precision in the HD mode was better than that in the EK mode. Also for quantification purposes it seems to be better to use peak height than peak area, as the former had better reproducibility for most ions. However, for plotting calibration graph, using peak area provided a larger linear scaling than using peak height.

The linearity of the calibration graphs expressed as peak area *vs.* metal ion concentration was evaluated in the concentration range 10 μequiv.–1 mequiv. for the HD mode and 1 μequiv.–1 mequiv. for the EK mode. Fig. 7A displays typical calibration lines for K, Ca, Zn and Cd. Note that the sensitivity varies greatly from ion to ion. For most ions, a good linearity ($R^2 = 0.9995$–0.9999) could be obtained in the HD mode over a concentration range where the highest and lowest standard differed by a factor of 100. However, in the EK mode, the calibration graphs were hyperbola-shaped (*e.g.*, the Zn curve in Fig. 7B). In the EK mode the sensitivity was much better in the lower concentration range. Therefore, for quantitative analysis, the sample should be serially diluted

Table 2
Precision: comparison between HD and EK injection modes

Parameter	R.S.D. (%)[a]	
	Hydrodynamic injection	Electrokinetic injection
Migration time	0.29–0.76	0.62–2.24
Peak height	1.1–4.0, except for K, Cs, 5.0–6.4	1.2–4.3, except for Cu, 7.6
Peak area	Ni, Pb, Mg, Zn, Ba, Co, Fe, Cr, Sr, Mn, 1.7–4.8 Ca, Li, Cd, Cu, 5.3–6.3 Na, K, Cs, 6.5–8	Ca, Mg, Co, Cr, Sr, Cs, Fe, Na, Ba, 1.6–4.5 K, Li, Ni, Pb, Cd, 5.5–8.0 Cu, 21

[a] Electrophoretic conditions as in Fig. 2. $n = 5$.

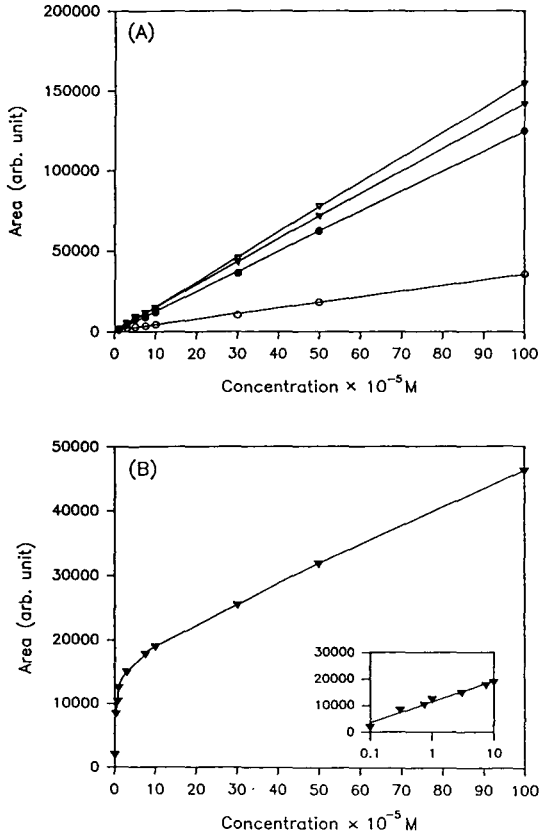

Fig. 7. Comparison of calibration graphs for selected metal ions in the (A) HD and (B) EK modes. ○ = K; ● = Ca; ▽ = Cd; ▼ = Zn. Only the Zn ion graph is shown in the EK mode. The inset is an enlargement for concentrations below 0.1 m*M*. Electrophoretic conditions as in Fig. 2.

such that the concentration of the analyte falls into the range where the calibration graph is linear.

The detection limit (DL) for the various metals was studied by diluting the standard solution serially and comparing the appearance of the peaks of each species in the electropherograms between the diluted standards and the diluent. The concentration that was one level higher in the series than that in which the S/N ratio fell below 3 was defined as the DL. The DL values for the various metals using the EK mode (which gave better sensitivity than the HD mode) are compared in Table 3. The better detection sensitivity in the EK mode probably was due to the "stacking" effect. The stacking effect occurred when the ion concentration in the sample plug was considerably lower than the leading electrolyte in the separation buffer. This phenomenon led to concentration of the analyte ions. Thus, the non-linearity of the calibration graph run in the EK mode could also be attributed to the stacking effect.

4. Conclusions

We have developed a rapid and reliable capillary electrophoretic method for the determination of seventeen metal ions. A complete separation of these metal ions can be accomplished in

Table 3
Detection limits of various metal ions

Metal	Detection limit		Metal	Detection limit	
	μM	ppb		μM	ppb
Na	0.001	0.02	Cd	0.1	11.2
Mg	0.01	0.2	Fe	0.3	17
K	0.01	0.4	Ni	0.5	29
Ca	0.01	0.4	Cs	0.5	66
Li	0.1	0.7	Ba	0.5	69
Mn	0.1	5.5	Pb	0.5	104
Co	0.1	5.9	Cu	2	127
Zn	0.1	6.5	Cr	4	208
Sr	0.1	9			

Minimum detectable concentration at $S/N > 3$; 5 s EK injection at 10 kV; separation conditions as in Fig. 2.

15 min with pyridine or imidazole as the background electrolyte and glycolic acid as the metal-complexing agent (at pH 4.0). Peak detection was done by indirect UV absorbance measurements at 210 or 254 nm. This method has excellent reproducibility for migration time and good precision for peak height and peak area in order to determine metal ion species and their concentrations accurately. The calibration linearity is good over a 100-fold range of concentration. With successive serial dilutions, real samples can be analysed at the sub-ppb to sub-ppm level. The results obtained so far show that the CE methods developed here are well suited for both qualitative and quantitative analyses for metals in water, food and soil samples. A CE method has also been developed for determining Ag and Al, but must be performed separately using 5 mM pyridine with the pH adjusted to 3.2 with sulphuric acid.

5. Acknowledgements

This work was supported by grant NSC81-0208-M002-535 from the National Science Council, Republic of China. We are grateful to Professor C.F. Lin of the Department of Environmental Sciences, National Taiwan University, for providing the soil samples.

References

[1] D.A. Skoog and J.J. Leary, *Principles of Instrumental Analysis*, Saunders, New York, 4th ed., 1992.
[2] Z. Yi, G. Zhuang and P.R. Brown, *J. Liq. Chromatogr.*, 16 (1993) 3133.
[3] F. Foret, S. Fanali, A. Nardi and P. Bocek, *Electrophoresis*, 11 (1990) 780.
[4] W.J. Wildman, P.E. Jackson, W.R. Jones and P.G. Alden, *J. Chromatogr.*, 546 (1991) 495.
[5] A. Weston, P.R. Brown, P. Jandik, A.L. Heckenberg and W.R. Jones, *J. Chromatogr.*, 608 (1992) 395.
[6] A. Weston, P.R. Brown, P. Jandik, W.R. Jones and A.L. Heckenberg, *J. Chromatogr.*, 593 (1992) 289.
[7] A. Weston, P.R. Brown, P. Jandik, A.L. Heckenberg and W.R. Jones, *J. Chromatogr.*, 602 (1992) 249.
[8] W. Beck and H. Engelhardt, *Chromatographia*, 33 (1992) 313.
[9] W. Beck and H. Engelhardt, *Fresenius' J. Anal. Chem.* 346 (1993) 618.
[10] A.R. Timerbaev, W. Buchberger, O.P. Semenova and G.K. Bonn, *J. Chromatogr.*, 630 (1993) 379.
[11] M. Aguilar, X. Huang and R.N. Zare, *J. Chromatogr.*, 480 (1989) 427.
[12] W. Buchberger, O.P. Semenova and A.R. Timerbaev, *J. High Resolut. Chromatogr.*, 16 (1993) 153.
[13] M. Chen and R.M. Cassidy, *J. Chromatogr.*, 640 (1993) 425.
[14] Y. Shi and J.S. Fritz, *J. Chromatogr.*, 640 (1993) 479.
[15] T.-I. Lin, Y.-H. Lee and Y.-C. Chen, *J. Chromatogr. A*, 654 (1993) 167.
[16] R.C. Weast, M.J. Astle and W.H. Beyer (Editors), *Handbook of Chemistry and Physics*, CRC Press, Boca Raton, FL, 69th ed., 1988.
[17] Y.-H. Lee and T.-I. Lin, unpublished results.

ELSEVIER

Journal of Chromatography A, 675 (1994) 237–239

JOURNAL OF CHROMATOGRAPHY A

Short Communication

New lateral reservoir flash chromatography system for the expeditious preparative purification of organic compounds

Gerard A. Potter

Drug Development Section, Cancer Research Campaign Laboratory, Institute of Cancer Research, Sutton, Surrey SM2 5NG, UK

(First received March 16th, 1994; revised manuscript received April 26th, 1994)

Abstract

A flash chromatography system which incorporates a lateral solvent reservoir attached to the main column is described which facilitates the preparative purification of organic compounds. This apparatus allows introduction of the eluting solvent into the column without dismantling the air-pressure inlet adaptor, and with minimal disturbance of the stationary phase.

1. Introduction

Flash chromatography is presently used routinely in organic chemistry research laboratories for the preparative purification of organic compounds [1]. Essentially it is a medium-pressure short-column chromatography system with moderate resolution, where the pressure is provided by an air-pump or gas cylinder. The main disadvantage of flash chromatography is that the apparatus requires constant disassembly and reassembly of the air-pressure inlet adaptor in order to introduce the eluting solvent into the column, which is both tedious and time consuming since the adaptor, which has to withstand positive air-pressure (ca. 0.5 atm), is commonly held in place with springs, clamps, or screw-thread devices. Furthermore, great care has to be taken when pouring solvent into the top of the column so as not to disturb the bed of adsorbent which forms the stationary phase, otherwise poor resolution results. The need to constantly dismantle the air-pressure inlet adaptor prompted the design of a system which would allow introduction of the eluting solvent without this inconvenience.

2. Results and discussion

The apparatus described here is a refinement of flash chromatography whereby solvent is introduced into the side of the column from a lateral solvent reservoir (Fig. 1). This permits the eluting solvent to be introduced into the column without disassembly of the air-pressure inlet adaptor. Consequently the preparative purification of organic compounds by this system is more operationally convenient and more rapid than conventional flash chromatography. The essential feature of the apparatus is that a solvent reservoir is attached to the side of the column so that the inlet is above the height of the stationary phase, with a tap (T_2) fitted at the

0021-9673/94/$07.00
SSDI 0021-9673(94)00402-U

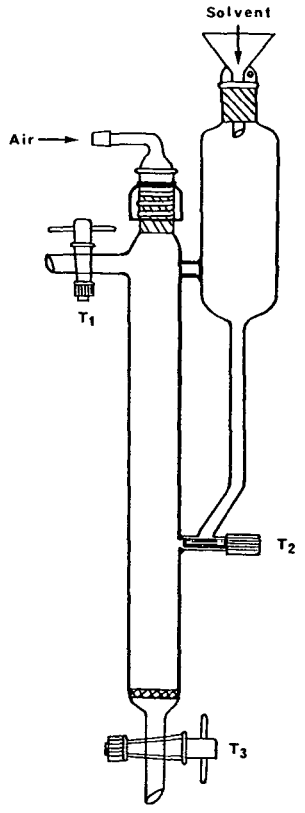

Fig. 1. Lateral reservoir flash chromatography apparatus.

reservoir to column inlet. A tap (T_1) is also required at the top of the column to release air-pressure from the pump. The solvent reservoir is configured so that its header volume is greater than that of the column elution volume to allow sufficient solvent header pressure to refill the column.

An important additional advantage of this means of introducing the eluting solvent from a lateral reservoir is that the Rotaflo side-inlet tap T_2 allows solvent to be introduced into the main column in a controlled fashion. Consequently there is minimal disturbance of the silica bed which forms the stationary phase, and this feature ensures optimal resolution is achieved consistently. In order to further examine this beneficial feature an orange coloured solution of azobenzene in diethyl ether was delivered from the lateral reservoir, after preparing the column using colourless hexane as loading solvent. The orange diethyl ether solution entered the main column as a distinct layer above the hexane, and only marginal mixing of the solvents at their interface was observed.

Gradient elution is also more convenient since the solvent polarity can be easily varied in the solvent reservoir. Variable or fixed aliquots can also be dispensed from the column, as required. Additionally the whole purification can be performed in less time than with conventionally flash chromatography since the next aliquot of solvent is introduced into the reservoir whilst the previous aliquot elutes from the column, and the column is then refilled simply by turning two taps.

3. Experimental

The apparatus consists of a column which incorporates an integral lateral reservoir as shown in Fig. 1, fitted with a Rodaviss air-pressure inlet adaptor and vented solvent filling funnel[a]. Air-pressure is provided by a Hi-Flow piston air-pump, obtainable from Merck (BDH Laboratory Supplies) or Fisons Scientific Equipment.

3.1. General procedure, column preparation

The bottom tap T_3 can be left open during the entire operation. With taps T_1 and T_2 closed, and the top of the column open, the main column is prepared in the usual fashion [1]. Typically, for a normal-phase purification using silica gel as the stationary phase (preferably Merck 15111), this is done by adding the silica gel through the top of the column as a slurry in a non-polar loading solvent, so that the final height of the compressed silica bed is at least 1 cm below T_2. This is then followed by the material to be purified, which is usually preadsorbed onto

[a] The complete apparatus is available as the Quick-Sep System from Radleys, Shire Hill, Saffron Walden, Essex CB11 3AZ, UK, under licence from Cancer Research Campaign Technology Ltd.

silica by evaporation from dichloromethane and then also added as a slurry in the loading solvent. The Rodaviss air-pressure inlet adaptor is then fitted, the air-pump switched on, and the loading solvent is eluted from the column down to tap T_2, then tap T_1 opened to release the air-pressure. As with conventional flash chromatography the top of the silica bed should not be allowed to run dry.

3.2. Column refilling

The lateral reservoir is filled with eluting solvent, and tap T_2 opened. The eluting solvent then enters the main column from the lateral reservoir, under gravity pressure, until it reaches just below the height of T_1, then T_2 is closed (Fig. 2).

3.3. Column elution

As soon as T_1 is closed the pump air pressure forces solvent through the stationary phase and the eluent collected in a receiver flask. Once the solvent reaches the level of T_2 the tap T_1 is opened to release the air-pressure, and the column is refilled again as previously described. Whilst the solvent from the main column is eluting the lateral reservoir is conveniently refilled, changing the solvent polarity as required, ready for the next refill. The column refill/elution modes are then repeated until the desired component elutes from the column. With practice these operations are performed swiftly and easily.

In summary, a new flash chromatography system that allows the eluting solvent to be introduced into the column without dismantling the air-pressure inlet adaptor and with minimal disturbance of the stationary phase is described which facilitates the preparative purification of organic compounds.

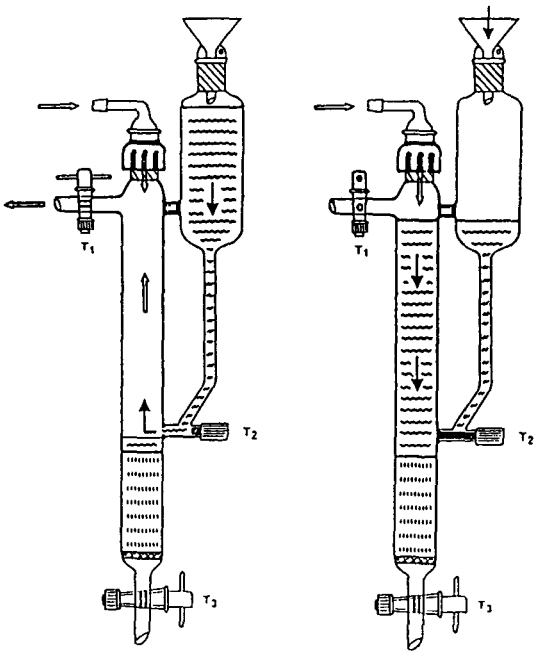

Fig. 2. Column operation; (a) refill mode and (b) elution mode.

References

[1] W.C. Still, M. Kahn and A. Mitra, *J. Org. Chem.*, 43 (1978) 2923.

ELSEVIER

Journal of Chromatography A, 675 (1994) 240–243

JOURNAL OF CHROMATOGRAPHY A

Short Communication

High-performance liquid chromatographic determination of flavone C-glycosides in some species of the Cucurbitaceae family

M. Krauze-Baranowska, W. Cisowski*

Department of Pharmacognosy, Medical Academy, ul. J. Hallera 107, 80-416 Gdańsk, Poland

(First received December 27th, 1993; revised manuscript received February 22nd, 1994)

Abstract

Flavonoid complexes occurring in the medicinal plants *Bryonia alba*, *Bryonia dioica* and *Lagenaria siceraria* were found to be flavone C-glycosides. Flavonoids of these species were compared by HPLC and separation conditions were elaborated for C-glycosides using isocratic and gradient elution. The content of the major C-glycoside, saponarin, was determined. The highest saponarin level (2.481%) was found in *Bryonia dioica*.

1. Introduction

HPLC is one of the methods used for the separation and determination of naturally occurring mixtures of flavonoids (aglycones and glycosides) [1–5]. It permits rapid separations of the flavonoid complexes occurring in the plant material, a feature important in chemotaxonomic studies [6]. This study was carried out from the chemotaxonomic standpoint by utilizing the HPLC analysis of flavonoid C-glycoside complexes in some species of the Cucurbitaceae family.

So far, investigations of flavonoids in the Cucurbitaceae family have revealed C-glycoside compounds together with flavonoid O-glycosides [7–10]. The C-glycoside flavonoids saponarin and isovitexin, isolated and identified by us in three species of Cucurbitaceae [9,10], owing to their rare dissemination in the plant kingdom, can provide good markers for chemotaxonomic investigations of this family. Three species have now been studied, namely *Bryonia alba* L., *Bryonia dioica* Jacq. and *Lagenaria siceraria* L. As yet, flavonoids have not been surveyed in *Lagenaria siceraria* and *Bryonia alba*, whereas in the flavonoid complexes of *Bryonia dioica*, saponarin and vicenin-2 have been found [8]. The species are used in therapy as antirheumatics and in homeopathy [11,12].

The purpose of this study was to demonstrate, with the aid of HPLC, the chemical affinity of the three species and to determine the concentration of saponarin, the predominant C-glycoside in the flavonoid complexes.

* Corresponding author.

0021-9673/94/$07.00
SSDI 0021-9673(94)00269-F

2. Experimental

2.1. Equipment

An HPLC system from Knauer (Berlin, Germany) was used, consisting of two Model 64-00 pumps, a solvent dynamic mixing chamber and a Model 87-00 UV detector, equipped with a Model 7125 injection valve (Rheodyne, Cotati, CA, USA) with a 20-μl sample loop, under computer control (Knauer HPLC, version 211a). The flavonoids were separated on a LiChrospher RP-18 (5 μm) column (250 × 4 mm I.D.) (Merck, Darmstadt, Germany) connected to a guard column containing the same stationary phase (5 μm) (50 × 4 mm I.D.) (Merck).

2.2. Reagents

The organic solvents were of HPLC grade (acetonitrile and methanol; Merck) or analytical-reagent grade (acetic acid; POCH, Lublin, Poland). Redistilled water was used. After preparation of the mobile phase it was filtered through a 0.49-μm filter (J.T. Baker, Phillipsburg, NJ, USA).

2.3. Elution

The flavonoids were separated by isocratic elution using methanol–water–acetic acid (30:70:3) and by gradient elution using solvent A (acetonitrile) and solvent B [water–acetic acid (97:3)] with the following gradient programme: 0 to 20 min, from 12 to 15% A in (linear gradient), and from 20 to 45 min, 15% A (isocratic elution). A re-equilibration period of 10 min was used between individual runs. Elution was carried out at room temperature with a flow-rate of 1.3 ml/min and UV detection at 330 nm (sensitivity 0.008 AUFS).

2.4. Reference compounds

Flavone C-glycosides (Table 1) were isolated from plant material by preparative column and thin-layer chromatography. Their structures were established on the basis of classical (m.p., PC, TLC, hydrolysis) and spectroscopic methods (FD-MS, LSI-MS, EI-MS, UV, IR, ^{1}H NMR, ^{13}C NMR and 2D NMR) [9,10].

2.5. Calibration

A stock solution of saponarin was prepared by dissolving 4 mg of the flavonoid in 10 ml of water–methanol (7:3, v/v). The volumes injected (20 μl) corresponded to amounts of saponarin in the range 1–8 μg. A calibration graph was obtained by plotting peak area (y) against concentration of standard solutions (x) (regression equation: $y = 1.724x - 0.299$, correlation coefficient $r = 0.9998$).

Table 1
Flavone C-glycosides from *Bryonia alba*, *Bryonia dioica* and *Lagenaria siceraria*

Compound	Species		
	Bryonia alba	*Bryonia dioica*	*Lagenaria siceraria*
Vitexin	+	+	−
Isovitexin	+	+	+
Isoorientin	−	+	+
Saponarin	+	+	+
Lutonarin	+	+	−
Saponarin 4′-O-glucoside	−	−	+
Saponarin caffeic ester	−	+	−
Unidentified			
C-Glycoside flavonoid	−	+	−

2.6. Sample preparation

The plant material was a flowering herb collected in the garden of Medicinal Plants, Medical Academy, Gdańsk, Poland. After drying, the material was powdered and purified by extraction with chloroform in a Soxhlet apparatus. The flavonoids were extracted from the material with methanol (Soxhlet apparatus, 3 h, 100 ml). For quantitative determinations, samples of either 0.5 g (*Bryonia dioica*) or 1 g (*Bryonia alba*, *Lagenaria siceraria*) were taken. The methanolic extracts were concentrated under reduced pressure and the dry residues were dissolved in water–methanol (7:3, v/v) (100 ml with *Bryonia* and 10 ml with *Lagenaria*). The solutions were then filtered through a 0.45-μm filter (J.T. Baker) and injected.

3. Results and discussion

The conditions for the HPLC analysis of the complexes of flavone C-glycosides occurring in some species of the Cucurbitaceae family were established. The structures of the C-glycosides isolated from the plant material are shown in Fig. 1.

The procedures leading to the separation of the complexes of flavonoid C-glycosides are based on solvents typical for the RP-HPLC of flavonoids [13,14]. The best results were obtained with methanol–water–acetic acid (30:70:3, v/v/v). Under these conditions, the complex of flavone C-glycosides of *Lagenaria siceraria* was separated (Fig. 2). For the remaining species, a good separation of lutonarin, saponarin and isoorientin was obtained, whereas vitexin and isovitexin gave poorly resolved

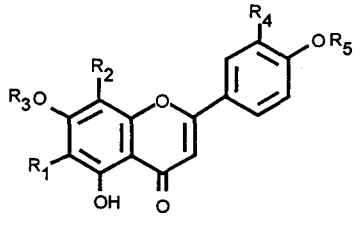

compound	R_1	R_2	R_3	R_4	R_5
vitexin	H	glucose	H	H	H
isovitexin	glucose	H	H	H	H
saponarin	glucose	H	glucose	H	H
saponarin 4'-O-glucoside	glucose	H	glucose	H	glucose
saponarin caffeic ester	glucose	H	caffeoylglucose	H	H
isoorientin	glucose	H	H	OH	H
lutonarin	glucose	H	glucose	OH	H

Fig. 1. Structure of flavone C-glycosides from *Bryonia alba*, *Bryonia dioica* and *Lagenaria siceraria*.

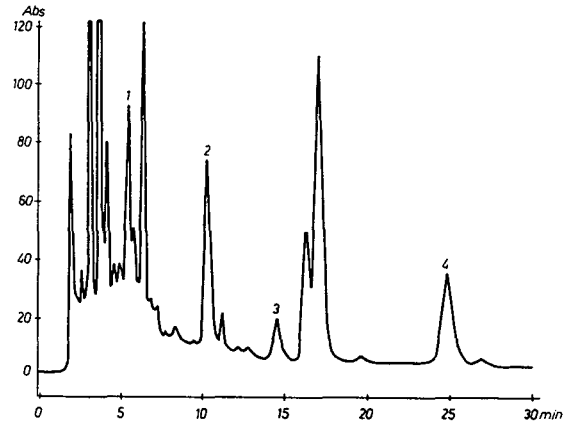

Fig. 2. HPLC of flavone C-glycosides from *Lagenaria siceraria* (isocratic elution). Peaks: 1 = 7,4'-O-diglucosyl-6-C-glucoside of apigenin; 2 = saponarin; 3 = isoorientin; 4 = isovitexin.

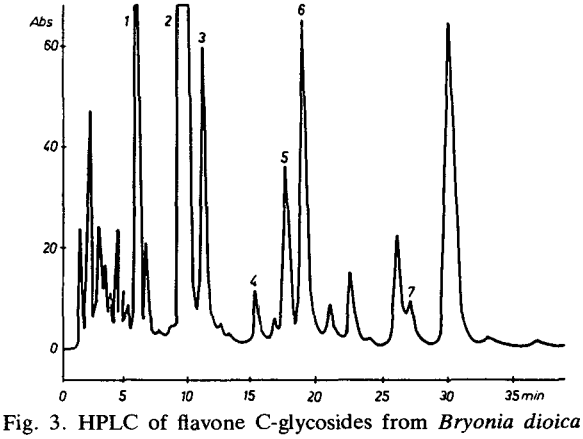

Fig. 3. HPLC of flavone C-glycosides from *Bryonia dioica* (gradient elution). Peaks: 1 = lutonarin; 2 = saponarin; 3 = isovitexin; 4 = vitexin; 5 = isovitexin; 6 = caffeic ester of saponarin; 7 = unidentified.

Table 2
Determination of saponarin in plant material

Species	Amount of saponarin (% dry material) ($n = 5$)	Standard deviation (%)
Bryonia alba	1.142	0.0495
Bryonia dioica	2.481	0.0280
Lagenaria siceraria	0.064	0.0037

peaks. To separate flavone C-glycosides from *Bryonia dioica* and *Bryonia alba*, programme for gradient elution were developed with the acetonitrile–3% acetic acid system. The best separations of the C-glycosides from *Bryonia dioica* (Fig. 3) and *Bryonia alba* were achieved using a linear gradient of acetonitrile in 3% acetic acid followed by isocratic elution. The determination of saponarin in the aforementioned species was carried out by isocratic elution using methanol–water–acetic acid (30:70:3). The results of quantitative analysis are given in Table 2. The high saponarin content in *Bryonia* allows it to be classified among those rich in flavonoids.

The flavonoid complexes occurring in the plants of the Cucurbitaceae family are mixtures that are difficult to separate and identify. The species investigated here, although fairly common, have been poorly surveyed for their flavonoid dyes. The present HPLC method permits good separations and identification of the flavonoids in these plants.

References

[1] F. Briancon-Scheid, A. Lobstein-Guth and R. Anton, *Planta Med.*, 49 (1983) 204.
[2] D. Strack, K. Fuisting and G. Popovici, *J. Chromatogr.*, 176 (1979) 270.
[3] G.J. Niemann, J.W. Koerselman-Kooy, J.W. Steijns and L.J. van Biederode, *J. Pflanzenphysiol.*, 109 (1982) 105.
[4] J.P. Bianchini and E.M. Gaydou, *J. Chromatogr.*, 218 (1981) 73.
[5] I. McMurrough, *J. Chromatogr.*, 218 (1981) 683.
[6] R. Hegnauer, *Chemotaxonomie der Pflanzen*, Birkhauser, Basle, 1989.
[7] H. Leska and K. Müller, *Pharmazie*, 305 (1988) 5.
[8] A. Proliac, A. Chaboud and I. Raynoud, *Pharm. Acta Helv.*, 7 (1989) 64.
[9] M. Krauze and W. Cisowski, *Pol. J. Chem.*, 66 (1992) 951.
[10] M. Krauze-Baranowska and W. Cisowski, *Pharmazie*, (1994).
[11] G. Penso, *Index Plantarum Medicinalium*, O.E.M.F., Milan, 1983.
[12] G. Charrete, *Homeopatische Arzneimittellehre für die Praxis*, Hippokrates Verlag, Stuttgart, 1987.
[13] F. Dondi, G. Grassini-Strazza and Y.D. Kahie, *J. Chromatogr.*, 462 (1989) 205.
[14] F. Dondi, Y.D. Kahie, G. Blo, C. Pietrogrande and P. Reschiglian, *J. Chromatogr.*, 461 (1989) 281.

ELSEVIER

Journal of Chromatography A, 675 (1994) 244–247

JOURNAL OF CHROMATOGRAPHY A

Short Communication

Direct stereochemical resolution of 3,4-dihydroxyphenylserine using a chiral crown ether stationary phase

Masahiko Okamoto*, Ken-Ichi Takahashi, Tadashi Doi

Environmental Health Science Laboratory, Sumitomo Chemical Co., Ltd., 1-98, 3-chome, Kasugade-naka, Konohana-ku, Osaka 554, Japan

(First received September 10th, 1993; revised manuscript received April 8th, 1994)

Abstract

The direct stereochemical resolution of the four stereoisomers of 3,4-dihydroxyphenylserine was achieved on a high-performance liquid chromatographic chiral stationary phase based on a chiral crown ether. The effects of pH and temperature were investigated. The role of the crown ether ring in separating the analyte is also described.

1. Introduction

3,4-Dihydroxyphenylserine (DOPS) is a synthetic amino acid that can exist in four possible stereoisomeric forms: *threo-* and *erythro*-DOPS and their enantiomeric isomers, the L- and D-forms (Table 1). Only L-*threo*-DOPS is postulated to have beneficial effects on the freezing phenomenon or akinaesia in Parkinson's disease [1,2] and orthostatic hypotension in familial amiloid polyneuropathy [3].

The enantiospecific synthesis of L-*threo*-DOPS requires the determination of enantiomeric purity, often when one enantiomer is present in a large excess of the other. For this purpose, a method has to be developed that would allow the chromatographic separation of these optical isomers, preferably without derivatization.

This is the first report on the direct optical resolution of DL-*threo*-DOPS. The enantiomeric ratio of L-*threo*-DOPS can be determined accurately by this method. The system is also able to resolve the diastereomeric pairs of DOPS and the four corresponding isomers.

Table 1
Structures of the four stereoisomers of 3,4-dihydroxyphenylserine (DOPS)

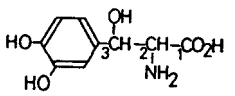

Compound	Absolute configuration
L-*threo*-DOPS	2*S*,3*R*
D-*threo*-DOPS	2*R*,3*S*
L-*erythro*-DOPS	2*S*,3*S*
D-*erythro*-DOPS	2*R*,3*R*

* Corresponding author.

0021-9673/94/$07.00
SSDI 0021-9673(94)00348-D

2. Experimental

2.1. Chemicals

DL-*threo*-DOPS was purchased from Sigma (St. Louis, MO, USA). The four stereoisomers of DOPS was kindly provided by Research Laboratories, Sumitomo Pharmaceuticals (Osaka, Japan). Perchloric acid was obtained from Wako (Osaka, Japan).

2.2. Apparatus

The chromatographic system consisted of a Hitachi L-6000 solvent-delivery module, a Rheodyne Model 7125 injector equipped with a 20-μl loop, a Hitachi L-4000 UV–Vis detector set at 220 nm and a Shimadzu C-R3A integrator. The column temperature was controlled by an Eyela Uni Cool UC-65 circulating water-bath (Tokyo Rikakikai, Tokyo, Japan). The column consisted of a 150 × 4 mm I.D. stainless-steel column packed with a chiral stationary phase composed of a chiral crown ether coated on a polymeric support [Crownpak CR(+) and CR(−); Daicel, Tokyo, Japan].

2.3. Chromatographic conditions

The mobile phase was prepared by addition of perchloric acid to HPLC-grade water until the required pH was obtained. The flow-rate was 0.4 ml/min and the injection volume was 5 μl. To prevent corrosion and decomposition of the stationary phase, the column was washed every night with HPLC-grade water.

2.4. Samples

The chromatographic standards were prepared in distilled water (1 mg/ml) and filtered through a 0.45-μm Millipore filter before injection on to the column.

3. Results and discussion

Fig. 1a shows the enantiomeric separation of DL-*threo*-DOPS using a Crownpak CR (+) column and perchloric acid at pH 1.0 as the mobile phase, a column temperature of 2°C and a flow-rate of 0.4 ml/min. Shinbo *et al.* [4] have reported that this column is very powerful for the direct optical resolution of a variety of natural amino acids. No resolution was obtained using several other columns, such an Enantiopac and Ultron ES-OVM and Cyclobond-I, -II and -III. The resolution factor (R_s) from the data in Fig. 1a was calculated as 2.58. The enantiomer with the longest retention time was assigned as L-*threo*-DOPS by co-chromatography with authentic samples of the respective enantiomers.

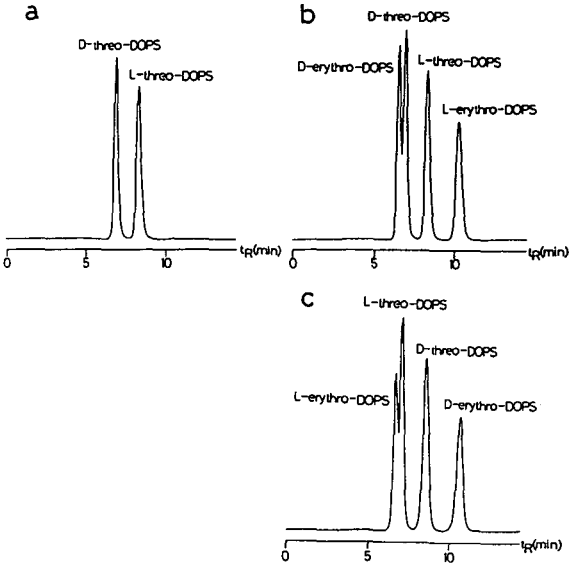

Fig. 1. (a) Chromatographic resolution of DL-*threo*-DOPS. Column, Crownpak CR(+). (b) Chromatogram obtained for the four possible stereoisomers of DOPS. Column, Crownpak CR(+). (c) Separation of the four possible stereoisomers of DOPS. Column, Crownpak CR(−). Other conditions are given in the text.

We carried out recovery tests of the D-*threo*-isomer from L-*threo*-DOPS to establish whether the enantiomeric ratio could be determined accurately. D-*threo*-DOPS was added to L-*threo*-DOPS to give a concentration of the former between 0.05% and 0.5%. The added D-*threo*-DOPS was recovered quantitatively at all concentrations by this procedure (Table 2). Hence the method allows the proportion of D-*threo*-DOPS in a sample to be measured precisely.

The resolution of DL-*threo*-DOPS can be reg-

Table 2
Results of recovery tests of D-*threo*-DOPS from L-*threo*-DOPS

Calculated (%)	Found (%)	Recovery (%)
0.05	0.05	100.0
0.1	0.10	100.0
0.2	0.21	105.0
0.5	0.48	96.0

ulated in two ways, by varying either the column temperature or the pH of the mobile phase. Temperature has a strong influence on the retention and chiral selectivity of this column [4]. The retention and resolution changes in the temperature range 2–40°C are given in Table 3. The stereoselectivity and retention decrease with increasing temperature. At 40°C the chiral resolution effect of the column was removed.

Variation of the pH of the mobile phase between 1.0 and 2.0 influences the resolution of DL-*threo*-DOPS, as demonstrated in Table 4. The resolution increases with decreasing pH, whereas the retention times are hardly affected. This effect is consistent with the proposed chiral recognition mechanism in which inclusion complexes are formed between a protonated primary amino group in the vicinity of the chiral centre of the analyte and the polyether rings of the chiral stationary phase [5]. In a highly acidic media, both the primary amino and the carboxylic acid groups of the solute appear to be completely protonated. Therefore, an inclusion complex with the chiral stationary phase would be readily formed and not be repelled by the oxygen atom of the crown ether ring.

Table 3
Influence of temperature on the enantiomeric resolution of DL-*threo*-DOPS

Temperature (°C)	t_R(min)	R_s
2	7.0, 8.5	2.61
10	6.3, 7.1	1.74
20	5.6, 6.0	1.00
40	4.8	No resolution

Column, Crownpak CR(+); mobile phase, perchloric acid (pH 1.0); R_s = resolution factor, calculated from $R_s = 2(t_2 - t_1)/(W_1 + W_2)$, where t_1 and t_2 are the retention times of the enantiomers and W_1 and W_2 are the widths of the peaks at their bases.

Table 4
Influence of pH on the enantiomeric resolution of DL-*threo*-DOPS

pH	t_R(min)	R_s
1.0	7.0, 8.5	2.58
1.3	7.1, 8.3	2.18
1.5	6.9, 7.9	1.86
2.0	5.9, 6.5	1.20

Mobile phase, perchloric acid; temperature, 2°C; other conditions as in Table 3.

Under the optimum conditions mentioned above, we attempted to separate the four possible stereoisomers of DOPS. A typical chromatogram is shown in Fig. 1b. In these separations, the elution of the D-isomer prior to the L-isomer was observed, as described in the manufacturer's instruction manual. The enantiomeric elution order is reversed on using the Crownpak CR(−) column, under the same conditions (Fig. 1c). In the determination of the optical purity of L-forms in D-forms, we can use these columns effectively by switching from the (+) to the (−)-column.

In conclusion, excellent resolution can be obtained for the stereoisomers of DOPS by using a chiral crown ether as the chiral bonded phase. The optical purity of small amounts of D-*threo*-DOPS can be also determined directly, rapidly and accurately by this HPLC method. This method will be applicable to probing the enantiomeric distribution of the antipode of L-*threo*-DOPS in biological media and to determining the enantiomeric purity of synthetic L-*threo*-DOPS.

Acknowledgements

The authors express their thanks to Sumitomo Pharmaceuticals for the gift of the four stereoisomers of DOPS and their colleagues Mr. Takao Nakagawa, Ms. Sanae Sakaguchi and Naoko Takagi for their skilful assistance.

References

[1] H. Narabayashi, T. Kondo, A. Hayashi, T. Suzuki and T. Nagatsu, *Proc. Jpn. Acad. B*, 57 (1981) 351.
[2] H. Narabayashi, T. Kondo, F. Yokochi and T. Nagatsu, in *VIII International Symposium on Parkinson's Disease*, New York, 1985, Abstracts, p. 26.
[3] T. Suzuki, S. Higa, S. Sakoda, M. Ueji, A. Hayashi, Y. Tanaka and A. Nakajima, *Eur. J. Clin. Pharmacol.*, 23 (1982) 463.
[4] T. Shinbo, T. Yamaguchi, K. Nishimura and M. Sugiura, *J. Chromatogr.*, 405 (1987) 145.
[5] D.W. Armstrong, *J. Liq. Chromatogr.*, 7 (1984) 353.

ELSEVIER

Journal of Chromatography A, 675 (1994) 248–252

JOURNAL OF CHROMATOGRAPHY A

Short Communication

Direct isomeric separation of a 3-hydroxyproline-containing prodrug, L-693 989, by high-performance liquid chromatography with a porous graphitic carbon column

Carrie Bell, Eric W. Tsai*, Dominic P. Ip, David J. Mathre

Department of Pharmaceutical Research, Merck Research Laboratories, Sumneytown Pike, West Point, PA 19486, USA

(First received January 4th, 1994; revised manuscript received April 12th, 1994)

Abstract

The use of high-performance liquid chromatography (HPLC) with a porous graphitic carbon (Hypercarb) column for the direct separation of a positional isomer of L-693 989, a 3-hydroxyproline-containing prodrug, is described. The isomer peak was isolated by HPLC and analyzed by mass spectrometry and proton nuclear magnetic resonance spectroscopy. An authentic sample of the isomer was also synthesized for chromatographic comparison. The results confirm that the peak in question is a 4-hydroxyproline isomer which is difficult to separate from L-693 989 compound with the silica-based reversed-phase columns. The observed chromatographic elution supports the retention mechanism based on the unique electronic donor–acceptor interaction between the lone-pair electrons of the analyte (donor) and the delocalized electron conduction bands on the graphitized carbon stationary phase (acceptor).

1. Introduction

L-693 989 is a 3-hydroxyproline-containing, semi-synthetic phosphate prodrug that possesses potent antifungal and antipneumocystis activity (Fig. 1) [1–3]. In the initial development stage, the synthesized bulk drug contained a small amount (*ca.* 7%) of the 4-hydroxyproline isomer (L-702 303). The first batches of L-693 989 were prepared from the fermentation product, L-688 786 [1], which contained *ca.* 7% of the 4-hydroxyproline isomer (L-700 098) as a minor fermentation by-product. Although the amount of the 4-hydroxyproline isomer in the starting material could be quantitated by high-performance liquid chromatography (HPLC), we were unable to resolve the isomer at the prodrug stage using a variety of reversed-phase columns such as the Nova-Pak C_{18}, Vydac (C_{18} and C_4) and Zorbax RX (C_8 and C_{18}). With all of these columns, the 4-hydroxyproline isomer co-eluted with L-693 989. The amount of the 4-hydroxyproline isomer in the bulk drug was monitored by proton nuclear magnetic resonance (^{1}H NMR) spectroscopy in a fashion similar to that observed for the L-688 786/L-700 098 natural products [4]. A more quantitative method for determining the amount of the isomer, however, was needed in order to ensure the purity of the bulk drug, and to demonstrate the selectivity of a

* Corresponding author.

0021-9673/94/$07.00
SSDI 0021-9673(94)00347-C

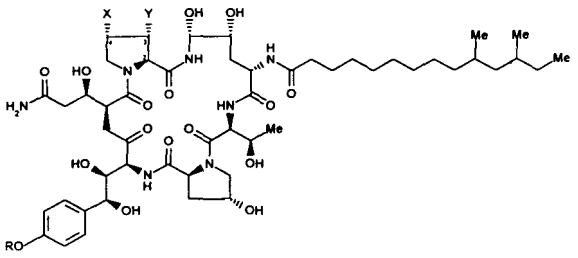

Compound	X	Y	R
L-693 989	H	OH	$-P(=O)(OH)_2$
L-688 786	H	OH	H
L-702 303	OH	H	$-P(=O)(OH)_2$
L-700 098	OH	H	H

Fig. 1. Molecular structures of L-693989 and related compounds.

quantitative assay for L-693 989 in dosage forms. Our research on a different type of HPLC column, the porous graphitic carbon (PGC), demonstrated a direct separation of the isomer from L-693 989.

PGC is a newly developed column packing material, recently made available for HPLC [5–9], with retention properties resembling that of a classical silica-based reversed-phase system. It is considered a "pure" reversed-phase material because it contains a strongly hydrophobic adsorbent with a flat surface consisting of hexagonal layers of covalently bonded carbon atoms and no unreacted silanol groups [6]. The advantages of PGC include unique selectivity, column stability in the pH range of 0 to 14, solvent compatibility (it does not swell with organic solvent), hardness to withstand high pressures (mechanical stability), surface homogeneity and reproducible performance. The pharmaceutical and biomedical applications of PGC have several literature precedents [10–15]; however, the number of literature applications with the PGC column is still very sparse. Resolution of chiral compounds using a PGC column with mobile phase additives has also been illustrated [16,17]. One of the significant features of PGC is the capability for the direct separation of positional isomers due to its unique possession of conduction bands of delocalized electrons as described by Bassler and co-workers [18,19]. In these studies, the retention mechanism on the PGC stationary phase for the separation of positional isomers of cresol and some natural products has been shown via an electronic donor–acceptor interaction between the electron-rich solutes (donor) and the delocalized electron-conduction bands of PGC (acceptor). This unique retention mechanism has inspired us to utilize the PGC column for a direct separation of L-693 989, which contains several electron-rich substituents, and its 4-hydroxy positional isomer. The isolation and data to support the identification of the isomer peak by mass spectrometry (MS) and ^1H NMR are presented in this study. The retention mechanism on the PGC column for isomeric separation is also proposed.

2. Experimental

2.1. Chemicals and reagents

L-693 989 ($C_{50}H_{80}N_8O_{20}PK$) was manufactured by Merck Research Labs. (Rahway, NJ, USA) [20]. Acetonitrile (HPLC grade), potassium phosphate and ammonium acetate (reagent grade) were purchased from Fisher Scientific (Philadelphia, PA, USA). All solvents and reagents were used as received without further purification. Deionized water with at least 18 MΩ purified by a Milli-Q system (Millipore, Bedford, MA, USA) was used for mobile phase and standard preparations.

2.2. Instruments and chromatographic conditions

Separation

A Hewlett-Packard (Avondale, PA, USA) 1090 LC system connected to a variable-wavelength UV detector (Applied Biosystems 783A, Foster City, CA, USA) was used for the chromatographic separation and isolation. A Shandon Hypercarb (Keystone Scientific, State College, PA, USA) analytical column (5 μm particle size, 100 mm × 4.6 mm I.D.) with a mobile phase

of 0.02 *M* potassium phosphate, pH 6.8–acetonitrile (55:45) delivered at a flow-rate of 1.5 ml/min was used to separate the 4-hydroxyproline isomer from L-693 989. The separation was carried out at ambient temperature with 10-μl injections of 0.3 mg L-693 989/ml in water. The wavelength was set at 220 nm for UV detection.

Isolation and identification

The isomeric fractions were collected by HPLC for identification with a more volatile mobile phase (0.02 *M* ammonium acetate, pH 6.8–acetonitrile; 55:45) and a larger injection volume (50 μl). The collected fractions of L-693 989 and its isomer were evaporated to remove the solvent with a rotary evaporator. Ammonium acetate solid was further removed by vacuum. The resulting samples were analyzed by MS and NMR spectroscopy. MS analyses were performed on a ZAB mass spectrometer with both fast atom bombardment (FAB) positive ion and negative ion modes using glycerol as a FAB matrix. ^{1}H NMR spectra were generated with a Bruker 400 MHz spectrometer using $C^2H_3O^2H$ as the solvent.

3. Results and discussion

3.1. Separation of the isomer

Because of the similar physical and chemical properties (such as hydrophobicity) of L-693 989 (3-hydroxyproline) and L-702 303 (4-hydroxyproline), direct separation of the two isomers by HPLC with the reversed-phase columns is difficult. Several reversed-phase columns, including Nova-Pak C_{18}, Vydac C_{18}, Vydac C_4, Zorbax RX-C_8 and Zorbax RX-C_{18} were investigated to support the determination of the 4-hydroxyproline isomer. The 4-hydroxyproline isomer co-eluted with L-693 989 in all the above instances. The concept of using the PGC column in this study is based on its unique retention mechanism which is dominated by the electronic interaction between the solute and the stationary phase rather than the hydrophobicity of the solute which normally is the key factor for reversed-phase chromatography. The difference in electronic properties influenced by the surrounding group for the title compound (mainly on the 3-hydroxy group) and its 4-hydroxyproline isomer renders the direct separation of the isomers on the PGC column feasible (see section 3.3).

Under the optimized chromatographic conditions described in the Experimental section, the two isomers were well separated with L-693 989 eluting at *ca.* 6 min followed by the isomer (L-702 303) at *ca.* 10 min. A typical chromatogram is shown in Fig. 2. L-693 989 exhibited shorter retention than the isomer counterpart indicating that the electronic donor–acceptor interaction was weaker for L-693 989. This result was in agreement with the hypothetical retention mechanism (see below). Two small peaks eluting before L-693 989, which have not been identified, will not be discussed in this study.

Prior to the isolation and identification of the

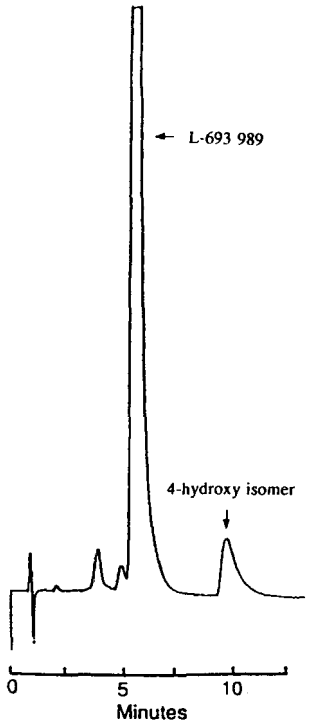

Fig. 2. Typical chromatogram of the resolved 4-hydroxy isomer from L-693989 on a porous graphitic carbon column. Chromatographic conditions are described in the Experimental section.

isomer peak, there were two indicators which supported the proposed peak identity of L-702 303. First, the HPLC area percent of the peak in question correlated well with the percent of 4-hydroxyproline isomer present in different lots of bulk drug (between 2 and 9%) as determined by ^{1}H NMR spectroscopy. Second, an experiment was done by adding a 0.1 *M* NaOH solution to the bulk drug solution to investigate the degradation behavior of L-693 989 and the peak of interest. Both peaks decreased in peak size and formed two base-induced degradates [1,4] eluting prior to the major drug peak (relative retention times were 0.57 and 0.70). These observations suggested that the peak of interest is chemically closely related to L-693 989. Based upon these observations, it is reasonable to suggest that the peak in question is the 4-hydroxyproline isomer of L-693 989. Although the peak could be proposed as the 4-hydroxy isomer, it was preferable to isolate the fractions for further characterization to gain additional support of the peak identity before an L-702 303 authentic sample was synthesized for chromatographic comparison.

3.2. Identification of the isomer peak

Fractions were collected by HPLC to provide samples for MS and ^{1}H NMR identification (see Experimental). Results of the MS analysis showed that both the front (L-693 989) and end (isomer) fractions exhibited an identical parent *m/z* of 1183 for the positive ion (K^+ salt) mode and 1143 for the negative ion (anion, without K^+ salt) mode. These two sets of mass spectra confirmed that the two components were isomers. Identification of the isomer was determined by ^{1}H NMR [4]. The structure of the isomer was confirmed by an authentic sample of the 4-hydroxyproline isomer which was later synthesized.

After the MS and ^{1}H NMR studies, the chromatographic behavior of the authentic sample was also compared. It was found that the peak in question matched perfectly with the authentic sample in terms of chromatographic elution. This observation further supports the proposed identity of the isomer peak.

3.3. Retention mechanism

The retention of the isomers on the PGC column observed in this study could be explained based on the electronic donor–acceptor interaction between the solute (donor) and stationary phase (acceptor) similar to that described by Bassler and co-workers [18,19]. The lone-pair electrons on the solute and the unique feature of delocalized electron conduction bands of the graphitized carbon play a key role in the retention of the PGC column. In our study, the substituent groups near the active–OH group (electron donor) on the proline ring, which affected the electronic activity due to the steric hindrance, governed the isomeric separation and the elution order of the two isomers.

L-693 989, the 3-hydroxyproline derivative, exhibited the electron donating group (–OH) next to a bulky substituent on the 2-position of the proline derivative leading to a large steric hindrance to the electronic interaction between the 3-hydroxyproline isomer and the graphite stationary phase. On the other hand, the 4-hydroxyproline isomer (–OH away from the bulky group) encountered less steric effect than the 3-hydroxy counterpart. Consequently, L-693 989 should elute faster than the 4-hydroxyproline isomer L-702 303 because of less electronic donor–acceptor interaction. The observed chromatography was in good agreement with the proposed retention mechanism. It was also consistent with the retention order reported for the separation of positional isomers of substituted phenols [18].

Alternatively, instead of the bulky steric effect, it was thought that the possibility of hydrogen bonding formation between the 3-hydroxy group and the neighboring–OH group on the ornithine residue could also explain the observed elution sequence. Because the lone-pair electrons on the 3-hydroxy (L-693 989) would become less available due to the hydrogen bonding interaction, there was less electronic donor–acceptor interaction between L-693 989 and the

graphite stationary phase, resulting in shorter retention. The 4-hydroxyproline isomer was less likely subject to the hydrogen bonding because of the unfavorable location of the lone-pair electrons on the active 4-OH group. Thus, it would possess more electronic donor–acceptor interaction and thereby a longer retention time than the 3-hydroxyproline isomer. Although speculative, both phenomena of steric hindrance and hydrogen bonding supported the retention sequence of the isomeric separation observed in this study.

4. Conclusions

The unique electronic feature of the porous graphitic carbon column enables the direct isomeric separation of L-693 989. This successful isomeric separation has exploited further the application of the relatively newly developed PGC column. Chromatographic data as well as the instrumental analysis by MS and ^{1}H NMR spectroscopy have supported the hypothesis that the peak in question is the 4-hydroxyproline isomer, a semi-synthetic fermentation minor. The retention mechanism on the graphite column is based on the electronic donor–acceptor interaction between the compound of interest and the graphite's delocalized electron conduction bands. Steric hindrance and/or hydrogen bonding formation from the neighboring group on the ornithine residue affects the electronic property of the active lone-pair electrons which plays an important role in the separation of the positional isomers.

Acknowledgements

The authors like to thank Dr. H.Z. Ramjit for the MS analysis, Dr. S.M. Pitzenberger and Dr. R.A. Reamer for the ^{1}H NMR analysis and Dr. R.E. Schwartz and Dr. M.L. Hammond for the valuable comments and discussions.

References

[1] R.E. Schwartz, D.F. Sesin, H. Joshua, K.E. Wilson, A.J. Kempf, K.A. Goklen, D. Kuehner, P. Gailliot, C. Gleason, R. White, E. Inamine, G. Bills, P. Salmon and L. Zitano, *J. Antibiot.*, 45 (1992) 1853.
[2] J.M. Balkovec, R.M. Black, M.L. Hammond, J.V. Heck, R.A. Zambias, G. Abruzzo, K. Bartizal, H. Kropp, C. Trainor, R.E. Schwartz, D.C. McFadden, K.H. Nollstadt, L.A. Pittarelli, M.A. Powles and D.M. Schmatz, *J. Med. Chem.*, 35 (1992) 194.
[3] D.M. Schmatz, M.A. Powles, D.C. McFadden, L. Pittarelli, J. Balkovec, M. Hammond, R. Zambias, P. Liberator and J. Anderson, *Antimicrob. Agents Chemother.*, 36 (1992) 1964.
[4] O.D. Hensens, J.M. Liesch, D.L. Zink, J.L. Smith, C.F. Wichmann and R.E. Schwartz, *J. Antibiot.*, 45 (1992) 1875.
[5] M.T. Gilbert, J.H. Knox and B. Kaur, *Chromatographia*, 16 (1982) 138.
[6] J.H. Knox and B. Kaur, *J. Chromatogr.*, 352 (1986) 3.
[7] J.H. Knox and B. Kaur, *Eur. Chromatogr. News*, 1 (1987) 12.
[8] P. Ciccioli, R. Tappa, A. Di Corcia and A. Liberti, *J. Chromatogr.*, 206 (1981) 35.
[9] P. Ciccioli and A. Liberti, *J. Chromatogr.*, 290 (1984) 173.
[10] G. Gu and C.K. Lim, *J. Chromatogr.*, 515 (1990) 183.
[11] M.F. Emery and C.K. Lim, *J. Chromatogr.*, 479 (1989) 212.
[12] C.S. Creaser and A. Al-Haddad, *Anal. Chem.*, 61 (1989) 1300.
[13] F.Y.K. Ghauri and C.F. Simpson, *Anal. Proc.*, 26 (1989) 69.
[14] J.E. Mama, A.F. Fell and B.J. Clark, *Anal. Proc.*, 26 (1989) 71.
[15] J.C. Berridge, *J. Chromatogr.*, 449 (1988) 317.
[16] A. Karlsson and C. Pettersson, *J. Chromatogr.*, 543 (1991) 287.
[17] B.J. Clark and J.E. Mama, *J. Pharm. Biomed. Anal.*, 7 (1989) 1883.
[18] B.J. Bassler, R. Kaliszan and R.A. Hartwick, *J. Chromatogr.*, 461 (1989) 139.
[19] B.J. Bassler and R.A. Hartwick, *J. Chromatogr. Sci.*, 27 (1989) 162.
[20] J.M. Balkovec, M.F. Loewe and D.J. Mathre, *US Pat.*, 5233023.

ELSEVIER

Journal of Chromatography A, 675 (1994) 253–256

JOURNAL OF CHROMATOGRAPHY A

Short Communication

Interfacing high-performance liquid chromatography and cold-vapour atomic absorption spectrometry with on-line UV irradiation for the determination of organic mercury compounds

Ralf Falter, Heinz Friedrich Schöler*

Institut für Sedimentforschung, University of Heidelberg, INF 236, D-69120 Heidelberg, Germany

(First received November 26th, 1993; revised manuscript received April 18th, 1994)

Abstract

A liquid chromatographic method with on-line UV irradiation was developed for the determination of organic mercury compounds by cold-vapour atomic absorption spectrometry (AAS). Methyl-, ethyl-, phenyl- and inorganic mercury were separated on RP C_{18} columns. An UV-irradiation lamp was used for the on-line destruction of the organomercury compounds. Sample and $NaBH_4$ solution were continuously fed to the reaction vessel where mercury was reduced. The volatilized mercury was swept into the absorption cell of a cold-vapour AAS system by nitrogen. The detection limit for methylmercury is 80 pg absolute ($S/N = 3$).

1. Introduction

In recent years various high-performance liquid chromatography (HPLC) methods for the determination of inorganic and organomercury have been developed. The most simple method is the interfacing of HPLC with UV detection. The use of RP C_{18} columns with chelating agents such as substituted dithiocarbamates or thiols enabled simultaneous separation and detection by UV absorption [1–5]. Another, but more selective method was the coupling of HPLC with atomic absorption spectrometry (AAS) or atomic fluorescence spectrometry (AFS), to suppress interferences which occur with UV detection [6,7]. The most difficult procedure was the transformation of the usually stable organomercury complexes into elementary mercury for detection. Several powerful oxidizing solutions like potassium dichromate or peroxodisulphate with following reduction have been used on-line to increase the detection limits. Former papers reported about oxidizing photodigestion by UV irradiation with high-pressure UV lamps (150 W) for batch samples [8–10].

A new method was developed to avoid the on-line wet oxidation, by using a 8-W low-pressure UV lamp with a surrounding PTFE tubenet, to reach detection limits for the investigated organo mercury compounds in the range of 80 pg absolute. Three chelating agents have been tested.

* Corresponding author.

0021-9673/94/$07.00
SSDI 0021-9673(94)00386-N

2. Experimental

2.1. Apparatus

A schematic diagram of the detection system is shown in Fig. 1. The HPLC system consists of a LDC Analytical pump module with a Rheodyne injector (20-μl sample loop), Model ConstaMetric 3200 and a LDC analytical membrane degasser. The detection was carried out on a cold-vapour AAS mercury monitor 3200 (the absolute detection limit of the detector for elementary mercury is 15 pg) by LDC Analytical with integration software LDCtalk. The 8-W UV lamp and the irradiation PTFE coils were obtained from ICT. The peristaltic pump was made by Ismatec and the gas–liquid separator was part of the cold-vapour mercury generator module by LDC Analytical. The drying tube (7 cm × 1 cm I.D.) was filled with calcium chloride. For lengthening the reducing time of the sodium borohydride a PTFE reaction tube (1.5 m × 0.8 mm I.D.) was used. Three RP C_{18} columns were used for the experiments: (1) Chromosphere ODS (5 μm) 30 × 4 mm, (2) Chromosphere ODS (5 μm) 15 × 4 mm and (3) Chromosphere ODS (3 μm) 8 × 4 mm.

2.2. Reagents

Mercury chloride and methylmercury chloride were purchased from Merck, ethylmercury chloride from Alfa and phenylmercury chloride from Aldrich. All compounds for the eluents like methanol, acetonitrile, HPLC-grade water, acetic acid, ammonium acetate and the reducing substances tin(II) chloride and sodium borohydride were of analytical-reagent grade (Baker). 2-Mercaptoethanol, sodium pyrrolidinedithiocarbamate and cysteine from Merck were used without further purification. Before application the sodium borohydride solution was purified from mercury by bubbling with nitrogen for 1 h.

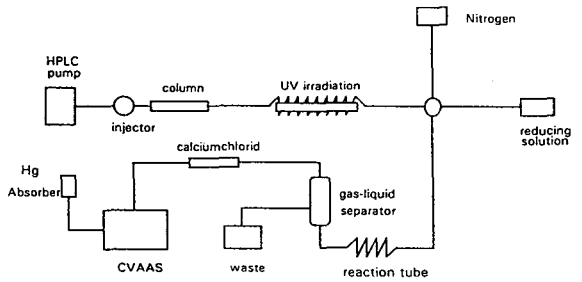

Fig. 1. The HPLC–cold vapor (CV) AAS system coupled with on-line UV irradiation and mercury vapour generator for the separation and detection of mercury compounds.

2.3. Preparation of solutions

The stock solutions of methyl-, ethyl-, phenyl- and inorganic mercury were prepared in water, stored in the dark and refrigerated. The standards were prepared weekly. The eluent was prepared by using acetonitrile–water (65:35, v/v) buffered with ammonium acetate–acetic acid at pH 5.5 containing 0.5 m*M* pyrrolidinedithiocarbamate. A solution of 1% sodium borohydride adjusted to pH 13 with 1 *M* NaOH was used for reduction.

2.4. Irradiation PTFE coil

Several lengths of irradiation coils were tested. The irradiation coil consisted of a PTFE tube of 0.3 mm I.D. A hand-knitted net of 5, 10, 15 and 20 m length is commercially available. For the shorter lengths we knitted the net ourselves. The UV lamp has a length of 30 cm and a diameter of 15 mm and was put in a box for eye protection. The irradiation coils were pulled over the lamp and to better exploit the irradiation they were enveloped with aluminum foil. The PTFE coil shows no change after 1000 operation hours.

3. Results and discussion

3.1. Selection of the complexing agent

2-Mercaptoethanol, cysteine and sodium pyrrolidinedithiocarbamate (SPDC) form stable complexes with organic and inorganic mercury compounds [11–15], which can be separated by HPLC and reduced by tin(II) chloride or sodium

borohydride after on-line oxidation by UV irradiation [3]. After gas–liquid separation, the mercury vapour was detected with AAS. Fig. 2 shows a typical chromatogram for inorganic mercury, methylmercury, ethylmercury and phenylmercury with and without on-line UV irradiation of the mercury pyrrolidindithiocarbamate complexes. The comparison of the two chromatograms shows that with UV irradiation the sensitivity is considerably increased. The inorganic mercury peak has the same area in both chromatograms, so that under these conditions a supplementary UV irradiation does not improve the peak height.

2-Mercaptoethanol, cysteine and SPDC as complexing agents are tested by different eluent conditions, reduction with tin(II) chloride and sodium borohydride as reducing compounds (see Fig. 3). We found that the best results are obtained by using the SPDC as complexing compound with sodium borohydride reduction. An advantage is the order of separation of the different mercury compounds with SPDC, because Hg^{2+} is eluted at the end. With 2-mercaptoethanol, Hg^{2+} is eluted first and might cover in higher concentrations the methylmercury peak during elution [12].

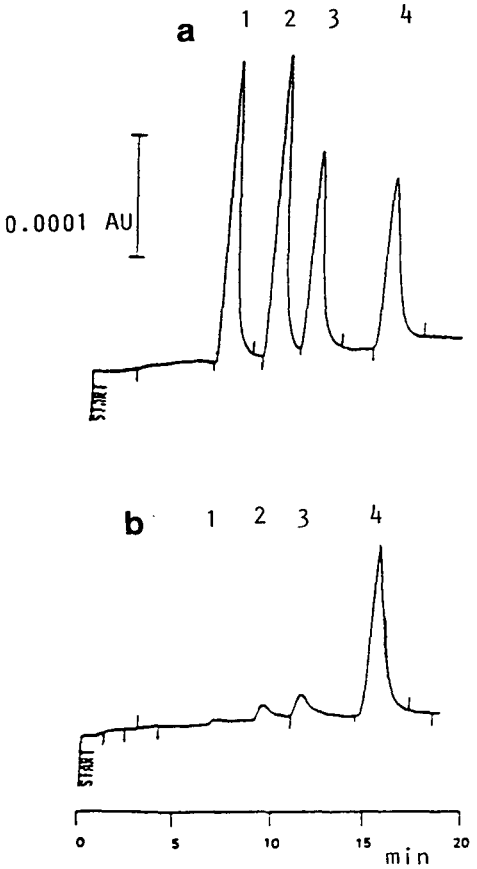

Fig. 2. Comparison between a separation with and without UV irradiation of mercury–SPDC complexes by HPLC–cold-vapour AAS. (a) UV irradiation (90% at 254 nm; reaction coil length 10 m); (b) without UV irradiation. Chromatographic conditions: mobile phase, acetonitrile–water (65:35, v/v) containing 25 mmol ammonium acetate, 0.5 mmol SPDC and acetic acid up to pH 5.0. Column, Chromosphere ODS (5 μm) 30 × 4 mm; flow-rate, 0.9 ml/min; 20-μl sample loop. Peaks: 1 = CH_3Hg^+ (5 ng as Hg); 2 = $CH_3CH_2Hg^+$ (4.5 ng as Hg); 3 = $C_6H_5Hg^+$ (5.5 ng as Hg); 4 = Hg^{2+} (4 ng).

3.2. Selection of the UV-irradiated reaction coil length

The irradiation source is a glass tube filled with argon and mercury under low pressure (about 10^{-3} Torr; 1 Torr = 133.322 Pa). The low-pressure mercury lamp transmits 90% of the light at 254 nm. The reaction coil is a handmade knitted PTFE coil (0.3 mm I.D.) which covers

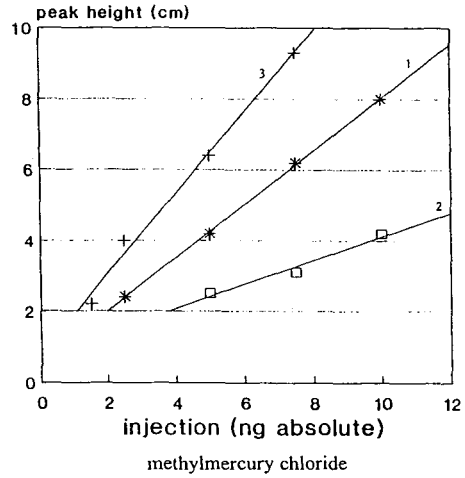

Fig. 3. The increase of the peak height for 2-mercaptoethanol (1), cysteine (2) and sodium pyrrolidinedithiocarbamate (3) as complexing compound. Sodium borohydride for reduction.

the lamp. The peak width, the peak height, the irradiation coil length, the reducing tube and the flow-rate of the eluent had to be optimized in order to achieve maximum sensitivity. There was good linearity for the SPDC–methylmercury complex (regression coefficient $r = 0.994$) between 200 pg and 20 ng Hg absolute (20-μl injection). One must also take into consideration that the pressure of the eluent pump increases with the length of the irradiation coil, so that we have an upper limit at 20 m coil length. Consequently the procedure for SPDC is optimized with an eluent flow of 0.9 ml/min (tested range between 0.5 and 1.5 ml/min), nitrogen flow 120 ml/min (tested range between 50 and 200 ml/min), a 10-m irradiation coil (tested range between 0 and 200 cm) and a reducing tube (tested range between 20 and 200 cm).

3.3. Detection limits for direct injection

The limit of detection for the four tested compounds (Hg^{2+} and the three organomercury compounds) are the same [80 pg Hg absolute ($S/N = 3$)]. This means: Hg^{2+} forms a stable compound with SPDC which is completely destroyed by sodium borohydride and serves as reference basis; the other organomercury compounds need an additional oxidizing step for a complete destruction (*e.g.* UV irradiation). From that we infer the conversion is almost 100%. Comparing to Sarzanini *et al.* [16] the enhanced sensitivity is due to the quantitative destruction of the organomercury compounds.

The relative standard deviations for the methylmercury, ethylmercury and inorganic mercury measurement at 5 ng level are 5%, for phenylmercury 6%.

4. Conclusions

The HPLC–AAS coupling with on-line UV irradiation is a new powerful method for the determination of methylmercury and other organomercury compounds. All components are commercially available. In comparison to earlier methods ours is a simpler one and overcomes the wet oxidation problem by using the on-line UV irradiation. Therefore this procedure does not have the problem of an increasing volume as wet oxidizing has.

References

[1] H. Irth, G.J. de Jong, U.A.Th. Brinkman and R.W. Frei, *Anal. Chem.*, 59 (1987) 98.
[2] W. Lengseth, *Anal. Chim. Acta*, 185 (1986) 249.
[3] J.C. Gaston Wu, *Spectroscopy Lett.*, 24 (1991) 681.
[4] K. Tajima, M. Fujita, F. Kai and M. Takamatsu, *J. Chrom. Science*, 22 (1984) 244.
[5] H. Hintelmann and R.D. Wilken, *Water, Air Soil Pollution*, 56 (1991) 427.
[6] H. Hintelmann and R.D. Wilken, *Appl. Organometallic Chem.*, (1994) in press.
[7] M. Fujita and E. Takabatake, *Anal. Chem.*, 55 (1993) 454.
[8] W. Dorten, P. Valenta and H.W. Nürnberg, *Fresenius' Z. Anal. Chem.*, 317 (1984) 264.
[9] R. Ahmed, K. May and M. Stoeppler, *Fresenius' Z. Anal. Chem.*, 326 (1987) 510.
[10] F.H. Frimmel, D. Sattler and K. Quentin, *Vom Wasser*, 55 (1980) 11.
[11] H. Morita, M. Sugimoto and S. Shimomura, *Anal. Sci.*, 6 (1990) 91.
[12] M. Hempel, H. Hintelmann and R.D. Wilken, *Analyst*, 117 (1992) 669.
[13] W. Holak, *J. Liq. Chromatogr.*, 8 (1985) 563.
[14] E. Munaf, H. Haraguchi, D. Ishii, T. Takeuchi, M. Goto, *Anal. Chim. Acta*, 235 (1990) 399.
[15] W. Lengseth, *Fresenius' Z. Anal. Chem.*, 325 (1986) 267.
[16] C. Sarazanni, G. Sacchero, M. Acteo, O. Abollino and E. Mentasti, *J. Chromatogr.*, 626 (1992) 151.

ELSEVIER

Journal of Chromatography A, 675 (1994) 257–260

JOURNAL OF CHROMATOGRAPHY A

Short Communication

Identification of leather preservatives by gas chromatography–mass spectrometry

D. Muralidharan, V.S. Sundara Rao*

Central Leather Research Institute, Adyar, Madras-600 020, India

(First received December 24th, 1993; revised manuscript received February 21st, 1994)

Abstract

A gas chromatographic method with mass-selective detection was developed for the identification of nine leather preservatives based on phenolic, chlorinated phenolic and heterocyclic compounds. The application of this method to the identification and confirmation of the active ingredients present in commercial formulations is described.

1. Introduction

Pentachlorophenol (PCP) was widely used as a leather preservative owing to its dual functions as a bactericide and fungicide and also its cost effectiveness. However, considering the toxicity of PCP, mostly due to contaminants present in the technical-grade product [the most toxic being the tetrachlorodibenzodioxin (TCDD)], the German Government banned the use of PCP as a leather preservative and set a maximum allowable limit of 5 mg/kg of leather [1]. Simultaneously, the US Government also banned PCP and decreed that leathers and leather products should not contain residues of PCP, its derivatives or any other pesticide that is not registered in the USA under the US Federal Insecticide Fungicide and Rodenticide Act (FIFRA) for use as biocides in raw materials, semi- or fully-finished leathers or leather goods.

The USA and Germany have suggested several substitutes for PCP, of which *o*-phenylphenol (OPP), thiocynatomethylthiobenzothiazole (TCMTB), benzalkonium chlorides (BAC) and *n*-octylisothiazolin-3-one (OITZ) are mainly used in the leather industry [2–4]. In the international leather trade it is essential to know which preservative is used to protect leather from fungal growth and this has necessitated screening and selecting the approved preservatives from commercially available products for use during leather processing. This can be accomplished only by identifying the active ingredients by suitable analytical techniques. As the commercial formulations are complex mixtures, it is necessary to isolate the active principle prior to its identification. Even though chromatographic methods (TLC, GC, HPLC) are the techniques of choice for this purpose [5–12], additional complementary spectral data such as IR, NMR and MS data are essential for confirmation. This paper describes a GC–MS method for the identification of leather preservatives (phenolics,

* Corresponding author.

0021-9673/94/$07.00
SSDI 0021-9673(94)00276-F

chlorinated phenolics, heterocyclic compounds, etc.).

2. Experimental

2.1. Gas chromatograph

A Hewlett-Packard Model 5890 Series II gas chromatograph fitted with an HP-5 (cross-linked 5% phenyl–methylsilicone) capillary column (25 m × 0.32 mm I.D.) with a 0.17-μm film thickness and an HP 5971A mass-selective detector was used.

2.2. Chromatographic conditions

The injector temperature was 300°C, the interface temperature 280°C, the analyser temperature 187°C and the foreline pressure 90 mTorr. The column oven temperature was programmed from 120 to 220°C at 10°C/min. The carrier gas was helium and the inlet pressure was 80 kPa. A splitting ratio of 1:10 was used.

2.3. Chemicals and reagents

p-Chloro-*m*-cresol (PCMC) (Riedel-de Haën), *p*-chlorophenol (4CP) and 2,4,6-trichlorophenol (TCP) (BDH), *o*-phenylphenol (OPP) (Bayer), pentachlorophenol (PCP) (Fluka) and thiocyanatomethylthiobenzothiazole (TCMTB) (Buckman Labs.) were used. *n*-Octylisothiazolin-3-one (OITZ) and methylene bisthiocyanate (MBT) were prepared in the laboratory. Diiodomethyl *p*-tolyl sulphone (DIMPTS) was extracted from Amical-48 (Angus Chemical). All other chemicals were of analytical-reagent grade.

2.4. Analytical procedure

The different preservatives 4CP, PCMC, TCP, OPP and PCP (25 mg each) were dissolved in 10 ml of *n*-hexane and acetylated with acetic anhydride and triethylamine at 60°C for 30 min [13], washed with water and the hexane layer was dried over anhydrous sodium sulphate and evaporated nearly to dryness. A 25-mg amount of each of MBT, TCMTB and OITZ and 50 mg of Amical-48 were added to the acetylated mixture, dissolved in chloroform, made up to 10 ml and further diluted tenfold with chloroform. Portions of 1 μl were injected into the GC–MS system.

Commercial leather preservative formulations based on phenols and chlorophenols were acidified to pH 2 with dilute sulphuric acid, extracted with *n*-hexane and the *n*-hexane extract was subjected to acetylation as described above and analysed by GC–MS. Other formulations were extracted with chloroform and injected directly without derivatization.

3. Results and discussion

The total ion chromatogram (TIC) of the mixture of nine leather preservatives mainly used in tanneries is shown in Fig. 1 and their mass spectral data are presented in Table 1. Phenolic compounds were acetylated prior to injection into the GC column to prevent adsorption of compounds which may lead to tailing of the peaks. For diiodomethyl *p*-tolyl sulphone obtained form the commercial formulation Amical-48, two peaks were obtained, one at 9.9 min (*m/z* 422) corresponding to the molecular ion and another at 6.45 min (*m/z* 296), which indicated the compound to be iodomethyl *p*-tolyl

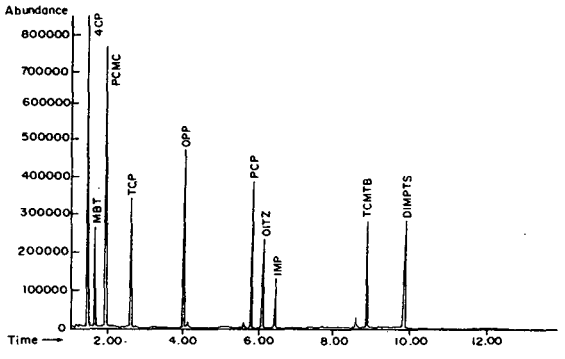

Fig. 1. Total ion chromatogram of leather preservatives. Chromatographic conditions and compound details are given in the text. Time in min.

Table 1
Retention time and mass spectral data for leather preservatives

Compound	t_R (min)	m/z[a]
4CP	1.49	Ac. 170, *128*, 99, 73, 65, 43
MBT	1.64	130, *72*, 58, 45
PCMC	1.97	Ac. 184, *142*, 107, 77, 43
TCP	2.60	Ac. 240, 238, 198, *196*, 167, 132, 97, 43
OPP	4.04	Ac. 212, *170*, 169, 141, 115, 89, 63, 43
PCP	5.87	Ac. 308, 268, *266*, 264, 237, 167, 165, 130, 95, 60, 43
OITZ	6.14	213, 196, 180, 156, 129, 115, 114, 102 *101*, 87, 58, 41
TCMTB	8.93	238, *180*, 166, 136, 108, 69, 45
DIMPTS	9.93	422, 267, 231, *139*, 127, 91, 65, 39

[a] AC = Acetate; values in italics are base peaks.

sulphone. This may be due to an impurity in the formulation. For TCMTB, in addition to the major peak at 8.9 min (m/z 238, 180), a small peak at 8.5 min with a fragmentation pattern of m/z 238, 206 and 180 was obtained, which can be attributed to the –N=C=S group. The absence of an ion at m/z 206 in the mass spectra of the major peak indicated that an –S–C≡N group is present in TCMTB. The chromatogram and mass spectra were stored in a library for reference purposes.

Commercial preservative formulations based on phenolics and chlorinated phenolics may contain sodium salts of these compounds, which are insoluble in hexane. Hence acidification prior to extraction was essential. During the screening of various commercial leather preservative formulations, the active ingredients of two unknown samples were identified by GC–MS. Even though sample 1 was claimed to be a non-PCP-based preservative, the TIC indicated two peaks (Fig. 2) and the mass spectra confirmed the compounds to be tetrachlorophenol (t_R 4.17 min, m/z 232; acetate, m/z 274) and pentachlorophenol (t_R 5.92 min, m/z 266; acetate, m/z 308). Sample 2 on GC analysis gave several peaks (Fig. 3). The sample was identified to be a mixture of two isomers of chloroxylenol (t_R 2.46 and 2.67 min, m/z 156; acetate, m/z 198), two isomers of dichloroxylenol (t_R 3.5 and 3.8 min, m/z 190; acetate, m/z 232), trichloro-

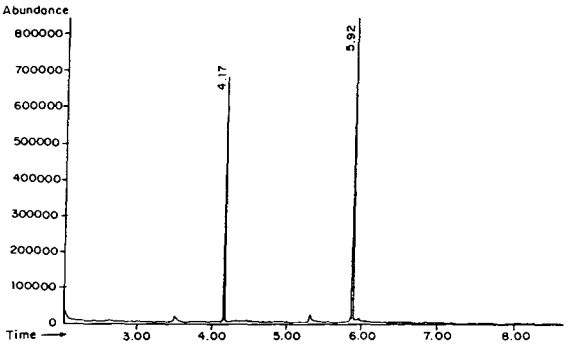

Fig. 2. Total ion chromatogram of a commercial leather preservative formulation (sample 1) obtained by GC–MS. Time in min.

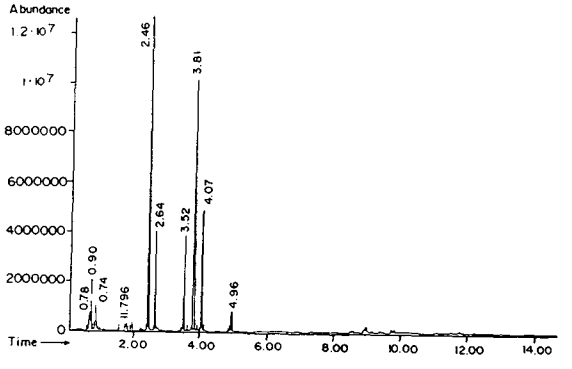

Fig. 3. GC–MS trace of a commercial leather preservative formulation (sample 2). Time in min.

xylenol (t_R 4.96 min, m/z 224, 225; acetate, m/z 268) and *o*-phenylphenol (t_R 4.1 min, m/z 170; acetate, m/z 212) from the mass spectral data, and this sample was free from pentachlorophenol. Our identification is supported by the fact that Antimould A2, a formulation based on a mixture of chloroxylenols and the sodium salt of orthophenylphenol [14], is available from Hodgson Chemicals.

This work clearly indicates that the unambiguous identification of leather preservatives can be achieved by GC–MS. The determination of preservative residues present at trace levels in leather and leather products can be carried out by GC–MS using selective-ion monitoring mode by choosing appropriate ions of individual compounds.

4. References

[1] *Pentachlorphenolverbotsverordnung (PCP-V) vom 12. Dezember 1989*, BGB1.IS.2235, Official Gazette, No. 59, 1989.

[2] V.H. Gattner, W. Lindner and H.U. Neuber, *Leder*, 39 (1988) 66.

[3] A.E. Russell, S. Pinchuck and D.R. Cooper, *J. Soc. Leather Technol. Chem.*, 69 (1985) 135.

[4] M. Tomaselli, A. Cozzolino and C. Liccardi, *Cuoio Pelli Mater. Concianti*, 66 (1990) 129.

[5] M. Tomaselli and A. Cozzolino, *Cuoio Pelli Mater. Concianti*, 67 (1991) 221.

[6] K. Ugland, E. Lundanes, T. Greibrokk and A. Bjorseth, *J. Chromatogr.*, 213 (1981) 83.

[7] M.J. Kennedy, *Analyst*, 111 (1986) 701.

[8] C.R. Daniels and E.P. Swan, *J. Chromatogr. Sci.*, 25 (1987) 43.

[9] C. Parbery and C.D. Taylor, *Analyst*, 114 (1989) 361.

[10] G. Blo, F. Dondi, A. Betti and C. Bighi, *J. Chromatogr.*, 257 (1983) 69.

[11] J.M. Van Deren and E.F. Weiss, *J. Am. Leather Chem. Assoc.*, 73 (1978) 498.

[12] E. Verdu, D. Campello, M. Almela and F. Maldonado, *Bol. Asoc. Quim. Esp. Ind. Cuero*, 43 (1993) 14.

[13] J. Hajslova, V. Kocourek, I. Zemanova, F. Pudil and J. Davidek, *J. Chromatogr.*, 439 (1988) 307.

[14] C.N. Calnan, *Fungicides on Leather*, Leather Conservation Centre, Northampton, 1985, p. 12.

ELSEVIER

Journal of Chromatography A, 675 (1994) 261–266

JOURNAL OF CHROMATOGRAPHY A

Short Communication

Determination of high- and low-molecular-mass plasticisers in stretch-type packaging films

Laurence Castle*,[a], Sue M. Jickells[a], Janet Nichol[a], Sue M. Johns[b], John W. Gramshaw[b]

[a]*Food Science Laboratory, Ministry of Agriculture, Fisheries and Food, Norwich Research Park, Colney, Norwich NR4 7UQ, UK*

[b]*Procter Department of Food Science, University of Leeds, Leeds LS2 9JT, UK*

(First received February 21st, 1994; revised manuscript received April 5th, 1994)

Abstract

A single analytical procedure is presented for determination of so-called monomeric plasticisers such as di(2-ethylhexyl) adipate, polymeric plasticisers such as poly(butylene adipate), and secondary plasticisers such as epoxidised soybean oil. The plasticisers are extracted from the film with concurrent derivatisation. Ester linkages are cleaved by treatment with potassium hydroxide in ethanol, epoxide moieties are opened using hydrochloric acid generated *in situ* by addition of acetyl chloride and, lastly, hydroxy groups are converted to silyl ethers using bis(trimethylsilyl)trifluoroacetamide. This reaction sequence is conveniently performed sequentially on a single sample leading to products that can be measured in a single GC analysis. The method has been applied to samples of known provenance and in a large survey of retail stretch-type films. The combined method offers significant savings in time compared with the separate analytical methods published earlier for monomeric and polymeric poly(vinyl chloride) plasticisers. The method is quantitative and gives results in good agreement with these earlier procedures.

1. Introduction

Thin stretch-type plastics films are widely used for packaging food in both home-use and retail applications [1]. The most common base polymers are poly(vinyl chloride) (PVC), vinylidene chloride co-polymerised with vinyl chloride (PVDC) and polyethylene (PE). Plasticisers are used in PVC and PVDC films to impart the desirable stretch and cling properties [2] while PE films are naturally flexible but may require tackifying agents ("cling additives") to impart cling properties [3,4].

Plasticisers for PVC and PVDC are typically esters and are incorporated into the plastic at quite high levels —percentage levels— in order to modify the basic physical properties of the polymer. For this reason the migration of these additives has been the topic of numerous studies [5,6] and manufacturers have tended in recent years to use higher-molecular-mass plasticisers to reduce migration levels [7]. Thus for PVC, it is now common to find di(2-ethylhexyl) adipate (DEHA) wholly or partially replaced by polymeric plasticisers prepared from adipic acid and

* Corresponding author.

SSDI 0021-9673(94)00378-M

glycols such as propane-1,2-diol or butane-1,3-diol. There is also a tendency to use higher levels of epoxidised soybean oil (ESBO) since this heat stabiliser has useful characteristics as a secondary plasticiser [8].

These changes have been successful in reducing migration levels but present the analyst with some difficulties. The polymeric plasticisers in particular are too high in molecular mass to be analysed successfully by GC and they lack a convenient chromophore for HPLC analysis. There are numerous methods published for the determination of the individual plasticisers. One of our laboratories has published methods for the analysis of plastic films and foods for DEHA [9], polymeric plasticisers [10] and ESBO [11,12]. It is time-consuming, however, to apply two or more separate methods if polymeric plasticisers are to be characterised according to their base monomers and then both monomeric and polymeric plasticiser levels are required. Bodies that require this information include industries' own quality control laboratories and enforcement authorities charged with ensuring food contact plastics meet applicable regulations. The present paper overcomes this analytical problem by the use of selective derivatisation procedures to allow a combined analysis of the additives to be performed.

2. Experimental

2.1. Materials

PVC films with declared plasticiser levels were available from earlier studies [7,13] and had been supplied by various manufacturers of stretch-type PVC films. The films were either production samples from the period 1987–1991 or experimental film formulations. The plasticisers DEHA, poly(propylene adipate) (PPA) and poly(butylene adipate) (PBA) were commercial samples obtained from these film manufacturers as were samples of the heat stabiliser and secondary plasticiser ESBO.

Bis(trimethylsilyl)trifluoroacetamide (BSTFA) was from Pierce (Chester, UK) and ethanol (99.9%, v/v) was from Hayman (Witham, UK). Acetonitrile (HPLC grade) and chloroform (glass-distilled grade) were from Rathburn (Walkerburn, UK). Triheptadecanoin, butane-1,4-diol and acetyl chloride were from Sigma (Poole, UK).

2.2. Methods

A known area of film (0.25 dm^2) was weighed, cut into small pieces and placed in a crimp-cap vial (20 ml capacity) along with internal standards butane-1,4-diol (3 mg) and triheptadecanoin (1 mg) dissolved in chloroform (250 μl). The chloroform was evaporated just to dryness under a stream of nitrogen at 40°C whereupon ethanolic potassium hydroxide (0.2 *M*, 2 ml) was added and the vial then capped and heated for 1 h at 80°C. Acetyl chloride (100 μl) was then added to the mixture and the vial contents heated for a further period of 2 h at 60°C. An aliquot of the supernatant (5 μl) was transferred by syringe to a tapered vial (1.6 ml capacity) and derivatised by the addition of acetonitrile (100 μl) and BSTFA (100 μl) followed by a period of heating at 80°C for 2 h and a further period of 24 h at ambient temperature. The tapered vials were loaded directly into the GC autosampler (Fisons A200S, Crawley, UK) for analysis.

GC analysis employed a CPSil 5CB fused-silica capillary column (Chrompack, London, UK) of dimensions 18 m × 0.25 mm I.D., 0.12-μm phase. The column was installed in a Carlo Erba Mega Series 2 gas chromatograph (Fisons, Loughborough, UK) operated with hydrogen as the carrier gas at 1 ml/min. The column was held at 60°C for 4 min after injection and then programmed to rise at 40°C/min to 260°C (held 1 min) then at 50°C/min to 290°C to clean. Injections of 1 μl in volume were made in the split mode (20:1) with the injector block at 240°C. The flame ionization detector was held at 300°C. Quantitation was on the basis of integrated peak area ratios of analytes *versus* the internal standard(s) and used standard curves prepared by the analysis of plasticiser standards taken through the full analytical method. GC–MS analysis for confirmation of peak identity used a Hewlett-

Packard 5890II GC fitted with a 7673 autosampler and an HP5971 mass-selective detector.

3. Results and discussion

3.1. The reaction scheme selected

The concurrent GC analysis of monomeric and polymeric plasticisers is made possible by the chemistry shown in Fig. 1. The aim of the first reaction was to break down the polymeric plasticisers to their more volatile base monomer units, adipic acid (as the diethyl ester) along with the C-3 or C-4 diol for PPA and PBA, respectively. The conditions also convert high-molecular-mass epoxidised triglycerides such as ESBO to the individual epoxy fatty acid ethyl esters. The basic conditions of potassium hydroxide in ethanol were chosen so as to leave the epoxy moieties in ESBO intact [14]. The second step chosen was the acid-catalysed opening of these epoxide groups to the isomeric 1,2-ethoxyalcohols. This was conveniently achieved by the addition of acetyl chloride to the basic ethanolysis solution to generate an excess of HCl under anhydrous conditions. Finally, an aliquot of the reaction mixture was treated with BSTFA to provide good chromatography on a robust non-polar GC phase, by converting the polar hydroxy functions to the silyl ethers.

3.2. Measurement of DEHA and polymeric plasticisers

A typical chromatographic trace is shown as Fig. 2. DEHA was quantified as the TMS ether of 2-ethylhexanol and PPA and PBA as the TMS ethers of propane-1,2-diol and butane-1,3-diol respectively (Fig. 1). The yield of diethyl adipate was used as a check on the DEHA, PBA and PPA results since these three plasticisers combined should account for the total adipate found when calculated on a mole basis. In this work

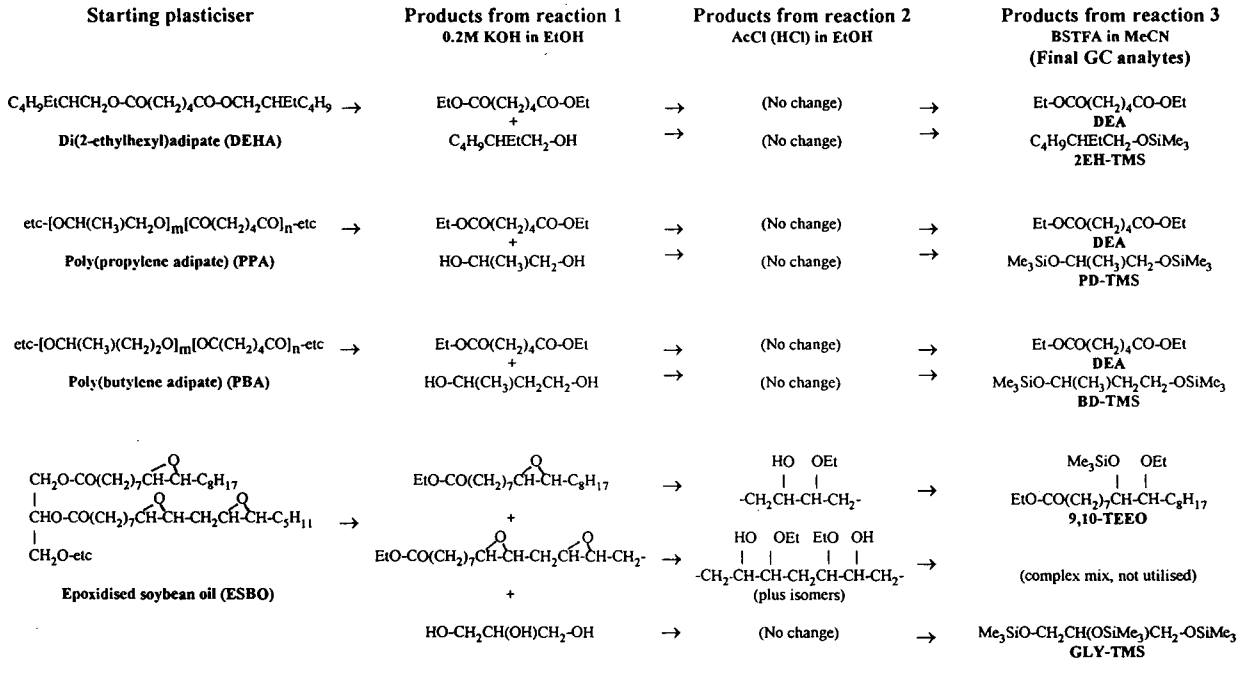

Fig. 1. Chemistry of analysis. DEA = Diethyladipate; 2EH-TMS = trimethylsilyl (TMS) derivative of 2-ethylhexanol; PD-TMS = TMS derivative of propane-1,2-diol; BD-TMS = TMS derivative of butane-1,3-diol; GLY-TMS = TMS derivative of glycerol; 9,10-TEEO = 9-trimethylsilyloxy-10-ethoxyethyl octadecanoate (and 10,9-isomer).

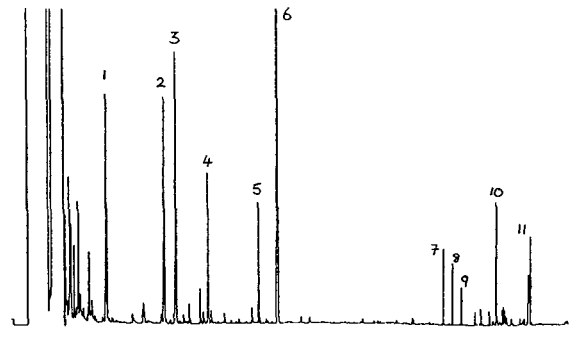

Fig. 2. GC trace of plasticiser standards taken through the method. Identification of peaks and the parent plasticisers: 1 = propane-1,2-diol-TMS from PPA; 2 = butane-1,3-diol-TMS from PBA; 3 = 2-ethylhexanol-TMS from DEHA; 4 = butane-1,4-diol-TMS internal standard; 5 = glycerol-TMS from ESBO and triheptadecanoin internal standard; 6 = diethyl adipate from DEHA, PPA and PBA; 7 = ethyl hexadecanoate from ESBO; 8 = ethyl heptadecanoate from triheptadecanoin internal standard; 9 = ethyl octadecanoate from ESBO; 10 = 9-trimethylsilyloxy-10-ethoxyethyl octadecanoate (and 10,9-isomer) from ESBO; 11 = complex products from diepoxide component of ESBO.

DEHA, PPA and PBA were the three main plasticisers encountered. If however the total yield of adipate did not tally as described above or if the chromatogram revealed the presence of phthalate, sebacate, azelate or citrate ethyl esters, for example, this served as an alert for the presence of alternative plasticisers such as di(2-ethylhexyl) phthalate, acetyl tributyl citrate, dioctyl azelate or dibutyl sebacate. These plasticisers are rarely found in PVC films for food contact but are used in certain other films, laminates, inks and varnishes [15, 16]. They can be quantified using the method described here with the appropriate standards.

3.3. Measurement of ESBO

The chromatogram in Fig. 2 shows a number of late-running peaks which are derived from ESBO and which were used to identify and quantify ESBO. GC–MS analysis identified ethyl hexadecanoate (peak 7) and ethyl octadecanoate (peak 9) derived from the saturated 16:0 and 18:0 fatty acids in ESBO. There were a number of other products identified by GC–MS and ascribed to the epoxy fatty acids in ESBO. The product of choice for determining ESBO was 9-trimethylsilyloxy,10-ethoxyethyl octadecanoate (TEEO, Fig. 1) derived from monoepoxy stearate (epoxidised oleate). The mass spectrum of this derivative showed no molecular ion but gave the expected [17] intense α-cleavage fragments at m/z 273 and 215 (base peaks) ascribed to positional isomers giving $[EtOOC(CH_2)_7CHOSiMe_3]^+$ and $[C_8H_{17}CHOSiMe_3]^+$ fragments from 9,10-TEEO and 10,9-TEEO respectively. These two isomers were the expected products arising from acid-catalysed attack of EtOH at the 10 and 9 carbons of the ESBO monoepoxy stearate (Fig. 1). The two isomers gave a single GC peak with good symmetry (peak 10). A number of closely related spectra were seen in the GC–MS analysis and these were attributed to positional and stereoisomeric forms of the derivatives from the diepoxy and triepoxy fatty acids in ESBO. These were less attractive for ESBO quantification because of their complexity (peaks 11, Fig. 2). This complexity was useful, however, as the characteristic fingerprint of peaks when expanded, served to confirm the presence of ESBO.

The fatty acid composition of soybean oil depends on source and cultivar. The 18:1 content can range from 14 to 35% [18] although a more typical 18:1 content is about 26% [19]. With this uncertainty, there is the possibility that only a semiquantitative calculation of ESBO can be made from the TEEO derivative unless the same ESBO as in the film is available as a calibration standard. Outside a manufacturer's own quality control laboratory this situation does not usually pertain. An alternative approach is to quantify ESBO via the TMS derivative of glycerol (Fig. 1). This should be done only if there is no evidence of triglycerides other than ESBO present in the plastic, and the triheptadecanoin internal standard should be omitted as it also yields glycerol. The butane-1,4-diol serves as the internal standard for glycerol.

3.4. Accuracy of the method

Results of analysis of film samples are shown in Table 1 along with information on plasticiser

Table 1
Comparison of results from the present method with known plasticiser levels

MFilm code	Composition as determined here (%, w/w)				Prior information (%, w/w)			
	DEHA	PPA	PBA	ESBO	DEHA	PPA	PBA	ESBO
Manufacturer A								
Film 1	18.3	<0.3	<0.3	7.8	17.6	na	na	7.3
Film 2	6.9	<0.3	7.4	3.8	10.2	na	na	na
Manufacturer B								
Film 3	<0.3	2.2	22.4	5.3	0	+	+	na
Film 4	24.0	<0.3	<0.3	6.7	+	0	0	+
Film 5	12.8	<0.3	2.4	5.7	na	na	na	na
Manufacturer C								
Film 6	9.8	5.7	2.4	7.8	10.0	9 (PPA + PBA)		8.0
Film 7	<0.3	21.7	<0.3	6.4	0	23 (PPA + PBA)		na
Film 8	12.0	5.0	<0.3	7.2	11.0	na	na	na

Levels as stated by the film manufacturer or determined in earlier studies using independent techniques. + = Stated as present by the manufacturer but no level revealed; na = no prior information available.

levels either supplied by the film manufacturers or obtained using alternative analytical methods [9–12]. There was good agreement in most cases indicating that the method presented here is reliable. The only major discrepancy was for film 2 where the manufacturer stated a DEHA content of 10.2% whereas our analysis indicated only 6.9%. Analysis by an independent technique [9] found 7% DEHA and so the manufacturer's figure appeared to be in error. For polymeric plasticiser analysis, the manufacturer of film 6 indicated a total polymeric content of 9% with both PPA and PBA used but gave no individual values. Analysis found 5.7% PPA and 2.4% PBA and so the total was very close to that expected. Similarly for film 7 where the manufacturer declared 23% polymeric plasticiser but did not state which type. PPA at 21.7% was found —again consistent with the declared composition.

For the determination of ESBO the agreement with the measured value and the expected value was good at 7.8 *versus* 7.3% and 7.8 *versus* 8% for films 1 and 6. The films had been supplied by two different manufacturers and the ESBO standard by a third manufacturer, at times separate by 2 or 3 years. This agreement between expected and found values suggests, therefore, that although the natural composition of soybean oil can vary quite markedly in principle, in practice the epoxy fatty acid composition of ESBO is rather consistent.

3.5. Precision and robustness of the method

In a survey of 170 films sold for home-use or used to package retail foodstuffs, every 10th film was analysed in triplicate. The precision of the method was in all cases ± 5% or better for DEHA, PPA, PBA and ESBO. The detailed results of this survey will be reported elsewhere. The limit of determination (LOD) was found to be about 0.3% (w/w) for each plasticiser in the films. The exact LOD value depended on the state of the film —some retail films had adhering food components and gave an LOD close to this 0.3% (w/w) figure while films sold on the roll for home-use were cleaner and had a lower LOD. The limiting factor in this LOD figure is dilution of the sample aliquot (5 μl) when reacted with BSTFA–MeCN (200 μl) according to Fig. 1. Since an additive below this 0.3% limit would serve almost no useful purpose as a plasticiser, the LOD figure is considered acceptable. The

lowest level of interest in practical terms is for ESBO in PVDC where a 1% level of the heat stabiliser would be typical [6].

In the aforementioned survey, the 170 film samples, along with replicates and calibration standards, were analysed without difficulties. A single capillary GC column was employed without any evidence of build-up of column residues. The whole procedure takes about 29 h but this is largely time required for the derivatisation and the method is not labour intensive. With the accuracy, precision and robustness thus established, it is considered that the combined method proposed here is suitable for general use and offers considerable time savings over the individual methods available to date.

Acknowledgement

The authors acknowledge the help of the PVC flexible film manufacturing industry for the supply of experimental materials.

References

[1] K.R. Osborn and W.A. Jenkins, *Plastics Films —Technology and Packaging Applications*, Technomic, Lancaster, PA, 1992.
[2] D.A. Tester, in R.H. Burgess (Editor), *Manufacture and Processing of PVC*, Applied Sci. Publ., London, 1982, p. 215.
[3] *Eur. Pat. Appl.*, 0 080 198 A2 (1983).
[4] UK Pat. Appl., 2 128 199 A (1984).
[5] Ministry of Agriculture, Fisheries and Food, *Survey of Plasticiser Levels in Food Contact Materials and in Foods; Food Surveillance Paper No. 21*, HMSO, London, 1987.
[6] Ministry of Agriculture, Fisheries and Food, *Plasticisers: Continuing Surveillance; Food Surveillance Paper No. 30*, HMSO, London, 1990.
[7] L. Castle, A.J. Mercer and J. Gilbert, *Food Addit. Contamin.*, 5 (1988) 277.
[8] T.C. Moorshead, *Plastics*, 22 (1957) 343.
[9] J.R. Startin, I. Parker, M. Sharman and J. Gilbert, *J. Chromatogr.*, 387 (1987) 509.
[10] L. Castle, A.J. Mercer and J. Gilbert, *J. Assoc. Off. Anal. Chem.*, 71 (1988) 394.
[11] L. Castle, M. Sharman and J. Gilbert, *J. Chromatogr.*, 437 (1988) 274.
[12] L. Castle, M. Sharman and J. Gilbert, *J. Assoc. Off. Anal. Chem.*, 71 (1988) 1183.
[13] L. Castle, A.J. Mercer and J. Gilbert, *Food Addit. Contamin.*, 8 (1991) 565.
[14] R.A. Barford, S.F. Herb, F.E. Luddy, P. Magidman and R.W. Riemenschneider, *J. Am. Oil Chem. Soc.*, 40 (1963) 136.
[15] L. Castle, A.J. Mercer, J.R. Startin and J. Gilbert, *Food Addit. Contamin.*, 5 (1987) 9.
[16] C. Nerin, J. Cacho and P. Gancedo, *Food Addit. Contamin.*, 10 (1993) 453.
[17] G.A. Ulsaker and G. Teien, *Analyst*, 111 (1986) 559.
[18] B. Holland, A.A. Welch, I.D. Unwin, D.H. Bass, A.A. Paul and D.A.T. Southgate, *McCance and Widdowson's The Chemical Composition of Foods*, Ministry of Agriculture, Fisheries and Food/Royal Society of Chemistry, Letchworth, 5th ed., 1991.
[19] T.P. Hilditch and P.N. Williams, *The Chemical Composition of Natural Fats*, Chapman & Hall, London, 1964.

ELSEVIER

Journal of Chromatography A, 675 (1994) 267–270

JOURNAL OF CHROMATOGRAPHY A

Short Communication

Analysis of silanised polyglycerols by supercritical fluid chromatography

Miroslav Macka[a,☆], Hans-Peter Mettler[a], Michael Bokel[a,*], Winfried Röder[b]

[a]*Department of Analytical Chemistry WAQ1, Lonza AG, 3930 Visp, Switzerland*

[b]*Research and Development, Macherey–Nagel AG, P.O. Box 224, 4702 Oensingen, Switzerland*

(Received February 16th, 1994)

Abstract

A supercritical fluid chromatography method for the analysis of polyglycerols is described. The oligoglycerols are baseline separated up to a degree of polymerization of $n = 5$ and peak maxima can be seen up to $n = 10$ on a SE-54 column. The higher oligoglycerols (presumably $n > 20$) are eluted too; an evaluation similar to that used in size-exclusion chromatography can be used.

1. Introduction

Polyglycerols are used as intermediates for polyglycerol fatty esters which find wide application as emulsifiers in food and personal care industries [1]. Polyglycerol is typically prepared by base-catalyzed polymerization of glycerol. A distribution of polymers is formed with the degree of polymerization (n) ranging from 1 up to 20 or higher, dependent on the reaction conditions (Fig. 1). Several structural isomers of each value of n are formed [1]. Glycerol and oligomers up to hexaglycerol were separated by paper chromatography [1]. An HPLC method with refractive index detection on a carbohydrate column was described for polyglycerols up to $n = 11$, higher polyglycerols are likely not eluted [2]. There has been no analysis method for higher polyglycerols. For the analysis of polyglycerol fatty esters, supercritical fluid chromatography (SFC) was used [3]. SFC is known for successful analyses of various oligo- and polymers [4,5]. It is therefore reasonable to investigate the applicability of SFC to the analysis of polyglycerols.

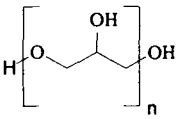

Fig. 1. Structural formula of polyglycerols.

2. Experimental

2.1. Materials

Two polyglycerol samples were obtained from

* Corresponding author.

☆ Present address: Department of Chemistry, University of Tasmania, GPO Box 252C, Hobart, Tasmania 7001, Australia.

0021-9673/94/$07.00
SSDI 0021-9673(94)00337-9

Lonza, USA: sample A with an average polymerisation degree of $n = 10$ and sample B with an average polymerisation degree of $n = 6$ (determined by hydroxyl number analysis). N-Methyl-N-trimethylsilyltrifluoroacetamide (MSTFA) was purchased from Fluka. All other chemicals used were reagent grade (Fluka). Supercritical fluid was carbon dioxide, SFC-grade UN1013, Scott Specialty Gases (< 5 ppm O_2, < 3 ppm H_2O).

2.2. Apparatus and chromatographic conditions

The system used was a Carlo Erba SFC 3000 chromatograph comprising a SFC 300 syringe pump and SFC 3000 GC oven equipped with an flame ionization detector (320°C). Columns used were (1) Macherey-Nagel SE-54, 10 m × 50 μm, $d_f = 0.25$ μm, integrated restrictor 2.1 ml/min CO_2(g) at 10 MPa and 25°C or (2) the same but 20 m long and with an integrated restrictor 2.6 ml/min CO_2(g) at 10 MPa and 25°C. The analyses were run isothermally at 80°C. The following pressure gradient was used: 0 min, 6 MPa; 3 min, 6 MPa; 53 min, 31 MPa; 60 min, 31 MPa.

Samples were derivatized with MSTFA (100 mg sample + 1.0 ml MSTFA) at 100°C for 10 min under stirring and directly injected. Injection was done in a time-split mode (*ca.* 130 ms effectively from an 0.1-μl loop), injection temperature was 30°C. Integration parameters were: acquisition speed, low; peak width (PW) = 10 s; peak threshold (PT) = 500 μV; minimum area (MA) = 20 000 μV/s.

3. Results and discussion

Preliminary experiments showed that high-temperature GC analysis of the polyglycerols after silylation or acetylation is difficult with $n \approx 6$–10 or greater. Also, size-exclusion chromatography partially separated oligoglycerols up to $n \approx 6$ whereas the higher polyglycerols were noticeably excluded from the column.

Chromatograms obtained after silylation with MSTFA are shown in Fig. 2. The assignment of the peaks to the corresponding number n of the structural unit is based on the analogy with previous high-temperature GC–MS analyses of acetylated and of silylated sample A which were similar to the SFC chromatograms up to $n = 6$ (higher oligomers could not be eluted from the non-polar GC column).

Chromatograms in Fig. 3 show the separation

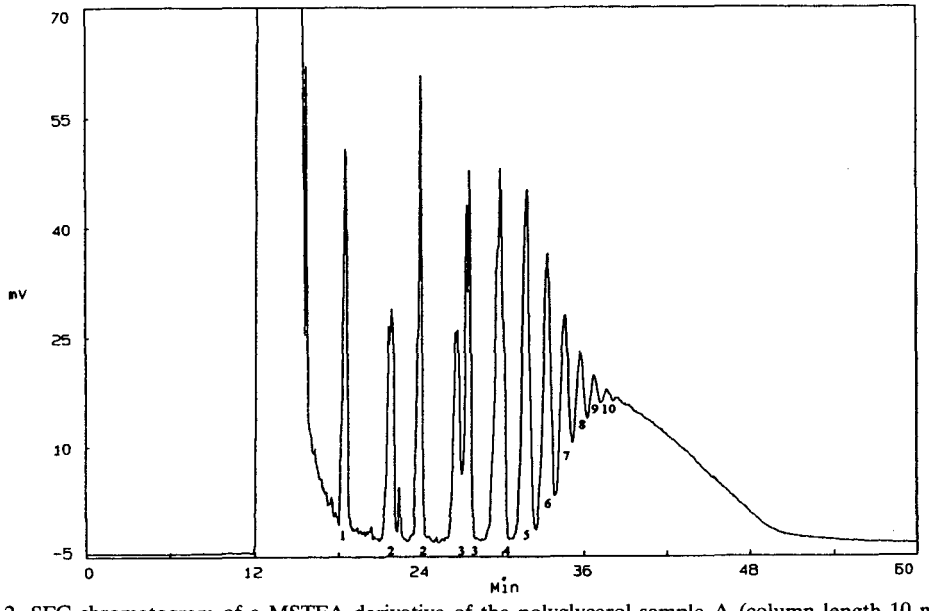

Fig. 2. SFC chromatogram of a MSTFA derivative of the polyglycerol sample A (column length 10 m).

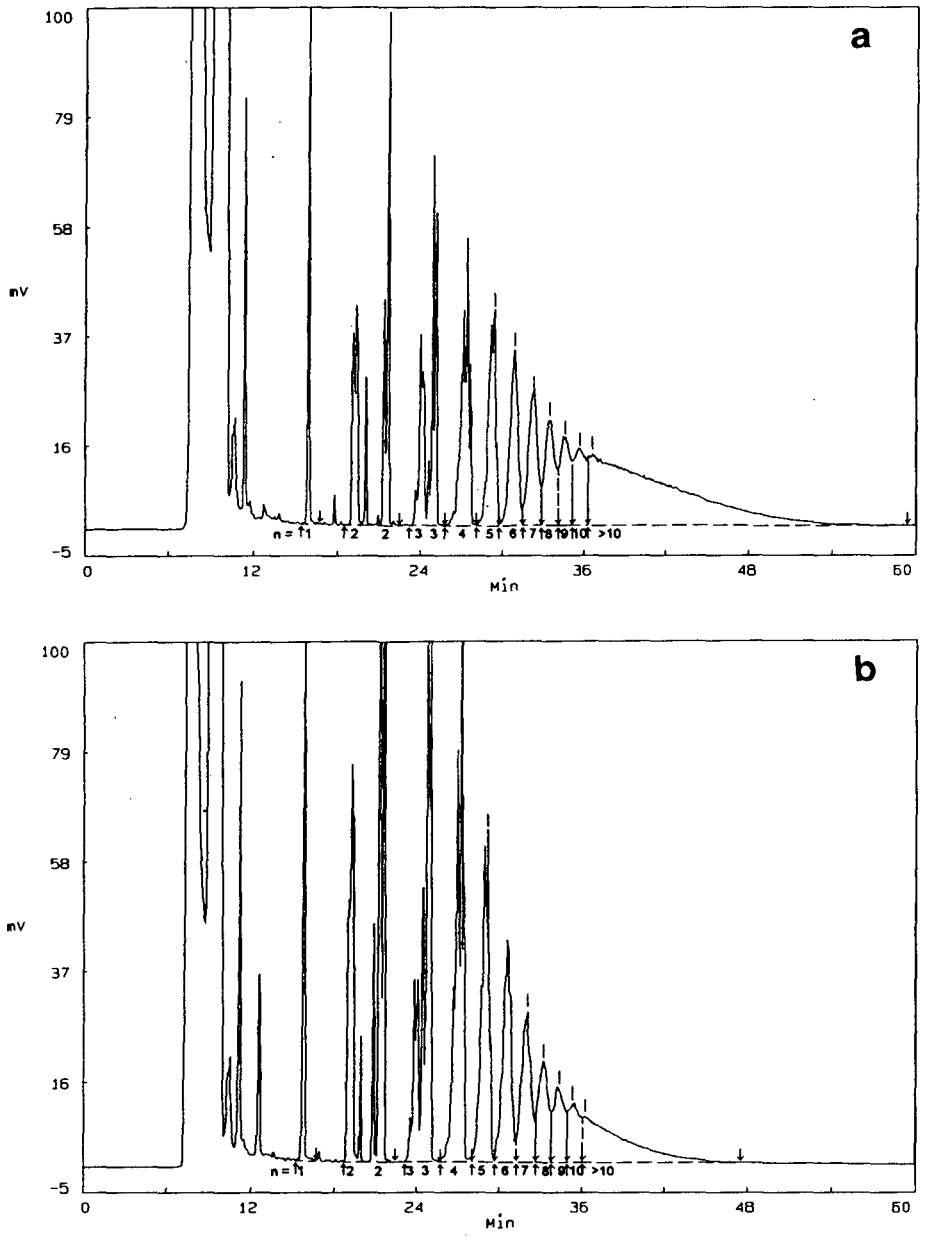

Fig. 3. SFC chromatograms of MSTFA derivatives of (a) polyglycerol sample A (column length 20 m) and (b) polyglycerol sample B (column length 20 m).

of the two samples A and B on a 20-m SE-54 column at 80°C. On this longer column, a better separation of the low ($n = 2$–4) oligomers can be observed whereas the higher polymers are not much affected (compare sample A in Fig. 2). A comparison of the chromatograms of the samples A and B clearly shows a different oligomer distribution.

The integrated areas of the chromatograms in Fig. 3 are shown in Table 1. Although the polyglycerol peaks of $n > 10$ are not separated at all, the differences in the areas under the curve

Table 1
Comparison of the relative peak areas of the two samples

n	Relative peak areas (%)	
	Sample A	Sample B
1	5.0	5.4
2	10.6	22.0
3	9.8	16.8
4	8.5	12.9
5	7.6	9.8
6	7.0	7.6
7	6.3	6.1
8	5.5	4.4
9	4.7	3.6
10	4.7	3.0
>10	30.2	8.4
Total	100	100

at $n > 10$ between the samples A and B are significant (30.2 and 8.4% relative, respectively).

4. Conclusions

Using SFC, silylated polyglycerols up to $n = 20$ (and presumably higher) can be eluted from the column which is a distinctive advantage compared to GC methods and also to the LC method on the carbohydrate column. Size-exclusion chromatography, another method that allows high polyglycerols to be eluted, does not separate the low oligomers as good as SFC. This method is therefore very useful for the comparison of samples of different origin. For oligomers of $n > 10$ which are not separated by the SFC method an "envelope" curve corresponding to the oligomer distribution is obtained. In this case, an evaluation similar to that used with size-exclusion chromatography can be applied.

References

[1] H. Behrens and G. Mieth, *Nahrung*, 28 (1984) 815–835; and references cited therein.
[2] T.N. Kumar, Y.S.R. Sastry and G. Lakshminarayana, *J. Chromatogr.*, 298 (1984) 360–365.
[3] T.L. Chester, D.P. Innis, *J. High Resolut. Chromatogr. Chromatogr. Commun.*, 9 (1986) 178–181.
[4] B. Wenclawiak, *Analysis with Supercritical Fluids —Extraction and Chromatography*. Springer, New York, 1992.
[5] L.Q. Xie, K.E. Markides and M.L. Lee, *Anal. Biochem.*, 200 (1992) 7–19.

ELSEVIER

Journal of Chromatography A, 675 (1994) 271–275

JOURNAL OF CHROMATOGRAPHY A

Short Communication

Chromatographic studies of metal complexes VII. Thin-layer chromatography of cobalt(III) complexes

R.K. Ray*,[a], George B. Kauffman[b]

[a]Department of Chemistry, Rama Krishna Mission Vivekananda Centenary College, Rahara-743 186, 24-Parganas (North), West Bengal, India

[b]Department of Chemistry, California State University, Fresno, CA 93740, USA

(First received June 3rd, 1993; revised manuscript received April 26th, 1994)

Abstract

Thin-layer chromatography of a variety of inert cobalt(III) complexes of different charges (+ 3, + 2, + 1, 0, −1, −3) shows that silica gel is charged negatively in contact with water. Cationic complexes do not move on an anionic silica gel bed; strong adsorption is observed between the complex cation and the negatively charged silanol group of the silica gel. Such strong binding can be reduced considerably by using electrolytes such as KI, KCl, K_2SO_4, etc. In the case of neutral and anionic complexes no such binding is observed. A close connection between R_F values and charges of complexes was observed.

1. Introduction

The movement of cationic complexes on stationary phases may be correlated with the (1) overall charge of the complex species [1–4], (2) stereochemistry of the complex species [1,5], (3) concentration and composition of the mobile phase [1,6], (4) nature of the stationary phase (paper, silica gel, cellulose powder, alumina, etc.) [1,6,7], (5) surface tension of the developer (mobile phase) [8], (6) viscosity of the developer (pure solvent or mixed solvents) [8], (7) dielectric constant of the developer [8–10], (8) ion-pair formation between the complex cation and anion present in the developer solvent or between the complex cation and the anionic stationary phase [2,11], (9) equivalent conductance of the electrolyte [11] and (10) joint effect of the surface tension of the developer and the anionic conductance of the electrolyte present in different developers [11].

The present paper describes the separation by TLC of a number of cationic, neutral and anionic cobalt(III) complexes with aqueous salt solutions as eluents. These separations are based on outer-sphere association between the complex cation and the anion present in the developer.

2. Experimental

2.1. Materials

The complexes were synthesized according to published procedures [12,13]. Their purity was established by elemental analysis and spectral

* Corresponding author.

0021-9673/94/$07.00
SSDI 0021-9673(94)00191-B

measurements. Both the homo- and the heteroligand cobalt(III) biguanide complexes are very stable in the solid state as well as in solution [12,13].

2.2. Procedure

Merck silica gel H was used as the adsorbent. Other experimental techniques have been described elsewhere [14].

3. Results and discussion

The surface of silica gel consists of silanol ($\equiv$Si–OH) sites whose hydrogen atoms can be exchanged for cations [6,15]. From enthalpy, entropy and free energy change values for the exchange reaction between the metal ions and hydrogen atoms of the gel Dugger *et al.* [15] found that the bond energy of the gel varies directly with the charge density of the unhydrated ion. The fact that such adsorbed metal ions cannot be eluted by simple washing with water is evidence of the coordination of the silanol oxygen via exchange of the hydrogen atoms by the metal ion [16,17].

The degree of adsorption of complex cations on silica gel was found to be dependent upon the charge and charge distribution of the complex ion. Furthermore, the amount of acid liberated by sorption of the metal complex cation corresponds to the charge of the complex ion [11,18,19]:

$$(\equiv \text{Si–OH}) + \text{M(en)}_3^{n+} \rightleftharpoons \text{M(en)}_3(\text{O–Si}\equiv)_n + n\text{H}^+$$

When cobalt(III) complexes of different ıarges (-3 to $+3$) were developed with water, ıe anionic and neutral complexes moved easily ı the silica gel and exhibited high (*ca.* 0.9) R_F ılues, but the cationic complexes trailed from ıe point of application. Such strong adsorption : cationic complexes could be reduced by using ther different electrolyte solutions or acidic ılvents [1–4,20].

Acidic solvents, however, were found to be unsuitable, particularly for cobalt(III) biguanidine complexes, since spectrophotometric studies showed substantial modification of electronic spectra. Thus acidic developers do not give R_F values of genuine complexes. It should be noted that for the $[Co(bigH)_3]^{3+}$ ion $\lambda_{max} =$ 480 nm, with $\epsilon = 203$ in water and in different electrolyte solutions, but in acidic solvents it becomes 490 nm, with $\epsilon = 125$, corresponding to the $[Co(H_2O)_2(bigH)_2]^{3+}$ ion [21]. The formation of the $[Co(H_2O)_2(bigH)_2]^{3+}$ ion is also evident from the immediate shift in the absorption maxima of $[Co(OH)(H_2O)(bigH)_2]^{2+}$ from 480 nm to 490–495 nm by the addition of acid [22]. $[Co(H_2O)(bigH)_2]^{3+}$ may dissociate further to $[Co(H_2O)_4(bigH)]^{3+}$ and finally to Co^{2+} with simultaneous release of biguanide if the concentration of acid present in the developer solvent is much greater [22]. Because $[Co(bigH)_3]^{3+}$ and $[Co(H_2O)_2(bigH)_2]^{3+}$ have the same charge, their mobility on silica gel is almost identical (R_F values of 0.72 and 0.68, respectively). Biguanide is more basic ($pK_1 =$ 13.0) than ethylenediamine ($pK_1 = 9.93$) because of an exceptionally high enthalpy of protonation [23,24]. Therefore protonation takes place at the free basic imino group ($=$NH) of the biguanide molecule to the cobalt atom. This causes a strain in the chelate ring, resulting in its rupture from the central metal atoms [21,22,25,26].

Protonation of the complex $[Co(bigH)_3]^{3+}$ ion will naturally facilitate bond breaking by exerting a pull on the electrons of the outer shells of the adjacent atoms of the molecule; thus the metal–nitrogen bond becomes weaker and finally breaks (Fig. 1).

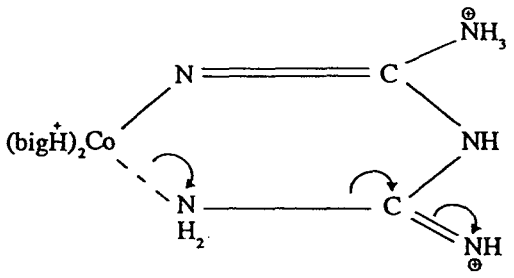

Fig. 1. Protonation of $[Co(bigH)_3]^{3+}$

The addition of pyridine (py) in aqueous KCl developer lowers the R_F values of cationic complexes (Table 1). Because pyridine is a base, it easily removes a proton from the silica gel ($\equiv$Si–OH), making the adsorbent more negative:

$$\equiv Si\text{–}OH + py \rightarrow \equiv Si\text{–}\overline{O} + pyH^+$$

Therefore cationic complexes exhibit much lower R_F values.

In this study we observed a peculiar but definite fact: when cationic complexes were developed with 0.1 *M* KCl or 0.1 *M* KI, the R_F values showed a regular increase with the decrease in the cationic charges (Fig. 2, line ABCD), but a reverse order of R_F values resulted when the same cationic complexes were developed with 0.2 *M* K_2SO_4 solutions (Fig. 2, line EFGH). A similar variation of R_F values was also noted when sodium thiosulfate ($Na_2S_2O_3$) and potassium sodium tartrate ($KNaC_4H_4O_{6)}$ solutions were used as mobile phases (Table 1). The change of R_F values with higher concentration of electrolyte is also shown (Fig. 2, line IJKL). Some of our results corroborate those of Baba *et al.* [20] on another group of cobalt(III) complexes.

In water silica gel becomes negative so that it can hold all the complex cations on its surface, resulting in low R_F values. Adding electrolytes (KI, KCl) to the developer can reduce such strong binding, and the migration of the complex cations on the silica gel bed becomes easy. As expected, the order $R_F + 1 > R_F + 2 > R_F + 3$ is

Table 1
R_F values of cobalt(III) complexes with developers of different concentrations

Complex	R_F								
	KI		KCl		K_2SO_4, 0.2 *M*	K_2SO_4, 0.2 *M* + KCl, 0.2 *M*	$Na_2S_2O_3$, 0.2 *M*	$KNaC_4H_4O_6$, 0.2 *M*	KCl + pyridine (100:5, v/v, 0.2 *M*)
	0.1 *M*	0.2 *M*	0.1 *M*	0.2 *M*					
$[Co(bigH)_3]Cl_3$	0.28	0.72	0.40	0.72	0.90	0.95	0.90	0.91	0.62
$[Co(MebigH)_3]Cl_3$	0.28	0.71	0.38	0.69	0.89	0.96	0.89	0.89	0.60
$[Co(PhbigH)_3]Cl_3$	0.30	0.72	0.40	0.74	0.90	0.95	0.90	0.92	0.64
$[Co(nPr\text{-}bigH)_3]Cl_3$	0.29	0.70	0.40	0.71	0.89	0.97	0.89	0.91	0.59
$[Co(\alpha\text{-}alan\overline{O})(bigH)_2]Cl_2$	0.41	0.52	0.51	0.62	0.73	0.75	0.72	0.73	0.66
$[Co(\beta\text{-}alan\overline{O})(bigH)_2]Cl_2$	0.43	0.53	0.52	0.63	0.75	0.76	0.73	0.74	0.64
$[Co(leuc\overline{O})(bigH)_2]Cl_2$	0.40	0.50	0.49	0.61	0.74	–	0.73	0.75	0.56
$[Co(meth\overline{O})(bigH)_2]Cl_2$	0.40	0.51	0.50	0.61	0.72	0.74	0.71	0.74	0.58
$[Co(val\overline{O})(bigH)_2]Cl_2$	0.41	0.50	0.51	0.60	0.73	0.74	0.71	0.72	0.60
$[Co(IDA)(bigH)_2]Br$	0.52	0.68	0.62	0.72	0.83	0.75	0.86	0.84	0.62
$[CoCO_3(en)_2]Cl$	0.53	0.69	0.61	0.71	0.84	0.95	0.83	0.82	0.61
$[Co(NO_2)_3(NH_3)_3]$	0.82	0.91	0.87	0.92	0.92	0.94	0.93	0.94	0.92
$[Co(gly\overline{O})_3]$	0.83	0.93	0.89	0.93	0.95	0.96	0.94	0.95	0.93
$K[Co(NO_2)_2(gly\overline{O})_2]$	0.95	0.96	0.97	0.98	0.96	–	0.97	0.98	0.97
$NH_4[Co(NO_2)_4(NH_3)_2]$	0.94	0.95	0.96	0.98	0.96	–	0.96	0.98	0.98
$Na_3[Co(NO_2)_6]$	1.00	1.00	1.00	1.00	1.00	–	1.00	1.00	1.00
$K_3[Co(Ox)_3]$	1.00	1.00	1.00	1.00	1.00	–	1.00	1.00	1.00

α-alanOH = α-Alanine; β-alanOH = β-alanine; bigH = biguanide; en = ethylenediamine; glyOH = glycine; $IDAH_2$ = iminodiacetic acid; $KNaC_4H_4O_6$ = potassium sodium tartrate; leucOH = leucine; MebigH = methylbiguanide; methOH = methionine; OxH_2 = oxalic acid; PhbigH = phenylbiguanide; nPr-bigH = *n*-propylbiguanide; valOH = valine; – = not tried.

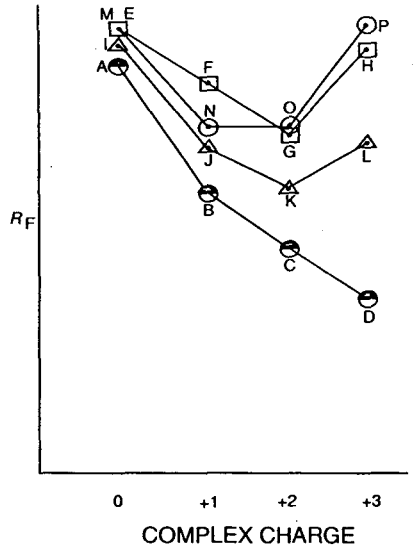

Fig. 2. Complex charge *versus* R_F. ◓ = 0.1 *M* KCl developer; △ = 0.2 *M* KCl developer; □ = 0.2 *M* K_2SO_4 developer; ○ = 0.2 *M* KCl + 0.2 *M* K_2SO_4. (i) A, E, I and M are the spots of $[Co(NO_2)_3(NH_3)_3]$ when developed with 0.1 *M* KCl, 0.2 *M* KCl, 0.2 *M* K_2SO_4 and 0.2 *M* KCl + 0.2 *M* K_2SO_4, respectively. (ii) B, J, N and F are the spots of $[Co(IDA)(bigH)_2]Br$ when developed with 0.1 *M* KCl, 0.2 *M* KCl, 0.2 *M* KCl + 0.2 *M* K_2SO_4 and 0.2 *M* K_2SO_4, respectively. (iii) C, K, G and O are the spots of $[Co(\alpha\text{-alan-}\overline{O})(bigH)_2]Cl_2$ developed with 0.1 *M* KCl, 0.2 *M* KCl, 0.2 *M* KCl + 0.2 *M* K_2SO_4 and 0.2 *M* K_2SO_4, respectively. (iv) D, L, H and P are the spots of $[Co(bigH)_3]Cl_3$ developed with 0.1 *M* KCl, 0.2 *M* KCl, 0.2 *M* K_2SO_4 and 0.2 *M* KCl + 0.2 *M* K_2SO_4, respectively.

observed (Table 1). If the concentration of the electrolyte in the developer is high (0.2 *M* KI or KCl), much greater R_F values for all the complex cations are observed (Table 1). We ascribe this effect to ion-pair formation between the complex cobalt(III) cation and the anion of the developer electrolyte because it is known that ion-association constants increase with increasing charge on the ion and decrease with increasing size of the ion [27,28]. Studies of the outer-sphere dissociation constants of $[Co(NH_3)_6]^{3+}$, $[Co(en)_3]^{3+}$ and $[Co(bigH)_3]^{3+}$ have shown these constants to follow the order [28,29]: $I^- < Br^- < Cl^- \leqslant SO_4^{2-}$. Interestingly, the R_F values for cobalt(III) complexes follow this order. In essence, the anion of the developing electrolyte reduces the overall charge of the complex cation and thus allows easy passage of the complex ion along the anionic silica gel:

$$[Co(bigH)_3]^{3+} + X^- \rightleftharpoons \{[Co(bigH)_3]^{3+} \cdot X^-\}^{2+} \quad \text{(low}[X^-]\text{)}$$

$$\downarrow X^-$$

$$[\{[Co(bigH)_3]^{3+} \cdot X\}^{2+} \cdot X^-]^+ \quad \text{(high } [X^-]\text{)}$$

$$[Co(bigH)_3]^{3+} + SO_4^{2-} \rightleftharpoons \{[Co(bigH)_3]^{3+} \cdot SO_4^{2-}\}^+$$

That such an assumption is not unusual is verified by running additional experiments using 0.2 *M* KCl + 0.2 *M* K_2SO_4 mixed developer solvent (Table 1) where $[Co(LH)_3]^{3+}$ (LH = bigH, etc.), $[Co(gly\overline{O})_3]$ and $[Co(NO_2)_3(NH_3)_3]$ show R_F values of almost 1 (Fig. 2, line MNOP). Therefore formation of the neutral species by $[Co(bigH)_3]^{3+}$ in mixed developer solvent is not unlikely:

$$\{[Co(bigH)_3]^{3+} \cdot SO_4^{2-}\} + Cl^- \rightleftharpoons [\{[Co(bigH)_3]^{3+} \cdot SO_4^{2-}\} + Cl^-]^0$$

4. Conclusions

The degree of adsorption of the cationic complexes on negative silica gel ($\equiv Si\text{–}\overline{O}$) was dependent on the charge and charge distribution of the complex ion. Such strong binding can easily be reduced by using ionic electrolytes. The variation in R_F values for a particular cationic complex in different electrolytes indicates different ion-pair formation between that complex cation and the anion present in the developer solvent, resulting in considerable reduction of the overall effective charge of the complex cation. The larger the association constant (K_A) of the cationic complex, the larger is the R_F value. Such K_A values increase with increasing charge of the ion and decrease with increasing size of the ion [28]. Our results fully agree with the above-mentioned theory.

Acknowledgements

R.K.R. is grateful to Professors R.L. Dutta and D. Banerjea for laboratory facilities. The

authors are also indebted to the referees for valuable suggestions for improving this article.

References

[1] R.L. Dutta, R.K. Ray and G.B. Kauffman, *Coord. Chem. Rev.*, 28 (1979) 23.
[2] R.K. Ray and G.B. Kauffman, *J. Chromatogr.*, 442 (1988) 381.
[3] R.K. Ray and G.B. Kauffman, *Inorg. Chim. Acta*, 162 (1989) 45.
[4] R.K. Ray and G.B. Kauffman, *J. Chromatogr.*, 504 (1990) 464.
[5] T. Baba and H. Yoneda, *Bull. Chem. Soc. Jpn.*, 43 (1970) 2478.
[6] L.F. Druding and G.B. Kauffman, *Coord. Chem. Rev.*, 3 (1968) 409.
[7] M. Lederer and M. Battilotti, *J. Chromatogr.*, 89 (1974) 380.
[8] A. Paul and P.B. Janardhan, *Bull. Chem. Soc. Jpn.*, 40 (1967) 1131.
[9] A.M. Ghe and A. Placucci, *Ann. Chim. (Rome)*, 49 (1959) 1769.
[10] M. Qureshi and M.A. Khan, *Talanta*, 13(1966) 117.
[11] R.K. Ray, M.K. Bandyopadhyay and G.B. Kauffman, *J. Chromatogr.*, 469 (1989) 383.
[12] P. Rây, *Chem. Rev.*, 61 (1961) 313.
[13] A. Syamal, *J. Sci. Ind. Res.*, 37 (1978) 661.
[14] R.K. Ray and G.B. Kauffman, *Transition Met. Chem.*, 17 (1992) 141.
[15] D.L. Dugger, J.H. Stanton, B.N. Irby, B.L. McConnell, W.W. Cummings and P.W. Maatman, *J. Phys. Chem.*, 68 (1964) 757.
[16] R.L. Burwell, R.G. Pearson, G.L. Haller, P.B. Tjok and S.P. Chock, *Inorg. Chem.*, 4 (1965) 1123.
[17] B.J. Hathaway and C.E. Lewis, *J. Chem. Soc., A*, (1969) 1176.
[18] F. Vydra and V. Markova, *J. Inorg. Nucl. Chem.*, 26 (1964) 1319.
[19] F. Vydra and V. Markova, *Collect. Czech. Chem. Commun.*, 30 (1965) 2382; 32 (1967) 1614; 32 (1967) 3530.
[20] T. Baba, H. Yoneda and M. Muto, *Bull. Chem. Soc. Jpn.*, 41 (1968) 1965.
[21] D. Banerjea and B. Chakraborty, *J. Inorg. Nucl. Chem.*, 26 (1964) 1233.
[22] B. Chakraborty and A.K. Sil, *J. Indian Chem. Soc.*, 55 (1978) 452.
[23] L. Fabbrizzi, M. Micheloni, P. Paoletti and G. Schwarzenbach, *J. Am. Chem. Soc.*, 99 (1977) 5574.
[24] L. Fabbrizzi, M. Micheloni and P. Paoletti, *Inorg. Chem.*, 17 (1978) 495.
[25] D. Banerjea, *Indian J. Chem.*, 26A (1987) 543.
[26] B. Chakraborty and P.K. Das, *Indian J. Chem.*, 16A (1978) 583.
[27] M.T. Beck, *Coord. Chem. Rev.*, 3 (1968) 99.
[28] F. Basolo and R.G. Pearson, *Mechanisms of Inorganic Reactions*, Wiley, New York, 2nd ed., 1967, p. 37.
[29] M.K. De and R.L. Dutta, *J. Indian Chem. Soc.*, 52 (1975) 67.

ELSEVIER

Journal of Chromatography A, 675 (1994) 276–281

JOURNAL OF CHROMATOGRAPHY A

Short Communication

Diphenyltin dichloride as a chromogenic reagent for the detection of flavonoids on thin-layer plates

Alois Hiermann*, Franz Bucar

Institute of Pharmacognosy, University of Graz, Universitätsplatz 4/I, A-8010 Graz, Austria

(First received January 20th, 1994; revised manuscript received March 18th, 1994)

Abstract

Among several complexation reagents, diphenyltin dichloride (DTC) proved to be a useful chromogenic compound for both the qualitative and quantitative analysis of flavones and flavonols on thin-layer plates by forming fluorescent complexes of different colour. For qualitative analysis, comparative detection with DTC and diphenylboric acid 2-aminoethyl ester can indicate the position of the glycosidated hydroxyl of kaempferol and luteolin glycosides. Fluorimetric densitometry showed high sensitivity to flavonols with a free 3-hydroxyl group and flavones containing two adjacent hydroxyl groups in ring B.

1. Introduction

Different chromogenic reagents such as NH_3, $AlCl_3$, $Al_2(SO_4)_3$, $ZrOCl_2$, diphenylboric acid 2-aminoethyl ester (Naturstoffreagens A, NA), 2,6-dichloroquinonechlorimide and EDTA are available for the detection of flavonoids on thin-layer plates in order to reveal the spots of these compounds and also to obtain information about their degree of oxidation and substitution patterns [1–8]. For example, when detected with NA on cellulose layers, 3,5-dihydroxyflavones fluoresce at 510–527 nm if two adjacent hydroxyl groups in ring B are missing, but at 560–567 nm with 3′,4′-dihydroxy groups [6].

We report here on investigations on further chromogenic compounds that are able to form fluorescent flavonoid complexes and provide structure information. Some chromogenic reagents were chosen as they were already known in flavonoid analysis [$FeCl_3$, $SbCl_3$, $Be(NO_3)_2$, $Na_2B_4O_7$] [2,6,9] but had not been thoroughly investigated for their ability to form complexes with different types of flavonoids. Additionally we took some similar reagents {$FeSO_4$, $Bi(NO_3)_3$, $SnCl_2$, Ph_2SnCl_2 ($SnCl_4$ has already been used for detection of flavonoids on thin-layer plates [10])}. First their complexes with flavonoids in methanolic solutions were investigated for stability and for the ability to show structure-dependent bathochromic shifts of the UV bands compared with pure methanolic flavonoid solutions. Fluorescence studies were also carried out. In the course of these investigations it turned out that these reagents caused bathochromic shifts of flavonoid UV bands and also caused fluorescence. Among those examined, diphenyltin dichloride (DTC) proved to be the most suitable. DTC also was adapted as a spray

* Corresponding author.

0021-9673/94/$07.00
SSDI 0021-9673(94)00278-H

reagent for the TLC of flavonoid compounds. The best results were obtained with a 2% solution in acetone–methanol (1:1). Different flavonoids varying in degree of oxidation and substitution pattern (isoflavone, flavanone, flavone and flavonol aglycones and glycosides) were investigated on silica gel layers after detection with DTC by fluorimetric densitometry and compared with diphenylboric acid 2-aminoethyl ester as a chromogenic reagent. The fluorescent colours on polyamide and cellulose layers were also determined.

2. Experimental

2.1. Materials

All flavonoids except kaempferol-3-O-glycosides, kaempferol-3,7-O-dirhamnoside and kaempferol-7-O-rhamnoside were obtained from Carl Roth (Karlsruhe, Germany). Kaempferol-3-O-rhamnoside, kaempferol-3-O-glucoside and kaempferol-3-O-glucuronide were isolated from *Epilobium angustifolium* and kaempferol-7-O-rhamnoside and kaempferol-3,7-O-dirhamnoside from *Prunus spinosa*. The identity of the isolated compounds was confirmed by UV, ^{1}H NMR and mass spectrometry.

Organic solvents and inorganic reagents were of analytical-reagent grade from Merck (Darmstadt, Germany). Diphenyltin dichloride was of zur Synthese purity from Merck. Diphenylboric acid 2-aminoethyl ester was purchased from Carl Roth.

2.2. UV spectrophotometry

UV spectrophotometry was carried out on a Kontron Uvikon 810 spectrophotometer. The absorbances of 0.02 mmol l^{-1} solutions were determined between 220 and 500 nm in comparison with pure solvent (scan speed 100 nm min^{-1}). To 2.0 ml of methanolic flavonoid solution 0.05 ml of reagent solution [1% (w/v) in methanol] were added.

2.3. Spectrofluorimetry

Measurements were carried out on a Perkin-Elmer LS-5 luminescence spectrometer between 200 and 900 nm with 0.02 mmol l^{-1} methanolic solutions. To 2.0 ml of flavonoid solution 0.05 ml of DTC solution [1% (w/v) in methanol] were added. Because of the very intense fluorescence, solutions of kaempferol, its 7-O-glycosides and luteolin had to be diluted tenfold.

2.4. Preparation of spray reagents for TLC

A 2% (w/v) solution of DTC in acetone–methanol (1:1, v/v) was used as a chromogenic reagent for TLC. Spraying was repeated twice with intermediate drying of the TLC plates in a cold stream of air. To enhance and stabilize the fluorescence, spraying with a 5% (w/v) ethanolic solution of polyethylene glycol (PEG) 4000 (Merck) and with "Paraffin dünnflüssig" (Merck) followed [11]. Detection with diphenylboric acid 2-aminoethyl ester (Naturstoffreagens A, NA) was carried out in the same way except that a 1% (w/v) methanolic solution of NA was used. Measurements were made 15 min after spraying.

2.5. TLC procedures

Volumes of 1 μl of 0.0035 mol l^{-1} methanolic flavonoid solutions were applied with Blaubrand intraEND single-use 1-μl micropipettes (Brand, Wertheim, Germany) to TLC plates: silica gel (precoated aluminium-backed TLC plates, Kieselgel 60 F_{254}, 20 × 20 cm; Merck); polyamide (precoated plastic-backed thin layer plates, Polygram polyamide 6-UV_{254}, 20 × 20 cm; Macherey–Nagel, Düren, Germany); and cellulose (precoated plastic-backed TLC plates, Polygram cel300; Macherey–Nagel).

Samples were applied as spots 3 mm in diameter at intervals of 10 mm and with a distance of 15 mm from the lower edge and 15 mm from the side edges. Chromatography was carried out over a distance of 8 cm in a 20 × 20 cm twin-trough chamber with a stainless-steel lid (Camag, Muttenz, Switzerland) under saturated conditions.

Flavonoid aglycones were separated on silica gel plates using (I) toluene–methanol–2-butanone–acetylacetone–cyclohexane (20:15:10:5:50, v/v) and flavonoid glycosides using (II) ethyl acetate–formic acid–water (68:8:8, v/v) as mobile phase. On polyamide layers flavonoids were separated with (III) toluene–methanol–2-butanone–acetylacetone (40:30:20:10, v/v) and (IV) water–2-butanone–acetone–formic acid (60:30:9:1, v/v). On cellulose layers, (V) 10%, (VI) 20% and (VII) 30% (v/v) acetic acid were used as mobile phases. When separation was complete the plates were dried in a warm stream of air and detected as described above.

2.6. Densitometric analysis

Measurements were carried out on a Shimadzu CS-9000 dual-wavelength flying spot scanner. TLC lanes were scanned at a wavelength of 436 nm in the fluorescence mode using filter 3 (split width 10 × 1 mm). During measurement the TLC plates were fixed to a 20 × 20 cm glass plate to the back of which a plastic tube (2 mm I.D.) was attached in several loops. The temperature of the TLC plates was controlled by the flow-rate of ice-cooled water which was pumped using a Minipuls 2 pump (Gilson, Villiers-le-Bel, France) through the plastic tube. The relative standard deviation (R.S.D.) range of the densitometric measurements was 4.3–7.1% (5.2% on average) ($n = 4$). A calibration plot for 0.02–0.4 μg of quercetin (3,5,7,3′,4′-pentahydroxyflavone) showed good linearity between 0.16 and 2 μg [method of linear regression, y (area units) = ax (μg) + b, $y = 102510x - 9156$, standard deviation of a (S.D.$_a$) = 1812, standard deviation of b (S.D.$_b$) = 1905, correlation coefficient (r) = 0.99887, nine calibration points, $n = 4$]. The limit of detection of quercetin (TLC system I) with DTC was 20 ng, which matched that with NA detection.

3. Results and discussion

3.1. Absorbance measurements in solution

In preliminary studies, the influence of different complexation reagents [$Be(NO_3)_2$, $SnCl_2$, $Na_2B_4O_7$, $SbCl_3$, $Bi(NO_3)_3$, $FeSO_4$, $FeCl_3$, Ph_2SnCl_2] on the UV spectra of various flavo-

Table 1
UV absorbance and spectrofluorimetric measurements of different flavonoid–DTC complexes in methanolic solutions (0.02 mmol l^{-1})

Compound	UV [λ_{max} (nm)]		Fluorescence [λ_{max} (nm)]	
	Band I (MeOH)	Band I with DTC	Excitation	Emission
Aglycones				
Genistein (5,7,4′-OH-isoflavone)	327sh	327sh	420	475
Dihydrofisetin (3,7,3′,4′-OH-flavanone)	310	311sh	425	487
Apigenin (5,7,4′-OH-flavone)	335	337	390	491
Luteolin (5,7,3′,4′-OH-flavone)	349	366	420	505
Kaempferol (3,5,7,4′-OH-flavone)	367	424	424	474
Quercetin (3,5,7,3′,4′-OH-flavone)	370	433	436	496
Rhamnetin (3,5,3′,4′-OH-7-OMe-flavone)	369	432	443	504
Myricetin (3,5,7,3′,4′,5′-OH-flavone)	374	446	437	515
Glycosides				
Kaempferol-3-O-glucoside	351	352	422	484
Kaempferol-7-O-rhamnoside	366	423	424	474
Quercetin-3-O-rhamnoside	350	360	432	480
Myricetin-3-O-rhamnoside	352	362	438	490

noids in methanolic solutions was investigated in order to obtain information about the mechanism of complexation. Bathochromic shifts of band I were recognized with all flavonols with a free 3-OH group. Further investigations were carried out with DTC–flavonoid complexes and the results are given in Table 1.

The flavonols showed a marked shift of band I (from +54 to +72 nm) when DTC was added. 3′,4′-Dihydroxyflavones without a 3-OH group and also 3-O-glycosidated flavonols which contained two adjacent hydroxyl groups in ring B showed only smaller shifts (10–17 nm). Compounds that did not contain one of these structural elements did not show substantial shifts of band I. Hence complexation of DTC with 4-keto, 3-hydroxy (in the case of flavonols) and *o*-dihydroxy groups in ring B (in the case of flavones and flavonols) might be assumed. Detailed complexation studies with DTC and flavonoids have not yet been carried out. Measurements over a period of 20 min showed no decrease in intensity or bathochromic shift. None of the flavonoid–DTC complexes were acid resistant as the bathochromic shifts disappeared when 1 mol l^{-1} hydrochloric acid was added.

3.2. Spectrofluorimetric measurements in solution

Fluorescence was characterized by the determination of the λ_{max} of excitation and emission (Table 1). According to these results the intense spectral line of the mercury lamp at 436 nm was

Table 2
Visual analysis of flavonoids on silica gel plates after detection with DTC

Compound	Vis	UV (366 nm)
Aglycones		
Genistein (5,7,4′-OH-isoflavone)	Dark yellow	Olive
Dihydrofisetin (3,7,3′,4′-OH-flavanone)	Yellow[a]	Ochre[a]
3-OH-flavone	Green[a]	Blue
5-OH-flavone	Dark yellow[a]	Olive
7-OH-flavone	Not visible	Blue[a]
Apigenin (5,7,4′-OH-flavone)	Olive[a]	Light green[a]
Luteolin (5,7,3′,4′-OH-flavone)	Yellow	Yellow
Kaempferol (3,5,7,4′-OH-flavone)	Light yellow	Turquoise
Kaempferide (3,5,7-OH-4′-OMe-flavone)	Light yellow	Turquoise
Quercetin (3,5,7,3′,4′-OH-flavone)	Light orange	Light orange
Rhamnetin (3,5,3′,4′-OH-7-OMe-flavone)	Light orange	Light orange
Myricetin (3,5,7,3′,4′,5′-OH-flavone)	Light orange	Orange
Morin (3,5,7,2′,4′-OH-flavone)	Light yellow	Light green
Glycosides		
Luteolin-5-O-glucoside	Light yellow	Green
Luteolin-7-O-glucoside	Yellow	Yellow
Luteolin-7,3′-O-diglucoside	Light yellow[a]	Green[a]
Kaempferol-3-O-rhamnoside	Yellow[a]	Olive[a]
Kaempferol-3-O-glucoside	Yellow[a]	Olive[a]
Kaempferol-3-O-glucuronide	Yellow[a]	Olive[a]
Kaempferol-3,7-O-dirhamnoside	Yellow[a]	Olive[a]
Kaempferol-7-O-rhamnoside	Light yellow	Turquoise
Kaempferol-7-O-neohesperidoside	Light yellow	Turquoise
Quercetin-3-O-rhamnoside	Dark yellow	Yellow
Quercetin-3-O-glucoside	Dark yellow	Yellow
Myricetin-3-O-rhamnoside	Dark yellow	Yellow

1 μl of 0.0035 mol l^{-1} methanolic flavonoid solutions; solvent systems I and II.
[a] Weak.

chosen for fluorimetric densitometry. Conspicuous was the intense fluorescence when DTC was added to solutions of kaempferol, its 7-O-glycosides and luteolin.

3.3 Measurements on TLC plates

Visual analysis showed above all intense fluorescing spots of 3′,4′-dihydroxy flavone and 3-hydroxy flavones with (yellow or orange fluorescence) or without (green or turquoise fluorescence) *o*-dihydroxy groups in ring B (Table 2).

In comparison with NA fluorescence, the colours with DTC were similar but generally tended to shorter wavelengths (*e.g.*, light orange instead of orange for quercetin; turquoise instead of green for kaempferol). Kaempferol, kaempferide and the 7-O-glycosides of kaempferol fluoresced very intensely turquoise, whereas the 3-O-glycosides of kaempferol showed a weaker greenish fluorescence. Obviously the hydroxyl at C-3 was necessary for complexation of flavonols lacking two adjacent hydroxyls in ring B. The fluorescent colours on polyamide and cellulose layers (TLC systems III to VII) were commensurate with those on silica gel.

In order to determine the fluorescence intensities, densitometric measurements on DTC-de-

Table 3
Fluorimetric densitometry of different flavonoids detected with DTC and NA on silica gel layers

Compound	R_F (I)	DTC	NA
Aglycones			
Genistein (5,7,4′-OH-isoflavone)	0.31	–[a]	0.6
Dihydrofisetin (3,7,3′,4′-OH-flavanone)	0.17	1.7	0.8
3-OH-flavone	0.63	57	52
5-OH-flavone	0.76	0.5	1.8
7-OH-flavone	0.37	–[a]	–[a]
Apigenin (5,7,4′-OH-flavone)	0.33	4.8	101
Luteolin (5,7,3′,4′-OH-flavone)	0.25	343	236
Kaempferol (3,5,7,4′-OH-flavone)	0.30	311	156
Kaempferide (3,5,7-OH-4′-OMe-flavone)	0.33	131	90
Quercetin (3,5,7,3′,4′-OH-flavone)	0.21	90	45
Isorhamnetin (3,5,7,4′-OH-3′-OMe-flavone)	0.30	98	24
Rhamnetin (3,5,3′,4′-OH-7-OMe-flavone)	0.31	70	23
Myricetin (3,5,7,3′,4′,5′-OH-flavone)	0.09	52	24
Morin (3,5,7,2′,4′-OH-flavone)	0.10	385	288
Glycosides	R_F (II)		
Luteolin-5-O-glucoside	0.30	231	222
Luteolin-7-O-glucoside	0.47	299	79
Luteolin-7,3′-O-diglucoside	0.10	1.2	64
Kaempferol-3-O-rhamnoside	0.73	5.5	64
Kaempferol-3-O-glucoside	0.55	13	69
Kaempferol-3-O-glucuronide	0.45	8.1	61
Kaempferol-3,7-O-dirhamnoside	0.44	5.8	85
Kaempferol-7-O-rhamnoside	0.79	309	266
Kaempferol-7-O-neohesperidoside	0.27	309	221
Quercetin-3-O-rhamnoside	0.66	55	50
Quercetin-3-O-glucoside	0.49	66	42
Myricetin-3-O-rhamnoside	0.53	50	54

1 μl of 0.0035 mol l^{-1} methanolic solutions; solvent systems I and II; λ_{ex} = 436 nm; AUC (peak area) × 10^{-3}; R.S.D. = 5.2% (on average) (n = 4).
[a] Not quantifiable.

tected flavonoids were made on silica gel layers and compared with those for NA as a chromogenic reagent. Before *in situ* measurements the fluorescence was enhanced and stabilized by spraying with PEG 4000 (5% ethanolic solution) and liquid paraffin according to ref. 11. Preliminary investigations showed that additionally a constant temperature was necessary to obtain sufficient fluorescence stability. Therefore, all measurements were carried out at 20°C (temperature of TLC plates), which decreased the R.S.D. to 5.2% (on average) ($n = 4$). Measurements at the "normal" instrument temperature (varying from 25 to 32°C) gave R.S.D.s up to 10.4% ($n = 4$).

Flavones with two adjacent hydroxyl groups in ring B (luteolin) and flavonols (especially kaempferol and morin) formed the most intensely fluorescent complexes (Table 3).

In comparison with NA detection, the peak areas of DTC complexes of these compounds were up to four times larger. When detected with DTC glycosidation in position 7 or 5 had no marked influence on the fluorescence intensity compared with the corresponding aglycones (see, *e.g.*, kaempferol, kaempferol-7-O-rhamnoside and kaempferol-7-O-neohesperidoside). Methylation of the hydroxyl at the 4′-position (compare kaempferol and kaempferide) reduced the fluorescence but it still was higher than that of NA-detected kaempferide. On the other hand, kaempferol-3-O-glycosides and luteolin-7,3′-diglucoside showed a weak fluorescence. Glycosidation in these positions did not have such an influence when detected with NA. Hence for qualitative analysis comparative detection with DTC and NA can indicate the position of the glycosidated hydroxyl groups of kaempferol and luteolin glycosides.

Quantitative measurements of quercetin–DTC and –NA complexes every 5 min over a period of 40 min indicated a decrease in the DTC peak area of 3.8% within 15 min and a further 3.5% in the following 25 min. The decreases with NA detection were 13.8% and 3.1%, respectively. The R.S.D. range of densitometric measurements was 4.3–7.1% (5.2% on average) ($n = 4$). Densitometric measurements were best made at least 15 min after spraying.

Our investigations showed that DTC is suitable for both the qualitative and quantitative analysis of 3′,4′-dihydroxy flavones and of flavonols, especially kaempferol and its glycosides with a free 3-OH group.

References

[1] T.A. Geissmann, *The Chemistry of Flavonoid Compounds*, Pergamon Press, Oxford, 1962.
[2] J.B. Harborne, T.J. Mabry and H. Mabry, *The Flavonoids*, Chapman & Hall, London, 1975.
[3] P.P.S. Schmidt, *J. Chromatogr.*, 157 (1978) 217.
[4] R. Neu, *Fresenius' Z. Anal. Chem.*, 142 (1954) 335.
[5] R. Neu, *Fresenius' Z. Anal. Chem.*, 151 (1956) 328.
[6] H. Homberg and H. Geiger, *Phytochemistry*, 19 (1980) 2443.
[7] I.M. Hais and K. Macek, *Handbuch der Papierchromatographie*, Gustav Fischer, Jena, 1958.
[8] M. Billeter, B. Meier and O. Sticher, *J. Planar Chromatogr.*, 3 (1990) 370.
[9] T. Hayashi, K. Hara, S. Kawai and T. Ohno, *Chem. Pharm. Bull.*, 18 (1970) 1112.
[10] H. Jork, W. Funk, W. Fischer and H. Wimmer, *Dünnschichtchromatographie*, Vol. 1b, VCH, Weinheim, 1993.
[11] H. Jork, W. Funk, W. Fischer and H. Wimmer, *Dünnschichtchromatographie*, Vol. 1a, VCH, Weinheim, 1989.

ELSEVIER

Journal of Chromatography A, 675 (1994) 282–285

JOURNAL OF CHROMATOGRAPHY A

Short Communication

Prediction of the lipophilicity of some plant growth-stimulating amido esters of ethanolamine using reversed-phase thin-layer chromatography

Simion Gocan*, Florin Irimie, Gabriela Cîmpan

Analytical Chemistry Department, "Babeş-Bolyai" University, 11 Arany Janos Street, 3400 Cluj-Napoca, Romania

(First received October 5th, 1993; revised manuscript received March 17th, 1994)

Abstract

Using reversed-phase high-performance thin-layer chromatography with octadecylsilane-bonded silica gel as the stationary phase and methanol–water as the mobile phase, several new compounds (amido esters of ethanolamine) were studied. The R_M values were plotted *versus* methanol molar fraction (x) and a linear correlation was obtained, $R_M = a_0 + a_1X$, characterized by high values of the correlation coefficient, r. The R_M values for $X = 0$ (organic solvent content), $(R_M)_{X=0} = a_0$, can be used to elucidate the lipophilicity of the studied compounds. The log P values were calculated using fragmental constants. A good correlation was found between a_0 and log P, with $r = 0.929$.

1. Introduction

Lipophilicity can be determined by the traditional partition method between *n*-octanol and water [1,2]. The octanol–water system is used in most partition studies but the determination of the partition coefficient by equilibration methods [3] is difficult. The difficulties can be overcome by using chromatographic methods, especially reversed-phase thin-layer chromatography (RP-TLC) [4–7]. Martin and Synge [8] and Consden *et al.* [9] derived a relationship between the partition coefficient P and R_F values in partition chromatography. Bate-Smith and Westall [10] introduced the term $R_M = \log(1/R_F - 1)$, which leads to a linear correlation between the partition coefficient (log P) and R_M values. The correlations between log P and log k' or R_M are frequently linear for non-ionic and ionic compounds [11–13]. When a compound contains one or more dissociable polar substituents, the pH [14,15] and the ionic strength of the eluent [16–18] modify the apparent lipophilicity. The hydrophobic properties of seventeen aniline and phenol derivatives were characterized by Gullner *et al.* [19] by means of RP-TLC and RP-HPTLC retention data. Cserháti *et al.* [20] studied the lipophilicity of aniline and 36 ring-substituted aniline derivatives by RP-TLC. The R_M values were determined under different experimental conditions, including the addition of salt solutions to the silica gel or to the eluent. Two linear

* Corresponding author.

0021-9673/94/$07.00
SSDI 0021-9673(94)00274-D

correlations between the R_M and log P values [21] and between R_M and the sum of the lipophilicity values of the substitutents $\Sigma\pi$ [22] were obtained. These correlations were in all instances inferior to those obtained in salt-free systems.

The purpose of this study was to determine the lipophilicity for fourteen new plant growth-stimulating amido esters of ethanolamine using RP-HPTLC and to establish the correlation between the R_M values for a zero organic solvent content of the eluent and the calculated log P values.

2. Experimental

The structures of the amido esters of ethanolamine studied are shown in Fig. 1. These compounds were synthesized in our laboratory (Department of Organic Chemistry) [23] and they are new plant-growth stimulators. The compounds showed growth-stimulating activity in the Moewus test with *Lepidium satium* similar to that of the reference substance indoleacetic acid [24].

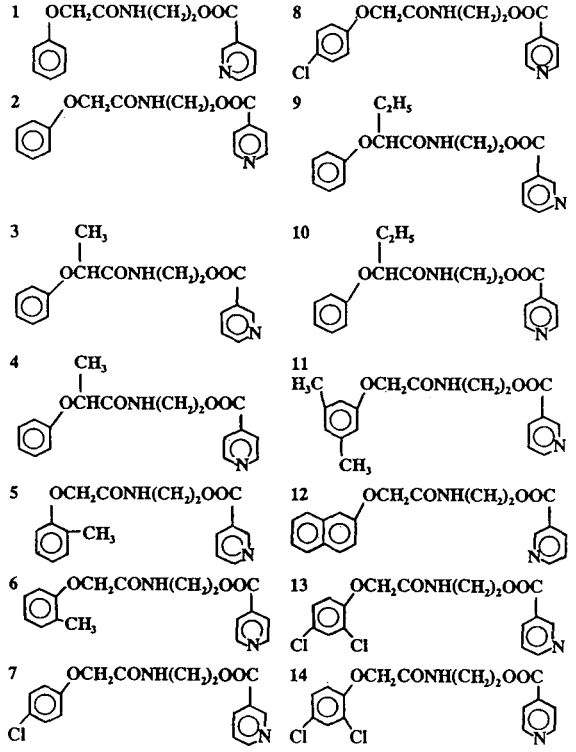

Fig. 1. Structures of the amido esters of ethanolamine studied.

HPTLC plates (10×10 cm) precoated with silica gel (RP-F_{254s}) were obtained from Merck (Darmstadt, Germany). Methanol for chromatography was obtained from Reactivul (Bucharest, Romania).

Solutions of the compounds in methanol (1 mg/ml) we prepared and 2 μl per spot were applied to the starting line, 1.5 cm from the bottom edge of the plate. The applied spots were dried in a gentle stream of air. The plates were developed in a previously equilibrated glass chromatographic chamber for 30 min. The migration distances of the eluent between start and the front was 8 cm in all instances.

The spots were revealed under UV light at 254 nm (Camag universal UV lamp).

3. Results and discussion

C_{18}-bonded silica gel was used as a non-polar stationary phase and methanol–water as a polar mobile phase. The experimentally measured R_M values with different concentrations of methanol (in terms of the molar fraction X) in the mobile phase are presented in Table 1.

It is well known that in binary aqueous organic eluents, *e.g.*, methanol–water, methanol has a decisive influence on the overall chromatographic distribution equilibria reflected in the R_M values of the investigated solutes.

A good linear correlation ($R_M = a_0 + a_1X$) was found between R_M and X, characterized by high values for the correlation coefficient, r. The R_M values extrapolated to zero organic solvent content, $(R_M)_{X=0} = a_0$, are different and depend on the structures. The intercept value a_0 can be correlated with the lipophilicity of the compound, and the slope a_1 can be considered as a measure of the strength of the mobile phase or, in other words, a_1 is the mobile phase contribution to the solute retention (Table 1).

Table 1
Dependence of R_F values (first row in each pair) and R_M values (second row) of some amido esters of ethanolamine on methanol molar fraction in aqueous solutions, X

Sample No.[a]	$X/(1-X)$							Log P
	0.800/0.200	0.640/0.360	0.509/0.491	0.400/0.600				
1	0.78 −0.549	0.62 −0.213	0.52 −0.053	0.31 0.347	1.13	−2.12	−0.981	2.090
2	0.76 −0.501	0.60 −0.176	0.50 0.000	0.29 0.389	1.17	−2.12	−0.984	2.090
3	0.78 −0.545	0.61 −0.194	0.50 0.000	0.29 0.389	1.23	−2.24	−0.988	2.497
4	0.78 −0.549	0.59 −0.158	0.48 0.035	0.29 0.389	1.25	−2.25	−0.992	2.497
5	0.73 −0.432	0.51 −0.017	0.40 0.176	0.19 0.630	1.57	−2.52	−0.985	2.594
6	0.75 −0.477	0.54 −0.070	0.40 0.176	0.20 0.602	1.58	−2.60	−0.991	2.594
7	0.73 −0.432	0.54 −0.070	0.40 0.176	0.20 0.602	1.53	−2.49	−0.988	2.814
8	0.74 −0.454	0.53 −0.052	0.39 0.194	0.20 0.602	1.57	−2.55	−0.992	2.814
9	0.76 −0.501	0.56 −0.105	0.43 0.122	0.21 0.575	1.53	−2.57	−0.987	3.027
10	0.77 −0.525	0.56 −0.105	0.41 0.158	0.21 0.575	1.59	−2.66	−0.993	3.027
11	0.70 −0.368	0.48 0.035	0.34 0.288	0.15 0.753	1.76	−2.69	−0.988	3.039
12	0.71 −0.389	0.48 0.035	0.34 0.288	0.15 0.753	1.78	−2.74	−0.989	3.374
13	0.67 −0.308	0.42 0.140	0.28 0.410	0.11 0.908	2.00	−2.92	−0.989	3.479
14	0.68 −0.327	0.42 0.140	0.27 0.432	0.10 0.954	2.11	−3.09	−0.989	3.479

[a] See Fig. 1.

The log P values were calculated according to the method described by Rekker [25] using the fragmental constants and the relationship log $P = \Sigma f_i n_i + \Sigma k_n C_m$, where f_i is fragmental constant for fragment i, n_i is the number of identical fragments, k_n is the number of identical proximity effect corrections and C_m is the proximity effect correction type m. The resulting values for the studied compounds are present in Table 1.

Arranging the compounds according to their increasing values of log P, the same trend results for the corresponding a_0 values. Exceptions were observed for certain compounds, but these were within the experimental error limits. The intercept values were correlated with log P values, and the linear regression is plotted in Fig. 2. In this way, the following linear expression was obtained: $a_0 = 0.140 + 0.603$ log P. The statisti-

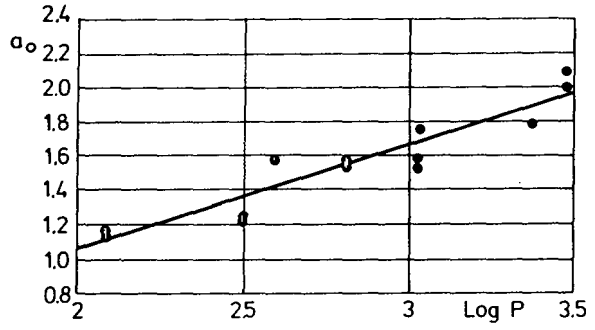

Fig. 2. Correlation between a_0 and log P values.

cally supported correlation coefficient was $r = 0.929$.

4. Conclusions

RP-HPTLC is a suitable method for the determination of the intercept values $(R_M)_{X=0} = a_0$, which may be used as lipophilicity parameter for several compounds. A good correlation between a_0 and log P with $r = 0.929$ was found.

References

[1] C. Hansch and S.M. Anderson, *J. Org. Chem.*, 32 (1967) 2583.
[2] R.N. Smith, C. Hansch and M.A. Ames, *J. Pharm. Sci.*, 64 (1975) 599.
[3] A. Hulshoff and J.H. Perrin, *J. Chromatogr.*, 120 (1976) 65.
[4] C.B.C. Boyce and B.V. Milborrow, *Nature*, 208 (1965) 537.
[5] G.L. Biagi, M.C. Guerra, A.M. Barbaro and M.F. Gamba, *J. Med. Chem.*, 13 (1970) 511.
[6] G.L. Biagi, A.M. Barbaro and M.C. Guerra, *J. Chromatogr.*, 41 (1969) 371.
[7] T. Cserháti, Y.M. Darwish and Gy. Matolcsy, *J. Chromatogr.*, 270 (1983) 97.
[8] A.J.P. Martin and R.L.M. Synge, *Biochem. J.*, 35 (1941) 1358.
[9] R. Consden, A.H. Gordon and A.J.P. Martin, *Biochem. J.*, 38 (1944) 224.
[10] E.C. Bate-Smith and R.G. Westall, *Biochim. Biophys. Acta*, 4 (1950) 427.
[11] A.M. Barbaro, M.C. Guerra, G. Cantelli Forti, G. Aicardi, G.L. Biagi, P. DaRe, P. Valenti and P.A. Borea, *J. Chromatogr.*, 242 (1982) 1.
[12] T. Hanai, K.C. Tran and J. Hubert, *J. Chromatogr.*, 239 (1982) 385.
[13] M. Kuchar, V. Ryholec, M. Jelinkova, V. Rabek and O. Nemeček, *J. Chromatogr.*, 162 (1979) 197.
[14] B. Rittich, M. Polster and O. Králik, *J. Chromatogr.*, 197 (1980) 43.
[15] Gy. Vigh, J. Varga-Puchony, J. Hlavay and E. Papp-Hites, *J. Chromatogr.*, 236 (1982) 51.
[16] T. Cserháti, Y.M. Darwish and Gy. Matolcsy, *J. Chromatogr.*, 241 (1982) 223.
[17] T. Cserháti, M. Szögy and L. Györfi, *Chromatographia*, 20 (1985) 253.
[18] E. Pap and Gy. Vigh, *J. Chromatogr.*, 258 (1983) 49.
[19] G. Gullner, T. Cserháti, B. Bordás and K. Valkó, *J. Liq. Chromatogr.*, 12 (1989) 957.
[20] T. Cserháti, B. Bordás and M. Szögy, *Chromatographia*, 21 (1986) 312.
[21] C. Hansch and A. Leo, *Substituent Constants for Correlation Analysis in Chemistry and Biology*, Wiley, New York, 1979.
[22] C. Hansch, A. Leo, S.H. Unger, K.H. Kim, D. Mikaitani and E.J. Lien, *J. Med. Chem.*, 16 (1973) 1207.
[23] F. Irimie, S. Mager, E. Brown and M. Horn, *Rev. Roum. Chim.*, in press.
[24] F. Irimie, *Thesis*, "Babeş-Bolyai" University, Cluj-Napoca, Romania, 1993.
[25] R.F. Rekker, *The Hydrophobic Fragmental Constants*, Elsevier, Amsterdam, 1977.

ELSEVIER

Journal of Chromatography A, 675 (1994) 286–287

JOURNAL OF CHROMATOGRAPHY A

Book Review

Capillary zone electrophoresis (*Electrophoresis Library*, edited by R.J. Radola, Vol. 3), by F. Foret, L. Křivánková and P. Boček, VCH, Weinheim, 1993, XIV + 346 pp., price DM 228.00/£93.00, ISBN 3-527-30019-8.

Capillary Zone Electrophoresis is the third volume in a series devoted to electrophoresis entitled *Electrophoresis Library*. The first two volumes are *Analytical Isotachophoresis* and *The Dynamics of Electrophoresis*. This series was created to provide readers with firm guidance in the field of electrophoresis, and deals with selected techniques or important areas of application. The present volume is devoted to capillary zone electrophoresis (CZE).

The book is divided into ten chapters comprising 346 pages. The first two chapters, introduction and brief history, are very concise and to the point. The historical perspective gives credit where it is due. The third chapter deals with fundamental concepts and theoretical principles. This is a comprehensive chapter which presents a good review of electrophoresis theory and deals with such topics as mobility, effect of temperature, ionic strength, current and so on. While Chapter 3 deals with pure theory, Chapter 5 deals with principles of capillary electrophoresis (CE) techniques such as zone electrophoresis, isotachophoresis, isoelectric focusing, micellar electrokinetic chromatography and electrophoresis in sieving media. The explanations of each technique are brief and the reader is referred to literature reviews and publications to supplement the book discussions and explanations. Chapter 4 deals with the phenomena accompanying electrophoresis and Joule heat before it discusses electroosmosis, diffusion and electromigration dispersion. This chapter could have been organized in a more simplified form to generate a streamlined discussion. The overall organization of the book, in my humble opinion, could have been better. For example, practice of CE (Chapter 6) is discussed ahead of instrumentation (Chapter 7). In Chapter 6 the readers are reminded of diffusion, Joule heating and other topics that were discussed in a previous chapter, however, it also contains an excellent discussion of CE practice and is rich in references. Most of these references, however, are prior to 1991. I realize that writing a book takes time, and the authors cannot chase after every reference that appears in the scientific literature, but for a book published in 1993, the reader expects to see more references from 1991 and some from 1992. The chapter on the instrumentation system is adequate and reviews the basic CE instrumentation, including detection, in a satisfactory manner. I question the book's organization because commercial instrumentation, Chapter 9, does not follow Chapter 7, which deals with instrumentation. Instead, Chapter 9 follows advanced systems for improvement of selectivity, sensitivity and identification (Chapter 8). The last chapter of the book, Chapter 10, deals with applications, which makes up one-third of the book, is

SSDI 0021-9673(94)00437-E

divided into 17 sections dealing with different groups of compounds in a tabulated form and is rich in references, 331, up to 1991.

Overall, the book is a good reference for CZE users. The scientific discussions are sound and to the point; however, the English needs some attention (see for example, the second paragraph on page 22). Thin capillary is used in Chapter 2 to denote narrow capillary and non-constant for variable. On page 114, Figure 6-13, there is an error in the caption which states that pressure generated in a hand-held syringe can easily exceed 500 atm. Should it not read 500 p.s.i.?

Among the books that have been published to date on CZE, this one ranks in the upper half of the list.

H.J. Issaq

Frederick, MD, USA

Author Index

Journal of Chromatography A

Request for Manuscripts

Susumu Honda will edit a special, thematic issue of the *Journal of Chromatography A* entitled

Chromatographic and Electrophoretic Analyses of Carbohydrates

Both reviews and research articles will be included.
Topics such as the following will be covered:

- Gas chromatography and gas chromatography–mass spectrometry of carbohydrates
- Supercritical fluid chromatography of carbohydrates
- Thin-layer chromatography of carbohydrates
- Liquid chromatography of carbohydrates
  - Separations based on various modes including adsorption, hydrophilic interaction, hydrophobic interaction, ion exchange, ligand exchange, size exclusion, bioaffinity, etc.
  - Derivatization
  - Preparative liquid chromatography
  - High-performance liquid chromatography–mass spectrometry
- Electrophoresis of carbohydrates
  - Gel electrophoresis
  - Capillary zone electrophoresis
  - Micellar electrokinetic capillary chromatography
  - Ultrasensitive detection
  - Derivatization
  - Capillary electrophoresis–mass spectrometry
- Chromatography and electrophoresis in glycobiology
  - Release of carbohydrates from glycoconjugates
  - Monosaccharide composition analysis
  - Oligosaccharide mapping
  - Oligosaccharide sequencing
  - Automated analysis of carbohydrates

Potential authors of reviews should contact Roger Giese, Editor, prior to any submission. Address: Mugar Building Rm 122, Northeastern University, Boston, MA 02115, USA; tel.: (+1-617) 373-3227; fax: (+1-617) 373-8720.

The deadline for receipt of submissions is **November 15, 1994**. Manuscripts submitted after this date can still be published in the Journal, but then there is no guarantee that an accepted article will appear in this special, thematic issue. Four copies of the manuscript, citing this issue, should be submitted to the Editorial Office, *Journal of Chromatography A*, P.O. Box 681, NL-1000 AR Amsterdam, The Netherlands. All manuscripts will be reviewed and acceptance will be based on the usual criteria for publishing in the *Journal of Chromatography A*.

Intelligent Software for Chemical Analysis

Edited by **L.M.C. Buydens** and **P.J. Schoenmakers**

Data Handling in Science and Technology Volume 13

Various emerging techniques for automating intelligent functions in the laboratory are described in this book. Explanations on how systems work are given and possible application areas are suggested. The main part of the book is devoted to providing data which will enable the reader to develop and test his own systems. The emphasis is on expert systems; however, promising developments such as self-adaptive systems, neural networks and genetic algorithms are also described.

Contents:

1. Introduction. Automation and intelligent software. Expert systems. Neural networks and genetic algorithms. Reader's guide. Concepts. Conclusions. **2. Knowledge-based Systems in Chemical Analysis** (P. Schoenmakers). Computers in analytical chemistry. Sample preparation. Method selection. Method development. Instrument control and error diagnosis. Data handling and calibration. Data interpretation. Validation. Laboratory management. Concluding remarks. Concepts. Conclusions. Bibliography. **3. Developing Expert Systems** (H. van Leeuwen). Introduction. Prerequisites: Knowledge acquisition. Knowledge engineering. Inferencing. Explanation facilities. The integration of separate systems. Expert-system testing validation and evaluation. Concepts. Conclusions. Bibliography. **4. Expert-System-Development Tools** (L. Buydens, H. van Leeuwen, R. Wehrens). Tools for implementing expert systems. Tool selection. Knowledge-acquisition tools. Concepts. Conclusions. Bibliography. **5. Validation and Evaluation of Expert Systems for HPLC Method Development - Case Studies** (F. Maris, R. Hindriks). Introduction. Case study I: Expert systems for method selection and selectivity optimization. Case study II: System-optimization expert system. Case study III: Expert system for repeatability testing, applied for trouble-shooting in HPLC. Case study IV: Ruggedness-testing expert system. General comments on the evaluations. Concepts. Conclusions. Bibliography. **6. Self-adaptive Expert Systems** (R. Wehrens). Introduction - maintaining expert systems. Self-adaptive expert systems: Methods and approaches. The refinement approach of SEEK. Examples from analytical chemistry. Concluding remarks. Concepts. Conclusions. Bibliography. **7. Inductive Expert Systems** (R. Wehrens, L. Buydens). Introduction. Inductive classification by ID3. Applications of ID3 in analytical chemistry. Concluding remarks. Concepts. Conclusions. Bibliography. **8. Genetic Algorithms and Neural Networks** (G. Kateman). Introduction. Genetic algorithms. Artificial neural networks. Concepts. Conclusions. Bibliography. **9. Perspectives.** Limitations of Intelligent Software. Dealing with intelligent software. Potential of intelligent software. **Index.**

ELSEVIER SCIENCE B.V.

© 1993 366 pages Hardbound
Price: Dfl. 350.00 (US $ 200.00)
ISBN 0-444-89207-9

ORDER INFORMATION

For USA and Canada
ELSEVIER SCIENCE INC.
P.O. Box 945
Madison Square Station
New York, NY 10160-0757
Fax: (212) 633 3880

In all other countries
ELSEVIER SCIENCE B.V.
P.O. Box 330
1000 AH Amsterdam
The Netherlands
Fax: (+31-20) 5862 845

US$ prices are valid only for the USA & Canada and are subject to exchange rate fluctuations; in all other countries the Dutch guilder price (Dfl.) is definitive. Customers in the European Community should add the appropriate VAT rate applicable in their country to the price(s). Books are sent postfree if prepaid.

Send your article on floppy disk!

All articles may now be submitted on computer disk, with the eventual aim of reducing production times and improving the reliability of proofs still further. Please follow the guidelines below.

With revision, your disk plus one final, printed and exactly matching version (as a printout) should be submitted together to the editor. **It is important that the file on disk to be processed and the printout are identical.** Both will then be forwarded by the editor to Elsevier.

The accepted article will be regarded as final and the files will be processed as such. Proofs are for checking typesetting/editing: only printer's errors may be corrected. No changes in, or additions to the edited manuscript will be accepted.

Illustrations should be provided in the usual manner and, if possible, on a **separate** floppy disk as well.

Please follow the general instructions on style/arrangement and, in particular, the reference style of this journal as given in the "Guide for Authors".

The preferred storage medium is a 5¼ or 3½ inch disk in MS-DOS or Macintosh format, although other systems are also welcome.

Please label the disk with your name, the software & hardware used and the name of the file to be processed.

For further information on the preparation of compuscripts please contact:

Elsevier Science B.V.
Journal of Chromatography A
P.O. Box 330
1000 AH Amsterdam, The Netherlands
Phone: (+31-20) 5862 793 Fax: (+31-20) 5862459

ELSEVIER SCIENCE

PUBLICATION SCHEDULE FOR THE 1994 SUBSCRIPTION

Journal of Chromatography A and *Journal of Chromatography B: Biomedical Applications*

MONTH	1993	J–M	J	J	A	
Journal of Chromatography A	652–657	658–669	670/1 + 2 671/1 + 2 672/1 + 2	673/1 673/2 674/1 + 2 675/1 + 2 676/1	676/2 677/1 677/2 678/1	The publication schedule for further issues will be published later.
Bibliography Section		681/1	681/2			
Journal of Chromatography B: Biomedical Applications		652–655	656/1 656/2	657/1 657/2	658/1 658/2	

INFORMATION FOR AUTHORS

(Detailed *Instructions to Authors* were published in *J. Chromatogr. A*, Vol. 657, pp. 463–469. A free reprint can be obtained by application to the publisher, Elsevier Science B.V., P.O. Box 330, 1000 AH Amsterdam, Netherlands.)

Types of Contributions. The following types of papers are published: Regular research papers (full-length papers), Review articles, Short Communications and Discussions. Short Communications are usually descriptions of short investigations, or they can report minor technical improvements of previously published procedures; they reflect the same quality of research as full-length papers, but should preferably not exceed five printed pages. Discussions (one or two pages) should explain, amplify, correct or otherwise comment substantively upon an article recently published in the journal. For Review articles, see inside front cover under Submission of Papers.

Submission. Every paper must be accompanied by a letter from the senior author, stating that he/she is submitting the paper for publication in the *Journal of Chromatography A* or *B*.

Manuscripts. Manuscripts should be typed in **double spacing** on consecutively numbered pages of uniform size. The manuscript should be preceded by a sheet of manuscript paper carrying the title of the paper and the name and full postal address of the person to whom the proofs are to be sent. As a rule, papers should be divided into sections, headed by a caption (*e.g.*, Abstract, Introduction, Experimental, Results, Discussion, etc.). All illustrations, photographs, tables, etc., should be on separate sheets.

Abstract. All articles should have an abstract of 50–100 words which clearly and briefly indicates what is new, different and significant. No references should be given.

Introduction. Every paper must have a concise introduction mentioning what has been done before on the topic described, and stating clearly what is new in the paper now submitted.

Experimental conditions should preferably be given on a *separate* sheet, headed "Conditions". These conditions will, if appropriate, be printed in a block, directly following the heading "Experimental".

Illustrations. The figures should be submitted in a form suitable for reproduction, drawn in Indian ink on drawing or tracing paper. Each illustration should have a caption, all the *captions* being typed (with double spacing) together on a *separate sheet*. If structures are given in the text, the original drawings should be provided. Coloured illustrations are reproduced at the author's expense, the cost being determined by the number of pages and by the number of colours needed. The written permission of the author and publisher must be obtained for the use of any figure already published. Its source must be indicated in the legend.

References. References should be numbered in the order in which they are cited in the text, and listed in numerical sequence on a separate sheet at the end of the article. Please check a recent issue for the layout of the reference list. Abbreviations for the titles of journals should follow the system used by *Chemical Abstracts*. Articles not yet published should be given as "in press" (journal should be specified), "submitted for publication" (journal should be specified), "in preparation" or "personal communication".

Vols. 1–651 of the *Journal of Chromatography*; *Journal of Chromatography, Biomedical Applications* and *Journal of Chromatography, Symposium Volumes* should be cited as *J. Chromatogr.* From Vol. 652 on, *Journal of Chromatography A* (incl. Symposium Volumes) should be cited as *J. Chromatogr. A* and *Journal of Chromatography B: Biomedical Applications* as *J. Chromatogr. B*.

Dispatch. Before sending the manuscript to the Editor please check that the envelope contains four copies of the paper complete with references, captions and figures. One of the sets of figures must be the originals suitable for direct reproduction. Please also ensure that permission to publish has been obtained from your institute.

Proofs. One set of proofs will be sent to the author to be carefully checked for printer's errors. Corrections must be restricted to instances in which the proof is at variance with the manuscript.

Reprints. Fifty reprints will be supplied free of charge. Additional reprints can be ordered by the authors. An order form containing price quotations will be sent to the authors together with the proofs of their article.

Trace Element Analysis in Biological Specimens

Edited by **R.F.M. Herber** and **M. Stoeppler**

Techniques and Instrumentation in Analytical Chemistry Volume 15

The major theme of this book is analytical approaches to trace metal and speciation analysis in biological specimens. The emphasis is on the reliable determination of a number of toxicologically and environmentally important metals. It is essentially a handbook based on the practical experience of each individual author. The scope ranges from sampling and sample preparation to the application of various modern and well-documented methods, including quality assessment and control and statistical treatment of data. Practical advice on avoiding sample contamination is included.

In the first part, the reader is offered an introduction into the basic principles and methods. Quality control and all approaches to achieve reliable data are treated as well.

The chapters of the second part provide detailed information on the analysis of thirteen trace metals in the most important biological specimens.

The book will serve as a valuable aid for practical analysis in biomedical laboratories and for researchers involved with trace metal and species analysis in clinical, biochemical and environmental research.

Contents:

© 1994 590 pages Hardbound
Price: Dfl. 475.00 (US$ 271.50)
ISBN 0-444-89867-0

ORDER INFORMATION
ELSEVIER SCIENCE B.V.
P.O. Box 330
1000 AH Amsterdam
The Netherlands
Fax: (+31-20) 5862 845
For USA and Canada
P.O. Box 945
Madison Square Station
New York, NY 10159-0945
Fax: (212) 633 3680
US$ prices are valid only for the USA & Canada and are subject to exchange rate fluctuations; in all other countries the Dutch guilder price (Dfl.) is definitive. Customers in the European Union should add the appropriate VAT rate applicable in their country to the price(s). Books are sent postfree if prepaid.

ELSEVIER SCIENCE